Publisher: State and Provincial Joint Engineering Lab. of Advanced Network Monitoring and Control (ANMC)

Cooperate:

Xi'an Technological University (China)

West Virginia University (USA)

Huddersfield University of UK (UK)

Missouri Western State University (USA)

James Cook University of Australia (Australia)

National University of Singapore (Singapore)

Approval:

Library of Congress of the United States

Shaanxi provincial Bureau of press, Publication, Radio and Television

Address:

4525 Downs Drive, St. Joseph, MO64507 , USA

No. 2 Xuefu Road, weiyang District, Xi’an, 710021, China

Telephone: +1-816-2715618 (USA) +86-29-86173290 (China)

Website：www.ijanmc.org

E-mail：ijanmc@jianmc.org

xxwlcn@163.com

ISSN: 2470-8038

Print No. (China): 61-94101

Proceedings

2017 International Conference on Computer Network, Electronic and Automation

ICCNEA 2017

Xi'an, China
23-25 September 2017

IEEE Computer Society Order Number E6156
ISBN-13: 978-1-5386-3981-8
BMS Part # CFP17M07-CDR

Additional copies may be ordered from:

IEEE Computer Society
Customer Service Center
10662 Los Vaqueros Circle
P.O. Box 3014
Los Alamitos, CA 90720-1314
Tel: + 1 800 272 6657
Fax: + 1 714 821 4641
http://computer.org/cspress
csbooks@computer.org

IEEE Service Center
445 Hoes Lane
P.O. Box 1331
Piscataway, NJ 08855-1331
Tel: + 1 732 981 0060
Fax: + 1 732 981 9667
http://shop.ieee.org/store/
customer-service@ieee.org

IEEE Computer Society
Asia/Pacific Office
Watanabe Bldg., 1-4-2
Minami-Aoyama
Minato-ku, Tokyo 107-0062
JAPAN
Tel: + 81 3 3408 3118
Fax: + 81 3 3408 3553
tokyo.ofc@computer.org

Individual paper REPRINTS may be ordered at: <reprints@computer.org>

Editorial production by Juan E. Guerrero
Cover art production by Annie Jiu
Printed in the United States of America by Applied Digital Imaging

IEEE Computer Society
***Conference Publishing Services* (CPS)**
http://www.computer.org/cps

Organizing Committees

General Chair:

Ph.D. Weiguo Liu
Prof. and President of Xi'an Technological University, China
Director of State and Provincial Joint Engineering Lab. of Advanced Network and Monitoring, China

Chairman:

Ph.D. Houbing Song
Golden Bear Scholar and Professor, SM IEEE
Department of Electrical and Computer Engineering, West Virginia University, USA.
Director of Security and Optimization for Networked Globe Laboratory, USA

Dr. Jianguo Wang
Prof. and Dean, Xi'an Technological University, China
Vice-Director of State and Provincial Joint Engineering Lab. of Advanced Network and Monitoring, China

Program Chair:

Prof. George Yang
Missouri Western State University, USA
4525 Downs Drive，St. Joseph, MO 64507
Phone: (816) 271-5618 (office)

Prof. Zhongsheng Wang
Xi'an Technological University, China
No. 4 North Jinhua Road, Xi'an 710032,Shaanxi Province, China
Tele:+86-29-86173290 (office)

Program Committees

Ph.D. and Prof. George Yang, Missouri Western State University, USA
Ph.D. Houbing Song, SM IEEE Department of Electrical and Computer Engineering Director, West Virginia University, USA
Ph.D. Linhuo Shi, Toyoda Gosei North America Corporation, USA Ph.D. and Prof. Zhijie Xu,University of Huddersfield, UK
Ph.D. and Prof. Changyuan Yu, National Univ. of Singapore (NUS) Ph.D. and Prof. Y.W.Liu Rm, Hong Kong polytechnic University , China Ph.D. William S. Cheung, The University of Hong Kong. , China
Prof. Mao Wenlin, Xi'an JiaoTong University, China
Ph.D. and Prof. Hongyi Sun, City University of Hong Kong, China Dr. and Prof. Yaping Lei, Xi'an Technological University, China Prof. Li Yibo, Shenyang Aerospace University, China
Prof. Wang Chongqing, Nanjing University of Aeronautics And Astronautics, China Ph.D. and Prof. Yuhai yang, Beihang University, China
Ph.D. Mei Li, China university of Geosciences (Beijing) , China
Ph.D. and Prof. Wenhui Chen, Northwestern Polytechnical University (NPU), China Ph.D. and Prof. Guohua Geng, Northwest University (NWU), China
Dr. Samadhan J Jadhao, Indian Veterinary Research Institute, India Dr. Ahm Omar, Menoufia University, Egypt
Dr. Ahmed Nabih Zaki Rashed, Menoufia University, Egypt Prof. Zhen Luo, Soong Sil University, South Korea
P.h. D Nikunj Batheja, Indian Institute of Technology Kanpur, India

Message from General Chair

The International Conference on Computer Network, Electronic and Automation (ICCNEA) is a high-level international forum for engineers and scientists to state their innovative ideas and research results. It is also a multi-track international forum for academics, practitioners and research students to exchange their ideas, techniques, methods, and state-of-the-art applications for the latest computer network, electronic and automation. Initially, formed as a scientific venue for advanced network, electronic and automation, the conference will keep expanding and become a pedigree that attracts all over the world researchers to exchanges academic views. This is the first occurrence of ICCNEA and it will be a series conference, which will be held annually. The first session will be held in the beautiful ancient city of Xi 'an, Shaanxi, China, and it will be held all over the world afterwards. For this conference, ICCNEA solicits high-quality papers in the following disciplines: computer technology, network technology, electronic engineering, control and automation. The conference had received over 378 papers, and accepted 102 papers after two rounds of double-blind reviews. The acceptance rate of the contributed papers is about 27%. The ICCNEA 2017 conference invited four keynote speakers on advanced network engineering, monitoring and control, automation and control, electrical and computer engineering. The four of them will give an excellent speech to the conference, one of them is from Singapore and the others are from the USA.

The ICCNEA 2017 conference will be held in the beautiful city of Xi'an. The conference is mainly organized by the School of Computer Science and Engineering, Xi’an

Technological University, China, State and Provincial Joint Engineering Lab. of Advanced Network and Monitoring, China, supported by the Department of Electrical and Computer Engineering, West Virginia University, USA, Security and Optimization for Networked Globe Laboratory, USA, Missouri Western State University, USA, University of Huddersfield, HD1 3DH, UK and National Univ. of Singapore (NUS). The conference was supported by the IEEE CPS and IEEE computer society. Without the support of these universities, IEEE and all authors, the conference would not have been held successfully. On behalf of the conference general chair, I would like to say thank you.

Welcome to Xi’an.

Ph.D. Weiguo Liu
Prof. and President of Xi'an Technological University, China
Director of State and Provincial Joint Engineering Lab. of Advanced Network and Monitoring, China

Message from Program Chair

On behalf of the Technical Program Committee, it is our great honor and pleasure to welcome you to the ICCNEA 2017 in Xi'an, one of the famous historical and top tourist cities in the world.

ICCNEA 2017 has attracted excellent contributions covering research topics in a wide range of computer science, network, Electronic and Automation. Paper submissions and reviews were organized in 4 regular sessions and 2 special sessions. A total of 378 manuscripts were received. Each paper was assigned to at least two independent reviewers by program chair or the general chair. After being thoroughly reviewed, 102 manuscripts were accepted, and the acceptance rate is about 27%. All the accepted papers will be presented either in the oral speech or in the form of projections, and about 83 authors will attend the conference, which will spread over the three days of Sep. 23-25, 2017.

Apart from paper presentations, the ICCNEA2017 invited 4 keynote speakers and 3 experts from the industry and academia, who will share with us their visions and insights in the field of advanced network, electronic and automation. This year, we will have 2 half-day cutting-edge tutorials offered by the keynote and leading experts on the topics of research frontiers, while four branches section will address and demystify issues of interests to many colleagues ranging from all of the authors. We believe each participant will significantly benefit from such rich technical content and the featured events hosted by the experts. We thank the keynote speakers, IEEE CPS, IEEE computer society, organizers and authors for making this possible.

We are greatly indebted to the general chair and the program Committee who have been involved in organizing the review as well as forming the final program, and to the many reviewers who volunteered their time on quality review to ensure good quality of the accepted papers. We sincerely thanks to all the authors for preparing and submitting their papers to the ICCNEA 2017, which makes the event a reality while contributing to the high quality papers. Finally, the smooth review process would not be possible without the timely support and assistance from the IEEE Conference Publishing Services (CPS) and IEEE Computer Society.

Prof. George Yang

Missouri Western State University, USA 4525 Downs Drive
St. Joseph, MO 64507
Phone: (816) 271-5618 (office)
Email: yang@missouriwestern.edu

Welcome Message

Ladies and Gentlemen,

Welcome to the 2017 International Conference on Computer Network, Electronic and Automation (ICCNEA) and the beautiful city of Xi'an, Shaanxi, China.

First, I would like to express my sincere appreciation of the conference organizers for their hard work. Their efforts and services made this conference possible. If there are any places that need to improve, please provide them with your constructive suggestions.

There are tremendous developments every second in the fields of advanced network, electronic and automation. An academic conference is a valuable and efficient platform for us to exchange ideas, to meet new researches, and to develop new friendship and collaboration. I am really glad to see this time we have many researchers attending this conference to present their cutting-edge accomplishments. I firmly believe that we can make the conference a premium event in our research area. Hopefully, with the contribution of everyone, the conference will become an annual event with widespread impacts.

The conference is sponsored by Xi'an Technological University and State and Provincial Joint Engineering Lab. of Advanced Network and Monitoring Control, Located in Xi'an,

China, Department of Electrical and Computer Engineering, West Virginia University, USA, Director of Security and Optimization for Networked Globe Laboratory, USA. Xi'an Technological University is a multi-discipline technology-focused university currently with 26,000 undergraduate and graduate students as well as 1800 faculty and staff members.

Finally, I hope you find the conference informative and inspirational to your research. Please enjoy the discussions with your colleagues. Also, please enjoy the beautiful city of Xi'an, the most popular travel destinations in China

Thank you very much.
Dr. Jianguo Wang
Prof. and Dean, Xi'an Technological University, China
Vice-Director of State and Provincial Joint Engineering Lab. of Advanced Network and Monitoring, China

Table of Contents

Design and Implementation of the Comprehensive Information Platform for Smelting Enterprises

Ma Dandan
College of Electrical and Information Engineering,
Beihua University
Jilin， China
madandan11@126.com

Bai Jing
College of Electrical and Information Engineering,
Beihua University
Jilin， China
jlbyj@163.com

***Abstract*—According to the development of information technology and the management of metallurgical enterprises, the paper puts forward the design scheme of the information platform for metallurgical enterprises, introduces the structure and function of the new type of metallurgical information platform. It realize loop online collection, hierarchical data computation, distributed database management and global WEB publishing capability. And improve the level of production automation, reduce energy consumption and improve the competitiveness of enterprises**.

Keywords-metallurgical; enterprise information technology; networking; cloud services; big data

I. THE MEANING OF THE METALLURGY ENTERPRISE INFORMATION SYSTEM

In the era of big data[1-4], metallurgy enterprise information [5] is the development direction of the future. Metallurgy enterprise information is the future of information technology which can be applied to the whole process of the design of products, manufacture, managements and sales, as an object to development and utilization of information resources, as the main content to reform the enterprise production, management and marketing and other business process, as the goal of the dynamic development process in order to improve enterprise's economic benefit and competitiveness. Enterprise information is an event involving enterprise survival and the development and also is the enterprise management innovation accelerator; Information management and system innovation management, management innovation supplement each other, promote each other; information is the enterprise technological progress lifter; Information is also the multiplier of enterprise competitiveness; information is the safe valve of enterprise funds operation ; Information is the enterprise products to the world and the direct train of transnational management.

II. THE DESIGN OF METALLURGY ENTERPRISE INFORMATION SYSTEM FRAMEWORK

A real enterprise information system [6-8] must be a comprehensive, integrated information management system and a complete enterprise information system should be composed of horizontal and vertical two aspects. The lateral needs to cover supply productions, sales and finance, personnel, equipment maintenance, projects management and so on each link. The longitudinal should be from the bottom of the production equipment, production lines and materials control system to extend upward to the enterprise the highest level of [9-10].A real enterprise information system must be a comprehensive, integrated information management system.

For metallurgical enterprises, the application of a five-layer system architecture may be the best choice. The five systems are: level 1 system: the equipment control system; level 2 system: the process control system; level 3 system: workshop manufacturing execution system (MES);level 4 system: the enterprise resource planning system (ERP);level 5 systems: the enterprise management system and decision support system (DSS). The five layers of system are mutual integration and coordinate with each other, forming a complete enterprise information management system.

Among the three layers system of DCS and MES and ERP, business system regards production scheduling and production management as the core, and finally with enterprise ERP forms one of the multilevel network application system, which regards composition control and scheduling management and operation management as a whole. And the MES and ERP are the main system of the business application system .

MES built up the communication between DCS and ERP information with it around production process continuity of information collection, processing and handling and completed all kinds of production data and business plan transmission and so on by developing and producing various kinds of real-time database, DCS, PLC, instrument and meter, key equipment and the ERP system data interface. What MES levels mainly have are detailed scheduling, resource allocations and state managements, distribution of production units , processes managements, human resource managements, maintenance managements, quality management, document control, products tracking and inventory managements, performance analysis and data acquisitions etc.

ERP system achieves the enterprise resource planning that regards finance as the core and makes enterprise resources becoming a reasonable plan and allocation and management, makes the enterprise logistics, cash flow,

information flow be the integration of management, so as to guide the enterprise management, management, decision-making, specific function in business process management, sales and distribution, purchasing and inventory, financial management, customer relationship management, production management, human resource management, cost control and material management etc.

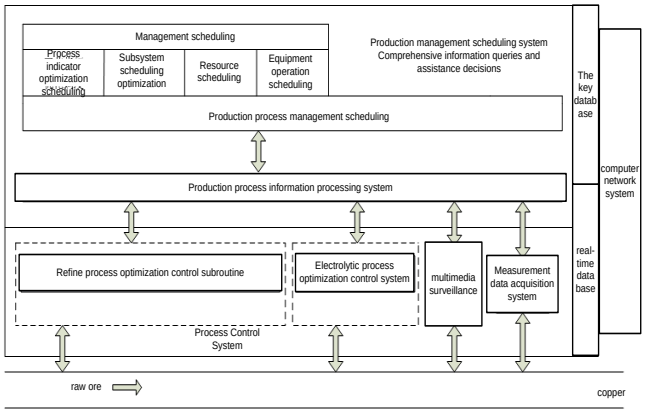

Figure 1. The integrated optimization scheduling system structure

Business systems first need timely data obtained from the production site information and guide the production scheduling, when necessary, it can according to a new technological process and process parameters optimization control strategy; secondly, it need to surround production scheduling and management to complete the relevant business operations and accept the production planning, production scheduling commands and controls instructions, and generates the necessary daily scheduling, production statistics etc. ERP system is the comprehensive information management system which is applied to all ranges , on the one hand, it accepts the production data from the MES level, on the other hand , it issued production plan to production department , according to the production and operation situation, you can adjust the plan and guide management decisions. As shown in figure 1 integrated optimization scheduling system structure.

At the management level, the manager leader needs to comprehend enterprise's production and management as a whole and production, supply and sale , people, goods of the process of production to correct and prevents the contents of abnormal timely. In the face of numerous business application systems, to facilitate the competent leadership, we need a comprehensive platform for the display, only need one account, a password to query and browse all information within the scope of his authority. Implementation through a comprehensive display platform based on ERP system to achieve and complete the comprehensive analysis of the production and management, by means of data mining, such as graphics, trends, dashboard intuitive form, we can provide it for management decision makers. Fig. 1 for integrated optimization scheduling system structure.

III. CLOUD SERVICES AND THE INTERNET OF THINGS IN THE APPLICATION OF METALLURGICAL INFORMATION TECHNOLOGY

The template is used to format your paper and style the text. All margins, column widths, line spaces, and text fonts are prescribed; please do not alter them. You may note peculiarities. For example, the head margin in this template measures proportionately more than is customary. This measurement and others are deliberate, using specifications that anticipate your paper as one part of the entire proceedings, and not as an independent document. Please do not revise any of the current designations.

Cloud services and the Internet of things are a hot field of information industry at home and abroad in recent years, our government thinks highly of it and we will vigorously support it. Both them will play a positive role in energy conservation and emissions reduction and enterprise innovation. Cloud service is not a new, specific IT technology, its characteristics is based on the Internet, especially high-speed Internet, which can be able to provide reliable, convenient and cheaper services for using. The users can choose the most suitable way for their own using according to their own needs , such as to pay on time, to pay according to the need, to pay according to times, to pay according to the users. And the system is flexible and scalable. For example, if users are less, system can be used fewer, if users are more, system can be used more. When you need more storage space, you can apply to the system. Cloud services can make users access to the standardized interface (Web browser or Console) you can use on-demand, self-service ways to visit cloud computing center and storage resources. By purchasing a cloud computing service, users can greatly reduce the investment in infrastructure, accelerate the system deployment, reduce management and operational costs. Cloud computing center offers a variety of data protection solutions, including online backup, offline backup and disaster in another place, and we can according to customer demands to set up the flexible backup and disaster plan in order to ensure the data availability.

Establish energy metering cloud computing service center in the whole country's industry. Energy metering cloud storage is the cloud computing system which regards data storage and management as the core. First, establish a computer cloud computing center. Cloud computing center includes monitoring system server and database system and a number of internal substation. Cloud computing can accept several enterprise database system data and have the cloud storage and release functions. The center also has the remote data list, remote diagnosis expert analysis evaluation, region or industry operation regulation and financial supervision even provides query interface of government and society, diagnosis and fault diagnosis of BBS and other functions. Fig. 2 is a cloud computing center network structure:

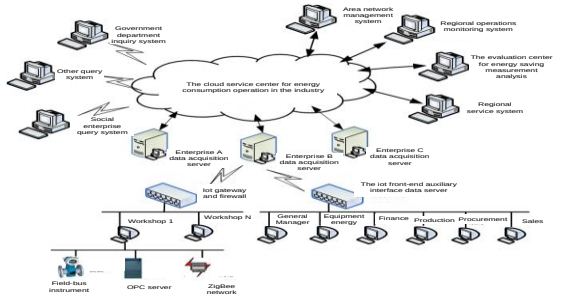

Figure 2. The cloud computing center network structure

Establish an intelligent integrated information networking platform, which has multiple levels and intelligent interface in the internal of the enterprise. And it uses the framework of wireless Internet of things and includes instrument bus data acquisition system, the database to form a system, data storage, computing analysis and networking WEB publishing and other functions. Through field bus and all kinds of Internet interface and wireless communication mode to realize the automatic equipment and instrument measurement and using the network security and redundant technology to form the independent stable and energy management network, people can achieve circulating online acquisition, hierarchical data computation, the distributed database management and the global WEB publishing function.

IV. METALLURGY ENTERPRISE INFORMATION DATA PROCESSING METHOD

Before you begin to format your paper, first write and save the content as a separate text file. Keep your text and graphic files separate until after the text has been formatted and styled. Do not use hard tabs, and limit use of hard returns to only one return at the end of a paragraph. Do not add any kind of pagination anywhere in the paper. Do not number text heads-the template will do that for you.

Finally, complete content and organizational editing before formatting. Please take note of the following items when proofreading spelling and grammar:

A. The raw data tracking

Define abbreviations and acronyms the first time they are used in the text, even after they have been defined in the abstract. Abbreviations such as IEEE, SI, MKS, CGS, sc, dc, and rms do not have to be defined. Do not use abbreviations in the title or heads unless they are unavoidable.

Because the information data of metallurgical enterprise is giant. In order to analysis the data and management effectively and clearly , we will make a raw data classification and start original information tracking analysis. We can track from five lines, which are from material into products, from energy consumption into products, from equipment into products, from releasing into the products, from human into products. And it is asked ensuring the energy management network and control network (DCS) and office automation (OA) three network to run and relate independently of each other. At the same time, we must pay attention to network security problem and the key area to be strictly on guard and defend to the last. And we can use the instrument of OPC server and distributed database systems for information collection and storage. When using a satellite synchronous timing, we should check the time of information systems to make each unit be a time synchronization system, which can guarantee the circulation of online data acquisition systems to have a valid time tag. Information acquisition system block diagram is shown in fig. 3.

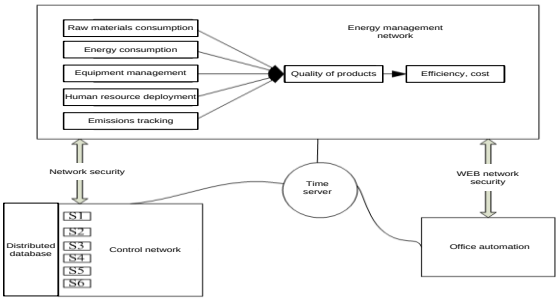

Figure 3. The information acquisition system diagram

B. Simple and flexible data entry interface

Information platform must have a flexible data access way. The current popular ways are OPC, FTP, ODBC, Matrix and other data acquisition ways; For Mobile devices, Mobile system design should be considered to use USB, infrared, Bluetooth, wireless access system.

C. The optimization of reliable distributed extensible database system

Almost every database product has a clustering solution. Oracle RAC is the most popular products in the industry. the biggest characteristic of its architecture is the Shared storage architecture (Shared-disk).The whole RAC cluster is built on a shared memory device, and the nodes are interconnected by high speed network. RAC Oracle provided very good high availability features. Oracle apparently aware of the problem, in the Oracle MAA (Maximum Availability Architecture) architecture, the ability of ASM to integrate multiple storage devices, ability makes the shared memory at the bottom of RAC have linear expansion of the processing ability of the cluster is no longer dependent on large storage and availability.

Using the Oracle database to define the data points (Data point) and common data points (Generic Data point)and Constant and the derivative data points (Derived Data point) and other data types. It can improve the utilization rate of database in that way to adopt flexible data storage method and through the substitution of value, data limitation and so on to ensure the data acquisition of continuous and reliable or through derived through Summarization concept.

D. The hierarchical data calculation

The basis of information system data calculation is divided into three layers: cycle (Loop), formula (MEVAS),

Excel. Loop (Loop) is to collect data in the field for online calculation. Including mathematical processing, logic operation, comparison operation, threshold processing, quantitative analysis, time data processing and a variety of standard functions and so on. At the same it can provide interfaces for users who write personalized processing function. And the calculated data can be used as the basis of formula data to be stored in the database.

The formula (MEVAS) is based on the database to store data. It offers a large number of rich data analysis(rich reporting system), information processing formula and so on. And it provides users with the results of the analysis as the basis of information reporting various performance value. This data can be generated according to needs rather than in advance for data storage and reduce the burden of the database system.

The analysis reports are showed in Excel format and are based on formula (Mevas) and data points (Datapoint) data and so on or software, which provides various query template. It is compatible with Excel charts and Macro computing model, which is convenient and flexible to generate reports to meet the needs of users. Such as energy prediction and energy cost analysis.

E. Global WEB data release function

The client can use IE browser to visit system such as real-time information, alarm information, historical data, a variety of graphical information, production statistics, energy performance reports, etc; Interface with real-time system man-machine conversation interface style is consistent; WEB browsing has permission limits, only the legitimate users can access and use the system.

The release function can classify each sampling point data statistics to produce all kinds of statements, including daily, monthly, annual reports etc. Reports can query and print something at any time. And it also can start history query of each sampling point data and analysis and so on.

The statistical analysis of Information analysis system refers to make use of historical data and real-time data, rely on the data mining technology, analysis the situation of the production and then control the production costs and formulate energy consumption quotas. System can flexible choose statistical time and set up the statistical conditions. System provides the fuzzy query of statistical results , provides function of historical data contrast and also provides printing etc. System can record directly and produces the following results: the price of energy and raw materials and quality, the input and output of energy and raw materials and products of quality and quantity. We can query directly what is sent from the energy management WEB site to the company.

V. CONCLUSIONS

"Information technology to improve the industry development" is the guiding ideology of manufacturing enterprises development in our country. We can establish a comprehensive information platform in metallurgical enterprise and build five layer information management architecture. The cloud technology and internet technology is applied to the enterprise information management. Using advanced data storage, analysis and management technology is bound to improve the management level of metallurgical enterprises and production automation level. Saving energy improves the competitiveness of the enterprises. In the days of extending enterprise scale and competing intensely, by strengthening and perfecting the enterprise information construction and we can ensure that strengthening enterprise resources, planning, production and sales, efficiency, the development direction of decision-making management is correct.

ACKNOWLEDGMENT

This paper is supported mostly by the Jilin Province department of education Science and Technology Plan Project(Grant NO.201656),partially by the Jilin Province department of education Science and Technology Plan Project(Grant NO.201632).

REFERENCES

[1] Chen Xiaohong, Fu Taotao, Cao Yu. Enterprise circular economy evaluation system-Take the case of a large smelter[J].Science Research Management,2012, 33(1) : 47-55.

[2] Lin Ziyu, Lai Yongxuan, Lin Chen, Xie Yi, Zhou Quan. Cloud database research[J].Journal of Software,2012, 23(5) : 1148-1166.

[3] Ma Qianling, Guo Quan. Environmental impact assessment of copper smelting enterprises[J]. Nonferrous Metals,2009, 61(1) : 125-128.

[4] Yu Min, Cheng Xianhai. The marketing management of smelting enterprise should be informationized as soon as possible[J].Non-Ferrous Mining and Metallurgy,2009, 25（2） : 98-101.

[5] He Feiyong, The planning and research of the information system of the Zhuzhou smelts group company[J].Hunan Nonferrous Metals,2011, 27(3) : 74-78.

[6] [6]Shi Yingjie, Meng Xiaofeng.Overview of query technology in cloud data management system[J].Chinese Journal of Computers,2013, 36(2) : 209 -225.

[7] Wu Aixiang, Yu Zhitan.The establishment of the nonferrous metal strategic alliance[J].Metal Mine,2004, (6) : 1-4.

[8] Wang Chengliang, Li Ren, Wang Zhuding.Power distributed computing system model for service oriented architecture[J].Journal of Chongqing University,2011, 34(2) : 69-73.

Design of Monitoring System for Rural Drinking Water Source Based on WSN

Zexin Lin
College of Electronic Engineering
South China Agricultural University
Guangzhou 510642, P.R.China
995480993@qq.com

Huili Yin, Sheng Jiang
College of Electronic Engineering
South China Agricultural University
510642, P.R.China
76576676 @qq.com, 410252413 @qq.com

Weixing Wang(Correspondence author)
College of Electronic Engineering
South China Agricultural University
Guangdong Engineering Research Center for Monitoring Agricultural Information
weixing@scau.edu.cn

Guohui Jiao, JiepingYu
College of Electronic Engineering
South China Agricultural University
Guangzhou 510642, P.R.China
1035390779 @qq.com, 489398737@qq.com

***Abstract*—In order to solve the existing traditional rural drinking water monitoring in a lot of manpower, material resources, real-time, this paper introduces a WSN based on the rural drinking water source monitoring system design, the system consists of five parts: water quality monitoring, soil monitoring node node, node, routing node and gateway server. Water quality monitoring node, soil monitoring nodes send the collected data to the gateway node through the wireless module sent directly, or through the routing gateway node to the gateway node, each node of the data collection, unified by the GPRS module to upload server. The system can periodically detect the water quality and the important indicators of the soil in the rural water sources, and combine the water pollution with the soil non-point source pollution to realize on-line monitoring and provide guidance for pollution control. Network test shows that the designed system can realize data acquisition and remote transmission, stability, range of dissolved oxygen system for 1.09%~1.86% acquisition error, pH error is in the range of 0.64%~1.68%, Cu concentration in the range of error is 1.98%~2.22%, Cu concentration in the range of error is 1.58%~ 2.01%.**

Keywords-Wireless sensor network; Water quality monitoring; Soil monitoring; Rural drinking water; Water source

I. INTRODUCTION

Wateris the source of life, a direct impact on human health. In rural areas, due to the lack of safety awareness and professional knowledge, the lack of attention to the safety of drinking water, agricultural great significance to the accelerating of the agricultural production process using pesticides, fertilizers, garbage, human and animal manure and other improper handling, often cause drinking water Or non-point source pollution of the soil in the water source [1, 2].

Domestic monitoring of rural drinking water is mainly concentrated in the process of drinking water for all aspects of sampling, so that artificial collection and then to the laboratory processing methods [3], need to spend a lot of manpower and material resources, and the existence of time difference, Could not determine whether the recent water pollution or long-term non-point source of water pollution caused by water pollution and so on limitations.

With the rise of Internet of Things, wireless sensor networks are widely used. Wireless sensor networks, nodes through the wireless channel connection, self-organizing network topology, collaboration between nodes, timeliness, with a strong flexibility[4, 5].

At present, wireless sensor networks are used in many water quality detection scenarios, but basically are focused on the monitoring of a single small-scale water [6-8], However, the water quality and soil linkage of rural drinking water sources proposed in this paper can not only detect water and soil pollution in a large scale and real time, but also play a guiding role in governance.

II. SYSTEM STRUCTURE

The overall framework of the system as shown in Fig .1, in the drinking water source to deploy water quality testing nodes, soil detection nodes and gateway nodes. The gateway node has a timer, the timer will wake up the monitoring node, and the gateway waiting for all monitoring nodes to upload data; water quality and soil nodes on the sensor to collect data through the wireless sensor module to the gateway node; gateway to confirm all monitoring nodes Have been uploaded after the data, notify the monitoring node to sleep and the monitoring node data through the GPRS module upload background server.

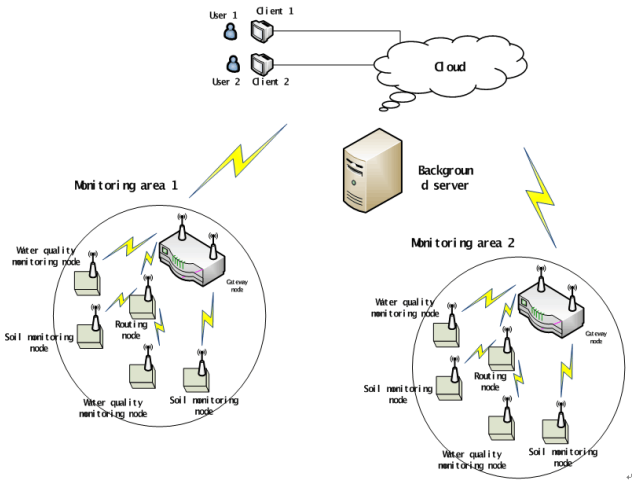

Figure 1. System block diagram

III. SYSTEM HARDWARE DESIGN

A. *Water Quality Monitoring Node*

The water quality monitoring node is composed of a processor module, a sensor module, a GPRS module, a wireless communication module, a power supply module and a solar charging module. The hardware structure is shown in Fig .2.

Water quality monitoring node usingSTM32F103VET6 processor module to do the main control center, the chip has low power consumption, high stability, real-time strong, cost-effective features, can achieve equipment management, task scheduling, data fusion processing [9].

As the water source is generally wide area, and the requirements of the power supply is more demanding, so the choice of wireless communication module WLK01L32 as a hub between the routing node, the module power consumption is low, in the receiving mode, the current is about 8mA; Point-to-point send and receive time is 20ms ~ 30ms; transmission distance, open ground up to 2km; and support for wireless wake-up function [10], for our system is very suitable.

The ATK-S1216F8-BD positioning module is used to obtain the GPS position of the water quality monitoring node, which is a high performance GPS / Beidou dual mode positioning module, which is small in size and has FLASH and backup battery inside. It can be kept within half an hour Ephemeris data, support TTL level, can be directly connected with STM32F103VET6 serial port [11].

Taking into account the lack of rural drinking water supply conditions, the system uses battery-powered and designed solar charging module, the battery power toadd.

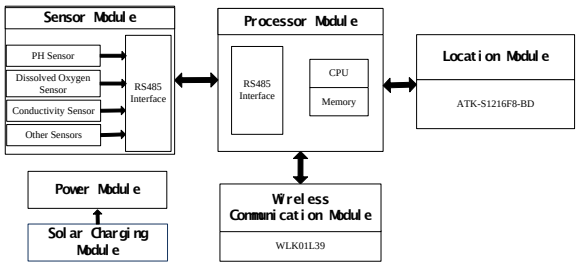

Figure 2. Water quality monitoring node hardware block diagram

It is very important to dissolve oxygen, pH, ammonia, phosphorus and other heavy metal ions in rural drinking water. The system uses ASI's water quality ion selective electrode series sensor probe to collect dissolved oxygen, pH, conductance Rate, ammonia, copper ions, cadmium ions and zinc ions, the physical sensor shown in Fig. 3, the sensor collected data, through the RS485 conversion module to transfer data to the processor module, the processor module to send data packets sent by the wireless communication module To the gateway node, or through the routing node forwarded to the gateway node.

Figure 3. Sensor physical map

B. *Soil Monitoring Node Nodes*

The soil monitoring node is composed of a processor module, a sensor module, a wireless communication module, a GPRS module, a humidity supply module, a power supply module and a solar charging module. The hardware structure is shown in Fig. 4.

Considering the monitoring of soil contamination, the sensor needs to be buried in the soil, and the system uses a five-in-one integrated sensor that monitors temperature, pH, conductivity, copper ions and cadmium ions.

The system selected sensors are required for soil moisture, thus increasing the humidity sensor and humidity supply module. The humidity sensor uses Star et al. CSF11 soil moisture sensor, the sensor operating current less than 50mA, the response time of 1S, in the water range of 0-100% error is ±2%. When the detection of soil moisture is insufficient, the CPU will call the humidity supply module to add moisture to the soil, humidity supply module mainly

by the control circuit, solenoid valve and distilled water supply device.

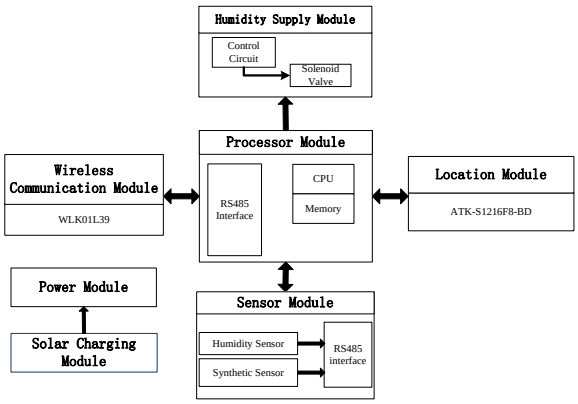

Figure 4. Hardware Block Diagram of Soil Monitoring Node

C. *Routing Node*

In order to reduce the packet loss rate and improve the robustness and reliability of the network, the routing node is added to the monitoring node and the gateway node. The role of the routing node is to forward the packet from the monitoring node to the gateway node. As shown in Fig .5, the routing node consists of a processor module, a wireless communication module, a positioning module, a power supply module and a solar module.

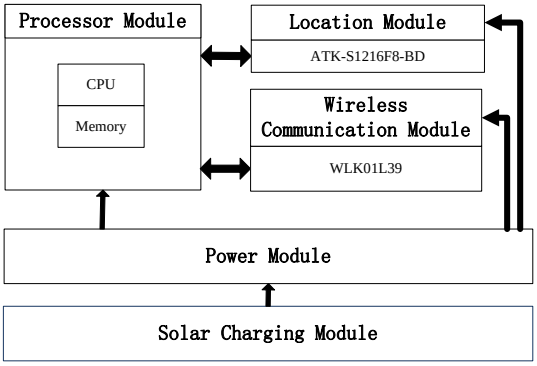

Figure 5. Routing node hardware block diagram

D. *Gateway Node*

As shown in Fig .6, the gateway node consists of a processor module, a wireless communication module, a GPRS module, a display module, a data memory, and a power supply module.

Taking into account the actual needs, in the gateway node to increase the display module and data memory, so as to monitor the data can also be observed changes. Display module main LCD capacitive screen and key module, through the key module to control the LCD screen and flip the screen and other functions. With the SD card as the primary external data memory power-down cause data loss.

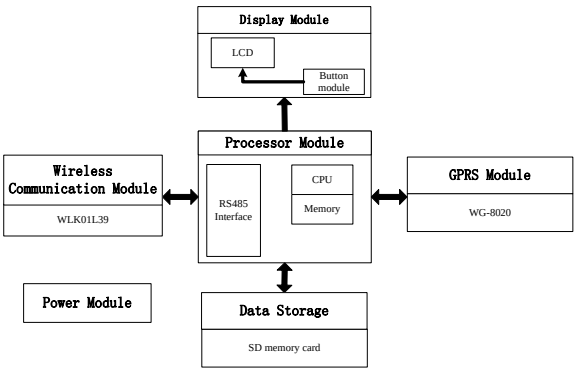

Figure 6. Gateway node hardware block diagram

IV. SOFTWARE DESIGN

A. *Monitor the Node Program*

Monitoring node program flow shown in Fig .7, the node starts to determine whether the first boot, if the first boot waiting for the gateway to download the synchronization package, access to system time, node number and other information into sleep, if not the first The next boot is to collect the appropriate data and get GPS information packaged sent to the gateway, and then enter the sleep state to wait for the next wake up.

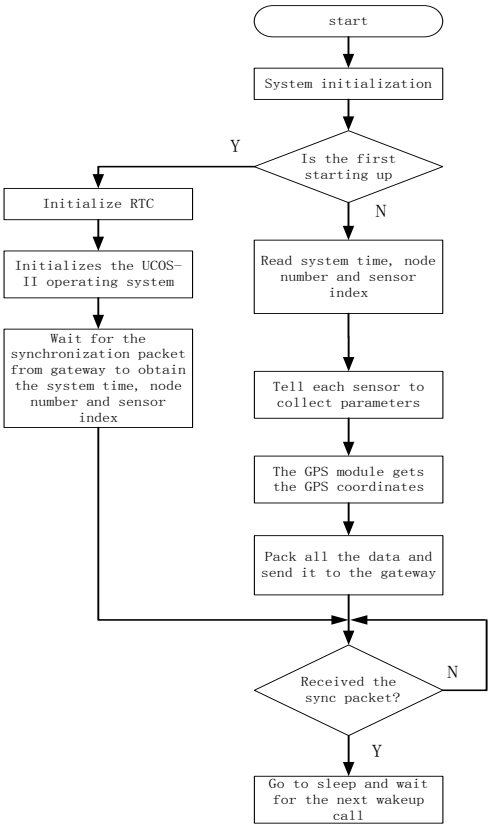

Figure 7. Monitors the node program flow

B. Gateway Node Program

Gateway node hardware program flow shown in Fig .8, the node starts to check whether the first start, if it is the first start from the server to obtain time and node information table, send the synchronization package to the entire network to synchronize the entire system Time and name the node number. The gateway node receives the data of the monitoring node to register the node number and save the data to the SD card. When all the nodes are set up or the set acquisition period arrives, the gateway node sends all the data to the upload server and sends the synchronization packet to all the nodes in the system.So that all nodes into the dormant state, after their own into the sleep state, waiting for the next wake up.

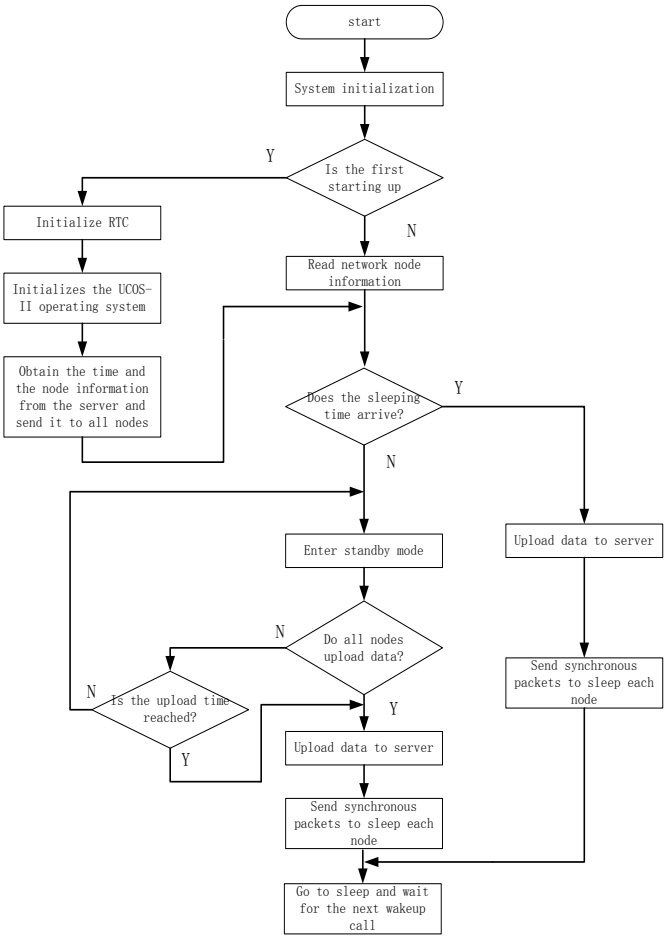

Figure 8. Gateway node program flow

C. Routing Node Program

Routing node program flow shown in Fig.9, the routing node to receive data packets to determine whether the packet has been forwarded, if not forward will record the packet information and forward, if the packet is discarded, received the gateway Synchronize the packet when the synchronization package forwarded automatically into the sleep state waiting for the next wake-up.

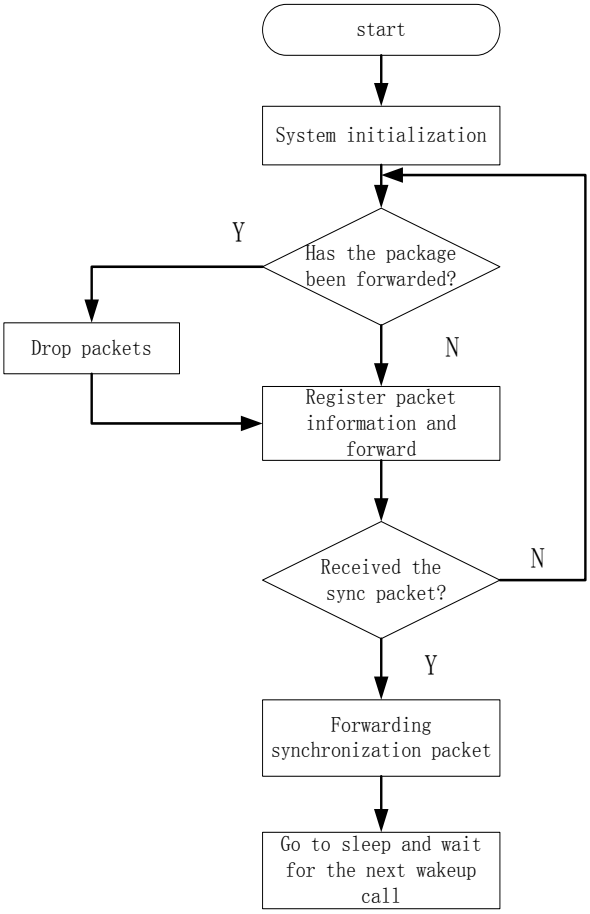

Figure 9. Routing node program flow

V. NETWORKING TEST RESULTS

The system selects South China Agricultural University the deployment of two water quality monitoring node, two soil monitoring nodes and two nodes, a gateway node of the network test, simulation tests were carried out for a period of three months, in order to ensure the accuracy of monitoring parameters of the system, each a week on water quality and soil sampling monitoring points to the professional laboratory testing, table 1 is pH, dissolved oxygen of water node 1 and the same time to collect comparative laboratory measurements, fig .10 and 11 respectively in January 1, 2017 to April 1, 2017 1 soil monitoring node of copper ions variation and soil monitoring node 2 cadmium ion change map. By contrast, the error range of the dissolved oxygen obtained by the system is 1.10%~2.20%, the error range of pH is 0.64%~1.67%, the error range of Cu ion concentration is 1.98%~2.22%, and the error range of Cd ion concentration is 1.58%~2.01%.

TABLE I. SPECIFICATIONS OF WATER QUALITY SENSORS

Test index	Laboratory test	Acquisition node data	error
pH	9.58	9.42	1.67%
	9.61	9.65	0.64%
	9.54	9.62	0.84%
	9.55	9.41	1.47%
	9.65	9.58	0.73%
dissolved oxygen /mg/L	8.15	8.03	1.47%
	8.13	8.3	2.09%
	8.2	8.02	2.20%
	8.16	8.32	1.96%
	8.21	8.3	1.10%

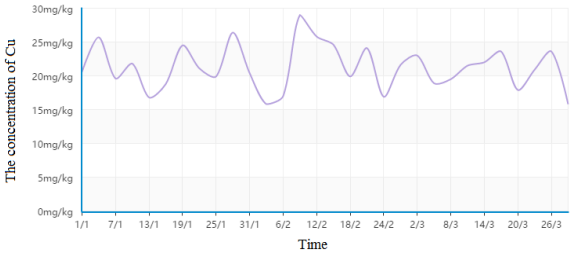

Figure 10. Variation of Cu concentration in soil monitoring node 1

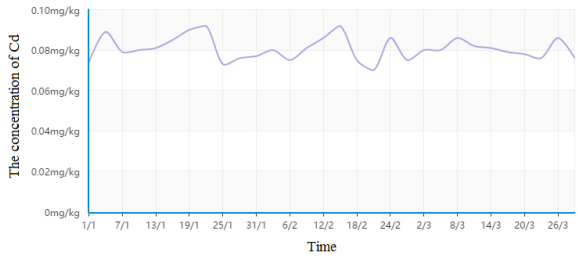

Figure 11. Variation of Cd concentration in soil monitoring node 2

VI. CONCLUSIONS

Based on the wireless sensor network, the system designs the water quality monitoring node, the soil monitoring node, the routing node, the gateway node and the background server. The various parts communicate with each other through the wireless communication module. The gateway is the control center. When the gateway receives all the nodes Information detection data after uploading the server and broadcast the synchronization package, so that all nodes in the network sleep waiting for the next wake-up collection. The system solves the problems of large amount of manpower, material resources and real-time difference in the traditional rural drinking water monitoring. Through the monitoring of water quality and soil linkage, the system has a certain guiding effect on the pollution control problem in the monitoring process.

ACKNOWLEDGMENT

This research was financially supported by Science and Technology Planning Project of Guangdong Province, China (2014-17) and Science and Technology Program of Guangzhou, China （201605030013）

REFERENCES

[1] Xianglan Cao. Cause analysis and treatment of rural water pollution[J]. Modern rural science and technology, 2014(03):68.

[2] Tao Jiang, Gang Chen. Analysis and research of rural drinking water safety [J]. Heilongjiang Science and Technology of Water Conservancy, 2014(09):261-262.

[3] Shoufeng Zhang.Problems and optimization methods of water quality environmental monitoring [J]. Technology and enterprise, 2015(12):102.

[4] Long Hui. Research on Development of Wireless Sensor Networks[J]. Microcontrollers & Embedded Systems, 2011(06):9-12.

[5] Zhuojing Yang, Hongzhi Sun, Chenghong Ren. Overview of application technology in Wireless Sensor Networks [J]. China Science and Technology Information, 2010(13):127-129.

[6] Gao Juan, Hua Luo, Hua Liping, etc. Analysis of Surface Water Quality Monitoring Condition and Its Countermeasures[J]. Journal of Capital Normal University(Natural Science Edition), 2006(01):75-80.

[7] CHEN Yan, YAN Yun-hao, TAN Ting, etc.Design of multi-parameter water quality monitoring terminal based on WSNs[J]. Transducer and Microsystem Technologies, 2014(10):83-86.

[8] JIANG Peng. Survey on Key Technology of WSN-Based Wetland Water Quality Remote Real-Time Monitoring System [J]. Chinese Journal of Sensors and Actuators, 2007(01):183-186.

[9] Weijiang Ma. The Design of Aerodynamics Data Acquisition System Based on STM32[D]. Southwest Jiao Tong University, 2010.

[10] Li Liangbin, Jiang Sheng, Wang Weixing, etc. Design of wireless sensor network node for monitoring water quality of rural water supply plant[J]. Journal of Hunan Agricultural University(NaturalSciences), 2016(02):212-216.

[11] Xingyi Electronic Technology Co., Ltd.. ATK-S1216F8-BD Module user manual [Z]. 2016.

Single Image Dehazing Based on Deep Neural Network

Dewei Huang, Kexin Chen
College of Electronic Engineering, South China Agricultural University, Guangzhou, China
E-mail: huangdewei@stu.scau.edu.cn; 285078375@qq.com

Jianqiang Lu
College of Electronic Engineering, South China Agricultural University, China;
Guangdong Engineering Research Center for Monitoring Agricultural Information, China;
Science and Technology Program of Guangzhou, Chian.
E-mail: Ljq@scau.edu.cn

Weixing Wang
College of Electronic Engineering, South China Agricultural University, China;
Guangdong Engineering Research Center for Monitoring Agricultural Information, China;
Science and Technology Program of Guangzhou, Chian.
Corresponding author
E-mail: weixing@scau.edu.cn

***Abstract*—This paper proposes a single image dehazing based on deep neural network that is to deal with haze image. In this paper, we build up a deep neural network to restore the hazy image.We test our method both objective and subjective and compare with classical method for dehazing. Our test shows that our method works better than the others in reducing Halo effect and also our method does well in restore colorful of input image. Finally, our method process faster.**

Keyword-Dehazing; Deep neural network; Imagedepth map

I. INTRODUCTION

Outdoor images taken in bad weather usually had loses contrast and becomes blur which is resulting from the fact that light is absorbed and scattered by the turbid medium such as particles and water droplets in the atmosphere during the process of propagation [1]. These hazy image become useless in detection or finding some interesting information. Using dehazig method can restore the hazy image and get more detail so that more interesting information shows in the restored image. It does make sense to do research in image dehazing.

Image dehazing can be divvied into two kinds that one is based on traditional image processing method such as the enhancement of histogram[2,3], and Retinex[4]. However, this kind doesn't care about how the haze comes so that the result always loses a lot of information or cannot remove haze clearly. And the other kind is based on atmospheric scattering model that concerned about how the haze occurs in the image and then estimate the parameters for the model to dehazing. Tan [5] maximum the local contrast of the image based on Markov Random Field (MRF) to gain clear image, but the image is always over-saturated. Fattal[6] is based on Independent Component Analysis to remove haze, but they failed while the haze is dense. With a large number set of statics, He et al. [7,8] propose dark channel prior (DCP) that in the non-sky area, at least one color channel has some pixels whose intensities are very low and trend to zero. They make a big progress in haze removal because this approach is simple and effective. However, they may fail when image has large area of sky or white scene. Guided filtering is proposed[9,10] to improve the dark channel later. Tarel et al.[11] make an approach which is based on the median filter, but this approach cannot handle the edge of the image. Zhu et al.[12] assume that the relationship between transmission and brightness and contrast is linear, but this model is not so clear.

In this paper, we propose a new method to dehazing that based on deep neural network. We using a lot of clear image and its real depth map the feed our network so that it can describe the relationship between input image and its depth map correctly. As the result, our dehzing result becomes better and faster.

II. DEHAZING METHOD

A. Atmospheric Scattering Model

Atmospheric scattering model [13] is wildly used in dehazing and it can be described as quation (1)(2) shown:

$$\mathrm{I}(x) = J(x)t(x) + A(1-t(x)) \tag{1}$$

$$t(x) = e^{-\beta d(x)} \tag{2}$$

Where I(x) is input image with haze; J(x) is output image what we wanted; t(x) is transmission map; A is global air light; d(x) is depth map; β is coefficient which can be described as constant. There are three unknown variables in equation so that we cannot solve the model unless we estimate transmission map and global air light. In this paper, we try to estimate transmission map from depth map, and estimate the rest coefficient for our dehazing method.

From equation (1)(2), we know that depth map play an import role in dehazing method. Narasimhan [14]points that β can be described as constant in the same environment so we can try to estimate transmission map by depth map. From discussion above, we can restore hazy image if we know depth map and air light.

B.Depth Map Estimating Based on Deep Neural Network

We can use two deep neural network to estimate depth map based on Davied Eigen' work. One is to estimate raw depth map and the other is to refine it. The structure of our neural network is shown in Fig.1. We do some improvement based on Davied's work.

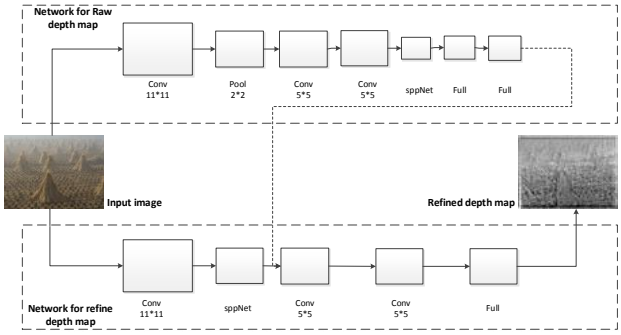

Figure 1. The network for getting depth map

As shown in Fig.1. we firstly build up a deep neural network to estimate raw depth map and it consist of seven layers. Input image is sent to first convolutional layers and then do max pooling for it. We do out the result to two convolutional layers later. In order to fit any size of the input image, we do spatial pyramid pooling (SPP)net for the result and the do two times of fully connect.

We ever try to use raw depth map to restore hazy image, but it does a bad work. We should build up another network to refine the raw depth map.Our refine network is shown in Fig.1. We firstly feed input image in convolutional layers and SPP net to fit the output size of the raw depth map. This result and the raw depth map as input for rest layers. We feed them in a convolutional layers and fully connection layers so that to refine the depth map.

C.Training Details

The last layer is need linear regression so we use linear active function at the last layers. However, active function of the other layer should do some preprocess. In the programming, always make transformation for the input image so that all of the value is between 0 and 1. From discussion above, it seems that Sigmoid function is a good choice, but it will easily cause gradient disappearance; Reluhas good performance is positive axis and has sparsity in negative axis. Based on analysis above, we cut down the RuLu while the input is larger than 1. Sigmoid ,ReLu and our active function is shown in Fig.2.

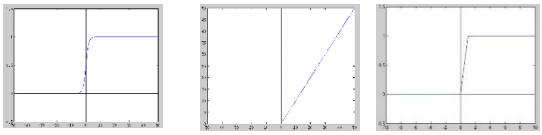

a. Sigmoid b. ReLu c. Ours

Figure 2. Active function

Our loss function is as equation (3), it is a scale-invariant loss function that is proposed by [15].

$$D(y, y^*) = \frac{1}{2n}\sum_{i=1}^{n}(\log y_i - \log y_i^* + \alpha(y, y^*))^2 \tag{3}$$

Where y and y^* respectively are training data and its predicted data and in our paper it mean the real depth map and the predict depth map. The $\alpha(y, y^*)$ is described as equation(4)

$$\alpha(y, y^*) = \frac{1}{n}\sum_i(\log y_i^* - \log y_i) \tag{4}$$

We build up the loss function what we required and it is shown in equation (5)

$$L(y, y^*) = \frac{1}{n}\sum_i D_i^2 - \frac{\lambda}{n^2}(\sum_i D_i)^2 \tag{5}$$

Where λ is set to 0.5.

D. Estimate Air Light

We try to reformat the equation (1) and it is shown as equation (6):

$$J(x) = \frac{I(x) - A}{t(x)} + A \tag{6}$$

We has estimated transmission map and now need to estimate the air light. Air light can be consider as constant in the same environment, such Ancuti compare the input image and its semi-inverse image in CIE color space and marke some special point and then chose the brightest as air light; He et al. mark the top brightest 0.1% in the dark channel and then pick the brightest in input image. Another researcher consider the air light is not constant in the same environment, such Yang Xun using linear interpolation to estimate air light in the direction of attenuation of illumination.

We do preprocess to the input image so that the estimate value of air light would be exactly. In this paper, we consider air light is a constant and that can get from the input image. In the image the white color is getting close to 1 and if we chose the brightest pixel directly from input image, we can almost get a very value that closed 1. We first set a threshold to remove the high value and the get the ighest value in the processed image. The step of our method is shown in Fig.3, we remove the value which is higher than the threshold in each R, G, B channel and then combine them. After does this preprocessing, the top highest value would be removed. We chose top 0.1% highest value from processed image and compute the average as air light.

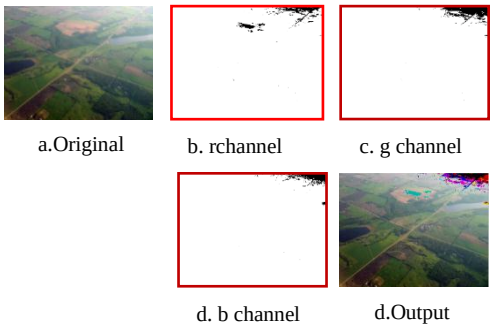

Figure 3. Estimate air light

III. EXPERIMENTAL RESULT AND ANALYSIS

A. Prepare Training Data

In this paper, we use natural hazy image and some synthetic image to train our model and as the result our method can get more suitable for dehazing. Expending the training data can lead our method has more generalization ability. The natural image, we get from the open source and token image by ourselves.

Synthetic hazy image can consider as the inverse processing of dehzing, so we need clear image and its depth map to estimate hazy image. Saxena et al. has built up a large database that include a large number of clear image and its real depth map. The database is wildly used in researching. They use professional device to get the depth map so that it is exactly precision and also this database is suitable in synthetic hazy image. The step to synthetic hazy image is shown in Fig.4.

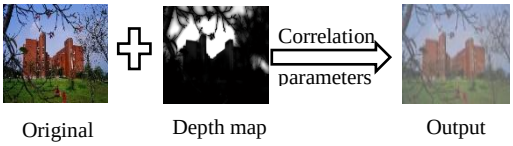

Figure 4. Synthetic hazy image

From equation (1), we know that when $I(x) = A, t \to 0$. It means that air light is very close to the pixel value when transmission value is very small and close to 0. As the result, we can chose the value as air light where the depth value is highest.

B. Experimental Result

Using the model that we have trained before to estimate depth map and air light and then put them into equation (6) to get clear image. We compare with He's method and Tarel's method objectively and subjectively. Our test environment is in Ubuntu 14.04 operating system with Intel Xeon(R) CPU E5-2620 v4 @ 2.10GHz ×16 and GTX TIAN X. We use Tensorflow and Matlab2014Ra to do simulation.

C. Qualitative Analysis

Having done a large number of test, wo select three of them to shown in this paper. Fig.5, 6 and 7 is our test result with Tarel's method, He' method and our method. It is obvious that all of them do efficiency in dehazing. Our statistics shows that Tarel's method cannot remove the hazy thoroughly and it seems some haze remain in the output image; He's image do better than Tarel's method but it fail in color restoration. The output image will be dark in He' method. Our method does better than the other method subjectively. Our method perform better in haze removal and color restoration and also our method can show more details in the output image.

Figure 5.a: Input image; b: He's method; c: Tarel's approach; d: ours

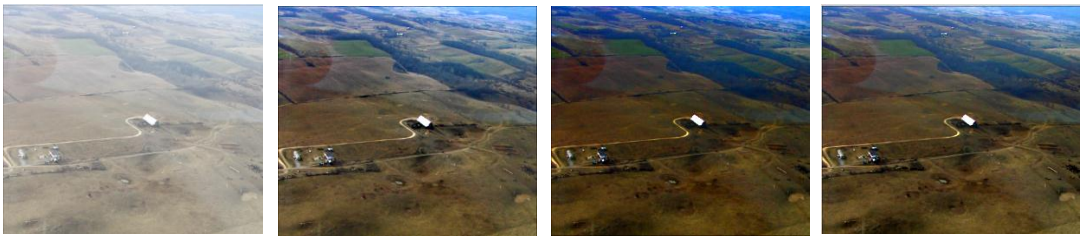

Figure6.a: Input image; b: dark channel; c: Tarel's approach; d: ours

a. Original b. Tare's c. He's d. Ours

Figure 7.a: Input image; b: dark channel; c: Tarel's approach; d: ours

D. Quantitative Analysis

Firstly, we use MSE assessment to compare the three method in this paper, and the MSE is as equation (7) shown.

$$MSE=\frac{\sum_{0?i<M}\sum_{0?j<N}(f_{ij}-f_{ij}^{'})^2}{M\times N} \quad (7)$$

where f_{ij} is input image, $f_{ij}^{'}$ is the output image, M and N is the numbers of x and y axis. The smaller of this value, the better of the output image.

We also use Hu Zi'ang's[16]assessment to evaluate the methods and this assessment is shown in equation (8)

$$Q=\frac{S\times Hist}{e^{-L}} \quad (8)$$

Where $Hist$ is histogram similarity function and when $Hist$ is closed to 1, it is better.; L is edge intensity function which is using Canny to gain and the bigger of L ,the better; S structure similarity function; the bigger of Q the better ntegratedly. We the get two table is shown in Table Iand II for Fig.5, 6, 7.

TABLE I. MSE FOR EACH METHOD

Test image	Tarel'	He's	Ours
Fig 5.	0.412 6	0.250 9	0.102 2
Fig 6.	0.618 6	0.471 0	0.149 4
Fig 7.	0.109 1	0.095 8	0.100 5

TABLE II. COMPREHENSIVE EVALUATION

Test image	Tarel's	He's	Ours
Fig 5.	0.455 7	0.674 9	1.028 9
Fig 6.	0.237 0	0.349 6	1.005 3
Fig 7.	2.541 0	1.941 6	1.476 3

From table I, it is easily to find that Tarel's method always has the highest value of MSEandthat means Tarel's method performs worse than others. Our score of MES is smaller in Fig.5 and 6 while is bigger in Fig.7. However, our score in Fig.7 is almost the same as He' method. In conclusion, it can consider that our method performs better than other's in MSE. From table 1, it is easily to find that Tarel's method always performs worsethan other's. our method has better than others, sometime it is as same as He's method.

Based on the analysis above, it can consider that our method is better than the two others and it is the same as which we analysis subjectively.

E. Running time

If a method cannot process in real time, we cannot applicate it in product. We chose different size of picture to run these three method. We run these three method 20 times and the get the average shown in table III.

TABLE III. RUNING TIME/S

Image size	Tarel's	He's	Ours
400×600	0. 9682	0.793 2	0.321 9
479×640	1.1363	1.041 0	0.445 9
768×1024	3.0295	2.601 9	0.930 8
1461×2560	13.5192	12.148	1.7567

When the image size become larger and larger, the running time of our method doesn't change very much but the others become slower and slower. That is because our method need just need to initial the model. Our method can process in real time.

IV. CONCLUSION

In this method, we propose a single image dehazing based on deep neural network that is to deal with haze image which token under the bad weather. We pay much time in training the mode that is for getting the depth map of input image. As a result, when we applicate our method is almost just need to initial the model that we have trained.The weight of our neural network that come from a real natural image and its depth, so that it can do good at getting depth map. Our method can do good in color restoration and dehzing.

ACKNOWLEDGEMENT

This research was financially supported by Science and Technology Program of Guangzhou, China （201605030013）.

REFERENCES

[1] Narasimhan S G, Nayar S K. Vision and the Atmosphere[J]. International Journal of Computer Vision, 2002, 48(3):233-254.

[2] Stark J A, Fitzgerald W J. An alternative algorithm for adaptive histogram equalization[J]. Graphical Models and Image Processing, 1996, 58(2): 180-185.

[3] Stark J A. Adaptive image contrast enhancement using generalizations of histogram equalization[J]. Image Processing, IEEE Transactions on, 2000, 9(5): 889-896.

[4] Rahman Z, Jobson D J, Woodell G A. Multi-scale retinex for color image enhancement[C]// International Conference on Image Processing, 1996. Proceedings. IEEE, 2002:1003-1006 vol.3.

[5] R. T. Tan. Visibility in bad weather from a single image. In Proc. CVPR, 2008

[6] R. Fattal. Single image dehazing. ACM Transactions on Graphics, 27(3), 2008

[7] K. He, J. Sun, and X. Tang. Single image haze removal using dark channel prior. In Preoccupy, 2009.

[8] K. He, J. Sun, and X. Tang. Single image haze removal using dark channel prior. IEEE TPAMI 33(12): 2341-2353, 2011.

[9] K. He, J. Sun, and X. Tang. Guided image filtering. In Proc. ECCV, pages 1-14, 2010.

[10] K. He, J. Sun and X. Tang. Guided image filtering. IEEE TPAMI, 35(6): 1397-1409, 2013.

[11] J. P. Tarel, and H. Nicolas. Fast visibility restoration from a single color or gray level image. In Proc. ICCV, 2009.

[12] Zhu Q, Mai J, Shao L. A Fast Single Image Haze Removal Algorithm Using Color Attenuation Prior.[J]. IEEE Transactions on Image Processing A Publication of the IEEE Signal Processing Society, 2015, 24(11): 3522-33.

[13] Stark J A, Fitzgerald W J. An alternative algorithm for adaptive histogram equalization[J]. Graphical Models and Image Processing, 1996, 58(2): 180-185.

[14] Narasimhan S G, Nayar S K. Contrast restoration of weather degraded images[J]. IEEE Transactions on Pattern Analysis & Machine Intelligence, 2003, 25(6):713-724.

[15] Eigen D, Puhrsch C, Fergus R. Depth Map Prediction from a Single Image using a Multi-Scale Deep Network[J]. Computer Science, 2014:2366-2374.

[16] Hu Zi'ang, Wang Weixing, Lu Jiangqiang, et al, Image Dehazing using Visual Information Loss Prior[J], Journal of Image and Gaphics, 2016, 21(6):711-722.22.

Research on Balanced Energy Consumption of Wireless Sensor Network Nodes Based on Clustering Algorithm

Jie Huang
College of Information and Communication Engineering
Hezhou University
Hezhou,China
huangjie0773@163.com

***Abstract*—A multi-cluster-head based clustering routing algorithm is researched and realized in order to achieve better balance the energy consumption of wireless sensor network nodes as well as promote the stability and extend the service life of the network. By taking cluster as the basic unit, it divides the wireless sensor network into multiple clusters, each of which includes a main cluster head node, an assistant cluster head node, a cluster management node and several ordinary nodes. The article elaborates the energy consumption model of the wireless sensor network, the network topological structure of the multi-cluster-head based clustering routing algorithm and the method for realization. In addition, it conducts simulation and analysis on the multi-cluster-head based clustering routing algorithm. According to the results, the algorithm can achieve preferable balance on energy consumption of various nodes in the wireless sensor network, which effectively extends the service life and improves the stability of the wireless sensor network. It has good application prospects.**

Keywords---Wireless sensor network; Balanced energy consumption; Clustering algorithm; Multi-cluster-head; Data fusion

I. INTRODUCTION

The wireless sensor network is composed by large quantities of sensor nodes deployed within the supervision region, which forms a multi-hop self-organizing network system with wireless communication, in order to coordinate perception as well as collect and manage the information of the perceived objects within the coverage of the network [1, 2]. Operating in unattended environment for a long term, the nodes of the wireless sensor network are generally powered with batteries. Due to the limited energy of batteries, nodes lose efficacy with the exhaustion of energy in batteries. There are unbalanced energy consumptions between cluster head nodes and ordinary nodes in a cluster, in which the former ones need to receive and integrate the data of other nodes in the cluster, and then send the data to the base station in a way of single-hop or multi-hop. Cluster head nodes generally consume more energy considering that they need to receive and transmit data frequently. Ordinary nodes in the cluster generally have less energy consumption considering that they need only to perceive information and send it to cluster head nodes. Cluster head nodes in different clusters have unbalanced energy consumptions [3]. Due to unbalanced energy consumptions among various nodes in the wireless sensor network, the ones with more energy consumption will die soon, which gives rise to influence on the stability and the topological structure of the wireless sensor network and shortens the service life of the network [4]. The preferable balance on energy consumptions among various nodes in the wireless sensor network plays an important role in extending the service life and improving the stability of the wireless sensor network.

II. THE MODEL FOR ENERGY CONSUMPTION OF WIRELESS SENSOR NETWORK NODES

The energy consumption of wireless sensor network nodes includes the calculation energy consumption and the communication energy consumption, in which the latter one occupies larger proportion in node energy consumption [5]. TABLE I shows the energy consumption of a communication module.

TABLE I. ENERGY CONSUMPTION OF A WIRELESS COMMUNICATION MODULE

State of the wireless communication module	Energy consumption[mW]
Sending	14.73
Receiving	12.29
Idle	12.10
Dormant	0.015

The energy consumed for sending the data of m bit by the node in the wireless sensor network is as shown in (1) and (2).

$$E_{fs}(m,d) = mE_{elec} + m\varepsilon_f d^2 (d \le d_0) \quad (1)$$

$$E_{fs}(m,d) = mE_{elec} + m\varepsilon_n d^4 (d > d_0) \quad (2)$$

The E_{elec} in (1) and (2) is the energy consumed for sending the data of 1 bit by the node; ε_f is the energy consumption magnification times within unit distance in condition of free space model as the transmission channel; ε_n is the energy consumption magnification times within unit distance in condition of multi-route attenuation model as

the transmission channel; d is the distance between the sending node and the receiving node. The energy consumed for receiving the data of m bit by the node is as shown in (3). The energy consumed for integrating the data of m bit by the node is as shown in (4).

$$E_{js}(m) = mE_{elec} \tag{3}$$

$$E_{rh}(m) = mE_r \tag{4}$$

The E_r in (4) is the energy consumed for integrating the data of 1 bit by the node. The energy consumption of the cluster head node in the wireless sensor network usually includes the energy consumed for data transmission with ordinary nodes in the cluster, the energy consumed for data integration to the data in the cluster as well as the energy consumed for data transmission between the cluster head node and another cluster head node or the base station. The energy consumption of the cluster head node is as shown in (5) and (6).

$$E_{ct}(d) = nE_{elec} + pE_r + mE_{elec} + m\varepsilon_f d^2 \quad (d \le d_0) \tag{5}$$

$$E_{ct}(d) = nE_{elec} + pE_r + mE_{elec} + m\varepsilon_n d^4 \quad (d > d_0) \tag{6}$$

The d in (5) and (6) is the distance between the cluster head node and the base station or between different cluster head nodes. The energy consumption of the cluster head node is related to the quantity of ordinary nodes in the cluster and the distance between the cluster head node and the base station. Large quantity of nodes in the cluster leads to large energy consumption for data integration between the cluster head and the data in the cluster. In condition that the single-hop method is adopted for the direct data transmission between the cluster head and the base station, the cluster heads far away from the base station consume more energy during data transmission with the base station. In condition that the multi-hop method is adopted for data transmission between the cluster head and the base station, the cluster heads closer to the base station consume more energy. Due to unbalanced energy consumptions of different cluster heads, the ones with large energy consumption will become failure nodes or death nodes very soon, giving rise to influence on the stability and the service life of the wireless sensor network.

The energy consumption for ordinary nodes in the cluster mainly involve in the energy consumption for data transmission with cluster heads, with the energy consumption expression as shown in (7) and (8).

$$E_{ct}(d) = aE_{elec} + bE_{elec} + b\varepsilon_f d^2 \quad (d \le d_0) \tag{7}$$

$$E_{ct}(d) = aE_{elec} + bE_{elec} + b\varepsilon_n d^4 \quad (d > d_0) \tag{8}$$

The d in (7) and (8) is the distance between ordinary nodes and cluster head nodes in the cluster. Considering that there are different distances between various ordinary nodes and cluster head nodes in the cluster, the ordinary nodes closer to cluster head nodes consume less energy, and the ones far away consume more energy. Due to the unbalanced energy consumptions for ordinary nodes, the ordinary nodes with larger energy consumption will become failure nodes or death nodes very soon, giving rise to the stability and the service life of the wireless sensor network. The effective balance on the energy consumption of various nodes in the wireless sensor network plays a very important role in improving the stability and extending the service life of the wireless sensor network.

III. CLUSTERING ALGORITHM BASED ON MULTI-CLUSTER-HEAD

A. Clustering Algorithm for Single-cluster-head

Clustering algorithm refers to the division and management on the wireless sensor network with unit of cluster. A cluster includes cluster head nodes and ordinary nodes. In which cluster head nodes conduct management on ordinary nodes in the cluster and receive the data from the ordinary nodes in the cluster; in addition, cluster head nodes integrate and transmit data, in order to effectively reduce network energy consumption and extend the service life of the network [6,7]. LEACH algorithm is a typical clustering routing algorithm; the nodes in the cluster collect data and send the data to cluster head nodes, which integrate the data and directly send the integrated data to the base station [8]. Each node in the wireless sensor network selects a value from 0-1 randomly; in condition that the randomly selected value by the node is less than the threshold value $T(n)$, the node is selected as the cluster head node [9]. The expression for calculation of the threshold value $T(n)$ is as shown in (9) .

$$T(n) = \begin{cases} \frac{p}{1 - p \times \mathrm{mod}(r, 1/p)} & n \in G \\ 0 & \end{cases} \tag{9}$$

The p In (9) is the proportion of cluster head nodes in all the nodes of the wireless sensor network; $\mathrm{mod}(r, 1/p)$ is the number of the selected cluster head nodes in current round of circulation; G is the set of the unselected cluster head nodes in recent $1/p$ round; r is the round of the

network. The design of $T(n)$ can effectively balance the energy consumptions of various nodes in the cluster [10].

There may be single or multiple cluster head nodes in each cluster in the clustering algorithm. In condition of cluster division and management in a way of single cluster head, compared with other ordinary nodes in the cluster, cluster head nodes need to consume more energy due to frequent receiving of the data of other nodes in the cluster as well as integrating and transmitting of data. The energy consumed by cluster head nodes is different from that of ordinary nodes in any cluster. Due to different numbers of ordinary nodes in different clusters as well as different distances between cluster head nodes and the base station, different cluster head nodes consume different energies in the wireless sensor network. In order to effectively balance the energy consumption among nodes in the wireless sensor network and avoid premature failure or death of cluster head nodes due to too much consumption, the wireless sensor network needs to select cluster head nodes at set interval of t. In condition of too large t value, cluster head nodes may lose efficacy or die due to too much consumption, leading to influence on the topological structure and the service life of the wireless sensor network. In condition of too small t value, the wireless sensor network consumes large quantities of energies due to frequent selection of cluster head nodes, shortening the service life of the wireless sensor network. It is critical to select a suitable t value for the balancing of the energy consumption among various nodes in the wireless sensor network. However, it is difficult to accurately select and set a suitable t value. The re-selection of cluster head nodes in the whole wireless sensor network needs to consume a lot of energy consumption of nodes, which gives rise to the service life of the network. The reduction on the energy consumed for re-selection of cluster head nodes plays a critical role in extending the service life of the wireless sensor network. The energy consumption of cluster head nodes in the clustering algorithm of single cluster head includes data receiving related energy consumption, data integrating related energy consumption and data transmission related energy consumption [11]. Data receiving related energy consumption mainly includes the energy consumed for receiving the data of other nodes by cluster head nodes; data integration related energy consumption mainly involves in the energy consumed for integrating the data in the cluster by cluster head nodes; data transmission energy consumption mainly refers to the energy consumed for the transmitting of the data in the cluster to the base station or other cluster head nodes by cluster head nodes. The energy consumption of ordinary nodes in the cluster mainly involves in data transmitting related energy consumption. Effective reduction of energy consumption of cluster head nodes plays a critical role in balancing the energy consumption among various nodes in the wireless sensor network.

B. Clustering Algorithm for Multi-cluster-heads

A multi-cluster heads based clustering algorithm is designed aiming at the characteristics of single-cluster-head based clustering algorithm, with the topologic structure of the wireless sensor network as shown in Fig. 1. Each cluster includes a main cluster head node, an assistant cluster head node, a cluster management node and several ordinary nodes.

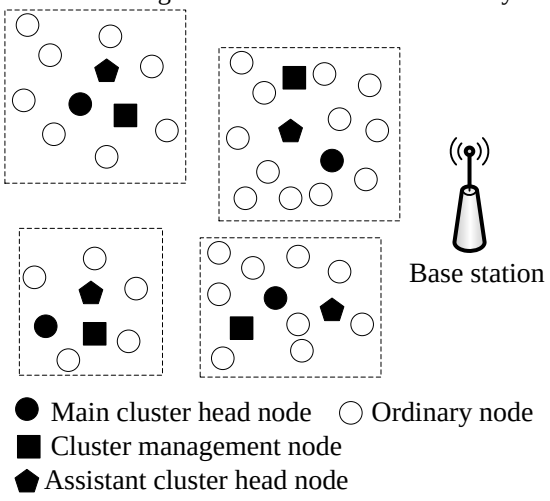

Figure 1. Topologic structure of the wireless sensor network

The basic process of the clustering algorithm is listed as follows.

Step 1: Select main cluster head nodes. Select several main cluster head nodes from the wireless sensor network by adopting the cluster head selection algorithm, and assumes that each node can perceive its own residual energy.

Step 2: Add the nodes into corresponding main cluster head node network by taking cluster as the unit, and send related information such as the residual energy of the nodes to main cluster head nodes for saving.

Step 3: According to the residual energy of various member nodes, the main cluster head node selects two nodes with the highest residual energy as the assistant cluster head node and the cluster management node.

Step 4: The main cluster head node sends the information of various member nodes and main cluster head nodes in the cluster to cluster management nodes for saving.

Step 5: The assistant cluster head node receives the data of various ordinary nodes in the cluster and integrates the data, and then transmits it to main cluster head nodes. The energy consumption of assistant cluster head nodes is as shown in (10).

$$E_{fct}(d) = aE_{elec} + bE_r + cE_{elec} + c\varepsilon_f d^2 \tag{10}$$

The d in (10) is the distance between the assistant cluster head node and the main cluster head node

Step 6: The main cluster head nodes receives the data of the assistant cluster head node, and sends the data to the base station or other cluster head nodes in a way of single-hop or multi-hop. The energy consumption of the main cluster head node is as shown in (11) and (12).

$$E_{zct}(d) = kE_{elec} + zE_{elec} + z\varepsilon_f d^2 \quad (d \le d_0) \tag{11}$$

$$E_{zct}(d) = kE_{elec} + zE_{elec} + z\varepsilon_n d^4 \quad (d > d_0) \quad (12)$$

In which the d in (11) and (12) is the distance between the main cluster head node and the base station or between different main cluster head nodes.

Step 7: In the wireless sensor network, it is necessary to reelect cluster head nodes in time in condition of too much energy consumption due to unbalanced energy consumption among cluster head nodes in the cluster, in order to avoid the influence on the stability and the service life of the wireless sensor network caused by failure or death of cluster head nodes. Considering that various cluster head nodes consume different energy consumptions, it is unnecessary to reelect cluster head nodes for the ones with sufficient residual energy, but it is needed to reelect cluster head nodes in time for the ones with insufficient residual energy. The reelection of cluster head nodes in the whole range of the wireless sensor network at regular intervals needs to consume a lot of energy of nodes. This algorithm conducts management and reelection to cluster head nodes in the cluster by taking cluster as the basic unit, in order to effectively reduce the energy consumed for reelection of cluster head nodes. Cluster management nodes in the cluster inquire the residual energy of the main cluster head node and the assistant cluster head node in the cluster at regular intervals. In condition that the residual energy of the main cluster head node or the assistant cluster head node is lower than the preset threshold value, cluster management nodes give a warning message to the main cluster head node, to reelect cluster head nodes in the cluster. In condition of accidental failure or death of the main cluster head node or the assistant cluster node, cluster management nodes take over the functions of the main cluster head node or the assistant cluster head node temporarily and reelect cluster head nodes. The energy consumption of cluster management nodes is as shown in (13).

$$E_{cgl}(d) = jE_{elec} + kE_{elec} + k\varepsilon_f d^2 \quad (13)$$

In which the d in (13) is the distance between cluster management nodes and the main cluster head nodes or between different assistant cluster head nodes.

Step 8: In order to better balance the energy consumption among various nodes in the cluster and reduce the energy consumption for data integration of the assistant cluster head node, ordinary nodes in the cluster conduct integration to collected data and then send the integrated data to the assistant cluster head node. The energy consumption of ordinary nodes in the cluster includes data transmission energy consumption and data integration consumption, with related expression as shown in (14).

$$E_{pt}(d) = mE_r + pE_{elec} + p\varepsilon_f d^2 \quad (14)$$

The d in (14) is the distance between ordinary nodes and the assistant cluster head node in the cluster.

IV. Experimental Analysis

The nodes in the wireless sensor network with too much energy consumption lead to premature failure or death, giving rise to influence on the topological structure and the service life of the network. Balanced energy consumption of nodes leads to large quantities of survival nodes in the wireless sensor network as well as stable topological structure and long service life of the network. Simulation is conducted through simulation software, obtaining the relationship between the number of the survival nodes and the time of the network as shown in TABLE II.

TABLE II. Changes of Number of Survival Nodes with Time

Time[s]	Number of survival nodes
0	200
2000	200
5026	199
10000	196
20000	189
30000	185
40000	173

According to TABLE II, no node died within the first 2000s during the operation of the network; the 1st node died at the 5026s during the operation of the wireless sensor network. The change on number of died nodes in the network is gentle during 10000s-40000s, without sudden death of large quantities of nodes, and there are sufficient surviving nodes in the network and balanced energy consumption among various nodes in the wireless sensor network.

V. Conclusions

In the wireless sensor network, the nodes with too much energy consumption will become premature failure nodes or death nodes due to unbalanced energy consumption among various nodes. Increased number of failure nodes and death nodes give rise to the topological structure of the wireless sensor network, shortening the service life of the wireless sensor network. This article researches and realizes a multi-cluster-head based clustering routing algorithm. By taking cluster as the basic unit, it divides the wireless sensor network into multiple clusters, each of which includes a main cluster head node, an assistant cluster head node, a cluster management node and several ordinary nodes. The assistant cluster head node is in charge of integrating the data in the cluster. The main cluster node is in charge of sends the data in the cluster to the base station or other cluster head nodes in single-hop or multi-hop. The cluster management node conducts management to the main cluster head node, the assistant cluster head node and ordinary nodes in the cluster; in addition, the cluster management nodes conducts supervision on the residual energy of the main cluster head node and the assistant cluster head node, and determines if it is necessary to reelect cluster head nodes in the cluster according to the residual energy of the main cluster head node and the assistant cluster head node. According to the results of simulation and test, the multi-cluster-head based

clustering routing algorithm proposed in this article can preferably balance the energy consumption among various nodes in the wireless sensor network, which effectively extends the service life of the wireless sensor network and improves the stability of the network.

ACKNOWLEDGMENT

This work was financially supported by the National Natural Science Foundation of China (Grant No. 6154055).

REFERENCES

[1] Y. Xu, L.J. Chen and L.X. Gan, "Principles and Applications of Wireless Sensor Network," Beijing, Tsinghua University Press, 2015, pp. 23-36.

[2] M.N. Yang, D. Yang and C. Huang, "An Improved HEED Clustering Algorithm for Wireless Sensor Network,"Journal of Chongqing University, vol. 35, Aug. 2012, pp. 101-106.

[3] X.L. Lu, Y.Y. Wang, H.B. Wang and B.G. Xu, "Energy-balanced Unequal Clustering Algorithm in Wireless Sensor Network, " Computer Science, vol. 40, May. 2013, pp. 78-81.

[4] C.X. Yang, L. Gao and C. Lu, "Research on the Clustering Algorithm of a Balanced Energy Consumption of Nodes for WSN," Journal of Jiamusi University(Nztural Science Edition), vol. 33, Nov. 2015, pp. 925-928.

[5] X.Q. Wang, Y.J. Ou and N.L. Huang, "Design and Implementation of ZigBee Wireless Sensor Network," Benjing, Chemical Industry Press, 2012, pp. 125-150.

[6] L. Kang and Z.S. Dong, "An Improved Unequal Clustering Algorithm Based on Cluster Head Classification," Chinese Journal of Sensors and Actuators, vol. 28, Dec. 2015, pp. 1841-1845.

[7] Z.Y. Tao and S.F. Jiang, "Clustering Algorithm for Wireless Sensor Networks with Mobile Clusterheads," Computer Engineering and Applications, vol. 52, Mar. 2016, pp. 75-78.

[8] H.B. Yu, W. Liang and P. Zeng, "Intelligent Wireless Sensor Network System," Beijing, Science Press, 2013, pp. 161-173.

[9] Z.Y. Sun and C. Zhou, "Adaptive Clustering Algorithm in WSN Based on Energy and Distance," Journal of Northeast Dianli University, vol. 36, Feb. 2016, pp. 82-86.

[10] C.S. Zhang, J. Xing and S.Q. Zhao, "Energy-efficeent Uneven Clustering Algorithm, " Computer Engineering and Applications, vol. 52, Apr. 2016, pp. 106-109.

[11] J.Z. Li, H.T. Wang and A. Tao, "An Energy Balanced Clustering Routing Protocol for WSN," Chinese Journal of Sensors and Actuators, vol. 26, Mar. 2013, pp. 396-401.

Research on Wireless Sensor Network Coverage Based on Improved Particle Swarm Optimization Algorithm

Li Changxing
College of Science
Xi'an University of Postsand Telecommunications
Xi'an, China
shuxueshiyanshi@163.com

Zhang Long-yao
College of Science
Xi'an University of Postsand Telecommunications
Xi'an, China
prczly@foxmail.com

Zhang Qing
College of Science
Xi'an University of Postsand Telecommunications
Xi'an, China
137376870@qq.com

***Abstract*—In order to improve the network coverage, this paper presents the research on wireless sensor network coverage based on improved particle swarm optimization algorithmfor wireless sensor nodes that are randomly deployed in a certain area.In this paper, we use the regional network coverage as the target objective function, and combine various improved particle swarm optimization algorithms to optimize the deployment location of all nodes to enhance the area coverage. The experimental results show that the influence levelof different perceived radius on the optimization performance of the network coverage is different. At the same time, the optimization performance comparison graph of improving the network coverage by using the standard particle swarm optimization algorithm, the chaos particle swarm optimization algorithm and the breeding particle swarm optimization algorithm is given, and it is proved that the latter twoalgorithms solve the wireless sensornetwork coverage better than the firstalgorithm.**

Keywords-Wirelesssensor;Node;Network coverage; Particle swarm optimization;Perceivedradius

I. INTRODUCTION

Wireless Sensor Networks (WSN) consists of a number of inexpensive, low-energy sensor nodes, as a platform for physical world and human information exchange [1-2].Due to the limited computing power, sensing range and transmission range of each sensor, the wireless sensor network transmits the collected data to the cluster head sensor by multi-hop to monitor whether there is an anomaly in the area [3].The deployment of sensor nodes is very important, it affects the network coverage, communication costs and management resources, so WSN node deployment strategy is an urgent problem [4].

Particle swarm optimization (PSO) algorithm is widely used in multi-dimensional function optimization problem. It has the characteristics of simple structure, easy implementation, no gradient information and few parameters. It has become a hot research algorithm in the field of intelligent optimization at home and abroad [5-7].LinZhu-liangpresented particle fire optimization based on forest fire detection system of wireless sensor network [8] improved the network performance. However, the PSO algorithm is prematurely convergent and easy to fall into the local optimal value.Therefore, the improved particle swarm algorithm is continually proposed by researchers:According to the PSO algorithmdoes not have traversal type, the chaotic map is added to the standard particle swarm optimization algorithm. When the algorithm is premature, the chaotic search of the population makes it possible to jump out of the local optimal [9]; Chaos Particle Swarm Optimization (CPSO) algorithm improves the accuracy and efficiency of solving.Liu Wei-tingproposed a wireless sensor network coverage optimization based on the CPSO algorithm [10].Although the PSO algorithm has overcome the shortcomings of the local optimum, the ability of the algorithm to keep the population diversity is relatively general and the convergence speed is not improved obviously.According to the shortcomings of early convergence and late iterations of PSO algorithm, Li Ji proposed the Breeding Particle Swarm Optimization (BPSO) algorithm, and introduced the genetic algorithm (GA) into the PSO algorithm to increase the diversity of the particles, using the adaptive inertia weight to improve the convergence rate of the algorithm [11].Wang Jun proposed a three-dimensional cross-particle swarm optimization algorithm for wireless sensor networks [12]. Although the population diversity is better maintained, the ability to jump into local optimum is general.

Based on the above analysis, this paper respectivelystudies the coverage of wireless sensor networks based on PSO, CPSO and BPSO, and embodies the advantages and disadvantages of the algorithm.A wireless sensor coverage based on improved particle swarm optimizationis proposed for wireless sensor nodes that are randomly deployed in a certain area.The network coverage is used as the objective function, combined with the particle

swarm optimization algorithm, and the deployment location of all nodes is optimized to enhance the area coverage.The experimental results show that the influence level of different perceived radius on the optimization performance of the network coverage and the optimization performance comparison graph of improving the network coverage by usingthe standard particle swarm optimization algorithm, the chaos particle swarm optimization algorithm and the breeding particle swarm optimization algorithm, and prove that the latter two algorithms solve the network coverage better than the first algorithm.

II. WIRELESS SENSOR NETWORK COVERAGE MODEL

A. Node and Node Set Coverage

Suppose there is a monitoring area for the two-dimensional plane A.In the region A, thesensor nodes with the same parameters are placed, and the coordinates of each node are (x_i, y_i), where $i = 1,2,\mathrm{L}\ ,N$.So that the sensor radius of each sensor node r, communication radius R.In this paper, in order to ensure the connectivity of the wireless sensor network, considering the wireless interference and other factors, the communication radius is set to twice the perceived radius, which is $R = 2r$.The sensor node set is denoted by $C = \{c_1, c_2, \mathrm{L}\ , c_N\}$, where the monitoring field of the i sensor node is centered on the position coordinate (x_i, y_i) and r is the circle of the monitoring radius, denoted by $c_i = \{x_i, y_i, r\}$.

Assuming that a detection area A is digitally discredited into $m \times n$ pixels whose coordinate are denoted by $(x_j, y_j), j = 1,2,\mathrm{L}\ , m \times n$.The distance between the j pixel and the i sensor node is $d(c_i, p_j) = \sqrt{(x_j - x_i)^2 + (y_j - y_i)^2}$.Assuming that the event at which the j pixel is covered by the i sensor node is r_{ij}, the probability of occurrence of event r_{ij} is $\mathrm{P}\{r_{ij}\}$, then the probability [8] that the pixel (x_j, y_j) is covered by the sensor node c_i is:

$$P_{\mathrm{cov}}(x_j, y_j, ci) = \begin{cases} 1, & if\ d(c_i, p_j) < r \\ 0, & otherwise \end{cases} \tag{1}$$

However, in the practical application, the interference of the monitoring environment, noise and other factors makes the sensor nodes with a certain probability distribution, according to reference [13] we can see the node monitoring probability distribution is as follows:

$$P_{\mathrm{cov}}(x_j, y_j, ci) = \begin{cases} 1, & if\ d(c_i, p_j) \le r - re \\ e^{(-\alpha_1 \lambda_1^{\beta_1})/\lambda_2^{\beta_2} + \alpha_2}, & if\ r - r_e < d(c_i, p_j) < r + r_e \\ 0, & otherwise \end{cases} \tag{2}$$

In equation (2), r_e $(0 < r_e < r)$ is the measurement uncertainty parameter of the sensor node, $\alpha_1, \alpha_2, \beta_1, \beta_2 > 0$ is the measurement parameter about the characteristics of the sensor node, where $\lambda_1 = r_e - r + d(c_i, p_j), \lambda_2 = r_e + r - d(c_i, p_j)$.The model reflects the characteristics of infrared and ultrasonic sensor isometric devices.Considering that the target pixel j is simultaneously covered by multiple sensor nodes, the joint monitoring probability [14] is:

$$P_{\mathrm{cov}}(C\,\mathrm{ov}_j) = 1 - \prod_{c_i \in C\,\mathrm{ov}_j} (1 - P_{\mathrm{cov}}(x_j, y_j, c_i)) \quad i = 1,2,\mathrm{L}\ N;\ j = 1,2,\mathrm{L}\ , m \times n \tag{3}$$

Where Cov_j is the set of sensor nodes that measure the target pixel point j.

B. Monitor Area Coverage

From the above assumptions, the region A has $m \times n$ pixels. In this paper, we use the joint monitoring probability of the node set to measure whether each target pixel is covered, so that P_{th} is the expected coverage threshold, then

$$P_{\mathrm{cov}}(Cov_j) = \begin{cases} 0, & if\quad P_{\mathrm{cov}}(Cov_j) < p_{th} \\ 1, & if\quad P_{\mathrm{cov}}(Cov_j) \ge p_{th} \end{cases} \tag{4}$$

Where $P_{\mathrm{cov}}(Cov_j) = 1$ indicates that the target pixel j is overwritten; otherwise, the target pixel j is not overwritten.This paper establishes a grid intersection that represents the coverage of the sensor, where the grid intersection is also called the sampling point [14].The effective coverage points $(\mathrm{N}_{effective})$ are calculated by the formula (2-4), and the number of sampling points of the whole sensor field is $m \times n$, so the coverage rate ϕ_p of the monitoring area A can be calculated as follows:

$$\phi_p = \frac{\mathrm{N}_{effective}}{m \times n} = \frac{\sum_j P_{\mathrm{cov}}(Cov_j)}{m \times n} \tag{5}$$

C. Optimization Model of Wireless Sensor NetworkCoverage

According to the above analysis, this paper takes the monitoring area coverage as the objective function, the node in the monitoring area as the constraint condition, and establishes the wireless sensor network coverage optimization model according to the formula (2-5):

$$\text{Maxmize}\quad \phi_p = \frac{\mathrm{N}_{effective}}{m \times n} = \frac{\sum_j P_{\mathrm{cov}}(Cov_j)}{m \times n} \qquad s.t.\quad \begin{cases} 0 \le x_i \le m \\ 0 \le y_i \le n \end{cases} \tag{6}$$

III. NETWORK COVERAGE OPTIMIZATION BASED ON IMPROVED PARTICLE SWARM OPTIMIZATION

A. Standard Particle Swarm Algorithm Principle

A group of M particles in the D dimension search space at a certain speed flight, PSO algorithm initialize a group of random particles, through the iterative to find the optimal solution. Where the speed of each generation of particles, the location update formula [5-6] as follows:

$$v_{ij}(n+1) = W * v_{ij}(n) + c1 * rand * (pbest_{ij} - x_{ij}) + c2 * rand * (gbest - x_{ij}) \quad (7)$$
$$i = 1,2,\mathrm{L}\ M;\ j = 1,2,\mathrm{L}\ D$$

$$x_{ij}(n+1) = x_{ij}(n) + v_{ij}(n+1), \quad (8)$$
$$i = 1,2,\mathrm{L}\ M;\ j = 1,2,\mathrm{L}\ D$$

Where v_i is the velocity vector of the i particle; x_i is the current position of the i particle; $pbest_i$ is the position of the optimal solution found by the i particle; $gbest$ is the position of the optimal solution currently found by the whole population; $c1, c2$ is the learning factor to respectivelyadjust the particle attractionstrength; $rand$ is the random number between $(0,1)$; W is the inertia coefficient, which is calculated as follows:

$$W(t) = 0.9 - \frac{t}{\max number} \times 0.5 \quad (9)$$

B. Coverage Optimization Design Based on PSOAlgorithm

Assuming that the monitoring area A is divided into several pixels with an area of 1, N sensor nodes are randomly deployed in the monitoring area. The coverage optimization based on the PSO algorithm is as follows:

Step1: Calculate the coverage of each pixel node for each sensor node according to (2);

Step2: Calculate the joint coverage of each pixel node for each sensor node according to (3);

Step3: According to (4-5) to calculate the coverage of the region, it istheobjective function, in the particle swarm algorithm also known as fitness.

Assuming that there are M particles, since the N sensors are deployed in the two-dimensional space, each particle has $D = 2 \times N$ -dimensional solution space that is $x = (x_1, x_2, \mathrm{L}\ x_D)$. The PSO algorithm is as follows:

Step1: Randomly generate the position and velocity of each particle in the monitoring area;

Step2:Update the position and velocity of each particle according to (7-9);

Step3: Calculate the fitness of each particle according to the optimization objective function;

Step4:Compare the particle fitness and the fitness ofits own best position, if better, and then set the new $pbest$;

Step5:Compare the fitness of each particle and the fitness of the best position in the population, if better, set the new $gbest$;

Step6:Until the maximum number of iterations is reached, the algorithm stops, otherwise proceed to step 2;

Step7: Output the optimal fitness and the corresponding particle position.

C. Chaotic Particle Swarm Algorithm

The main idea of the chaotic particle swarm algorithm is to generate a large number of initial groups by using the traversal type of chaotic motion, and select the optimal initial population to generate chaotic perturbations to the current particle individuals, so that the local extreme value interval can be jumped out. The random motion state usually obtained from the deterministic equation is called chaos. In this paper, Logistic map is used, which is a typical chaotic system. The iterative formula is:

$$z_{D+1} = \mu z_D (1 - z_D), D = 0,1,2,\mathrm{L} \quad (10)$$

The Logistic system is completely in the chaotic state when the control parameter $\mu = 4$ and $0 \le z_0 \le 1$ .The mapping of the chaotic to the optimization variables is:

$$x_{ij} = xmin_j + z_D \times (xmax_j - xmin_j), \quad (11)$$
$$i = 1,2,\mathrm{L}\ M,\ j = 1,2,\mathrm{L}\ D$$

Where $xmin \le x \le xmax$ and $x_i = (x_{i1}, x_{i2}, \mathrm{L}\ , x_{iD})$. According to the idea of chaos search, a small amount of chaotic perturbation is added to the current optimal solution, which is

$$z^{'} = (1 - \gamma)\psi^{*} + \gamma z \quad (12)$$

Where $\psi^{*} = \frac{x^{*} - xmin}{xmax - xmin}$ is the optimal chaotic vector formed by the current optimal solution x^{*} mapping, γ is the adjustment parameter of $[0,1]$, and $z^{'}$ is the vector obtained by adding a small amount of chaotic perturbationat the present optimal solution x^{*} [15-17].

D. Coverage Optimization Design Based on CPSO Algorithm

Step1:Randomly generate a D-dimensionalvector $z_1 = (z_{11}, z_{12}, \mathrm{L}\ , z_{1D})$ between $[0,1]$; generate M vectors $z_1, z_2, \mathrm{L}\ , z_M$ according to (10). According to (11), their components are carrier to the range of the optimal variables. Calculate the fitness of the initial particle swarm, and chose the better M_0 solutions as the initial solutions and randomly generate M_0 initial velocities.

Step2: Compare the particle fitness and the fitness ofits own best position, if better, and then set the new $pbest$;

Step3: Compare the fitness of each particle and the fitness of the best position in the population, if better, set the new $gbest$;

Step4: Update the position and velocity of each particle according to (7-9);

Syep5:The population optimal position $gbest$ is updated by a small amount of chaotic perturbations. If the number of current iterations is greater than or equal to $2/3$ times the total number of iterations, which is $MaxC \geq (2/3)MaxDT$ .A small amount of chaotic perturbation is added to the optimal position of the population according to (12), and the new chaotic variable is carried to the optimization variable according to (11).

Step6: Until the maximum number of iterations is reached, the algorithm stops, otherwise proceed to step 4;

Step7: Output the optimal fitness and the corresponding particle position.

E. The Principle of Cross Particle Swarm Algorithm

The main idea of the breeding particle swarm optimization algorithm: in the iterative process, the first half of the particles with good fitness directly into the next generation, and the latter half of the particles will be two pairs of pairs, and use the same crossover operation with the genetic algorithm to generate the same number of offspring with the parent number, and then compared with the parent, the better half of the fine particles into the next generation. This ensures that the number of particles remain unchanged.The breeding operation not only enhances the diversity of particles but also avoids the local optimum value, which helps to speed up the iterative convergence [18].

According to the breeding operation of the genetic algorithm, the position and velocity formula of the offspring particles are as follows:

$$\begin{aligned} child_1(x) &= pb \times parent_1(x) + (1-pb) \times parent_2(x) \\ child_2(x) &= pb \times parent_2(x) + (1-pb) \times parent_1(x) \end{aligned} \tag{13}$$

$$\begin{aligned} child_1(v) &= \frac{parent_1(v) + parent_2(v)}{\left| parent_1(v) + parent_2(v) \right|} \times parent_1(v) \\ child_2(v) &= \frac{parent_1(v) + parent_2(v)}{\left| parent_1(v) + parent_2(v) \right|} \times parent_2(v) \end{aligned} \tag{14}$$

Where $child(x), parent(x)$ represents the position of the offspring particles and the parent particles, $child(v), parent(v)$ respectively represents the velocity of the offspring particles and the parent particles, x is the position of the particle of the optimized variable, v is the velocity of the particle, pb is the D-dimensional vector of the value between $[0,1]$ [11].

F. Coverage Optimization Design Based on BPSO Algorithm

Step1: Population initialization. Randomly generated the location of each particle, speedin the monitoring area;

Step2: Calculate the fitness of each particle according to the optimization objective function;

Step3: Compare the particle fitness and the fitness ofits own best position, if better, and then set the new $pbest$;

Step4: Compare the fitness of each particle and the fitness of the best position in the population, if better, set the new $gbest$;

Step5: Update the position and velocity of each particle according to (7-9);

Step6: Calculate the fitness of the updated particles, and sort them from large to small;

Step7: The first half of the particles with good fitness directly into the next generation, the latter half of the two pairs of particles to match, anduse the same genetic algorithm with the cross operation, according to (13-14) to generate the same number of parents with the child Generation, and then compared with the father, the better the first half of the fine particles into the next generation;

Step8: Data merges to form new offspring particles and updates individual extremes and global extremes;

Step9: Until the maximum number of iterations is reached, the algorithm stops, otherwise proceed to step 2.

IV. SIMULATIONS

A. Experimental Environment and Parameter Setting

By using a computer with a frequency of 2.30GHZ, the wireless sensor network coverage optimization simulation is carried out in MATLAB2014a environment.In this paper, we assume that the region is a square with a length of 20meters and a total of 20 sensor nodes with the same performance and the same size. The perceived radius of the sensor r be 3 meters, the communication radius R be $2 \times r = 6$ meters. Sensor node measurement uncertainty parameter $r_e = 0.4 \times r = 1.2$, $\alpha_1 = 1, \alpha_2 = 0, \beta_1 = 1, \beta_2 = 1.5$. In the particle swarm optimization algorithm, let the learning factor $c_i, i = 1,2$ be 2 and the maximum number of iterations $MaxDT$ be 1000 .The 20 wireless sensor nodes are randomly distributed in the area as shown in Fig.1, where $*$ is the node position, and the circle represents the perceived range of the node, and the corresponding network coverage is 53.75% .

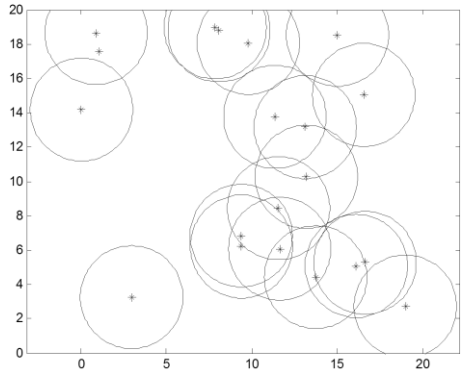

Figure 1. Monitoring area random distribution graph

B. Influence of Perceptual Radius on Network Coverage Optimization Performance

Under the same parameters and experimental environment, letthe number of particles M be 40 and the dimension D be $20\times 2=40$. By setting different perceive radius, the influence degree of different perceived radius on the network coverage optimization performance is analyzed.At the value of the node sensing radius r be $2,2.5,3,3.5,4,5$ meters, the PSO algorithm optimizes the network coverage of the monitoring area as shown in Fig .2. The number of iterations and the optimal coverage of the corresponding algorithmare as shown in Table I.The following data conclude that the higher the sensor node perceived radius, the higher the wireless sensor network coverage optimization performance.When perceivedradius r be 3.5 meters, the network coverage has reached more than 90%, the monitoring area is almost all covered, and achieve the desired coverage effect. At the beginning of the network coverage growth rate is faster, with the increasing in perceived radius, network coverage growth rate has slowed, the number of iterations less and less.

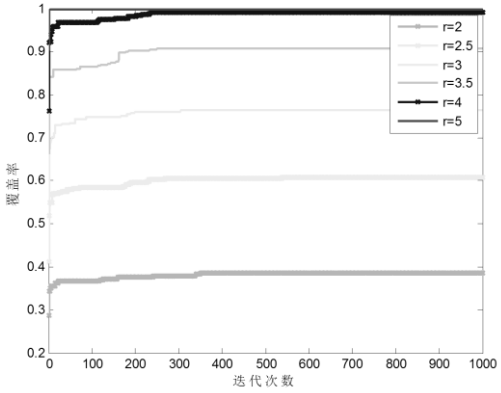

Figure 2. Theiteration graph of the different radius

TABLE I. THE NETWORK COVERAGE OPTIMIZATION PERFORMANCE OF DIFFERENT SENSING RADIUS

Area A network coverage optimization performance test						
Node perceived radius(m)	2	2.5	3	3.5	4	5
Number of iterations	351	539	305	249	236	4
Optimal coverage(%)	38.5	60.75	76.5	90.75	99.25	100

C. Performance Comparison of Network Coverage Based on PSO / CPSO / BPSO Algorithm

Under the same parameters and experimental environment, using respectively the standard particle swarm, chaos particle swarm and breeding particle swarm optimization algorithm to optimizethe regional network coverage. And the resulting node deployment situation isshown in Fig .3, Fig.4, and Fig .5. The corresponding optimal network coverage is $77.75\%,78\%,80\%$, and optimization performance comparison results shown in Fig. 6.

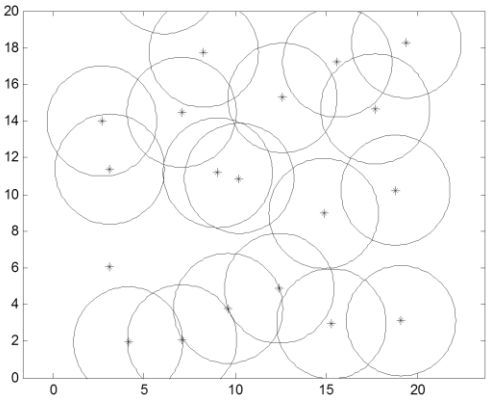

Figure 3. Optimized deployment graph for wireless sensor nodes based on standard particle swarm optimization

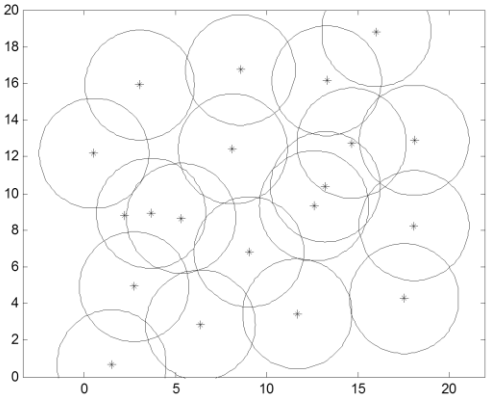

Figure 4. Optimized deployment graph for wireless sensor nodes based on chaos particle swarm optimization

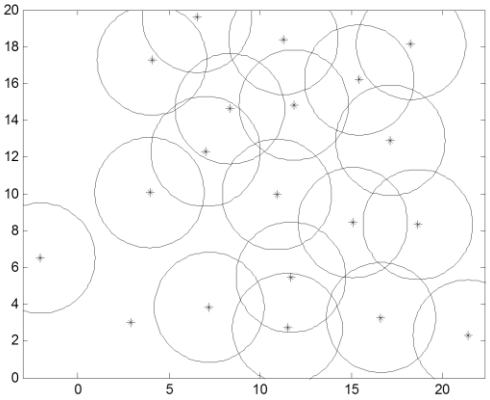

Figure 5. Optimized deployment graph for wireless sensor nodes based on breeding particle swarm optimization

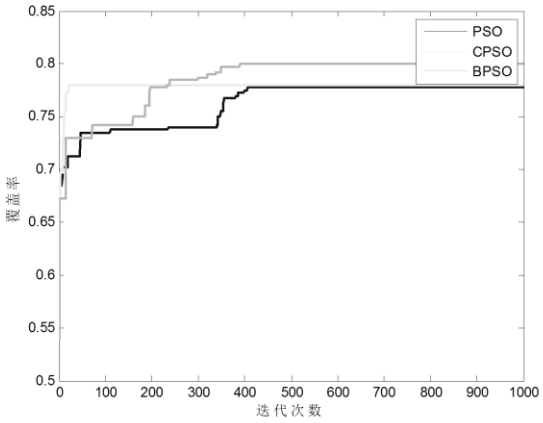

Figure 6. The comparison graph of the coverage performance of wireless sensor networks based on PSO / CPSO / BPSO algorithm

It can be seen from Fig.6 that the PSO algorithm has the lowest optimization result and the BPSO algorithm has the highest optimization result. The CPSO algorithm has the most number of iterations and the BPSO algorithm has the least number of iterations.It is shown that the PSO algorithm is easy to be trapped in the local optimum;the convergence degree of the late evolution is low; the ability that CPSO algorithm avoids falling into the local optimal is strong; the BPSO algorithm strongly maintains the population diversity and improves the convergence rate to a large extent.

V. CONCLUSIONSS

In this paper, we improve the coverage of wireless sensor networks by improving particle swarm optimization. Firstly, the mathematical model of wireless sensor network node, node set and region coverage is established, and the regional coverage formula is the optimization objective function.Then, the area coverage is taken as the fitness function, and the optimal deployment strategy and optimal coverage are solved in the particle swarm optimization algorithm.Finally, the simulation data show that the larger the node perceived radius, the better the network coverage optimization performance.By comparing the optimal performance of the three algorithms, such as standard particle swarm, chaotic particle swarm and cross particle swarm,it is proved that the latter two algorithms solve the network coverage better than the first algorithm.

ACKNOWLEDGMENT

This work was partially supported by Scientific Research Program Funded by Shaanxi Provincial Education Department of China (Program No. 16JK1696).The specific information of the project is as follows:

Project Name: Mining of Maximal Association Rules Based on Soft Set Logical Formula and Its Application.

Item Number: 16JK1696.

Project Category: Shaanxi Provincial Education Department special research project.

Project amount: 20,000.

Starting and ending time: June 2016 to December 2017.

REFERENCES

[1] LI Jian-bo,MU Bao-chun.Moving Node Localization Algorithm Based on Cooperated Prediction for Wireless Sensor Networks[J].Computer Application Research,2017,34(1):186-187.

[2] JAIN S, KUMAR A, MANDAL S, et al. B4:experience with a globally-deployed software defined WAN[J].ACM SIGCOMM Computer Communication Review,2013, 43(4):3-14.

[3] LIANG Bang-wei. Fault Diagnosis of Wireless Sensor Node for Railway Monitoring[D].Dalian:Dalian University of Technology,2015:1-3.

[4] MAO Yong-yi,CHEN Peng. WSN Intelligent Node Location Algorithm Based on Multi-power Mobile Anchor. Xi'an: Journal of Xi'an University of Posts and Telecommunications, 2016,21(3):48-53.

[5] ZHANG Li-biao.Research Based on Particle Swarm Optimization[D].Jilin:Jilin University,2004:1-28.2004101033.htm.

[6] LI Jian-yong. TheStudyofParticleSwarmOptimization[D].Zhejiang:Zhejiang University.2004:16-22.

[7] GAO Fang. ResearchonIntelligentParticle Swarm Optimization Algorithm[D].Harbin:Harbin Institute of Technology,2008:11-26.

[8] LIN Z L, MA S P, TAO Z Y. Research on Particle Swarm Optimization Strategy for Forest Fire Detection System Based on Wireless Sensor Networks[C].Control and Decision Conference, 2009:3608-3612.

[9] LIU Dao-hua,YUAN Si-cong,LAN Yang,et al.Method of Particle Swarm Optimization Based on the Chaos Map[J].Journal of Xidian University,2010,37(4):764-769.

[10] LIU Wei-ting,FAN Zhou-yuan.Coverage Optimization of Wireless Sensor Networks Based on Chaos Particle Swarm Algorithm[J].Computer Application,2011,31(2):338-361.

[11] LI Ji,SUN Xiu-xia,LI Shi-bo,et al. Improved Particle Swarm OptimizationBased on Genetic Hybrid Genes[J].computer engineering,2008,34(2):181-183.

[12] WANG Jun,LIShu-qiang,LIU Gang. Three- dimensional Localization Method of Agriculture Wireless SensorNetworks Based on Crossover Particle Swarm Optimization[J].Journal of Agricultural Mechanization,2014,45(5):233-238.

[13] LIN Zhu-liang,FENG Yun-jing.Optimization Strategy of Wireless Sensor Networks Coverage Based on Particle Swarm Algorithm[J].Computer Simulation,2009,26(4):190-193.

[14] LI Z M, LIN L. Sensor Node Deployment in Wireless Sensor Networks Based on Improved Particle Swarm Optimization[C].International Conference on Applied Superconductivity and Electromagnetic Devices,2009:215-217.

[15] GAO Shang,YANG Jing-yu.Research on Chaos Particle Swarm Optimization Algorithm[J].Pattern Recognition and Artificial Intelligence,2006,19(2):266-270.

[16] TANG Xian-lun. Theory and Application of Chaotic Particle Swarm Optimization Algorithm[D].Chongqing: Chongqing University,2007:40-42.

[17] LIAO Hui.Analysis and Application of Chaotic Particle Swarm Optimization Algorithm[D].Guangdong University of Technology,2011:22-33.

[18] WEI Yuan-yuan,YAO Jin-jie. Application of Modified Particle Swarm Algorithm with CrossoverOperator in the Space Flight Target Localization[J].Journal of Projectiles, Rockets and Guidance,2010,30(5):162-164.

Improved Statistical Analysis Method Based on Big Data Technology

Hongsheng Xu[1,2*]
[1]Luoyang Normal University
[2]Henan key Laboratory for Big Data Processing & Analytics of Electronic Commerce
Henan LuoYang, China
E-mail: 85660190@qq.com

Ke Li
Luoyang Normal University
Henan LuoYang, China
E-mail: 85660190@qq.com

Ganglong Fan[1,2]
[1]Luoyang Normal University
[2]Henan key Laboratory for Big Data Processing & Analytics of Electronic Commerce
Henan LuoYang, China
E-mail: 85660190@qq.com

***Abstract*—Big data technology refers to the rapid acquisition of valuable information from various types of large amounts of data. It can be divided into 8 technologies: data acquisition, data access, infrastructure, data processing, statistical analysis, data mining, model prediction and results presentation. The paper presents improved statistical analysis method based on big data technology. A statistical analysis model in big data environment is designed to extract useful information features from large amounts of data based on the Hadoop system by using its distributed storage and parallel processing mechanism.**

Keywords-Big data; Statistical analysis; Hadoop; Data acquisition; Data mining

I. INTRODUCTION

With the rapid growth of the scale of statistical data, data characteristics become increasingly complex, data collection channels are diverse, and statistical related field research has entered the era of big data. How to efficiently collect sample data, mine information, extract useful information features from large amounts of data, and provide information to relevant departments in a timely manner has become one of the focuses of current statistical research [1]. Compared with foreign countries, there are some problems in the statistical analysis of our country, such as the low degree of integration of information resources, the lack of data sharing and incomplete information. With the advent of the era of big data, research and application of data analysis and mining of large pay more and more attention, big data mining and analysis will help the statistics department in reasonable time collection, management and analysis of massive data.

Statistical analysis of the eight methods, one index, comparative analysis, index comparative analysis, also known as comparative analysis, is the most commonly used method of statistical analysis. It is a comparative method to reflect the differences and changes in the number of things.

Big Data refers to the large data size exceeds the commonly used software tools at run time can withstand the collection, management and data processing ability of data sets; data is currently stored mode and ability, computing and storage and processing capacity can not meet the existing data sets generated by the relative concept of scale.

With the development of information technology, more and more data are accumulated. In fact, the data itself is meaningless and can only really work if it is used for analysis. Therefore, it can be said that the more important behind the surge of data is implicit information, and people want to be able to analyze these data at a higher level in order to make better use of these data. The massive data is the development trend of data analysis and data mining is becoming more and more important, from the mass of data to extract useful information is important and urgent, this will require the processing to be accurate, high precision, and the processing time is shorter, get valuable information quickly, therefore, promising research of massive data, too worthy of extensive research.

In the large data environment, facing the collection and statistics of massive data, traditional methods can not meet the needs of large-scale data set processing [2]. Based on the Hadoop system, using the distributed storage and parallel processing mechanism, and it is the design of the statistical data environment analysis model, to extract useful features information from massive data, realizing the sharing of data resources, to provide information service for the relevant decision-making departments.

Statistics is a data processing engineering, dealing with large data sets, the statistical sample becomes large, complex data feature makes statistical work has become cumbersome, and data mining is a process to get useful information from a large number of data, the use of modern information technology and mining algorithm, can effectively useful for data acquisition and processing. It might be accurate data statistical model for processing data for a large data mining under the condition of understanding, relevant data processing and analysis of mining data after introducing the statistics, two kinds of methods are combined. The paper

presents improved statistical analysis method based on big data technology.

II. DISCUSSION ON THE INTEGRATION OF BIG DATA AND STATISTICAL ANALYSIS

Partial least squares regression is a new multivariate statistical analysis method. It was first proposed by Wood and Abano in 1983. In the past ten years, it has developed rapidly in theory, method and application. Many statisticians are beginning to focus on their theoretical research, and its growing potential in applications is attracting more and more attention.

According to the data contained in the prior information in the background, the data set can be divided into homogeneous and heterogeneous (homogeneity) (heterogeneity), this paper introduces the two kinds of data integration punishment analysis method; it summarizes both considering network structure (Network), the method of punishment. The regression coefficient of integration analysis has two meanings: the first is the variable level, and the ordinary single data set model; second is the data set level, the same explanatory variables with a regression coefficient associated with each data set is connected by the regression coefficient. This is also the particularity of integration analysis. The significance of variables is no longer a regression coefficient, but a set of regression coefficients. Therefore, a special variable selection method is needed.

Packet analysis comparison index contrast, but the overall statistical units have a variety of characteristics, which makes the unit in the same overall range have many differences, statistical analysis not only on the total number of features and quantitative analysis of the relationship, but also the overall was analyzed deeply inside. Packet analysis is based on the statistical analysis of the objective requirements, the overall research in accordance with one or several marks is divided into several parts, collate, observation, analysis, to reveal the inherent relationship between it.

Big data technology refers to the rapid acquisition of valuable information from various types of large amounts of data. It can be divided into 8 technologies: data acquisition, data access, infrastructure, data processing, statistical analysis, data mining, model prediction and results presentation. At the same time, three computing models, batch processing, stream processing and interactive analysis, are formed by these techniques, as is shown by equation(1) [3].

$$P(\beta;\lambda,\gamma)=\lambda\sum_{j=1}^{p}\left\|\beta_j\right\|^{\gamma}=\lambda\sum_{j=1}^{p}\left(\left(\sum_{i=1}^{M}(\beta_j^{(i)})^2\right)^{1/2}\right)^{\gamma} \quad (1)$$

The classification is to find out a set of data objects in the database of the common characteristics and in accordance with the classification model can be divided into different classes; its purpose is through the classification model, mapping the data item to touch a given category. Can be applied to the prediction of application involves classification, trends, such as the Taobao shops will be users over a period of time in the purchase are divided into different classes, recommended Association class products to users according to the situation, so as to increase the sales of shops.

Hadoop has developed into a collection containing multiple sub items. The core content is the MapReduce and Hadoop distributed file systems (DHFS). It also includes Common, Avro, Chukwa, Hive, Hbase, and other sub projects, they provide high-level services on the core layer, and play an important role in the promotion of Hadoop applications.

Big data has been defined as the fourth paradigm of scientific inquiry. After hundreds of years of experimental science, thousands of years ago before the theory of science and decades ago computational science, the data explosion gave birth to data intensive science, theoretical, experimental and computational simulation paradigm of unity. Big data has been hailed as "non competitive" factors of production. Big data has "inexhaustible," the characteristics of the continuous re-use, restructuring and expansion of the continuous release of its potential value, in a wide range of open, sharing, and constantly create new wealth. The root is that the value of big data is to predict future trends in unknown areas and non specific factors, to solve long-term, universal social problems. The current big data technology and applications are still limited to historical and real-time data association analysis, limited to meet short-term, specific market demand. The process of solving paradoxes is just the course of theory and method. While people try to solve the paradox of effort, just big data push air plant.

Data mining is from a large, incomplete, noisy, fuzzy and random data to extract implicit, believable, novel, people do not know in advance, but is potentially useful patterns of advanced treatment process. Data mining is a cross subject formed by the integration of many fields, such as statistics, artificial intelligence, database and visualization technology [4]. In addition to describing relationships and rules, one of the most important tasks of data mining is analysis. According to the laws found in past and present data, this model can sometimes be considered as a key attribute of time.

The partial least squares regression theory is the greatest contribution of Umea University Organic Chemistry Department wood its founder professor Wood taught the moral education in sweden. Under his guidance, as is shown by equation (2), and the Department has published many doctoral dissertations on the theory and applications of partial least squares regression. He and his collaborators have also conducted extensive theoretical discussions and developed SLMCA-P data analysis software running under Windows to support partial least squares regression calculations and interpretation of results. Perhaps this is true. Partial least squares regression is widely used in the field of chemical engineering.

$$\xi_{ij}(k)=\left[1+\left|\frac{\Delta x_i(k)}{\sigma_i}-\frac{\Delta x_j(k)}{\sigma_j}\right|\right]^{-1} \tag{2}$$

Where x is often in the use of ordinary multiple flyback when Wei, is the number of samples should not be too small. In the general statistics book, the number should be more than two times the number of variables. However, in some of the scientific research experiment, there are often many important variables must be considered, but because of the condition fee and time limit, the number of available samples is far less than the variable. The general multiple regression model is incapable of modeling when the number of sample points is less than the number of variables.

Integration analysis is also an effective way to solve the "size" problem. It integrates multiple data sets and increases the sample size. It is an effective way to solve the small sample problem. This problem is very common in big data, on the one hand, due to large data sparsely, low value density, the marginal value of information is not the amount of data with increased; on the other hand is the high dimensionality of the data highlight the Internet and cloud computing for data acquisition and storage to bring convenience, small study on the factors associated with the phenomenon may be collected, dimensions will be high, as is shown by equation(3), and "noise purification" is an urgent problem to be solved. Integrated analysis is a variable selection method combined with integration analysis, dimension reduction is an effective way to extract information, not only can be applied to model selection, correlation analysis between data sets can, in order to better identification of signal and noise.

$$P(\beta;\lambda,a,b)=\sum_{j=1}^{p}P_{MCP}\left(\sum_{m=1}^{M}P_{MCP}(\left|\beta_j^{(m)}\right|;\lambda,a);\lambda,b\right) \tag{3}$$

The key to processing and analyzing large data lies in the distributed storage function and powerful computing power. The basis of data processing is data storage, and the key to data analysis lies in the powerful processing ability. Hadoop is a scalable and reliable computing system, open source distributed, the framework can be realized by simple calculation model of massive data processing in computer cluster, compared with on high performance servers, Hadoop good scalability, while the nodes in the cluster can provide local storage and calculation.

III. IMPROVED STATISTICAL ANALYSIS METHOD BASED ON BIG DATA TECHNOLOGY

Time series is a series of values that change and develop in the same time in time. They are formed in chronological order, forming a time series, also called a dynamic series. It can reflect the development and change of social economic phenomena. Through the compiling and analysis of time series, we can find out the law of dynamic change, and provide the basis for predicting the future development trend [5]. The time series can be divided into absolute number, time series, relative number, time series, and average time series.

A large collection of data received from the client is using multiple databases (Web, App or sensor form) data, and the user can perform simple queries and processing work through these databases. For example, the electricity supplier will use traditional relational databases such as MySQL and Oracle to store every transaction data. In addition, NoSQL databases such as Redis and MongoDB are also commonly used for data collection. In the process of collecting data, the main characteristics and challenges is the high number of concurrent, because at the same time there may be tens of thousands of users to access and operate, such as train ticketing website and Taobao, visit their concurrent at the peak reached millions, so in the end need to support the deployment of a large number of data acquisition. And how to load and distribute between these databases requires deep thinking and design.

The missing value ratio, which is based on data columns that contain too many missing values, is less likely to contain useful information. Therefore, you can remove columns with missing data columns greater than a certain threshold. The higher the threshold is, the more efficient the dimensionality reduction method is, the less the lower dimension, the lower variance is similar to the filtering method, which assumes that the data column changes very little and the information contained in the column is very small. As a result, all columns with small variance are removed. One thing to note is that the variance is related to the range of data, so you need to normalize the data before using the method.

Data collection center is mainly through the deployment in the cloud server cluster environment to complete data acquisition, data are stored in HDFS distributed database; statistics management department to set up the server cluster, in order to ensure the scalability of the system, can also be incorporated into the base layer of the server at any time in the cluster computing tasks by using MapReduce the mechanism of distribution and processing; statistical analysis center is mainly intelligent algorithm pool, through the analysis of the application of algorithm for the data collection.

Statistics is an ancient discipline, has more than 300 years of history, in the natural science and social science development has played an important role in statistics; it is a strong vitality and discipline, as is shown by equation (4), and it all rivers run into sea with the growing development and learn widely from others'strong points, specific discipline each door. Without exception, the arrival of the big data era has brought opportunities for the development of statistical disciplines, but also made statistical disciplines face major challenges. How to deeply understand and grasp the development opportunity, how to better understand and deal with this great challenge, so we need to clarify the concept of "big data features clear big data; put forward the

new concept of statistical thinking process to re-examine the statistics [6].

$$w_{i+1}^{1}(t+1)=\left(1-wd_{i}^{1}(t)\right)x_{i}^{1}(t)-rs_{i}\alpha N^{1}(t) \quad (4)$$

The regression analysis reflects the attribute value of the data in the database, and finds the dependence between the attribute values through the relation between the function and the data mapping [7]. It can be applied to the prediction of the data sequence and the study of the correlation. In marketing, regression analysis can be applied to every aspect. Through the regression analysis of the quarterly sales, we forecast the sales trend in the next quarter and make targeted marketing changes.

Time series speed index. According to the absolute number of time series can be calculated speed indicators: there is development speed, growth rate, average speed of development, the average growth rate. Dynamic analysis is method. In statistical analysis, it is difficult to make a judgement if there is only one period index value. If the time series is worked out, dynamic analysis can be carried out to reflect the changing law of its development level and speed.

Hadoop provides a stable and reliable analysis system and shared storage for statistical analysis. It contains two core technologies: MapReduce and HDFS [8]. MapReduce implements data processing and analysis, and HDFS is responsible for data sharing and storage. In large data environment, the basic framework of statistical work includes data acquisition center and statistical analysis processing center.

IV. Experiments and Analysis

Analysis of statistics based on large data, the statistical object is often structured and unstructured mixed data, such as text, image, audio and video, here is the basic idea of the design is the use of the underlying mining model through data collection, management middleware, implementation layer analysis, screening and sorting out the valuable data and information finally, the statistical results of visualization.

Partial least squares regression can solve many problems that can not be solved by ordinary multiple regression. In the application of ordinary multiple linear regression, we are often faced with many restrictions, and the most typical problem is the multiple correlation between the self changing and the most [9]. Many experienced system analysts have noticed this problem. In order to describe and analyze systems more fully, as far as possible without omitting some of the most important system characteristics, analysts tend to selects relevant indicators more carefully.

Factor analysis is using the index. Factor analysis is the research object is divided into various factors, the overall research object as the factors common result, through the analysis of various factors, the influence degree of the research object in the general changes of factors were determined [10]. The factor analysis can be divided into the factor analysis of the change of the total index according to the statistical index of the object under study, and the factor analysis of the change of the average index.

Statistics and analysis of the main use of the distributed database, or distributed computing analysis and classification of common summary of mass data storage within the cluster, in order to meet the demand analysis of the most common, in this regard, some real-time requirements will be used EMC GreenPlum, Oracle Exadata, and MySQL based storage Infobright so, some of the batch, or based on semi-structured data needs can use Hadoop, as is shown by equation(5).

$$q_{ii}=\lim_{h\to 0^{+}}\frac{p_{ij}(h)}{h}=\begin{cases}\lambda_{i},\ \text{j=i+1},\\ u_{i},\ \text{j=i-1},\\ 0,\ |i-j|\geq 0.\end{cases} \quad (5)$$

The purpose of using large statistics is to infer the average or quantile of economic, social or social, economic or social indicators. The emphasis of statistics is on the representativeness of samples, which are generally met by probability sampling. Although there is a large data sample mass, can provide a wealth of information, but strictly speaking, big data is not a sample, on the contrary there will be lack of large data sample representation, information redundancy, noise and other problems, this situation is very easy to bring system error analysis results.

Big data based on the analysis of massive data to produce value, then how to get massive data to make big data really landing it. One of the most important aspects of this is data openness. Now to promote data openness and it is more importantly, through the sharing of data to produce more value. Data opening can improve the efficiency of social operation, and actively integrate the public data of all parties, and establish urban planning based on big data to ease traffic and social security issues. The opening of data can stimulate great commercial value, and the opening of data is open to the public, and anyone can use it to create new business opportunities.

People familiar with multivariate statistical analysis know that there are two broad categories of multivariate statistical analysis methods. One is the model based approach, which is mainly represented by regression analysis and discriminate analysis. It is characterized by the separation of independent variable and dependent variable in the set of variables. Data analysis is often used to find the functional relationship between dependent variables and independent variables. A model is established for prediction. The other is the cognitive method, which is represented by principal component analysis and cluster analysis, and canonical correlation analysis belongs to this method. The main feature of this kind of method is not in the original case according to the independent and dependent variables of the points, and through data analysis, can simplify the data structure and the similarity between observed variables or sample points.

V. SUMMARY

The paper presents improved statistical analysis method based on big data technology. Balance analysis is a method to study the equivalence of quantitative changes in social economic phenomena. It arranges the two sides of the unity of opposites according to their constituent elements, and gives the whole concept, so as to facilitate the whole situation to observe the balance relation between them. Balance relationship exists widely in economic life, to the national macro economy, small personal income. Balance analysis functions: one is the balance to reflect the social economic phenomenon from the number of equivalence relations, analysis of the ratio between the various phase to adapt to the situation; the two is to reveal the factors and development potential is not balanced; the three is the balance between the individual indicators can be calculated from the given index in the unknown.

At present the government with the e-government platform can realize the sharing of data resources, but the enterprise between the government and the lack of data sharing platform, causing the information isolation, in this regard, the statistics department to build a full range of safety statistics data sharing and distributed storage analysis platform, implementation of statistical information exchange across the region, and to meet the real time share mass data processing.

ACKNOWLEDGMENT

This paper is supported by Henan key Laboratory for Big Data Processing & Analytics of Electronic Commerce, and also supported by the science and technology research major project of Henan province Education Department (13B520155, 17B520026).

REFERENCES

[1] Patricia L. Mabry. Making Sense of the Data Explosion. American Journal of Preventive Medicine, 2011, 40(5),pp.12-30.

[2] Viktor Mayer-Schonberger,Kenneth Cukier,Big Data: A Revolution That Will Transform How We Live, Work and Think, Hodder & Stoughton,2013.

[3] Letouzey, S. Huberlant, P. Mares et al.. Assessment of Quality of Life of Patients Supported for Genital Prolapse Surgery: Feasibility of a Computerized Data Collection. The Journal of Minimally Invasive Gynecology, 2011, 18(6).

[4] W. Aigner, A. Rind, S. Hoffmann. Comparative Evaluation of an Interactive Time-Series Visualization that Combines Quantitative Data with Qualitative Abstractions,Computer Graphics Forum, 2012, 31,pp.3-15.

[5] B. Zhu, L. Xu, D. Faries et al.. PMH83 Comparison of Total Health Care Costs Between Remitters and Non-Remitters for Schizophrenia Patients from a Prospective Longitudinal, Observational Study in the Presence of Missing Data. Value in Health, 2012, 15(4),pp.100-120.

[6] Hassibi,Khosrow & De, Big Data, Data Mining, and Machine Learn, John Wiley Sons, 2014.

[7] Ahmed M. Abdel-Khalek, Mostafa A. Elseifi, Kevin Gaspard et al.. Model to Estimate Pavement Structural Number at Network Level with Rolling Wheel Deflectometer Data. Transportation Research Record: Journal of the Transportation Research Board, 2012, 2,pp.30-41.

[8] Lee, Keon Myung & Park, Seung Jong & Lee, Soft Computing in Big Data Processing, Springer, 2014.

[9] Yanqing Lv, Jianmin Gao, Zhiyong Gao and Hongquan Jiang, "Multifractal information fusion based condition diagnosis for process complex", Process Mechanical Engineering, (2012),pp.1-8.

[10] Bauckhage C, Kersting K. Data mining and pattern recognition in agriculture, KI-Künstliche Intelligenz, 2013, 27(4): 313-324

Evaluating Performance of Broadband NetworkBased on Indexes of TCP Messages

Xin Wang
Information Engineering Institute
The College of Arts and Sciences Yunnan Normal University
Kunming, China
E-mail: wangxin.bupt@139.com

Keguang Yang
Information Engineering Institute
The College of Arts and Sciences Yunnan Normal University
Kunming, China
E-mail: 504469132@qq.com

Yali Liu
Information Engineering Institute
The College of Arts and Sciences Yunnan Normal University
Kunming, China
E-mail: 3138022@qq.com

Yi Gao
Information Engineering Institute
The College of Arts and Sciences Yunnan Normal University
Kunming, China
E-mail: 13577046394@126.com

***Abstract*—Qos of broadband network is important. ISPs have some methods for evaluate it. But they are not efficient enough. This paper present a new method in which delay and scale of windows of TCP messages are used for evaluating performance of broadband. Comparison between delay or scale of window s of samples is the core idea of the method. There are two kinds of comparison.One is absolute terms of above-mentioned indexes,another is score,that is relative term. We can grade samples according to their scores. It is helpful for locating probably fault situation for ISPs.**

Keywords-QoS;Broadband;RTT;TCP;Scale of Window

I. INTRODUCTION

A. What is Broadband Access Network

The Internet known as the information superhighway, has indeed established a worldwide borderless cyber society. Nowadays, Internet is acknowledged worldwide as an essential component for electronic communication services. The rapid increase in the use of the Internet has changed the way we live, the Internet has become an important factor in people's daily life. Higher speed access network is necessary for huge amount of data.

Broad communication involves participants including users, ISPs and content providers. When users access Internet, the data will go through many parts of the network as showed in Fig. 1[1]. In fact, users' feeling about the Quality of Service (QoS) relates to ISPs' network, web sites, Content Delivery Network (CDN) servers and so on. However, occasionally the scenarios under which Internet is sold to customers is not fair and unfortunately Internet subscribers are not well informed on the InternetQoS provided to them by Internet service providers ISPs[2].

Usually, access network includes all line and equipment between Broadband Remote Access Server(BRAS) and hosts, as Fig. 1 shows. It is more and more difficult for ISPs to maintain the access network because of its more and more complexity. As reliance on Internet networks, in promoting socioeconomic development, increases the QoS of Internet networks also becomes very critical and important. How to evaluate effectiveness of a broadband access network is a hot topic. J. Sharad mentioned in an article[3]that we can track of the values of two important variables associated with a TCP connection: the sender's congestion window and the connection Round Trip Time (RTT). This paper will talk about them with other methods.

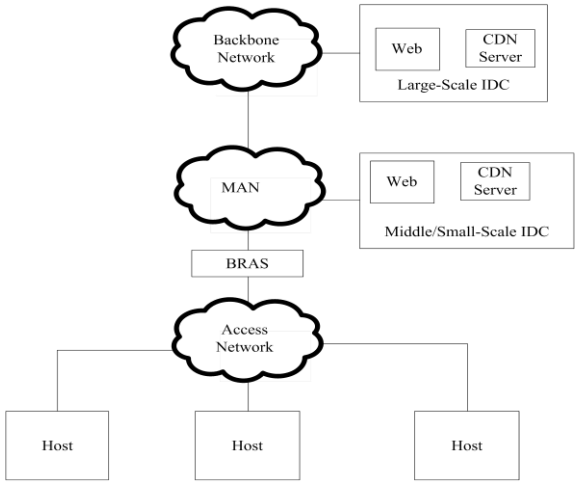

Figure 1. Structure of Broadband Network

B. An Existing Method

Monitoring RTT provides important insights for network troubleshooting and traffic engineering. The common monitoring technique is to actively send probe packets from selected vantage points (hosts or middleboxes).Active probing from selected vantage points for efficientRTTmonitoring of all the links and any round-trip path between any two switches in the network[4].

In a standard released by Ministry of Industry and Information Technology of the People's Republic of China concerns to measuring broadband access velocity. In the standard, a measure platform accesses to BRAS as showed in Fig.2[5]. Three models are presented including client speed-measurement, web page speed-measurement and control speed-measurement. The measurement process is described as follows. Firstly, users visit the special measurement web page, or use the measurement client to communicate with the measurement platform. Secondly, users download some special files from the platform. Lastly, the formula to calculate the access rate isEq.5

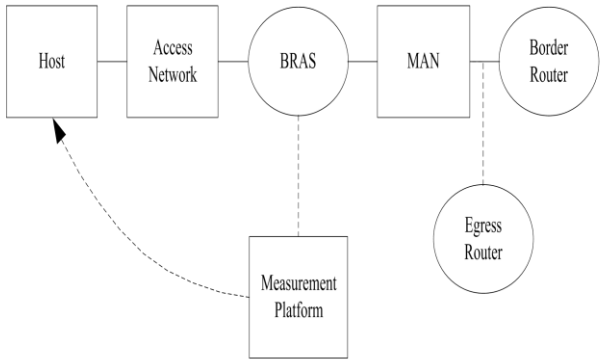

Figure 2. Architecture of Access Rate Measurement System

$$V = \frac{L}{T} \tag{1}$$

V (Byte/s) is the access rate, L (Byte) is the length of the downloaded file, and T(s) is the spent time for downloading the file.

Above-mentioned is a briefand direct way, and it is easy to draw a conclusion without complex devices. But this way has two shortcomings. At first, the conclusion cannot point out what is the main factor infecting the velocity. At last, too much platforms are not easy managing because there are many BRAS on the network.

II. A NEW METHOD

In this method, we can use some indexes of TCP messages including handshake-delay, wave-delay and scale of windows for measuring efficiency of the network. The following part will elaborate the method.

A. *Handshake-delay and Wave-delay*

1) *Definition of Handshake-delay and Wave-delay*

Su Q. and etc. mentioned some ways for measuring RTT in anarticle[6].According to their theories, we present two indexes, they are handshake-delay(T_1) and wave-delay(T_2)result from Eq.2 and Eq.3. And parameters being used for calculating them are shown in Figure 3. T_1 is handshake-delay of a upstream TCP message which is from Core Router (CR) to content server, for example, CDN.T_2 is Wave-delay of a downstream TCP message which is from CRto host, for example, PC[7]. We had capturedmessages in CR for a month.According to statistics and analysis, we divided T_1 and T_2into twelve intervals as Table 1 shown. T_1 and T_2 are defined as Eq.2 and Eq.3. Unit of them is millisecond.

$T_{hu}$is handshake-RTT of upstream, $T_{wu}$is wave-RTT of upstream, T_{hd} is handshake-RTT of downstream, and T_{wd} is wave-RTT of downstream. They can be calculated by time stamp of upstream or downstream. INT means bracket function. For instance, time stamp of downstream TCP message's ACK from content server minus time stamp of upstream TCP message's SYN from host can get T_{hu}.As shown in Fig. 3.

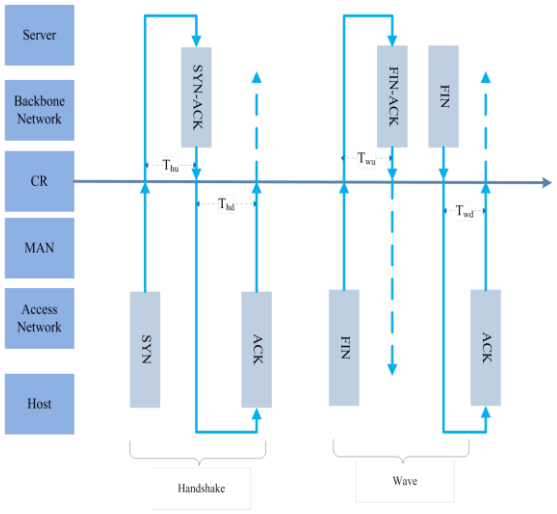

Figure 3. Definition of Delay

$$T_1 = \mathrm{INT}\left(\frac{T_{hu} + T_{wu}}{2}\right) \tag{2}$$

$$T_2 = \mathrm{INT}\left(\frac{T_{hd} + T_{wd}}{2}\right) \tag{3}$$

According to the value of T_N(including T_1 and T_2), T_N is divided into *i* intervals, $T_{N\text{-}i}$including $T_{1\text{-}i}$ and$T_{2\text{-}i}$ stands for the count ofT_N in No. *i* intervals in unit time. $T_{N\text{-}i}$ has no unit.

TABLE I. INTERVALS OF TN

T_N	<10	40	80	160
$T_{N\text{-}i}$	$T_{N\text{-}1}$	$T_{N\text{-}2}$	$T_{N\text{-}3}$	$T_{N\text{-}4}$

T_N	320	640	1280	2400
$T_{N\text{-}i}$	$T_{N\text{-}5}$	$T_{N\text{-}6}$	$T_{N\text{-}7}$	$T_{N\text{-}8}$

T_N	6000	18000	32000	>32000
$T_{N\text{-}i}$	$T_{N\text{-}9}$	$T_{N\text{-}10}$	$T_{N\text{-}11}$	$T_{N\text{-}12}$

For example, $T_{1\text{-}7}$ is 14 if 200 T_1 are recorded and 14 of them are between 1280ms and 2399ms in the unit time.

2) *Analysis of Handshake-delay and Wave-delay*

Probe at CR is able to collect aforesaid timestamp of TCP messages for calculating $T_{1\text{-}i}$ and $T_{2\text{-}i}$ in unit time. Then the statistics are inserted into a database consists of quintuples.

These quintuplesare defined according to a TCP message's parameters including source IP, source port, destination IP, destination port and name of the service. These parameters are easy being captured by probes based on Field Programmable Gate Array(FPGA).Table II shows THE data structure.

TABLE II. DATA STRUCTUREOFTN STATISTICS

Time Stamp	IP_{Source}	P_{Source}	$IP_{Destination}$	$P_{Destination}$	Service Name
2 Byte	4 Byte	4 Byte	4 Byte	4 Byte	20 Byte
	Quintuple				

T_1	T_2
12 Byte	12 Byte

Note: Structure of T_1 and T_2 is shown in Table I

Calculating accumulative total probability distribution of $T_{1\text{-}i}$ and $T_{2\text{-}i}$ as Eq.5

$$T_{S-N} = \sum_{i=1}^{12} (T_N)_i \tag{4}$$

T_{S-N} (N=1 or 2) is the sum of T_1 or T_2 in a quintuple in unit time.

$$P_{N-m-t} = \frac{\sum_{i=1}^{m} T_{N-i}}{\sum_{i=1}^{12} T_{N-i}} * 100\% \tag{5}$$

P_{N-m-t} (N=1 or 2) is accumulative total probability distribution of $T_{N\text{-}i}$ in *m* intervals,and T_{N-i} (i= 1 ~ 12) is the probability distribution of No.*i* interval.

Table III demonstrates how to use Eq.5.

TABLE III. THE DISTRIBUTION OF T2

T_2	<10	40	80	160
$T_{2\text{-}i}$	65	40	18	20
$P_{2\text{-}m\text{-}t}$	31.55%	50.97%	59.71%	69.42%

T_2	320	640	1280	2400
$T_{2\text{-}i}$	9	6	12	16
$P_{2\text{-}m\text{-}t}$	73.79%	76.70%	82.52%	90.29%

T_2	6000	18000	32000	>32000
$T_{2\text{-}i}$	12	7	1	0
$P_{2\text{-}m\text{-}t}$	96.12%	99.51%	100.00%	100.00%

$T_{N\text{-}A}$is defined as Eq.6 and score of $S_{N\text{-}k\text{-}t}$ is defined as Eq.7.$T_{N\text{-}A}$ means average of $T_N$and $S_{N\text{-}k\text{-}t}$ means the score of time delay of No. *k*sample.

$$T_{N-A} = \frac{\sum_{k=1}^{n} (T_{S-N})_k}{n} \tag{6}$$

$T_{1\text{-}A}$ is average T_1 of *n* samples,*n* is the number of samples with same destination IP, same destination Port and same name of the servicebut different source IP. $T_{2\text{-}A}$ is average T_2 of *n* samples,*n* is the number of samples with same BRAS or same port of BRAS, or same VLAN of portbut different source IP. $T_{S\text{-}N}$comes from Eq.4

$$S_{N-k-t} = \frac{100 * (I - \sum_{m=1}^{I} P_{N-m-t})}{I * x} + 100 * \frac{1-x}{2} \tag{7}$$

$S_{N\text{-}k\text{-}t}$(*N*=1 or 2) is the score of No. *k* sample. P_{N-m-t} results fromEq.5. *I* and *x* are parameters. Because there are 12 intervals for $T_{1\text{-}i}$ ($T_{2\text{-}i}$), so I equals 12. In addition, shorter time-delay means better QoS, so *x*=-1. For example, in the specified time, if the accumulative total probability distribution of $T_2$is shown in Table 3, the score of No. *k* sample is 75.5.

According to Eq.2 and Eq.3, T_1indictsefficiency of transferring data of uplink from CR to content server and T_2 indicts efficiency of transferring data of downlink from CR to host in the unit time. Two parameters could beused for evaluating the QoS. The comparison between $T_N$and $T_{N\text{-}A}$(from Eq.6), the comparison between T_N from different IP, different BRAS, different VLAN etc. in same time quantums, the comparison between T_N in different time quantums is helpful to locate the situation of fault. For the same reason, the comparison between $S_{N\text{-}k\text{-}t}$(from Eq.7) is helpful to locate the situation of fault. For example, if user-a blame to the speed when he was playing an online-game, we can score speed of users-b who playing same game on same server in the same VLAN-a during the same time. If a and b's scores were almost same, and users-c who playing same game on same server in others VLAN-b acquire higher score. So we can draw a conclusion that there may be something wrong with VLAN-a. Conversely, if user-a's score was obviously lower than users-b's , we can find maybe something wrong with user-a's equipment. Moreover, if user-a acquire different scores when he played same game on same server, without reconfiguring his equipment, in different time quantum. We can draw a conclusion that the difference dues to time but not equipment.

B. Scale of Windows

1) Interview

When CRs communicate with content servers or host, they can use sliding windows scheme in order to enhance efficiency of per TCP connection. Larger windows means more effective[7]. That is to say, more data can be transferred in unit time[8]. So we can grade scale windows

according to their score, using similar method to mentioned-above.

2) Definition of Scale of Windows

$W_1$is defined as scale of windows of upstream TCP messages and $W_2$is defined as scale of windows of downstream TCP messages in a quintuple[9]. They also are divided into 12 intervals according to our statistics and analysis base on captured packets in CR for a month, as shown in Table IV.W_{N-i} including W_{1-i} and W_{2-i} stands for the count of W_N in No. *i* intervals in the unit time. Neither of $W_N$and W_{N-i}has unit.

TABLE IV. INTERVALS OFWN

W_N	0	500	1000	1500
W_{N-i}	W_{N-1}	W_{N-2}	W_{N-3}	W_{N-4}

W_N	2000	2500	3000	7500
W_{N-i}	W_{N-5}	W_{N-6}	W_{N-7}	W_{N-8}

W_N	11520	16000	32000	>32000
W_{N-i}	W_{N-9}	W_{N-10}	W_{N-11}	W_{N-12}

For example, W_{1-7}equals500 if 2000 TCP connections of upstream are recorded and 500 of their scale of windows are between 2500 and 3000 in the unit time.

3) Analysis of Scale of Windows

We construct a table similar to Table II shown as Table V.

TABLE V. DATA STRUCTUREOFWN STATISTICS

Time Stamp	IP_{Source}	P_{Source}	$IP_{Destination}$	$P_{Destination}$	Service Name
2 Byte	4 Byte	4 Byte	4 Byte	4 Byte	20 Byte
	Quintuple				

W_1	W_2
12 Byte	12 Byte

Now we can use Eq.8 for calculating the count of windows in a quintuple in unit time .

$$W_{S-N} = \sum_{i=1}^{12} W_{N-i} \tag{8}$$

We can acquire the accumulative total probability distribution of W_{N-i}in *m* intervals, as Eq.9 shown

$$P_{N-m-w} = \frac{\sum_{i=1}^{m} W_{N-i}}{\sum_{i=1}^{12} W_{N-i}} * 100\% \tag{9}$$

P_{N-m-w} (N=1 or 2) is accumulative total probability distribution of W_{N-i} in *m* intervals, W_{N-i} (i= 1 ~ 12) is the probability distribution of No.*i* interval.

Table VI demonstrates how to use Eq.9.

$W_{N-A}$is defined as Eq.10 and score of S_{N-k-w} is defined as Eq.11. W_{N-A} means average of $W_N$and W_{N-k-w} means the No. *k*sample's score of scale of windows .

$$W_{N-A} = \frac{\sum_{k=1}^{n} (W_{S-N})_k}{n} \tag{10}$$

W1-A is average W1 of n samples,n is the number of samples with same destination IP, same destination Port and same name of the service but different source IP. W2-A is average W2 of n samples,n is the number of samples with same BRAS or same port of BRAS, or same VLAN of port but different source IP. WS-N comes from Eq.8.

We also are able to calculate score of scale of windows for any sample based on Eq.11 similar to Eq.7.

$$S_{N-k-w} = \frac{100 * (I - \sum_{m=1}^{I} P_{N-m-w})}{I * x} + 100 * \frac{1-x}{2} \tag{11}$$

But it is important that *x*=+1in this scene because scale of windows and efficiency of network is positive correlation. This is different from delay. The latter is negative correlation.There is an example in Table VI similar to TableIII.

In Table VI, the values of P_{2-m-w} are as same as them in Table III, but the score of the scale of windows is only 24.5. We can estimate such a result because it is obviously that about one third of samples' scale of windows equals 0 in unit time. That means congestion during that time quantum[10] .

Thus comparison between $W_N$and W_{N-A}, the comparison between W_N from different IP, different BRAS, different VLAN etc. in same time quantums, the comparison between W_N in different time quantums is helpful to locate the situation of fault. For the same reason, the comparison between score of scale of windows is also helpful to locate the situation of fault. The example is similar to which are mentioned-above and it is not necessary to repeat.

TABLE VI. THE DISTRIBUTIONOFW2

W_2	0	500	1000	1500
$W_{2\text{-}i}$	65	40	18	20
$P_{2\text{-}m\text{-}w}$	31.55%	50.97%	59.71%	69.42%

W_2	2000	2500	3000	7500
$W_{2\text{-}i}$	9	6	12	16
$P_{2\text{-}m\text{-}w}$	73.79%	76.70%	82.52%	90.29%

W_2	11520	16000	32000	>32000
$W_{2\text{-}i}$	12	7	1	0
$P_{2\text{-}m\text{-}w}$	96.12%	99.51%	100.00%	100.00%

III. CONCLUSION

Delay and scale of windows are two important index when TCP messages are transferred on the Internet. This paper puts forward a new method using them for evaluating the QoS of broadband network. Following steps describe the method. Firstly, TCP messages in CR are captured. Secondly, delay and scale of windows are calculated. Thirdly, data from step 2 are used to calculate $T_{N\text{-}A}$,$W_{N\text{-}A}$and scores of T_N or W_N. Lastly, comparison between T_Ns, $W_N$sand scores can be used to locate fault.

But there is a problem should overcome. Though 20 Bytes are distributed to service name in quintuples mentioned in Table II and Table V, it is difficult to classify different services. Next we should devote our energies to abstracted huge amount of services to a limited quantity.

In addition, there are others indexes should be used for evaluating performance, for example, zero-windows delay. Because indexes relate to each other, we had better research more methods considering interdependencyof indexes.

ACKNOWLEDGMENT

This study was partially supported by Research of Wired Broadband Access Based on Analysis of TCP/IP funded by the Science Foundation of Yunnan Provincial Department of Education (No. 2015Y523)

REFERENCES

[1] YDB 118-2012, “Broadband speed test method—User experience of Internet surfing”,Ministry of Industry and Information Technology of the People’s Republic of China,Beijing, 2012, p.2(In Chinese).

[2] ITU-T Y.1545.1,“http://handle.itu.int/11.1002/1000/13199”,2017

[3] S. Jaiswal,G. Iannaccone, C. Diot, J. Kurose, D. Towsley, ”Inferring TCP connection characteristics through passive measurements,” Joint Conference of the IEEE Computer and Communications Societies. IEEE, 2004:1582-1592 vol.3.

[4] Atary, Alon, and A. Bremler-Barr. "Efficient Round-Trip Time monitoring in OpenFlow networks." IEEE INFOCOM 2016 - the, IEEE International Conference on Computer Communications IEEE, 2016:1-9.

[5] YD/T 2400-2012,”Test methods for connection speed in broadband network- Fixed broadband access”,Ministry of Industry and Information Technology of the People’s Republic of China,Beijing, 2012, p.5(In Chinese).

[6] Q.Su, J. Gong, X.Hu,“RTT Estimation with Sampled Flow Data”, Ieice Transactions on Communications, 2015, E98.B(9):1848-1857.(In Chinese)

[7] Z. Wang,X. Zeng, X. Liu, M. Xu, Y. Wen, L. Chen, "TCP congestion control algorithm for heterogeneous Internet", Journal of Network & Computer Applications 68.C(2016):56-64.

[8] W. Richard Stevens,“TCP/IP IllustratedVolume1-The Protocols”, Addison Wesley,Inc. New York, 2011,pp. 242-253

[9] W.F. Zhao,”Study on RTT-Based End-to-End Network Congestion Control,”Ph.D., Tianjin University of Technology, China 2014, p.9. (In Chinese)

[10] S. Islam, M. Welzl, S. Gjessin, J. You,”OpenTCP: Combining congestion controls of parallel TCP connections,” 2016 IEEE Advanced Information Management, Communicates, Electronic and Automation Control Conference(Xian, China, October 10-13,2016).Vol.1:p.195

Designing of Intelligent Parking Lot Based On MQTT

Zhongsheng Wang
College of Computer Science and Engieering
Xi'an Technological University
Xi'an China
59483672@qq.com

Kang Han
College of Computer Science and Engieering
Xi'an Technological University
Xi'an China
744324414@qq.com

Zhichao Lian*
College of Computer Science and Engieering
Xi'an Technological University
Xi'an China
965941167@qq.com
*The Corresponding Author.

***Abstract*—With the development of economy and the improvement of people's living standards，people's lives are getting inseparable from cars, the contradiction between the number of parking spaces and the increasing demand for parking is becoming more and more outstanding. It is necessary to design a intelligent parking system. This paper analyzes the drawbacks of the traditional parking system ,and design the main functions and solutions of the intelligent parking. This paper present the whole architecture of the system, and discusses the key technologies: ZigBee networking, MQTT protocol, Node.js, and mobile client technology. This paper proposed an effectively way of urban parking problem.**

Keywords-Intelligent Parking System; ZigBee; MQTT; Node.js; O2O

I. FOREWORD

With the development of economy, the number of motor vehicles increased rapidly, the contradiction between the number of parking spaces and the increasing demand for parking is becoming more and more outstanding. Traditional parking lots do not meet the demand of parking. So intelligent parking system for improving the traffic management situation plays a vital role[1].

Traditional parking lots have been unable to meet the needs of modern parking development in terms of parking efficiency, energy consumption, safety performance, yard management operations, most conventional parking systems have the following problems:

The parking system only records the number of parking vehicles or remaining parking spaces, parking can not provide location specific information.If the parking lot is large, it is difficult for the owner to quickly find the right parking space.

The car park can not provide spare parking spaces online display function. For an open car park, the owner can not understand whether the parking lot will have spare parking spaces, until the owner arrived at the parking lot only found there have been filled. This is undoubtedly a waste of time and resources.

There is little resource sharing between parking systems.The current system of each parking lot is separate of the "information island" [2], the parking system can not share data,even if some parking lot is full, and some parking lots have a lot of free parking spaces, and the system can not provide optional parking options from other parking lots.

Therefore, it is necessary to develop and design a complete intelligent parking management system [3].It can

effectively reduce the pressure of parking, alleviate the problem of modern city traffic jam and parking.

II. SYSTEM FUNCTION

The intelligent parking management system aims at the shortcomings of the traditional parking area,combined with the research status of intelligent parking system at home and abroad, add the following functions for the system：

A. Free parking spaces online view function

In the O2O mode, the user can remotely view the parking spaces in the parking lot via the PC website or the terminal of the mobile phone. When the parking spaces are parked or left, the parking status changes are displayed on the user terminal in time.Users can ahead through mobile phones and other mobile terminals to check information, and pre-set parking spaces,make a planned arrangement to eliminate the blindness of the search for parking spaces.

B. Parking Reservation Function

Through the mobile terminal to view the free parking spaces, the user can mark and make reservations.And the user-marked parking spaces will limit the other vehicles parked, until the user arrives at their booking the parking spaces and operate through the mobile terminal ,then car into place.

C. Parking guidance function

Users can view the parking lot layout and parking situation through the mobile terminal, and according to the guide to find a pre-appointment or vacant parking spaces.

D. Parking lot information sharing and parking spaces recommended function

When the user through the mobile terminal to reserve parking spaces, the system controls the hardware, take coercive measures to protect the parking spaces, such as raising a row of piles or lever to prevent other users from entering.But this is obviously a waste of public resources, it is better practice, only to mark the reservation of parking spaces, when the user reservate parking spaces occupied by other users, the system can recommend parking spaces for the user to provide optional parking program.

III. SYSTEM STRUCTURE

The intelligent parking system is divided into three parts [4]: data source, data processing and release, as shown in Figure 1.

First of all, the original data in the system are derived from the data source layer, through the infrared, ultrasonic and other equipment to collect parking sensor data[5].The collected sensor data be sent to the PC host computer through ZigBee sensor network for centralized data preprocessing.

Second, the data service layer runs on the server, receives the sensor data from the PC host computer,and finally processes it conversion to parking status information stored in the database.The Webservice specification is used to publish the data interface to provide data sharing.

Finally, in the distribution layer, the system supports a variety of clients, users can easily view the parking lot parking information, and use parking spaces, parking guidance and other functions.

IV. SYSTEM DESIGN AND KEY TECHNOLOGIES

The system to achieve the idea is: in accordance with the O2O concept [6], offline use ZigBee for data collection, with Arduino controller control hardware, online use Node.js to deal with data storage and data distribution, with the mobile phones and other mobile terminal APP.Through this way, parking space resource management is realized.The overall structure of the system shown in Figure2.

The system mainly uses ZigBee data transmission, MQTT message push, Node.js data service, mobile client and other key technologies.

A. ZigBee WSN

In the intelligent parking system, the lower computer uses the ultrasonic sensor to detect the distance to determine whether there is parking on the parking spaces.

Through the Arduino controller to manipulate the sensor acquisition data,then send to the PC host computer. The data on the host computer for pre-processing (to eliminate noise), the final submission to the server.On the other hand, the host computer can also receive server control information, and through the ZigBee network to send control information to

the Arduino controller, finally achieve reverse control. This system can not only obtain the sensor data through the mobile terminal to view the function of parking spaces online, but also through the mobile phone control system hardware, to achieve the function of parking spaces.Ultrasonic sensors and Arduino controller, ZigBee and the host computer are using serial communication protocol to exchange data.

B. MQTT message push

Intelligent parking system requires data to be independent two-way flow.In the host computer and server communication process, the sensor data changed due to parking spaces or leave, host computer initiative to inform the server, the server to receive new data and storage.On the other hand, the user sends feedback data to operate the parking space, the server can take the initiative to notify the host computer, then the host computer transfer the user control instruction data to the ZigBee network, inform the Arduino controller operation related hardware.

Because of the HTTP protocol has a passive type, the simple use of the HTTP protocol can only ensure that the sensor data is correctly submitted to the server, but can not guarantee that the server data changes can take the initiative to notify the server, unless the client long polling (the host computer to send HTTP requests to obtain the latest server data).But this way is very costly system resources. Therefore, it is more reasonable to use MQTT protocol, which has the characteristic of message subscribing mechanism, to communicate between server and host computer.

MQTT (Message Queuing Telemetry Transport, Message Queue Telemetry), with lightweight release and subscripte messaging mechanisms to support two-way messaging.In the MQTT protocol, there are three types of roles for subscribers, publishers and proxies. The first two are presented in the form of MQTT clients, and the latter is presented in the form of MQTT proxy servers.The relationship between the subscriber and the publisher is coordinated by the MQTT agent. The mechanism is that the MQTT proxy server maintains the relationship between the MQTT clients. When client issues a message, the proxy server first receives the message,queries the user who subscribes to the type of message, and forwards the message to the subscriber, who can then actively receive the message. The system communication model is shown in Figure 3.

The system uses the Python-based open source tool Paho to implement the MQTT client on the host computer, interacts with the MQTT proxy server running on the server, and completes the message push to the host computer。 Using the HTTP protocol to achieve the host computer to the server communication, when the sensor data changes beyond a certain threshold,send HTTP requests, and then submit the data to the server.Generally speaking, through the HTTP protocol and the MQTT protocol, the data can flow automatically between the server and the host computer.

C. Node.js data service

The server uses Node.js technology, can achieve service mount, data operation, data distribution and other functions.

Service mount.In the Node.js environment can be simultaneously loaded MQTT proxy server and HTTP server to push the message to the host computer, but also allows the host computer to send HTTP requests to submit the sensor data.In the Node.js environment, you can use Mosca [8] to build MQTT proxy server and creating MQTT client. when the database update message, notify the host computer to perform the appropriate action.

Data operation.MongoDB is a NoSql database based on distributed file storage. you can store relatively complex data types, suitable for large data query services.In the intelligent parking system, the server receives the sensor data and then maps the sensor data to the occupancy status information of the parking spaces according to certain rules, expressed in JSON format and stored in MongoDB.

Data distribution. Webservice provides an interactive specification for applications running on different systems or platforms. RESTful Webservice is widely used in mobile Internet applications due to its lightweight, efficient, easy-to-use and easy-to-use design.Express lightweight Web framework using the Node.js platform,You can design APIs that conform to the Rest specification for quick and easy data distribution and sharing.Mobile client can obtain parking space information from the database by call REST API, then displayed on the mobile device.

In short, in the Node.js environment, the functions can be easily achieved [9], the overall organizational structure shown in Figure 4.

D. Mobile client technology

Using Java, Swift, React Native [10] and other technologies can develop App for each platform, get the parking status by calling the Rest API provided by the server, and use the third party SDK to integrate some useful functions.For example, the use of Baidu map SDK for the App integrated map and navigation functions [11] [12]; use Alipay SDK can be integrated for the App online payment function. the user through the App can quickly view the parking lot layout and parking spaces of the current occupation of information, advance booking parking spaces.

V. CONCLUDING REMARKS

Based on the analysis of the existing parking system and the advanced technology, this paper puts forward the overall architecture of an intelligent parking system according to the O2O model, and focuses on the key technologies that may be used.The system can provide free parking spaces online parking, parking spaces online booking, the user parking guide, the nearby parking lot recommended and intelligent billing system and other functions, to achieve automatic parking management, to ease the growing car ownership to bring the city parking pressure.

According to the development trend of information technology, the future intelligent parking lot mainly from the following aspects to deepening:

Break the information island. Rely on the Internet technology, data sharing between the parking lot and build a unified IOT platform, integration and effective use resources .

To achieve a high degree of automation. Through the mobile self-help payment, use the sensor technology to automatic billing, and use the computer vision technology to achieve rapid identification, realize the parking lot unattended management, saving human resources.

Accurate parking guidance.Through the sensor location technology, the parking area layout can be automatically generated, which can provide more accurate parking guidance and reverse search for users.

The mobile terminal supports more features. Such as parking automatic navigation, automatic payment, in accordance with the parking spaces back to the car and other functions.

Overall, with the development of Internet of Things technology, parking system will become more and more intelligent, "urban parking difficult" problem will gradually slow down.

ACKNOWLEDGMENT

This work is supported by the special fund of Department of Education shaanxi province, NO. 2013-23.

REFERENCES

[1] Teng Guo. Research and implementation of intelligent parking management system [D]. Beijing: North China University of Technology, 2015.1-4.

[2] Xiong Yao. Problem of information islands and PLM solutions [D]. Nanjing: Nanjing University of Aeronautics & Astronautics, 2005.5-9.

[3] Mang Dang. Design and implementation of an open-air parking lot management system [D].Zhou Zheng: Zhengzhou University, 2014.27-31.

[4] Yangwei Li, Jiao Pengpeng. City intelligent parking management system based on [J]. traffic information security, 2014.32 (4): 160-164.

[5] Wenjing Cai. Wireless data acquisition system based on ZigBee technology, [D]., Hangzhou Dianzi University, 2011.1-5.

[6] Yiqing Lu, Chen Li. O2O business model and development prospect of [J]. enterprise economy, 2013. (11): 98-100.

[7] Collina, M. Introducing the QEST broker: Scaling the IoT by bridging MQTT(PIMRC),2012,IEEE,23rd

[8] Mcollina. MQTT broker as a module [EB/OL].https://github.com/mcollina/mosca

[9] Stefan Tilkov. Node.js: Using JavaScript to Build High-PerformanceNetwork Programs[J]. IEEE Internet Computing,2010,14(6).1-15.

[10] A JavaScript library for building user interfaces [EB/OL].http://facebook.github.io/react/

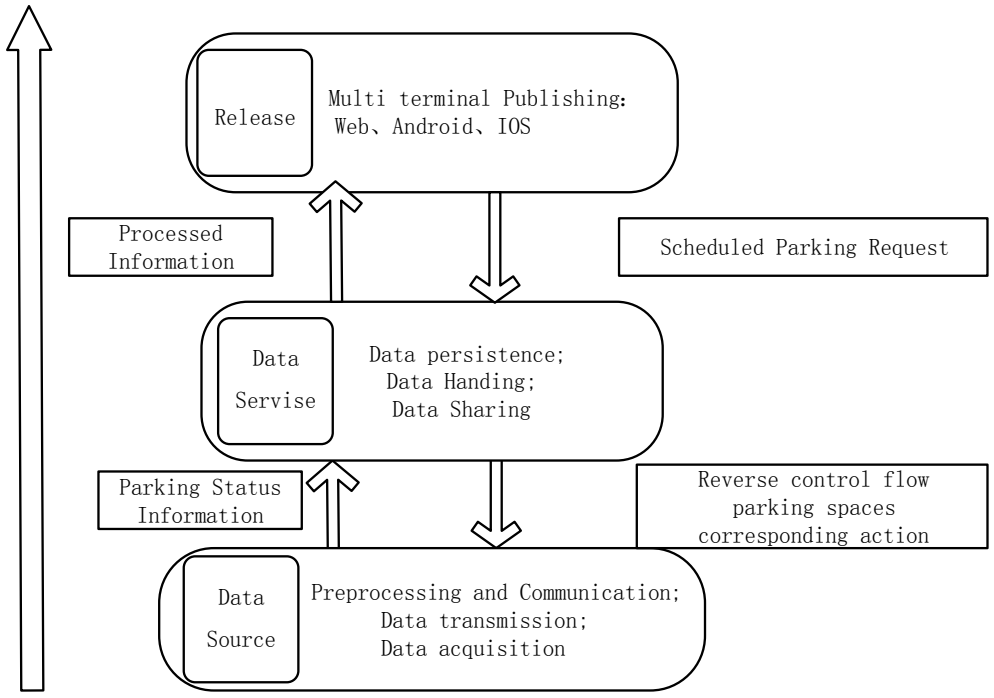

Figure 1. System overall framework

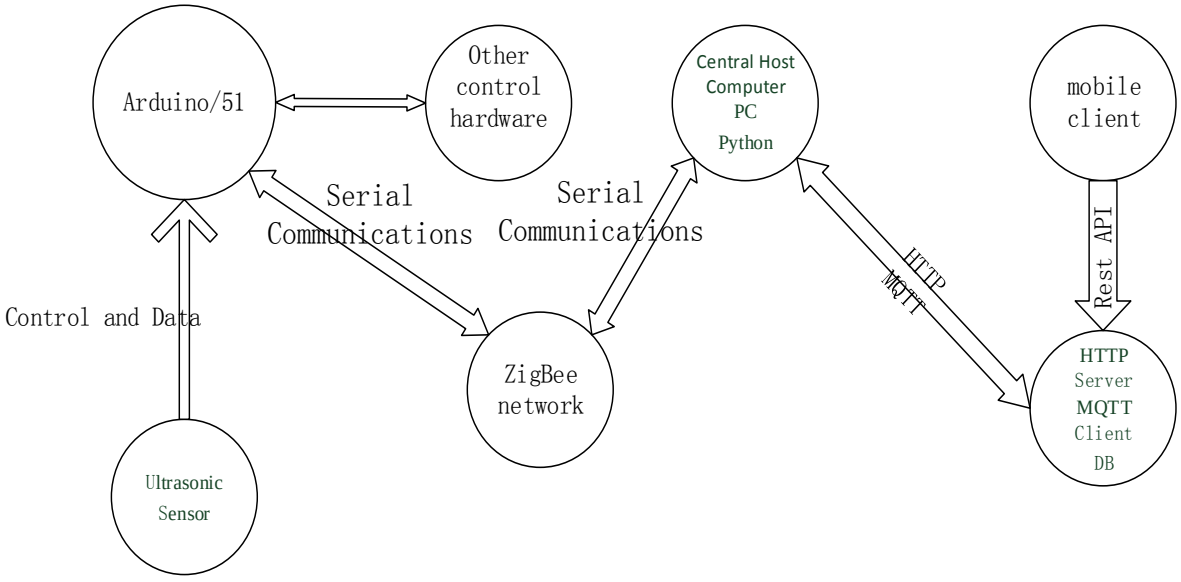

Figure 2. The overall structure of the intelligent

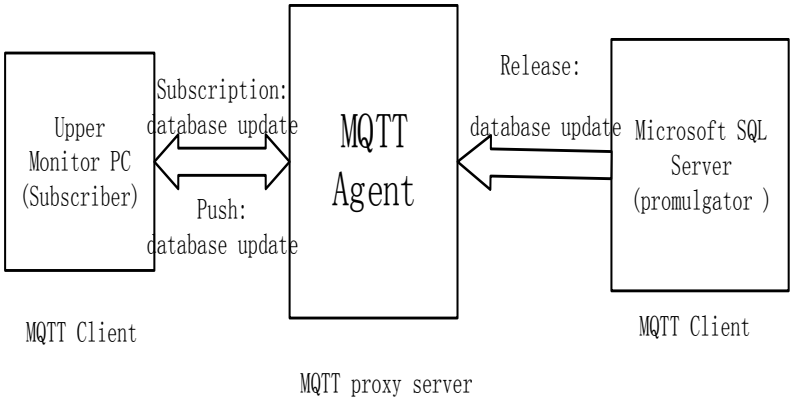

Figure 3. Figure 3 MQTT protocol communication model

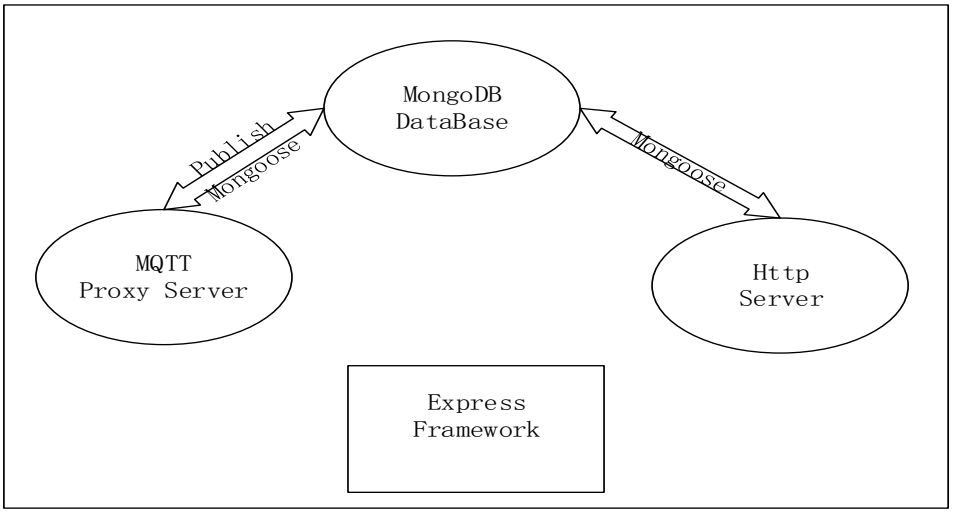

Figure 4. organization structure of node.js environment

BOOST Inductor Optimizing Design Based on Finite Element Simulation

Qi Wang
School of Electronic Information Engineering
Xi'an Technological University
Xi'an， China
e-mail: wangqi@xatu.edu.cn

Tian Gao
School of Electronic Information
Northwestern Polytechnical University
Xi'an， China
e-mail: gtonline@sina.com.cn

Abstract—As the role of energy storage and filtering in DC/DC converter, the inductor is widely applied in switching power supply designs. BOOST inductor affects the input/output ripple voltage and current. Improper parameter design can cause inductor saturation easily, so the inductor design is the emphasis and difficulty in the Boost circuit design. In this paper, combining the traditional parameter calculation and finite element simulation, a design process of the BOOST inductor is given in detail, and the correctness of the design was validated by the experiments. It provides a more convenient and effective design approach of Boost inductor design.

Keywords- Inductor; Optimizing design; Finite element simulation; BOOST

I. INTRODUCTIONS

With the continuous development of power electronic technology, the switch power supply with miniaturization, lightweight and high reliability has become the research direction and trend at present. As an important part of switch power supply, magnetic components are not only the key determinants of switch power supply volume and weight, but also are the important reasons of affecting the reliability of switch power supply[1]. So how to design magnetic components with parameters meeting the performance requirements, small volume, light weight and low loss, has become the focus of research. Inductor, which plays the role of energy storage and filtering in DC/DC converter, is widely applied in switching power supply design[2]. The conventional design method has the disadvantages of long production cycle and it is also difficult to achieve the best effect[3]. Through an example of BOOST inductor design, this article gives the structure diagram of inductance model, then analyzes the distributions of the magnetic field, energy density and temperature field. In the way of combining the traditional parameter calculation and finite element simulation, the optimization design is carried out, and the correctness of the design is verified by experiments.

II. PARAMETER CALCULATION OF BOOST INDUCTOR

The BOOST converter circuit is shown in figure 1.

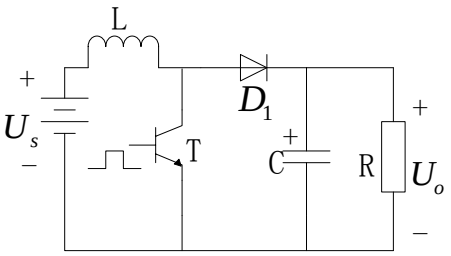

Figure 1. BOOST converter circuit

When the switch tube T is connected, the input voltage U_s is applied on the BOOST inductor L, so the inductance current i_L increases linearly and the electric energy is stored in the inductor coil L in the form of magnetic energy[4-6]. The increase of the inductor current i_L is expressed as,

$$\Delta i_{L+} = \frac{U_s}{L} t_{on} = \frac{U_s}{L} DT_s \tag{1}$$

When the switch tube T is disconnected, the magnetic field in the coil L will change the voltage polarity of the coil L, so as to keep the inductance current i_L unchanged. At this time, the voltage on the BOOST inductor L is ($U_s - U_0$)[7]. Because U_s is less than U_0, i_L will reduce linearly and the reduction is expressed as follows.

$$\Delta i_{L-} = \frac{U_0 - U_s}{L} t_{off} = \frac{U_0 - U_s}{L} (1-D)T_s \tag{2}$$

In the continuous mode, the input current i_L is not fluctuating, and the ripple current decreases with the increase of inductor L, while the input current i_L is fluctuating in discontinuous mode. But the current i_T of the switch tube is always fluctuating in the continuous or discontinuous mode, and the peak current is relatively large[8-9].

The technical indicators in this design are as follows. Input power: $P_{in} = 5.0KW$, switching frequency: f_s=65kHz,

efficiency: $\eta \geq$ 90%, AC input voltage range: 220VAC±20%, power grid frequency: f =50Hz, output voltage: U_0 =380V, output power: $P_0 = 4.5KW$.

A. Calculation of ripple current and peak current

Because the maximum current is expressed as formula (3), the ripple current ΔI and the peak current I_{pk} can be calculated as formula (4),(5).

$$I_i = \frac{\sqrt{2}P_{in}}{U_{i\min}} = \frac{\sqrt{2}\times 5000}{176} \approx 40.17A \tag{3}$$

$$\Delta I = I_i \times 18\% = 40.17 \times 0.18 \approx 7.23A \tag{4}$$

$$I_{pk} = I_i + \frac{1}{2}\Delta I = 40.17 + \frac{1}{2}\times 7.23 = 43.785A \tag{5}$$

B. Calculation of maximum duty cycle with minimum input voltage

$$D_{\max} = \frac{U_0 - U_{i\min(peak)}}{U_0} = \frac{380-249}{380} \approx 0.345 \tag{6}$$

In the formula, the output voltage of the Boost circuit is expressed in U_0, and $U_{i\min(peak)}$ indicates the peak voltage after rectified with the minimum input voltage, where $U_{i\min(peak)} = 176\times 1.414 = 249$V.

C. Calculation of critical inductance

$$L \geq \frac{U_{\text{in}} \times D_{\max}}{f_s \times \Delta I} = \frac{249\times 0.345}{65\times 10^3 \times 7.23} \approx 183\text{uH} \tag{7}$$

In the design, the inductance value of BOOST is 200 μH.

D. Selection of magnetic core specifications

Firstly, magnetic potential energy of magnetic core is calculated.

$$E = \frac{1}{2}LI_{\text{pk}}{}^2 = \frac{1}{2}\times 200\times 43.785^2 \approx 191712 \text{ Vus} \tag{8}$$

Then the design output capability of the magnetic core A_p is calculated.

$$A_p = \frac{2E\times 10^2}{K_m B_m J} = \frac{2\times 191712\times 10^2}{0.4\times 7000\times 500} \approx 27.39 \quad cm^4 \tag{9}$$

In the formula, B_m is the maximum working magnetic flux density, here taking B_m=0.7T; J is the current density, taking J=500; K_m is the core window of the fill factor, taking K_m=0.4.

After consulting the magnetic core table provided by the magnetic core manufacturer, the final choice which is close to the value of A_p above is the Fe-Si-Al core (CS777060) with three rings folded around. A single standard magnetic ring parameters are $\phi 77.8/\phi 49.2/12.7$ (outside diameter / inside diameter / height, unit: mm) and the permeability is 60. The basic parameters of magnetic core are as follows. A_ε =1.77 × 3=5.31 cm^2, A_ω =17.99 cm^2, l_ε =20 cm, A_p =95.53 cm^4, $A_L = 204\text{nH}/N^2$, and the saturation magnetic flux density B_s =1.05T.

E. Calculation of winding turns

$$N = \sqrt{L/A_L} = \sqrt{200000/204} \approx 31.3 \tag{10}$$

Taking the winding turns into an integer, the value of this design is 32 turns.

F. Determination of winding wire diameter

$I_{av} = \frac{P_{in}}{U_{i\min}} = 28.41A$

Because the average current , the current density J =500 A/cm^2, the sectional area of the winding wire $S_1 = \frac{I_{av}}{J} = 5.682mm^2$. In order to keep a certain margin, the cross-sectional area of the wire is taken S_1' =6 mm^2.

With the penetration depth of the switching frequency Δ =0.26 mm, according to the principle of the wire diameter selection ($\Phi \leq 2\Delta$), the paint package line of the bare wire diameter Φ =0.50 and cross-sectional area S=0.1963 is chosen. The maximum diameter of the wire Φ =0.56, so the number of parallel wire is:

$$n = S_1'/S = 6/0.1963 \approx 30.56 \tag{11}$$

Taking it into an integer, there are 31 enameled wires of Φ 0.56 paralleled winding.

III. OPTIMIZATION DESIGN AND SIMULATION OF INDUCTANCE

A. *Optimization design and modeling of BOOST inductor*

The BOOST inductor is designed by using PExprt design software of Ansoft company. Enter the technical parameters of the BOOST inductor[10], select the ring magnetic core of Magnetics, and finally come to the following design, as shown in table 1.

Considering from the temperature, power loss, cost and other aspects synthetically, the second options is chosen as an optimization scheme with the resulting optimal parameters as follows.

1) The magnetic core uses 55906A2 with size as Φ77.8/Φ49.2/15.(outside diameter × inside diameter × length, unit: mm), and the core material is Fe-Si-Al----Kool Mu(60μ);

2) The BOOST inductance is 205.99 uH and the winding turns is 49, winding with 2 strands round wires of AWG#10.

3) The maximum working magnetic flux density is 0.592T and the change of magnetic flux density is 0.132T.

4) The DC resistance of the winding coil is 8.432 $m\Omega$ and the DC loss is 6.841 W, while the AC resistance of the winding coil is 20.98 $m\Omega$ and the AC loss is 0.053 W.

5) The maximum temperature of the magnetic core is $67.72°C$ and the filling percentage of the winding window is 30.17%.

6) The core loss is 8.688 W, the winding loss is 6.894 W and the power consumption is 15.582 W.

TABLE I. BOOST INDUCTOR DESIGN SCHEME

Magnetic core model	Core material	Wire number	Wire strands	Volume（mm^3）	Turns	Temperature（℃）	Power consumption（W）
55906A2	High Flux(60μ)	AWG10	2	45286.5	49	62.62	13.7050
55906A2	Kool Mu(60μ)	AWG10	2	45286.5	49	67.72	15.5824
55866A2	High Flux(60μ)	AWG10	2	35400.0	56	65.03	14.9794
55866A2	Kool Mu(60μ)	AWG10	1	35400.0	53	69.71	20.2220
55906A2	Kool Mu(60μ)	AWG13	2	45286.5	49	76.96	17.2283
55866A2	Kool Mu(60μ)	AWG13	2	35400.0	53	78.49	16.4724
55906A2	Kool Mu(90μ)	AWG13	1	45286.5	35	77.14	15.7932
55866A2	Kool Mu(90μ)	AWG13	1	35400.0	35	80.47	16.3466
55906A2	Kool Mu(125μ)	AWG13	1	45286.5	25	82.53	15.6534
55866A2	Kool Mu(125μ)	AWG13	1	35400.0	25	98.88	18.2142

The schematic diagram of the BOOST inductor model is shown in Figure 2. It can be seen the winding process from the figure. First, 1 strands of AWG#10 are used to make 49 turns around the circle and the lead thread (or tail) is connected. Then 1 strands of AWG#10 are used to circle the 49 turns of the wire and the lead thread (or tail) is connected. Finally, the 2 strands of thread lead into a leading thread and the end of the line lead into a tail. The insulation layers are required between the winding and the winding and between the layer and the layer. The thickness of the former is 0.68mm, and the thickness of the latter is 0.683mm.

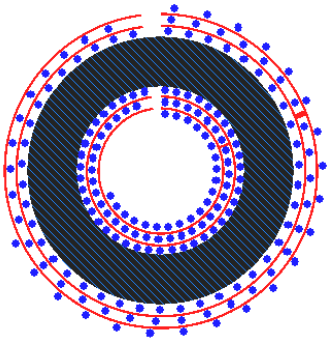

Figure 2. Schematic diagram of BOOST inductance model

B. *Simulation analysis of BOOST inductor model*

The transient magnetic field simulation results of BOOST inductor are as follows by the finite element analysis software Maxwell 2D.

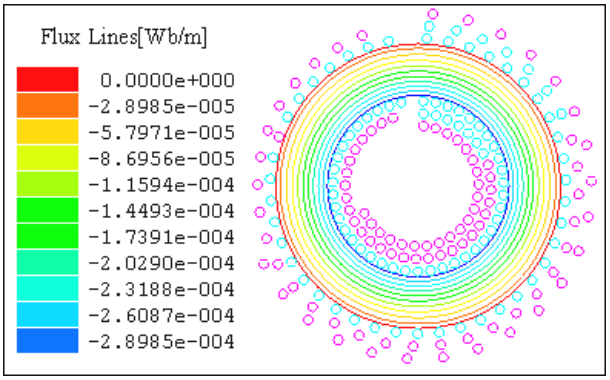

Figure 3. Magnetic field lines distribution

Figure 3 is the distribution of magnetic field lines. It can be seen that the magnetic field lines of the toroidal cores are closed lines and form concentric circles which are the pairwise disjoints. The magnetic field lines near the

outer diameter of the toroidal core are relatively few so as that the magnetic field is weak. On the contrary, if the distance from the inner diameter is shorter, the distribution of the magnetic field lines is more intensive and the magnetic field is also increased. So the magnetic field near the inner diameter of the core is the strongest, and the magnetic induction intensity is maximal.

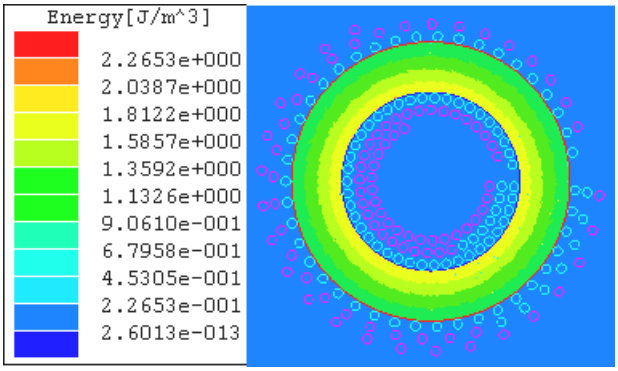

Figure 4. Energy density distribution

Figure 4 shows the distribution of the magnetic core energy density. The energy is mainly concentrated in the inner ring while a small number around the magnetic core. The maximum value of the energy density is located in the inner core of the magnetic core, and its value is about $2.04\ J/m^3$.

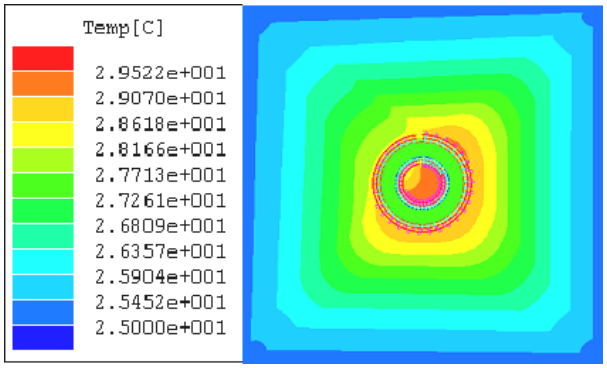

Figure 5. Temperature field distribution

Figure 5 is the temperature field distribution of magnetic core. In the figure, the ambient temperature is 25 ^{o}C, and the maximum temperature of the inductance model is 29.522 ^{o}C. Because the winding coil is easy to produce heat to cause the temperature increased sharply, the temperature is high in the place of many winding coils. So in the internal ring with the highest temperature, the winding coil is too concentrated that the heat can not spread out. On the contrary, in the external ring, the temperature around the coil is high enough to make the heat radiating outwards and reducing the temperature. As a result, in the process of winding, should be selected as far as possible. The winding loss can be reduced because the larger diameter wires heat difficultly can carry a large current to make the temperature rise smaller. Besides, when the component is arranged, the wires should be far away from the components which are liable to cause heat.

IV. Experimental Results Analysis

In accordance with the above data, a BOOST inductor has been made, which can form a BOOST control circuit with a dedicated power factor correction chip. The rationality of this BOOST inductor design can be verified by the experiments on this BOOST control circuit.

Figure 6, Figure 7 and Figure 8 are the driving signals and the inductor current waveforms under different powers. The channel 1 indicates the drive signal waveform of the MOSFET tube, and the channel 2 indicates the inductor current waveform.

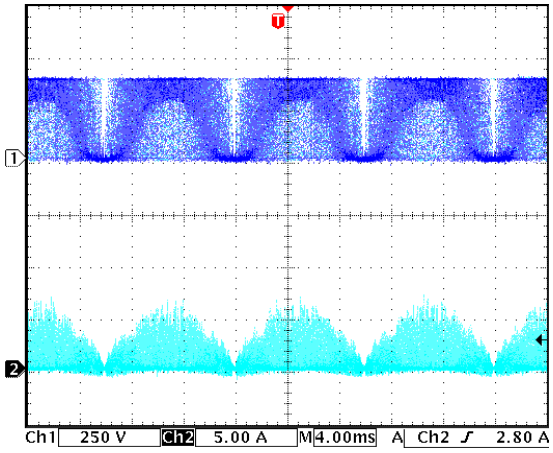

Figure 6. Waveform when the output current is 0.5A

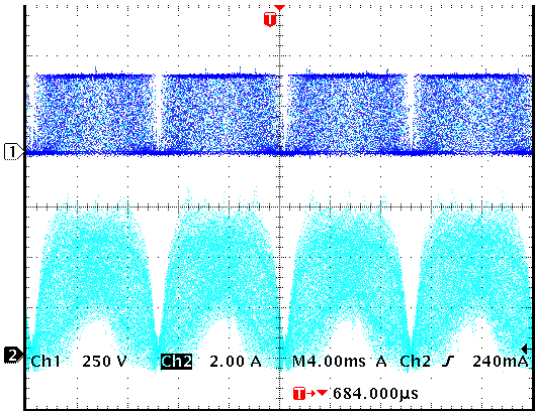

Figure 7. Waveform when the out put current is 2A

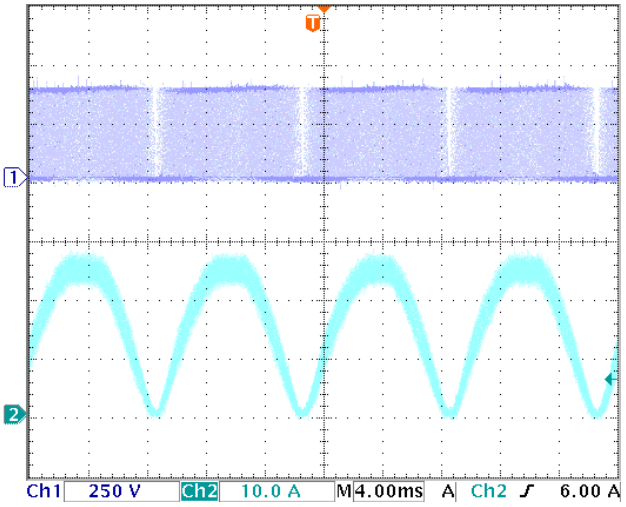

Figure 8. Waveform when the output current is 13A

From the figures, it can be seen that the inductor current is working in the discontinuous mode when the power is small, and with the increase of the power, the inductor current is in the continuous mode. When the input power reaches 5kW, the output current is 13A, the power factor is as high as 0.96, and the work efficiency is as high as 92.1%.

V. CONCLUSION

In engineering practices, the design of conventional parameters is more complicated, and the results may not be the best. By using the combination of traditional parameter calculation and finite element simulation, the paper gives the detailed design steps of the BOOST inductance, establishes the inductance model, and carries on the related electromagnetic simulation analysis to the model. Finally, through the prototype test, the results show that the BOOST inductor design is reasonable and feasible.

ACKNOWLEDGEMENTS

The work described in this paper is supported in part by the key industry problem plan of Shaanxi Province Industry Science and Technology under grant 2016GY-074.

REFERENCES

[1] [1] Hu Yanshen, Xie Yunxiang, “Engineering Design of Boost Inductance with Sendust Core”, Electrotechnical Application, vol.25, no. 7, (2006), pp.83-86.

[2] [2] Liffran, Florent, “A Procedure to Optimize the Inductor Design in Boost PFC Applications”, 13th International Power Electronics and Motion Control Conference, Poznan, POLAND(2008), September 01-03.

[3] [3] Sartori, Hamiltom Confortin; Hey, Helio Leaes; Pinheiro, Jose Renes, “An Optimum Design of PFC Boost Converters”, 13th European Conference on Power Electronics and Applications, Barcelona, SPAIN (2009), September 08-10.

[4] [4] Ye, Yuanmao; Cheng, Ka Wai Eric, “Single-switch Single-inductor Multi-output Pulse Width Modulation Converters Based on Optimised Switched-capacitor”, IET Power Electronics. vol.8, no.11, (2015), pp.2168-2175.

[5] [5] Kim, Dong-Hee; Choe, Gyu-Yeong; Lee, Byoung-Kuk, “DCM Analysis and Inductance Design Method of Interleaved Boost Converters”, IEEE Transactions on Power Electronics, vol.28, no.10, (2013), pp.4700-4711.

[6] [6] Nussbaumer, Thomas; Raggl, Klaus; Kolar, Johann W, “Design Guidelines for Interleaved Single-Phase Boost PFC Circuits”, IEEE Transactions on Industrial Electronics, vol.56, no.7, (2009), pp.2559-2573.

[7] [7] Feng, Gaohui; Yuan, Liqiang; Zhao, Zhengming, “Transient Performance Improvement in the Boundary Control of Boost Converters Using Synthetic Optimized Trajectory”, Journal of Power Electronics, vol.16, no.2, (2016), pp.584-597.

[8] [8] Kim, Jung-Won; Yi, Je-Hyun; Cho, Bo-Hyung, “Enhanced Variable On-time Control of Critical Conduction Mode Boost Power Factor Correction Converters”, Journal of Power Electronics, vol.14, no.5, (2014), pp.890-898.

[9] [9] Cao, Guoen; Kim, Hee-Jun, “Improved Bridgeless Interleaved Boost PFC Rectifier with Optimized Magnetic Utilization and Reduced Sensing Noise”, Journal of Power Electronics, vol.14, no.5, (2014), pp.815-826.

[10] [10] Thirumurugan, V.; Manoharana, S, “Optimized interleaved boost converter with high step up voltage gain for photovoltaic applications”, Optoelectronics and Advanced Materials-rapid Communications, vol.9, no.5-6, (2015), pp.613-618.

Research on Stability of Power Carrier Technology in Streetlight Monitoring System

Zhang Liguang
School of Electronic Information Engineering
Xi'an Technological University
Xi'an， China
zhangliguang@xatu.edu.cn

Tong Xiaolong
School of Electronic Information Engineering
Xi'an Technological University
Xi'an， China
xinyuan1994@live.cn

Abstract—Based on the analysis of low voltage power line carrier network topology and the characteristics of the communication channel, the concept of splitting the data bus is proposed in streetlight monitoring system. The secondary network bus strategy is adopted to solve the problem of signal relay in the control of streetlights. Because the network topology of the streetlamp control system is a complex and strong transition diagram, the traditional bus monitoring scheme is easily invalidated in the network. In this paper, the problem of optimal path planning in data transmission is realized by using an ant colony algorithm which has a strong adaptive ability.

Keywords-Power carrier; Signal relay; Adaptive routing forwarding; Ant colony algorithm

I. INTRODUCTION

In recent years, the government has actively promoted the construction of urbanization. With a large number of people quickly swarming into the city, the urban is becoming larger and larger. As a business card, the traditional street lamp control technology has been far from meeting the needs of modern city construction. The digital intelligence of street lamp control becomes the requirement of modern city street lamp construction. In order to realize the digital intelligence of street lamp control, the communication problem of street lamp control system must be solved firstly. At presently, the research of power carrier technology in streetlight monitoring system has become a hot pot. The power carrier technology has its special technological advantages, which is suitable for the communication of lamp control system. But the disadvantages of the power carrier technology are not to be ignored. This paper puts forward the information forwarding scheme based on data relay and adaptive routing, to improve the communication quality of street lamp control system.

II. THE SYSTEM TOPOLOGY OF STREETLAMP CONTROL

The network topology of street lamp control system is closely related to the location distribution of street lamps. Urban lighting systems are powered by independent transformers. The lamps used in one area are powered by a special transformer, and the street lamps are powered by it. Structure of streetlamp control network is a three-layer control network. It consists of monitoring center, concentrator and lamp control devices. The system topology is shown in figure 1. The communication network of street lamp control system is based on the digital communication network of the electric carrier. The communication sub-station is an important node, which mainly completes the transfer of information between the lamp terminal and the control center. Because of its special system structure and network model, the lamp control system has a certain technical problem to realize information communication with the power line carrier technology. Usually, the electric carrier communication is used between the lamp terminal and the concentrator. GPRS communication is used between the concentrator and the control center. The communication substation is usually set in the special transformer. The communication substation links all the light branches of this transformer. The problem of the carrier signal cannot pass through the transformer is effectively solved. The network topology of the street lamp control system is composed of radial structure and bus structure.

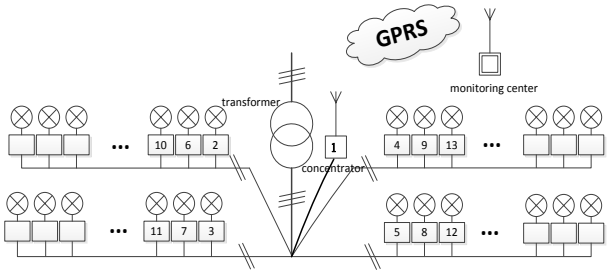

Figure 1. Streetlamp control system topology diagram

There are also significant limitations in the use of power lines as an information transfer medium. Low voltage power lines have the following problems: There are also significant limitations in the use of power lines as an information transfer medium[1]. Low voltage power lines have the following problems:

1) The electromagnetic environment is complex. The power line has poor shielding performance and is easily disturbed by external environment. There are a variety of noise disturbances on the power lines, which have strong time denaturation and different properties. It makes the electromagnetic environment of the communication channel extremely complex. The quality of the signal transmission is severely affected by electromagnetic interference[2].

2)The communication distance is limited. Signal transmission distance is the impedance characteristic of the electric power network and signal intensity attenuation restricts the. Signal transmission must consider the physical communication channel length and the impedance matching of the power supply grid.

3) The signal attenuation is serious. The attenuation of high-frequency signals on low voltage lines is a difficult problem to overcome by the power line carrier communication. Signal attenuation is affected by carrier frequency, interference in line, transmission distance. The reliability of signal transmission is affected by the random and fast effect of signal attenuation. [3]

III. THE RESEARCH OF THE RELAY PLAN

Due to the limited transmission distance of the low voltage power carrier module, a point-to-point communication cannot be carried out when the transmission distance reaches a certain level. Transmission signals can be badly distorted and can't even be transmitted efficiently. Therefore, relay transmission must be carried out by means of signal relay.

Because of the limits of the distribution of street lamps, the network transmission structure of the street lamp control system can only be bus structure. The forwarding of a lamp terminal signal can only be resolved by signal relay. It is especially important to ensure that the signal is real-time and stable during transmission. Based on this, this paper designs a two-level bus transport solution to solve this problem. The so-called secondary bus transmission refers to the separation of signal relay and signal transmission according to the characteristics of the power carrier technology. [4]

A. Network node topology analysis

Since there are more lamps on the same circuit branch, the remote street lamp terminal cannot establish direct data link with concentrator. The relay transmission of the signal to the control terminal at the remote side of the branch is required. By selecting the suitable relay nodes, the transmission scheme is adopted to establish the data link between the concentrator and the lamp control terminal. [5] The schema topology is shown in figure 2.

As shown, a remote power carrier branch that requires signal relay. Establish the data link between node 12 and concentrator 1 by using node 3, node 6, and node 10 as the relay. The signal from the node 12 is passed through the relay to the concentrator 1. This will solve the problem of the short supply of power carrier technology.

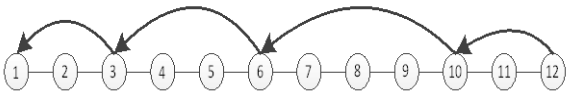

Figure 2. The relay partition topology of the street lamp

B. Subnet partitioning principle

When the number of street lamps in a branch is larger, it is not reasonable to transfer the signal from each terminal to the concentrator through the relay node. If every street lamp terminal establishes a data link directly through the relay and concentrator, this will lead to a significant reduction in signal transmission efficiency and increased communication latency. It will not meet the real-time traffic requirements of the streetlamp control system. In order to solve this problem, the concept of communication subnet in computer network communication was introduced in the lamp control system. A physical subnet is divided into multiple logical subnets by routing Repeaters. A node in each subnet serves as a relay node for data communication. The data from each control terminal is uploaded to the relay node and then uploaded to the concentrator by the relay node. The data routing protocol is used to separate subnets. Each logical subnet has a relay node. The repeater in the logical subnet is responsible for the forwarding of all terminal nodes in the subnet. Continuous transmission is adopted between the relay devices.

In order to guarantee the independence and stability of the data signals between the subnets, the frequency of transmission between the subnet is different from that in the subnet. In order to improve the security and stability of the information transfer, the relay and terminal signal transmission is separated. All nodes in each subnet transmit data over a fixed frequency. The adjacent subnets communicate in different frequencies to avoid the interference of signals between neighboring regions. The relay nodes communicate with a particular frequency, which is different from the frequency of communication within the region. In order to establish the data link between the concentrator and the control terminal, the repeater and the repeater are using point-to-point communication.

IV. RESEARCH ON ROUTE FORWARDING RULES

The routing protocol of the data forward must be studied if the relay scheme of the reasonable power line carrier is established. The geographical distribution of streetlamps leads to the monitoring network of streetlamps only as a bus network. There is only one communication channel. But we can choose different relay nodes, which can change the path of data transmission. According to the data routing protocol, the communication network independently selects the data forwarding path. This improves the availability of data transmission paths and the stability of data transfer. By means of data relay and data routing, the carrier's communication distance can be improved[6].

In the street lamp communication network, each street lamp acts as a node, and any two adjacent nodes are within the range of power line carrier communication. If there is only one data path between adjacent nodes, then the street lighting network can be regarded as an undirected graph G=(V,E), Where V represents the set of all valid communication nodes, and E is a collection of valid paths between any two nodes in the network.Dij represents the communication distance between node i and j, that is, the number of hops between the node i and the node j, and $i,j \in V,(i,j) \in E$, Wij indicates the probability that ants will connect directly to node j from node i. In a street light network with n node, the number of effective paths N from

the most remote node n to node 0 can be calculated by the network topology of the street lamp:

$$N = 1 + (n-2) + \frac{(n-2)(n-3)}{2} + \frac{(n-2)(n-3)(n-4)}{6} \quad (1)$$

Path planning requires a stable communication channel between the concentrator and any terminal devices. Because the communication channel of the street lamp system is easily disturbed, the noise distribution in the channel is random. It leads to the selection of the signal's relay device for diversity. The topology of the communication network can also be complex and variable.In order to adapt to the complex diversity of the network topology of lamp control system, the routing algorithm should be adaptive. The routing algorithm should choose the appropriate forwarding path according to the control requirement, so that the communication can be real-time and stable. The optimal path selection algorithm in the control system mainly has the ant colony algorithm, the flood algorithm and so on. How to select the relay node is the core of the study.

A. The basic principle of ant colony algorithm

Ant colony algorithm (ACA), also called ant colony optimization (ACO), is an emerging algorithm developed in recent years. It is primarily through the transfer of information between ant groups to find the optimal path. The principle is a good adaptive feedback mechanism. The ant colony algorithm uses a single artificial ant to find the optimal solution. When an ant completes its complete search, it will release pheromones on the path it passes. At the same time, more ants are given the pheromones to strengthen some of the route. In order to avoid stopping the search, the pheromones on the path will evaporate as a factor[8].

The algorithm is a heuristic stochastic optimization algorithm. Adopt positive feedback mechanism to achieve distributed global optimization. The continuous update path of the pheromones will eventually converge to the optimal path. The algorithm does not require a large number of probability calculations or a complex mathematical model to predict the system. The algorithm is used to improve the reliability and robustness of the communication system. The routing problem (RP) is one of the typical applications of this algorithm.

B. Establish the carrier communication mathematical model

Ant colony algorithm is applied to the carrier wave communication routing for diameter and the choice of relay points, first of all, according to the characteristics of the ant colony algorithm and carrier communication channel characteristics, to establish an appropriate mathematical model. The carrier communication based on the streetlamp control system has the characteristics of the spacing of the nodes and the distance between any two communication nodes. The distance between each two nodes can be normalized, and the distance between each node is 1. The communication distance between any two nodes is calculated from the location of the nodes. Each node is remembered as an element I in the ant colony algorithm. Bi(t) means the number of ants in the element I at time t. τ(ij) means the information on the t time path (I, j). N represents the number of nodes in the entire network. M is the total number of ants in the colony. Tabuk is the path the ant has traveled.

Lamp control communication has the nature of one-way non-return. A mathematical model for the carrier communication in street lamps is described using a directed graph. Using a lamp network with eight nodes as an example, the colony algorithm for carrier communication has shown in figure 3. There is a line segment indicating the distance between any two nodes, and the length is marked on the line segment. The data on the carrier communication of the street lamp control system can only be transmitted in one direction. When the concentrator sends data to the lamppost as a concentrator, only the left is valid for the line segment. When the lamp terminal sends a reply message, it is available to the right of the line segment.

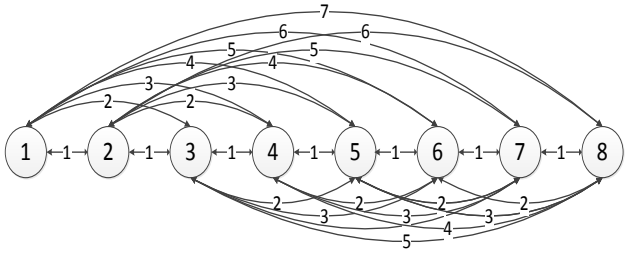

Figure 3. A directed graph of carrier communication ant colony algorithm

C. The implementation of ant colony algorithm

Considering the particularity of the power carrier communication network, it is necessary to improve the classic ant colony algorithm to achieve the control requirement of the street lamp control system. In the initialization phase of the network, the pheromones on each path are equal and set τ(ij) = const. The optimization of ant colony algorithm is achieved through a directed graph. The ant routing algorithm based on ant colony optimization has three phases, routing detection, routing selection and routing maintenance of [9].

1) Routing Detection

In the routing phase, a data packet are generated by the source node, which is called search ant. When the ant find a path, it leaves pheromones on every node passing by. When the ant reaches the destination node, it will produce a backward ant. The backward ant return the pheromone written by the search ant to the source node, and then the search ant death.

By formula (4), it can be seen that at least N of this iteration is needed when the network completes a traversal. In order to avoid excessive iterations and increase the time of travel establishment, the relay nodes in the network should be as few as possible. In the condition of data transmission error rate, the communication distance from any node j to concentrator node 0 needs to be minimum.Then:

$$D_{0j} = \{\min\{D_{0j}\} \mid D_{0j} \in V\} \quad (2)$$

During the routing phase, the main task of the artificial ant is to find the repeater node, which makes the D0j value the smallest, in N efficient paths. When routing is established, the m artificial ant is randomly placed on m different nodes. Each ant finds a local optimal solution within its own search scope. And find the optimal path in the region. When searching for the optimal path, the artificial ant k is placed in the node i, and the probability of the node j as the next node is :

$$P_{ij}^{k} = \frac{(\tau_{ij})^{\alpha}(\eta_{ij})^{\beta}}{\sum_{l \in U_j^k}(\tau_{ij})^{\alpha}(\eta_{ij})^{\beta}} \quad (3)$$

In the formula, τ_{ij} means the pheromone concentration on path (i,j) at time t, and η_{ij} is the problem heuristic information value. In communication networks, η_{ij} is positively related to the distance between two nodes. The number of nodes skipped at each time is the maximum, and the number of hops Dij is the minimum during communication. The further the node is from the source node, the more likely it is to be selected. Each node has a route forward table. The routing table is based on this node's address code and the difference between this node and the next node address, and the following formula should be satisfied:

$$s = \begin{cases} \arg_{u \in allowd_k} \max\{[\tau(r,u0)]^{\alpha} \cdot [\eta(r,u0)]^{\beta}\} & if \quad q \le q_0 \\ \arg_{u \in allowd_k} \max\{[\eta(r,u0)]^{\alpha}\} & else \end{cases} \quad (4)$$

$$(ID_u - ID_r) \cdot (ID_d - ID_u) > 0 \quad (5)$$

In the formula, $\eta(r,u) = \|ID_u - ID_r\|$, ID_r is the node where ants are explored. ID_u is an alternative destination node in the area where ants are explored. $\tau(r,u)$ is the pheromone content that exists on the selected node. $\eta(r,u)$ is the physical distance between the source node r and the destination node u. Due to the limited communication distance of each node in carrier communication, it is necessary to set a suitable destination node according to the specific situation, so as not to waste too much routing setup time.

When the bit error rate reaches the upper error limit, the target node modification mechanism will be triggered. Move the destination node to the previous node where the ants arrive. The ants are generated from the node and return the pheromone to the source node. The current node is considered as the optimal node and the pheromone and table list are updated.

2) Route Selection

The optimal relay node in the whole network has been determined at the route discovery phase. Routing is forwarding according to the selection table of each node. In the forwarding process, the pheromone of the forwarding node is constantly strengthened, and a positive feedback mechanism is formed, so that the subsequent data forwarding is always in the optimal state. Pheromone update formula:

$$\tau_{ij}^{new} = (1-\rho)\tau_{ij}^{old} + \sum_{k=1}^{m} \Delta\tau_{ij}^{k} \quad (6)$$

In the formula, $0 < \rho \le 1$ is the volatilization rate of pheromone traces; $1-\rho$ is the survival rate of pheromone traces; $\Delta\tau_{ij}^{k}$ is the pheromone increment relea. And satisfy the following formula:

$$\tau_{ij}^{k} = \begin{cases} \frac{Q}{L^k} & \forall (i,j) \in T^k \\ 0 & else \end{cases} \quad (7)$$

In the formula, Q is constant; T^k is the tour completed by the first k ant, and its length is L^k; L^k is defined as the total length of all the edges contained in T^k.

The routing option is to determine the next step based on the routing table information of each node. Each node records statistics about its status and the transition probability of its neighbors. Each node maintains its current estimate of the best path. If a node receives a message, it first looks for the node's path information in its own routing table. If there is, forward this information directly to the destination node. If not, the data is sent to the next neighbor node based on the probability transfer information in the routing table. The packet is forwarded from the source node to the destination node via a limited route forward. In the process of forwarding, the value of the information element in the table is strengthened, and a positive feedback mechanism is formed to improve the forward probability of the optimal node. After numerous mathematical iterations, each node can choose the best forward path and continuously reinforce the process. [10]

3) Route Maintenance

The optimal path from the source node to the destination node has been established, so there is not necessary to set up a special packet for routing maintenance. Routine packets will be able to complete the management maintenance of the path. In carrier communication, the channel environment is complex, and the disturbance of the channel is likely to cause a large change in the transmission distance of the node. Some nodes may suddenly drop out of the streetlights network, causing the data link to be blocked. This requires certain measures to maintain the communication stability of the entire network system. For ant colony algorithms, when some nodes are found out of the network, the information

element of the node is marked as 0. The node will select the other path from its routing table, and the data will be forwarded. Eventually, another possible forward path is formed and the path is enhanced to complete the switch. If the street lamp network has a wide range of interference, the communication node has an uncontrollable data link. The active node will restart the routing discovery, reroute the routing selection, and complete the network's self-organizing self-recovery. [11]

V. CONCLUSIONS

According to the above analysis, the application of low voltage power carrier on lamp control system has certain complexity. The physical connection of the streetlamp control system limits the topology of the communication network. The power carrier communication network structure of the street lamp control system can only be the bus structure. Signal relay must be carried out for carrier signals transmitted over long distances. This relates to the selection of the relay and the forwarding path. In this study, the proposed secondary bus transmission scheme was proposed. In order to manage the large network of network nodes, the relay is divided into different logical subnets. Different levels of the bus use different frequency transmitting signals. Different frequency transmission signals are also used between different logical subnets. In order to improve the reliability of signal relay, the method of data routing between relay is adopted. The ant colony algorithm is the optimal choice for the subnet division and route relay.

ACKNOWLEDGEMENTS

Supported by Scientific research plan projects of Shaanxi Education Department, (NO.16JK1362)

REFERENCES

[1] LIU-Xiaosheng,ZHOU-Yan,QI-Jiajin. Automatic routing method of power line carrier communication [J] . Journal of the Chinese electrical engineering project, 2006, 26(21) : 76-81

[2] ZHANG-Yunxia. The research of intelligent lamp control system based on carrier communication. Harbin: master's thesis of Harbin institute of technology..2008

[3] WANG-Heyi,DING-Jianli,TANG-Wansheng. A routing algorithm based on ant colony optimization [J]. Computer application,2008,28(1) : 7-13.

[4] DUAN-Haibin. The principle and application of ant colony algorithm [M]. BeijingSciencePress,2005.12

[5] SONG-Tao,JIANG-Wei,ZHAO-Qinxue. Low voltage distribution network power line carrier communication routing algorithm [J]. 2016,16(02):169-173.

[6] WEN-Wenbo,DU-Wei. A general analysis of the ant colony algorithms [J]. Automation in Petro-Chemicalindustry, 2002, 19(01):19-22.

[7] Yuan Yabo,Liu Yi, Solving shortest path problem with modified ant colony algorithm. Computer Engineering and Applications[J].2012,52(06):8-12

[8] Shah S, Kothari R, Chandra S.Debugging ants : how ants find the shortest route[C]//2011 8th International Conference on Information, Communications and Signal Processing (ICICS), 2011:1-5.

[9] Zakzouk A A A, Zaher H M, El-Deen R A Z.An ant colony optimization approach for solving shortest path problem with fuzzy constraints[C]//2010 The 7th International Conference on Informatics and Systems (INFOS), 2010:1-8.

[10] Stutzle, Hoes.MAX-MIN ant system.Future Generation Computer System Journal[J],2000,16(8):889-914.

[11] Zheng Weiguo,Tian Qichong,Zhang Lei,An Improved Ant Colony Algorithm Based on Pheromone Intensity, Computer Simulation [J].2010,27(7):191-193.

Fuel Cell Test System Based on AVR Single-chip Computer

Wei Zhang
Automation and Electrical Engineering Institute of Linyi University
Linyi, Shandong, China
E-mail: zhwei369@163.com

***Abstract*—Fuel cell technology is considered to be the 21st century of choice for clean and efficient power generation technology, due to a fuel cell itself is a very complex physical and chemical process, the input output are different kinds of physical quantities, so a practical fuel cell must have accurate monitoring and control the performance of these physical quantities. Are briefly introduced in this paper the characteristic and principle of the fuel cell, the function of fuel cell system and the fuel cell test system are analyzed, and made a specific fuel cell test system implementation scheme. The system Atmega32 is the core, can finish the collection work of various data quantity very well, theapplication fuel cell inspection meter can complete to the battery voltage and the current measurement. This system has great flexibility, except for the detection of PEMFC, it can also be adapted to different types of fuel cell detection.**

Keywords-Fuel cell; Data acquisition; Serial communication; Detection system; Control.

I. INTRODUCTION

Fuel cell compared with the traditional energy of today, with many advantages, such as high energy conversion efficiency, can extract the hydrogen from other renewable resources, use of non pollution. Therefore, many countries around the world into a lot of human and financial resources to make research and development. Due to the fuel cell itself is a very complex physical and chemical process, the input output are different kinds of physical quantities, so a practical fuel cell must have precise monitoring and controlling the performance of these physical quantities. Tell from this meaning, fuel cell monitoring control system not only in the development stage of a fuel cell system is very important, even if is in the after put into use for is indispensable for maintain the normal work of the fuel cell. The fuel cell is directly converted into electricity by electrochemical method.. It does not process through the heat engine, high energy conversion efficiency (40% - 60%); environment friendly, almost no emissions of sulfur and nitrogen oxides; carbon dioxide emissions also than conventional power plants less 40% above. Because of these outstanding advantages, fuel cell technology is considered as the first clean and efficient power generation technology in twenty-first Century.

II. FUEL CELL PRINCIPLE

The fuel cell is a device that directly transforms the chemical energy of the fuel into electrical energy by electrochemical reaction.. The fuel cell is composed of platinum based metal as the anode, cathode and ion conducting electrolyte.. The hydrogen oxygen fuel cell, for example: when the anode and the cathode is connected with the load, hydrogen oxidation at the anode, oxygen is reduced at the cathode, anode to produce proton transmission through the isolation membrane to the cathode, cathode with oxygen to form water, electrons from the anode through the load flow to the cathode to form an electrical circuit, to generate electricity and drive load. The difference between the fuel cell and the primary battery and the two battery is that the battery can continuously provide the power to provide the fuel to the battery continuously.. And the final product of the battery reaction is only water, and the environment is not polluting. Its schematic diagram as shown.

Anodic reaction (battery cathode) :

$$H_2 \longrightarrow 2H^+ + 2e^- \tag{1}$$

Cathodic reaction (the positive electrode of the battery) :

$$2H^+ + \frac{1}{2}O_2 \longrightarrow H_2O + h\,e\,a \tag{2}$$

The general chemistr:

$$H_2 + \frac{1}{2}O_2 = H_2O \tag{3}$$

III. THE ANALYSIS OF THE FUEL CELL SYSTEM

A. System

Fuel cell system of PEM fuel cell system in addition to the core part of the cell stack, still need some auxiliary system to work normally.

1) The battery pack, it is the heart of the battery system, it converts the chemical energy of fuel into electricity output outward to load.

2) The supply of hydrogen and oxygen (air) system, the system function is to provide battery with fuel and oxidant;

3) Battery pack water and heat management subsystem, main is to make sure the battery internal water/heat balance state, control the temperature of the fuel cell in a proper range;

4) The output power adjustment system, including the stability of the dc voltage, overload protection and ac dc

variable communication subsystem to meet the needs of users;

5) Automatic control system, because of the fuel cell is a automatic generating equipment, so the function of automatic control subsystem is the key control parameters of each subsystem test, adjustment and control, to ensure that the battery system is stable, reliable operation. The system should also include the start of the battery system, Parking program and failure measures. From a hardware perspective, automatic control system by a variety of sensors, actuators, and executive control software.

B. The Physical State of Fuel's Impact on Performance

The physical state of the fuel (temperature, humidity, purity, pressure, etc.), electrical load, heat load, and the conditions of the environment can affect the working state of the fuel cell. For fuel, different types of fuel have different calorific values. Even the same type of fuel, in the different humidity, under the pressure of the fuel, the reaction of the situation may change with the time of the changes. The fluctuation of electrical load seriously affects the performance of the battery. And, in the power supply process, each part of the response to transient changes are different. Environmental conditions have a serious impact on the performance of the battery. Such as: air temperature and pressure will affect the content of oxygen. Because of the PEM fuel cell for proton exchange membrane to maintain certain humidity, so must the input fuel cell reaction air humidification, then the relative humidity of the air also on the battery performance will play a key role. Fig .1 , Fig .2 shows the characteristic

Curves of fuel cell at different temperatures and pressures.

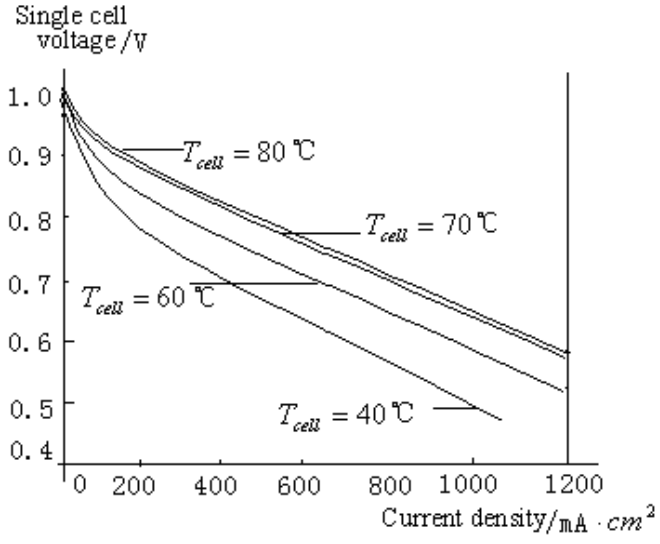

Figure 1. Temperature on the performance of the battery

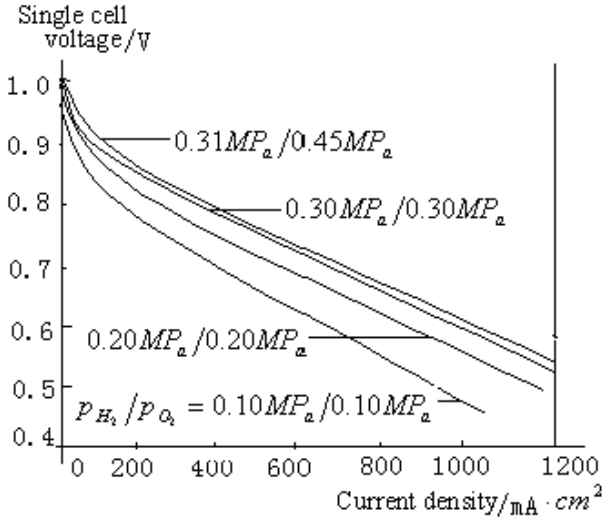

Figure 2. Pressure on the performance of the battery

Therefore, the development of a reasonable test method and evaluation method requires that every parameter is measured. In addition, some parameters must be controlled, so as to determine the causes of the fuel cell performance.

IV. THE HARDWARE DESIGN OF FUEL CELL TEST SYSTEM

A. Block Diagram Of Fuel Cell Test System

The diagram of the fuel cell test system is shown in Fig .3.

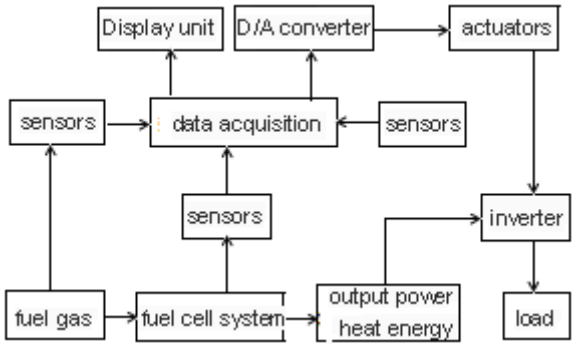

Figure 3. Fuel cell test system schematic diagram

As shown in Fig .3 shows, the fuel cell test system is mainly composed of industrial computer, sensors, data acquisition part, and the executing agency. In this system, sensors used to detect need to test the various physical quantities, send test results to data acquisition system, industrial control is the core of the test system, which receives data from the data acquisition system, and analyze them, according to the result of analysis to control the actuator to complete the corresponding action.

B. Choice of Industrial Computer

By IPC-880 EVOC company production of the (R) Pentium 4 microprocessor and 2.0GHz frequency, 2G ram is

used in the system, from the performance to meet the large amount of data, fast processing.

C. Data Acquisition Card:

The fuel cell testing system needs to collect a lot of data. The data obtained by the sensor is generally standard electrical signal, and can be sent to the data acquisition card directly. If it is not a standard signal, it is also required to preprocess (enlarge or convert). In this system we use data acquisition card:

PCL-813, A/D conversion card is the 32 channel single ended isolated, the main role is to complete the fuel cell simulation of the detection work, the detection results of the industrial computer. PCL-813 each channel can achieve high voltage isolation. 500VDC high-voltage isolation can protect the PC and peripherals caused by high voltage input damage. In addition, each channel two DC - DC converter and software programmable gain control, the system more stable and flexible.

PCL-733, 32 isolated bidirectional digital input channels, can detect the running state of the fuel cell, in a timely manner to timely detection of data sent to the IPC, to make corresponding adjustment.

PCL-726, 6 channel, 12 bit analog output card (D/A). Use it to the results of the industrial computer processing output to the executive body, to control the actuator to make the appropriate action to ensure fuel cell security work.

PCL-734, 32 way isolated digital output card, the output driver is strong, the output channel high voltage isolation can reach DC 1000V, wide output range DC 5~40V. When the abnormal reaction of fuel cell occurs, the main responsibility of the fuel cell is emergency shutdown, and the damage of fuel cell is prevented..

D. Sensor Selection

In any test system, the sensor is essential. It can convert various types of physical quantities to standard electrical signals.. Currently, there is no accepted commercial to sensors work in a fuel cell gas environment, in the fuel cell test system, measurement of physical quantities is very complex, hence the need for the large number of sensors. However, the problem is more than that, because the fuel cell involves a complicated physical and chemical reaction, the working condition is harsher, it is also very high for the sensor requirements. In addition to the general situation of the selection of the sensor constraints, but also to consider the accuracy, life, reliability and cost of these four aspects. In this system, we have chosen the sensor, which can meet the needs of the whole system.

V. FUEL CELL INSPECTION GAUGE

A. Use Reason

The PEM fuel cell each film can only generate about 1 volts of the voltage, so the use of fuel cells is often a stack of hundreds of film (called fuel cell group). The working status of each film is directly affected by the working status of the whole battery group. So it is necessary to monitor the voltage of each film in time. If a piece of film of the voltage changes (generally considered is lower than 0.4 V), means that the film appeared problem, need emergency shutdown operation (by IPC instructions) to the battery pack, otherwise it will lead to the collapse of the cell stack. In order to better detection of fuel cell of each single battery voltage, prevent the occurrence of reverse polarity. We have developed a single-chip microcomputer to control the data acquisition module -- fuel cell patrol instrument, in the running on batteries, use it to detect the battery voltage of each battery group, once a battery voltage dropped to a certain value (such as 0.4V), open cell, and examined.

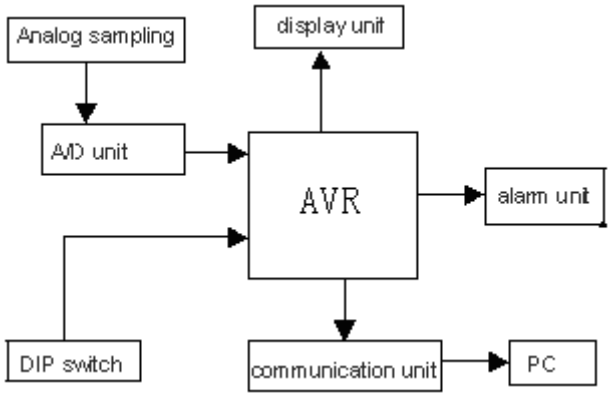

Figure 4. Inspection instrument structure

B. The Composition of the Inspection Instrument

The fuel cell inspection meter is the core of the AT89S51 microcontroller, the periphery has 12 bit A/D converter AD574, the multi-channel switch CD4051, uses the photoelectric isolation, guarantees the data accurately, reduces outside interference. Its structure is shown in Fig .4.

Fuel cell patrol instrument is through the voltage of each battery is detected to track the running state of the battery, guide the battery operation, through single day minimum voltage setting alarm value for battery alarm and control.

C. Communication of the Inspection Instrument

Inspection instrument operation is to communicate with the host computer through the RS-232 interface, communication baud rate setting for 2400Bit/s. The content of the communication with the following aspects: read and write inherent data and read test data. Inherent data have battery nodes and alarm voltage. The detection of a data read, read and writes data to the communication protocol. Inspection instrument of single battery voltage value mining binary coded transmission because of inspection instrument of single node voltage value is too large and just to record, did not control, purpose of doing so is to improve the transmission speed. Each of the data contains 8 bytes, the first 5 data bits, there is a decimal point, and the decimal point is fixed. Data bits followed two transmission is voltage or current. If it is 00h, transmission of data is current or voltage, the last byte is the parity bit to check the transmission of data is correct. Fuel cell sends data program flow as shown in Fig .5.

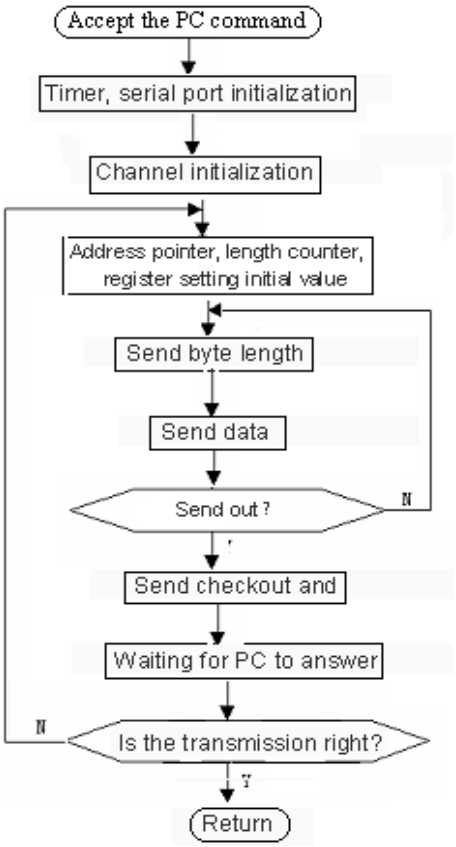

Figure 5. Fuel cell inspection instrument sends data program flow char

VI. SOFTWARE DESIGN AND PROCESS

A. Through the CD4097 Single Cell Selection Control Module

The low three bits of the B port are respectively connected to the coding control of the CD4097 layer, and the selection channels are controlled, the B port is 3, 4 and 5 bits are connected to the coding control end of the high CD4097.. Choose which group to control the selection of the channel to choose which group.

```
Rl=0xFFFF;
[P_IOB_Data]=R1; / / B port data vector set,
IOA low, output data
[P_IOB_Atrib]=R1; / / set attribute vector A port,
[P_IOB_Dir]=R1; / / set attribute vector A port set high
PP:R1+=1; / / strobe and strobe, word one analog channel
...
//CPU call processing module, analog-to-digital conversion module
JMP PP
```

B. Driver Digital Tube Display Module

Here for the reliability design of the transistor drive circuit of LED displays in each of the light emitting diode through 5 to 20 mA current to achieve the normal brightness, SPCE061A input current can reach 12mA and output up to 5mA, in fact, without driving circuit can reach normal brightness. The process showed that the use of dynamic, namely six display one by one rotation, the each sustained 1ms, 10ms or 20 seconds cycle again, of course, can be appropriate to make changes, but the refresh rate not less than 30 frames / S. So, because of the persistence of vision, we see is the 4 display in the display at the same time.

C. CPU Alarm Processing Module

When the voltage of the fuel cell is lower than O.2V or above CPU, the 1.5V output control signal controls the peripheral circuit to send an alarm signal, and the program is as follows:

```
Baojing: .Proc
r3=[P_IOB_Data];
r3 =OxOO80;// use B port 8 bit control Light emitting diode
[P_IOB_Data]=r3 ;
r4=0x0001;
[i]=r4:
CALL Xianshi
RETF;
.ENDP
```

VII. SUMMARY

This paper introduces the fuel cell testing system and the hardware design scheme, design based on industrial computer as the core, it greatly saving hardware cost, while improving the automation degree of the system to meet the system of data acquisition and processing fast and accurate requirements. The test system has been verified by practice, and its work is accurate and reliable, and can basically complete the detection of fuel cell parameters.

REFERENCE

[1] Hou Ming, Yi Baolian. Progress and perspective of Fuel Ceii Technology [J]. Journal of Electrochemistry. 2012 01.P1-13

[2] Xiao Gang. Fuel cell technology [M].BeiJing: Electronics Industry Press. 2009.P128-136

[3] Liu Zhixiang, Qian Wei, Guo Jianwei. Proton exchange membrane fuel cell material [J].Progress in Chemistry. 2011.21.P487-500

[4] Wei Dong,Zheng Dong,Chu Leimin. Design of battery voltage detection system for fuel cell [J]. Chinese Journal of Power Sources, 2010.0..P658-660

[5] Yang Zhongjun,Liu Jingyi;,Zong Xuejun. Study on fault detection of proton exchange membrane fuel cell [J].Renewable Energy Resources. 2015.01.P128-132

[6] Li Fang, Li Di, QIU Huiting Zhang Ming. Fuel cell detection system based on virtual instrument and CAN [J].Microcomputer Information. 2009.16.P84-85

[7] Chen Wei, Wang Guofu, Zhang Faquan, Ye Jincai. Design and implementation of battery detection management system based on ARM[J].Video Engineering,.2015.05..P61-64

[8] Zhang Hui, Study on proton exchange membrane fuel cell [J]. Chinese Journal of Power Sources. 2015. 04.P763-764

[9] Peng Yuejin.Study on Key Technology of Proton Exchange Membrane Fuel Cell [D]. Southwest Jiaotong University, 2016.

[10] Gavin D. J. Harper. Fuel cell projects for the evil genius[M]. The McGraw-Hill Companies, Inc.2008.P112-118

Design of Temperature Sensitive Structure for Micromechanical Silicon Resonant Accelerometer

Heng Li, Libin Huang* , Qinqin Ran
School of Instrument Science and Engineering,
Southeast University
Nanjing, China
E-mail: 1113762274@qq.com
*101010566@seu.edu.cn

Songli Wang
Aviation Key Laboratory of Science and Technology on Inertia, FACRI
Xi'an, China
E-mail: 618gdb104@facri.com

***Abstract*—A micromechanical silicon resonant accelerometer (MSRA) is a potential micro accelerometer with high accuracy. One of the most important factors affecting its performance is temperature. To research the effect of temperature on micromechanical silicon resonant accelerometer, this study based on the original micromechanical silicon resonant accelerometer, designs a chip-level temperature-sensitive structure which a pair of temperature resonators is arranged on both sides of the force resonator of the original accelerometer to ensure symmetry of the MSRA, as well as compares and selects the appropriate structure, fundamental frequency, and size. The ANSYS simulation is used to verify the rationality of the structure design. The MSRA is fabricated using the Deep Dry Silicon on Glass technique and packaged in metal shell, a measurement circuit is designed and a full temperature test is conducted. The results show that the resonant frequency of the temperature resonator is strongly sensitive to temperature changes but not sensitive to acceleration, and that it can reflects temperature change in the package cavity. Therefore, the temperature resonator can achieve accurate temperature measurement of accelerometer and can be used in temperature compensation.**

Keywords-Accelerometer; MEMS; Resonant; Temperature error; Temperature measurement structure

I. INTRODUCTION

A micromechanical silicon resonant accelerometer (MSRA) with high sensitivity and resolution has frequency as its output signal, as well as the advantages of wide dynamic range, anti-interference ability, and high stability. Given its significant advantages and high-precision measurement, it has become one of the most popular high-precision Micro Electro-Mechanical Systems [1-4]. The publicly reported MSRA with the highest performance, has a scale factor stability of 0.14 ppm and a bias stability of 0.19μg, was developed by the Draper laboratory [2]. Hyeon Cheol Kim from Seoul National University designed inertial-grade vertical-and lateral-types of differential accelerometers. The out-of-plane resonant accelerometer shows a bias stability of 2.5μg, a scale factor of 70 Hz/g, and a bandwidth of 100Hz. The in-plane resonant accelerometer indicates a bias stability of 5.2μg, a scale factor of 128Hz/g and a bandwidth of 110Hz [3]. Lin He and Yong Ping Xu from the National University of Singapore developed an MSRA with a bias stability of 5μg, a scale factor stability of 3 ppm, and a scale factor of 100Hz/g [5].

Temperature is one of the most important factors affecting MSRA performance, and temperature compensation is commonly used to suppress temperature error. References [6-9] proposed different temperature compensation methods, have made some compensation effect. To achieve temperature compensation, the first step is to measure the temperature of the MSRA. The traditional method generally measures the temperature outside the MSRA; however, this method is affected by the temperature gradient and temperature delay, and exists a large error to accurately reflect temperature changes. Guoming Xia proposed an MSRA with an integrated temperature measurement structure [10]. Fan Wang established a platinum resistance on the MSRA glass substrate to measure temperature [11]. Both designs are available for the real-time temperature measurement of MSRA.

This study designed a chip-level temperature sensitive structure based on the original MSRA structure and it can achieve the real-time temperature measurement of MSRA.

II. DESIGN OF TEMPERATURE RESONATOR STRUCTURE

A. Fundamental Frequency of Temperature Resonator Structure

Both force resonator and temperature resonator exist in the MSRA with temperature sensitive structure. A coupling exists between two resonators if their frequencies are identical. To eliminate or decrease the coupling, a large frequency difference between the force and temperature resonators can be designed so that the operating frequencies of the two do not coincide with their respective operating ranges. A MSRA without a temperature-sensitive structure is shown in Fig .1. The MSRA consists of proof mass, leverage, and support system, as well as stress-sensitive resonators. Two identical double-ended tuning forks (DETFs) are symmetrically arranged and connected by the proof mass, which converts the acceleration into an inertial force magnified by leverage. One resonator's frequency will increase under the tensile force, whereas the other will decrease under the compressive force. The acceleration will be calculated from the frequency difference between the two resonators. Table I shows the resonant frequency of the

upper and lower force resonators at axial accelerations utilizing ANSYS.

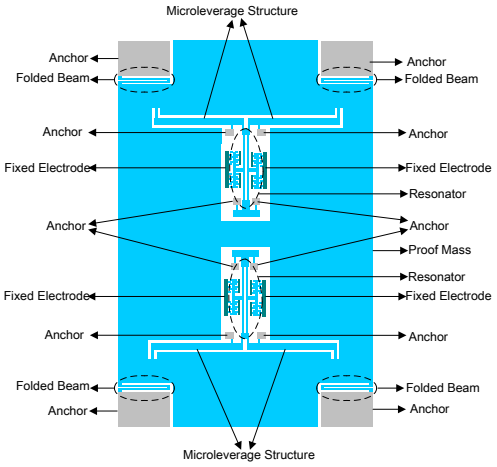

Figure 1. A MSRA without temperature sensitive structure

TABLE I. RESONANT FREQUENCY OF FORCE RESONATOR AT AXIAL ACCELERATIONS

Acceleration [g]	Frequency of force resonator 1 [Hz]	Frequency of force resonator 2 [Hz]
20	27,646	30,702
10	28,439	29,972
0	29,208	29,233
-10	29,957	28,453
-20	30,687	27,661

Table I shows that the resonant frequency range of the temperature resonator should be either less than 27,646 Hz or more than 30,702 Hz.

B. *Comparison of Temperature Resonator Structure*

As Fig .2 shows, micro electrostatic silicon resonator has two main forms: tuning fork (Fig .2a) and folding beam (Fig .2b).

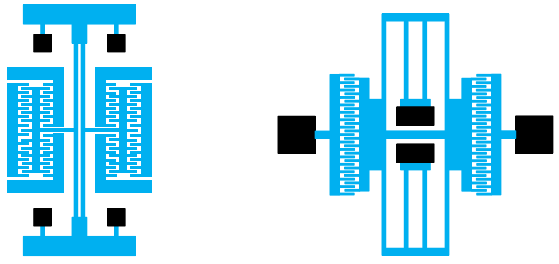

(a) Tuning fork (b) Folding beam

Figure 2. Vibration beam structure forms of temperature resonator

Considering process limitation, the thickness of the temperature resonator is 80μm and the width is 10μm, and the length of the vibration beam is 1400μm and the distance is 20μm. With the same size of vibration beam, a comparative analysis of resonant frequency at different temperatures is performed on the tuning fork and folding beam resonators as shown in Table II.

TABLE II. RESONATOR FREQUENCY OF TUNING FORK AND FOLDING BEAM AT DIFFERENT TEMPERATURES

Temperature [℃]	Frequency of tuning fork resonator [Hz]	Frequency of folding beam resonator [Hz]
60	29,531	16,660
40	29,402	16,670
20	29,086	16,680
0	28,527	16,690
-20	27,653	16,700
-40	26,365	16,710

Table II indicates that the tuning fork resonator is more sensitive to temperature changes. Improving the scale factor can reduce the difficulty of signal detection. Therefore, the use of tuning fork resonators as temperature resonators to measure temperature changes in MSRA is more appropriate.

C. *Design of a MSRA with Temperature Sensitive Structure*

In Fig .3, a pair of temperature resonators is arranged on both sides of the force resonator to ensure symmetry of the MSRA. The resonant beams of temperature resonators are parallel to the resonant beams of force resonators.

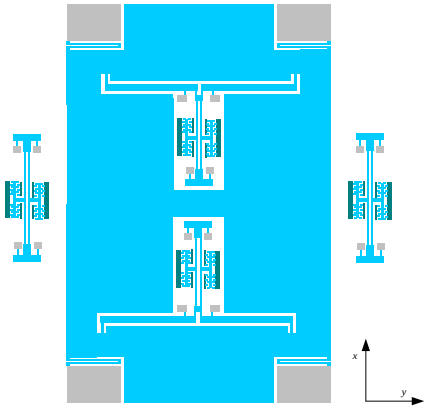

Figure 3. MSRA with Temperature Sensitive Structure

FINITE ELEMENT ANALYSIS OF TEMPERATURE RESONATOR STRUCTURE

A. *Working Modes Analysis*

ANSYS is used to perform the mode analysis on the MSRA with temperature resonator. The working modes of the resonators are shown in Fig .4. From the finite element method, the resonant frequency of the upper and lower force resonators is 29,223 and 29,210 Hz, respectively; whereas the resonant frequency of the left and right temperature resonators is 22,740 and 22,739Hz, respectively. Owing to the accumulated errors of ANSYS, a slight difference in fundamental frequency exists between the upper and lower force resonators and between the left and right temperature resonators.

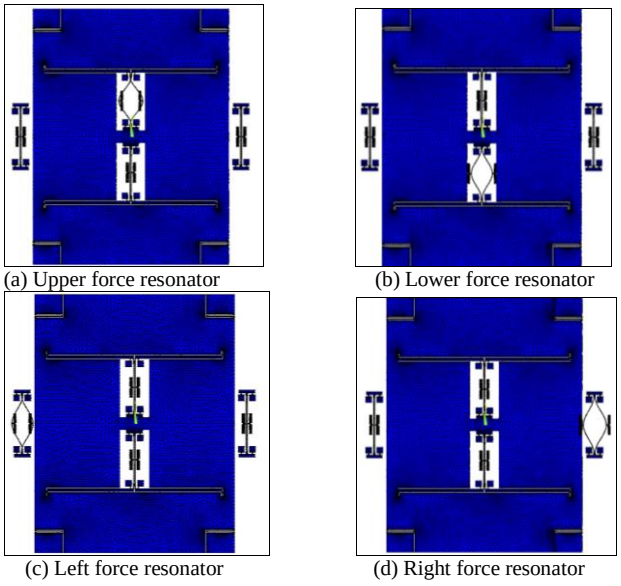

(a) Upper force resonator (b) Lower force resonator

(c) Left force resonator (d) Right force resonator

Figure 4. The working modes of the resonators of MSRA with temperature resonator

B. Thermal Simulation

Thermal simulation is implemented by ANSYS software and the relationship between the temperature and the resonant frequency is shown in Table III.

TABLE III. THE RELATIONSHIP BETWEEN TEMPERATURE AND THE RESONANT FREQUENCY

Temperature [℃]	Resonant frequency [Hz]
-40	21,634
-30	21,887
-20	22,138
-10	22,385
0	22,629
10	22,871
20	23,111
30	23,348
40	23,582
50	23,814
60	24,044

According to Table III, the maximum operating frequency at 24,044 Hz is less than the minimum operating frequency of the force resonator (27,646 Hz), so that the structural parameters of the temperature resonator are reasonable.

C. Effect of Acceleration on Resonant Frequency of the Temperature Resonator

The force resonator is sensitive to acceleration and temperature; however, as a temperature sensitive element, the temperature resonator should be sensitive to temperature but not to acceleration. The use of ANSYS to apply different accelerations under the three axis on the MSRA and the effect of acceleration on the temperature resonator are shown in Table IV-Table VI.

According to Table IV, Table V and Table VI, the temperature resonator is insensitive to acceleration, making the temperature resonator suitable to be used as a temperature-sensitive element to measure MSRA temperature.

TABLE IV. X-AXIAL ACCELERATION ON TEMPERATURE RESONATOR

Acceleration [g]	Frequency under x-axial acceleration [Hz]	
	Left resonator	*Right resonator*
20	22,739.802,9	22,736.207,1
10	22,739.798,5	22,736.212,6
0	22,739.795,2	22,736.219,1
-10	22,739.792,9	22,736.226,5
-20	22,739.791,5	22,736.235,0

TABLE V. Y-AXIAL ACCELERATION ON TEMPERATURE RESONATOR

Acceleration [g]	Frequency under y-axial acceleration [Hz]	
	Left resonator	*Right resonator*
20	22,739.985,5	22,738.939,2
10	22,739.985,5	22,738.939,2
0	22,739.795,2	22,738.219,1
-10	22,739.985,5	22,738.939,0
-20	22,739.985,5	22,738.939,0

TABLE VI. Z-AXIAL ACCELERATION ON TEMPERATURE RESONATOR

Acceleration [g]	Frequency under z-axial acceleration [Hz]	
	Left resonator	*Right resonator*
20	22,739.796,4	22,736.220,2
10	22,739.796,4	22,736.220,2
0	22,739.795,2	22,736.219,1
-10	22,739.794,6	22,736.218,5
-20	22,739.794,0	22,736.217,9

III. FABRICATION AND PACKAGING

The MSRA is fabricated using the Deep Dry Silicon On Glass (DDSOG) technique. Silicon and glass are the structural layout and the substrate of the MEMS device, respectively. Silicon-glass bonding process is used to combine the silicon mass and glass substrate. The main process is: (a) Etching the bonding area on silicon wafer. (b) Depositing the metal electrodes on glass substrate. (c) Bonding the glass substrate to silicon wafer. (d) Thinning and polishing on silicon wafer. (e) Deep reactive-ion etching through silicon wafer to release the structure. A small structural stress is generated because of the use of monocrystalline silicon as a structural material; and the gap between the silicon structure and the glass substrate is sufficiently large, resulting in minimal parasitic capacitance. In addition, DDSOG can achieve metal deposition and processing to the metal wire product. Fig .5 shows the local structure of the improved temperature resonator under the 3D video microscope.

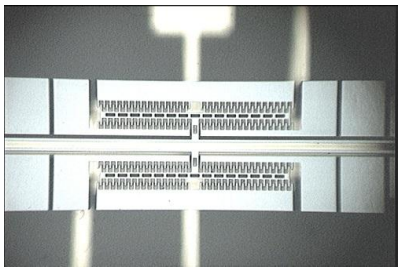

Figure 5. The local structure of the temperature resonator under the 3D video microscope

Accelerometer structure is packaged in metal shell. In the atmosphere the damping of resonator is so large that it should affect oscillation of resonator. The vacuum encapsulation of the MSRA is implemented.

IV. EXPERIMENT

Control and Detection Circuit of Temperature Resonator

Fig .6 shows that the circuit of the temperature resonator mainly includes the analog driving and digital frequency measurement sections. The analog driving section is comprised of the interface circuit, phase, and amplitude control circuit. The phase control circuit is implemented by an analog phase-locked loop used to suppress noise. On the one hand, the output signal is for driving the resonator vibration. On the other hand, for field-programmable gate array (FPGA) measures the instantaneous frequency. Amplitude control circuit utilizes the direct-current automatic generation control circuit to extract the amplitude signal from the interface circuit output signal, and compares it with the reference voltage. Afterwards, the amplitude control signal, through the adder, controls the amplitude of the drive signal to achieve steady oscillation at the resonant frequency. The digital frequency measurement section is mainly implemented by the digital circuit. Frequency measurement algorithm is written in FPGA, so that the output frequency signal of the phase-locked loop can be measured on time. The measurement results are transmitted via the universal asynchronous receiver/transmitter to the PC for display and recording. Figs .7 and 8 show the driving circuit board and the frequency measurement module with the same shape and size, respectively.

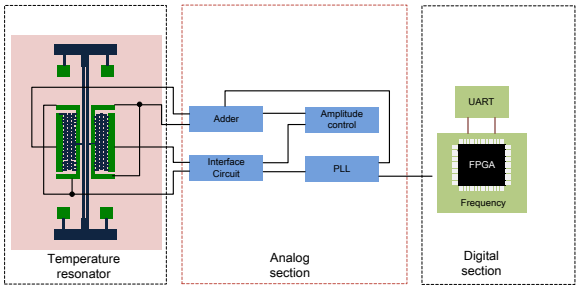

Figure 6. The control and detection circuit of temperature resonator

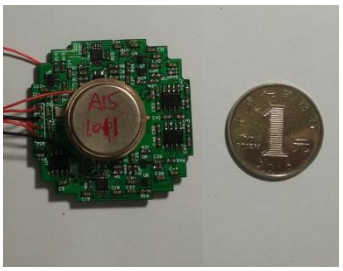

Figure 7. The structure and driving circuit

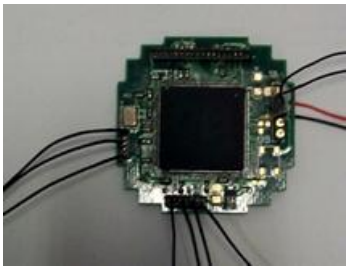

Figure 8. The frequency measurment module

Full Temperature Experiment

The accelerometer operates from -40 ℃ to 60 ℃. To verify the effect of the temperature sensitive structure, the accelerometer is placed in the temperature control box. The variable temperature range in the temperature control box is from −60 °C to 100 °C, and the temperature control accuracy is 0.1 ℃. The experiment procedure is as follows:

1) Energize the temperature resonator but not the force resonator;

2) Decrease the temperature to −40 ℃ and keep the temperature for 120 min;

3) When the temperature resonator output is stable, use a 1 Hz sampling frequency to record the result in 30 s and calculate the average as the temperature resonator output at the point of the current temperature;

4) Increase the temperature to −20 ℃ and keep the temperature for 120 min;

5) When the temperature resonator output is stable, use 1 Hz sampling frequency to record the result in 30 s, and calculate the average as the temperature resonator output at the point of the current temperature;

6) Increase the temperature to 0 ℃ and keep the temperature for 120 min;

7) When the temperature resonator output is stable, use 1 Hz sampling frequency to record the result in 30 s, and calculate the average as the temperature resonator output at the point of the current temperature;

8) Increase the temperature to 20 ℃ and keep the temperature for 120 min;

9) When the temperature resonator output is stable, use 1 Hz sampling frequency to record the result in 30s, and calculate the average as the temperature resonator output at the point of the current temperature;

10) Increase the temperature to 40℃ and keep the temperature for 120 min;

11) When the temperature resonator output is stable, use 1 Hz sampling frequency to record the result in 30s, and calculate the average as the temperature resonator output at the point of the current temperature;

12) Increase the temperature to 60℃ and keep the temperature for 120 min;

13) When the temperature resonator output is stable, use 1 Hz sampling frequency to record the result in 30s, and calculate the average as the temperature resonator output at the point of the current temperature;

After processing the data, we obtain the values of the full temperature points of the temperature resonator, as shown in Table VII.

TABLE VII. THE EXPERIMENT RESULTS UNDER FULL TEMPERATURE OF TEMPERATURE RESONATOR

Temperature [℃]	Resonant frequency [Hz]
60	27,975.343,43
40	27,078.624,69
20	26,049.472,18
0	25,097.384,74
20	23,841.168,93
-40	23,080.606,04

According to Table VII, the fundamental frequency of the temperature resonator is greater than the design value, which is mainly affected by the processing errors and the packaging stress. The frequency of the temperature resonator changed significantly with the temperature changes. Furthermore, the trend is monotonic, which means that the temperature resonator frequency reflects the temperature changes.

V. CONCLUSION

To solve the serious problem of temperature effect on the output frequency of MSRA, we based the study on the original MSRA and designed a chip-level temperature-sensitive structure. The temperature resonator is strongly sensitive to temperature changes but not sensitive to acceleration. Therefore, the temperature resonator can realize the real-time temperature measurement of MSRA and can be used in temperature compensation.

VI. ACKNOWLEDGMENT

This work was financially supported by the National Natural Science Foundation of China (Grant No.61101021) and Aeronautical Science Foundation of China (Grant No.20140869004).

REFERENCES

[1] Seok, Seonho, H. Kim, and K. Chun, "An inertial-grade laterally-driven MEMS differential resonant accelerometer," Sensors, vol.2,pp.654-657,2004.

[2] Hopkins, R., J. Miola, and R. Setterlund, "The silicon oscillating accelerometer: A high-performance MEMS accelerometer for precision navigation and strategic guidance applications," Proceedings of Annual Meeting of the Institute of Navigation, pp.1043-1052, 2005.

[3] Hyeon Cheol Kim, Seonho Seok, Ilwhan Kim, Soon-Don Choi, and Kukjin Chun, "Inertial-grade out-of-plane and in-plane differential resonant silicon accelerometers (DRXLs)," in Proc. 13th Tntemational Conference on Solid-state Sensors, Actuators and Microsystems, pp.172-175, 2005.

[4] Chul Hyun, Jang Gyu Lee, and Taesam Kang, " Precise oscillation loop for a resonant type MEMS inertial sensors,"in Proc. SICE-ICASE International Joint Conference, pp.1953-1958, 2006.

[5] He L, Xu YP, and PalaniapanM, "A cmos readout circuit for soi resonant accelerometer with 4 μ g bias stability and 20- μ g/$\sqrt{}$Hz resolution, " IEEE J Solid-State Circuits,vol.43, 2008, pp.1480-1490.

[6] Falconi C, Fratini M, "CMOS microsystems temperature control," Sensors & Actuators B Chemical,vol. 129, 2008, pp.59-66.

[7] Anping Qiu, Jinhu Dong, "Temperature Effect and Compensation of Silicon Micro Resonance Accelerometer ," Nanotechnology and Precision, vol.10, 2012, pp.215-219.

[8] Wei Wang, Yan Wang, Haihan Zhuang, Chaoyang Xing, "Temperature Characteristics of Silicon Micro Resonance Accelerometer ," Journal of Chinese Inertial Technology, 2013, pp.255-258.

[9] Fan Wang, Jingxin Dong, Shuming Zhao, Bin Yan, "Microstructure and Process Design of Anti-temperature Drift of Silicon Micro-vibrating Beam Accelerometer," Journal of Chinese Inertial Technology, 2014.

[10] Guoming Xia, Anping Qiu, Qin Shi, Jing Zhang, Yan Su,and Henggao Ding, "A micro silicon resonant accelerometer based on chip intergrated precision temperature structure,"2013.

[11] Fan Wang, Jingxin Dong, Shuming Zhao, "Micro silicon resonant accelerometer temperature sense and closed-loop control," Optics and Precision Engineering, vol.22, 2014, pp.1590-1597.

Separating Signals with Specific Temporal Structure

Yongjian Zhao
School of Information Engineering
Shandong University (Weihai)
Weihai, China
E-mail: zhaoyj@sdu.edu.cn

Haining Jiang
School of Information Engineering
Shandong University (Weihai)
Weihai, China
E-mail: jian123cn@sdu.edu.cn

Bin Jiang
School of Information Engineering
Shandong University (Weihai)
Weihai, China
E-mail: jiangbin@sdu.edu.cn

Meixia Qu
School of Information Engineering
Shandong University (Weihai)
Weihai, China
E-mail: qumx@sdu.edu.cn

***Abstract*—Blind signal extraction is particularly attractive to solve signal mixture problems while only one or a few source signals are desired. Many desired biomedical signals exhibit distinct periods. A sequential method based on second order statistics is introduced in this paper. One can choose to recover one source signal or all signals in a specific order. The validity and performance of the proposed method are confirmed by computer simulations.**

Keywords-Component; Period; Order; Mixture; Extraction; Simulation

I. INTRODUCTION

In recent decades, blind signal separation (BSS) has been studied extensively and has become an increasingly important technique for signal analysis [1-3]. Indeed, BSS is a technique aiming to transform multivariate random signal into components that are mutually independent in complete statistical sense. Traditional BSS approach always separates all source signals from their mixtures simultaneously. In many applications, a large number of original sources are available while only one or a few are desired [4,5]. A typical example is the cocktail party problem, which is the phenomenon of being able to focus one's auditory attention on a particular stimulus while filtering out a range of other stimuli. This means the same way that a partygoer can focus on a single conversation in a noisy room. This effect is what allows most people to extract the desired single voice and throw away the others. In such cases, only one source signal is considered interesting and the others are regarded as interfering noise. As a result, simultaneous BSS approach will introduce large computational burden. It is important to introduce an effective approach which enables us to recover the desired source signal, which is potentially interesting and contain useful information, from its mixtures exclusively. This problem is referred to as blind signal extraction (BSE), which is indeed a particular class of BSS.

Recently, several approaches have been proposed for the solution of BSS/BSE problem, which are generally based on the second or higher order statistics of the data [6-8]. For example, Cichocki presented a classical BSE algorithm based on the stochastic property of source signals [3, 4]. It can extract a source signal, whose absolute kurtosis value is the largest among all mixed signals, as the first output. However, it must be mentioned that the high order statistics (HOS) based techniques often have high computation [4, 6]. Second order statistics (SOS) based techniques have the advantage of requiring shorter data records due to their reduced small sample estimation errors, and do not limit the number of Gaussian sources that can be separated to one [5, 9]. SOS based techniques have generally represented the preferred approach to solving the BSS/BSE problem [4, 5]. Recently, there is a trend to exploit BSS/BSE approaches based on SOS techniques.

In many BSS/BSE applications, one is not complete blind about the original sources or the mixing process. In other words, one can know a priori knowledge about one source signal in advance. Fortunately, in many applications such as biomedical signal processing, this type of knowledge is often readily available. A typical example is that the human heart contracts at regular intervals. In fact, when a biomedical source signal is periodic, its fundamental period can be measured based on methods such as heart instantaneous frequency estimation techniques.

Many natural signals such as speech signals or biomedical signals have significant temporal structures [8, 10]. It is valuable to exploit the second order correlations based on time delay for source extraction. Our work is motivated by the observation that majority of measurements obtained from many biomedical applications exhibit some degree of periodicity. In this paper, we focus on separating one or a few desired source signals, which are time delayed correlation, from the observed sensor signals. By analyzing the linear autocorrelation feature of the desired source signal, we have novel insights about source extraction. An objective function based on linear autocorrelation of the desired signal is first designed. Optimizing the objective function, a flexible BSE method is introduced correspondingly. Compared to the traditional BSS/BSE method, the proposed techniques have many good properties in terms of computing time and

flexibility. For example, only desired source signal is recovered, lots of computing time and resources can be saved; source signals can be recovered in a specific order according to some properties of source signals. The validity and performance of the introduced techniques are confirmed by computer simulations.

This manuscript is organized as follows. In section II, a constrained optimization problem is introduced based on second order correlations of the desired source. Solving the constrained optimization problem, a batch fixed-point learning algorithm is deduced for estimating the desired source signal with linear autocorrelations. Section III demonstrates the proposed techniques with computer simulations. Some conclusions are drawn in the final section.

II. PROPOSED ALGORITHM

Denote the observed sensor signals $x[k] = [x_0[k], x_1[k], \cdots, x_{n-1}[k]]^T$ described by matrix equation

$$\xi[\kappa]=A\sigma[\kappa] \tag{1}$$

where A is an n*m unknown mixing matrix, $s[k] = [s_0[k], s_1[k], \cdots, s_{m-1}[k]]^T$ is a vector of unknown temporally correlated sources (zero-mean and unit-variance), k is the time index, m is the number of sources and n is the number of mixtures. Since the BSS problem is blind, it is difficult to develop new technology. For simplicity, in the following we assume m=n. Fig .1 shows a general BSS architecture for separating all source signals from the observed sensor signals at a time.

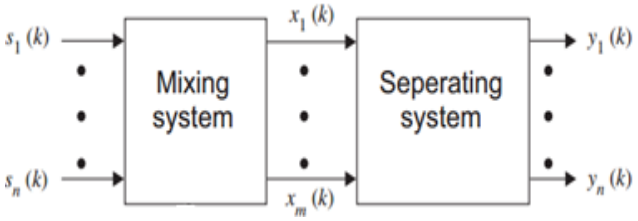

Figure 1. Traditional BSS techniques.

To cope with ill-conditioned cases and make algorithm fast and simple, a linear transformation known as preliminary whitening is often exploited to whiten the sensor mixtures[11,12]. That is to say, one may transform the observed vector x linearly so that a new vector is obtained. As a result, the generated vector becomes white. In other words, components of the new vector are uncorrelated and their variances equal unity. A typical whitening solution is as follows

$$\tilde{x}(k) = Vx(k) = VAs(k) \tag{2}$$

so that $E\{\tilde{x}(k)\tilde{x}(k)^T\} = I$, where V is called whitening matrix. Therefore, after the sensor signals are whitened, the components of $\tilde{x}(k)$ are unity and uncorrelated.

To formulate the BSS problem, one must construct a suitable objective function that is greatly dependent on the parameters of the specified neural network model in (1). Optimizing the objective function will deduce approach to recover all source signals from their sensor mixtures at a time. To recover one source signal exclusively, one should introduce specific prior information about the desired signal into the objective function, thus causing a constrained optimization problem. The use of such prior information about the source signal leads us to call BSE as semi-blind separation [13,14]. Optimization of such an objective function should cause the outputs of the model to satisfy the desired statistical conditions. As a result, the output will be the desired source signal. In general, SOS based approach assumes that the original sources are not correlated with each other and every source signal has a different temporal structure.

It is very often the case with biomedical measurements that we have some prior information about the source signals which we wish to extract from the sensor mixtures. Indeed, many physiologically relevant signals or patterns have certain temporal, spectral or time–frequency characteristics, and in the case of multi-channel (body surface, volumetric) measurements also particular spatial projections. It is efficient and indeed possible to incorporate such prior information into the BSS/BSE model using only minor modifications of the estimation procedures, essentially by imposing constraints on the model, which can act on the spatial projections, or work on the temporal dynamics of the source waveforms. The idea is that we may be able to guide the BSS/BSE solution to include an expected outcome. By introducing prior information into the traditional BSS system shown in Fig .1, we develop improved BSS/BSE techniques to estimate the unknown portions based on the assumptions as have already been covered, thus helping us to interpret the output results. In this paper, we suppose that the desired source signal has property of linear autocorrelations. Our work is to estimate the desired source signal with specific temporal structure from a large number of mixtures exclusively. The main criterion of source extraction is to find a specific vector w, and apply a demixing operation by applying vector w to the signal mixtures. In our work, a single neural processing unit is introduced as follows

$$\tilde{y}(k) = w^T\tilde{x}(k) \tag{3}$$

$$\tilde{y}(k-\tau) = w^T\tilde{x}(k-\tau) \tag{4}$$

Where $w = (w_0, \cdots, w_{n-1})^T$ is the weight vector and τ is a time delay in time.

To estimate one source signal with linear autocorrelation from its mixture exclusively, we introduce the following constrained optimization problem based on second order correlations of the desired source

$$\max_{\|w\|=1} J(w) = E\{\tilde{y}(k)\tilde{y}(k-\tau)\}$$
$$= E\{(w^T\tilde{x}(k))(w^T\tilde{x}(k-\tau))\} \quad (5)$$

where J(w) is called objective function. The parameter τ can be selected as an optimal prior time delay based on some information of the desired source signal. In some cases if the optimal time delay cannot be obtained, the time delay is often set to 1.

Optimizing the objective function contrast J(w) in (5), one can further deduce a batch learning BSE algorithm. The gradient of J(w) with respect to w can be deduced as

$$\frac{\partial J(w)}{\partial w} = E\{\tilde{y}(k-\tau)\tilde{x}(k) + \tilde{y}(k)\tilde{x}(k-\tau)\}. \quad (6)$$

According to the Kuhn–Tucker conditions[1,7], one can note that at a stable point of the optimization problem in (5), the gradient of $\frac{\partial J(w)}{\partial w}$ at w must point to the direction of w. In other words, one can optimize the objective function in (5) by the classical fixed-point algorithm[1,2]. To solve problem in (5), we utilize the fixed-point algorithm that, after each iteration, enforces the constraint $ww^T = 1$ dividing by its norm, then obtaining the following updating rule

$$w \leftarrow E\{\tilde{y}(k-\tau)\tilde{x}(k) + \tilde{y}(k)\tilde{x}(k-\tau)\}$$
$$w \leftarrow w/\|w\|. \quad (7)$$

Approach in (7) is a batch fixed-point learning algorithm, which is utilized to recover the desired source signal with linear autocorrelations. One can find that this approach is very simple. Most of all, in contrast to classical fixed-point algorithm [1,2], it do not need to choose any learning step sizes. After the first desired source signal is recovered, one can exploit a deflation process to remove it from the signal mixtures. Then the remained mixtures may experience another separating process to recover next signal. This procedure can be repeated until each desired source signal is recovered from its mixture. In other words, our work can recover source signals in a prescribed order, which is efficient in many applications. In addition, each source signal can be extracted using different BSE method, according to distinct feature of original sources. A general architecture of batch learning BSS techniques is shown in Fig.2.

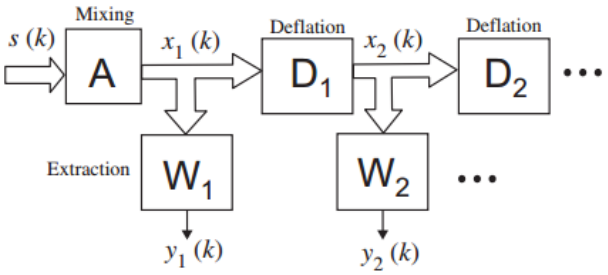

Figure 2. Batch learning BSS techniques.

III. Computer Simulations

To confirm the performance of the proposed approach, we performed extensive computer simulations. Due to space constraint, only one simulation is illustrated here. The real-world ECG data, distributed by De Moor[15], are a well-known electrocardiogram measured from a pregnant woman (shown in Fig .3). Many classical BSS/BSE approaches utilize these data to verify their separating performance. For the sake of comparison, we also perform simulation on the real-world ECG data.

The electrocardiogram measurements are recorded over 10 s and sampled at 250 Hz with 8 electrodes located at the abdomen and thorax of a pregnant woman. Actually, although in De Moor's homepage he claims the sampling frequency is 500 Hz, Barros et al. [3] believe it is 250 Hz. One can see the heart beat of both the mother (stronger and slower) and the fetus (weaker and faster). The fetal electrocardiogram (FECG) is the recording of the fetal heart's electrical activity, which contains valuable clinical information about the healthy condition of the fetus [3–5]. However, in the dimensional mixtures shown in Fig.3, the desired FECG signal is very weak, which is often contaminated by a variety of noise, such as the maternal electrocardiogram (MECG) with extremely high amplitude, the mother's respiration, and thermal noise from electronic equipment. In fact, even the accurate occurrence time or shape of each complex of FECG is often not easy to obtain, especially when the fetus is in early phase. Therefore, non-invasive extraction of FECG has become vital important from a clinical point of view. However, it must be mentioned that the measured FECG is always contaminated by a large number of other signals and artifacts. Separating FECG by conventional BSS methods may produce hundreds of recordings, which may result in heavy computational load. Our main purpose is to extract a clear FECG signal exclusively, which is the recording of the fetal heart's electrical activity and provides valuable clinical information about the heart performance. Since the FECG signal is always corrupted by a variety of noise, how to develop an efficient method to extract a clear FECG as the first output has become a difficult task.

Figure 3. ECG signals obtained from a pregnant woman.

The fetal influence in channel 1 is clearly stronger than that in the other channels [3,5,6]. The fetal heart should strike every 0.5 s or so [5,6]. By carefully examining the autocorrelation of the sensor signal in channel 1, we find that it has a peak at τ=112 sampling period. In fact, it is the optimal time delay for extracting the FECG signal. To estimate the desired FECG, we first whitened the sensor signals and initialized the weight vector by $w = [1,0,\cdots,0]^T$. In the first simulation, we adopted the optimal time delay as τ=112. The FECG estimated by our algorithm is FECG1 as shown in Fig .4. To compare the performance of our algorithm, we also ran the algorithms in [2] and [5], which were classical methods for FECG extraction. The extracted signals were FECG2 and FECG3 accordingly as shown in Fig .4. In contrast, the algorithm proposed in this paper can separate clear FECG. The signals extracted by the other algorithms contain some contributions of the mother's breathing artifacts. To further compare the performance of our algorithm with the other algorithms in [2] and [5], we selected slightly wrong delays as τ=114. The simulation results are shown in Fig .5. The signals estimated by the proposed algorithm and algorithms in [2] or [5] are FECG4, FECG5 and FECG6 accordingly. From the comparison results shown in Fig.5, one can find that the signal extracted by algorithms in [2] or [5] for τ=114 (FECG5 and FECG6 accordingly) is mostly the respiration artifact. Obviously, the algorithm proposed in this paper outperforms the other two algorithms, as expected, and again the algorithm in [5] performs poorly. The computer simulations illustrate that the proposed algorithm is not sensitive to the estimation error of the time delay as long as the error is not too large, which is valuable in practical applications.

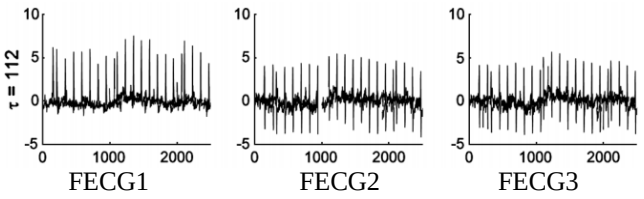

Figure 4. The extracted FECG signals using τ=112.

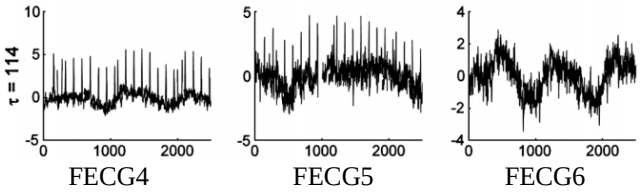

Figure 5. The extracted FECG signals using τ=114.

IV. Conclusions

In recent decades, the BSE technique has received extensive research attention in various fields such as biomedical signal analysis, speech processing, data mining, and so on. In many applications, the desired biomedical signal exhibits specific temporal structure. In general, it is apparent that BSS/BSE techniques using temporal structure are suited to biomedical signal analysis very well. The temporal and time-frequency information exploited is clearly relevant in biomedical signals. The second order statistics based method is less expansive for the calculation than traditional higher order statistics. If one has specific information on the source signals, it is desirable to exploit BSS/BSE techniques based on the use of second order statistics.

In this paper, we introduce a sequential BSE algorithm for blind separation of source signals with distinct periods, based only on second order statistical information. Indeed, the proposed approach exhibits computational advantages over traditional BSS approach when one's purpose is to recover only one or a few source signals from dimensional mixtures. It must be pointed out that the source signals recovered by the traditional BSS method are subject to the ambiguities of permutation and scaling. Through the proposed algorithm in this paper, after one source signal is estimated, one can choose a deflation process to eliminate it from its mixtures. Then the remained mixtures can experience another estimating process to recover the next signal. In other words, the source signals can be recovered in a specific order according to proper features of original sources. In addition, based on the proposed techniques, different methods can be utilized at different stages of the extraction process. This means that source estimation can be completed according to the features of original source that one wants to estimate at a particular stage, which is important in practice. The simulation results have shown the presented approach can recover the desired signal from its

mixtures in a better and faster way. Time structure based techniques will be readily adaptable to provide more valuable applications to biomedical signal processing. The BSE techniques can be in fact utilized to estimate a lot of meaningful information from a set of sensor signals through just a few assumptions about the underlying sources and their mixing process, which is the objective of further research.

ACKNOWLEDGMENT

This work is supported by the National Natural Science Foundation of China (11473019), Natural Science Foundation of Shandong (ZR2014AM015)

REFERENCES

[1] James C J, Hesse C W. Independent component analysis for biomedical signals. Physiological Measurement, 2005, 26(1): 15-39

[2] Barros A K, Cichocki A. Extraction of specific signals with temporal structure. Neural Computation, 2001, 13(9): 1995-2003

[3] Lu W, Rajapakse J C. ICA with reference. Neurocomputing, 2006, 69(16–18): 2244-2257

[4] Lu W, Rajapakse J C. Approach and applications of constrained ICA. IEEE Transactions on Neural Networks, 2005, 16(1): 203-212

[5] Huang D S, Mi J X. A new constrained independent component analysis method. IEEE Transactions on Neural Networks, 2007, 18 (5): 1532-1535

[6] Mur A, Dormido R, Duro N A. An unsupervised method to determine the optimal number of independent components. Expert Systems with Applications, 2017, 75: 56-62

[7] Redif S, Weiss, Stephan. Relevance of polynomial matrix decompositions to broadband blind signal separation. Signal processing, 2017, 134: 76-86

[8] Zhang Z L. Morphologically constrained ICA for extracting weak temporally correlated signals. Neurocomputing, 2008, 71(7–9): 1669-1679

[9] Shi Z W, Zhang C S. Blind source extraction using generalized autocorrelations. Neural Networks, 2007,18(5):1516-1524

[10] Liu W, Mandic D P. A normalized kurtosis-based algorithm for blind source extraction from noisy measurements. Signal Processing, 2006, 86(7): 1580-1585

[11] Liu W, Mandic D P, Cichocki A. Blind second-order source extraction of instantaneous noisy mixtures. IEEE Transactions on Circuits and Systems, 2006, 53(9): 931-935

[12] G. Chabriel, M. Kleinsteuber, E. Moreau. Joint matrices decompositions and blind source separation. IEEE Signal Processing, 2014, 31 (3): 34–43

[13] Giri R, Rao B D, Garudadri H. Reweighted algorithms for independent vector analysis. IEEE Signal Processing Letters, 2017, 24(4): 362-366

[14] Parah S A, Sheikh J A, Assad U I. Realisation and robustness evaluation of a blind spatial domain watermarking technique. International journal of electronics, 2017, 104(4): 659-672

[15] De Moor D. Daisy: database for identification of systems. http://www.esat.kuleuven.ac.be/sista/daisy

Study on The Mechanical Properties of Hydrostatic Guide-way

Enxiu Shi
Xi'an University of Technology
Xi'an, china
E-mail: shienxiu@163.com

Rongshen Zhang
Xi'an University of Technology
Xi'an, china
E-mail: 379461906@qq.com

Hailong Wang *
Xi'an University of Technology
Xi'an, china
E-mail: 497481197@qq.com
*The corresponding author

***Abstract*—Hydrostatic guide-way is used on CNC machine tools because of its advantages. In order to meet the requirements of ultra-precision CNC machine tool for precision and high speed, a new type hydrostatic guide-way with high liquid resistance is put forward. The simulation has been done how the position, width and depth of the ring on oil seal edge of hydrostatic guide-way effect on the oil chamber pressure. It is verified that the chamber's pressure of hydrostatic guide-way can be enhanced significantly if the position, width and depth of the ring are appropriate. It is reasoned that the carrying capacity and stiffness of hydrostatic guide-way are improved when a ring is set on its oil seal edge. The conclusion can be got that the new type hydrostatic guide-way has a better carrying capacity and stiffness because of the ring if its position, width and depth are appropriate.**

Keywords-Hydrostatic guide-way; Oil film stiffness; Carrying capacity; High liquid resistance; Oil-pad

I. INTRODUCTION

The development of machining in ultra-precision, high-speed, nanotechnology and informatization has promoted the evolution of CNC machine tool. Hydrostatic guide-way are widely used in large, heavy-duty and super precision machining tool[1] because of the advantages such as good bearing capacity, better absorption vibration, proper stiffness and so on. How to improve the oil film stiffness of hydrostatic guide-way is becoming the main problem to improve the machining accuracy of machine tool, for which the fluctuation of oil film thickness from the change of load affect the accuracy of machine tool during application process. Many researches about features of hydrostatic guide-way have been done: references [2] and [3] analyzed the influence of oil chamber depth on guide-way performance; references [4] and [5] analyzed the effect of machining accuracy and parameter as the location of oil chamber on guide-way respectively. Oil thinness has been controlled through changing oil viscosity based on the relationship between capillary restrictor flows [6]. References [7] have research to improve the carrying capacity and stiffness of hydrostatic guide-way by designing a new type of resistive oil edge of it.

In this paper, in order to improve stiffness and carrying capacity of hydrostatic guide-way, a new structure of hydrostatic guide-way with high liquid resistance, which has an oil ring on oil seal edges, has been put forward based on local pressure loss. The simulation about the influence of oil ring structure parameters on oil film stiffness and carrying capacity of the hydrostatic guide-way has been done, and the experiment has done. The result from simulation and experiment show that the new hydrostatic guide-way proposed has played an active role in improving the carrying capacity of hydrostatic guide-way.

II. THE FACTORS OF INFLUENCING THE CARRYING CAPACITY AND STIFFNESS OF HYDROSTATIC GUIDE-WAY

An oil-pad of hydrostatic guide-way is composed by oil chamber and oil seal edges. Until now, most of oil seal edges is used parallel plate shown as Fig .1, which oil-film is circular. The pressures of oil-film is p_0, the gap is h_0. The oil flow can be expressed as follow:

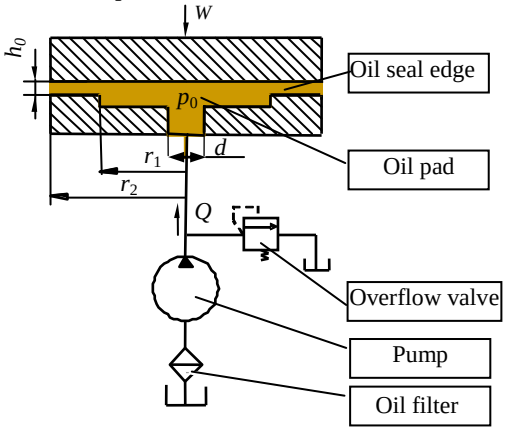

Figure 1. The schematic diagram for hydrostatic guide-way with quantitative oil supply

$$Q = \frac{p_0}{R_{h0}} \tag{1}$$

Where, R_{h0} is the liquid resistance designed and is presented as $R_{h0} = 6\mu \ln(r_2 / r_1)/(\pi h_0^2)$;

When W is loaded on slider of hydrostatic guide-way, the pressure of oil chamber changes because of the oil film thickness or the gap changing:

$$W = pA_e = \frac{p_0 A_e}{1+\lambda_0(1-\varepsilon)^3} \tag{2}$$

Here, p is oil chamber's pressure; A_e is the effective bearing area, $A_e = \pi(r_2^2-r_1^2)/2\ln(r_2/r_1)$; ε is the relative displacement between the guide surface, $\varepsilon=e/h_0$; λ_0 is the liquid resistance ratio, $\lambda_0=R_h/R_{h0}$. R_h is liquid resistance, $R_h = 6\mu\ln(r_2/r_1)/(\pi h^2)$.

The stiffness of hydrostatic guide-way stiffness can be expressed as:

$$s = \frac{\partial W}{h_0 \partial \varepsilon} = \frac{3pA_e\lambda_0(1-\varepsilon)^2}{h_0[1+\lambda_0(1-\varepsilon)^3]^2} \tag{3}$$

According to equation (2) and (3), the carrying capacity and stiffness of hydrostatic guide-way can be improved by increasing p or A_e. But increasing A_e will lead to increase the volume of hydrostatic guide-way or decrease the width of oil seal edge. The carrying capacity and stiffness of hydrostatic guide-way will be weak because of the chamber's pressure p when the width of oil seal edge is increased. The pressure p can be increased by increasing liquid resistance of hydrostatic guide-way from equation (1). It is inferred that the performance of hydrostatic guide-way can be improved through increasing liquid resistance.

III. ANALYSIS ON THE MECHANISM OF LOCAL PRESSURE LOSS FOR A RING

When oil flows through the channel with variable cross-section, its hydraulic energy is lost as the pressure being decreased gradually because of oil's viscosity. Therefore, pressure is related to not only the shape of channel but also the length of channel. While oil goes through the oil seal edge with ring of hydrostatic guide-way, two kinds of hydraulic energy losing will be occured: linear pressure loss and local pressure loss. A hypothesis is put forward that a ring set on the oil seal surface of the hydrostatic guide-way will improve the carrying capacity of hydrostatic guide-way.

A. *The Effect of the Ring's Width on the Local Pressure Loss*

For proving the hypothesis above, the simulation for streamline of the oil through the ring is done and the generation mechanism of local pressure loss is analyzed. The result is as Fig .2. Here the width of oil ring is changed.

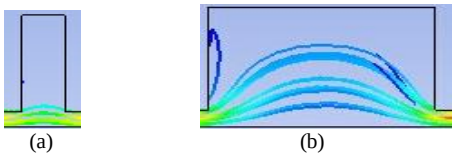

(a) (b)

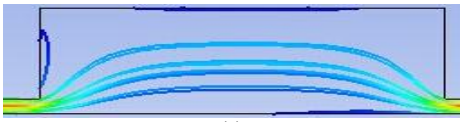

(c)

Figure 2. The influence of oil ring on the flow characteristics

It is found: while oil going through the channel, there is no enough length for local pressure loss if the ring's width is too small as (a). There is enough length for it if the width is increased as (b). Not only local pressure loss but also linear pressure loss will be caused if the width is too big as (c), but linear pressure loss decrease greatly because of the gap between oil seal edge increasing. The result is that the total pressure loss is decreased. So, the ring's width should be neither small nor large. Accordingly, its depth should be as same as its width.

B. *The Effect of the Ring's Depth on the Local Pressure Loss*

For analyzing the relationship between the local pressure loss and the ring's depth h_2, the model as Fig .3 is built and the pressure difference between inlet A and outlet B is simulated while h_2 being set as 0.2,0.5,0.8,1.0,1.3, 1.5mm, its width l_2 as 0.2, 0.5 and 0.8mm, l_1 as 0.1mm. The result is shown as Fig .4.

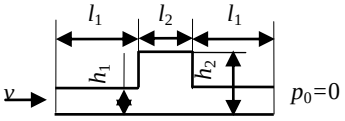

Figure 3. The Model of the Boundary Conditions for Parallel Plate with Oil Sink

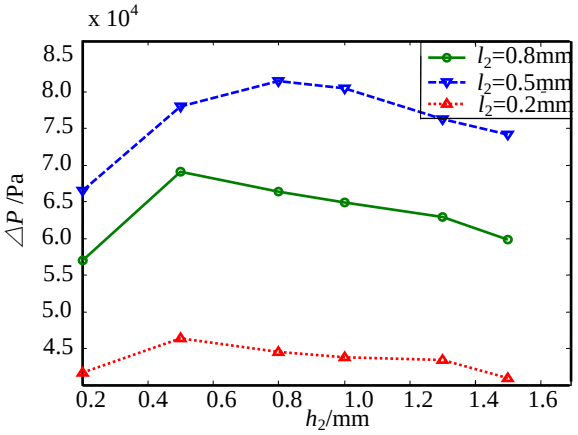

Figure 4. The Relationship between the local pressure loss and the ring's depth

It is found that local pressure loss is the highest when l_2=0.5 and h_2 is from 0.5 to 1mm.

C. The Effect of the Ring on the Local Pressure Loss

Orthogonal simulating how set h_2 and l_2 to make the local pressure loss be the biggest is done while h_2 and l_2 are set from 0.3 to 1.0mm by step 0.1mm. The result is as Fig .5.

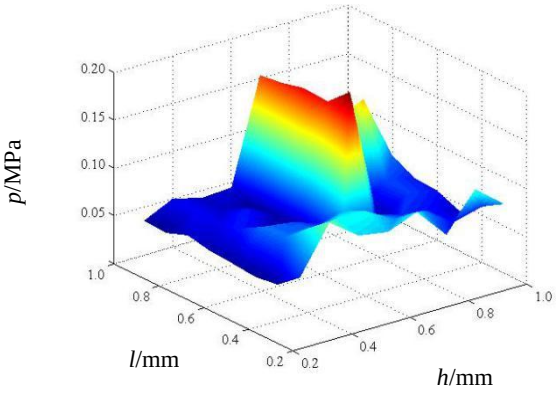

Figure 5. The pressure distribution when the width and depth of ring are changed

It is known from the result above that the local pressure loss is the biggest when h_2 is 0.5mm and l_2 is from 0.5~0.8mm about.

IV. THE INFLUENCE OF OIL RING'S PARAMETERS ON THE OIL CAVITY PRESSURE ANALYSIS

To prove the result above, the model of oil-film for hydrostatic guide-way Fig.1 is made as Fig.6: r_1=45mm, r_2=60mm, h_0=0.05mm, h=2mm, d=3mm,the length of inlet is 20mm. The pressure of the chamber is simulated while changing the ring's parameter such as its width, depth and the distance from the chamber. For doing this, some hypothesis should be given as follow:

①Oil is incompressible and steady flow;

②No relative slide between oil and solid;

③The pressure at outlet of oil film is zero.

④Ignore the inertia of oil and Thermal deformation of the work-table;

The condition for simulating is: the velocity of oil at the inlet is 100mm/s，the surface which oil contacts with work-table is Wall type, outlet is Opening type and the pressure is 0Pa, oil's density is 875kg/m3, its dynamic viscosity is 0.035Pa.s.

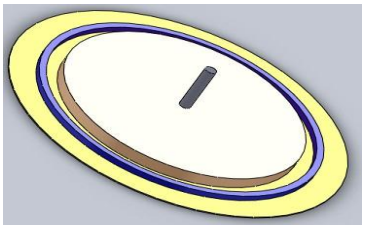

Figure 6. The model of fluid file with ring

A. The Effect of the Position of the Ring on the Chamber Pressure

The chamber's pressure is simulated while the distance from the ring to the chamber is changed as 1,3,⋯,13 mm but its width and depth are set as 0.5mm according to section 2. The results is shown as Fig .7 .

It is verified from the simulation above that the pressure is changed while changing the distance between the ring and the chamber. But the pressure is the highest when the distance is 5mm about. So the distance is taken as 5mm for following simulation.

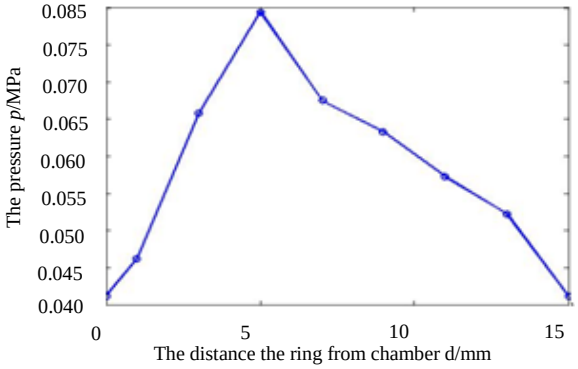

Figure 7. The curve for the effect of the ring's position on the chamber's pressure

B. The effect of the ring's width on the chamber's pressure

For analyzing the effect the ring's width on the chamber's pressure, the depth is set as 0.5mm, and the distance the ring from the chamber is set as 5mm according to section A. The chamber's pressure is simulated as Fig .8 when the width is changed from 0.1 to 1.0mm by step 0.1mm.

The bigger the width is, the higher the pressure is if it is smaller than 0.6mm about. But the bigger the width is the lower the pressure is when the width is bigger than 0.6mm,. The pressure is the highest while the width is from 0.3 to 0.6mm. The ring's width can be set 0.5mm while simulating following.

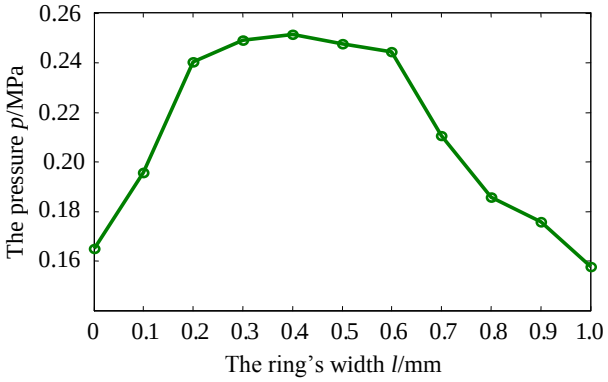

Figure 8. The curve for the effect of the ring's width on the chamber's pressure

C. *The Effect of the Ring's Depth on the Chamber'S Pressure*

For analyzing the effect the ring's depth on the chamber's pressure, the width is set as 0.5mm, and the distance is set as 5mm. The chamber's pressure is simulated as Fig .9 while the depth is set from 0.1 to 1.0mm by step 0.1mm.

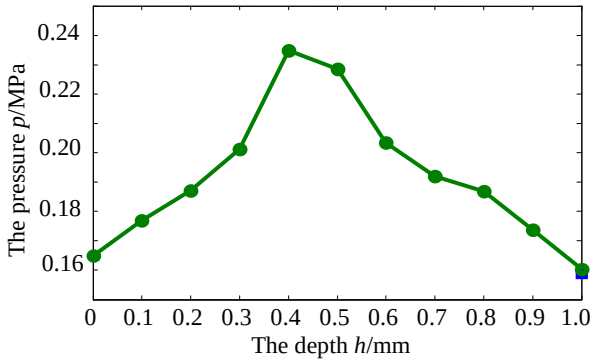

Figure 9. The curve for the effect of the ring's depth on the chamber's pressure

It is shown clearly that the changing trend of the chamber's pressure by the ring's depth is similar to that by its width, and the pressure is the biggest when the depth is 0.4mm~0.5mm.

It is proved from above that the chamber's pressure can be increased when a ring is set in the oil seal edge of hydrostatic guide-way. In another words, hydrostatic resistance of hydrostatic guide-way is increased when a ring is set. So the design of a ring is the same important as that of the chamber for hydrostatic guide-way. The ring's width, depth and position should be chosen while designing the hydrostatic guide-way.

V. THE ANALYSIS OF HYDROSTATIC GUIDE-WAY STIFFNESS

The closed hydrostatic guide-way fluid solid coupling simulation model is constructed in this paper to verify the simulation result above for hydrostatic guide-way. Four chambers were constructed on both up and down to reduce computation. The oil chamber was designed on guide-way as (a) and (b) in Fig.10. The lower chamber, which its length and width are 60mm and 30mm and the resistive edge width is 15mm and the distance between two chambers is 35mm, is for bearing only. The upper chamber's length and width are 70mm and 10mm and the resistive edge width is 10mm. The size of hydrostatic guide-way is: width 300mm, length 200mm, height 80mm. The fluid model is designed according to hydrostatic guide-way and slide block. The oil ring on the oil seal edge is 5mm far away from the oil chamber, its width and depth are 0.5mm. The model is shown as Fig .11. The condition for the fluid-soild model is shown as Fig .12.

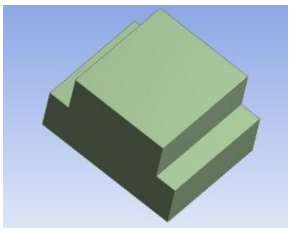

(a) The slide block

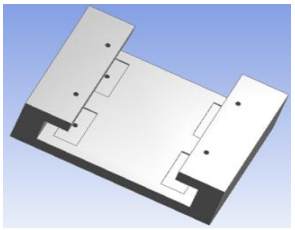

(b) hydrostatic guide-way without ring

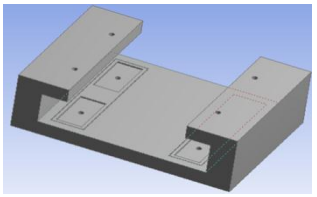

(c) hydrostatic guide-way with a ring

Figure 10. The solid model for closed hydrostatic guide-way

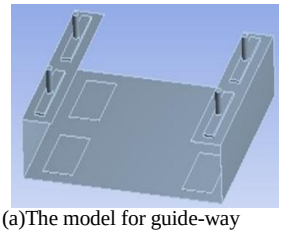

(a)The model for guide-way without a ring

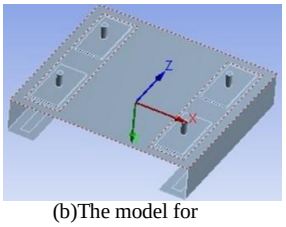

(b)The model for guide-way with a ring

Figure 11. The oil film model for closed hydrostatic guide-way

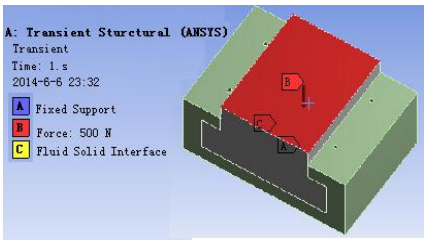

Figure 12. The edge condition of hydrostatic guide-way entity domain

For simulation the pressure of oil-chamber and displace of slider, the edge condition of hydrostatic guide-way is set as Fig .12. The chamber's pressure and the slider's displacement will be obtained when the force is loaded on the slider as Fig .13 and Fig .14. The bearing capacity and stiffness of hydrostatic guide-way with and without oil ring can be get while the force on slider is changed during the simulation as Fig .15 and 16.

It is proved from the simulation result that the bearing capacity and stiffness can be improved if a ring is set on the oil seal edge of hydrostatic guide-way. In the other hand, the liquid resistance can be increased when a ring is set on the oil seal edge of guide-way. The hydrostatic guide-way with high liquid resistance has better bearing capacity and stiffness.

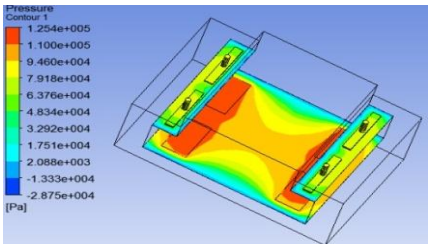

(a)The pressure distribution of guide-way without ring

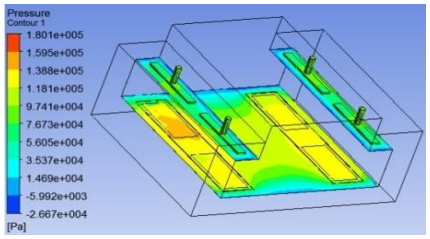

(b)The pressure distribution of Guide-way with a ring

Figure 13. The oil-film pressure distribution for hydrostatic guide-way

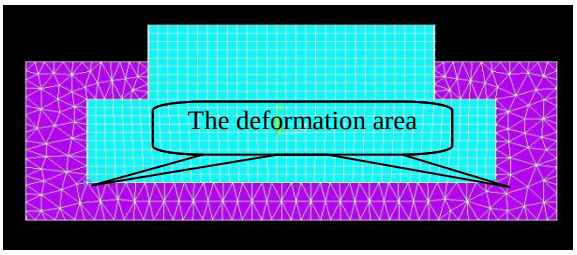

(a) The deformation area

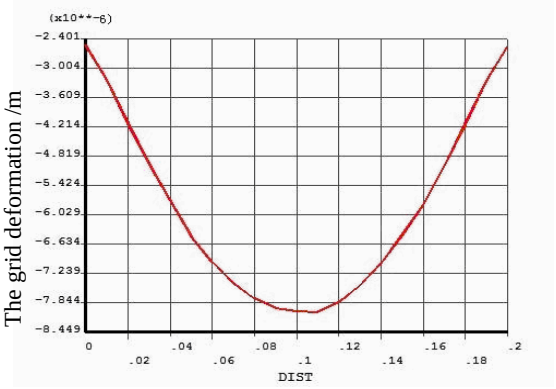

The grid at the longitudinal direction /m

(b)This is for hydrostatic guide-way without ring

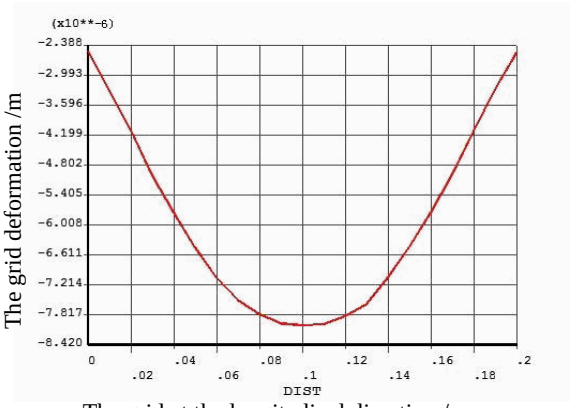

The grid at the longitudinal direction /m

(c) This is for hydrostatic guide-way with a ring

Figure 14. The grid's deformation at the longitudinal direction

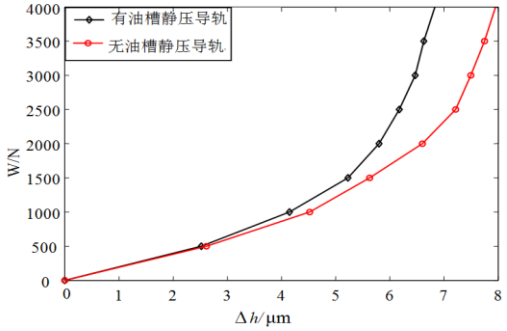

Figure 15. The curve for the relationship between oil-film thickness variation Δ h and force W

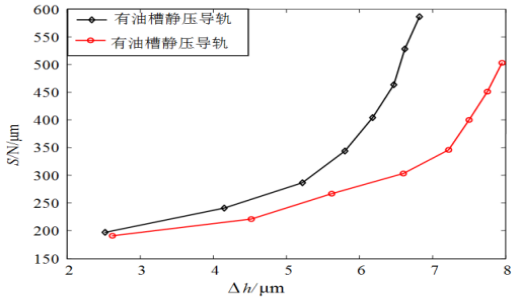

Figure 16. The curve for the relationship between thickness variation Δ h and stiffness S

VI. THE CONCLUSION

Hydrostatic guide-way is the most important supporting component for ultra-precision CNC machine tools, and its carrying capacity and stiffness are important performance parameters. In order to meet the requirements for ultra-precision CNC machine tool of ultra-precision, high-speed, a new type hydrostatic guide-way with high liquid resistance is put forward based on the generation mechanism of local pressure loss. The simulating has been done how the width,

depth and position of the ring, which is on the oil seal edge of hydrostatic guide-way, effect on the oil chamber pressure. It is verified from the result that the chamber's pressure of hydrostatic guide-way can be enhanced significantly if the position, width and depth of the ring are appropriate. It is reasoned that the carrying capacity and stiffness of the hydrostatic guide-way are improved when a ring is set on its oil seal edge.

The conclusion can be got that the new type hydrostatic guide-way with a high liquid resistance has a better carrying capacity and stiffness because of a ring set on the oil seal edge if its position, width and depth are appropriate.

ACKNOWLEDGMENT

This research was financially supported by the Shaanxi Province Natural Science Foundation (No.014JM2-5067), haanxi Province Education Department key laboratory scientific research plan (No.13JS072).

REFERENCES

[1] Chun Hong Park, Chang Kyu Song, Jooho Hwang, etc. Development of an Ultra Precision Machine Tool for Micromachining on Large Surfaces [J]. International Journal of Precision Engineering and Manufacture, 2009, 10,pp:85-91

[2] Junpeng Shao, Limin Zhou, Hongmei Li, etc.. Influence of The Oil Cavity Depth on Dynamic Pressure Effect of Hydrostatic Thrust Bearing[C]. 2009 International Conference on Intelligent Human-Machine Systems and Cybernetics,pp:11-14.

[3] N. Heinrichson and I. Ferreira. The Infuence of Injection Pockets on The Performance of Tilting-Pad Thrust Bearings [J]. Journal of Tribology, 2007, 191,pp:895-903.

[4] Fei Xue,Wanhua Zhao,Yaolong Chen, Zhiwei Wang. Research on Error Averaging Effect of Hydrostatic Guideways [J]. Precision Engineering, 2012, 36(1),pp:84‐90.

[5] T.A.Osman, M.Dorid, Z.S. Safar, etc.. Experimental Assessment of Hydrostatic Thrust Bearing Performance [J]. Tribology International, 1996, 29, pp:233-239.

[6] A.Bouzidane, M. Thomas. An Electrorheological Hydrostatic Journal Bearing for Controlling Rotoration [J]. Computers and Structures, 2008, 86,pp: 463-472.

[7] T Satish C. Sharma, Saurabh K. Yadav. Performance Analysis of A Fully Textured Hybrid Circular Thrust Pad Bearing System Operating with Non-Newtonian Lubricant[J]. Tribology International, 2014,77, pp:50.64.

[8] Xiaobo Zuo, Jianmin Wang, Ziqiang Yin, etc. Comparative performance analysis of conical hydrostatic bearings compensated by variable slot and fixed slot[J]. Tribology International. 2013. 66:83‐92.

[9] Zhang Y Q, Yu X D, Yang X D, et al. Viscosity Influence Research on Load Capacity of Heavy Hydrostatic Bearing [C]. 3rd International Conference on Advanced Design and Manufacture, Nottingham, UK, 2010, 63-66.

[10] Satish C. Sharma, Saurabh K. Yadav. Performance analysis of a fully textured hybrid circular thrust pad bearing system operating with non-Newtonian lubricant[J]. Tribology International, 2016,77:50‐64

Multi - point Cooperative Multicast Video Design and Research

Wang Tao
Wuxi Environmental Science and Engineering Research Center,
School of Internet of Things Engineering,
Wuxi City College Of Vocational Technology,
Wuxi, Jiangsu
Wang_830@163.com

Abstract—Internet era in the context of increasing popularity of mobile terminals, network video browsing has become an indispensable feature of wireless terminals. However, in order to improve the reliability of video multicast, this paper increases the gain system from the overlapping access points in the coverage area, because of the low reliability of the inter-link interference between the wireless networks. Improve the fairness of the system, and propose and design a multi-point broadcast scheme based on network coding and multi-access point collaboration. The program will first divide each video segment into the same segment and divide the access point completely and not completely interfere with the two models. The video multicast problem when the transmission range between the access points is overlapped is modeled as Linear programming optimization problem, a two-stage heuristic algorithm is designed to solve the problem. By using multiple access points to get the gain of space and time diversity, the reliability of data transmission is improved, and data is transmitted in parallel by allowing access points that interfere with , To improve the system utility. Finally, the simulation experiment is used to verify the validity of the number of packets to be decoded, the total amount of packets received and the fairness.

Keywords-Video multicast; network coding; multi-point access collaboration; Linear programming optimization, heuristic algorithm; fairness

I. INTRODUCTION

With the rapid development of mobile devices such as tablets and smart phones, the popularity of mobile devices continues to increase. Watching video via the Internet is becoming an important feature of these devices. Recent studies have shown that [1], the main data flow on the Internet is the multimedia data stream. For example, YouTube and Netflix traffic in the overall share of the Internet traffic reached 20-30%. Because of the low link reliability of wireless network, it will have a great impact on the video quality received by the user, so it is significant to study the reliability of video data stream transmission [2].

At present, the most common method of video data transmission reliability is the message feedback mechanism, the automatic repeat request (Automatic Repeat reQuest, ARQ) is the most commonly used [3]. In order to reduce the overhead of ARQ message, the [4-6] method is proposed by combining Hybrid-ARQ with erasure code and ARQ. But in general, all of the methods using feedback packets can lead to additional costs and increase the energy consumption of nodes. In addition, the feedback mechanism is not feasible for some applications. For example, in multicast applications, the cost of deploying a feedback mechanism is high, because it is a waste of time to transmit a feedback message to each receiver. The use of random linear network coding [7] (Random Linear Network Coding, RLNC) and fountain code [8], such as network coding without feedback packets which can improve the reliability of data transmission. For example, the RLNC method uses the random coefficient to fuse the original message, the destination node receives a sufficient number of encoded messages and decodes the encoded messages. Thus, the source node does not need to know what the destination node is missing.

II. SYSTEM MODEL

A. Setting and objectives

It is assumed that the video server in the research environment sends the video stream to an m adjacent WiFi access point, and then transmits to the wireless users such as smart phone, tablet and desktop. Suppose the access point is connected to the video server via a wired link. The reliability of these wired links is high, so it will not become the bottleneck of data transmission. Thus, we can further assume that the video message at the access point can be transmitted to the user at any time. In this paper, the system model and the labeling method are shown in Figure 1, respectively.

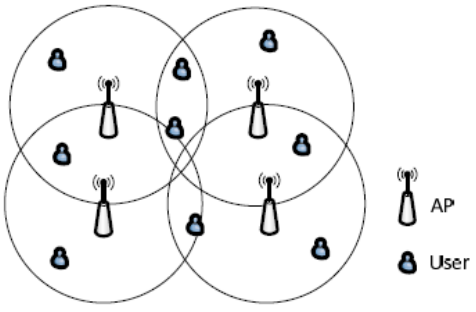

Figure 1. System model

When the data is transmitted by wireless link, some of the destination node may lose the transmitted video message. We show $\grave{o}_{ij}$ the probability of deletion of the link between the access points i to j and the access points to J. Each access point has a circular coverage area. In addition, the

overlap region of WiFi access points may overlap with each other. As a result, these WiFi devices will interfere with each other, and if the access point transmits the message at the same time, then the user node located in the overlap region will not be able to receive the message correctly. The purpose of this paper is to improve the fairness of the video multicast to the user by properly scheduling access points. Specifically, we want to maximize the expected value of the number of messages received by the user.

B. *Interference model [5] [6]*

In this paper, we consider two kinds of interference models: complete interference and incomplete interference between access po(1) complete interference graph: in this model, each access point interferes with all other access points. In other words, the interference graph is a complete graph. In order to avoid interference between the access points when the interference graph is complete, the access point can not be scheduled at the same time.

III. SCHEME

A. *Video coding*

improve the reliability of data transmission in the absence of feedback packets, the RLNC mechanism is adopted in this paper. First, each video is divided into the same size packets. Then, we use RLNC to encode the packets of each segment. Figure 2 (a) in the video is divided into multiple message segments, figure 2 (b) gives the original video encoding message. For simplicity, we do not show a factor in the graph. For example, the graphic $p_1+p_2+p_3+p_4$ is expressed $\alpha_1 p_1+\alpha_2 p_2+\alpha_3 p_3+\alpha_4 p_4$ as α_1 to α_4 a random coefficient. Therefore, the encoded messages of each segment in Figure 2 are not the same. The coding process is carried out on the video server, and the coded message is transmitted to the access point through a high reliability wired link.

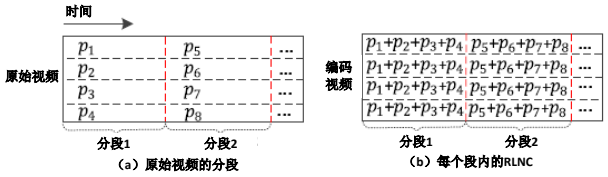

Figure 2. Network coding mechanism

B. *Access point scheduling algorithm under complete interference graph [7] [8] [9]*

The goal of this paper is to achieve fair scheduling by maximizing the expected value of the number of messages received by the user. In other words, we want to maximize the number of messages received at each access point. As shown in the following section, the problem of solving the above problem can be solved in polynomial time when the data transmission range of the access point is not overlapped. Conversely, if the scheduling of a WiFi access point overlaps, I It may exist the number of parallel transmissions. Therefore, the time complexity of this scheduling is very large. To this point, we propose a two-phase scheduling algorithm for access points. In the first stage, we use linear programming optimization theory to determine the optimal scheduling scheme when the access point does not overlap. Then in the second stage, we use the results of the first phase as the initial solution, and then allow the interference of the access points to a certain degree of parallel transmission, which aims at improving the overall utility. In the second stage, we use linear programming theory to determine the parallel transmission scheme which can improve the overall utility.

1) phase 1 (no overlapping scheduling scheme): we obtain the basic solution of the problem at this stage, and does not allow access to parallel transmission. The optimal scheduling scheme is obtained by solving the following linear programming problem without transmission overlapping:

$$\max \quad y \tag{1}$$

$$s.t \quad \sum_{j\in B} x_j \le 1 \tag{2}$$

$$r_i = \sum_{j\in C(i)} b\cdot x_j\left(1-\varepsilon_{ji}\right), \forall i \in U \tag{3}$$

$$y \le r_i, \forall i \in U \tag{4}$$

We show that the access point can be represented as a time proportional to the data transmission. The main constraint of this scheduling is that the access point can not transmit data at the same time. Thus, the sum of the time allocated to the access point shall not exceed 1, as shown in the constraint (2). We represents the transmission bandwidth of the access point as B. Therefore, if the user is located within the transmission range of the access point, the number of messages received by the user from the access point is $b\cdot x_j\left(1-\grave{o}_{ji}\right)$. . Since we do not allow parallel transmission, the total expected value of a message received by a user is equal to the sum of the expected value of the number of messages received by the user from the point of access to the user. The constraint (3) calculates the total expected value of the message received by each user. Constraint (4) is fairness constraint which represents the total expected value of the message received by the user. In order to achieve fair scheduling, the number of messages received by the user should be close to the expected value. Therefore, we do not maximize the expected value of the total amount received by users , but maximize the minimum expected value. To this point

C. *Access point scheduling algorithm under the condition of incomplete interference graph [9]*

There is no interference between nodes in the interference graph. According to graph theory, we need to find the maximum independent set at the same time. However, the determination of the maximum independent set is a NP problem [11]. So we will search for maximal independent sets instead of maximal independent sets. A maximal independent set is an independent set that is no longer an independent set when the other nodes are added to the collection. For an $|S|$ independent set of overlapping scheduling, there may be a $2^{|S|}-1$ parallel transmission. Thus, the time complexity of the scheduling problem is very similar to that of the complete interference graph. In this paper, a 3 stage algorithm is used to schedule the access points under the condition of incomplete interference graph, and the time complexity is low.

1) phase 1 (finding the maximal independent set): we first construct the interference graph of the access point. We use the nodes in the interference graph to represent each access point. If the node of a two node is isturbed, the two nodes are connected. In order to avoid interference between access points, we can only allow some nodes that do not interfere with the simultaneous transmission of data. A common scheduling method is to use large independent sets that can be determined in polynomial time, rather than the largest independent set.

Detection algorithm of Maximum independent Set is shown in algorithm 2. In this algorithm, the B UN marked access points are put into the set A. In order to determine the independent set, the algorithm searches for the smallest node in each iteration, and puts it into an independent set. Then, the algorithm removes the adjacent nodes j from the set and marks the nodes. Repeat the process until the collection is empty. After an independent set is determined, all the nodes in the independent set are marked in the collection. Then, the non tagged nodes are added to the collection, and then run the set of nodes that have never been marked by the algorithm to look for other independent sets. Repeat this process until al.

Algorithm 2: maximum independent set detection
1：input： B , $N(j)\forall j \in B$;
2： $S=\{\}$, $A=B$;
3：Remove the label of the node
4：while B （There are not marked nodes in） do
5： while A Not empty do
6： $I=\{\}$
7： j Finding the lowest node ;
8： Mark the right node;
9： $I=I\cap j; A=A/N(j)$;
10： $S=S\cup I$;
11： Put the UN marked nodes in the

IV. EXPERIMENTAL EVALUATION[10]

In this section, through the performance proposed by a comprehensive simulation, it can evaluate the performance of the scheme when receiving messages, the number of decoding messages and the fairness.

A. *Simulation settings*

We deploy the simulator in the MATLAB environment and evaluate the performance of the various algorithms under 1000 network topologies with random link delivery rates. The simulation results presented in this paper are the average of the 50 simulation results. We assume that the wireless link delivery rate is independent of each other. The nodes are randomly deployed on a square area of 20 x 20 meters, and the rate of the link between them is calculated according to the Euclidean distance between the access point and the user. For the two nodes with interval distance, the Rayleigh fading model [12] is used to calculate the probability of successful delivery:

$$P=\int_{T^*}^{\infty}\frac{2x}{\sigma^2}e^{-\frac{x^2}{\sigma^2}}dx \tag{5}$$

$$\sigma^2 @\frac{1}{(4\pi)^2 L^{\alpha}} \tag{6}$$

Among them, the link loss index, the decoding SNR threshold.

B. *Simulation results [4]*

We first evaluate the performance of the method of complete interference graph and then demonstrate the evaluating results under the condition of incomplete interference graph. Finally We compare the scheme with the present more typical video multicast scheme.

(1) Completely interference graph: we will set the number of nodes as 10, and the number of access points will change from 3 to 7, which evaluate the impact of access point of the user node. The results is shown in Figure 3 (a). When we increase the number of access points, the total amount of received messages has increased. This is because when we increase the number of access points, each user will be covered by more access points. Thus, each user has at least one high quality wireless channel with a probability of rise. As a result, the number of messages delivered to the user increases successfully.

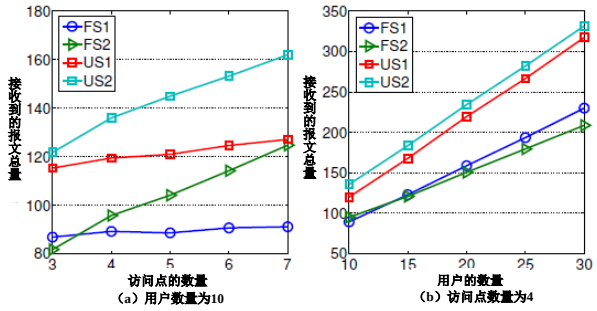

Figure 3. The total amount of messages received by the user in the complete interference graph

From Fig. 1 (a), the total amount of received messages in the unfair method is the largest. This is because we set the objective function to maximize the amount of messages received at the time of optimization. In the second phase of the fair scheduling method, we allow some nodes to transmit data in parallel, thus increasing the number of messages received by users. Fig. 1 (a) proves the validity of the parallel access point. When there are 3 access points, the number of received messages of FS2 is less than FS1. This is because many users are more likely to be covered by a single access point. Thus, phase 2 cannot increase the number of messages received. On the other hand, FS2 aims to increase fairness.

We set the number of access points as 4, and the number of users ranges from 10 to 30, which evaluate whether the number of users have impact on the total amount of received messages, and the results are shown in Figure 3 (b). As we expect, the total amount of the received message increases with the increasing of the number of users.

V. CONCLUDING REMARKS

The main application of wireless devices such as smart phones and tablet is to watch video through the Internet. In this paper, we use multiple access point cooperation and network coding mechanism to transmit the video data stream to the client node. After a plurality of access points, the client node can obtain spatial and temporal diversity, and then receive more messages. In addition, after using the network coding mechanism, all transmission messages are of equal importance. As a result, reliable transmission of data can be achieved even without feedback mechanism. Compared with previous video multicast schemes that do not allow access point to be transmitted in parallel, this method supports the parallel transmission of data with interference access points, which effectively improves the performance of the system. In the next step, we will consider the impact of video encoding hierarchical structure on the performance of the system, through searching matched available resources to video encoding hierarchical structure of available used in user channel conditions, modulation encoding and system to optimize the performance of the system, which proposed for wide band wireless network layered video multicast transmission mechanism.

ACKNOWLEDGMENT

The author are grateful for financial support from the funding project :

(1) outstanding young teachers and principals outside the training project Department of Education , Jiangsu Province

(2) Education Science Planning Leading Group Office ,Jiangsu Province (grant no.D/2016/03/62)

REFERENCES

[1] Han, Z. Guo, and D. Zhang. Multispectral palmprint recognition using wavelet-based image fusion[C]. In ICSP, 2010:2074–2077.

[2] Y. Hao, Z. Sun, T. Tan, and C. Ren. Multispectral palm image fusion for accurate contact-free palmprint recognition[C]. In Proc. ICIP, 2008: 281–284.

[3] Kisku, P. Gupta, J. Sing, and C. Hwang. Multispectral palm image fusion for person authentication using ant colony optimization[C]. In IEEE Workshop on Emerging Techniques and Challenges for Hand-Based Biometrics, 2010:1–7.

[4] Lin P, Bi J, Wolff S, et al. A west-east bridge based SDN inter-domain testbed[J]. IEEE Communications Magazine, 2015, 53(2): 190-197.

[5] Yu K, Li F Y, Wu X, et al. The heterogeneity of inter‐domain Internet application flows: entropic analysis and flow graph modelling[J]. IEEE Transactions on Emerging Telecommunications Technologies, 2015, 26(5): 760-771.

[6] Dong M, Ota K, Liu A, et al. Joint optimization of lifetime and transport delay under reliability constraint wireless sensor networks[J]. IEEE Transactions on Parallel and Distributed Systems, 2016, 27(1): 225-236.

[7] Larsson P, Rasmussen L K, Skoglund M. Throughput Analysis of Hybrid-ARQ—A Matrix Exponential Distribution Approach[J]. IEEE Transactions on Communications, 2016, 64(1): 416-428

[8] Wang Q, Jing Y. Closed-Form Average SNR and Ergodic Capacity Approximations for Best Relay Selection[J]. IEEE Transactions on Vehicular Technology, 2016, 65(4): 2827-2833.

[9] Bai C, Leeson M, Higgins M D, et al. Throughput and energy efficiency‐based packet size optimisation of ARQ protocols in bacterial quorum communications[J]. IEEE Transactions on Emerging Telecommunications Technologies, 2016, 27(8): 1128-1143.

[10] Li Jiao, Shang Tao, and. Secure quantum repeater network coding scheme based on identity authentication [J]. Journal of electronics, 2016, 44(3): 560-564.

[11] Niu Fanglin, Li Baoming, Chen Fuliang, et al. An improved design of fountain codes based on partial information [J]. 2016, 44(2): 295-300.

[12] Choi M, Sun W, Koo J, et al. Reliable video multicast over Wi-Fi networks with coordinated multiple APs[C]//IEEE INFOCOM 2014-IEEE Conference on Computer Communications. IEEE, 2014: 424-432.

[13] Tassi A, Chatzigeorgiou I, Lucani D E. Analysis and optimization of sparse random linear network coding for reliable multicast services[J]. IEEE Transactions on Communications, 2016, 64(1): 285-299.

[14] Tang Qiang, Xie Mingzhong, Luo Yuansheng, et al. An algorithm for constructing minimal connected dominating set based on two hop independent neighbor covering [J]. mini computer system 2016, 37(6): 1245-1249.

[15] Khreishah A, Khalil I, Wu J. Universal Network Coding-based Opportunistic Routing for Unicast[J]. IEEE Transactions on Parallel and Distributed Systems,2015,26(6):1765-1774.

Optimization of Matching on Torque Converter with Engine Based on Improved Radar Chart Method

Zhenbao Wang
College of mechanical Science and Engineering
Jilin University
Changchun, China
E-mail: wangzhenbao1989@126.com

Sicheng Qin
College of mechanical Science and Engineering
Jilin University
Changchun, China
E-mail: qsc925@hotmail.com

***Abstract*—In order to comprehensively evaluate the performance of matching between engine and torque converter, a series of matching evaluation indexes were developed according to the ideal matching principle and a standardized treatment for every index was put forward. Considering the different importance of each indexes in different applications, weight of each index was given by using comprehensive method, The evaluation method of the hydraulic torque converter and engine matching was established based on the improved radar map method. The objective function was constructed based on the sum of each evaluation index and the perimeter of radar map. With a hydraulic torque converter of ZL50 loader as an example, the effective diameter of circular circle on hydraulic torque converter was optimized in view of the shovel loading cycle condition. The original size of torque converter effective diameter was 0.340 m. After optimization, the effective diameter of hydraulic torque converter was 0.350 m, and the matching performance of engine and torque converter was increased by 7.4%. The results show that the optimal matching scheme can be improved by using the improved radar map method.**

Keywords-Torque converter; Matching; Improved radar chart method; Optimization; Wheel loader

I. INTRODUCTION

Hydraulic torque converter as a kind of hydraulic transmission device works with the engine in the course of work. After the matching of hydraulic torque converter and engine, it can be considered as a new power installation and its performance greatly depends on whether the matching of them is reasonable. Thus, it is necessary to make a comprehensive evaluation for the performance of the joint work [1, 2].

Aiming at the deficiency existing in the matching evaluation method of engine and hydraulic torque converter, this paper makes a further improvement on the traditional radar chart [3, 4]. Through the formulation of dimensionless matching evaluation index and the empowerment by principal component analysis, this paper establishes the comprehensive evaluation method of the matching of a hydraulic torque converter and engine. Based on it, the objective function is constructed. And aiming at shovel mucking drive cycle, the diameter of the effective circulating circle of the hydraulic torque converter of ZL50 loader is optimized.

II. EVALUATION INDEX OF MATCHING PERFORMANCE

According to the matching principle of hydraulic torque converter and engine, this paper selects five evaluation indexes of matching performance and standardizes each index, which is shown in table I [5, 6].

TABLE I. EVALUATION INDEXES OF MATCHING PERFORMANCE

Evaluation indexes	Formula
Maximum torque output coefficient a_1	$T_1/T_{\max}$
Maximum power output coefficient a_2	$P_1/(P_{eH}\eta_{\max})$
Width of the efficient workspace a_3	$(n_{w2}-n_{w1})/n_{\max}$
Power output coefficient a_4	$\bar{P}_1/(P_{eH}\bar{\eta})$
Coefficient of fuel consumption a_5	$(g_{\max}-\bar{g}_e)/(g_{\max}-g_{\min})$

In the table I: T_1 refers to the crossover point torque between load parabola and engine's net torque curve when the transmission ratio of hydraulic torque converter $i=0$; $T_{\max}$ refers to the maximum net output torque of engine; P_{eH} refers to the maximum net output power of engine; $\eta_{\max}$ refers to the peak efficiency of the hydraulic torque converter; P_1 refers to the maximum output power of the hydraulic torque converter; n_{w1} and n_{w2} refer to the corresponding turbine speed when the efficiency of the hydraulic torque converter η_1 is equal to 0.75; $n_{\max}$ refers to the maximum output speed of turbine shaft; $\bar{\eta}$ refers to the average efficiency of the hydraulic torque converter when η_1 is greater than or equal to 0.75; $\bar{P}_1$ refers to the average output power of the turbine shaft of hydraulic torque converter when η_1 is greater than or equal to 0.75; $\bar{g}_e$ refers

to the average effective fuel consumption rate; $g_{\max}$ refers to the maximum fuel consumption rate of engine; $g_{\min}$ refers to the minimum fuel consumption rate of engine.

According to the definition of each formula in table I, the greater the value of each evaluation index, the better the matching performance of the corresponding engine and hydraulic torque converter. Because of the different importance of each evaluation index, the evaluation index should be weighted. This paper uses principal component analysis to empower each index [7, 8].

III. CONSTRUCTION OF EVALUATION FUNCTION BASED ON THE IMPROVED RADAR CHART

A. Drawing of Improved Radar Map

This paper perfect the traditional radar chart further. The construction method is as follows [9, 10]:

1) The standardized evaluation index is weighted. The weight is sorted from large to small and the obtained weight after sorting is q_1, q_2, q_3, q_4, q_5, each index value is sorted anew according to the corresponding order, which is e_1, e_2, e_3, e_4, e_5. According to the weight, the corresponding sector angle $\theta_j = 2q_j\pi$ of e_j index in radar chart can be obtained.

2) Determine the index shaft. Firstly, we should draw a unit circle. And then we should draw a horizontal ray from the center of the circle O. The ray and circle intersect at point A. Then we should draw rays OB, OC, OD, and OE in order under ray OA, and then draw diagonals of sectors AOB, AOC, BOD, COE, and DOE. The diagonals and circle intersect at points M1, M2… M5. Lines OM1, OM2… OM5 are taken as the index shaft.

3) we should mark e_1, e_2, e_3, e_4, e_5 in the index shaft according to the length and then the points A', B', C', D', E' can be obtained in order. Finally we should connect point A'-B'-C'-D'-E'. The improved radar chart with comprehensive evaluation can be obtained, which is shown in Fig. 1.

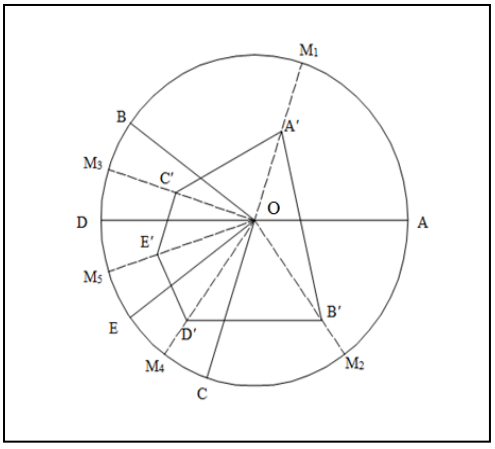

Figure 1. Improved radar map

B. Construction of Objective Function

According to the construction method of radar chart, the better the matching performance of the engine and hydraulic torque converter, the larger the perimeter of pentagon ABDEC. Based on the perimeter of pentagon, the optimization function is constructed:

$$\begin{cases} f(D) = \sum_{k=1}^{5} \alpha_k C_k \\ C_k = l_{A'B'} + l_{A'C'} + l_{B'D'} + l_{C'E'} + l_{D'E'} + \sum_{j=1}^{5} q_j e_j \\ L_{A'B'} = \sqrt{e_1^{\,2} + e_2^{\,2} - 2e_1 e_2 \cos\frac{\theta_1 + \theta_2}{2}} \\ L_{A'C'} = \sqrt{e_1^{\,2} + e_3^{\,2} - 2e_1 e_3 \cos\frac{\theta_1 + \theta_3}{2}} \\ L_{B'D'} = \sqrt{e_2^{\,2} + e_4^{\,2} - 2e_2 e_4 \cos\frac{\theta_2 + \theta_4}{2}} \\ L_{C'E'} = \sqrt{e_3^{\,2} + e_5^{\,2} - 2e_3 e_5 \cos\frac{\theta_3 + \theta_5}{2}} \\ L_{D'E'} = \sqrt{e_4^{\,2} + e_5^{\,2} - 2e_4 e_5 \cos\frac{\theta_4 + \theta_5}{2}} \end{cases} \quad (1)$$

In the Equation (1): α_k is the weight of each working period, which is determined by the job time allocation. C_k is the sum of the perimeter of matching radar chart and each evaluation index of each working period. $l_{A'B'}$, $l_{A'C'}$, $l_{B'D'}$, $l_{C'E'}$, and $l_{D'E'}$ are the length of each side of the pentagon.

C. Program Design

The effective circular circle diameter of hydraulic torque converter is taken as the optimization variable to optimize the matching performance of the engine and hydraulic torque converter. Using MATLAB to prepare the calculation program, the calculation of the block diagram shown in Fig. 2.

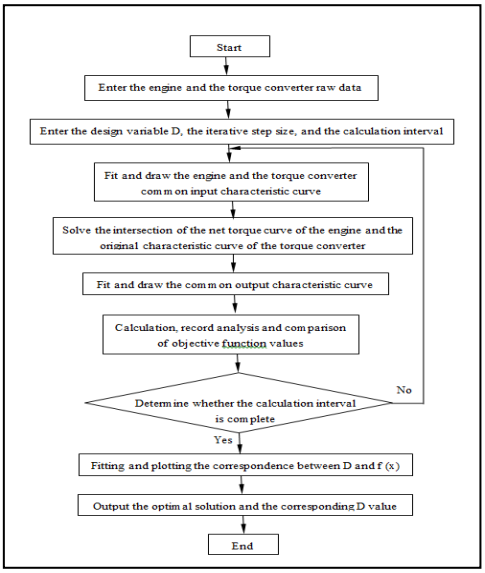

Figure 2. Figure 2. Program flowchart of matching evaluation

IV. Optimization Analysis

In this paper, the torque converter of ZL50 loader is taken as an example to optimize the matching performance of I shovel cycle.

1) According to the net output torque of the engine and the original data of hydraulic torque converter of each working period, the common work input and output characteristics of the engine and hydraulic torque converter are calculated [11,12].

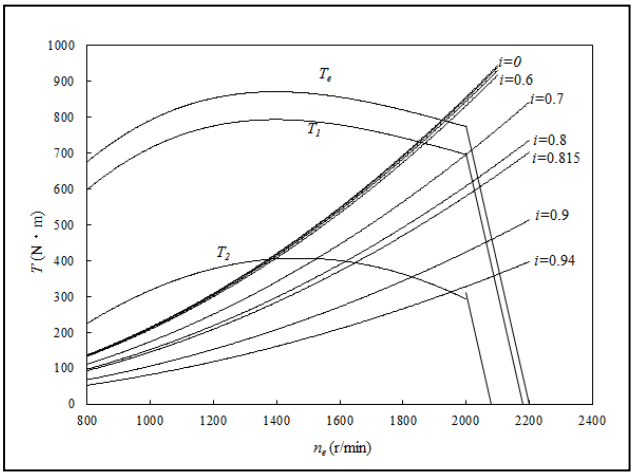

a. Input characteristics

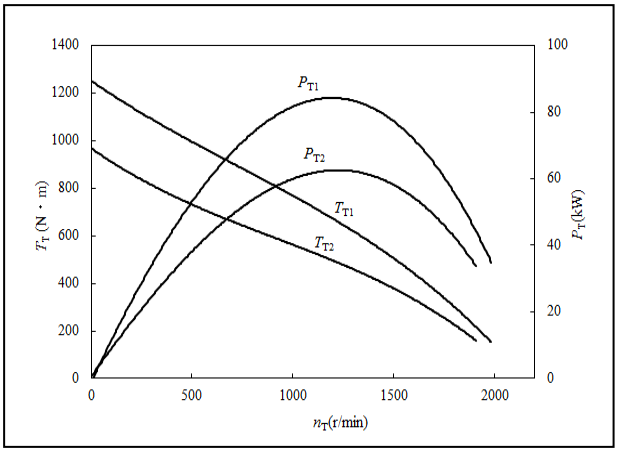

b. Output characteristics

Figure 3. Characteristics of engine working together with torque converter

2) Evaluation indexes of each working period are calculated respectively.

3) The above steps should be repeated, and then the evaluation index value of different diameters D should be calculated respectively.

4) The weight of matching evaluation index is determined. The evaluation matrix is constructed by obtained matching scheme by diameters of different circular circles:

$$\boldsymbol{U}=\begin{bmatrix}0.837 & 0.919 & 0.519 & 0.786 & 0.570\\ 0.879 & 0.944 & 0.525 & 0.815 & 0.609\\ 0.918 & 0.975 & 0.530 & 0.842 & 0.627\\ 0.932 & 0.987 & 0.539 & 0.853 & 0.661\\ 0.937 & 0.984 & 0.549 & 0.878 & 0.697\\ 0.940 & 0.988 & 0.560 & 0.876 & 0.729\\ 0.950 & 0.980 & 0.569 & 0.899 & 0.741\\ 0.959 & 0.978 & 0.579 & 0.905 & 0.749\\ 0.963 & 0.973 & 0.589 & 0.904 & 0.744\\ 0.961 & 0.966 & 0.600 & 0.896 & 0.737\\ 0.941 & 0.960 & 0.610 & 0.883 & 0.745\\ 0.922 & 0.955 & 0.622 & 0.869 & 0.749\\ 0.890 & 0.980 & 0.631 & 0.888 & 0.735\\ 0.848 & 0.935 & 0.650 & 0.833 & 0.699\end{bmatrix} \quad (2)$$

In the Equation (2): $u_{rj}=\sum_{k=1}^{5}\alpha_k a_{jk}$, a_{jk} is the a_j index of each working period. The weight vector of principal component analysis can be obtained through the calculation:

$$W=[0.238,0.203,0.114,0.236,0.209] \quad (3)$$

5）According to the formula (1), the corresponding objective function values of diameter of different circular circles are calculated. The results are shown in Fig. 4.

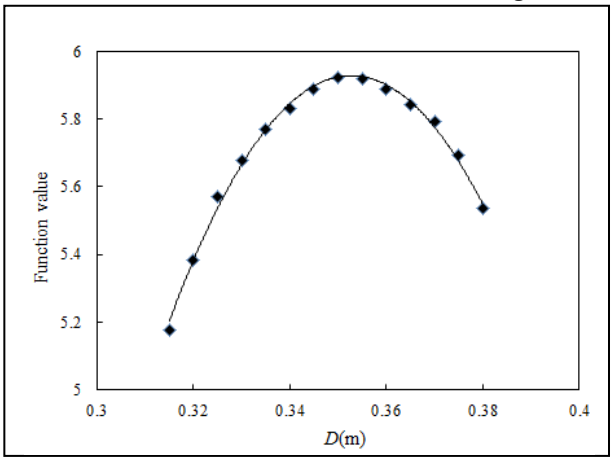

Figure 4. Corresponding relationship of D Values with objective function values

According to the Fig. 4 we can see that when D =0.350m, the matching performance of hydraulic torque converter and engine is optimal.

TABLE II. CALCULATION VALUES OF EVALUATION INDICATORS BEFORE AND AFTER OPTIMIZATION

Evaluation indexes	Before optimization	After optimization	Increased proportion (%)
A_{11}	0.902	0.935	33.7
A_{12}	0.982	0.985	16.7
A_{13}	0.51	0.54	6.1
A_{14}	0.82	0.886	36.7
A_{15}	0.579	0.667	20.9
A_{21}	0.982	0.997	83.3
A_{22}	0.975	0.967	-32
A_{23}	0.611	0.641	7.7
A_{24}	0.922	0.934	15.4
A_{25}	0.884	0.879	-4.3

According to the table II, we can see that after optimization, the matching performance of all is improved to some extent except a_2. In the optimization process, the gap between the function value and the ideal value is decreased gradually. We can use the following formula to calculate the degree of improvement of matching performance before and after the optimization:

$$y = \frac{f' - f}{f^{\max} - f} \tag{4}$$

In the Equation (4): f and f' are the function values before and after the optimization respectively; $f^{\max}$ is the ideal value. By using the upper calculation, after the optimization, the overall matching performance is increased by 7.4%. The performance evaluation radar map for the performance evaluation of the engine and the hydraulic torque converter is shown in Fig. 5.

V. ACKNOWLEDGMENT

The work reported in this paper is supported by the National Key Technology Research and Development Program of the Ministry of Science and Technology of China (Grant No. 2013BAF07B04)

VI. CONCLUSION

This paper utilizes the improved radar chart method to optimize the matching performance of hydraulic torque converter and engine and links up the interaction of multiple dimensionless evaluation indexes. The angle of each sector also embodies the importance of different indexes and avoids the irrationality of equal distribution. After the optimization, the overall matching performance can be increased by 7.4%. The results show that it is effective and feasible to adopt the improved radar chart method to evaluate and optimize the matching performance of hydraulic torque converter and engine and also it can provide the reference for the selection of matching schemes.

REFERENCES

[1] Y. Chen, X.K. Chen, and Y. Lin,"Application of improved radar chart evaluation method on evaluation of automobile comprehensive performances,"Journal of Jilin University (Engineering and Technology Edition), vol.41, pp.1522-1526, 2011.

[2] H.R. Wu, L. Feng, and H.S. Zhang,"Computer aided calculation of matching between engine and hydraulic torque converter," Proceedings of 2010 2nd International Conference on Future Computer and Communication, Wuhan, 2010, vol. 2, pp. 6-9.

[3] J. Murin,"Some properties of a diesel drive line with hydrodynamic torque converters of the latest generation,"Mechanism and Machine Theory, pp. 99-117, 2005.

[4] K. Chen, and G.Q. Wu,"Genetic algorithm-based multi-objective optimization for the matching of torque converter with engine, "Automotive Engineering, vol.36, pp. 532-536, 2014.

[5] L. Chang,"Optimization of power matching on torque-converter with diesel engine for wheel loader, "Transactions of the Chinese Society for Agricultural Machinery, vol.41, pp. 25-29, 2010.

[6] C.F. Li, H.Y. Chen, and G. Tao, et al,"Arithmetic of the cooperating point of engine and torque converter,"Transactions of the Chinese Society for Agricultural Machinery, vol.40, pp.11-15, 2009.

[7] L. Chang,"Optimization of power matching on torque-converter with diesel engine for wheel loader based on performance evaluation mesh figure,"Transactions of the Chinese Society of Agricultural Engineering, vol. 28, pp.50-54, 2012.

[8] Q.D. Yan, S.C. Liu, and W. Wei, et al,"Evaluation for matching between hydrodynamic torque converter and engine based on improved radar chart method,"Journal of Jilin University (Engineering and Technology Edition), vol.46, pp.1510-1516, 2013.

[9] D.K. Elif, and G. Züal,"The usability analysis with heuristic evaluation and analytic hierarchy process,"International Journal of Industrial Ergonomics, vol. 39, pp. 934-939, 2009.

[10] R. Banuelas, and J. Antony,"Modified analytic hierarchy process to incorporate uncertainty and managerial aspects,"International Journal of Production Research, vol.42, pp. 3851-3872, 2004.

[11] M.F. Qi, Z.G. Fu, and Y. Jing, et al,"A comprehensive evaluation method of power plant units based on information entropy and principal component analysis,"Proceedings of the CSEE, 2013, vol. 33, pp. 58-64.

[12] P.C. Qiao, and Z.G. Wu,"Power quality synthetic evaluation based on improved radar chart," Electric Power Automation Equipment, vol.31, pp. 88-92, 2011.

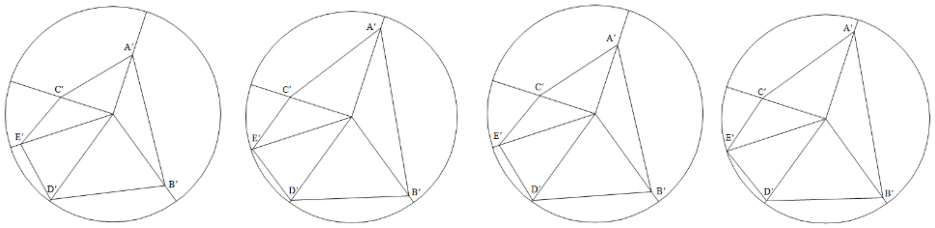

Figure 5. The radar map of engine and torque converter matching performance evaluation of before and after optimization

Optimal Waveform Design for Smart Jamming Focused on CA-CFAR

Xia Xingyu
Luoyang Electronic Equipment Test Center of China
Luoyang, China
13383886001@163.com

Yan Li
Luoyang Electronic Equipment Test Center of China
Luoyang, China
wispyl@163.com

Hao Daoliang
Luoyang Electronic Equipment Test Center of China
Luoyang, China
dearlord@live.com

Wang Xiaoyang
Luoyang Electronic Equipment Test Center of China
Luoyang, China
xywang_2016@163.com

***Abstract*—Focused on CA-CFAR anti-jamming mechanism, the method of optimal waveform design is studied to increase detection threshold for reducing true target detection, which can also improve the detection rate of false targets. Based on the relationship of signal to interference (ISR) and reference distance, the amplitude of jamming waveform is designed to follow Rayleigh distribution and finite interval random, and the interval is designed as random interval based on minimum interval. In addition, the interference region is designed as dense false targets region and sparse false targets region. Through modeling and simulation of CA-CFAR and smart jamming, the method of designing optimal waveform is explored, which will provide reference for other related waveform design.**

Keywords-CA-CFAR; Smart jamming; Waveform design; False alarm probability

I. PREFACE

CFAR is designed to suppress false alarms caused by different noise, clutter, or ECM, which can be used to enhance the performance of a threshold or gain control device. CFAR detection performance is directly related to the background clutter distribution type. When the CFAR detector and the clutter distribution type match it can ensure good detection performance, otherwise it will lead to a serious loss of CFAR or high false alarm probability. When the background clutter follows the Rayleigh distribution, the mean class, OS class and adaptive CFAR detection method can get better detection performance[1-2].

II. CA-CFAR MECHANISM

When χ^2 is used to testify the clutter distribution type, it is necessary to know the distribution function of the clutter. First, the parameters of the clutter distribution should be estimated with the samples. The probability density of the Rayleigh distribution is:

$$f(x)=\frac{x}{\sigma^2}\exp(-\frac{x^2}{2\sigma^2}),x\geq 0 \qquad (1)$$

where σ^2 is average power of the clutter. The parameter σ of the distribution is estimated from the observation sequence x using the moment estimation method. The estimated value is

$$\sigma=(\frac{2}{\pi})^{\frac{1}{2}}\frac{1}{N}\sum_{i=1}^{N}x_i \qquad (2)$$

A. CA-CFAR Constant False Alarm Mechanism

The clutter interference environment assumed by the CA-CFAR detector is that the probability density function of clutter amplitude after detection follows the Rayleigh distribution.

The specific method is to use a digital shift register tapped delay line to obtain output x of the detection cell and output x_i of N reference cells simultaneously. The output x_i of reference cells averaged to obtain estimates of the average, with the output x of the detected cell is divided by the valuation of the average value, to complete the normalization. The result is independent of the clutter amplitude, so we can get constant false alarm processing effect[3-5]. The schematic diagram is shown as Fig .1.

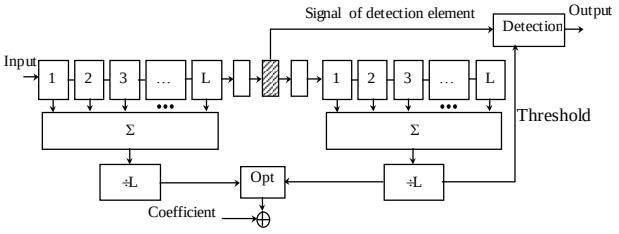

Figure 1. Example of a ONE-COLUMN figure caption.

The maximum likelihood estimate is the average of the known samples which is obtained by derivation, see (3). The expression of the final detection threshold is (4).

$$\hat{\beta}^2=\frac{1}{N}\sum_{i=1}^{N}x_i \qquad (3)$$

$$\hat{T} = \frac{\alpha}{N}\sum_{i=1}^{N} x_i \tag{4}$$

We can get the false alarm probability as (5) and the product factor as the (6) after derivation.

$$\bar{P}_{fa} = \int_{-\infty}^{\infty} e^{-\frac{\hat{T}}{\beta^2}} p_{\hat{T}}\left(\hat{T}\right) \mathrm{d}\hat{T} = \left(1+\frac{\alpha}{N}\right)^{-N} \tag{5}$$

The required threshold product factor to a given expected mean false alarm probability is

$$\alpha = N\left(\bar{P}_{fa}^{-\frac{1}{N}} - 1\right) \tag{6}$$

The average false alarm probability $\bar{P}_{fa}$ does not depend on the actual jamming noise power, but only on the average number N of nearby neighbor samples and the threshold product factor α. Therefore, CA-CFAR technology shows the characteristics of constant false alarm probability.

B. CA-CFAR Simulation in Clustering

Condition setting: clutter signal follows the Rayleigh distribution, the number of reference cells is 20, the number of protection cell is 3, the detection cell is 1, the false alarm probability is 10^{-3}. The detection threshold variation is obtained by the constant false alarm processing to the collection data, as shown in Fig .2. The suppression effect of CA-CFAR on clutter is obvious.

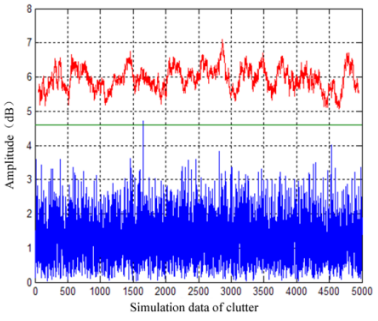

Figure 2. CA-CFAR Simulation in Clustering.

III. SMART JAMMING WAVEFORM DESIGN AND SIMULATION OF CA-CFAR COUNTERMEASURE EFFECT

Smart jamming, a new type of jamming besides barrage jamming and deception jamming, can get bigger radar processing gain due to its consistency with radar signal, which has been widely concerned and studied, and has been developed and progressed rapidly[9-10]. This paper focuses on the study of smart multiple false-targets jamming and waveform optimization. For the traditional or existing jamming mode, how to go beyond their defects and drawbacks in countering CFAR, bringing the new processing methods into the smart jamming and improving the performance of smart jamming is the goal of this study.

A. Smart Jamming Waveform Design

The false target group is generated dynamically, amplitude of which is follow the Rayleigh distribution.The false target group is divided into sparse region, dense region, sparse region three parts and designed respectively. The dense false target region is mainly used to enhance the threshold suppression target. The sparse false target regions mainly provide the multiple false targets threshold. The false target Interval is set to more than 8 times the length of the radar distance resolution, and frequency shift range is set to megahertz level. Waveform model is shown as (7).

$$F(T,S,P) = \begin{cases} S_i >= S_0 \,\&\, P_i >= P_0, \forall T_i < T_{m-j} \\ S_i <= S_0 \,\&\, P >= n * P_0, n > 2, \forall T_{m-j} < T_m < T_{m+j} \\ S_i >= S_0 \,\&\, P_i >= P_0, \forall T_i > T_{m-j} \\ P_i \sim raylrnd \,\&\, \sum_{i=1}^{N} P_i = P_{jam} \end{cases} \tag{7}$$

where S is the false target interval; P is the false target power; P_0 is the radar detection sensitivity; S_0 is the equivalent of the radar distance unit; T_m is the target position; N is the false target quantity; n is the power product factor.

B. Influence of Random Properties on Waveform Design

Condition setting: The radar signal is LFM signal; the smart jamming waveform on time domain after pulse compression is shown in Fig .3; there are 20 reference units, 3 protection units and 1 detecting unit; the false alarm probability is 10^{-3}. The target's echo signal and the jamming signal is dynamically generated. The number of fake targets is around 100 while the real target is in the middle of the fake targets.

The influence of interval stochastic on waveform design: The interval of fixed interval false targets varies from 80 to 200 with successive increments. By contrast, the interval of random interval false targets is the minimum interval plus a random increment, and the smallest interval also changes from 80 to 200 with successive increments. When the interval is 100, the effect of random false targets with fixed intervals and the ones with minimum interval on CFAR is illustrated in Fig .3. We can see that the false targets with fixed interval will raise the detecting threshold and the false target cannot be detected. While the false targets with stochastic characteristic can not only raise the threshold of detecting, but also disturb radar's detecting for some false targets can pass the detection threshold.

As the interval increases until reaching up to 170m, the random characteristics of smart jamming false targets are more obvious than ones of fixed interval. However, when the interval is larger than a certain distance, the validity of the fixed interval and the random interval will be similar to the same.

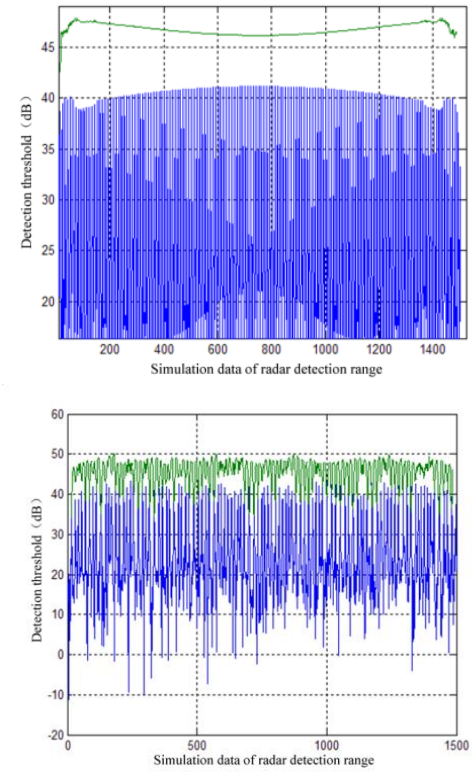

Figure 3. Simulation of the effect of fixed and random interval false targets on CFAR.

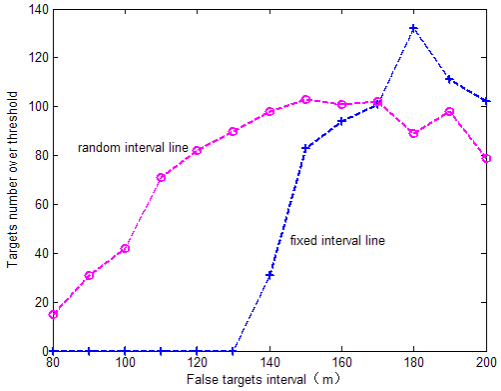

Figure 4. Comparison of the effect of fixed and random interval false targets on CFAR.

Influence of energy stochastic on waveform design: As is shown in Fig .5, the false targets of fixed interval and equal amplitude can restrain the CFAR as well as raise the threshold of detecting, but false targets cannot pass the detecting threshold. When the amplitude has stochastic characteristics, some false targets will pass the detecting threshold and achieve the effect of suppression. However, with the increase of false targets' interval, the amplitude stochastic characteristic is below equal interval, for the amplitude of the sharp signal decreases as the increase of interval, resulting in the reduction of the number of false targets which pass threshold.

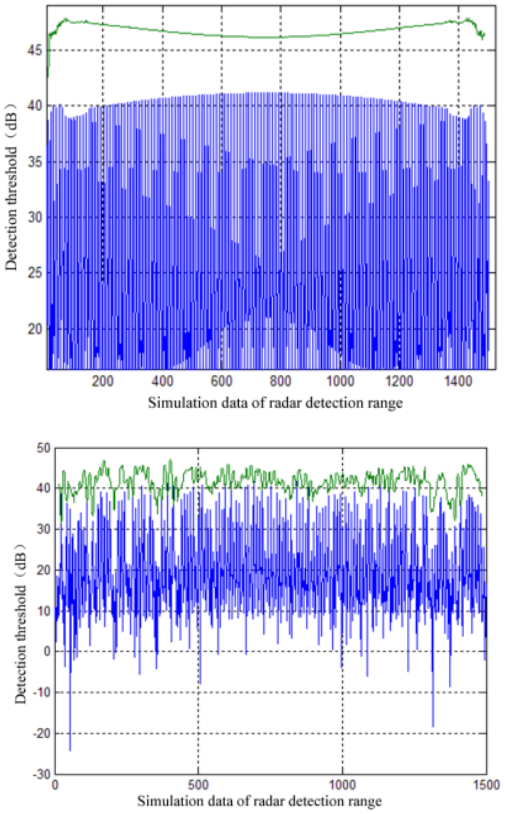

Figure 5. Parity and random amplitude false targets pass CFAR.

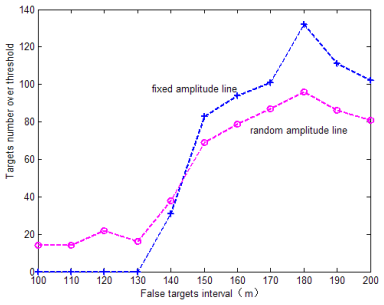

Figure 6. Comparison of CFAR performance between parity and random amplitude false targets.

C. *Modeling and effect analysis of confrontation CA-CFAR*

Simulation of sparse/dense partitioning settings and under different noise-signal ratio: When the noise-signal ratio is -40dB or 20dB, the sparse and dense false targets jamming area are set up and waveform are shown in Fig .7. The threshold after the CA-CFAR sliding window is shown in Fig .8.

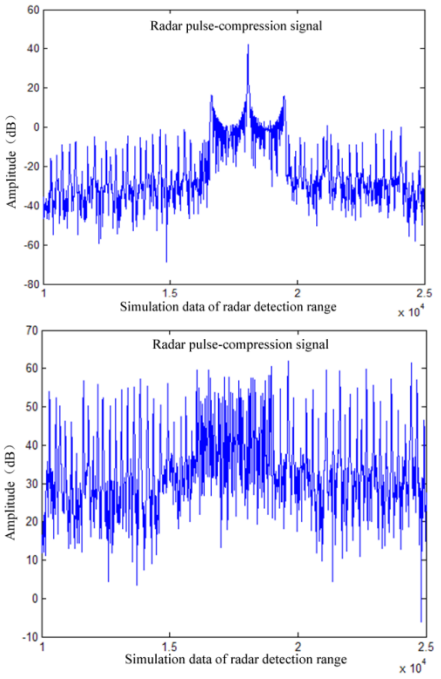

Figure 7. Waveform under the condition that noise-signal ratio is -40dB and 20dB respectively.

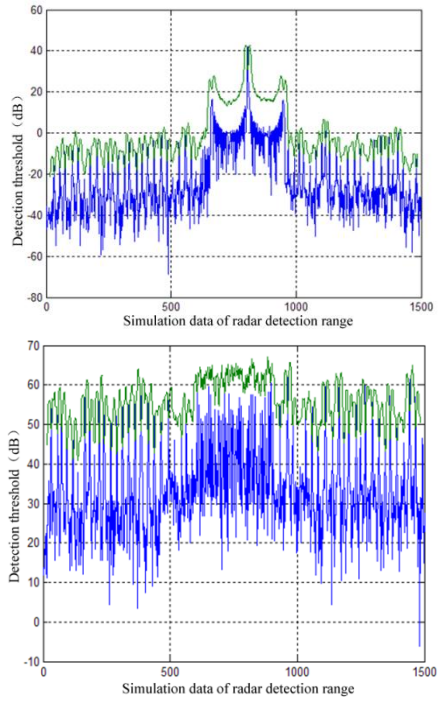

Figure 8. CFAR sliding window detection threshold under the condition that noise-signal ratio is -40dB and 20dB respectively.

Simulation results show that the dense area can elevate threshold after distinguishing dense and sparse false targets' setting, while the sparse area increases the false targets' number which pass the threshold and has the jamming effect.

Simulation of minimum interval under stochastic span condition: The minimum intervals of the dense zone false targets vary from 80m to 150m, while which of sparse zone vary from 150m to 200m. Noise-signal ratio changes from -40dB to 20dB. The number of false targets is illustrated in Fig. 9. We can see that in each definite interval, the number is basically maintained at a relatively stable order of magnitude. As the internal increases, the number presents an incremental trend.

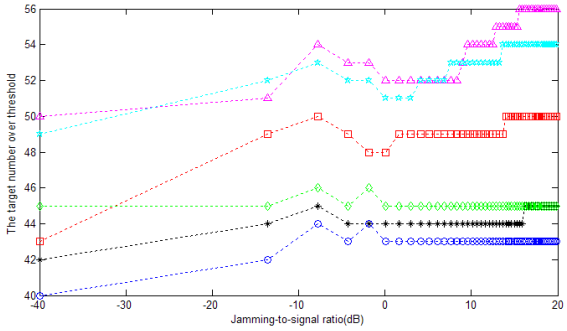

Figure 9. Simulation of the number of false targets passing threshold under the condition that false targets have a random span.

Through the above dense area and sparse area simulation we can see that dense false targets mainly have the effect of raising the threshold of detection, while sparse areas can make a large number of false targets pass the threshold, resulting in suppressing real targets.

Simulation of jamming effect under comprehensive condition: By using Monte-Carlo simulation, we can obtain statistical results of the number of real target passing CA-CFAR threshold. Then we can obtain its quantity in different noise-signal ratio under condition of sparse area and dense area false targets' interval, as shown in Figure 10. We can see that in order to achieve a better suppressing effect, the noise-signal ratio should be larger than 5dB. In the dense area, the false targets's interval should be about 8 times times the radar distance resolution, while in the sparse area it should not be less than 15 times.

IV. CONCLUSION

Based on the relationship of signal to interference (ISR) and reference distance, the amplitude of jamming waveform is designed to follow Rayleigh distribution and finite interval random. Then, the interval is designed as random interval based on minimum interval and the interference region is designed as dense false targets region and sparse false targets region. The jamming waveform design method can break through the uniformity of the false targets to resist the time trap technology, which will generate realistic interference effect. Meanwhile, this method can change fixed amplitude to random, which will not only cause the false targets through detection threshold to increase false alarm probability, but also raise the detection threshold to suppress real target.

REFERENCES

[1] Bassem R.Mahafza, Atef Z.Elsherbeni, MATLAB Simulations for Radar Systems Design, Beijing: Publishing House of Electronics Industry, 2016.

[2] HE You, GUAN Jian, MENG Xiangwei, Radar Target Detection and CFAR Processing, Beijing: Tsinghua University Press, 2011.

[3] Mark A.Richards, Fundamentals of Radar Signal Processing, Beijing: Publishing House of Electronics Industry, 2010.

[4] QI Xiaohui,LU Dan,JIN Tao, "Improved Signal Detection Method Based on CFAR at Active Jamming Background", Science Technology and Engineering, vol.12, No.18,pp.4413–4417, Jun 2012.

[5] Yuan Hui, Tao Jianfeng, An Le, "Two CFAR Detectors Based on Cell Selection", Computer Measurement &Control, vol.21,pp. 1057-1059, April 2013.

[6] YANG Yong, FENG Dejun, XIAO Shunping,"Impact Analysis of CFAR Detection for Dense Multiple False Targets Jamming", Moden Defence Technology,Vol.41,No.1, pp. 126-130,Feb 2013.

[7] WANG Teng, XU Xiang-dong, FAN Congwang, QIN Zhenjie", Performance Analysis of CA-CFAR Detector Under Two Detection Modes", Journal of Air Force Radar Academy, Vol.23, No.5, pp. 356-358, Oct. 2009.

[8] FENG Dejun, YANG Yong, XU Letao, "Impact analysis of CFAR detection for active decoy using interrupted-sampling repeater" , Journal of National University of Defense Technology, vol.38, No.1 pp.63–68, Feb.2016.

[9] MENG Yueyu, WU Hu, CHENG Siyi, CHI Jianing, "Effecticeness evaluation of smart noise jamming against active radar seeker", Journal of Projectiles, Rockets, Missiles and Guidence vol. 35, pp. 173–176, Feb 2015.

[10] DAI Xiaojun, XU Caihong, "computer simulation of jamming PD radar", Modern Electronics Technique, vol.35, pp.39–41, Sep 2013.

Research and Implementation for a class of Large-Scale Full-Range Power System Real-Time Simulator

Gu Wei
Electric Power Research Institute of Guizhou Power Grid Co., Ltd
GuiYang, China
215669483@qq.com

Zhang Yan
China Electric Power Research Institute
Beijing, China
zhangyan2010@epri.sgcc.com.cn

Wang JiHua
Beijing Sifang Automation Co., Ltd.
Beijing, China
wangjihua@sf-auto.com

Gui JunGuo, Xu MeiMei
Electric Power Research Institute of Guizhou Power Grid Co., Ltd
GuiYang, China
215669483@qq.com, xumemei_1986@163.com

***Abstract*—In order to realize intensive research and analysis of the whole bulk power system, which contains all electronic elements not only includes generator, electronic grid system, but also includes power generation system, based on the thermodynamics and dynamics theory in power generation system and the electromechanical and electromagnetic transient theory in electronic grid system, we established a class of Large-Scale Full-Range Power System Real-Time Simulator (LFPSRS). The definition of LFPSRS is given, structure of the emulated objects is described, and physical and logical structures of LFPSRS are listed. Finally, the experiment results prove that the system is superior to the traditional simulation system. We confirmed that the proposed LFPSRS can play a major role in the further research on the whole bulk power system.**

Keywords-component; power system; RealTime; simulator; transient theory; coordination

I. INTRODUCTION

With the increasing of the power supply capacity in modern power system, the dynamic and static processes of power generation units have more and more important influence on the stability of power system. Power plants and power grids are be interdependent, mutual effect, the unity of opposite's entirety. The coordination control management between power plants and power grids has become an important issue that directly affects the security and stability of power systems. Therefore, it is a complex interdisciplinary issue that must be paid more attention in the development of large units and large power grids [1-3].

High fidelity simulator is an important tool for analyzing coordination problem in power system [4-6]. It is also an important basis for power grid dispatcher to determine the power grids operation mode, guide the power plants to increase or decrease load. The isolated power station simulator or the power grid simulator which is independent of power generation units cannot meet the needs of the research on the above problems. The establishment of Large-Scale Full-Range Power System Real-time Simulator with high reliability has become a research direction in the industry.

This paper introduces the limitations of the traditional power station and power grid simulation system firstly. Then we put forward the definition of a class of Large-Scale Full-Range Power System Real-Time Simulator. Immediately following the background, the framework of emulated objects structure, and the framework of physical and logical structure of this simulator are listed. A simulator is implemented, and an example is done to verify the effectiveness of this simulator. Finally, conclusion and prospect are given.

II. LIMITATIONS OF TRADITIONAL SIMULATOR

A. Power Plant Simulator

At present, the calculation environment of common power plant simulator, which is running in power plants, power companies or power training schools in China, is a common computer or a server computer with slightly higher performance. Considering the computing environment and the mathematical model size of the simulator for a whole power plant, the calculating step length for power plant simulator is in millisecond class. [7-8]

Taking the common thermal power station as an example, the power station simulation system is usually divided into four parts: boiler, turbine, generator and power grid. The mathematical model of boiler is based on thermodynamics theory whose calculating step length is always between 100ms~200ms. The mathematical model of turbine is based on dynamics theory, and its calculating step length is always between 50ms~100ms. Similarly, the calculating step length of the mathematical model for generator, power grid, which

is based on electromechanical and electromagnetic steady theory, is always between 10ms~50ms.

The simulator with the above computing environment is sufficient for power plant staff training, but it is insufficient for special researcher in power grid or generator. Such as, getting the instantaneous value of the system is impossible based on the above simulator.

B. Power Grid Simulator

Power system simulator, in a narrow sense, is refer to the simulation system of power grid. Although its running environment is varied, there are some common features in their system, such as, the basic theory is multi CPU parallel processing technology, and the performance of system depends on software instead of hardware, if the calculation step length and the bandwidth of I/O equipment is enough to meet the requirements. The system is designed on the basis of electromechanical transient and electromagnetic transient theory. The simulation calculation step length is all in microsecond class [9-10].

Take some current power grid simulator at home and abroad for example. The RTDS system, software of Canadian RTDS Company, use one CPU to simulate one power system component, the communication between CPUs is in parallel-serial-parallel mode. The digital simulation system (ARENE), developed by the French electric power company (EDF), takes the hardware, HP multi CPU parallel processing computer which is based on the HP-CONVE workstation, as its simulator calculation environment.

Grid simulation system can simulate more accurately transient changes of power system than traditional power plant simulator. Thus, not only effectively simulate the can be displayed in the system, but also the wave of instantaneous value can be generated too. Because the simulator is independent of dynamic power supply terminal simulation data, the simulator cannot make fully analysis of generalized bulk power system.

Combining the above two traditional simulation systems, it is necessary to build a high precision and large-scale power plant and power grid simulation system.

III. DEFINITION AND FRAMEWORKS OF LFPSRS

A. Definition

The Emulated objects range of Full-Range Power System Real-Time Simulator (FPSRS) includes prime mover, generator, power grid and other important components. Each component of the system is translated into digital mathematical simulation model, and it is implemented in their respective computing units by parallel mode. The high frequency communication interface between the computing units is used to realize the real-time data communication of each mathematical simulation model. The running simulator can deal with the external disturbance in time and achieve real-time operation effect. Considering the factors of thermodynamic theory, the calculation step length of prime mover model should be kept in milliseconds class. Considering the theory of electromechanical and electromagnetic, the calculation step length of generator and power should be kept in microsecond level.

When there are more than one set of prime mover model in the whole power grid model, and the running state of the system will interact with each other, the system constitutes a Large-Scale Full-Range Power System Real-Time Simulator (LFPSRS).

B. Framework

The framework of emulated objects in our simulator is listed briefly in Fig.1. The system is divided into power plant side and power grid side, which including all elements in the power system, some important elements are especially listed in the graph, such as power grid, generator, and prime mover. The icon of prime mover is displayed in brief with a turbine icon. In fact, according to the characteristic of different power plants, the prime mover may be boiler, steam turbine, water turbine, fan and so on.

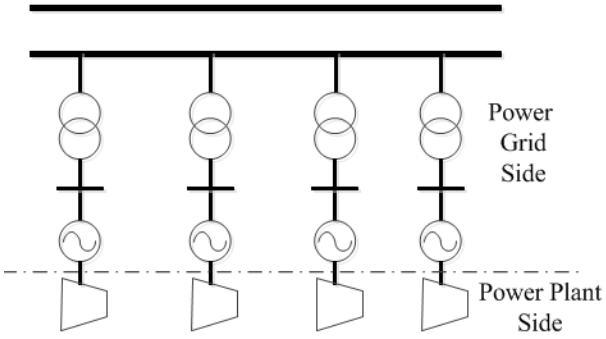

Figure 1. Framework of emulated objects stucture in LFPSRS

The physical structure of the simulator is shown as follows. The prime units in the simulator are model storage unit, model calculation unit, history backup unit, control area unit, and other physical interfaces, and so on. All the units communicate with each other via Ethernet.

The model storage unit contains all the models involved in the system, including prime mover, generator, transformer, power grid and so on. The calculation unit is running in parallel computing way, and then exchanges data through high speed communication protocol.

The processing power of the computing engine is divided into several levels. For example, some part of the engine can finish all calculation in millisecond level, which is designed for thermodynamics and dynamics model, and some done in microsecond level, which is used for electromechanical and electromagnetic transient model.

The control units provide storage space for all monitoring related files, display the monitoring interface, receive all the operation command and get and send to computer screen the result of request of operator etc. In short, this is the control center of the whole system.

The historical station unit is responsible for storing important experimental historical data. Other physical interface units leave space for subsequent access to other systems.

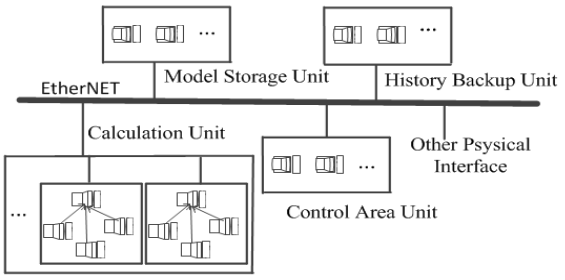

Figure 2. Framework of physical stucture of LFPSRS

The logical structure of the system is shown as follows. The bottom layer is the data module zone, which includes power plant database, power grid database and some user configuration files. The intermediate layer stores various models, such as, boil, turbine, primary system, secondary system and other computer configuration content. The top layer includes control engines and view methods of our system. For example, energy and flow balance calculation, transient calculation, stability calculation and some analysis in simulator.

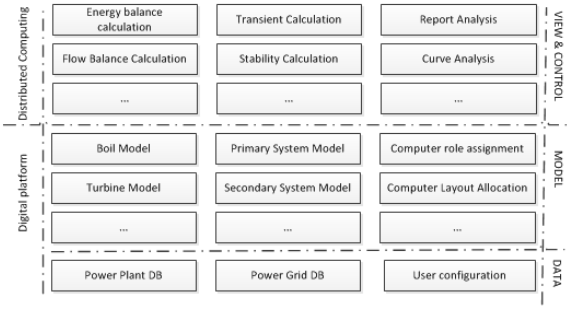

Figure 3. Framework of logical stucture of LFPSRS

IV. Implementation of LFPSRS

Based on the above theoretical foundations, a Large-Scale Full-Range Power System Real-Time Simulator is built successfully for Electric Power Research Institute of GuiZhou Power Grid Co., Ltd. In this simulator, the mathematical model of prime mover is implemented on CyberSim platform, simulation software developed by Beijing Sifang automation Co., Ltd. At the same time, the mathematical model of power grid and generator are running on Advanced Digital Power System Simulator (ADPSS), which is a digital simulation system developed by China Electric Power Research Institute. The simulator is a part of technology project (GZ2015-1-0001) in Guizhou Power Grid Co., Ltd.

We have done the following experiment on the above platform to verify the effectiveness of the system.

The real accident occurred in October 12, 2011. A cross road hard connecting pipe, between a switcher B phase and a current transformer on a bus line, fell off from the original position. The underside end of pipe affixed to the ground, the upper end is leaning on the porcelain bottle of switch port. Then one power plant triggered bus differential protection.

The fault phenomena are simulated and tested on the simulation system, and the results are shown as follows. In order to keep the simulation wave sit at the same start point on time axis to the wave of real system, we set the real system's wave start time on axis to zero, and make the time axis unit to millisecond.

The graph above and graph below in Fig.4 show the bus voltage waves from real system and simulator respectively.

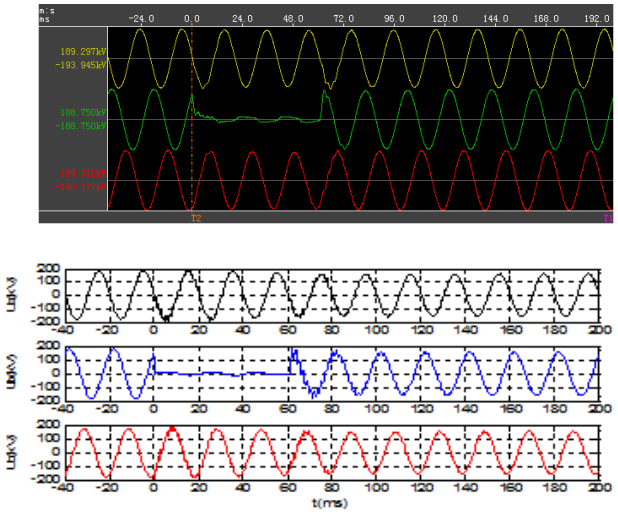

Figure 4. Voltage waves from real system and simulator

The graph above and graph below in Fig.5 show the bus current waves from real system and simulator respectively.

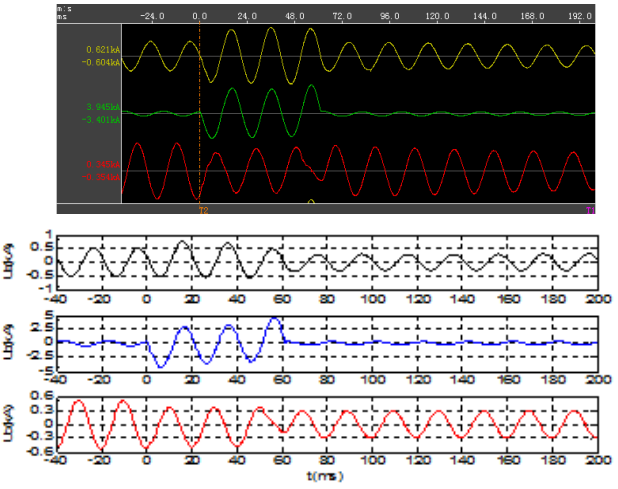

Figure 5. Current wave from real system and simulator

As shown in above graph, the voltage and current wave, which are drawn according to the result from LFPSRS, are similar to the recorded waves, which are collected from the real power system accident scene.

V. CONCLUSION

Considered the present research on the bulk power system, and combined with the characteristics of power plant part and power grid part respectively, we designed and implemented a class of Large-Scale Full-Range Power System Real-Time Simulator. This simulator has successfully solved the problems that previous conventional power plant simulation system cannot realize the instantaneous value of the system, and the traditional grid simulation system cannot demonstrate the relation with generator units. It provides a new research method for bulk power system research.

In this system, researchers can study in the coordination control management problem for bulk power system, and they can make a research on peak load adjustment mechanism for power plants, even for energy storage dispatch of wind energy, water energy and solar energy, and so on. In short, the LFPSRS simulator can play an important role in the research of bulk power system in the future.

REFERENCES

[1] Vipul N. Rajput, Kartik S. Pandya. Coordination of directional overcurrent relays in the interconnected power systems using effective tuning of harmony search algorithm [J]. Sustainable Computing: Informatics and Systems, 2017, 15(9): 1-15.

[2] Chao-Rong Chen, Cheng-Hung Lee, Chi-Juin Chang. Optimal overcurrent relay coordination in power distribution system using a new approach [J]. International Journal of Electrical Power & Energy Systems. 2013, 45(1): 217-222.

[3] Kehe Wu, Huan Zhou. A multi-agent-based energy-coordination control system for grid-connected large-scale wind–photovoltaic energy storage power-generation units [J]. Solar Energy. 2014, 107(9):245-259.

[4] Udo Spanel, Carsten Roggatz. DUtrain Power System Handler - the movement of an Operator Training Simulator Prototype towards an Operational Training System [J]. IFAC-PapersOnLine, 2016, 49(27): 170-177.

[5] Celis C, Pinto G R S, etc. A Steam Turbine Dynamic Model for Full Scope Power Plant Simulators [J]. Applied Thermal Engineering, 2017, 120(25): 593-602.

[6] R. Razzaghi, M. Mitjans, F. Rachidi, M. Paolone. An automated FPGA real-time simulator for power electronics and power systems electromagnetic transient applications[J]. 2016, 141(12):147-156.

[7] Lv ChongDe, Ren TingJin, Jiang XueZhi, etc. System simulation and modeling of large thermal power unit [M]. BeiJing:Tsinghua University Press. 2002 (in Chinese).

[8] Wang ZhengYi, Modeling Simulation and Optimal Control of Combustion Control System on Large-scale Thermal Power Unit [D], BeiJing: North China Electric Power University, 2016(in Chinese).

[9] CHEN Lei, ZHANG Kanjun, XIA Yongjun, HU Gang. Electromechanical-electromagnetic transient hybrid simulation on HVDC power transmission system based on ADPSS [J]. Power System Protection and Control. 2013 41(12) :136-142 (in Chinese)

[10] Song Yankan, Chen Ying, Huang Shaowei, etc. Electromagnetic transient parallel simulation algorithm and implementation for large-scale power system[J] . Electric Power Construction , 2015 , 36(12) : 9-15(in Chinese).

The Design and Research of Intelligent Search and Rescue Device Based on Sonar Detection and Marine Battery

Zhao Jian
Mechanical and Electrical Engineering Institute
Qingdao Binhai University
Qingdao, China
e-mail: 8431062676201691@qq.com

Zheng Li-nan
Mechanical and Electrical Engineering Institute
Qingdao Binhai University
Qingdao, China
e-mail: 1021090387@qq.com

Zhang Liang
Mechanical and Electrical Engineering Institute
Qingdao Binhai University
Qingdao, China
e-mail: 76201691@qq.com

Li Nan
Mechanical and Electrical Engineering Institute
Qingdao Binhai University
Qingdao, China
e-mail: 691525115@qq.com

***Abstract*—With the increasing number of Marine accidents, the task of maritime search and rescue is increasingly difficult. This paper studies a fast, accurate and scientifically valid intelligent equipment which breakthrough maritime search and rescue capability and level for maritime search and rescue. Using sonar detection technology combined with GPS navigation systems and Marine battery energy technology, intelligent search and rescue devices which we designed can quickly search for victims of life information. When the sonar equipment is searched for feedback, the GPS provides precise positioning to achieve accurate rescue. The search and rescue device is powered by Marine batteries, which is environmentally friendly and can be supplied for a long period of time. The Marine intelligent search and rescue equipment is equipped with fast speed and strong resistance to wind and waves, which have a long working characteristic and can reach the marine perils area quickly and realize efficient unmanned search and rescue.**

Keywords-Sonar Detection; Marine; Battery; Intelligent; Search and Rescue Device; Laser gyroscope; product design

I. INTRODUCTION

Maritime search and rescue is refers to the search and rescue operations taken by any maritime rescue force after obtaining maritime distress information in addition to the ship, which consists of two parts: maritime search and maritime rescue. Maritime search is refers to actions coordinated by the rescue coordination center or the rescue sub-center to utilize existing personnel and facilities to determine the position of the person in distress. Maritime rescue is refers to the rescue of any person in distress by any salvage force that can be used to provide initial medical care or other required services and to brought to safety place[1].Due to the continuity of sea search and maritime assistance in working hours and content, these two tasks are often referred to as sea search and rescue or referred to as maritime search and rescue.

II. THE PRESENT SITUATION OF THE TECHNICAL EQUIPMENT OF MARINE SEARCH AND RESCUE AT HOME AND ABROAD

The experience of the developed countries in the world shows that the perfect maritime search and rescue system and advanced equipment and facilities have a decisive role in ensuring maritime safety. After years of efforts, China's maritime search and rescue system construction has made great achievements, equipment level and search and rescue capabilities have been strengthened, China's maritime traffic safety situation improved significantly, the number and extent of ship traffic accidents were continue to decline[2]. However, we should also clearly see that the current situation of China's maritime traffic safety improved, mainly rely on administrative orders, insistent prevention and other measures to obtain. Management and rescue methods are extensive and costly.

Intensive, scientific and advanced, long-term maritime search and rescue system has not established yet, the maritime traffic safety situation is still preliminary and unstable. The number and quality of maritime search and rescue infrastructure and equipment, the ability to rescue the accident, especially the fast and effective rescue ability in the case of big waves, are also far from being able to adapt the development of social and economic and the demand of people's quality of life to improve, and there is a huge gap with the developed countries. Due to the gap in economic development, there is still a large gap between the technical equipment for maritime search and rescue and the developed countries. Of course, there are significant gaps in the number of search and rescue facilities due to the different functions of search and rescue organizations. The Search and rescue equipment quantity Contrast is shown in table 1.

TABLE I. SEARCH AND RESCUE EQUIPMENT QUANTITY CONTRAST FIGURE

country	Search and rescue equipment quantity			
	Wing plane	*Helicopter*	*small ship*	*Large ships*
China	2	6	28	12
Japan	29	46	350	169
America	150	62	1800	235

China's north sea, the east China sea and the south China sea rescue bureau have 40 existing professional rescue vessels, 18 emergency rescue teams and eight rescue helicopters including fixed wing aircraft. The U.S. coast guard is equipped with 13 large and medium-sized boats with a total of about 1,800 boats, with a total of about 1, 800, and a total of 212 aircraft with 5 fixed wing aircraft and helicopters. Japan's coast guard has 514 boat and 75 aircraft, with 29 fixed-wing aircraft and 46 helicopters. Therefore, the researching on intelligent rescue equipment can be applied to the complex situation and improving our maritime search and rescue capabilities has become the urgent needs to solve a big problem.

III. THE DESIGN AND RESEARCH OF INTELLIGENT SEARCH AND RESCUE DEVICE

In view of these problems， the nobody search and rescue machine has been researched and developed, which is high-performance, high-efficiency, low-cost, fast-to-reach area and long-time work. In this study, the maritime intelligent rescue device, the hull is a three-body structure, including the two wings and the main body. The wings and the main body make up the ocean battery, providing the system with electric energy. The rear of the main body set the propeller to provide propulsion for the rescue device. The storage space in front of the main body placed high calorie compressed food and fresh water. The storage space at the rear of the main body and the storage space of the wings store the life-saving supplies. A sonar detector is arranged above the main body for detecting survivors of the surrounding waters. The main body is also set up a GPS module to provide positioning information for the console. The middle of the main body is also equipped with warning lights. When the sonar detector detects the survivor, the UAV ejects life-saving supplies through the wings of the catapult and open the front of the front cover, and warning lights open at the same time. This intelligent search and rescue device is small, easy to transport, easy to use. The UAV can be used directly into the maritime area for work. This search and rescue device is mainly composed of detector, positioning lights, balance wings, power device, storage space and other structures. The structure and performance of each part will be described in detail below[3-5].Intelligent Search and Rescue Device Structure Chart is shown in Fig. 1.

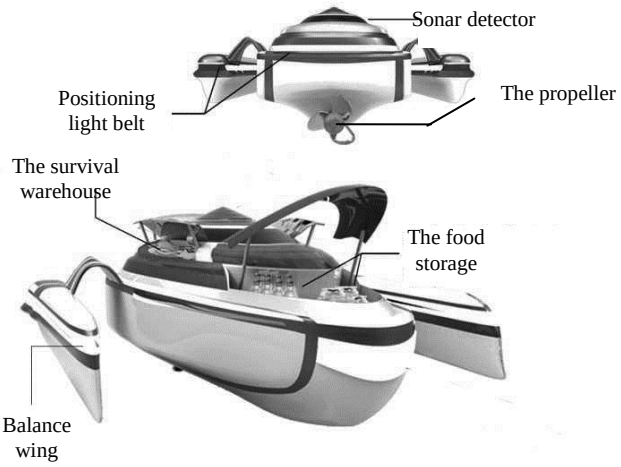

Figure 1. Intelligent Search and Rescue Device Structure Chart

A. *Detector*

Detector is located above the main body. Its role is mainly to detect a range of maritime survivors. The detector uses the active sonar technology to detect the underwater target. The detector can detect the range within one kilometer. It provides broad coverage in order to facilitate the first time rescue. Active sonar technology is refers to the sonar active launch acoustic "irradiation" target, and then receive the water reflection of the target to determine the target parameters. Active sonar technology is most of the use of pulse system, but also the use of continuous wave system[6-7]. It evolved from a simple echo detection instrument, which actively emits ultrasonic waves and then calculates echoes for the detection of survivors of sea floating when a shipwreck occurs. Sonar detection works is shown in Fig. 2.

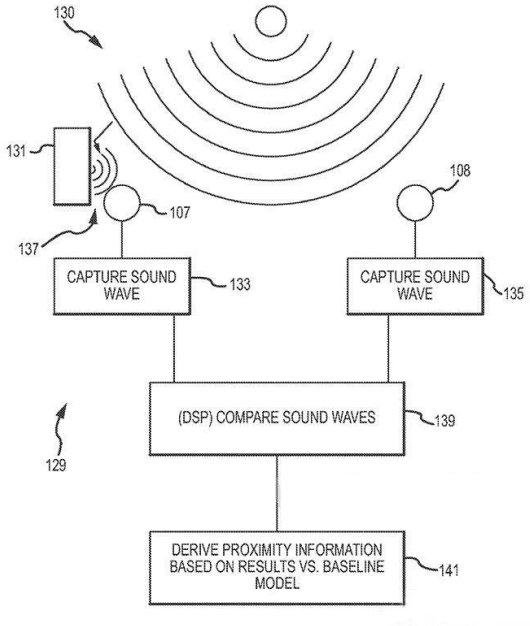

Figure 2. Sonar detection works

B. Positioning light belt

Positioning light belt is based on GPS technical. When the sonar get search feedback, the GPS provide real-time accurate positioning, so as to achieve accurate rescue by the search and rescue device[8]. As the scene of marine perils may be fog, big waves or search and rescue in the evening, as well as wind, flow and other natural factors affect the positioning accuracy will be affected, which led to the scene search is often very difficult. In order to find survivors, distress boats or lifeboats as soon as possible, then it need to locate the exact location to determine the target. The higher the positioning accuracy, the less the search time for the distress, the ship or the aircraft, and the search and rescue device as soon as possible to reach the exact location of distress and carry out search and rescue missions. The initiative rescue terminal of the search and rescue automatically open when the victims were found.

The process of micro-controller(MCU) active help terminal shown in Fig. 3.When the reed pipe conducts, the power supply begins to power the system[9].With MCU electricity self-inspection and the GPS unit power supply, It goes into the running state. After the GPS is on, it start to locate. At the time of the launch, MCU checks the GPS position. If GPS is invalid, it will select the location information stored in the MCU. If the GPS location is valid, it will select the location information of the current GPS. The MCU initiates the RF emission program. With Radio frequency emission module power supply, the MCU provides location data for launch after the modulation of radio frequency emission module. When the data is launched, the system is in low power and prepares for the next time[10].

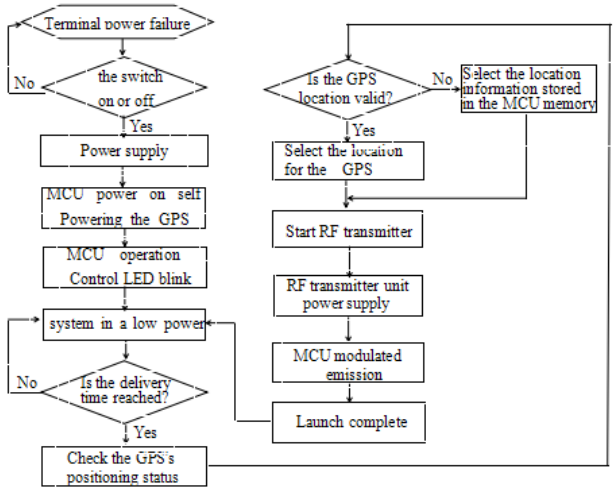

Figure 3. The process of micro-controller(MCU) active help terminal

The terminal positions through the GPS and sends the distress information including their own location coordinates to the nearby rescue ship or maritime rescue center through the maritime emergency rescue channel. Rescue ship quickly arrived at the waters of the waters to search and rescue after receiving the distress information or received the command of the shore command and control center. Under the guidance of the electronic chart, the rescuers can quickly find the staff and rescue them.

C. Balance wing

The balance of the rescuers depends on the wings. It is critical that the search and rescue machine balance on the surface of the water which is adjusted by the precise weight of the design and assembly. The center of buoyancy is above the center of gravity, and they are on the same vertical line. When the pitch and the horizontal, the force will form the recovery moment for the body. Maximizing the distance between the two hearts as much as possible, Its center of gravity is as close as possible to the bottom of the rescuers. The propeller on both sides of the rescuers are responsible for controlling the speed of surface navigation. The rudder plane is responsible for controlling the direction of the rescuers. According to the floating principle of the ship and the principle of the laser gyroscope, the search and rescue devices are always balanced on the surface of the water. The center of gravity and the center of buoyancy are on the same vertical line.

The laser gyroscope is designed to measure the angular velocity of the rotation by using the optical path difference. In a closed light path, two beams of light and light interference from the same source are sent clockwise and counterclockwise[11].By measuring the difference in the phase difference or interference pattern, the rotation angular velocity of the closed light path can be measured. The basic element of a laser gyroscope is a ring laser which made of triangular or square quartz closed optical path. there is one or a few with mixed gas pipe, two opaque mirror and one and a half. A monochromatic laser is produced by a high-frequency power source or a dc power source to excite the mixture. In order to keep the circuit resonant, the perimeter of the loop should be an integer multiple of the wavelength of light wave. A semi-transparent mirror is used to export the laser circuit, which is transmitted by a reflector to the two beams. The digital signal is formed from the Angle of the photoelectric detector and the input and output of the circuit. Because at high speed, the gyroscope's axis is stabilized in the fixed direction. Comparing this direction with the axis of the search and rescue device, the right direction of the search and rescue is accurate. Figure 4. The principle of laser gyroscope works is shown in Fig. 4.

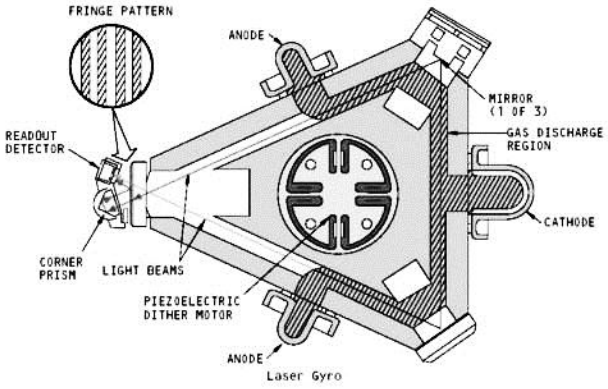

Figure 4. The principle of laser gyroscope works

D. Power plant

The energy for search and rescue devices use Marine batteries. The aluminum plate is negative, platinum is positive, water is electrolyte solution. Oxygen in the air reacts with aluminum that generates electricity. The Marine battery itself contains no electrolyte solution and positive active substance , which doesn't oxidize in the air and can be stored for a long time when the battery doesn't go into the ocean. When it is used, the battery can be turned into water, which is 20 to 50 times higher than the dry battery[12].The battery design cycle can last more than one year, avoiding frequent replacement of the battery. Even if you change it, you just replace a piece of aluminum. The size of the aluminum plate can be determined according to the actual needs.

E. Storage warehouse

The storage warehouse is divided into two parts---the survival warehouse and the food storage. The survival warehouse's position is located on both sides of the search and rescue device, which is stored in a life-saving appliance such as a compressed life jacket and waterproof glasses. The food storage is in the front space of the search and rescue unit, which stores high calorie compression food and fresh water[13].When Search and rescue device searched victims who is living , the survival warehouse was catapulted a life buoy through a catapult which keep the survivors afloat on the surface of the sea. After, the rescuers quickly ran to the survivors which opens storage automatically, and provides basic food and fresh water for survivors. Survivors can wait for ships or planes to rescue them.

IV. THE SEARCH AND RESCUE CAPABILITIES CONTRAST

The search and rescue capability of the ships, planes and ships that are currently available is determined by the search and rescue capability of the country. Search and rescue ability by the current location of the search and rescue individuals, ready to departure time, running speed, battery life, ability to resist the wind and waves, on-scene near and flow velocity, wave, wind speed and direction, air temperature, visibility, and so on factors .Search and rescue command center according to the above information is required, and the location of the object changes, determine the search area, select search and rescue individuals, choose the appropriate search pattern, make a search and rescue plan[14]. The Search and rescue equipment performance Contrast is shown in table 2.

TABLE II. SEARCH AND RESCUE EQUIPMENT QUANTITY CONTRAST FIGURE

	Search and rescue equipment performance		
items	***Rescue Aircraft***	***Rescue Ship***	***Intelligent Search and Rescue Device***
Sea area	Wide	Narrow	Wide
Sea limit	No	Yes	No
Wind and waves affect	No	Yes	No
Communication	Quick	Slow	Quick
speed			
Rescue speed	Quick	Slow	Quick
Rescue time	Long	Long	Short
accuracy	Common	Low	High
Emergency items provide	Not in time	Not in time	timely
Emergency speed	Quick	Slow	Quick
Cruising power	Weak	Common	powerful

As you can see from the analysis of the maritime search and rescue operations, a large amount of information is involved in the search and rescue mission and the search and rescue operations. The accuracy and rapid processing of this information will expedite the development of the search and rescue plan, improve the accuracy of the rescue plan, and coordinate the search and rescue work quickly and accurately.

A. Rescue Aircraft

The plane is flying fast, and be able to reach the disaster site quickly. This advantage is particularly acute in the case of a salvage mission at sea, when it is required to complete a rescue mission in a short period of time especially . In addition, the aircraft can search large areas of the sea and find the target in time. Also，it provides guidance for the accurate arrival of the salvage vessel. More importantly, the plane's involvement in the search and rescue operation was less affected by weather conditions such as wind waves. It is possible to use the Marine salvage facility when it is unable to sail to the area where the accident happened .The better aircraft have superior performance, have fast speed, long distance and good endurance ability. General aircraft have general performance , general speed , general voyage and general endurance ability. The poor plane has poor performance, slower speed , closer range and poor endurance[15] .

B. Rescue Ship

The ship referred here is a vessel that is specially used for salvage at sea or a professional salvage vessel. The salvage vessel is a special vessel, especially suitable for the field command. It is fast, resistant to wind and waves and can communicate with any distress vessel or boat on the maritime communication frequency. Professional salvage vessels are indispensable in maritime search and rescue operations. Search and rescue ship is excellent in performance, with fast speed and high wind resistance. General ship performance is general, with general speed, and general anti-wind grade . Poor ship have performance, slow speed, low wind resistance[16].

C. Intelligent Search and Rescue Device

The intelligent search and rescue device use sonar detector to detect underwater targets .The probe can detect a range within a kilometer. It can search for a wide range of areas and achieve the first time .It's supported by the GPS navigation system. When sonar is searched for feedback, the GPS provides precise positioning to achieve accurate rescue. Its main structure is aluminum and platinum with lightweight materials and small energy consumption .It can provide life-saving supplies, food and fresh water and can reach the

shipwrecks quickly, cost low, high efficiency. It uses Marine batteries and has a strong battery life and can work at sea for a long time.

V. CONCLUSION

Ship rescue and helicopter rescue are long and inflexible. This paper designs an intelligent search and rescue equipment which is able to accurately and accurately give the location of the drowning personnel. It combines GPS, sonar technology, Marine battery technology, database synchronization, wireless transmission, and so on, and implements three sets of equipment, such as active rescue terminal, receiving terminal and search and rescue display equipment. The active rescue terminal sends a distress signal containing its location information to the search and rescue vessel after the launch of the life jacket. Receiving terminal and search and rescue display equipment installed on search and rescue vessels. The search and rescue personnel can receive and display the position of the drowning personnel in real time and ensure the rapid implementation of the search and rescue work. The intelligent search and rescue devices which we designed is small, convenient to transport and convenient to use which needs to carry only some food and lifesaving goods. Intelligent search and rescue devices can be used directly to work in shipwrecks. Compared with the helicopter search and rescue, the intelligent search and rescue is low cost and high efficiency, which greatly reduces the search time. The intelligent search and rescue device uses a Marine battery to provide a steady stream of electricity for the search and rescue which has a long life and low cost and does not cause pollution. Using sonar detector, the search time was greatly reduced. The search and rescue vehicle uses sonar detector and GPS system, reduces the time of search and rescue greatly, and improves the search and rescue accuracy. Overall, the search and rescue with low cost, reasonable design, easy using, far signal range , accurate positioning and display high tracking performance, improve the efficiency of search and rescue work effectively.

REFERENCES

[1] Zhao Bing.Research and design of Marine search and rescue system[D].Fudan University.2013.

[2] Allen A. Leeway divergence [R].US Coast Guard Research and Development Center,2005.

[3] Zhao Dong.The design and implementation of the small scale maritime personal emergency search and rescue indicator[D].Xi 'an university of electronic science and technology,2014.

[4] LIU Hai-zheng, HAO Huai-ci, HAO Chun-yang. Search and rescue region prediction algorithm based on the Monte Carlo method [J]. Ship and ocean engineering ,2010,（2）:132-135.

[5] YU Wei-hong, Jia Chuan-ying. Maritime search and rescue search area method for determining [J]. Navigation of China,2006,（2）:34-37.

[6] Mohd Ansor Bin Yusof, Shahid Kabir.An Overview of Sonar and Electromagnetic Waves for Underwater Communication[J].IETE Technical Review 2012,(18):307-317 .

[7] WANG Li,Yang Peng. Design and implementation of virtual oscilloscope based on Lab VIEW[J]. Research and Exploration in Laboratory, 2010,29）:62-64.

[8] Ben A. Brushedtt ,Victoria c,Brian A.King. Determining the leeway drift characteristics of tropical Pacific island craft[Z]. Applied Ocean Research,.2014.

[9] Hu Bin,Study of automatic alarm system based on BeiDou[D].Shanghai ocean university,2016.

[10] Wang Dong-Dong,Chen Yong-jian, Ma Xiao-Feng.GPS and electronic chart based on the search and rescue location system[J].Avionics Technology, 2012, (43):14-19.

[11] Gebauer, A.Schreiber, K. U.Klügel, T.Schön, N.Ulbrich, U.High-frequency noise caused by wind in large ring laser gyroscope data[J].Journal of Seismology,2012,(12):777-786

[12] Wang Ming-hua.New ways of using Marine energy -- seawater batteries[J].Water Resources Research,2010.

[13] Cheng Cui-fang.The study of the key technologies of the water alarm and search system[D]. Jimei University,2016.

[14] Yan Jun-tao.GPS based self-positioning Marine search and rescue alarm system[D].Beijing university of posts and telecommunications,2014.

[15] Addoms Allen,Christophe Maisondieu,Michel Olagnon.Advances in search and rescue at sea[Z]. Ocean Dynamics.2013.

[16] Qian Jin-shan.The research of the method of maritime search and rescue[J].Chinese water transportation (lower half),2015,(9): 51-53.

Design of Low Voltage Power Line Carrier Communication System Simulation

Cheng Xiaoming
Chong Qing Electric Power Research Institute, Chong Qing, China
happy-xm169@163.com

Li songnong
Chong Qing Electric Power Research Institute, Chong Qing, China
lxpecolicee@163.com

Ye Jun
Chong Qing Electric Power Research Institute, Chong Qing, China
gtovictor@163.com

Sun Hongliang
Chong Qing Electric Power Research Institute, Chong Qing, China
cqepshl@sina.com

***Abstract*—Noise power line channel is the largest low-voltage power line interference sources, it is not a simple additive white Gaussian noise, but a time-varying noise, and with different environments and change, which is mainly the work of each of the grid kinds of electrical equipment generates, including instant asynchronous impulse noise such as background noise switching power supply or generation of amateur radio and frequency synchronization with the grid and grid-cycle pulse noise generated by the equipment.**

Keywords-Low-voltage power line interference; Channel measurement; Asynchronous impulse noise

I. INTRODUCTION

For the previous three kinds of noise, a narrowband noise due to the second type is usually over time (day or night) change change, OFDM system considering such noise as the background noise, the first three types of periodic pulse noise has a high repetition rate, and very low power spectral density (PSD), it can also be viewed as a background noise. These three types are divided into the background noise, which are the three spectral integrated spectrum, shown in Fig . 2-4. In an OFDM system for the noise or the usual solution is to avoid using these bands, or noise is the use of these bands on a low bit rate sub-channel.

Background noise is relatively stable A noise, but for the type 4 and 5, they are but it is time-varying, variations thereof are usually a few microseconds to several milliseconds. Compared with the fifth type of noise, the noise frequency and the grid frequency noise synchronization category 4, the repetition period is 50Hz or 100Hz, its Q short duration (a few milliseconds), the power spectral density (PSD) increases with frequency reduced. For these reasons, the first four kinds of noise model assumes that no error is generated when building models. And fifth, lasting from a few microseconds to a few milliseconds, the arrival time of a random, PSD sometimes higher than the background noise 50dB.

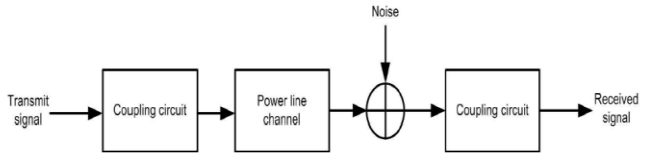

Figure 1. Graphical illustration of the PLC channel

Since the main purpose of this project is to study the low-voltage power lines in high-speed communication networks, so the main use of the high frequency range, typically between 500kHz ~ 20 coral z. The following high-frequency noise in time domain, the frequency-domain and time-varying characteristics were analyzed. First, the time-domain characteristics of high frequency noise of low frequency noise to reduce the influence of high frequency measurements, the selected test filter having high-pass characteristic, while simultaneously testing the selected sampling rate 100M Sample / s, the sampling points 2M points. The length of time for each measured time domain signal is 20ms, the equivalent of 50Hz frequency of a cycle length. Fig. 2-5 is a different place (laboratory and residential) and different times (peak and trough power) of the measured time-domain waveform.

From the high-frequency time-domain waveform measured, not difficult to find high and low voltage power line channel frequency noise has the following characteristics:

background noise: Background noise in residential areas during the peak and trough amplitude substantially identical, about 30mv; laboratory background noise amplitude at the peak time is about 100mV, and in the low power consumption of 30mV about. Amplitude and low frequency background noise when little difference. Impulse noise (2) and Frequency Synchronization: In Figure 2-5 (a), 2-5 (b) and 2-5 (d), the electrical equipment when working with power frequency generated by periodic synchronization impulse noise is very obvious, repetition frequency 100Hz, is also consistent with the low frequency band. Amplitude noise at the same time the laboratory is larger than the neighborhood, the noise amplitude at different times of peak

electricity than when a large trough. Among them, the neighborhood at the time of the pulse peak amplitude of the noise about 50mv, and the pulse peak amplitude of the noise when the lab reached 350mv above, even in the low power consumption, impulse noise rates are more than 100mv, from Fig. 2-5 (c), we see that in the ranks。 Man zone electricity trough, basically do not see impulse noise waveform. Thus, the pulse interference lab than to a large residential area.

II. LOW VOLTAGE POWER LINE CARRIER COMMUNICATION CHANNEL UNIVERSAL MODEL

We can see from Fig. 2-6, in a residential area, the periodic impulse noise and single-pulse noise z delete bands below 2.5, a major home appliances produced by interference in peak and trough periods, such interference power spectral difference can be more than 10dB; 2.5 heart z above the background noise is very flat, narrow-band shortwave broadcast signal to noise is a major disturbance in the 12MHz ~ 15 and 17 delete z coral z ~ 20MHz band can be seen narrowband noise, narrowband noise and stronger at night than at any other time, and shortwave radio transmission characteristics of these waves is the same. Background noise difference when peak and trough of about 3dB. From Fig. 2-6 (c) and FIG. 2-6 (d) we can see that, in the laboratory, the main disturbance is periodic impulse noise generated by the switching power supply from the computer, the spectrum performance of a certain discrete frequency reuse spectrum, the maximum magnitude higher than background noise disturbance around 40dB, and is widely distributed in the frequency domain can be achieved 8MHz; 9 deleted z above the background noise is very smooth. In the peak and trough periods, periodic impulse noise and background noise difference of about 10dB.Today, there are many different pairs of conductors of the transmission line, coaxial cable, stripline and the like. They can use the distribution parameter model shown in Figure 2.4 the four configuration will be described. However, for each transmission line parameters have different values, depending on which requires the cable structure, wire timber, type, etc. of insulating material is calculated.

$$s_k = s(kT/N) = \sum_{i=0}^{N-1} d_i \exp(\frac{j2\pi ik}{N}), 0 \le k \le N-1 \quad (1)$$

High-frequency power spectrum graphical comparison residential and laboratories in different periods can be found, the peak, the background noise power spectral density laboratory higher residential 10dB; trough when the electricity, the power spectral density of the background noise is almost the same . Above we see the performance of low voltage power line communication channel variability high frequency noise during long periods during the day and night, as well as peak and trough periods of time variability at low frequencies with the same kind of noise also showed short time degeneration. In order to observe this instantaneous time variability, we also add test data during the time window of the power spectrum estimation were calculated for each section of the power spectrum, and draw its power spectrum changes over time three-dimensional graphics. When the length of the time window 100us added, that the length of each segment is 10000. Figure 2-7 is a frequency characteristics at high frequencies corresponding figure.

III. NOISE DETAILED ANALYSIS AND MODELING

From Fig .2-7, we can more clearly see the power line noise channel with grid 50Hz frequency changes, changes in the power spectrum of the noise frequency is still 100Hz. This is observed in the time domain waveform is consistent with ours, this cyclical mainly by high-frequency noise and frequency synchronous periodic pulse noise. Frequency high frequency characteristics graph further observation and control of the power spectrum graphic Figure 2-6, at high frequencies, we can draw the following conclusions: (1) residential peak, impulse noise generated by electrical equipment can affect 2.5 delete z, within 10ms, impulse noise power spectral density at 10dB below; and 2.5 puncturing z above the background noise power spectrum is flat, changed slowly, within 24 hours of the power spectral density the magnitude of change in 5dB within; another less impulsive noise at night, when the broadcast signal is stronger, we can clearly see that the presence of narrowband noise (c) in Figure 2-7, it does not vary with the magnitude of the change in power frequency change.

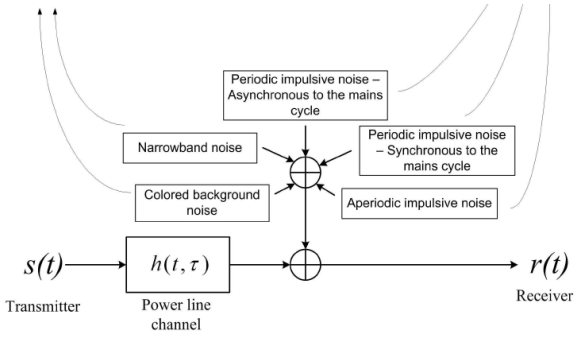

Figure 2. Noise Type observed in PLC systems

$$d_i = \sum_{k=0}^{N-1} s_k \exp(\frac{-j2\pi ik}{N}), 0 \le i \le N-1 \quad (2)$$

$$v_{guard} = 10\log_{10}(\frac{T_g}{T}+1) \quad (3)$$

$$x_g(n) = \begin{cases} x(n) & n = 0,\text{L}\ ,N-1 \\ x(N+n) & n = -N_g,\text{L}\ ,-1 \end{cases} \quad (4)$$

$$y_g(n) = x_g(n) \otimes h(n) + w(n) \tag{5}$$

$$Y(k) = \sum_{n=0}^{N-1} y(n) e^{-j2\pi kn/N}, k = 0,\mathrm{L}\ , N-1 \tag{6}$$

OFDM technology has the following advantages:

(1) the high rate data traffic through the serial-parallel conversion, so that the relative increase in each sub-carrier data symbols on the persistence length, so as to effectively reduce the radio channel time dispersion caused by ISI, equalization of the receiver is reduced within complexity, sometimes even without using the equalizer, but only to eliminate the adverse effects of ISI by employing a method of inserting a cyclic prefix.

(2) a conventional frequency-division multiplexing method, a frequency band is divided into a number of disjoint sub-frequency band transmitting data in parallel, to retain a sufficient guard bands between the respective sub-channels. The OFDM system due to the orthogonality between the subcarriers, allowing subchannel spectral overlap, as compared with the conventional frequency division multiplexing system, OFDM system can maximize the use of spectrum resources. When very large number of sub-carriers, the spectrum efficiency of the system can become 2Baud / Hz [4].

(3) each subchannel quadrature modulation and demodulation by using inverse discrete Fourier transform (IDFT, Inverse Discrete Fourier Transform) and discrete Fourier transform (DFT, Discrete Fourier Transform) method to achieve. In a large number of subcarriers of the system, may be implemented by a Fast Fourier Transform (FFT, Fast Fourier Transform). [5] With the development of large scale integrated circuit technology and DSP technology, IFFT and FFT are very easy to implement.

(4) the presence of wireless data services are typically asymmetric, i.e., the amount of downlink data transmission link is greater than the amount of uplink data transmission, which requires the physical layer supports asymmetric high-speed data transmission, OFDM system by using different number of subchannels to achieve uplink and downlink in a different transmission rate.

$$Y = XH + W \tag{7}$$

$$D_f \le \frac{1}{\tau_{\max} \Delta f} \tag{8}$$

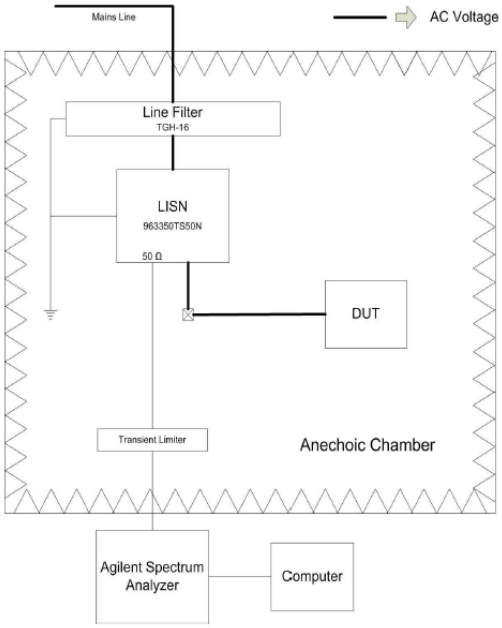

Figure 3. Pictorial description of the measurement setup

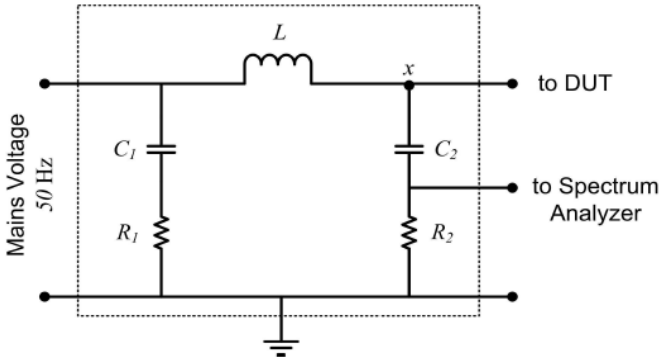

Figure 4. Block diagram of LISN

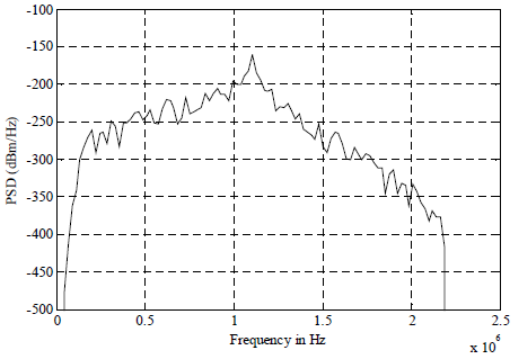

Figure 5. Measured PSD

IV. CONCLUSION

This chapter begins from the spread spectrum technology, analyzes the feasibility of spread spectrum communication in power line carrier communication, and the principle of spread spectrum technology for analysis. Reference TD-SCDMA system basic midamble sequence, designed for the detection of power line broadband channel characteristic measurement signal. Using broadband reference signal combined vector signal generators, network analyzers, and other software and hardware equipment, power line broadband channel sounding build and validate semi-physical simulation platform, as in the actual distribution network environment, the power line broadband channel characteristic measuring the accumulation of experience .

The use of semi-physical simulation platform for school laboratory and classroom building scene a lot of field measurements, analysis of power line channel transmission characteristics of the different environments, and features a three-dimensional graphic display of variable power line channel under different scenarios. At the same time in order to improve the efficiency of the data analysis, the use of MATLAB simulation software design based on off-line data analysis software GUI interface. It receiving end signal processing module integrated into the GUI interface, to implement graphical data analysis and processing, and at the same time from multiple dimensions of the channel parameters display.

ACKNOWLEDGMENT

This work is supported by State Grid Corporation of China technology project and cstc2016jcyjA0214

REFERENCES

[1] B.R.Saltzberg, “Performance of an efficient parallel data transmission system”, IEEE Transactions on Communications Technology, vol.15, no.6, December 1967, pp:805-811.

[2] E.Leung, P.Ho: “A successive interference cancellation scheme for an OFDM system”, Proc. IEEE ICC 98, Vol 1, June 1998, pp:375-3779.

[3] G.Santella, “Bit error rate performance of M-QAM orthogonal multi-carrier modulation in presence of time-selective multi-path fading”, in Proc’ 95, Seattle, WA, June 1995, pp:1683-1688.

[4] H.Steendam and M.Moeneclaey, “optimization of OFDM on frequency-selective time-selective radio channels”, in ISSSE’98, October 1998, pp:398-404.

[5] M.Russell and GL stuber, “Interchannel interference analysis of OFDM in a mobile environment”, in VTC’ 95, vol 2, pp:820-824.

[6] S.N.DIggavi, “Analysis of multicarrier transmission in time-varying channels”, in IEEE ICC’97, Montreal, pp:1191-1195.

[7] M.Septh, A.A.Fechtel, G.Fock, H.Meyer, “Optimum receiver design for wireless broadband systems using OFDM-Part I.”, IEEE Trans. On Communications, Nov, 1999, 47(11):1668-1677.

[8] Robertson, P., Kaiser, S., “Analysis of the loss of orthogonality through Doppler spread in OFDM systems”, GLOBECOM’99, Vol 1, 1999, pp:701-766.

[9] Li Ye, Leondard J. CImini Jr., “Bounds on the Interchannel Interference of OFDM in Time-Varying Impairments”, IEEE Transactions on Communications, Vol. 49, No.3, Mar, 2000, pp:401-404

[10] Yuping Zhao, Haggman, S.G., “Sensitivity to Doppler shift and carrier frequency errors in OFDM systems-the consequence and solutions”, In VTC’96, pp:1564-1568.

[11] Armatrong, J.; Grant, P.M; Povey, G., “Polynomial cancellation coding of OFDM to reduce intercarrier interference due to Doppler spread”, GLOBECOM 1998, vol.5, pp:2771-2776.

[12] Armstrong, J., “Analysis of new and existing methods of reducing intercarrier interference due to carrier frequency offset in OFDM”, on Communications, IEEE Transaction , Vol 47, issue 3, Mar 1999, pp:365-369.

Simulation Study Low Voltage Power Line Carrier Communication in Noisy Environments

Ye Jun
Chong Qing Electric Power Research Institute, Chong Qing, China
gtovictor@163.com

Li songnong
Chong Qing Electric Power Research Institute, Chong Qing, China
cqepshl@sina.com

Sun Hongliang
Chong Qing Electric Power Research Institute, Chong Qing, China
lxpecolicee@163.com

Hou Xingzhe
Chong Qing Electric Power Research Institute, Chong Qing, China
cqhhxz@163.com

***Abstract*—Studies have shown that there are a lot of low-voltage power line is one of the main obstacles to strong noise limit for data transmission quality. Power line noise can be divided into steady background noise, narrowband interference noise, sudden impulse noise and periodic noise. Background noise is distributed throughout the communication band, low-voltage power line up white Gaussian noise 22dB [133 or more. Sudden noise is generated by the random access or disconnect electrical equipment produced. Studies have shown that pulse interference effects on the quality of the low voltage power line carrier communication maximum. Literature statistics, intensity pulsed interference up 40dBuv.**

Keywords-Low-voltage power lin; Sudden impulse noise; Periodic noise

I. INTRODUCTION

With 10KV above high-voltage power lines, compared, 220V / 380V low voltage power line channel with harsh transmission environments, signal attenuation, interference characteristic strong, and time variability and other characteristics, and the power line burst interference seriously impact, making low-voltage power line carrier technology development is hampered. Overall, the low voltage power line carrier communication has the following aspects of the characteristics of children n4 151: 1, the signal attenuation low-voltage distribution network directly to the user, the load situation is complex, each node impedance mismatch, so the signal will produce reflection, resonance phenomena so that signal attenuation becomes extremely complex. For high frequency signals, low-voltage power transmission line is a line of non-uniform distribution of the various properties of the load randomly connected or disconnected at any position in this line. Therefore, the high-frequency signal transmission in low-voltage power line attenuation must exist. Studies have shown that the attenuation of the signal power line affected by the change in distance is fairly obvious, typically 10dB / km to 100dB / km. Meanwhile, the attenuation and the frequency of the signal, the phase of the commercial power supply, in general, as the frequency increases, the attenuation of the signal will also increase. It is reported that, when a communication frequency is greater than 100kHz, the frequency of each additional 1kHz, the attenuation increases O. 25dB [1 mendelevium. In some special frequency bands, due to the reflection, the resonant transmission line effects and the like, there will be a sudden surge attenuation.

Low power is a broad distribution network, and then on a wide range of load, leading to its channel incorporated into a variety of load impedance with constantly changing. Input impedance characteristics are important parameters for low voltage power line channel characteristics, research input impedance requirements for power transmission signal of great significance. Enter the low voltage power line carrier communication channel impedance n cho '173n81'1 cho means receives the signal transmitting device and a signaling device driver point distribution network equivalent impedance, it directly affects the size of the transmitted signal coupling efficiency. Figure 2-1 is a basic circuit diagram of the low voltage power line impedance measurement

Attenuation characteristic signal is a reflection of the communication channel characteristics also an important parameter, which represents the communication from the transmitting end to the receiving end of the signal energy loss, in practice the sake of convenience, in its logarithmic form usually expressed in dB. Channel attenuation characteristic consists of two parts n rip: signal transmitting means coupled between the channel attenuation characteristic signal attenuation characteristic in the channel transmission. Wherein, the coupling attenuation characteristic channel characteristic input impedance and coupling device about the parameters used in the design of the signal transmitting and receiving apparatus must be considered. Here focuses on the transmission channel attenuation characteristics. For high frequency signal, low-voltage power line is a non-uniform distribution of the transmission line, a variety of different properties at an arbitrary position of the load line of this random access or

disconnected. Therefore, the high-frequency signal transmission in low-voltage power line will inevitably decline. For low voltage power line communication, the attenuation of the signal is very serious. In general, PLC signal attenuation with frequency rises, increasing distance increases, but not monotonous. Low-voltage power line network branches and more load random access various properties or disconnected, the echo effect of multipath interference caused very serious, with great frequency selective fading. Under normal circumstances, the signal attenuation in 20dB or more, and sometimes reach 60dB. PLC channel to the extent that the various frequency signal attenuation PLC main basis to select the carrier frequency. Signal attenuation is mainly determined by the path through the network and the connected load. Some of the network load on certain frequencies constitutes a resonant circuit, to resonate. When a heavy load on the network, the line impedance can be achieved l Q or less, resulting in high attenuation of the carrier signal.

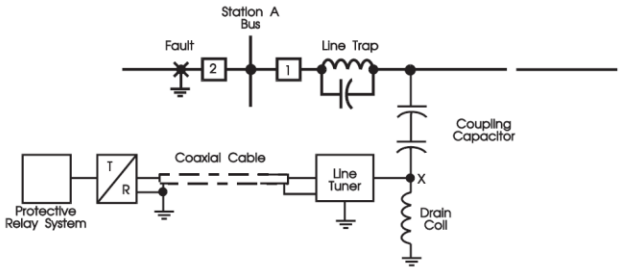

Figure 1. Basic Power Line Carrier

II. CHANNEL FADING CHARACTERISTICS

In general, the farther the signal transmission distance, the more severe attenuation, but because they do not match the load impedance, signal transmission occurs reflection, standing waves, scattering and other complex phenomena, these combinations of complex phenomena that signal attenuation with changes in the relationship between the distance becomes very complex, there may be larger than the attenuation at close distance dots. Distribution network directly to the user, the load situation is complex, does not match the impedance of each node, so that the signal can result in reflection, the resonance and other phenomena, so that the signal attenuation becomes extremely complex. In general, the pressure line signal attenuation 10dB / km, the low pressure can reach 100dB / km. Mainly related to the following four factors:

(1) the time-dependent signal attenuation;

(2) frequency-dependent signal attenuation;

(3) the distance related signal attenuation;

(4) the signal distribution network between different phases of decay; Q-phase signal attenuation values between 2-15dB. In addition, many parallel load distribution networks also have a great impact on the attenuation of the signal, especially those large capacitor for power factor adjustment; and when the load is small distribution networks (such as at midnight), you should consider disaster resistance coupled circuit, it will partition a considerable portion of power.

$$S(f)=\begin{cases}\dfrac{1}{\pi f_d\sqrt{1-(\dfrac{f}{f_d})^2}} & |f|<f_d \\ 0 & \text{else}\end{cases} \tag{1}$$

In general, loss of signal transmission is a function of frequency, as the frequency increases, the attenuation of the signal will also increase, which is the opposite of the noise, so the high frequency loss is greater than low frequency loss. However, in some special band, due reflection, resonance and transmission line effects and other factors, there will be a sudden surge attenuation. Single-phase test, for example, in the 140kHz, the hospital building power lines and industrial buildings difference signal attenuation 5dB, 20dB difference when 160kHz, 240kHz when in slow rise of 27dB. In different time periods, the same measurement parameter points will have different attenuation characteristics. In general, the attenuation was significantly higher than in the white decay phase. From the above analysis, the low-voltage power line on the attenuation characteristics of the signal is quite complex, it is difficult to find a simple formula to calculate the attenuation of the signal, but it also has its regularity can use, let the attenuation characteristics of the power line to conclude:

Attenuation size (1) is closely related to the time signal, i.e., a strong day / night sensitivity. For example, industrial areas, daytime than at night attenuation large, and in residential areas at night from 18:00 to 22:00 attenuation is greatest.

$$s(t)=\begin{cases}\sum_{i=0}^{N-1} d_i \operatorname{rect}(t-t_s-T/2)\exp(j2\pi f_i(t-t_s)) & t_s\le t\le t_s+T \\ 0 & t<t_s \wedge t>t_s+T\end{cases} \tag{2}$$

$$\frac{1}{T}\int_0^T \exp(j\omega_n t)\exp(j\omega_m t)dt=\begin{cases}1 & m=n\\ 0 & m\neq n\end{cases} \tag{3}$$

$$\begin{aligned}\hat{d}_j &= \frac{1}{T}\int_{t_s}^{t_s+T}\exp(-j2\pi\frac{k}{T}(t-t_s))\sum_{i=0}^{N-1} d_i\exp(j2\pi f_i(t-t_s)) \\ &= \frac{1}{T}\sum_{i=0}^{N-1} d_i\int_{t_s}^{t_s+T}\exp(2\pi j\frac{i-k}{T}(t-t_s))dt = d_j\end{aligned} \tag{4}$$

(2) signal attenuation and the frequency of the signal magnitude, in general, the signal attenuation with respect to increasing frequency increases, although this increase is not monotonic. For frequencies greater than 100KHz signal, M. 1. Chen and R. w. Donadlson derive frequency for each additional 1KHz, signal attenuation increases O. 25dB.

III. SIMULATION RESULTS

Transmission distance (3) signal attenuation and signal related, in general, the longer the distance signal transmission, the greater the signal attenuation. In the actual measurement, signal attenuation at 1 km and can even reach loodB.

Attenuation of a transmitting end and receiving end (4) is connected to the signal related to the same phase, when the transmitter and receiver connected to the same phase, the attenuation is generally on a different phase than smaller 2 to 15dB, in some cases next, the difference can even reach 40dB.

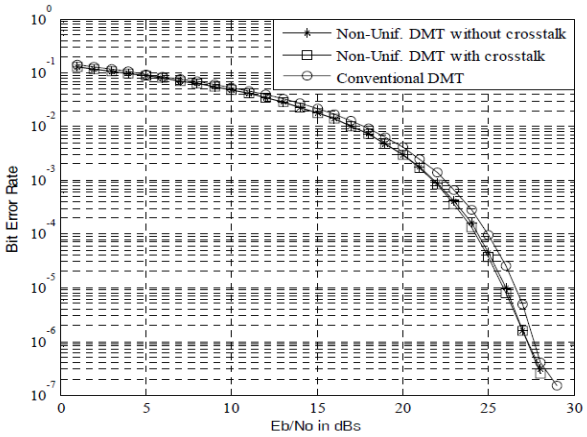

Figure 2. BER Performance comparison

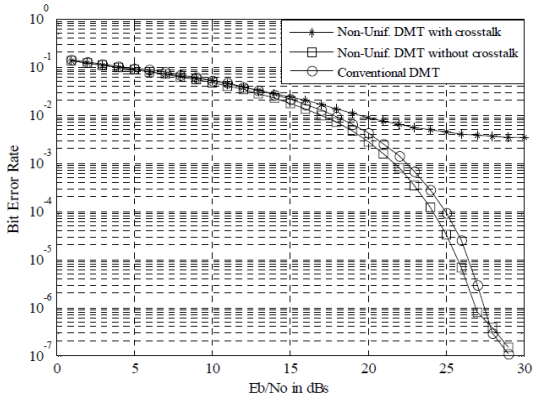

Figure 3. BER Performance comparison

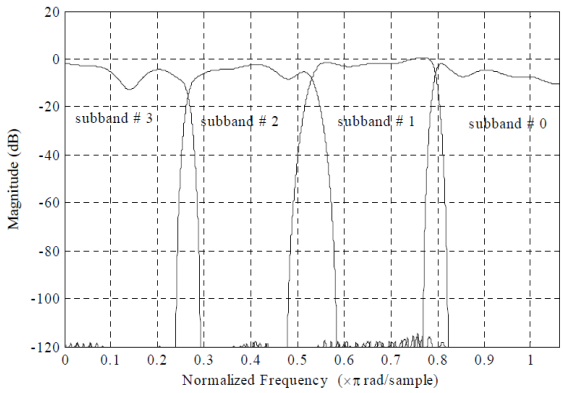

Figure 4. The Uniform bandwidth subbands of the in-home power line channel

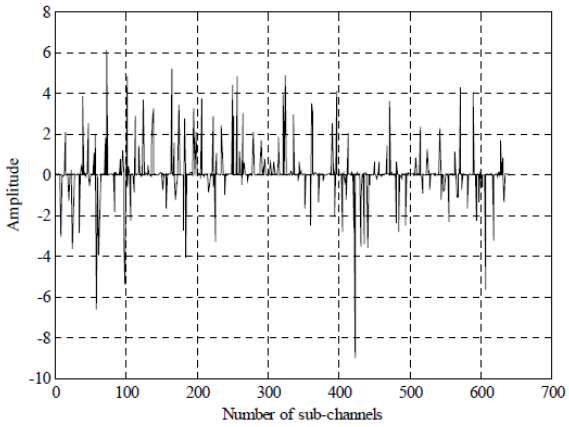

Figure 5. Impulse noise

IV. CONCLUSION

Noise on the power line noise into artificial and man-made noise. Artificial noise is a natural phenomenon, such as noise in the power line caused by lightning; artifacts from a variety of electrical, mechanical and electrical products and power lines themselves. The main power line noise is not additive white Gaussian noise pop child called larvae, its features are likely to change in a very short period of time. According to the band powerline communication studies at different stages of the power line noise z within 30 sampan classification can be divided into two parts: lookHz below and 100k a 30MHz. This paper studies a man-made noise in the 1MHz frequency range 30Hz.

ACKNOWLEDGMENT

This work is supported by State Grid Corporation of China technology project and cstc2016jcyjA0214

REFERENCES

[1] H. B. C » elebi, S. Guzelgoz, T. Guzel, H. Arslan, and M. K. Mihcak, Noise, atten- uation and multipath analysis of plc networks," in 2010 European Signal Processing Conference, Aug 2010, submitted.

[2] S. Guzelgoz, H. B. C » elebi, T. Guzel, H. Arslan, and M. K. Mihcak, Time frequency analysis of noise generated by electrical loads in plc," in IEEE International Conference on TElecommunications, ICT, April 2010, accepted.

[3] S. ¯Guzelgoz, H. B. C- elebi, and H. Arslan, \Articulating factors de¯ning rms delay spread in lv plc channels," IEEE Transactions on Power Delivery, submitted.

[4] Statistical characterization of the paths in multipath plc channels," IEEE Trans- actions on Power Delivery, submitted.

[5] M. Zimmermann, \An analysis of the broadband noise scenario in powerline networks," Int. Symp. Power-Line Commun. Appl., ISPLC, 2000.

[6] Balakirsky, \Potential limits on power-line communication over impulsive noise chan- nels," ISPLC, 2003.

[7] V. Degardin, M. Lienard, P. Degauque, A. Zeddam, and F. Gauthier, Impulsive noise on indoor power lines: characterization and mitigation of its e®ect on plc systems," in Electromagnetic Compatibility, 2003. EMC '03. 2003 IEEE International Symposium on, vol. 1, May 2003, pp. 166-169 Vol.1.

[8] D. Umehara, S. Hirata, S. Denno, and Y. Morihiro, \Modeling of impulse noise for indoor broadband power line communications," Proc. ISITA 2006, pp. 195-200.

[9] H. Meng, Y. Guan, and S. Chen, \Modeling and analysis of noise e®ects on broadband power-line communications," Power Delivery, IEEE Transactions on, vol. 20, no. 2, pp. 630-637, April 2005.

[10] G. Avril, M. Tlich, F. Moulin, A. Zeddam, and F. Nouvel, \Time/frequency analysis of impulsive noise on powerline channels," Home Networking, pp. 143{150.

Modeling of High-Frequency Low Voltage Power Line Carrier Communication Channel

Li songnong
Chong Qing Electric Power Research Institute, Chong Qing, China
e-mail:gtovictor@163.com

Hou Xingzhe, Zheng ke
Chong Qing Electric Power Research Institute, Chong Qing, China
e-mail:cqhhxz@163.com, cqetzk@sina.com

Liu Dong, Sun Hongliang
Chong Qing Electric Power Research Institute, Chong Qing, China
e-mail:cqepld@163.com

Meng Xin, Luo Zhishu
Chong Qing Electric Power Research Institute, Chong Qing, China
e-mail:cqepmx@126.com, cqeplzs@163.com

***Abstract*—Low-voltage power line channel characteristics are designed for low voltage power line carrier communication system foundation. The paper used to design and develop a system for measuring the electrical characteristics of the low voltage power line communication network used to do high, including the noise characteristics of the input impedance characteristics, signal attenuation characteristics and systems, etc., a lot of experimental research. On this basis, the establishment of a low-voltage power grid will be used as a high-frequency carrier communication channel model. The model provides a practical and effective platform for the research and design of low voltage power line carrier communication system network has laid a good foundation.**

Keywords-Channel capacity; channel modeling; Group delay; Power-line communication (PLC)

I. INTRODUCTION

Due to the low voltage power line as a communication medium has extensive applications (across households), solid (and distribution network in one) and economy (no special channel), etc., as early as the 1970s and 1980s 2O once attention of researchers. In recent years, with the rapid development of increasing user demand for a variety of communications and related technologies, low-voltage power line carrier communication is becoming a hot research workers in science and technology at home and abroad. However, the low-voltage power grid as a matter of high-frequency carrier wave communication channel to use, you first need to face is to understand the complexity of the electrical characteristics of the channel, this feature compared to communicate with dedicated communication channels have almost completely different electrical characteristics. In addition, low-voltage power network with millions of households connected to the characteristics of a variety of electrical equipment produced by complex noise propagation in the power line will be different degrees of interference carrier signal transmission channel. Therefore, carrier communication channel itself is the basis of the electrical characteristics of low voltage power line carrier communication studies.

Low-voltage power line channel characteristic mainly includes the following three aspects: impedance : 1,channel input characteristic signal access points; 2, signal in the channel transmission, due to impedance mismatches and signal reflections node generated by the refraction phenomena transmission induced attenuation and phase shift characteristics; 3, noise characteristics caused by a variety of electrical equipment.

Abroad in this regard has been done more research work, mainly focused on the measurement of various frequencies within the range of the channel characteristics, there are also reports the results of the corresponding l1]. There are also at low frequencies (≤500 kHz) some interesting research on the electrical characteristics of the distribution network carried out.

This paper studies within the frequency range of 100 kHz-3 MHz with the electrical characteristics of the grid. Use test device developed by a large number of experiments carried out on the basis of these experimental results, the establishment of a 500 kHz-3 MHz frequency band used low-voltage distribution network carrier communication channel model.

Low voltage distribution network is very complex geometries, different lines with different wire or cable, so the big difference between them, if not impossible, to describe a whole theoretically be also very difficult, it requires technical collaborative research. A theoretical study of the long-term goal is to describe the characteristics of each part of the network, which helps us to understand the characteristics of a gradual deepening of complex networks.

II. NOISE MEASUREMENT METHOD

Power line carrier transmission as communication signals, each element of the network connection lines to

study the basic transport properties, for the analysis of power line channel characteristics is necessary. Low-voltage distribution network generally consists of overhead lines and cable. In the vast rural areas, distribution station to supply users generally use overhead lines; and in densely populated urban areas, the general cable. However, for the average family of indoor power lines usually BV. BV are generally three wire-bound in a conduit or walking bridge (trough) inside. This is to some extent like a cable. This chapter first based on some assumptions, analysis of a simple two-conductor transmission line model, a common cable, the transfer function is derived. Then according to the three-line structure of the cable from the "crosstalk" perspective derived a three-conductor transmission line model, and proved to symmetrical three-conductor cables can become the equivalent two-conductor cable, finally introduces indoor wiring grounding specifications and discussed it three conductor cable conductor of the cable is equivalent to two impact.

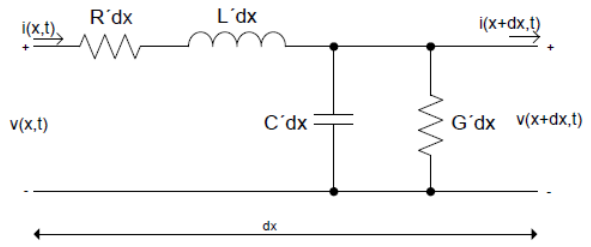

Figure 1. Elementary cell of a transmission line

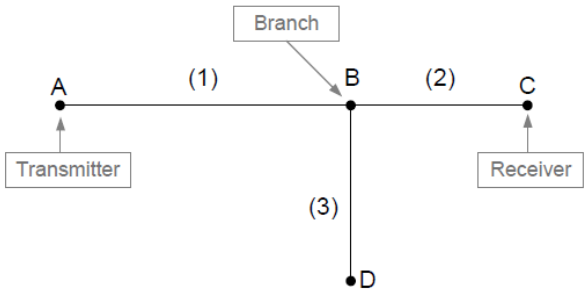

Figure 2. Topology of the sample network

III. PLC NETWORK STRUCTURE INSIDE THE CHAMBER

Today, there are many different pairs of conductors of the transmission line, coaxial cable, stripline and the like. They can use the distribution parameter model shown in Figure 2.4 the four configuration will be described. However, for each transmission line parameters have different values, depending on which requires the cable structure, wire timber, type, etc. of insulating material is calculated.

However, because the electromagnetic waves are in TEM mode propagation in the transmission line, the relationship between the parameters is the same. EM Mode refers to electric and magnetic fields are perpendicular to the direction of wave propagation in the cross section.

$$S_{21}=\frac{a(\omega)+b(\omega)Z_L}{c(\omega)+d(\omega)Z_L} \quad (1)$$

Noise low voltage distribution network is an important factor affecting the PLC reliable communications. But subject to the power line network designed from the beginning to consider restrictions, high-frequency signal transmission power lines are susceptible to external electromagnetic interference. Meanwhile, a variety of loads in a power grid access, will produce different characteristics of noise. Thus the need for different times, different frequencies, different scenarios make many measurements studies, statistical analysis of noise characteristics.

By 2.1 shows that the power line noise in accordance with the time / frequency characteristics and power spectral density characteristics can be divided into five. For the measurement of noise characteristics, the general coupler and oscilloscope / spectrum analyzer measurements. I.e., the noise signal by the coupling circuit is coupled to the oscilloscope, and the collected data is stored, and then import the data into a PC for analysis. The measuring principle is shown in Figure 2.6 below:

Low-voltage distribution network consists of a variety of different product types cables, transformers, consisting connection, while a variety of different types of electrical products access network terminal, the formation of different power line network topologies. Different power lines lay-line, such as overhead lines and underground cables, electrical transmission characteristics are also different. To sum up, the factors affecting the PLC network structure have : network location: Electricity demand in different regions differ, resulting in large differences in the structure of power line communication network. In the commercial and industrial clusters, the more general area of complex distribution networks, users with a high concentration. Distribution network structure of rural and urban differences also exist, but in all regions of the powerline communications needs are not the same;

Network Length: different supply network structures, transmission distance between the different position of the user and the transformer are not the same, resulting in a large difference in the same power line communication coverage area, this is particularly evident in rural areas; network design: low voltage distribution network architecture and the huge difference when degeneration, resulting in different network environments for each transmission. Meanwhile, the WAN connection (WAN) low-voltage distribution grid communications base position selection, it will lead to different users to communicate with

the radio region relative position change, thereby changing the structure of the communication network.

Based on the above analysis can be found, there is a big difference between the low voltage distribution network structure. Impossible to specify a typical network structure to analyze the entire grid, but can be used for some typical station area analysis, the definition of some of the same characteristics of the stage area network architecture to provide a reference for the laboratory simulation of real-world scenarios.

Noise low voltage distribution network is an important factor affecting the PLC reliable communications. But subject to the power line network designed from the beginning to consider restrictions, high-frequency signal transmission power lines are susceptible to external electromagnetic interference. Meanwhile, a variety of loads in a power grid access, will produce different characteristics of noise. Thus the need for different times, different frequencies, different scenarios make many measurements studies, statistical analysis of noise characteristics.

Fugyre 2.1 shows that the power line noise in accordance with the time/frequency characteristics and power spectral density characteristics can be divided into five. For the measurement of noise characteristics, the general coupler and oscilloscope/spectrum analyzer measurements. I.e., the noise signal by the coupling circuit is coupled to the oscilloscope, and the collected data is stored, and then import the data into a PC for analysis. The measuring principle is shown in Figure 2.6 below:

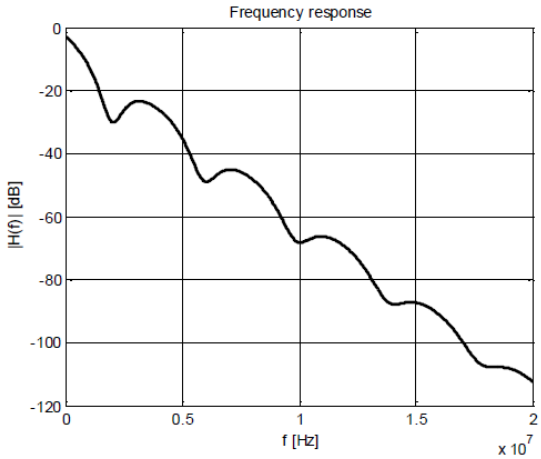

Figure 3. Simulation of the sample network

$$Attenuation(dB)_{f_i} = 20 \times \lg\left(\frac{U_{r,f_i}}{U_{s,f_i}}\right) \tag{2}$$

$$A(f,d) = e^{-(a_0 + a_1 f^k)\cdot d} \tag{3}$$

$$\gamma = \alpha + j\beta = \sqrt{(R + j\omega L)(G + j\omega C)} \tag{4}$$

$$H(f) = \sum_{i=1}^{N} \rho_i e^{-j2\pi f \tau_i} \tag{5}$$

$$\boldsymbol{CM}_{m,m} = \begin{array}{c} \\ t_1 \\ \text{M} \\ t_h \\ b_1 \\ \text{M} \\ b_k \end{array} \begin{array}{c} \begin{array}{cccccc} t_1 & \text{L} & t_h & b_1 & \text{L} & b_k \end{array} \\ \begin{pmatrix} 0 & \text{L} & 0 & c_{1,h+1} & \text{L} & c_{1m} \\ \text{M} & \text{O} & \text{M} & \text{M} & \text{O} & \text{M} \\ 0 & \text{L} & 0 & c_{h,h+1} & \text{L} & c_{hm} \\ c_{h+1,1} & \text{L} & c_{h+1,h} & c_{h+1,h+1} & \text{L} & c_{h+1,m} \\ \text{M} & \text{O} & \text{M} & \text{M} & \text{O} & \text{M} \\ c_{m1} & \text{L} & c_{mh} & c_{m,h+1} & \text{L} & c_{mm} \end{pmatrix} \end{array} \tag{6}$$

Connectivity matrix, the number of endpoints for the branch number of nodes is, the transfer order of the matrix. Order matrix values represent any node connectivity between states, when the value is 1, indicating that no other nodes relay nodes that can direct correspondence between the rows and columns. When the value is 0, the corresponding node can not communicate directly. By assumption we can see a direct link between any endpoint is not only connected to the neighboring branch node, so the matrix is zero matrix endpoints. Meanwhile, the same end-to-branch and branch node to node connectivity consistent port, so the matrix is a symmetric matrix, the matrix of end-to-value branch node are:

$$\boldsymbol{CM}_{m,m} = \begin{pmatrix} \boldsymbol{0}_{h,h} & \boldsymbol{CT}_{h,k} \\ \boldsymbol{CT}_{k,h}^{T} & \boldsymbol{CB}_{k,k} \end{pmatrix} \tag{7}$$

$$\boldsymbol{CB}_{k,k} = \begin{pmatrix} 0 & c_{12} & \text{L} & c_{1k} \\ c_{21} & 0 & \text{L} & c_{2k} \\ \text{M} & \text{M} & \text{O} & \text{M} \\ c_{k1} & c_{k2} & \text{L} & 0 \end{pmatrix} \tag{8}$$

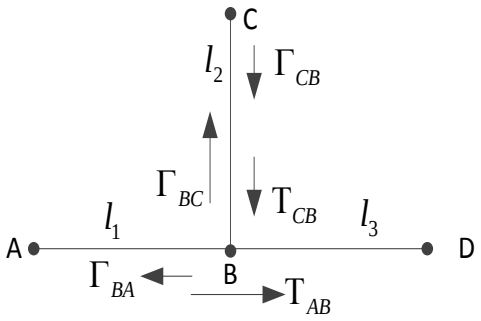

Figure 4. Transmissioin path of the sample network

$$A(f,d) = \exp((-a_0 - a_1 f^k)d) \quad (9)$$

IV. CONCLUSION

This chapter begins from the spread spectrum technology, analyzes the feasibility of spread spectrum communication in power line carrier communication, and the principle of spread spectrum technology for analysis. Reference TD-SCDMA system basic midamble sequence, designed for the detection of power line broadband channel characteristic measurement signal. Using broadband reference signal combined vector signal generators, network analyzers, and other software and hardware equipment, power line broadband channel sounding build and validate semi-physical simulation platform, as in the actual distribution network environment, the power line broadband channel characteristic measuring the accumulation of experience .

The use of semi-physical simulation platform for school laboratory and classroom building scene a lot of field measurements, analysis of power line channel transmission characteristics of the different environments, and features a three-dimensional graphic display of variable power line channel under different scenarios. At the same time in order to improve the efficiency of the data analysis, the use of MATLAB simulation software design based on off-line data analysis software GUI interface. It receiving end signal processing module integrated into the GUI interface, to implement graphical data analysis and processing, and at the same time from multiple dimensions of the channel parameters display.

ACKNOWLEDGMENT

This work is supported by State Grid Corporation of China technology project and cstc2016jcyjA0214

REFERENCES

[1] Ferreira, H.C., Grove, H.M., Hooijen, O. Vinck, A.J.. Power line communications: an overview, Proc. of IEEE ISPLC, 1996, pp. 558-563.

[2] Mlynek, P.; Misurec, J.; Koutny, M. The communication unit for remote data acquisition via the Internet. In Proceedings of the 7th WSEAS International Conference on Circuits, systems, electronics, control and signal processing (CSES'08). Puerto de La Cruz, Spain: WSEAS Press, 2008. s. 168-173. ISBN: 978-960-474-035-2.

[3] Misurec, J. The Data Acquisition via PLC in Energetics. In 32nd International Conference on Telecommunications and Signal Processing - TSP' 2009. 2009. s. 1-4. ISBN: 978-963-06-7716- 5.

[4] Krajsa, O.; Silhavy, P.; Koutny, M. Half- overlapped Filtered MultiTone modulation for PowerLine Communication systems. In Proceedings of the 13th WSEAS International Conference on Systems. Rhodos: WSEAS Press, 2009. s. 596-599. ISBN: 978-960-474-097- 0.

[5] Krajsa, O.; Silhavy, P. Half-overlapped Filtered MultiTone Modulation, its implementation and comparison with non-overlapped Filtered Multi-Tone modulation. In Proceedengs of The 7th WSEAS International Conference on CIRCUITS, SYSTEMS, ELECTRONICS, CONTROL & SIGNAL PROCESSING. 1. Puerto De La Cruz, Spain: WSEAS, 2008. s.272-277. ISBN: 978-960-474-035-2.

[6] Koutny, M.; Krajsa, O.; Mlynek, P. Modelling of PLC communication for supply networks. In Proceedings of the 13th WSEAS International Conference on Communication. Rhodos: WSEAS Press, 2009. s. 185-189. ISBN: 978-960-474-098- 7.

[7] Bingham, J.A.C. Multicarrier modulation for data transmission: An idea whose time has Come. IEEE Communication Magazine, vl.25. no.5. 1990, pp.5 - 14.

[8] Dostert, K. M. Power Lines As High Speed Data Transmission Channels – Modelling the Physical Limits, Proceedings of the 5th IEEE International Symposium on Spread Spectrum Techniques and Applications (ISSSTA 98), Sep. 1998, pp. 585-589.

[9] Hardy, M. E., Ardalan, S., O'Neal, J. B., Gale, L. J., Shuey, K. C. A Model for Communication Signal Propagation on Three Phase Power Distribution Lines. IEEE transactions on Power Delivery, Vol. 6, N ° 3, July 1991, pp. 945-951.

[10] H. Meng, S. Chen, L. Guan, C. L. Law, P. L. So, E. Gunawan, T. T. Lie. A Transmission Line Model for High- Frequency Power Line Communication Channel, IEEE Transactions, 2000, pp. 1290-1295.

[11] HRASNICA, H., HAIDINE, A., LEHNERT, R. Broadband Powerline Communications Network Design. [s.l.] : Willey , c2004. 275 s. ISBN 0-470-85741-2

[12] Babic, M.; Hagenau, M.; Dostert, K.; Bausch, J. Theoretical postulation of PLC channel model. Open PLC European Research Alliance (OPERA).2005

Design of Remote Eater Conservancy Information Monitoring System Based on Embedded Technology

Xiaoqing Shi
Shaanxi Railway Institute
Weinan, China
15304459101@189.com

Gangyu Gu
Weinan Technician College
Weinan, China
294244476@qq.com

Qianhua Huang
Shaanxi Weinan hi Tech Zone Engineering Quality
Safety Supervision and Management Station
Weinan, China
253389416@qq.com

***Abstract*—This paper studies the application of embedded system in water conservancy information remote monitoring, structured, modular scheme is adopted to improve the system of software and hardware design, debugging and implementation, and puts forward a set of embedded control, data acquisition and transmission, friendly interface in the integration of monitoring information management system design. This system based on the wide coverage of the GSM short message service provided mobile communication public transport hydrologic data, without networking, suitable for actual, system operation cost is low, the data transmission reliable and rapid. For water conservancy department of information management system of water resources to provide a complete set of hardware and software solutions, in areas such as DAMS, reservoirs, lakes has more broad application prospects.**

Keywords-Embedded systems; The remote water conservancy; Information monitoring; GPRS

I. PREFACE

With the rapid development of national economy, water conservancy project in the national economy role is more and more big, the flood control but also directly affect national economic development an important aspect. Because the information of flood prevention is not high, the error of artificial observation data is large, the system maintenance is difficult, easy to be wrong. In the event of abnormal weather, the flood control safety of major reservoirs and floodgates is a concern, while also causing great pressure on city flood control. At present, the state has put forward the goal of constructing "digital water conservancy", which is the policy of the ministry of water resources to promote and promote the modernization of water conservancy. We will fully implement the construction of water conservancy informationization to improve the work of flood prevention and flood prevention and flood prevention and flood control. In order to further improve the effectiveness and reliability of the flood control decision-making, the implementation of flood control and remote real-time monitoring system construction, can timely to possible or is happening flood dynamic monitoring, danger and disaster, informed the scene, in order to take corresponding preventive and remedial measures to ensure the safe operation of the reservoir. It is of great importance for leading decision making and reducing flood disaster, relieving the flood control pressure in the city, and safeguarding the safety of people's life and property. Under normal circumstances, such as dam water conservancy monitoring stations distributed in a wide range, and with the monitoring center distance is far, using the traditional way of cable connection, the circuit of the high cost of laying and construction cycle is long, and at the same time because of the physical factors such as canyon mountain barriers to using cables. The wireless monitoring solution addresses these problems well. Wireless monitoring solution without laying cable network, can quickly and easily deployed where various needs digital monitoring equipment, a new monitoring system or extensions to the existing monitoring system, has the very strong flexibility and expandability. The water flood control monitoring system USES the GSM/GPRS network communication lines, and USES wireless network technology to carry out remote monitoring of important water conservancy facilities such as reservoir DAMS. Can monitor at the same time on different positions in the water, will be monitoring the real-time collection of water conservancy information in a timely manner to the monitoring center, real-time dynamically, report the monitoring, timely find problems and processing, conform to the reservoir flood control, water supply, irrigation, power generation of the actual needs, and implement the requirements of modern water conservancy[1-2].

II. THE OVERALL STRUCTURE OF THE SYSTEM

This system adopts the pattern of decentralized monitoring and centralized processing. The entire monitoring control, transmission, and data reception processing system constitutes a system of distribution, including three large parts:

A. Field Monitoring Section

It is mainly based on the data collection equipment of the S3C2410 ARM9 chip, and has increased the GPRS

communication module which supports short message and data communication. The terminal data collection device can be sent to the monitoring center through GPRS Modem, while also receiving monitoring center commands for the operation.

B. Transport Links Section

The terminal data collection equipment and monitoring center communicate through GPRS Modem through GPRS wireless network.

C. Data Monitoring and Processing Centers

With access to mobile communication enterprise SP server, remote from the measured data, complete the hydrologic data processing, preservation, and other functions, also send control commands to the remote terminal of Modem equipment. When the alarm is called, the message can be forwarded to the remote operator's phone.

System function concrete realization process is: the data acquisition front-end at regular intervals to measure water level, water level, time and other useful information coding, according to the specific agreement for the accuracy of the sensor information processing, packaging, forming a short message, through the GPRS communication module will be sent to the monitoring center. Monitoring center will receive the message in the corresponding decoding and processing, the flow of statistical time out at a specific location, sent to various water control and decision making personnel and stored in the database for hydrologic information query in the future, the whole monitoring system structure as shown in Fig .1[3-5].

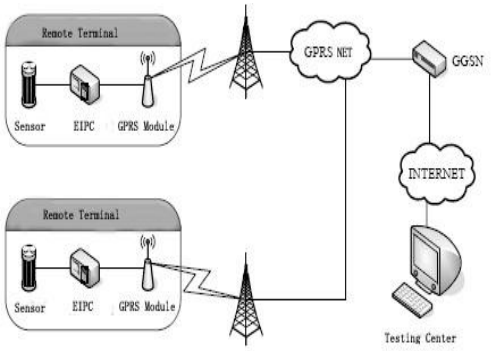

Figure 1 System structure diagram

III. THE MAIN FUNCTIONAL MODULE OF THE SYSTEM

In view of the present in the domestic area of water management in water conservancy information monitoring and sin problem, using the modern electronic technology and network communication technology, considering practicality, versatility, and scalability of the system, the system main function is divided into three modules.

A. Hydraulic Information Collection Module

General system of water conservancy projects in the field, even in remote mountainous area, information collection and communication influenced by natural environment conditions, all equipment shall be taken into account can continuous work in bad weather conditions, the encounter the most adverse circumstances can still achieve the most basic request of information transmission system design. In addition, because of incomplete and sin area field power supply facilities in a wide range of measuring point, low power consumption and low cost are put forward according to functional units and maintainability high demand.

B. GPRS Communication Module

For sin district of hydrologic data collection with measuring point, scattered layout, real-time demand is not high, the data transmission flow of small, send the low frequency characteristics, the existing cable communication mode hardware cost is too high. In recent years, with the rapid development of GSM, GPRS and CDMA technology, wireless data transmission speed and stability has been greatly improved, especially suitable for application in water conservancy information monitoring is not easy to wiring, a little quantity of monitoring data transmission field. Because GPRS technology can connect directly to the Internet via a gateway, the overhead machine does not need to receive a module of information, which greatly reduces the hardware cost and optimizes the composition of the system.

C. The Upper Machine Management Module

The management software is responsible for the data processing and the data processing. The database construction in the flood area is at the core of the construction of water resources real-time monitoring and management system. Sin area includes two aspects the contents of the database construction and the construction of the content of the construction of the database structure and database, the database structure refers to the anatomy of sin area, carry on the reasonable classification to the sin information, in accordance with the related theory and method of database design design is reasonable in structure, easy to implement in technology, and meet the application requirements of logical database and the physical database. Database content is according to the actual situation of sin area, using the database management system to provide the input tool will sin the data input to the database, the database become a have abundant information database warehouse, meet the requirements of sin daily management and decision support.

IV. SYSTEM HARDWARE DESIGN

The hardware components of this system are mainly composed of water level information collection devices, measurement and control units, communication module and monitoring center computer. We can see it in Fig.2.The measurement and control unit by A microprocessor, A/D, sensors, actuators, mainly to complete the data collection and processing, to control command decoding execution, etc. Communication module chooses special industrial GPRS communication module, complete to send and receive SMS text messages and connect the Internet network, etc, under a

communication module to realize the receiving and sending of information, upper monitor computer access to the Internet, from the Internet directly to in the form of short message sent to the hydrologic data and complete the control commands sent, finally will classify the collected data is stored in the corresponding database for inquiry calls. The water management department can obtain the water information in the flood area in time to make use of the water service.

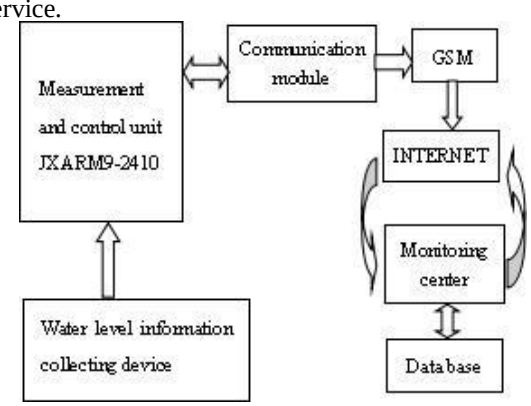

Figure 2 A structure diagram of the system hardware

V. RESEARCH AND IMPLEMENTATION OF TERMINAL NETWORK ACCESS

A. The Node Associated with the Terminal Access Network

Logically, GPRS is implemented by adding SGSN and GGSN new network nodes in the GSM network structure. Due to the addition of these two network nodes, the corresponding new interface needs to be added. Fig.3 illustrates the GPRS logical architecture. The GPRS network is a very complex system, and the following is an analysis of two entities that are concerned in the design of this article.

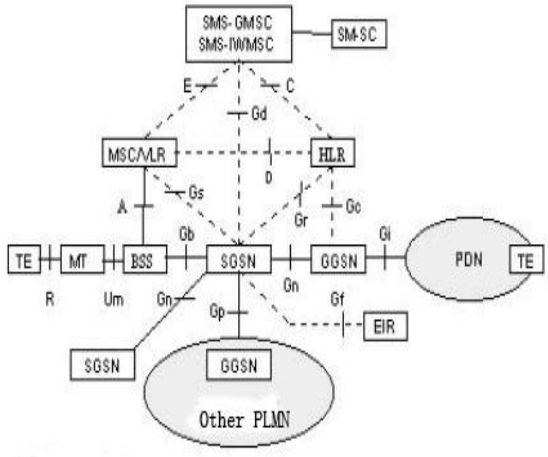

----Signaling interface
——Signalling and transport interfaces

Figure 3 The logical structure of GPRS backbone

The GPRS support node GSN is the most important network node in the GPRS network, including the functionality required to support GPRS. GSN has a mobile routing management capability that connects various types of data networks and can be connected to the GPRS register. GSN can complete data transfer and format conversion between mobile and various data networks. GSN is an independent device that resembles a router, and is integrated with MSC in GSM. Multiple GSN is allowed in a GSM network. There are two types of GSN: SGSN and GGSN. SGSN is the node that provides the business for the mobile terminal (MS). In activating the GPRS business, SGSN established a mobility management environment that included information about mobility and security aspects of the mobile terminal (MS). The main purpose of SGSN is to record the current location information of the mobile platform and to send and receive mobile packet data between the mobile and SGSN. GGSN is connected to the group data network by configuring a PDP address. It stores the routing information of the GPRS business users belonging to the node, and USES the information to send PDU to the current business access point of MS, known as SGSN, using tunnel technology. GGSN can query the user's current address information from the HLR through the Gc interface.

GGSN is primarily a gateway function that can be connected to a number of different data networks, such as ISDN and LAN. In addition, GGSN is also known as the GPRS router. GGSN can convert the GPRS packet packet from the GSM network to a remote TCP/IP or other network. The functions of SGSN and GGSN can be implemented both by a physical node and by different physical nodes. They all have IP routing capabilities and can be linked to IP routers. When SGSN and GGSN are located in different PLMN, they are connected through the Gp interface. SGSN can send location information to MSC/VLR through any Gs interface, and can receive calls from MSC/VLR via the Gs interface.

B. Process Analysis of GPRS Network for GPRS

The GPRS terminal designed in this paper collects and monitors the data collection from the RS232 serial port. The data is then uploaded to the server. Data transfer from the user terminal to the server: GPRS wireless terminal reads live device data from the user terminal through a serial port. The data is processed by GPRS terminal and sent to GPRS service support node (SGSN) by GPRS group data. SGSN communicates with the GPRS gateway support node (GGSN), which handles the grouping data and sends it back to the server on the Internet. GPRS backbone networks include GPRS service support junction (SGSN) and GPRS gateway support (GGSN). SGSN USES the base station subsystem (BSS) to complete the control of the mobile desk (MS), and locate MS by communicating with the register (HLR). SGSN and GGSN are connected via the IP backbone network in GPRS, where SGSN is between MS and GGSN and delivers data to MS and corresponding GGSN. GGSN is responsible for routing and encapsulation between GPRS and external data networks. GPRS network transport data mainly USES GPRS service support junction (SGSN) and GPRS gateway support junction (GGSN). Using GPRS network transfer data, you can view it as three processes, namely the

connection process, the data transfer process, and the termination process.

C. GPRS Terminal Communication Design

The GPRS module in this system USES the link layer PPP protocol for communication. The GPRS module communicates before the communication, then links the link to the TCP/UDP application transfer call. The process of data transfer by the network protocol stack is really a process of data encapsulation and data unmarshalling. When sending data, according to the application layer (user data) a (UDP) transport layer, network layer data link layer (PPP), a physical layer (serial) order data encapsulation: and when receiving data, decapsulation in reverse order. The implementation of the upper function needs to be applied to the underlying function, and the underlying function is to serve the upper function.

VI. SYSTEM SOFTWARE DESIGN

Linux, as an open source operating system, has unique advantages and extensive applications. Linux is highly flexible and can be tailored to suit a variety of application requirements. Linux was originally designed for desktop applications general-purpose operating system, not only inherited the characteristics of the Unix, including virtual memory mechanism, process support and user management, etc.; And many aspects exceed Unix, becoming the first choice for embedded development and the mainstream of the market in terms of open source, free, stable, etc. In addition, Linux is a portable cross-platform operating system that supports a wide range of different architecture processors. Linux can run whether it is a CISC, RISC, 32-bit, or 64-bit processor. The development of embedded Linux on the ARM platform is a bottom-up, step-by-step process, and of course some work can be done in parallel, typically with the following steps:

1) install and set up development tools on the host machine and set up a cross compilation environment;

Install the Bootloader on the target board.

3) configure and compile the kernel;

4) install and run the kernel by Bootloader;

5) device driver development;

6) prepare the contents of the root file system;

7) install the target root file system;

8) develop and run applications;

9) system integration.

This article USES the desktop Linux system RedHatLinux9.0 as the host development environment and communicates with the target board via the serial line and the network line. The host machine running terminal emulation program as the target board console (the console), and through the Ethernet transmission files and programs, in the form of a virtual terminal display target program running on the host. In this development mode, including the Bootloader, the kernel, the root file system, and the application are stored in the NANDFlash of the target board.

Using the terminal emulator minicom on Linux, you need to configure it properly before using it for the first time. Run minicom-s, select "Serialportsetup" under the Configuration menu, and select "Savesetupasdf1" to save the exit. Ethernet connections are used to download images of the kernel and root file system; After running embedded Linux on the target board, you can implement Linux's powerful network communication capabilities between the host and the target board. For example, you can mount a Shared directory and run the target program through NFS (network file system). You can also use TFTP (TrivialFileTransferProtocol) to transfer files and programs.

VII. CONCLUSION

Due to distribution is more dispersed, the monitoring stations of sin number, for the needs of multi-level management of water resources, a variety of information demand of modern sin district water resources management makes hydrologic monitoring system of the workload increased significantly, although general water automatic monitoring system to solve the traditional manual monitoring cycle is long, the disadvantages of low efficiency, small range but is common in the aspect of hydrologic data transmission investment costs, maintenance difficulties, easy to cause hydrologic data of the leaders, false positives, misstatement or omission, difficult to meet the practical requirements. To solve above problems, this article in to the area of informationization construction of sin based on the analysis of the basic content and characteristics of flood area based on ARM and GPRS hydrologic monitoring system for the overall structure of short message. To compile flood zones to monitor computer communication and data management software. The water conservancy information monitoring system is designed based on ARM and GPRS short information. Characteristics of this system is based on a wide coverage of the GSM short message service provided mobile communication public network transmission hydrologic data, without networking, suitable for actual, system operation cost is low, the data transmission reliable and rapid. In addition, the system is simple, intensive, and has good mobility.

REFERENCES

[1] Aacek, Szymensky. Embedded Internet Technology in Process Control Device.IEEE, 2002, 6(3):77-82.

[2] ARM Limited,ARM920T(Rev 1)Technical Reference Manual,2000.

[3] Wookey,Tak-Shing,Aleph One,Porting the Linux Kernel to a New ARM Platform,Guide to ARMLinux for Developers,2002：52-59.

[4] TC35 Cellular Engine Hardware Interface Description[S],Siemens Inc,2002.369.

[5] AT Command Set Siemens cellular engines V03.10[S].Siemens Inc,2002.284.

[6] Samsung Electronics Co. Ltd S3C2410X 32-Bit RISC Microprocessor User's Manual(Revision 1.2),2003.

[7] ARM Limited.ARM9TDMI Data Sheet. ARM Limited, 2002:34-36.

[8] Frank Vahid and Tony Givargis. Embedded System Design: A Unified Hardware/Software Approach. University of California: Department of Computer Science and Engineering, 2006:57-60.

[9] Samsung Electronics Inc. S3C2410X Data Sheet. Samsung Electronics Inc, 2003:4-45.

[10] Siemens Mobile. MC35 Hardware Interface Description. Siemens Mobile, 2004:13-16.

[11] Karim,Yaghmour.Buliding Embedded Linux Systems,2003.

Design of the Automatic Generative System of Examination Papers Based on ARM

Liancheng Guan
Information Construction office
Tianjin University of Technology and Education
Tianjin, China
E-mail: guanlc@tute.edu.cn

***Abstract*—With the development of network technology, the design for the automatic generative system of examination papers that is based on web has become a trend. In order to reduce the burden on teachers and avoid duplication of work, we design the system to automatically generate test papers. It is based on a constantly updated examination question bank system, according to the teachers' demands, which can automatically generate the test paper with a certain degree of difficulty, the number and value. The client configuration is simple and it can be free from geographic constraint. Users only need to go through their own identity authentication to enter the automatically generated system of test papers, and to manage and maintain examination questions, exam and user information and so on. The exam contents can be constantly enriched and improved and the data sharing among teachers can be easily performed. It will have important practical significance to improve work efficiency.**

Keywords-Automatic generative system; ARM; Management model; Database; Parameters.

I. INTRODUCTION

In the daily teaching work, especially before the midterm and final exams, first trouble and stressful issue before teachers is to design a set of scientific and reasonable examination papers. In general, a teacher wants to come up with an test paper, either to find out the questions in a huge examination question bank, and then, one by one, to put them on the paper, either to pick out a one from several books related to the subject.[1] Of course, there are some teachers now, or selecting and modifying the questions from the teaching plan of the usual lectures. Thus, it will be difficult to ensure the coverage areas and difficulty of the questions.

With the development of network technology, the traditional examination way is quickly replaced by paperless examination, which has become the mainstream now. Therefore, the development of the automatic generative system of examination papers will have a strong practical value.[2] The examination of the paper for learners is the primary method for the evaluation of teaching effectiveness. The number, difficulty and discrimination of the questions on the paper will eventually affect the reliability of teaching evaluation. [3] For a teacher, a good automatically generated system of test papers can reduce the burden on teachers, and avoid duplication of work to improve work efficiency. [4]

In this paper, the automatic generative system of examination papers is an application based on the internet network. This paper develops papers automatic generation system is based on Internet applications, the client configuration is simple and it can be subject to geographical constraints. Users only need to their own identity authentication to enter the automatically generated system of test papers, and to manage and maintain examination questions, exam and user information and so on. In addition, all test questions are based on a set of test database, its contents can be continuously enriched and improved, and the data sharing is very convenient among teachers.

II. ANALYSIS FOR USER'S REQUIREMENTS

For the automatic generative system of examination papers, first, it should be designed by the different kinds of type, the number of questions, the difficulty and score, in order to establish the corresponding the test database. Second, the papers is composed of random. Third, in a paper automatically generated, the knowledge keys involved can not occur. Fourth, the resulting paper should meet the requirements of the syllabus.

When the test paper is made, the questions are selected by the system in the questions database, they can meet user's requirements, and the efficiency and probability of success is high.

The user interface of this soft is friendly. The user's requirements can be set by way of human-computer interaction, such as: the scores for all kinds of questions in the test paper, the overall difficulty, the distribution of knowledge points and the proportion of various types of questions, and so on.

III. IMPLEMENTATION OF FFT PROGRAM OF DATA PROCESSING

Spectrum analysis is required by the data signal in many cases and the theoretical basis is the discrete Fourier transform (DFT). Fast Fourier transform analysis is the tool to analyze and process digital signal. This paper mainly introduces the decimation-in-time radix-2 FFT butterfly algorithm and its implementation of S3C2410X program.

According to the definition, $x(n)$ DFT of N point sequence is as shown in formula (1).

$$X(k)=\sum_{n=0}^{N-1}x(n)e^{-j\frac{2\pi nk}{N}}=\sum_{n=0}^{N-1}x(n)W_N^{nk}\quad ,k=0,1,\Lambda\ ,N-1 \tag{1}$$

and

$$W_N = e^{-j\frac{2\pi}{n}} \tag{2}$$

The basic idea of butterfly algorithm is that first conduct odd-even halving for the sequence until each subsequence becomes a term, then merge odd-even sequence combined with the butterfly diagram, and finally synthesize the original sequence DFT according to the sequence of $N/2$. Its mathematical description is shown as below:

Set the length of $x(n)$ as $N = 2^L$ and merge the odd-even sequence into two sub-sequences. The computational formula is shown as follows:

Odd sequence：

$$z(r) = x(2r+1) \tag{3}$$

Even sequence：

$$y(r) = x(2r) \tag{4}$$

In the formula (3) and (4), $r = 0,1,\Lambda\ ,\frac{N}{2}-1$. And DFT of $y(r)$ and $z(r)$ is $Y(k)$ and $Z(k)$, therefore the DFT of $x(n)$ can be expressed as:

$$\begin{cases} X(k) = Y(k) + W_N^K Z(k) \\ X(\frac{N}{2}+k) = Y(k) - W_N^k Z(K) \end{cases} \quad k = 0,1,\Lambda\ ,\frac{N}{2}-1 \tag{5}$$

In formula (5), W_N^k is known as the butterfly factor,that is,

$$W_N^k = e^{-j\frac{2\pi}{N}k} = \cos(\frac{2\pi}{N}k) - j\sin(\frac{2\pi}{N}k) \tag{6}$$

As the calculating diagram of formula (5) is like a butterfly as shown in Fig. 1, it is called the butterfly algorithm.

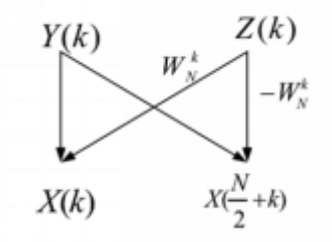

Figure 1. Tthe butterfly diagram of the calculating relation

Based on the above analysis, the callable function of butterfly algorithm is Bit_Reverse.Reversely rearrange the original sequence in accordance with the bit code. When $n = n'$, data is not exchanged; when $n \neq n'$, exchange $x(n)$ and $x(n')$. Taking $N = 8$ as an example, reversely rearrange $x(n)$ in accordance with the bit code $n = 0,1,\Lambda\ 7$ and the calculation results are as shown in Table 1 below.

TABLE I. 8-BIT CODE INVERTED SEQUENCE ADDRESSING

Source sequence bit code n	**Storage address**	**Bit code inverted sequence address**	**Bit code of new sequence** n'
0	000	000	0
1	001	100	4
2	010	010	2
3	011	110	6
4	100	001	1
5	101	101	5
6	110	011	3
7	111	111	7

The sequence of complex numbers which meets $N = 2^L$ is divided into L levels in FFT algorithm and each level can be subdivided into several groups which include a number of butterfly units. The number of levels is expressed as $stage = 1,2,\Lambda\ ,N/2$, the number of groups is expressed as $group = N/2, N/4,\Lambda\ ,1$, the butterfly unit is expressed as $s\_cnt = 0,1,\Lambda\ ,stage$ and the relationship between the butterfly computation data is as shown in equation (6).

$$\begin{cases} indexB = indexA + stage \\ indexA = indexB + 1 \end{cases} \tag{7}$$

For the number of levels $stage$ and the number of units s_cnt, the butterfly factor can be expressed as:

$$W_{stage\times 2}^{s\_cnt} = \cos(\frac{\pi}{stage}s\_cnt) - j\cdot\sin(\frac{\pi}{stage}s\_cnt) \tag{8}$$

Conduct successive iteration for the results combined with the butterfly algorithm. Reversely rearrange the original input data and conduct FFT calculation.

IV. THE DESIGN FOR THE AUTOMATIC GENERATIVE SYSTEM OF EXAMINATION PAPERS

The development of this system is based on Web, its design is more compact. The requirements on the server performance are not high. It provides a friendly interface and the simple operation in order to enable users to easily access. The function of the system is rich and its practicability is stronger. The interface of the management menu is shown in Fig. 2.

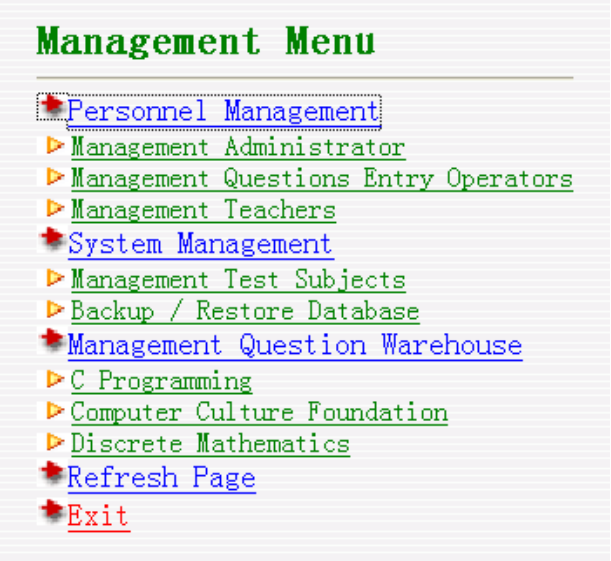

Figure 2. Management menu page

A. The Main Function of the System

The main functions of the automatic generative system of examination papers include the user management module, test subjects management module, system management module and question database management module, and so on. The system structure is shown in Fig.3.

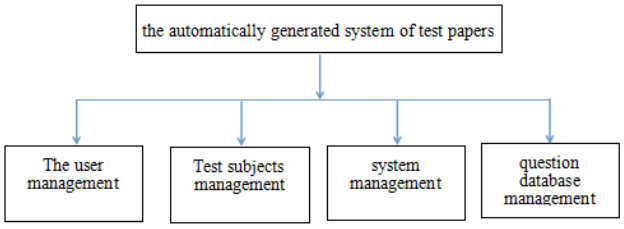

Figure 3. The structure of the automatic generative system of examination papers

The module includes the management of administrators, the teaching teachers, questions entry operators. The administrator can set teacher's teaching subjects. The administrators consider that the teachers registered in the system is the teaching teachers, who must also be registered for teaching the lesson. In order to ensure the security of the legitimate user account, the system provides a function to modify personal information. The teachers and administrators can modify their own login password in a timely manner through this function, its purpose is to ensure that their accounts are not stolen by others. The questions entry operators can only enter the questions and the additional information can not be modified by them.

The administrators can manage the test subjects, such as: delete and add the test subjects. The teachers can add, delete and query the examination information they is teaching the courses. After the parameters related to the examination papers are specified, it can automatically generate paper. Then, after the preview and edit, finally, the papers needed are printed out. Teachers can not modify or query the examination information of other teachers teaching the lesson.

The system management model includes the managements of the test database for various subjects and the backup / restore functions of the database. Once the system is damaged, the normal state will be quickly restored.

This model includs adding and modifying the description of the questions in the test database. To reduce the burden on teachers, the questions can be completed by the questions entry operators with a lower level. Considering the boring and repetitive questions entry work, the questions entry operators and the corresponding management modules are added. For system security reasons, the entry operators are only responsible for the examination questions. If the test database needs to be changed, the authorization can be applied, but other settings will be restricted for the system. After the teacher's identity of the corresponding subjects is verified, it is formally submitted to the database. So the deleting operation can only be done by the teacher.

B. The Protect of the System and Database Files

In order to prevent the unauthorized access to the automatic generative system of examination papers, there are many different interfaces on the home page, which are offered to the different people to log in. The permissions of the teachers, the administrators and the questions entry operators are divided, and the function of changing the password is provided. Especially, each page has the authentication check, and the purpose of checking the user's authority is to determine whether the page can be accessed. The login page for the automatically generated system of test papers is shown in Fig. 4.

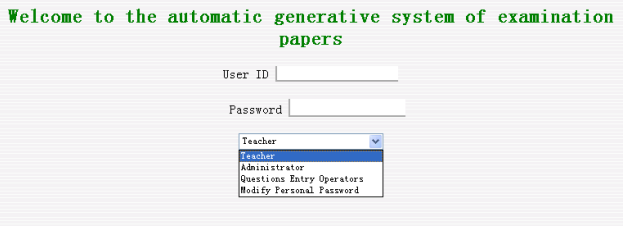

Figure 4. The login page for the automatic generative system of examination papers

The database files of the system are placed in the other directory, and use the irregular directory names and the

special file names, the purpose is to prevent the unauthorized users to download program files and database files.

In the event of an accident, in order to prevent the databases of the system from loss, the database backup and recovery features is added to the system. So the users can backup and recovery the database according to their need. In order to ensure the lawful rights of the users and the security of their accounts, the function of the personal information, which can be modified by users, has been increased. The landing system is available to all users through the function, the login password can be timely modified to prevent it from being stolen.

C. Setting the Major Parameters of the Examination Paper

Before the papers are generated, the examination name, the subjects and the type of questions, etc., which need to be set. If the number of questions is 0, this type means no test questions. The page of the test subjects and the questions, which need to be set, is shown in Fig.5.

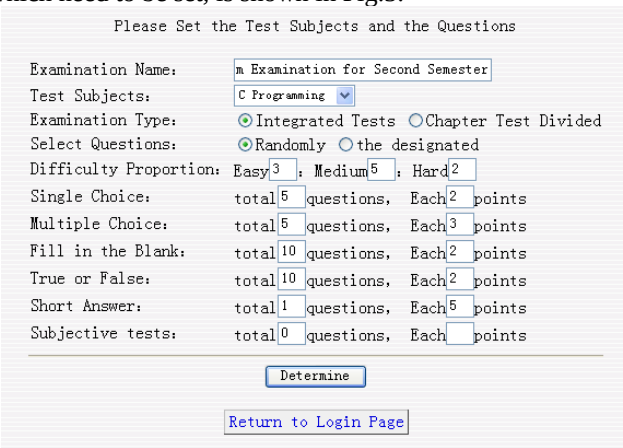

Figure 5. The page of the test subjects and the questions

After the test subjects and questions are set, the parameters of the papers need to be checked in order to ensure the correct parameter settings. After the confirmation, the user can click the button to generate the papers. If not satisfied, can click the Reset button and again set the parameters and confirm. The interface, which the parameters of the papers need to be confirmed, is shown in Fig. 6.

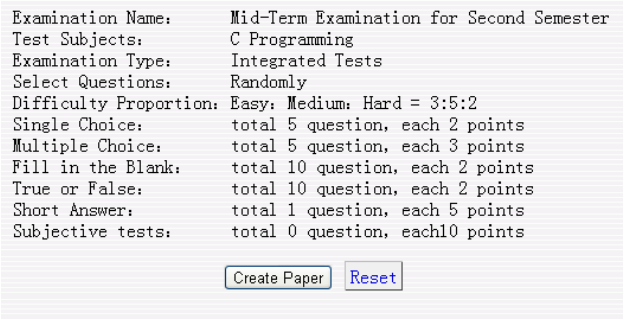

Figure 6. The parameters of the papers need to be confirmed

For the particular subject, if the papers randomly generated not be satisfied, the user can refresh the page to regenerate the new one. The display and printing button of the answer is at the bottom of the papers, the user can print directly to the answer.

V. CONCLUSION

This system is based on the Internet and suitable for the test papers automatically generated. it has a constantly updated examination question database and can constantly enrich and improve examination contents according to the teachers' demands. At the same time, it can also automatically generate the test paper with a certain degree of difficulty, the number and value. The client configuration is simple, and it can be subject to geographical constraints. Users only need to their own identity authentication to enter the automatically generated system of test papers, and to manage and maintain examination questions, exam and user information and so on. The data sharing among teachers can be easily performed.

ACKNOWLEDGMENT

This project was supported by Tianjin Education Science "Twelve- Five" Planned Research Topics ,Tianjin, China.(No.CE3008).

REFERENCES

[1] Sorensen H V, "On computing the split-radix FFT,"IEEE Trans on Acoustics, Speech and Signal Processing,vol.78,pp.1603-1624,2016

[2] YANG Xun, "Algorithmic research on online examination system," Computer Knowledge and Technology,vol.13,pp.45-46,2015.

[3] Qi Zhongqi, " Building of automatic creating system of examination papers in LAN," China Educational Technique &Equipment, vol.21,pp.77-78,2014.

[4] CHEN Sha and Yang Feng, " The design and research on the automatically generated system of test papers,"Market Modernization,vol.18,pp.128-129,2014.

[5] John G. Proakis and Dimitris G. Manolakis, Digital Signal Processing. Prentice Hall/Pearson, 2016.

[6] Wookey, Tak-Shing and Aleph One , "Porting the linux kernel to a new ARM platform,"Guide to ARMLinux for Developers, vol.33,pp.52-59,2014.

[7] Lin Y H, Liu Y S and Gao G. , "The IFC-based path planning for 3D indoor spaces,"Advanced Engineering Informatics, vol.27,pp.189-205,2016.

[8] Jun Lin,The Automatic Generative System. Beijing: Electronic Industry Press, 2015.

[9] Qingguo Zhou, Li Wang and Yanlong Wang, " A remote data acquisition and control system for Mossbauer spectroscopy,"Nuclear Instruments and Methods in Physics Research, vol.215,pp.577-580,2014.

[10] Mazinani M. and Abedzadeh M. , "Dynamic facility layout problem based on flexible bay structure and solving by genetic algorithm,"International Journal of Advanced Manufacturing Technology, vol.65,pp.929-943,2015.

Research on Image Denoising Adaptive Algorithm for UAV Based on Visual Landing

Pengrui Qiu[12]
[1]Faulty of Land Resource Engineering,Kunming University of Science and Technology,Kunming Yunnan,China
[2]Training Department, Kunming Metallurgy CollegeKunming Yunnan,China
E-Mail:80420631@qq.com

Shu Gan
Faulty of Land Resource Engineering
Kunming University of Science and Technology
Kunming Yunnan,China
E-mail:ganshu@qq.com

Xiping Yuan
Faulty of Land Resource Enagineering
Kunming University of Science and TechnoloAgyKunming Yunnan,China
E-Mail:yxpkm@163.com

Yu Lin
Department of Computer Science
Kunming Metallurgy College
Kunming Yunnan, China
E-Mail:15087048891@qq.com

Abstract*—UAV autonomous landing refers to the UAV lands on only depending on airborne navigation equipment and flight control system, and ultimately achieves a safe landing. To achieve self-landing, UAV must have the ability to self-navigation and positioning, so that the high-precision visual navigation positioning technology is the key to achieve UAV self-landing technology.This paper concentrating on the noise effects on the pictures obtained during visual landing process of UAV, it has introduced the gravity of classical physics to image pixel, come up with a mathematical expression for the strength of gravity between pixels, then conformed the adaptive window by the gravity between pixels and performed corresponding filtering processing. It is shown by the experimental results that this algorithm has a great improvement on image denoising and detail preserving when compared with the traditional median filtering *and switching median filtering algorithms.

Keywords-UAV; visual landing; median filter; image;gravity between pixels; adaptive window

I. INTRODUCTION

In recent years, with the rapid development of information technology, UAV (Unmanned Aerial Vehicle, UAV) technology is also developing rapidly. How to achieve the UAV's autonomous flight, especially the UAV's autonomous landing is the most urgent challenge that the current UAV industry need to solve. UAV autonomous landing refers to the UAV lands on only depending on airborne navigation equipment and flight control system, and ultimately achieves a safe landing. To achieve self-landing, UAV must have the ability to self-navigation and positioning, so that the high-precision visual navigation positioning technology is the key to achieve UAV self-landing technology[1][2]. In the acquisition of UAV landing images, it is vulnerable to be affected by random noise. The existence of noise will not only reduce the quality of the image, but also destroy the important information carried by the image, how to effectively eliminate such noise, accurately calculatethe UAV landing parameters, is an important issue in image processing field[3].

Median filtering is a non-linear processing technique based on the ranking theorythat can effectively eliminatenoise[4][5]. The median filter provides good denoising capability for some types of random noise, and better in protecting the edge of the imagethan the same size of linear smoothing filter. Although the traditional median filter has been widely used in denoising, there are many obvious problems. In order to overcome the shortcomings of the traditional median filter, many improved median filters such as the extreme value median filter [6], the switching median filter, the weighted median filter, the adaptive switching weights A mean filter, an improved median filter based on large and minimum values, and many others were produced[7]. These improved filters use some criteria to determine whether the current pixel is noise or not before filtering the image. If it is noise, executes the corresponding median filter processing; otherwise, no special treatment for the current pixel. In terms of denoising, the traditional median filter has been greatly improved. Based on these theories, this paper proposed an improved adaptive median filter algorithm, which not only has a stronger noise removal capability, but also can retain more details of the image information[8].

II. GRAVITATIONAL FORCE BETWEEN IMAGEPIXELS

Gravitational law points out that there is a gravitational interaction between any object, and the gravitational force between the two particles is proportional to the product of the two, inversely proportional to the square of the distance. The mathematical expression is shown in equation (1).

$$\Phi = -\frac{GMmr}{r^3} \quad (1)$$

Where: M is understood as the mass of the central body; G is the gravitational constant; formula(1) describes the gravitational force of the mass of m; r is the displacement vector of m relative to the elbow; r is the distance size of the two. The gravitational pull between image pixels is based on this theory, but it should be noted that the basic concepts and methods of introducing the law of gravitation are only considered in the mathematical sense, regardless of their physical constraints.

A. Distance of pixel

A, B is the two pixels of the image, the coordinates in the image are (x_1, y_1) and (x_2, y_2), D (A, B) is the distance between pixels A and B[9] [10].

1) Euclidean distance

$$\Delta(A,B)=[(x_1 - x_2)^2 + (y_1 - y_2)^2]^{1/2} \quad (2)$$

2) Distance of the city block

$$\Delta(A,B)=|x_1 - x_2| + |y_1 - y_2| \quad (3)$$

Distance of board

$$\Delta(A,B)=\max|x_1 - x_2| + |y_1 - y_2| \quad (4)$$

Where: The eight neighborhood of A is the pixel with D (A, B) = 1.

B. The Pixels Between the Gravitational Force

Assumption there is a digital image I (m, n), (m, n) ∈I (m, n) represents the gray value at the position (m, n). According to the law of gravity, I (m, n) can be described as the quality of the pixel at the position (m, n). A, B is random two pixels of the digital image, where the positions in the image are (m1,n1) and (m2,n2),and the corresponding gray values are I (m1,n1) and I (m2,n2). So we can get the formula of resulting pixel gravitational.

$$\Phi(m_1, n_1, m_2, n_2)=\kappa\frac{I(m_1,n_1)*I(m_2,n_2)}{r^2} \quad (5)$$

Including:k is the gravitational constant value of pixels, this paper use k = 1 ,r is the distance between the two pixels.

III. THE CONTENT OF THIS ARTICLE

A. Median Filter and Adaptive Window

This paper use the noise criterionis in the digital image I, if the gray value of the current pixel in the neighborhood window is the maximum value or the minimum value, the pixel is judged to be noise; otherwise, the pixel is a signal. The mathematical expression is shown in equation (6).

$$\Sigma=\begin{cases} 0 = I(m,n) = \min(W) \text{ or } I(m,n) = \max(W) \\ 1 \quad \text{others} \end{cases} \quad (6)$$

Including:I(m,n) is the gray value at the position (m, n); W is the neighborhood window which centered on I (m, n), It is a pixel gray value matrix which can be shown in equation (7). Here, the signal judgment S = 0 indicates that I (m, n) is noise and S = 1 is expressed as a signal.

$$\Omega=\begin{bmatrix} I(m-1,n-1) & I(m-1,n) & I(m-1,n+1 \\ I(m,n-1) & I(m,n) & I(m,n+1) \\ I(m+1,n-1) & I(m+1,n) & I(m+1,n+1) \end{bmatrix} \quad (7)$$

Select the 3 × 3 size of the adaptive window, the initial condition $AW=\begin{bmatrix} 0 & 0 & 0 \\ 0 & 0 & 0 \\ 0 & 0 & 0 \end{bmatrix}$ If the I= (m, n) value is not updated and the value of S at the position is 1, the 3 × 3 window data is skipped to the next position; if S = 0, I (m, n) is updated, calculate the maximum and minimum values of the 3 × 3 window W data firstly, and then calculate the gravitational force of I (m, n) of the pixels in its eight neighborhoods. The adaptive window AW is updated by Eq. (8).

$$A\Omega(\iota,\varphi)=\begin{cases} 1 \ I(m,n) = W_{min} \& \ t_2 < F(m,n,m+i,n+j) < t_1 \\ 1 \ I(m,n) = W_{max} \& \ t_4 < F(m,n,m+i,n+j) < t_3 \\ 0 \quad \text{others} \end{cases} \quad (8)$$

Including:i ∈ {-1,0,1}, j ∈ {-1,0,1}, and I, j can not be 0 at the same time.

After determining the matrix AW, update the window W which centered on I (m, n), and the expression between W and AW is shown in equation (9). Sort the window W non-zero elements, and then replace the original gray value with the original (m, n) position, the expression is shown in equation (10).

$$\Omega(\iota,\varphi)=\begin{cases} I(m+i,n+j) & AW(i,j) = 1 \\ 0 & AW(i,j) = 0 \end{cases} \quad (9)$$

$$I(\mu,\nu)=\underset{\substack{(i,j)\in|-1,0,1| \\ \text{and } W(i,j)\neq 0}}{\text{median}}\{W(i,j)\} \quad (10)$$

B. The Main Steps of the Algorithm

- Determine whether I (m, n) is noise according to the window W which the image is centered at a certain pixel I (m, n).
- If I (m, n) is a signal, I (m, n) is not updated and window W slides to the next position.
- If I (m, n) is noise, the adaptive window AW is calculated according to Eq. (8).
- When the adaptive window AW is not 0 either, the pixel I (m, n) is updated according to Eq. (9) (10).
- When the adaptive window AW all is 0, record the data that has been updated and the number equal to I (m, n). If the number is less than the threshold count, update I, otherwise I is not updated. The default count is 2; if the original image has a large area of gray value is 255 or a large area of gray value, count is 1.

IV. EXPERIMENTAL RESULTS AND ANALYSIS

Select the UAV image size as 200×200 pixels.Picture1 is the UAV original image and the UAV image which after add the noise density of 0.1,0.2,0.3,0.4 and 0.5 . Picture 2(a)is the process effect of the SM (switch median) filter, Picture2(b)is the processing effects of he TM (traditional rate) filter t.Picture2(c)is the processing effect of the algorithm.

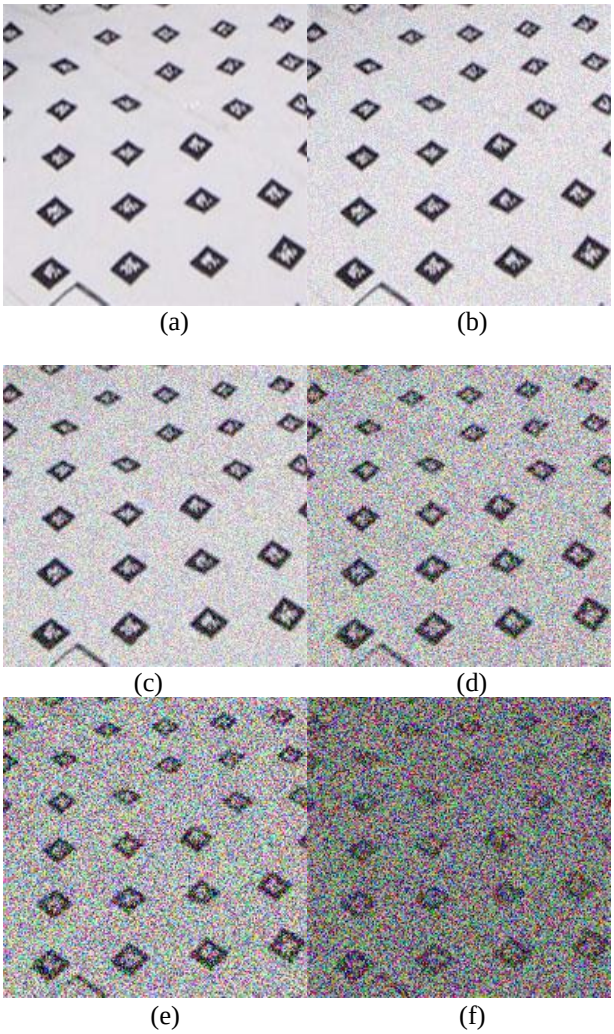

(a) (b)

(c) (d)

(e) (f)

Figure 1. UAV original image and the UAV image which after add the noise density of 0.1(b),0.2(c),0.3(d),0.4(e) and 0.5(f)

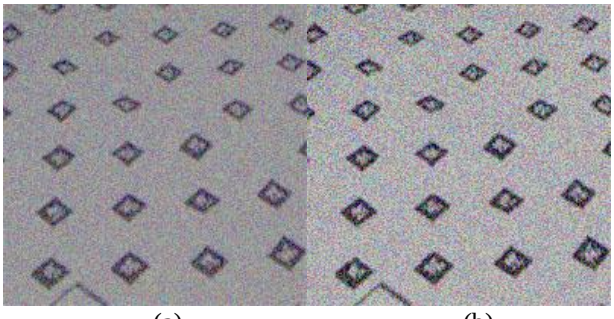

(a) (b)

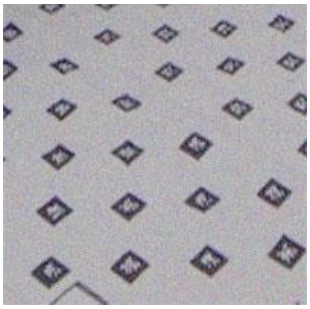

(c)

Figure 2. Picture 2(a)is the process effect of the SM (switch median) filter, Picture2(b)is the processing effects of he TM (traditional rate) filter t.Picture2(c)is the processing effect of the algorithm.

In the point view of the visual , it can be seen fromPicture2.This paper proposed the algorithm which has been greatly improved in removing salt and pepper noise and preserving the details of the image, especially under the interference of large noise, the effect of denoising is more obvious The meanings of the algorithm are quantitatively described by mean absolute elror (MAE) and mean square error (MSE) respectively. The definitions of MAE and MSE are given in Eqs. (11) and (12).

$$MAE=\frac{\sum\sum|X(i,j)-Y(i,j)|}{m*n} \tag{11}$$

$$M\Sigma E=\frac{\sum\sum|X(i,j)-Y(i,j)|^2}{m*n} \tag{12}$$

Including: x (i, j) is the original image; Y (i, j) is the filtered image; m, n is the number of rows and columns of the image.

In Fig .3, each map maps the MSE and MAE curves corresponding to the different algorithms.

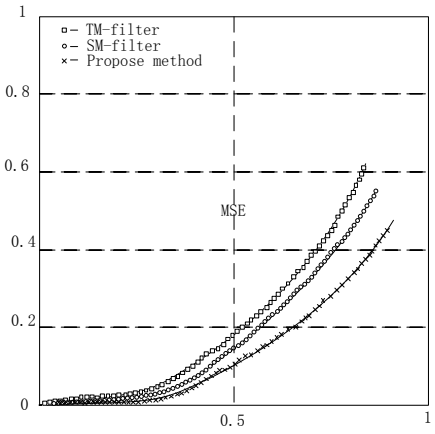

(a)

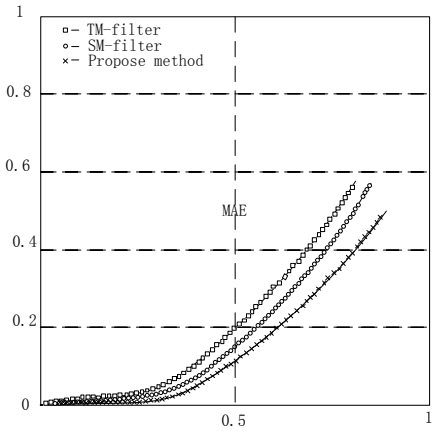

(b)

Figure 3. Picture3(a)is MSE curve, Picture3(b)is MAE curve use TM-filter,SM-filter and Propose method

It can be seen from the curve that the algorithm proposed from this paper is closer to the real data after image denoising, so the algorithm from this paper is better than the other two algorithms. The main reasons are as follows:

Detecting noise of pixels before filtering, onlyprocessing the pixels that are currently noise, and no noise-contaminated pixels are not processed, thus preserving more details of the image and reducing the degree of image blur. The median filter unconditionally treats all the pixels in the image, which may destroyed some unpolluted pixels while processing. When the contaminated pixels in an area of the image are processed, the shape of the adaptive window is controlled by the gravitational force between the pixels, thereby selectively filtering the pixels of the region, removing the interference of other noises, and more precisely gets the gray value of the current pixel. The median filter can not adapt to the local variation of the image when determining the size of the filter window El thus when the noise density is large, the processing effect is drastically deteriorated.

V. CONCLUSION

In this paper, we design an improved median filter, which introduces the concept of gravity in physics. By introducing the law of universal gravitation, this paper leads to the gravitational force of image pixel, and gives the mathematical expression of pixel gravitation. At the noise point, using the size of gravity between the pixels to determine whether the pixels in the neighborhood are noise or not. If the answer is yes, the data will be discarded; otherwise, the data is placed in the median filter data set. From the effect of image processing, graph of MAE and MSE, we can see that the algorithm proposed in this paper has greatly improved the denoising and detail reservation.

REFERENCES

[1] Xiangyu Yu,Lihua Guo.Image Registration by Contour Matching usingTangent Angle Histogram[J].IEEE computer society 2008.

[2] David G.Lowe.Distinctive image features from scale-invariant key-points[J].International Journal of Computer Vision,2004,60(2):90-110.

[3] S. T. Nuske, S. Choudhury , S. Jain, A. D. Chambers, L. Yoder,S. Scherer, L. J. Chamberlain, H. Cover, and S. Singh, “AutonomousExploration and Motion Planning for an Unmanned Aerial VehicleNavigating Rivers,” Journal of Field Robotics, June 2015.

[4] I. Sa and P. Corke, “System Identification, Estimation and Control for aCost Effective Open-Source Quadcopter,” in 2012 IEEE InternationalConference on Robotics and Automation (ICRA), 2012.

[5] G. M. Hoffmann, S. L. Waslander, and C. J. Tomlin, “Quadrotorhelicopter trajectory tracking control,” in AIAA guidance, navigationand control conference and exhibit, pp. 1–14, 2008.

[6] P. Pounds, R. Mahony, and P. Corke, “Modelling and control of alarge quadrotor robot,” Control Engineering Practice, vol. 18, no. 7,pp. 691–699, 2010.

[7] M. Achtelik, S. Weiss, and R. Siegwar, “Onboard IMU and MonocularVision Based Control for MAVs in Unknown In- and OutdoorEnvironments,” in Proceedings of the IEEE International Conferenceon Robotics and Automation (ICRA), May 2011.

[8] C. Zhang and J. M. Kovacs, “The application of small unmanned aerialsystems for precision agriculture: a review,” Precision agriculture,vol. 13, no. 6, pp. 693–712, 2012.

[9] M. Burri, H. Oleynikova, M. W. Achtelik, and R. Siegwart, “Real-timevisual-inertial mapping, re-localization and planning onboard mavs inunknown environments,” in Intelligent Robots and Systems (IROS),2015 IEEE/RSJ International Conference on, pp. 1872–1878, IEEE,2015.

[10] Akkoul S,Ledee R,Leconge R,et al.A new adaptive switching median filter[J].Signal Processing Letters,2010,17(6):587-590.

Design of Multi-channel Temperature Control Inspection System Based on PLC

Bi Xueqin
Institute of Electronic Information Engineering
Xi'an Technological University
Xi'an, China
bixueqin@126.com

Zhang Liguang
(Institute of Electronic Information Engineering
Xi'an Technological University
Xi'an, China
443032492@qq.com

Ma Xiaohui
Institute of Electronic Information Engineering
Xi'an Technological University
Xi'an, China
1300136901@qq.com

Abstract—The temperature control system is widely used in the field of industrial control, such as the boiler's temperature control system in Steel, chemical plants and thermal power plants. For the requirements of remote centralized management and security monitor in temperature control system, a temperature control inspection system consisted by down-computer clew and up-computer , is designed in this paper. In this system, a programmable logic controller (PLC) is use as up-computer, multiple AI smart meters are use as down-computer clew. The structure of the system hardware and the interconnection of the various parts are introduced simply, the design and implementation of communication system of down-computer is elaborated in detail, and the part of the communication system program is given. The actual operation shows that the remote monitoring function can be realized and design requirements be satisfied by the application of intelligent instruments of real-time collection, processing and feedback on the site temperature, and high efficiency, high universality and reliable stability are the advantages of the system.

Keywords-Programmable logic controller; Intelligent instrument; Temperature control system; Communication system; Inspection

I. INTRODUCTION

Programmable controller (PLC) is general automation device using computer technology as the core, and has been widely used in industrial production due to its high reliability, variable control program, and strong adaptability for all kinds of vicious environments [1]. But the PLC controller itself does not have the human-computer interaction devices such as display, and can't realize the online adjustment of the control parameters and the display of the system motion state. So an operation display system, which reading temperature by the intelligent meter, using PLC as the core, industrial computer as the control and operation center, is designed. The real-time display of the data and the on-line modification of the instrument set data can be realized in this design. Because in practical applications, the industrial site temperature need be reflected and controlled timely, the good communication between up-computer in the control room and down-machine in the industrial site is very important. In this design, the up-computer is industrial control computer, and the down-computer consists of a Siemens S7-200 PLC and 20 artificial intelligence temperature controllers which type is YuDian AI –708. The key to implement the above functions is the serial communication between PLC and the AI-708 instrument. Therefore, S7-200PLC and AI-708 instrument communication is the focus of this design.

II. SYSTEM STRUCTURE

The system network is divided into two layers, Ethernet and field-bus, shown as figure 1. The master station of data acquisition in the field is the Siemens S7-200 PLC, connected with industrial PC through the Ethernet. AIBUS network topology structure is used in the field-bus, the RS485 communication mode based on AIBUS communication protocol is used in the connection between PLC and intelligent instruments. Because RS485 is half – duplex communication[2-3], SMB87.7 should be reset when the data sending and set when the data receiving in order to avoid the conflict between data sending and receiving. AIBUS uses a 16-bit summation correction, supports a variety of baud rate such as 4800,9600, 19200, under the 19200 baud rate, the master station visits every AI – 708 needs 20ms on average. The interface of AI instrument is asynchronous-serial communication, and the interface level complies with the rules of RS232C and RS485 standards, the data format is a start bit, 8 data bits, no parity,1 or 2 stop bits. AI instrument have 20 connection ports, the third port (A) and fourth port (B) of AI instrument are connected with the port 3(＋) and

8(－) of PLC 485 communication port respectively. The first port and second port are connected with the positive and negative port of the 220V power supply, and the 17th port and 18th port are connected with 0-5V or 1-5V voltage signal[4-6]. The communication port must be ensured connected correctly before the communication with PLC.

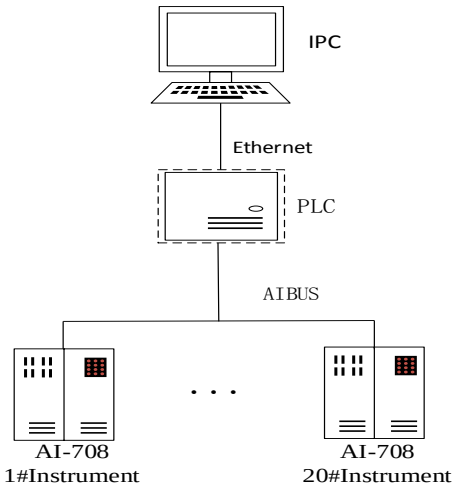

Figure 1. Detection system network structure

III. SOFTWARE PROGRAMMING OF COMMUNICATION BETWEEN PLC AND INTELLIGENT INSTRUMENT

Before compiling the serial polling communication program between PLC and the AI-708, the parameters of the communication must be defined. The serial communication port rate, information frame format, and PLC communication port communication mode should be set up, and communication message test control should be planned.

A. The structure of communication program between PLC and multiple smart meters

The serial polling communication between PLC and intelligent instruments is master - slave communication, PLC is the master, the intelligent instruments are slaves. The master initiates a communication request, the slave responds after receiving a communication request, the slave does not exchange data with the other slave or actively send data to the master. Free port mode communication of PLC involves sending instructions XMT and receiving instructions RCV[9]. Interruption will be generated at the end of these two instructions execution, so the whole process of communication can be controlled by sending and receiving complete interrupt. The interrupt events are shown in Table 1[7-8].

Initialization process is to set port 0 communication modes, serial communication information frame format and baud rate, message control etc. Specifically, it is completed by setting corresponding value for the four special registers listed in Table 2.

TABLE I. THE FREE PORT COMMUNICATION INTERRUPT EVENT

Event Number	Port	Interrupt Declaration	Priority Level
9	0	Transfer is completed	0
23	0	Receive information is completed	0
24	1	Receive information is completed	1
26	1	Transfer is completed	1

After initialization is completed, PLC sends a communication request to the 1# temperature controller, 1# AI-708 temperature controller receives the master request and sends the return data back to the master. At the same time, the main station generates a send-finished interruption of interrupt-9 after the XMT instruction sending the request. This PLC's interruption is connected to an interrupt 0 application, which executes receiving instruction RCV. When the return data from the instrument 1# AI is received completely, a complete interruption event of 23 can be produced. Connect this event with another break 1 program which processing and checking data, if the processing and checking pass, moves the data from data receive buffer to the specified area and clears the receive buffer; otherwise, clears the receive buffer directly. Then, PLC sends a communication request to the 2# AI instrument and processes the received data from the 2# AI, cleans the receive buffer, and then sends a communication request to the 3# AI instrument ,and so on. Until the PLC completes the processing accepted from 20# AI instrument, and cleans the receive buffer, send communication request to 1# AI instrument communication, and repeat.

TABLE II. REGISTERS COMMAND VALUES

register	set value	implication
SMB30	16#09	The baud rate is 9600, 8 data bits, 1 bit start, no check bit, 1 stop, port 0 is free port
SMB87	16#10	The timer is the message timer, using the interrupt condition to start the message detection
SMB90	0	Message wait time is 0
SMB94	16#10	The maximum number of characters to receive is 10

B. Serial communication baud rate, information frame format, port 0 communication mode and message detection control

Usually the temperature change in the field is slow, the polling frequency is too high to be practical, which only increases the burden of the PLC program. The values of registers in Table 2 are the best values by debugging repeatedly. The polling frequency of PLC can be reduced effectively by setting reasonable value for timeout testing timer T38, and the frequency of communication with online instrument can be reduced, so the load of PLC program is reduced, and the whole communication paralyzed causing by a device fault or communication line fault can be prevented.

The request instructions format of the master and return data format from station multiple slaves are shown as formula (1) and formula (2), where in the formula the baud rate is 9600 bits/s, one character frame is 10 bits (one start bit + 8 bits of data a + 1 stop bit), ignoring a few free bits between characters frames, The time passing one character can be calculated by the formula (1). It's about 1.42 ms. In this formula，B is the baud rate and N is the data number. The length of read and write instruction is 16 characters, and the time that the host sends a data is 22.72 ms[10]. The slave sends data instruction back after receiving the host instruction and time-delaying. The delay time is usually tens of milliseconds. This data is given by some instrument manufacturer, and can set within a certain range by user, and is fixed and not given by some instrument manufacturer. The delay time in this design is fixed. The time of return data can be calculated by the formula (2), where in the formula t is the delay time. If data formats returns from slaves are 20 characters, assuming that t is 20 ms, the T is 28.4 ms.

$$T = \frac{1}{B} \times N \tag{1}$$

$$T = \frac{1}{B} \times N \times \mathrm{t} \tag{2}$$

C. *Communication format between PLC and intelligent instrument*

PLC in Figure 1 collects the data of 20 pieces of smart meters with master-slave scanning communication protocol mode, each communication process is initiated by the master station, responded by the slave station to transmit information back, then a communication is completed. All kinds of instruction code and data in AI instrument are indicated by hexadecimal data formats. There are two standard communication instructions only, one is read instruction, the other is write instruction, through optimization design to AI instrument software communication instruction. It makes the PLC software writing easy, and can complete instrument operation 100%. The read instruction format for the AI instrumentation is shown in Table 3, and the write instruction format is shown in Table 4.

The address is codenamed by two identical bytes (the meter address + 80H) according to the AI instrument communication protocol. For example, the meter parameter Addr = 10 (16 decimal number is 0AH, 0A + 80H = 8AH), and the name of the instrument is 8AH 8AH. [11]

TABLE III. AI METER READING INSTRUCTION FORMAT

0	1	2	3	4	5	6	7
address	address	52H(82)	The parameter code to read	0	0	Check code	Check code
0~80H	0~80H	52H(82)	00H-56H	0	0	XX	XX

TABLE IV. AI METER WRITING INSTRUCTION FORMAT

0	1	2	3	4	5	6	7
address	address	43H（67）	The parameter code to write	Write in low bytes	Write several high bytes	Check code	Check code
0~80H	0~80H	43H（67）	00H-56H	XX	XX	XX	XX

Parameter code: the parameters of the instrument is replaced by a parameters code with an 8 bit binary number (one byte, written as hexadecimal number), it indicates the parameters name to be read/written in the instructions.

Check code: the check code uses 16 bits summation check method, and the check code of reading instruction can be calculated as formula (3) .

$$R * 2^8 + 82 + ADDR \tag{3}$$

The check code for writing instruction is the remainder of 16 binary addition calculations for the following formula (4).

$$W * 2^8 + 67 + K + ADDR \tag{4}$$

The Numbers in these two formulas are decimal, The ADDR in the formula is the parameter value of the meter, the range is 0~80, R is the parameter code to read, W is the parameter code to write, K is the parameter values to write. The check code is the remainder of the binary 16 bit integer addition to the above formula, the remainder is 2 bytes, its low byte is in front, and the high byte is follow. The parameter values to be written are represented by a 16-bit binary integer.

Return data: whether read or write, the instrument returns the following 10 bytes of data.

Measure Value (PV) + Given Value(SV) + Output Value(MV) and alarm status + read/write parameter value+ check code

The PV, SV and read parameter value takes 2 bytes each, represents a 16-bit signed binary complement integer, low byte in the former and high byte follow. The decimal integer cannot be shown, so need be processed in the upper machine by the user [12].The MV takes up a byte, eight bits of symbol binary number format, the numerical range -110 ~ +110, the state bit occupies a byte, the check code is two bytes, and all of them is ten bytes.

Return check code: the remainder (the numbers in the formula is decimal) when added by integer addition.

$$PV + SV + (S * 2^8 + MV) + C + ADDR \quad (5)$$

In the formula, S is the alarm state, C is the parameter value. In the calculation of the check code, each of the eight bytes consists of a 16-bit binary integer for addition, and the overflow number is ignored and the remainder is used as a check code. [13]

IV. Program operation and analysis

Communication program between PLC and intelligent instrument is written by using trapezoidal diagram, the instruction such as rising edge, timer, timer interrupt, is used in the program to insure the accuracy and stability. In order to make it more intuitive, trapezoidal diagram is converted into an instruction table form, and the program is as follows.

```
LD      S M0.0
ORB     VB122, VB101  //The AI meter address plus 80H is in VB122.
MOVB    VB101, VB102  // The current address of the instrument is in VB101.
MOVB    16#43, VB103  //Written instructions.
MOVB    16#0, VB104   //Write the set value.
LD      SM0.0
BTI     LW0           //The current meter address is given to LW0.
R       SM87.7, 1     //Enable the receive message function.
RCV     VB110, 0 //Receive the first address of the buffer, store the number of bytes received, and the next offset address is the first character received.
XMT     VB100,0 //The first address of the sender area, where the number of bytes is sent, the next offset address is the first character to be sent.
```

V. Conclusion

In guarantee the absolutely agree in the baud rate, information frame data bits number, start bit number, number of stop bits, odd/even check or without the check digit between the two communication site, the communication can be created in the process of debugging. The data exchange between PLC and 20 AI-708 smart meters is very stable, accurate and reliable. By adopting AIBUS agreement, the communication between S7-200 programmable controller and many intelligent instruments is implemented efficiently in the form of hexadecimal number, and the parameter setting is convenient, the control and operation of the industrial field device is easy. The temperature control system introduced in this paper can meet the different process requirements, and it's control method is convenient, practical and feasible. RS485 network can communicate serial polling with much more intelligent instruments. But the longer communication distance, the lower communication baud rate. The use of optical fiber and expensive consumables can be prevented by realizing the communication function only, and then the cost is reduced.

Acknowledgment

Supported by Scientific research plan projects of Shaanxi Education Department，（No.16JK1362）

References

[1] Xu Xiaotong."The temperature control system based on PLC designanalysis",Electronictest, vol.19,Sep.2016,pp.36-37,doi:10.1136/s10654-005-0060-67.

[2] Ying Bin."The study of temperature control system based on single chip microcomputer",Mechanical and electrical engineering, vol06,Dec.2015,pp.887-890,doi:10.1029/1471-2407-10-338.

[3] Li Zhongpeng,Yan Baorui and Xin Chunlin."A two-step extrusion unit temperature control system design based on theprofibus-dp/Modbus gateway",China plastic,vol.03,Jun.2015, pp.112-117,doi:10.1186/1471-2407-22.

[4] Jiang Wei,Xie Bin and Wu Fei."The design of temperature control system of machine intelligent stir-frying machine ismade by traditional Chinese medicine",Journal of hunan instituteof technology (natural science edition), vol.04,May.2014, pp.58-62, doi:10.1036/151-1207-362.

[5] Wu Hebao,Ke Chao and Zhu Dongjie."Research of the method of temperature measurement and control for material Enrichment", Journal of wuhan university of engineering,vol.10,Oct.2014, pp.47-51, doi:10.1156/1741-3107-52.

[6] Li Jie."A distributed temperature monitoring system based On Ethernet",The electronic commerce,vol.06,Aug.2015,pp.59-60, doi:10.1186/1532-1207-73.

[7] Zhang Yuanliang."Practical tutorials for integrated design of single chip machines"Beijing:China Machine Press,Dec.2013, pp.10-200, doi:10.1186/3531-2469-75.

[8] Bao Ligao."Design and implementation of small integrated PLC systems",Jilin university, vol.09, Apr.2013, pp.12-16, doi: 10.1055/1901-4307-66

[9] Liu Yanxia,Lu Qian and Ren Zihui."The automatic identificationsystem of the cargo for the group and PLC", Instrumentation technology and sensors,vol.06, May.2013, pp.55-58, doi:10.12066/1561-2707-121.

[10] Wang Hongyi."PLC data collection module design",.Inner Mongolia university of science and technology,vol.12,Sep. 2013,pp.36-38,doi:10.1096/1347-2547-187.

[11] Wang Maolei."The design and implementation of automatic control system of PLC based water plant",Software industry and engineering,vol.13,Jul.2013,pp.42-46,doi:10.1066/ 1714-2398-363.

[12] Wu Qi and Yang Jiangtao." Design and implementation of a thermostat temperature control system",Computer measurement and control, vol.08, Mar.2014, pp.2455-2458, doi:10. 1681/1741-3602-144.

[13] Ding Yuan,Zhong Youfa and Sun Yuwen."The system is based on thesingle-chip microcomputer control system", Zhejian gagricultural science, vol.10, Jun.2013, pp.1369-1371, doi: 10.1369/1524-2673-188.

Motion Simulation of Bionic Hexapod Robot Based on Virtual Prototyping Technology

Zhenyu Lei, Daxin Xin, Jin Hua
School of Electronic Information Engineering
Xi'an Technological University
Xi'an, China
zhenyulei2015@163.com, xdx661006@163.com, huahua_dz@aliyun.com

***Abstract*—Based on the principle of bionic hexapod, a 3D virtual prototype model of the bionic hexapod robot and the contact model between its feet and the ground are established by using MSC.ADAMS mechanical dynamics software to study the motion of the bionic hexapod robot on the horizontal ground. And then, the kinematics analysis of a single leg of the robot is made to realize the overall motion control of the robot. This paper analyzes the gait principle of the bionic hexapod robot and introduces the gait of the robot used. By simulating the straight motion of the robot, the angular velocity and angular acceleration in the legs of the virtual prototype model are obtained. The study is a theoretical foundation for the design of the physical model and motion planning of a bionic hexapod robot.**

Keywords-hexapod robot; bionic; virtual prototype; gait; simulation

I. INTRODUCTION

With the characteristics of high order, strong coupling, multivariable and non-linearity, the hexapod robot can adapt itself to the complex ground and dangerous operating environment, and can replace the human to fulfill some special tasks, thus liberating mankind and improving efficiency.

Because of these advantages, scientific research institutions in developed countries have been constantly improving and optimizing the structure and design of the hexapod robot. The Genghis[1] in the late 1980s and the Attila[2] in the early 1990s were autonomous planetary exploration robots developed by the Massachusetts Institute of Technology (MIT). They could walk on rough terrain. Scorpion[3,4], developed by the Fraunhofer autonomous Intelligence Institute of Germany in 2001, was able to perceive the external environment and had a strong ability to adapt itself to complex environment. The Silo-6[5] hexapod robot developed by the Spanish Association of industrial automation in 2009 could perform field clearance functions. In recent years, with the rapid development of high technology, especially intelligent technology in China, the research on robot has stepped into a new stage. For years, Nanjing Forestry University has developed a hexapod robot for disaster reduction[6,7], and a hexapod robot based on modular control unit has been developed by Harbin Institute of Technology.

Based on the biological prototype of the hexapod, the robot model and its walking gait were designed. In order to reduce research cost and time, we did our best to improve the quality of robot design. By using the simulation model established by the mechanical simulation software ADAMS, the model parameters of the robot can be adjusted easily, and the dynamics and kinematics simulation results of the robot motion process can be output directly. The study will provide some reference for the organization and motion control of the hexapod robot.

II. The Modeling Process of Hexapod Robot

A. *Prototype Structure of Hexapod*

Imitating the structure of six-legged insects in nature, the design of bionic hexapod robot is variable. Take beetles for example. A beetle generally has six legs which symmetrically distribute on its front, middle and rear sides of its body. Each leg consists of coxal, femur, tibia and foot. Coxal and the body are connected through the root joint. The coxal is connected to the femur through the hip joint. Femur and tibia are connected through the knee joint. A beetle is shown in Figure 1, and its leg structure is shown in Figure 2.

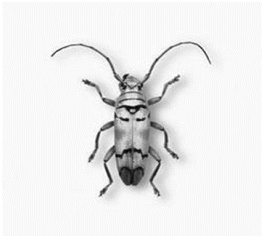

Figure 1. Beetle entity

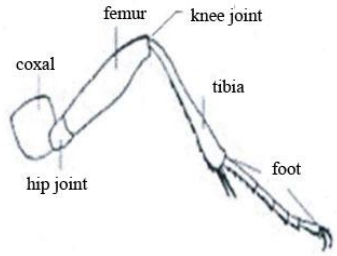

Figure 2. Schematic picture of leg structure

B. *Modeling and Simulation Process*

ADAMS, the automatic dynamics analysis of mechanical system, is the world famous virtual prototype analysis software. ADAMS was developed by Mechanical Dynamics Inc.company, which can complete the mechanical system modeling and solution operation. Simulation analysis

of static mechanics, dynamics and kinematics can be done after the ADAMS virtual prototyping model is created. It can measure each joint's displacement, velocity, acceleration and torque curve. The conceptual design of the bionic hexapod robot using ADAMS can help to carry out the research on and improvement of the robot's performance. The whole work includes the layout design and parameter design of the model. After the construction of each component, it is necessary to establish the link and constraint relationship between the separate devices, and to add the corresponding motion pair to the constraint. The final step is to set the simulation time and to post-process the simulation results, completing the analysis of the simulation results and modifying the design. The main work flow of hexapod robot modeling is shown in Figure 3.

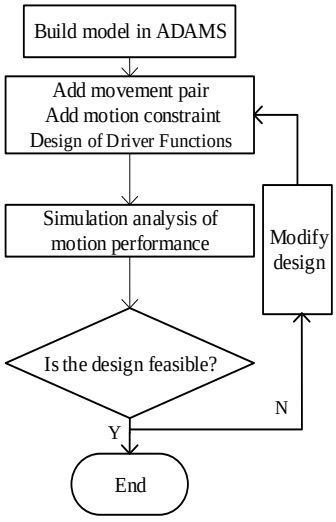

Figure 3. Modeling and simulation process

C. Construction of Bionic Hexapod Robot Model

In building the three-dimensional model in the mechanical dynamics simulation software ADAMS, in order to avoid too complex simulation model and difficult design, the model is simplified as follows:

1) The body of the robot is simplified into a uniform rectangular parallelepiped with the internal connection omitted. Keep the connection between the body and the root joint.
2) The coxal and the femur of the robot are simplified into a cylindrical structure, and the tibia into a truncated cone structure. The relative positional relationship between the joints in the leg structure is retained, and the connection between the coxal and the body is replaced by the revolute pair. The connection between the coxal, the femur and the tibia is also achieved by the revolute pair.
3) A cuboid is built at the bottom of the hexapod robot, Simulate the ground on which the robot walks, and establish the contact constraints between the foot and the ground.

Each leg of the hexapod robot has three degrees of freedom, and each degree of freedom needs rotational joints, so a total of eighteen revolute pairs are needed for the hexapod robot moving, swing and puting down its legs. The contact force creation dialog box is shown in Figure 4. Solid to Solid is selected as the Contact type, I solid as the robot's feet, and J solid as the ground. The various parameters are set as shown in Figure 4. The established model of a bionic hexapod robot is shown in Figure 5.

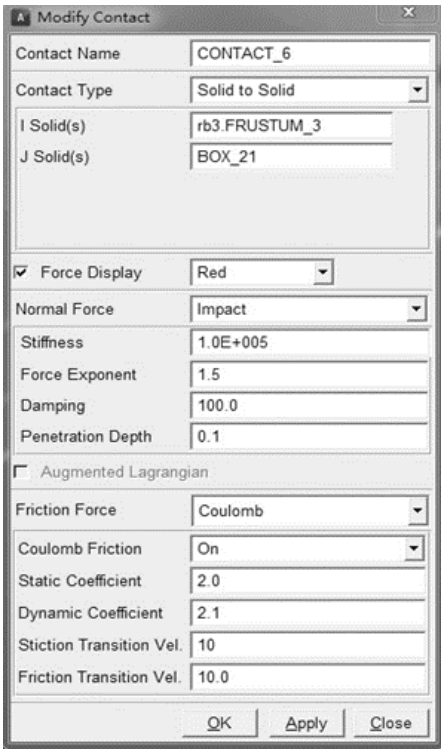

Figure 4. Creating a contact constraint dialog box

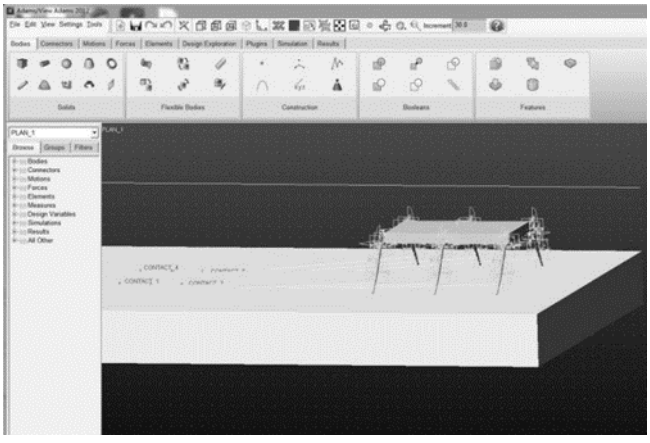

Figure 5. Bionic hexapod robot model

D. Kinematics Analysis of Hexapod Robot

The bionic hexapod robot is a multi-rigid body system, which satisfies the Newton-Euler equation, as in Formula (1).

$$m_i r^n = F_i^g - \sum_{i=1}^{n} T_{ij}(F_j^a + F_j^n) \quad (1)$$

$$J_i \bullet \omega + \omega_i \times (J_i \bullet \omega_i) = M_i^g - \sum_{j=1}^{n} [T_i^j (M_j^a + M_j^n) + C_{ij} \times (F_j^a + F_j^n)]$$

where $i = 1,2,\ldots,n$, C is the center of mass, force and moment are expressed in F, M, the association matrix is represented by T, the interaction between the external force of the superscript is indicated by g, the ideal effect of the hinge is represented by n and the interaction at the hinge is represented by a.

A forward kinematics analysis of a leg of a bionic hexapod robot is made. The single foot D-H parameters of the hexapod robot are shown in Table I. $\theta_1, \theta_2, \theta_3$ represent the rotation angles of the root joint, hip joint, and knee joint respectively. λ is the deflection angle of the root joint. The lengths of coxal, femur and tibia are represented by l_1, l_2, l_3. The distance between the common vertical lines is represented by d_i, α_i represents the twist angle of the joint axis, and the normal vertical length is a_i. The robot is shown in Figure 6.

TABLE I. SINGLE LEG D-H PARAMETER

连杆 i	变量 θ_i	扭角 α_i	距离 d_i	长度 a_i
1	θ_1	90°	$-l_1 \cos\lambda$	$l_1 \sin\lambda$
2	θ_2	0	0	l_2
3	θ_3	0	0	l_3

Each leg of the robot has 4 parameters $\theta_i, d_i, a_i, \alpha_i$, and they together determine the movement of each action. The $T = R(\theta)T(d_i)T(a_i)R(\alpha_i)$ represents the coordinate transformation, which is expressed by Formula(2).

$$T_{i-1}^{i} = \begin{bmatrix} c\theta_i & -s\theta_i c\alpha_i & s\theta_i s\alpha_i & a_i c\theta_i \\ s\theta_i & c\theta_i c\alpha_i & -c\theta_i s\alpha_i & a_i s\theta_i \\ 0 & s\alpha_i & c\alpha_i & d_i \\ 0 & 0 & 0 & 1 \end{bmatrix} \quad (2)$$

c is a cosine transform, and s is sine transform. The bionic hexapod robot is transformed from the coxal coordinates to the femur and then to the tibia. The total shift of the foot (p_x, p_y, p_z) of the robot relative to the entire base coordinate is shown in Formula (3).

$$T_0^3 = T_0^1 T_1^2 T_2^3 = \begin{bmatrix} n_x & o_x & a_x & p_x \\ n_y & o_y & a_y & p_y \\ n_z & o_z & a_z & p_z \\ 0 & 0 & 0 & 1 \end{bmatrix} \quad (3)$$

thus, the position coordinates of the robot foot can be obtained, as expressed in Formula(4).

$$\begin{aligned} p_x &= c\theta_1(l_3 c(\theta_2 + \theta_3) + l_2 c\theta_2 + l_1 s\lambda) \\ p_y &= s\theta_1(l_3 c(\theta_2 + \theta_3) + l_2 c\theta_2 + l_1 s\lambda) \\ p_z &= l_3 s(\theta_2 + \theta_3) + l_2 c\theta_2 - l_1 c\lambda \end{aligned} \quad (4)$$

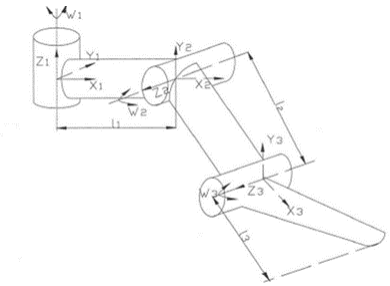

Figure 6. Single leg D-H coordinate system of bionic hexapod robot

III. Analysis of Gait Principle of Bionic Hexapod

A. *The basic concept of gait*

The swing phase is the position of the leg rising in the air from the ground. The support phase refers to the state of the leg landing. In the process of walking, the support phase and the swing phase alternate each other and the sequence of collections changing with time is called gait. Three-legged gait, four-legged gait and wave gait are three kinds of gait commonly used in the bionic hexapod robot. The time the hexapod robot takes to perform the whole gait during the moving process is called the gait cycle T. The duty factor β refers to the ratio of the support phase to the gait cycle in the period when the robot completes a gait cycle. The relationship between T and β is shown in Formula (5).

$$\beta = t / T \quad (5)$$

Step distance is the length of the center of gravity of a robot relative to the ground during moving, represented by λ. The foot travel refers to the distance the foot of a supporting phase moves forward or backward in the movement process of the bionic robot, which is represented by R.

The mathematical expression between the foot travel and the step distance is shown in Formula(6).

$$R = \lambda \bullet \beta \quad (6)$$

B. *Three-legged gait*

Because the three-legged gait is fast and stable, it is the most commonly used in the bionic hexapod robot movement. The walking mechanism of the three-legged gait is to divide the six legs of the robot into two parts, three legs into a part, and alternately move forward with a triangular support structure. The sketch map of the three-legged gait is shown in Figure 7.

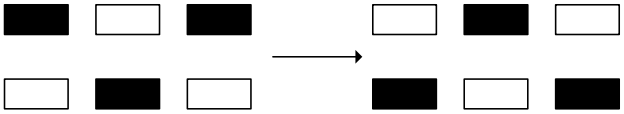

Figure 7. Three-legged gait sketch map

The black circle represents the support phase and the white circle represents the swing phase. The analysis of the movement of the hexapod robot is made as follows: 1,3,5 legs constitute a group, and 2,4,6 legs another group. When moving forward, 2,4,6 legs are in the swing phase and 1,3,5 legs in the support phase. First, the robot swings its 2,4,6 legs forward. And when the feet of the robot move down to the ground, 2,4,6 legs become the support phase while 1,3,5 legs become the swing phase. Such cycle repeats and the robot moves forward, which is shown in Figure 8.

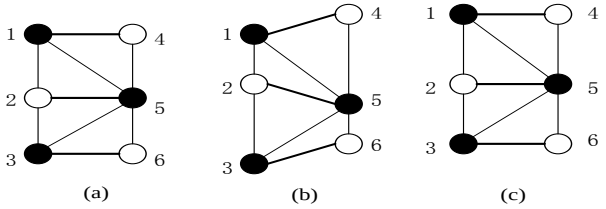

Figure 8. Sketch of three-legged gait in forward movement

IV. Motion Simulation of Bionic Hexapod Robot

After the model of the bionic six-legged robot is created and the corresponding revolute pairs and constraints are added, the corresponding drive is added to the root joint, hip joint and knee joint of the robot. The *step* function in ADAMS is adopted as the drive function. The format is $step(x, x_0, h_0, x_1, h_1)$, where x stands for argument time, x_0, x_1 represents the start time and end time respectively, and h_0, h_1 represents the initial value and final value of the function. Finally, after adding the corresponding drive function, a group of curves of each joint of the robot are measured. The angular velocity curve of the root joint is shown in the Figure9 (a), the angular velocity curve of the hip joint is shown in Figure9 (b), and the angular velocity curve of the knee joint is shown in Figure9 (c).

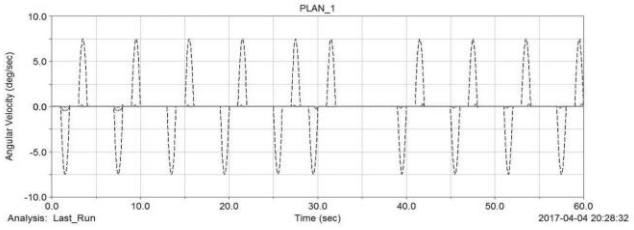

(a) angular velocity curve of the root joint

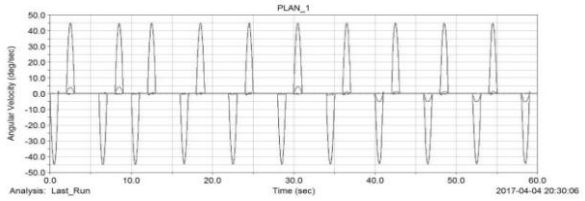

(b) angular velocity curve of the hip joint

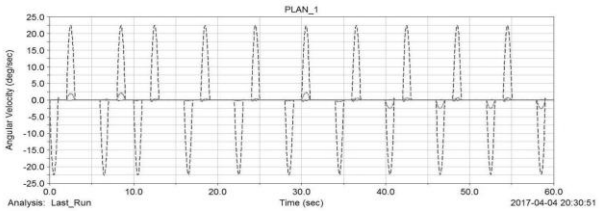

(c) angular velocity curve of the knee joint

Figure 9. Angular velocity curve of each joint

And the angular acceleration curve of this set is obtainded. The angular acceleration curve of the root joint is shown in Figure10 (a), the angular acceleration curve of the hip joint is shown in Figure10 (b), and the angular acceleration curve of the knee joint is shown in Figure10 (c).

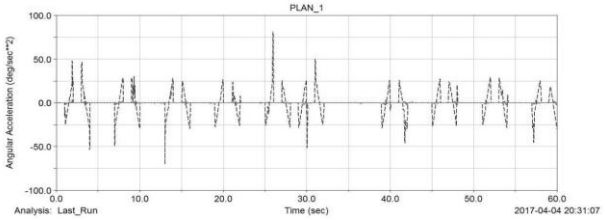

(a) angular acceleration curve of the root joint

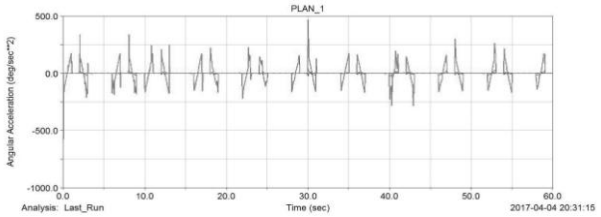

(b) angular acceleration curve of the hip joint

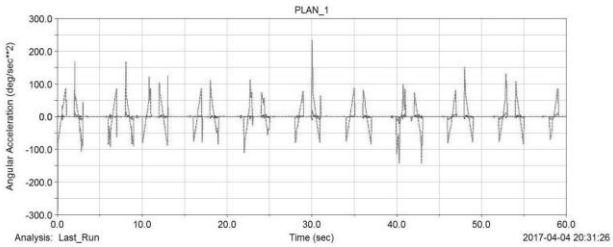

(c) angular acceleration curve of the knee joint

Figure 10 Angular acceleration curve of each joint

V. Conclusion

The experimental results show that the bionic hexapod robot prototype created by ADAMS is reasonable in layout, and the hexapod robot walks well under the driving function based on the three-legged gait. However, it can be seen from the simulation that the angular acceleration of the robot changes greatly at some time, indicating that the feet are subjected to greater impact. Therefore, when designing a physical prototype, it is advisable to add a damping equipment under the feet. The kinematic analysis obtained from the experiment provides a theoretical basis for the development of the physical prototype.

ACKNOWLEDGMENT

This work has been supported by Principal Fund of Xi'an Technological University(No.0850-302021410).

REFERENCES

[1] Brooks, R. A, "A robot that walks; emergent behaviors from a carefully evolved network.", Neural Computation, Vol. 1, No.2, pp. 253-262, 1989.

[2] Brooks, R. A, "Intelligence without Reason", Proceedings of the International Joint Conference on Artificial Intelligence, Sydney, Australia, 1991, pp.569-595.

[3] B Klaassen, R Linnemann, D Spenneberg, F Kirchner, "Biomimetic walking robot SCORPION: Control and modeling", Robotics & Autonomous Systems, Vol. 41, No.2, pp.69-76.

[4] Kirchner, F, "Q-learning of complex behaviours on a six-legged walking machine", Robotics & Autonomous Systems, Vol. 25,No.3, pp.253-262,1998.

[5] P. Gonzalez de Santos, et al, 'Minimizing Energy Consumption in Hexapod Robots", Advanced Robotics , Vol. 23, No.6, pp.681-704, 2009.

[6] Shuhai Jiang, Chenchen Pan, Liying Yuan, Qian Song, "Mechanism Design and Simulation of Hexapod Mitigation Rescue Bionic Robot", Journal of Computer Simulation, Vol.32, No.11, pp.373-377, 2015.

[7] Shuhai Jiang, Nan Zhang, "Analysis and Design of Forest Fire-Fighting Hexapod Bionic Robot Mechanism", Journal of Machinery Design and Manufacture, 2015, No.12, pp.208-212.

Research of Petroleum Well Fuel Pump Measurement & Control System Based on Internet of Things Technology

Shengquan Yang
School of Computer Science and Engineering
Xi'an Technological University
Xi'an, China
xaitysq@163.com

Ceng Gong
School of Computer Science and Engineering
Xi'an Technological University
Xi'an, China
1395861613@qq.com

***Abstract*—In order to realize remote automatic measurement and control of all petroleum well fuel pumps which are located in different regions of the crude oil production enterprises, this paper discusses and designs a petroleum well fuel pump measurement & control system based on internet of things technology. The measurement & control system uses a three-tier (perception layer, network layer and application control layer) form of the IOT (Internet of Things) structure, and then the function and feature of all layers are analyzed. As a focus, the hardware components and the control theory of the sensor instrument node and the aggregation instrument node, which are existed in the measurement & control system, are given and discussed also. In the end, programming flow chart of the node microcontroller and main design software module content of the IOT center computer are depicted and proposed. The enterprise experiment result shows that the system has the advantages of easy operation and maintenance, low labor intensity, high time efficiency of measurement & control and high precision with the traditional manual inspection methods of the petroleum well fuel pump to compare.**

Keywords - Internet of Things, Measurement & Control System, Sensor Instrument Node, Aggregation Instrument Node

I. INTRODUCTION

Fuel pumps are an important requisite external power transmission equipment for wells. As most of the wells are distributed in the desert and wild mountains, Oil-Fields enterprise management of its use field instruments to show monitoring, and carry out the early warning management by artificial way of power line patrol, that is inspectors daily check the operation of the group of oil wells ,record the relevant data, access to the pumps phase of the time running the flow pressure as well as temperature and other information[1]. With the oil field production and transmission pipe network is more and more wide， and the number of wells continues to expand, This approach gradually shows the lack of management, which shows great intensity of work labor, and shows some shortcomings of problem processing lag, for example :if the operating pressure of oil pump is abnormal, manual inspection line found that processing is not timely, it could cause the pipeline to burst, further, it causes a series of serious problems, such as property loss of oilfield enterprises and environmental pollution.

The internet of things is "things connected to things in the Internet", it is the automatic information acquisition equipment through various sensing devices, ZigBee wireless sensor network technology, 4G network transmission technology, RFID technology, video recognition technology, infrared sensors, GPS, laser scanners and etc. , intelligent network system, according to the agreement, and the need to realize the interconnection of the network of things, for information exchange and communication, in order to achieve intelligent identification, positioning, tracking, monitoring and management of intelligent network system[2] .

II. DESIGN OF PETROLEUM FUEL PUMP MEASUREMENT & CONTROL SYSTEM BASED ON INTERNET OF THINGS ARCHITECTURE

Measurement & control of petroleum well fuel pumps data is the foundation for the construction of the digital intelligent oil fields. The goal is to detect the running status and parameters of the well fuel pump equipments in real time and transmit the running data to the Internet of Thing control center through the intelligent correspondent node, and dedicated 4G network. On the one hand, the central machine analysis and process through the upper intelligent control software, if necessary, makes decision-making control, and then output to the equipment control agencies by a dedicate 4G network. On the other hand, the central machine can make gathered data store to the database server through the algorithm transforms and normalizes, at the same time, through the pubic 4G network or internet network for mobile terminals or desktop terminal users. Based on Internet To Things architecture of the equipment composition structure shown in Figure 1, the system is used a hierarchical design method to achieve real-time data collection and monitoring of pipeline pressure, flow and temperature and so on. It has the advantages of low cost ,automatic monitoring ability, which consists of 3 layers: the perception layer, the network layer and the application control layer.

A. The perception layer

The sensor signal of oil pump of the measurement and control in the oil field mainly include: various parts of the value switch of components inlet and outlet pressure of pumps, inlet and outlet temperature of pumps, the pump output flow and the pump body temperature an so on. The perception layer is composed of zigbee wireless subnet of pumps and wells in several areas. The zigbee wireless subnet consists of sensor instrument nodes, aggregation instrument nodes with zigbee correspondence module (zigbee wells

control correspondence instrument, also called gateway nodes). In this system, aggregation instrument node is the transfer station for each oil well's external correspondence, and its core component is the ZigBee wireless transceiver module. Aggregation instrument is a relatively independent processing unit, If the external network failure can not be connected with the Internet of things control center machine, if the external network fault occurs and can not connect with the Internet of things control center machine. It can automatically control the running state of the local oil pump according to the logical rule library running in the node. In addition, it can store the local measurement & control data for a period of time, and can query local sensors to display real-time or historical running data.

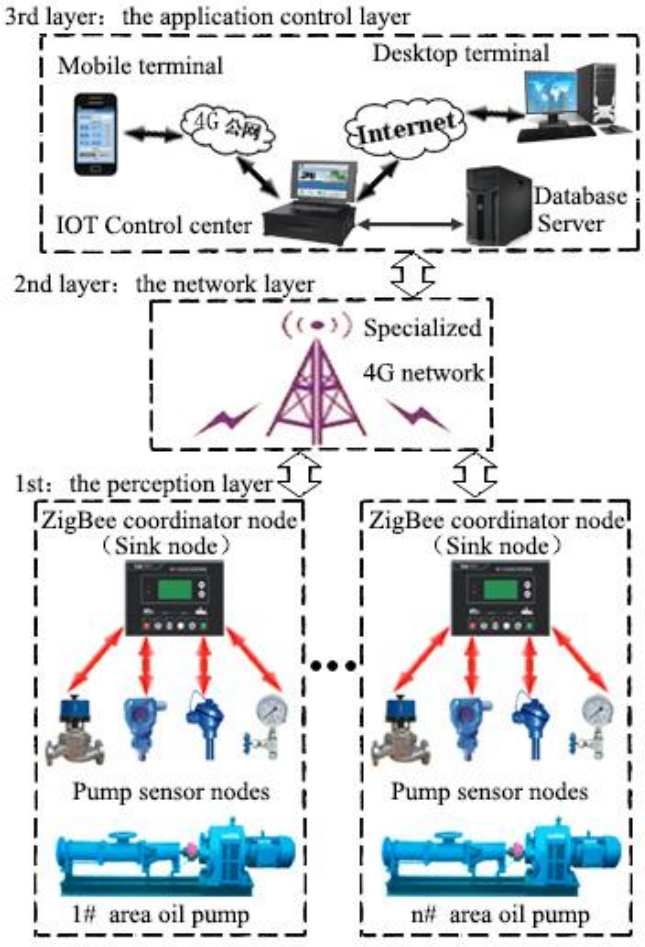

Figure 1. Organization structure of the system based on internet of things technology

B. *The network layer*

The network layer mainly completes the reliable transmission of the oil pump collection information or the central control signal of the Internet of things. In essence it is based on WLAN (Wireless Local Area Network, WLAN) wireless mesh protocol to form a larger network of aggregation instrument nodes, thus monitoring the oil pump in multiple regions. Its specific function is that mainly receives the information of the perception layer aggregation instrument node and can transmit to the control application layer by appropriate algorithm encryption as required, in addition, the information and control output of the application layer are transferred back to the aggregation instrument nodes of the perception layer, and the network layer acts as a bridge. As the oil wells of oilfield enterprises are mostly in the wild areas, these places often do not have public correspondence 4G network, so it is necessary to set up a dedicated wireless correspondence network to serve the system.

C. *The application control layer*

The application control layer is the highest level in the functional structure diagram of the system. It is the remote control center of the system. It realizes the automatic safety control of the oil pump on the basis of receiving and analyzing the information of each well. The application control layer is mainly composed of central machine of internet of things, database server, desktop terminal, mobile terminal and so on. The central machine of the Internet of things generally has wireless transceiver module, which can receive the equipment information transmitted by the 4G network and the base station at the transport layer in real time, according to the operating parameters of the pump to analyze and process through the software system. Different production wells are equipped with different pump power, operating parameters are not the same, by controlling the man-machine interface of the application control layer, various device parameters can be set up, and the regular rule library instructions are downloaded into the control correspondence instrument of the ZigBee well group as the local backup[3]. Application control layer receives the network layer data generally go through check, unpacking, reverse the encryption transformation , It can dynamically display oil well temperature, pressure and flow of data through intelligent computer graphics software system of powerful, it can predict the abnormal running of the equipment, and make the corresponding output actions quickly according to the equipment process, mobile terminals, such as mobile phones and handheld PDA, can be allowed to access the Web interface of the control system through the public 4G network, operating curves, data, etc. that can be accessed by the device under permission; in addition, each branch of the oilfield enterprise can also access the operation of the browsing system or remote control through the Internet. It is convenient for Oilfield Enterprises to manage oil pumps efficiently.

III. MEASUREMENT & CONTROL NODE HARDWARE OF PUMPS' INTERNET TO THING

A. *Sensor instrument node*

The main function of sensor instrument node is collecting current and voltage data, convert data to A/D, and process 1 times digital filtering, these sensors are equipped with wireless ZigBee correspondence module, they can

upload data to the aggregation instrument node, and accept the instructions of the aggregation instrument node to make the necessary adjustment output. Typical pump sensor instrument node consists of a sensor module, analog filter module, A/D conversion module, D/A output module, I/O control module, CPU processor, RFID wireless node module, storage module and power management module etc, the schematic diagram of the hardware is shown in Figure 2.

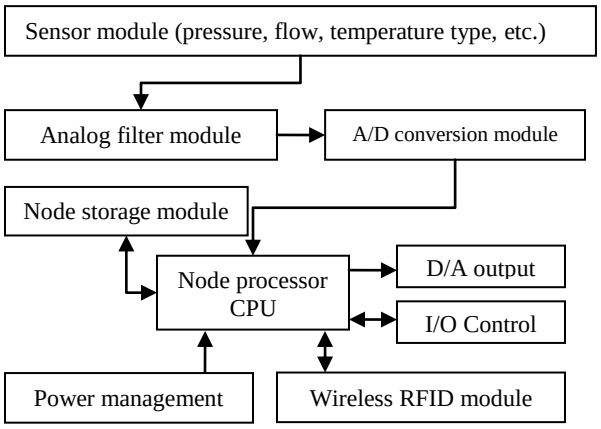

Figure 2. Hardware components theory block diagram of the fuel pump sensor instrument node

The pressure sensor of this system adopts Rosemount measuring accuracy 0.1% sensors, and the measuring range is 0~10 Mpa, the direct-current supply voltage is DC24V, the output sensing signal is 4 ~ 20mA, and the medium temperature is -20 ~ 90 ℃. The flow sensor adopts FD-M100AT sensor, the detection distance is 4~150 mm, the switching frequency is 1000Hz, the output mode is NPN, the response time is less than 0.5 ms, it can realize the detection of liquid flow in a severe environment, and is suitable for the field arrangement of an oil pipeline in an oil field enterprise. The temperature sensor uses the model DS18B20, its range is -55 ~ 125℃, can carry on the sampling to the temperature data, the quantification coding, the resolution generally may reach 0.0625, the work voltage is 3 ~ 5.5V, the sensor transforms the temperature into a digital format with only a maximum of 740ms, which is suitable for the low power consumption of sensor nodes.

B. Aggregation instrument node (Sink node)

Aggregation instrument node (ZigBee well control correspondence device, also known as gateway node or sink node, or Coordinator node), it is responsible for collecting local sensor signals, and interacting with data through the network layer and the central machine of Internet of things . When the central machine of the Internet of things sends a control instruction through data operation, after aggregation instrument node receiving, then send to the sensor node immediately through the wireless correspondence, the sensor node unpack according to the correspondence command information, carry out D/A output or I/O control. The aggregation instrument node is mainly composed of the upper layer wireless correspondence module, lower layer wireless correspondence module, node processor CPU, node LCD display module, node Key button control module, node storage module and power management module etc, its schematic diagram of the hardware is shown in Figure 3. The aggregation instrument node itself is a relatively independent local oil pump control instrument, and it has two patterns: Remote and Local, the normal situation is in the remote pattern. Once the correspondence delay or correspondence failure, the aggregation instrument node automatically transfers to the local pattern, and automatically regulates the oil pump according to the standby rule library of the instrument.

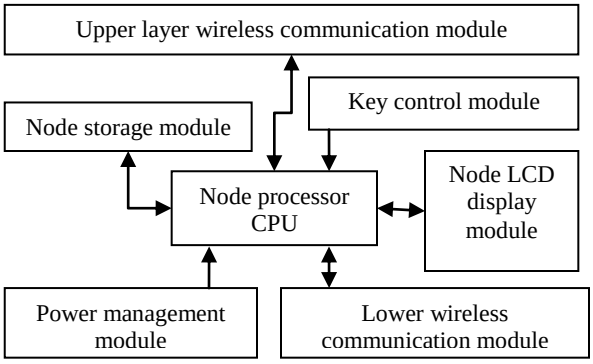

Figure 3. Hardware components theory block diagram of the IOT aggregation instrument node

The lower layer wireless correspondence module uses the CC1100 correspondence module, which can directly receive acquire information of the perception layer. The upper layer wireless correspondence module uses the SRWF508A wireless module, and the distance between the node and the network layer base station is 3.5km, by building wireless network, it is easy to realize long-distance transmission of information. The node storage module uses the AT 24C256 chip, which can extend the storage capacity through the interconnection of multiple chips. The node LCD display module can display the operation information and equipment status of the oil pump which is transmitted by the current sensor instrument node. It is convenient for user to view directly. Key button control module is convenient to operate the regulation rule library with the direct local manual input, set the working mode of the node, or directly issue a control command to start and stop the oil pump equipment, etc, it works in a matrix scan mode.

IV. SYSTEM SOFTWARE DESIGN

The software design of the intelligent wireless monitoring system for oil well pump is fundamental principle on reliability, safety and control robustness, design with modular, scalable upgrades as the guide. The software design mainly includes the program design of sensor instrument node, the programming of the aggregation

instrument node and the software design of the intelligent monitoring system of the Internet of things[4].

A. Node program design

The node program is mainly based on the design of microcontroller program. In this system, there are many similar working principle between the sensor instrument nodes and the aggregation instrument nodes, and their programming methods are similar, workflow of aggregation instrument node, the node program uses modular subroutine design patterns, it consists of a number of relatively independent subroutines called by the master loop program, each loop through these subroutines mainly completes the lower layer sensor data acquisition, correspondence layer, data storage and processing Key processing, wireless correspondence, data submitted to the upper node data display task, the maximum cycle time is set for each subroutine during the main loop operation, if occurs abnormity during the running the loop subroutine of the node, the system uses the stack to record the exception number in sequence, unify to the last step, carry out running exception handling subroutine by centralized stack mode. this can improve the efficiency of the program and peripheral wireless correspondence timely response[5].

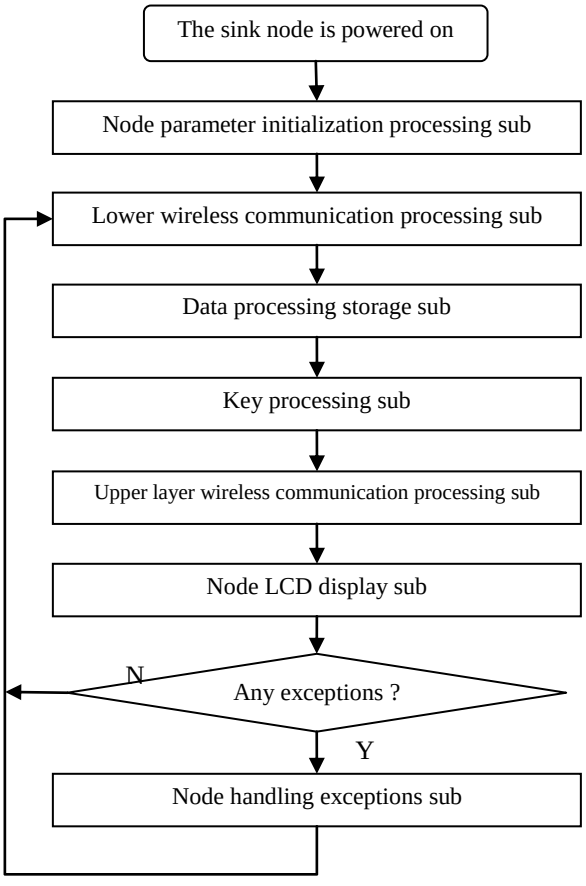

Figure 4. MCU control program flow chart of the IOT aggregation instrument node

The aggregation instrument node microcontroller program, using the C language syntax, MCU development environment to prepare, the code for its main loop program is as follows:

```
void main()     /* Main loop function definition */
{ GatherGaugeLoad();/*Aggregate node initialization */
  while (1)  /* Infinite loop until the node is powered down */
  { DownWirelessComm();/*Lower communication, collecting oil pump data */
    DataProcessSave();/*Data is normalized and saved */
    KeyInService();/*User Key processing */
    UpWirelessComm();/*Upper layer communication, execution of remote instructions */
    KeyInService();/*The node meter LCD displays the required data */
    if (RunError()!=0)    /* This round of abnormal */
      Exceptionhand();/*Handling exceptions that occur in the loop program */  }
}
```

The wireless correspondence networks of the sensor instrument nodes and the aggregation instrument nodes is based on the traditional MAC protocol in this system, it mainly realizes the establishment and maintenance of wireless data link between correspondence equipments, MAC data frame adopts time slot CSMA/CA mechanism, during running, it uses 3 parameters, namely the back index NB, the collision window CW and the back index BE to achieve reliable data transmission.

B. Software design of center monitoring system

According to the actual demand of the remote monitoring well group oil pump in oilfield enterprise, the central control system software of the Internet of things mainly consists of 7 modules, as shown in figure 5. It includes the system user management module, the network correspondence processing module, the data recording processing module, the process picture display module, the dynamic curve display module, the sensor node parameter module and the aggregation instrument node parameter module[6].

The system user management module is used to control the privileges of the user using the software, including remote desktop terminals and mobile end users, it can display or maintain the basic information record of the logged in user. Network communication processing module is the key module of the system, on the one hand, it performs exchange with the system's data in real-time through a dedicated network of network layer and the system's multiple aggregation instrument node, on the other hand, it provides data services for enterprise remote mobile terminals and desktop terminals through the public 4G network and Internet. The system control center adopts C/S design mode and adopts TCP/IP asynchronous correspondence mode, it handles network related work through proxy callback functions, it does not need to block or suspend threads when performing network operations. The system provides interfaces based on standard Modbus TCP RTU for Web based page access to remote desktops or mobile terminals. The main function of the data processing module is to normalize the data of all the oil station pump data monitored by the system, and then record the data in the database server

periodically (time can be set, usually 5min). Process picture display module is the man-machine interface system's main components, it uses virtual instrument technology to display the position of the corresponding position of each part of the oil pump and the sensing parameters in real time, and can prompt whether the system alarm or not, picture refresh time generally is 5S.

The function of the dynamic curve display module is showing the sensing parameters of each oil well in the form of curves, the dynamic curve shows the historical data curve, and also has a short running trend graph, system is built in fault diagnosis algorithm, can predict whether the future will be possible failure according to the trend of the curve, this make users prepare in advance and nip in the bud. The parameter module of sensor instrument node can set a series of parameters, such as the type of sensor, the mode of sensor operation and the communication mode of sensor network. The parameters module of the aggregation instrument node can set up a series of parameters, such as the working mode of each node of the oil station, the standby logic rule base and the correspondence mode of the node network[7].

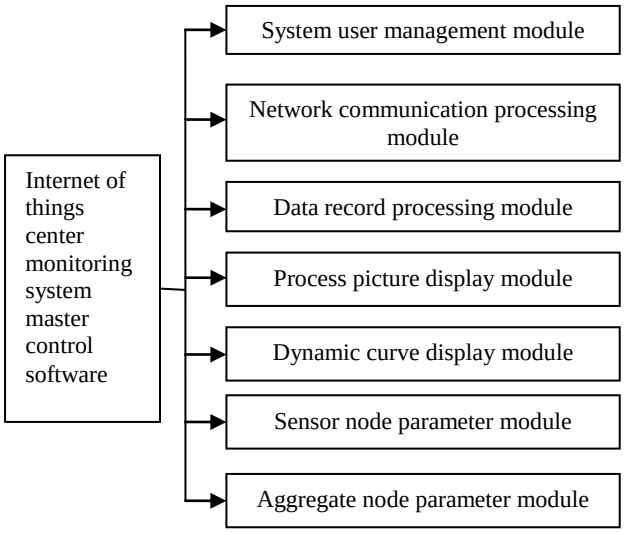

Figure 5. Module structure diagram of the IOT center computer monitor system software

V. PRACTICAL DEVELOPMENT AND EXPERIMENT OF THE SYSTEM

The author puts forward to the Internet of things theory framework in this paper, successful development and experiment have been made in the project of remote monitoring of oil well digital oil field in a subordinate oilfield enterprise of china. The key frame for the monitoring of the well pump operated by the system is shown in figure 6. The system can switch and control the 4 groups of petroleum well fuel pumps in different areas of the enterprise. The central software of the Internet of things is developed by using object oriented integrated programming tool Embarcadero, RAD, Studio and XE, the database system uses SQL Server 2008, remote desktop and mobile terminals use Visual Studio 2012 to develop B/S architectures for Web systems. Considering the safety of the special equipment controlled by the system, the mobile terminal only realizes the operation parameters and data of each oil pump and can not be remotely controlled. The system has been running for more than half a year. Compared with the traditional way of artificial inspection and management, the system is easy to operate, intelligent, equipment operation early warning, accurate and timely, it provides a powerful guarantee for the petroleum fuel production safety of the well group.

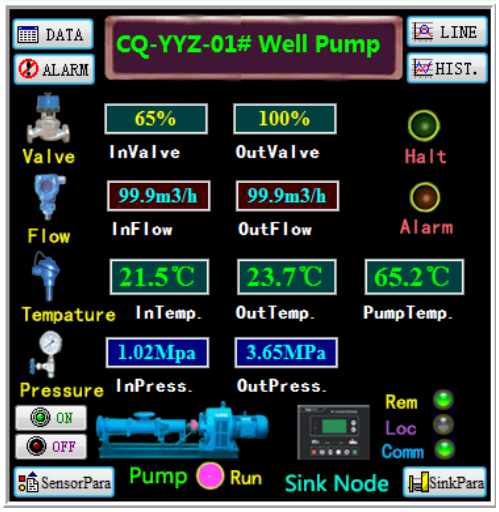

Figure 6. Remote monitoring main screen of the petroleum well based on IOT technology

VI. CONCLUSION

Design of petroleum well fuel pump measurement & control system based on Internet of things technology is an important part of digital oilfield construction, it can collect, transform and transfer information about the operation and monitoring of the petroleum fuel pumps in different areas, so as to realize remote real-time control, reducing the labor intensity of workers, improving the reliability of pump equipment operation. In addition it can realize trans regional cooperative work of oil well through internet to things, and closely connects to other parts of crude oil production, such as transportation, storage, and sales. It has realized the efficient integration of oilfield production and management technology.

ACKNOWLEDGMENT

This paper is supported by the State and provincial Joint Laboratory of Advanced Network and Monitoring Control , china (serial number: GSYSJ2016014)

REFERENCES

[1] HU Song,HE Xin-zhou,DU Li, “Petroleum equipment manufacturing industry in the internet of things technology application,” Manufacturing Automation, vol. 35, pp. 63-67, January 2013

[2] AN Jin-qiang, WEI Kai, WANG Li-qian, “Internet of things based accurate automation irrigation,” Journal of Northwest A&F

University (Natural Science Edition), vol. 41, pp. 220-223, December 2013

[3] ZHANG Nai-lu, LI Yong-jin, ZHANG Yu-xiang, "Gas station integrated information monitoring system based on internet of things," Journal of Xi'an Shiyou University(Natural Science Edition), vol. 28, pp. 103-105, June 2013

[4] ZHANG Kai-sheng, ZHAI Gong-chen, "Research of information monitoring platform based on internet of things technology," Computer Measurement & Control, vol. 21, pp. 1223-1227, May 2013

[5] WANG Guo-qiang, ZHANG Gen-bao, CHEN Jia-yan, "Research of running maintenance-alarm system of NC machine based on Internet of things technology," Application Research of Computers, vol. 30, pp. 3683-3688, December 2013

[6] LIU Bao-li, ZHANG Wen-dong, ZHUANG Wei, "Intelligent Security System Based on Internet of Things," Journal of Detection & Control, vol. 35, pp. 79-85, April 2013

[7] WANG Dong-Lai. "The Internet of Things the Design and Implementation of Smart Home Control System," Robots & Intelligent System (ICRIS), vol. 1, pp. 449 - 452, December 2016

Design of Control System for Dust - collecting Robot Based on DSP

Zhang Wei
Automation and Electrical Engineering Institute of Linyi University
Linyi，Shandong,China
Email:zhwei369@163.com

***Abstract*—With the rapid increase of labor cost in domestic service industry, it provides a powerful driving force for rapid development of service robot. Vacuum cleaner Robot as a service robot, you can replace the people to clean rooms, workshops, walls and so on. In this paper, the structure and function of the robot's measurement and control system, the type and function of the selected sensor are introduced. The structure of the motor control system and the driving principle of the motor are introduced. It can be self-navigation, detection of the wall, the room obstructions and can avoid, can travel most of the room space, you can detect the battery power and autonomy to return to charge, with strong application value.**

Keywords-control system; robot; sensor; DSP; communicate

I. INTRODUCTION

With the aging of the population and the improvement of social welfare system, resulting in a sharp rise in labor costs, labor costs in the domestic service industry compared to a substantial increase in the context of home service robot technology continues to mature, more practical, The cost will be further reduced, the price will be ordinary household consumer electronics products rather, or even cheaper. Therefore, it is expected that the home intelligent service robot will take advantage of leveraging domestic service market, the next 10 years as a high-end home service robot robotic consumer electronics products, will enter the home consumer electronic products directory[1]. Bill Gates once predicted that the robot will eventually enter the home, just like a personal computer as everyone has. Cleaning robot is a kind of service robot, you can replace people to clean rooms, workshops, walls and so on. Indoor cleaning robot's main task is to be able to replace people to carry out cleaning work, and therefore need to have some intelligence. Clean robots should be able to self-navigate, detect walls and obstructions in the room and be able to avoid; can travel most of the room space, you can detect the battery power and autonomy to return to charge, while requiring shape comparison Compact, stable operation, low noise; to have a user-friendly interface, easy to operate and control.

II. ROBOT SYSTEM STRUCTURE AND FUNCTION

In order to make the cleaning robot movement more smooth, to prevent the phenomenon of stuck, the vacuum robot designed to cylindrical or flat cylindrical shape, this design can make it free to enter the sofa, bed and furniture, some corner Are able to clean. Parallel to the ground with a circular chassis is supported by three wheels, left and right sides of the drive wheel, respectively, by the two micro-DC motor directly driven in front of the support wheel for the caster[2]. This shape and wheel layout of the robot makes it easy to turn in situ, greatly improving the walking dexterity, which is more prominent in the smaller space. A multisensor system consisting of collision, ultrasonic, and infrared sensors is used, with an infrared receiver on top of the robot; at the bottom edge of the robot. Every 45 °with a proximity sensor, used to detect the steps to prevent the fall; in front of the robot with a crash sensor, front and left and right with an ultrasonic sensor to detect the surrounding environment. The robot is equipped with a power management system, if the voltage is too low will stop cleaning, and to automatically charge. Robot processor is TI's TMS320LF2407A, it can quickly handle a variety of signals detected by the sensor, and can carry out rapid processing, the robot can quickly make a variety of reactions, the successful completion of the cleaning work.

Robot control system to complete the task: receiving sensors and encoders from the data, comprehensive treatment for cleaning path planning; drive left and right round before walking, cleaning control, vacuuming agencies to complete a variety of underlying control actions; design appropriate man-machine Interface that displays the robot status and running time on the LCD[3]. Therefore, the robot control system includes a sensor module and a motor drive module. Structure diagram of control system is Figure 1.

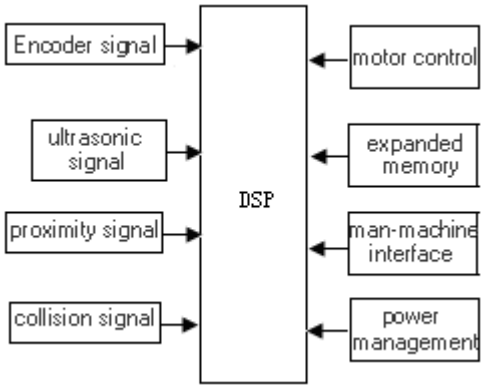

Figure 1. Structure diagram of control system

III. ROBOT HARDWARE COMPONENTS

A. *Microcontroller*

Traditional microprocessors such as 51 series, although the development cycle is short, low cost, but its real-time is not good, difficult to achieve complex control algorithm; In addition, the increase in peripheral circuit data conversion speed, the robot performance is not sufficient Play. Although the emergence of high-speed DSP makes the system modular and all-digital, so that the processing speed of the robot greatly accelerated, the system uses TI's TMS320LF2407A (hereinafter referred to as 2407) DSP chip, which is TI's DSP TMS320 series based on, Digital motor control and design. In addition to the general DSP's improved Harvard architecture, multi-bus structure and pipeline structure and other advantages, it also uses high-performance static CMOS technology, the voltage dropped from 5V to 3.3V, reducing power consumption[4]. And instruction execution speed increased to 40MIPS, almost all instructions can be completed in a single cycle of 25ns. It has the peripherals necessary for motor control applications: 32K on-chip FLASH, 2K single-access RAM, serial peripheral interface (SPI), serial communication interface (SCI), two event management modules (EVA / B), 16 Channel dual 10-bit A / D converter and CAN controller module. Each of the event managers includes the following resources: two 16-bit general purpose timers, eight 16-bit pulse width modulation (PWM) channels, three capture units for external events, quadrature encoder pulse (QEP) . As mentioned earlier, TI's 2000 series of DSP chips for the control area, 2407 of the PWM circuit has a dead-zone generation circuit, designed specifically for the bridge circuit, and the dead-band unit is programmable, making the peripheral hardware The circuit is greatly simplified, therefore, use the event manager PWM function to achieve the DC motor control is very convenient. It is particularly suitable for industrial control and small robot system, to meet the robot controller speed requirements. TMS320LF2407A as the core, the design of simple structure, stable performance of the cleaning robot body system[5].

B. *ultrasonic distance measurement module*

The basic principle of an ultrasonic transducer is to measure the time it takes to transmit and return from the sound wave to the receiver. First, the controller sends a 5μs wide pulse to stimulate the sensor to launch 40kHz high-frequency pulse, pulse issued after 750μs, the pin-level high; when the sensor receives the echo, the pin level is pulled low. From the high side of the width of the signal side to know from the launch to return to the time required for the width of 115μs ~ 18.5ms between. The formula s = vt / 2, where s represents the distance between the sensor and the target; t represents the time to launch to the recovery; v is the acoustic velocity, v = 340m / s. Thus, the distance between the sensor and the obstacle can be known[4]. A probe time of up to 20ms, 5 sensor query is completed, with l00ms, so two adjacent sensors using time-sharing to enable, will avoid mutual interference, and will not affect the speed of the robot. The ultrasonic ranging module KS103 adopted in the design adopts the SLAVE I^2C technology with innovative features. It communicates with the host computer through the standard I^2C interface, does not occupy the MCU timer, and can share the bus with other devices. With the temperature compensation function, high precision, the use of

temperature correction of the ranging command, the highest precision within a short distance of 1mm, the error is 0.152mm / 17cm; measurement of the blind area to a minimum of 1cm, no blind zone; with adjustable filter noise reduction technology, Power supply voltage is subject to interference or noise, you can still work, you can also send 0x70-0x75 a total of six levels of noise reduction instructions on the KS101B / KS103 configuration, effectively suppress the power supply noise on the ranging effect; Mode: with automatic sleep function, the module does not receive the host within 5s automatically enter the sleep command, at any time by the host I2C control instruction wake[6]. The maximum power consumption during sleep is: 500uA / 5.0V.

C. *Infrared Proximity Sensor*

Reflective photoelectric switch is composed of infrared LED light source and photosensitive diode or phototransistor and other photosensitive components, when there are obstacles to block the light can be reflected back, the output is low signal; when there is no obstruction to block, the light can not be reflected back, The output is a high level signal. The close-proximity infrared proximity sensor of the vacuuming robot consists of two groups of the same infrared transmitting and receiving circuit. Each group of circuit can be divided into high frequency pulse signal generation, infrared emission regulation and control, infrared emission driver, infrared receiver and other parts[7]. The infrared light emitted by the emission tube is reflected by the object and then received by the infrared receiving module. Through the internal processing of the internal integrated circuit to return to a digital signal input to the microcontroller I / O port. If the receiver receives the infrared pulse will return to the output low, otherwise it will output high. Through the I / 0 port detection, we can determine the existence of objects. The Si1143 infrared proximity sensor can detect close range of up to 50cm. If a suitable narrow-angle lens and an infrared filter are used in combination, the emission half-angle of the infrared LED is small enough that the emission beam Fully converged. At the same time, the infrared LED emission power is large enough, the maximum range of up to 1m. Si1143 infrared proximity sensor comes with three infrared LED driver, the host MCU can control its function through the I^2C interface, when the infrared emission of the LED is reflected by the proximity of the object is built-in infrared photodiode receiver, and then analog-digital conversion of light Strong signal is converted to digital signal, the calculated value can be compared with the set threshold value, if more than the threshold set the output from the INT interrupt signal to the main MCU, through the corresponding software to achieve specific operational functions[8].

D. *crash switch sensor*

Two slots on the photoelectric switch are distributed in the robot before the left and right to do. Such a layout allows the robot to perceive obstacles in three directions from the front, the front left, and the right, so that different responses are made depending on the direction of the obstacle. When the robot encounters obstacles, the spring under the action of obstacles, inward pressure collision switch swing arm, urging the reed to block the photoelectric switch light, the output low. When there is no obstruction, the reed under the action of the spring to restore the photoelectric switch light is not blocked, the output high.

Among the three sensors, the ultrasonic sensor is used to detect the front and left and right walls, obstacles. Two ultrasonic sensors on the left and the right are placed perpendicular to the walking direction for the walking plan of the robot. The distance between the robot and the wall is set to adjust the walking direction of the robot so that the distance between the two ultrasonic waves and the wall is approximately Equal to the set value, keeping the robot walking along the wall to maintain an appropriate distance, will not hit or away from the wall. The front two collision sensors and an ultrasound used to detect the first half of the environment; contact sensor with a large detection range, the signal without conditioning, taking up less resources, through contact collision, to detect those not detected by the ultrasonic sensor Bar-shaped obstacles such as furniture legs, etc. Proximity sensors are used to detect whether there is a cliff on the ground, in the robot at the bottom of the front, left front, right front and rear of a layout[9]. In addition to the above three sensors, the three wheels are equipped with a normally open switch sensor, when the wheel when the float,

the switch will close, the output low. When the wheels are floating, the robot can be stopped.

IV. Motor Control System

In the low power system, the DC motor has good linear characteristic and excellent control performance, suitable for point and speed control. In order to achieve positive and negative run of the DC motor, only need to change the polarity of the motor power supply voltage. The change in voltage polarity and the length of the run time can be achieved by the processor, while the current that provides the normal operation of the DC motor requires a drive circuit. H bridge drive circuit is the more commonly used driver circuit. Through the DSP to generate different duty cycle PWM pulse, precise adjustment of the motor speed. This type of circuit operates at the transistor saturation or cut-off state, avoiding the transistor in the linear amplification area of the work of the tube, can maximize efficiency; H-type circuit to ensure that the motor speed and direction can be achieved simple control.The Motor drive circuit is Figure 2.

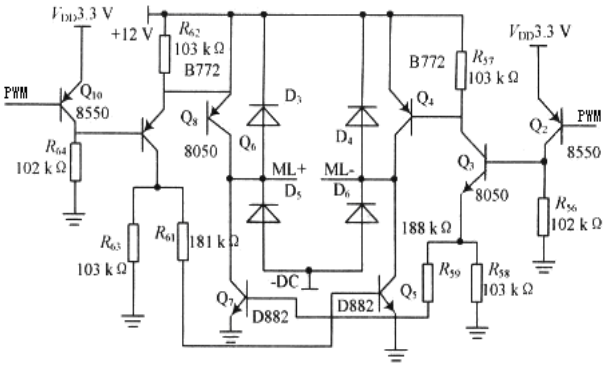

Figure 2. Motor drive circuit

With 2407 PWM output pin, you can control the speed of the motor. This part is mainly to ensure that the robot can move in the plane, while the wheel with the encoder, you can detect the distance traveled[10]. The dead reckoning can realize robot turning, indexing number hypothesis for N encoder robot; controller received pulse number is m; the wheel diameter is D; the distance between the two wheels of the wheel is W, forward distance:

$$S = \pi mD / N \qquad (1)$$

Pose a robot in the environment coordinates is (X (T), Y (T), φ(t)), then the n+1 sampling azimuth angle φn+1 and the n sampling values have the following relationship:

$$\varphi_{n+1} - \varphi_n = \frac{1}{W}\int_n^{n+T} [v_R(t) - v_L(t)]dt = \frac{1}{W}(\Delta S_{Rn} - \Delta S_{Ln}) \qquad (2)$$

V. Conclusion.

As a kind of service robot, the cleaning robot has huge market potential and wide application prospect. With the development of sensor technology and the continuous progress of microprocessors, prices are declining. This paper researches and designs a control system of the cleaning robot based on DSP, not only to meet the practical requirements, and on the basis of not increasing cost for the software provides a good hardware support, provide good technical support for better algorithms and software upgrade.

References

[1] Yun Chao.New Robot Control System [J]. China Information Industry-e Manufacturing, 2015 (6): 22-23.

[2] Liu Lei, Sun Xiaofei, Zhang Yu. Follow the electronic measurement technology [J]. STM32 car design based on intelligent remote control, 2015 (6): 31-33.

[3] Xiang Xianjun, Zhou Rongjing, Wang Yi. Detection of car control electronic measurement technology, [J]. STM32 intelligent system design based on the 2016, 39 (4): 86-89.

[4] Li Shuxia, Yang Juncheng, LIShu-Xia, et al. A path planning algorithm for indoor cleaning robot [J]. application of computer systems, 2014, 23 (): 170-172.

[5] Sun Guozheng. Interior cleaning robot design and path planning algorithm [D]. Huazhong University of Science and Technology, 2015

[6] Zhang Chao. Design of intelligent cleaning robot and its path planning [D]. Harbin Institute of Technology, 2012

[7] Zhongben Tao, Sun Yunfei. Application of storage and handling robot [J]. computer control system based on STM32 2016, 25 (7): 49-54.

[8] Liu Hai-tao, ZHANG Tie.Study on High Precision Robot Control System [J]. Machine Design and Manufacture, 2014 (1): 161-163.

[9] Ma Yan, SONG Ai-guo.Design of Control System of Force Feedback Rehabilitation Robot Based on STM32 [J]. Measurement and Control Technology, 2014, 33 (1): 74-78.

[10] Fan Lu-yi, WANG Dong-qing, LI Fang, et al.Design of palletizing robot control system based on STM32 [J]. Industrial Control Computer, 2014, 27 (11): 69-71.

Prediction of the Heat Load in Central Heating Systems Using GA-BP Algorithm

Bingqing Guo
China Electric Power Research Institute
Beijing, China
E-mail: bqguo@ epri.sgcc.com.cn

Jin Xu
Key Laboratory of Thermo-Fluid Science and Engineering, Ministry of Education,
Xi’ an Jiaotong University,
Xi’an, China
E-mail: xujin@stu.xjtu.edu.cn

Ling Cheng
China Electric Power Research Institute
Beijing, China
E-mail: chengling@epri.sgcc.com.cn

Lei Chen
Key Laboratory of Thermo-Fluid Science and Engineering, Ministry of Education,
Xi’an Jiaotong University,
Xi’an, China
E-mail: chenlei@mail.xjtu.edu.cn

***Abstract*—This paper presented the research on heat load prediction method of central heating system. The combined simulation data at Xi'an in January was used as the samples for training and predicting. This paper selected the daily average outdoor wind speed, the daily average outdoor temperature, date type, sunshine duration as input variables and the heating load value as output variable. After preprocessing of the historical data, the BP neural network algorithm and the GA-BP algorithm were employed to predict and verify heat load respectively. Based on the analysis of prediction results, it showed that the error between the predicted data and the actual value using the BP algorithm is large (maximum:-39.8%) and not suitable for heating load prediction while the error between the predicted data and the actual value using the GA-BP algorithm is small (maximum:-16.6%) and within the acceptable range. This paper provided a feasible method for heating load prediction.**

Keywords-Central heating; Heat load; BP network; GA-BP network; Heating network

I. INTRODUCTION

Global warming is one of the most important issues to handle in the energy sector, due to the high CO2 emissions from fossil fuel based power plants. The central heating sector can play a significant role in reducing the emissions [1], [2] and [3]. Central heating systems (CHS) are based on simple idea of central production of heat and further distribution of produced heat to final consumers [4], and. Primary energy use for central heat production is dependent not only on the availability of technology and on the considered environmental and social costs but also on the scale of central heat production. Every CHS comprises of three basic elements: heat source, distribution network and consumers, which are in most cases indirectly (through heating substations) connected to distribution network. To improve the efficiency of CHS, heat pumps were integrated in some models. The development of CHS is gaining more and more interest, but, in some case the space available for the integration is limited and the use of decentralized systems is necessary in order to improve efficiency of CHS and. Analysis was shown that regulation of the central-heating sector is necessary in principle, particular in terms of pricing. In order to be competitive with individual heating systems, CHS must use one of the five suitable strategic local energy resources: useful waste heat from thermal power stations (cogeneration); heat obtained from refuse incineration; useful waste heat from industrial processes; natural geothermal heat sources and fuels difficult to manage, such as wood waste, peat, straw, or olive stones and have advanced control which will lower operation and distribution costs. Models for the prediction of the temperature at critical points of central heating systems are paramount for heat suppliers to make optimal decisions on the water temperature at the supply point. Control of central heating systems is complex task and comprises of four different control sub-systems:

1) Heat demand control
2) Flow control
3) Differential pressure control and
4) Supply temperature control.

The performance of the CHS controller was characterized by an economic cost function based on predefined operation ranges. Temperature fault detection in CHS has changed from being slow and expensive to becoming fast and inexpensive. This is a basic condition for more efficient central heating systems in the future. The developed model, which manages detailed calculation of water flows, temperatures and heat losses in CH pipes, enables robust and accurate CH network state estimation. The central heating system for an building with many floors was analyzed and it was determined that under prescribed total mass flow rate, the mass flow rate of a floor increases with the increase in its heat load, while those of the other floors decrease and the temperature of supply water increases. A controlled case, for

one real thermal plant in the central heating system for the purpose of predicting the heat supply was shown that the model-based controller successfully regulates the outlet temperature of the boiler, and the total amount of heat duty has been well reduced due to the constraints on inputs considered in the control algorithm. Precise prediction of heat demand is crucial for optimizing CHS. In a central heating system, errors and deviations in customer substations propagates through the network to the heat supply plants. Based on the defined building types, the average absolute deviation of the predicted heat load was about 4–8% .The concept introduced a mass flow control model optimizing the primary and secondary water streams to achieve to achieve better results. The central heating mode not only improves the quality of life of the people, but also reduces the pollution to the environment, at the same time; it also improves the energy utilization rate and saves energy. There is a great significance to conduct research on the heat load prediction of central heating. Based on the quick and accurate prediction of heat load, making the heating system achieve fine management and improve the economy, efficiency and reliability of the central heating network to a great extent, also achieve the purpose of energy saving and environmental protection.

As early as 1984, Werner [5] in Sweden selected multiple central heating systems to be tested. The results showed the influence of outdoor temperature on the heat load of was about 60%. The heat loss of pipe could make the heat load increased by 5%-8%. Natural wind can make the heat load increase from 1% to 4%. The heat gain from solar radiation can reduce heat load from 1% to 5%. Living hot water consumption is different on working day and weekend and the average value of total heat load of 30%.

Arvastson [6] established a prediction model of the heat load based on the outdoor temperature. Erik Dotzauer [7] established a heat load prediction model based on user behavior. Peder Bacher [8] studied the prediction of thermal load at single building space. Therefore, they selected sixteen houses in Denmark Sandburg town as the object and an adaptive linear time series model using time series method. The study found great influence of the change of behavior patterns and weather forecast residents estimated on the uncertainty of the load. Also the influence of solar radiation was the largest. These factors lead to the heat load forecast deviation.

Vladimir D. Stevanovic [9] studied the prediction of the heat load in central heating system. They established a mathematical model in the complex system of heating pipe network. The model was based on the solution and carried out by hydraulic pressure and fluid velocity of high order accurate numerical prediction of the transient energy equation. It was found that the outside air temperature, the wind speed, the intensity of solar radiation, and the opening and closing state of the heating system may influence the value of heat load in the central heating system.

Krzysztof [10] modified the outdoor temperature through the intensity of solar radiation and natural wind speed, and focused on the study of the effects of these two factors on the heating load. The test selected the Poland Warsaw area. The results showed that the effect of natural wind on heating load was much weaker than the sun the effects of radiation and the solar radiation was the main factor affecting the heat load.

Because the method of artificial neural network prediction of nonlinear load has great advantages, so the artificial neural network forecasting method was also popular in the field of heating. Mattias B. Oohlsson[11], William J. stevenson[12] and Bradley P. Feuston [13] used the method of artificial neural network to predict the heat load of a large-scale construction of the United States. They selected temperature, sunshine, wind speed, time as input variables, which also marks the research of artificial neural network has begun to enter the field of heating. This paper is going to study on heat load prediction method of central heating system.

II. SELECTING THE INPUT AND OUTPUT VARIABLES

According to the BP neural network algorithm based genetic algorithm, the establishment of heating load forecasting model. To determine the input variables and output variables, the prediction model is trained on historical data. The trained model is used to predict the future load, it will need historical data as input variables, and the method of BP neural network optimized by genetic algorithm based on the mature training (GA-BP) model to predict, the output variable is the load forecasting the required value. This section applies the method to establish the central heating heat load prediction model. The input and output variables required respectively from the selection, pretreatment and analysis normalized.

Input variables are the original data or processed samples which directly affect the results of prediction. So selecting the right input variables is extremely important. The more practical and comprehensive of the input variables, the precision of the simulation neural network computing is higher. In this paper, the prediction of heat load is obtained by using the data of date, weather and history of the heat load.

The input variables of the heating system are the flow of water, supply-water temperature, return-water temperature, inlet pressure, outlet pressure and so on. The external conditions are outdoor wind speed, outdoor temperature, weather conditions and solar irradiation time. In the aspect of time, weekday and the day or night also matters. In the selection of input variables that affect the heating load, the degree of difficulty of data acquisition, and the fluctuation of the data itself need to be considered.

After simplifying the input variables, the daily average outdoor wind speed, the daily average outdoor temperature, date type and sunshine duration are determined as input variables.

The output variables of the central heating system are selected according to the different operation mode of the system. Main control operation modes are: (1) operation temperature is the major control parameter; (2) the pressure difference between supply and return water is the major control parameter. For the temperature parameter based system, the heating load value is selected as output variable. For the pressure difference parameters based system, the

pressure difference is selected. This paper selects the heating load of the day as the output variable of the neural network.

III. CASE STUDY ON LOAD PREDICTION OF CENTRAL HEATING SYSTEM

Based on the above analysis, the daily average wind speed, the daily average temperature, sunshine duration and the date type are the input variables and the heat load of the day is the output variable. First, the DeST is used to calculate the heating load of the whole heating season in Xi'an and the results is showed in Table 1. The data in Table 1 is the input and output variables of the network.

TABLE I. SAMPLE DATA

Date	*Wind speed (m/s)*	*Temperature(℃)*	*Sunshine duration (h)*	*Date type*	*Heat load (kW)*
1	0.4	2.12	7.1	0.7	32540
2	1.9	-1.69	6.5	0.7	43280
3	0.7	0.91	6.8	0.7	35620
4	0.6	1.57	6.9	0.4	33480
5	2.9	-2.25	6.4	0.4	45820
6	2.6	-2.24	6.5	0.4	45180
7	3.6	-2.98	5.8	0.4	48800
8	4.7	-3.25	3.6	0.4	51980
9	3.3	-2.82	6.2	0.4	47800
10	2.5	-2.02	6.5	0.4	44540
11	3.8	-3.01	4.3	0.4	49540
12	5.6	-3.45	2.7	0.8	55160
13	0.9	0.65	6.7	0.8	36760
14	3.1	-2.62	6.4	0.4	46960
15	2.4	-1.78	6.5	0.4	43860
16	3.2	-2.76	6.2	0.4	47480
17	0.5	1.78	6.9	0.4	32860
18	1.8	-1.08	6.5	0.4	41260
19	1.4	-0.38	6.6	0.8	39840
20	1	0.53	6.7	0.8	37200
21	1.1	-0.23	6.7	0.4	38120
22	1.2	-0.26	6.7	0.4	38380
23	1.5	-0.94	6.6	0.4	40360
24	3	-2.38	6.4	0.4	46280
25	1.9	-1.38	6.5	0.4	42060
26	0.3	2.55	7.2	0.8	31660
27	0.1	4.45	7.4	0.8	27420
28	0.4	1.91	7	0.4	32380
29	0.7	1.33	6.8	0.4	34180
30	0.1	5.9	7.5	0.4	23500
31	0.3	2.93	7.4	0.4	30060

In this paper, we use the data of the first 21 days of January shown in Table 1. as the training sample and the data of the following 10 days as the prediction samples. Then the data based on the training data and the date in the prediction samples was predicted and compared.

A Prediction of BP

The settings for the BP neural network are as follows: the layers of network structure are 3; input nodes are 4, hidden nodes are 15 and output node is 1, namely the structure of 4-15-1 network. Its main parameters are: learning efficiency: 0.1, the momentum factor: 0.65, the maximum number of training: 2000, square error of network training: 10-5. The results of the perdition of BP neural network and the actual load, absolute error, relative error of the results are shown in Fig. 1, Fig. 2 and Fig. 3.

It can be found from Fig. 1, 2 and 3 that the algorithm of BP neural network can predict the trend of heat load and its change characteristics, but the error between the actual value and the prediction load is large. The relative error range is from -39.8% to 6.5%. Only the prediction errors of two days of are less than 15% and cannot meet the actual needs. In order to improve the precise, we adopted the GA-BP algorithm.

B Prediction of GA-BP Algorithm

The main parameters of the training process of network connection weights in the optimization using Genetic algorithm are: population size is 100 N; maximum generation equals 60; neural network training times is 100; the momentum factor is 11; the maximum square error is 10-5. Through repeated training and learning algorithm, the weights optimized by genetic algorithm are revised using BP neural network algorithm. In the training of BP neural network, the number of BP neural network layers is 3; the number of input nodes is 4; the number of nodes in implicit layer is 15 and the number of the node in output layer is 1; the learning efficiency is 0.2, the momentum factor is 652; the maximum number of training network is 2000, the maximum square error is 10-5.

The results of the perdition of GA-BP neural network and the actual load, absolute error, relative error of the results are shown in Fig. 4, Fig. 5 and Fig. 6.

It can be seen that the predicted heating load curve using genetic algorithm and BP neural network algorithm is basically close to the real value, the relative error range is from -16.6% to -4.0%. So we can say that the GA-BP algorithm is superior to single BP algorithm from the prediction results.

IV. CONCLUSION

The method of GA-BP network optimizes the network weights and threshold and reduces the possibility of the training of BP neural network sunk into the local minimum, which improves the learning performance of the whole network. At the same time GA-BP also accelerates the training speed of the network and improves the learning efficiency. So using the GA-BP network provides a better method for heating load prediction.

ACKNOWLEDGMENT

This work was financially supported by the State Grid technology project “Research on the electric heating

planning and optimizing oepration of non municipal central heating district" (YD71-16-009).

REFERENCES

[1] D. Bättger, M. Gätz, N. Lehr, Hendrik Kondziellaa, Thomas Bruckner Potential of the power-to-heat technology in district heating grids in Germany. Energy Procedia, 46 (2014), pp. 246–253.

[2] M.A. Ancona, M. Bianchi, L. Branchini, F. Melino District heating network design and analysis. Energy Procedia, 45 (2014), pp. 1225–1234.

[3] A. Gebremedhin. Optimal utilization of heat demand in district heating system—a case study. Renewable Sustainable Energy Rev, 30 (2014), pp. 230–236.

[4] L. Di Luciaa, K. Ericssona. Low-carbon district heating in Sweden—examining a successful energy transition. Energy Res Soc Sci, 4 (2014), pp. 10–20.

[5] S.Werner, The heat load in district healing system. Swenden: Chalmers University of Technology, 1984

[6] L.Arvastson, Stochastic modeling and operational optimization in district heating systems. Lund University, 2001

[7] E.Dotzauer, "Simple model for prediction of loads in district-heating systems," Applied Energy, vol. 73, 2008, pp. 277-284, doi

[8] Bacher P, Madsen H, Nielsen HA. "Online short-term heat load forecasting for single family houses," Proc. 39th Annual Conference of the IEEE Industrial Electronics Society, IEEE Press,, 2013,pp.5741-5746

[9] Stevanovic VD, Zivkovic B, Prica S, et al. Prediction of thermal transients in district heating systems. Energy Conversion and Management, 2014, 50(9): 2167-2173

[10] Wojdyga K. An influence of weather conditions on heat demand in district heating systems. Energy and Buildings, 2015, 40(11): 2009-2014

[11] Ohlsson MB, Peterson CO, Pi H, et al. Predicting System Loads with Artificial Neural Networks--Methods and Results from" The Great Energy Predictor Shootout". ASHRAE Transactions-American Society of Heating Refrigerating Airconditioning Engin, 1994, 100(2): 1063-1074

[12] Stevenson WJ. Using artificial neural nets to predict building energy parameters]. ASHRAE Transactions., 2014, 100(3): 1076-1087

[13] Feuston BP, Thurtell JH. Generalized nonlinear regression with ensemble of neural nets: the great energy predictor shoot out. ASHRAE Transactions, 2012, (5): 1068-1080

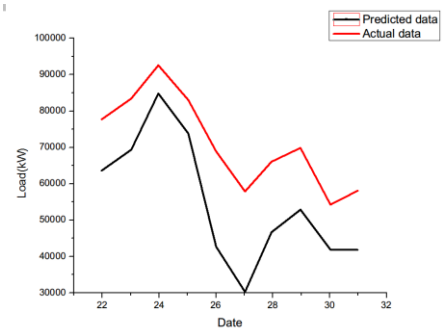

Figure 1. Predicted load by BP network and actual load

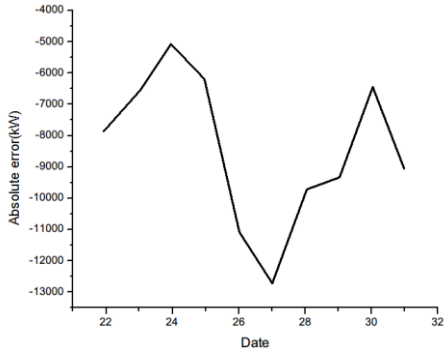

Figure 2. Absolute error of BP network

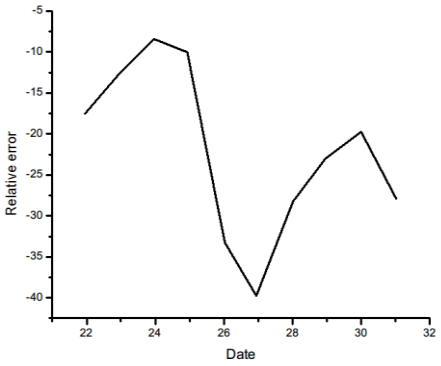

Figure 3. Relative error of BP network

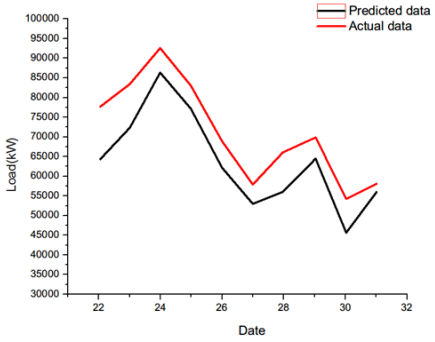

Figure 4. Predicted load by GA-BP network and actual load

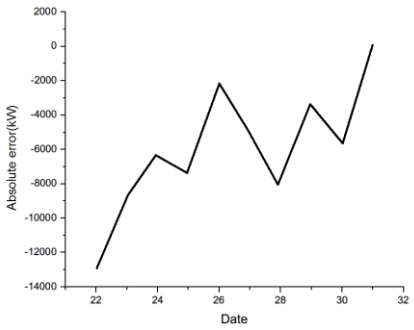

Figure 5. Absolute error of GA-BP network

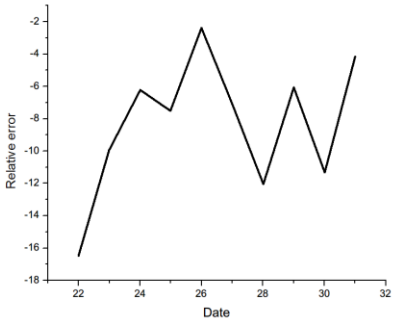

Figure 6. Relative error of GA-BP network

Research on Intelligent Monitoring Technology of Micro Hole Drilling

Yanhong Sun
College of Mechanical Engineering
Jilin Engineering Normal University
Changchun Jilin, China
E-mail: 343175460@qq.com

Mei Tian*
College of Mechanical Engineering
Jilin Engineering Normal University
Changchun Jilin, China
E-mail: 32593829@qq.com
*Corresponding author

***Abstract*—Aiming at the problem that the micro drills is easy to be broken in the process of drilling; it is difficult to detect the drill bit. The drilling torque signal is taken as the monitoring object. A new method for the on-line monitoring the micro-drill breakage based on BP neural network is proposed. After the three layer wavelet decomposition of the drilling torque signal, the energy feature vector is used as the input layer of the BP network, and the mapping model of the working state and the drilling force of the micro drill bit is obtained by using the network structure of the four layers. Using MATLAB software and Lab VIEW software, a micro drill on-line monitoring software system is constructed. The experimental results show that the accuracy of the wavelet neural network is very high, which is more than 90%, which shows the validity of the monitoring model and the popularization of the system.**

Keywords-Micro-role drilling; Micro-drill; Wavelet neural network; On-Line monitoring; Force

I. INTRODUCTION

Along with the development of technology at very fast speed, the micro-roles' application is tend to become more and more extensive[1]. The most practicable method among all drilling methods is still power drilling by the micro twist drills. During micro-role drilling ,the drill is subject to breaking, and the part containing broken drill will be scraped, therefore how to avoid micro-drill breakage has been a difficult technical problem[2-5]. Essential cause to drill breakage is that the drilling torque increases along with drill wear process and finally exceeds strength limit of the drill[6]. If the drilling torque can be predicted and the warning can be given on-line by drilling torque monitoring, micro-drill breakage will be avoided effectively.

Wavelet neural network is combining wavelet theory and neural network, which has the high auto-adapt character and robustness character[7].This paper carried out their nonlinearity mapping both micro-drill breakage and breakage signals based on BP neural network, whose input signal was the energy eigenvectors of torque by using wavelet packet transform. Furthermore, a kind of software system to on-line monitoring micro-role drilling has been constructed by using Matlab software and LabView software.

II. WAVELET NEURAL NETWORK

A. Wavelet and Wavelet Analysis

Wavelet is a kind of wave with finite length and zero-average value. The low frequency part of signal may be decomposed and analyzed by Wavelet analysis which came from signal analysis and the flex, parallel shift characters of the function. Wavelet packet analysis may process effectively decomposing to all frequency range signal, and be propitious to distill the characteristic of signal[8].

If $\varphi(t) \in L^2(R)$,it's fourier transform satisfies the following admissible conditions:

$$C_\varphi = \int_{-\infty}^{+\infty} \frac{|\hat{\varphi}(\omega)|^2}{\omega} d\omega < \infty \qquad (1)$$

$\varphi(t)$ is the basic wavelet or wavelet generating function. Continuous wavelet transform is defined as

$$\varphi_{a,b}(t) = \frac{1}{\sqrt{a}} \varphi\left(\frac{t-b}{a}\right) \qquad (2)$$

$$(WT_f)(a,b) = |a|^{-1/2} \int_R f(t) \overline{\varphi(\frac{t-b}{a})} dt \qquad (3)$$

$f(t) \in L^2(R)$ （$a, b \in R \ \ a > 0$）[8].

B. BP Neural Network

The structure of the BP network is shown in Fig.1. The network includes the input layer, hidden layer and output layer, the hidden layer can is composed of multiple layers, each layer has a plurality of nodes, front layer and a rear layer by weight connection, no coupling between nodes on the same layer[9].

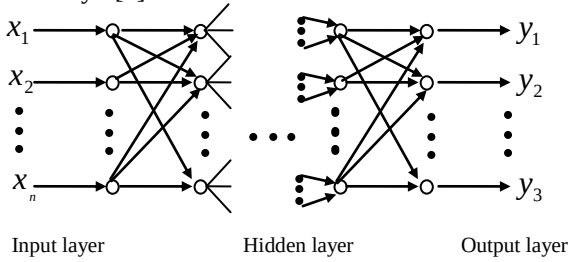

Figure 1. Neural network structure

BP neural network, as well as neural network whose error is transmitted in reverse, which has many layers framework, including input layer, output layer and some crytic layers. Its training steps are that the first step is to pick up a training sample among the muster and input to the neural network; the second step is to calculate network's output; the three step is to calculate the error between its input and its output ; next step is to adjust the network value in order to minish the error form output layer to former layers. Each training sample is trained by the method until the network's error becomes minimum[10].

C. *Wavelet Neural Network*

Wavelet neural network is relax combining wavelet analysis and neural network. It utilizes the local characteristic and the powerful distilling speciality of wavelet analysis or wavelet packet analysis which is used to be the label processor of neural network in time domain and frequency domain to decompose the signal to some independent frequency range. A new vector is given birth to be input signal to neural network, which is composed by all energy values in all frequency range. Applying those methods to construct wavelet neural network will make network structure more simple and comprehensible. And at the same time, network training time will be shortened and learning efficiency of network will be enhanced.

The flowchart of wavelet neural network is shown in Fig.2.

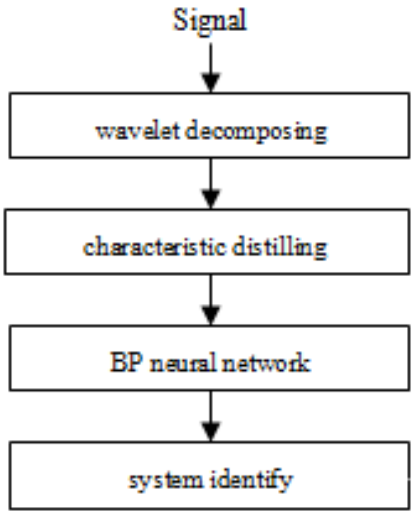

Figure 2. Flowchart of wavelet neural network

III. ON-LINE MONITORING EXPERIMENT SYSTEM DESIGN

A. *System Model*

Experiment indicated that essential cause to micro-drill breakage is that the drilling torque increases and finally exceeds strength limit of the drill. the torque signals both in fine condition and in breakage condition shown as Fig .3 were set up.

In this paper, the drilling torque signal is monitored and decomposed into three layers wavelet packet(shown as Fig .4), x_{ij} is the amplitude of the reconstruct signal, and E_{3i} is the energy signal of the third layer wavelet packet, whose calculating function is,

$$E_{3i} = \int |S_{3i}(t)|^2 dt = \sum_{j=1}^{N} |x_{ij}|^2 \quad (4)$$

Where, N is the data number; i is the sequence number, i=0 to 7.

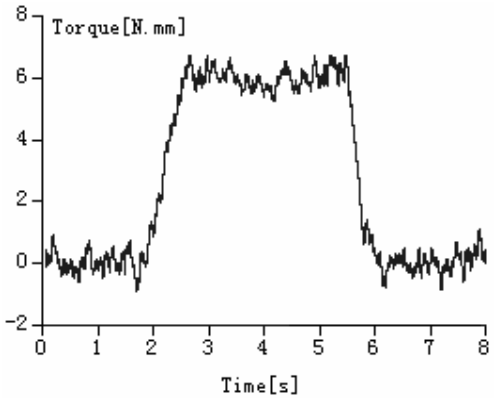

a. fine condition

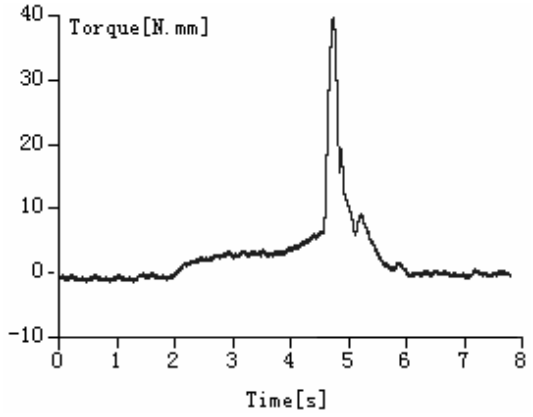

b. breakage condition

Figure 3. Torque signals of micro-drill

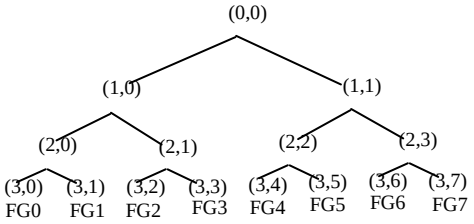

Figure 4. Three layers wavelet decompose tree

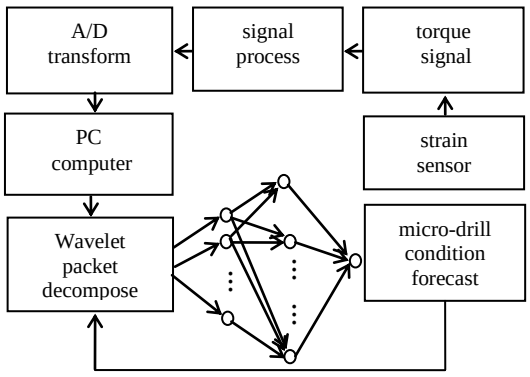

Figure 5. wavelet network monitoring model

The energy signal decomposed is input to three layers neural network for network training and learning, A mapped between energy variety and micro-drill breakage is built up, at last the monitoring liminal value may be calculated.

The experiment was carried out with a CNC precision micro-size drilling machine. For on-line monitoring drilling torque, total neural network system is shown as Fig .5. In the system, the data of drilling torque signal were collected by strain sensor, then it was transmitted to the industrial PC though NI6013 data acquisition board (16-bit resolution and 200 kHz sample frequency), and were processed in there by BP neural network in this paper. The network gave the judging result about micro-drill condition. In the experiment, the spindle rotating speed was 15000r/min; the feeding speed was 40mm/min. The workpiece material was stainless steal with 1.5mm thickness. The drill diameter was 0.4mm.

B. Network Training and Learning

This network has 8 input nodes and 1output node which judges micro-drill fine or breakage and 15 middle nodes calculated in the light of (2*n-1)principle[9](where, n is input nodes).The paper assumed that system error was 0.001, learning rate was 0.8, momentum gene was 0.7, maximum training time was 2000.

Under the experiment condition described above, drilling experiments were carried out. Then take that 50samples, including 40 training samples and 10 testing samples to train wavelet neural network, obtain network output corresponding to each sample.

After 326 times of training, the network converges to the precision requirement. After network training, degree of the network training results and comparison of micro drill actual cutting conditions, the comparison figure between the network output and the target network training was plotted as shown in Fig. 6. When the microdrill is in normal state, the expected output of the network is 0.1, while that of the breakage is 0.9. The results show that the output of the wavelet neural network can correctly reflect the cutting state of micro drills. The network has achieved good performance requirements.

Table1 is testing result.'+' showed testing true or '-'showed testing fault. Result made clear that true testing rate to checking out micro-drill breakage has attained 90%,the on-line monitoring system was proved efficiently.

TABLE I. DATASHEET TO NETWORK TESTING

No.	Input layer nodes data of BP neural network								Network output	Drills condition	Test result
	FG0	***FG1***	***FG2***	***FG3***	***FG4***	***FG5***	***FG6***	***FG7***			
1	11.62	19.27	26.52	179.8	375.2	725.5	1431	51.72	0.1098	fine	+
2	147.4	595.1	7581	595.5	166.2	8099	8951	11979	0.8508	breakage	+
3	96.33	408.7	7564	2317	170.6	9351	1655	556.1	0.1013	fine	+
4	149.8	3349	4979	2617	1471	5447	1359	14802	0.8856	breakage	+
5	96.00	1142	3033	798.5	146.5	6949	4607	2980	0.1101	fine	+
6	17.00	28.14	40.45	272.7	606.4	1356	3620	75.57	0.1024	fine	+
7	125.7	9285	17921	6974	1179	9684	6647	11820	0.9756	breakage	+
8	142.3	612.5	1607	850.0	215.4	7940	9133	2768	0.2427	fine	+
9	122.6	2794	6221	1397	1223	8757	4606	17890	0.8257	breakage	+
10	230.0	120.5	1949	3310	6113	3176	7143	1372	0.7283	breakage	-

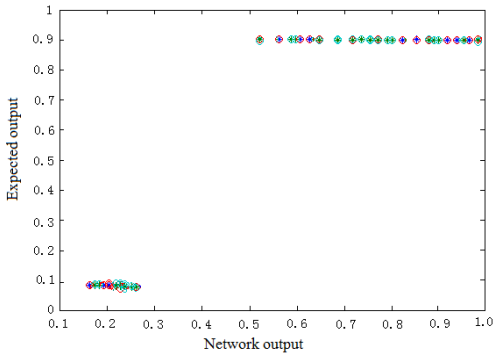

Figure 6. Comparison between target output and simulation results

In this paper, the data will be normalized after the network training, using the normalized equation(5) as follows:

$$x'_j = \frac{0.9-0.1}{x_{j\max} - x_{j\min}}(x_j - x_{j\min}) + 0.1 \qquad (5)$$

$x_{j\max}$、$x_{j\min}$ is the maximum and minimum values of the output characteristic，x'_j is normalized data.

C. *Comparative analysis of wavelet neural network and BP neural network*

The same experimental data are input to the BP neural network and wavelet neural network system for state identification and comparative analysis, as shown in Fig .7.

In order to better the accuracy comparison of two kinds of network, another 35 groups of samples were input to the two neural network model has been trained, then the network output and the actual state of the sample comparison, obtained results contrast Table II shows the. It is clear that the accuracy of the wavelet neural network to the new data is obviously higher than that of the BP network, which shows that the improved neural network has better robustness.

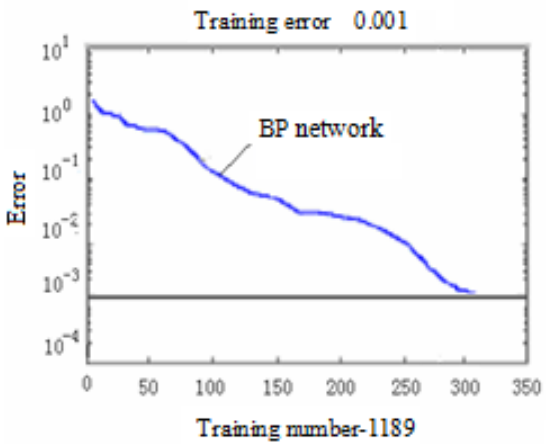

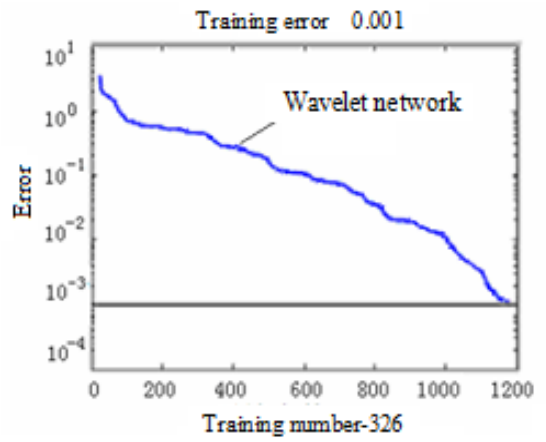

Figure 7. Velocity curves of the two networks drilling

TABLE II. NETWORKS CONTRAST

	normal		breakage		accuracy rate
	train	*test*	*train*	*test*	
BP network	20	15	20	15	87.0%
Wavelet network	20	15	20	15	93.3%

IV. MONITORING EXPERIMENT

According to data in Table I, anther 3 drill groups (10 drills each group) were taken to perform experiments using already trained network. Drills in first group did not employ on-line monitoring while drilling until breaking. Drills in other 2 drill groups were monitored on-line while liminal value was 0.75 for second drill group and 0.55 for third drill group. For each drill in second and third group, keep drilling until warning and drill backing off. Experimental results are shown in Table III.

TABLE III. ON-LINE MONITORING EXPERIMENTAL RESULTS

group No.	average holes drilled	breaking drills
1	49.6	10
2	45.1	1
3	40.7	0

V. CONCLUSION

A. The micro-drill monitoring method based on wavelet neural network is efficient under much model analysis and monitoring experiment.

B. Taking drilling torque as monitoring object and using strain sensor as measuring element are able to well monitoring drill wear states in drilling process. Therefore, it is convenience to use in practice.

C. On-line monitoring effect is relate to liminal value. Using low liminal value has well effect to forecast micro-drill breakage, but drilling role number is few

relatively. liminal value should be set up according to machining condition in practical drilling.

REFERENCES

[1] C. Yaxin. “Research on Micro-drilling Online Monitoring Based on Double Neural Network”[D]. Jilin University doctoral dissertation,2013, p. 25-37

[2] S. Yanhong. “Research on the Breakage Mechanism of Micro-drills and Drilling Forces Online Monitoring” [D]. Jilin University doctoral dissertation, 2009,pp. 18-34

[3] Y. Zhaojun, L. Xue, J. Qingxiang, and S. Yanhong. “Development of a rough set-based fuzzy neural network for online monitoring of microdrilling”[C]. Int J Adv Manuf Technol,vol.41, Jan.2007,pp. 219–225

[4] Z. Yonghai, G. Hui, H. Qi. “The study of drilling process based on finite elemnet method”[J].Natural Science Journal of Xiangtan University, Jan. 2012,pp. 108-112, (In Chinese)

[5] Y. Junchoi, M. Soopark, C. Namchu. “Prediction of drill failure using features extraction in time and frequency domains of feed motor current” [J]. International Journal of Machine Tools & Manufacture, vol.48, Jan.2008, p.29-39

[6] M. Sheelcheong, D.Woocho, K. Ehmann. “Identification and control for micro-drilling productivity nhancement” [J]. International Journal of Machine Tools & Manufacture, vol.39, Oct.1999,p. 1539-1561

[7] S. Yanhong, C. Yaxin. “Application of wavelet fuzzy neural network in microdrilling online monitoring” [C]. ICEICE, Aug.2011,p. 3001-3004

[8] T. Xianghong, l. Qiliang. “Time frequency analysis and wavelet transform: Second Edition”[M]. Mechanical Industry Press, Mar.2016 (In Chinese)

[9] Z. Shuxu, d. Zhanwu. “Neural network: theory, method and Application:First Edition” [M].Chinese Railway Press, May .2013(In Chinese)

[10] M. Rui. “Principle of artificial neural network: First Edition” [M].Mechanical Industry Press,Jan.2014(In Chinese)

A Diagnosis and Localization Method of Slime Pipe Blockage which Pressure Wave based on Wavelet Transform

Yuanbin Hou
College of Electrical and Control Engineering
Xi'an University of Science and Technology Xi'an
Xi'an, China

Jiao Dang
College of Electrical and Control Engineering
Xi'an University of Science and Technology Xi'an
Xi'an, China

Dong Li*
College of Electrical and Control Engineering
Xi'an University of Science and Technology Xi'an
Xi'an, China
E-mail: 349821997@qq.com
*The corresponding author

Hongxia Li
College of Electrical and Control Engineering
Xi'an University of Science and Technology Xi'an
Xi'an, China

***Abstract*—Aiming at the problem of blocked pipe in coal slurry pipeline transportation process, in the two phase of the project of 50MW unit in Shanxi Huangling coal gangue power generation company, the method of pressure wave slime pipeline blockage location is proposed based on *wavelet transform, which is the analysis of the pipeline* positioning principle based on the pressure wave method, the pressure wave is collected by the pressure sensor installed on the pipeline. Next, the abrupt change of the pressure signal is detected by the wavelet transform, which is integrated into the pressure wave method; Thus the pressure wave velocity and time difference are determined to realize the accurate location of the blockage point. The experimental platform of coal slurry pipeline transportation is built according to the proportion of 100:1, the simulation and experimental results show that the algorithm can be used for the location of the blockage fault in the viscous conveying pipeline system.**

Keywords-component slurry pipeline; Wavelet transform; Pressure wave method; Blockage fault location

I. INTRODUCTION

Slime is a by-product of coal washing industry; it is a kind of solid liquid two-phase flow which is separated from coal washing process, which accounts for 5-8%. The coal slurry pipeline transportation system is an important part in the process of boiler coal combustion, but the unstable quality of the coal slurry can lead to the blockage in the process of transportation. The blockage of the fault, the normal delivery of coal slurry, the safety and normal operation of the system will be a large extent, there are serious security risks. Therefore, it is very important to detect and diagnose the blockage fault of coal slurry pipeline.

There are many experts abroad to study the problem of viscous material conveying pipeline blockage, China University of Mining and Technology, many experts studied the coal slurry in the pipeline transportation, in 2009,Wu Miao, Pan Yue et al.[1] Put forward a method to calculate friction coefficient of high viscous materials in pipeline transportation through comparing the pressure at the different point on the same pipeline; in 2010, Feng Li, Liu Jiongtian et al[2] analyzed on Influencing Factors of Sedimentation Characteristics of Coal Slime Water; in 2016, Gao Jie, Hao Xuedi et al.[3] studied that the influencing factors of coal slime pressure loss in pipe flow at high pressure were investigated at a designed test facility. The experimental results show that pressure loss is directly proportional to flow rate, but inversely proportional to pipe diameter. It is also found that the pressure loss has a complex exponential relationship.

Secondly, experts at home and abroad have studied the problem of drainage pipeline or oil transportation, In 2012, Lee Jong-Hwi, Chu Ick-Chan et al.[4] discovered new technologies for preventing drainage pipe blockage in tunnel. there were so many methods to preventing drainage blockage, but the Quantum stick method and magnetic method are considered in this study. M. R. Khanarmuei, HRahimzadeh et al. in Indian [5] researched the effect of vortex formation on sediment transport at dual pipe intakes, experiments were performed on dual pipe intakes at three common intake withdrawal direction (vertical, horizontal and angle of 45°). Rushd, S. Sanders, S. A. in Canada [6] studied the parameter of the hydrodynamic roughness produced by a wall-coating layer of oil during the pipeline transportation of heavy oil-water mixtures. Ulanov, A.M. Bezborodov, S.A. in Russia[7] discovered the calculation method of pipeline vibration with damping supports made of the MR material. Lecreps, I. Orozovic, O. et al in

Australia[8] studied that physical mechanisms involved in slug transport and pipe blockage during horizontal pneumatic conveying. Other, in coal gangue power generation, many experts researched on blockage prediction of coal slurry transportation pipeline[9-11]. Also experts studied parameter characteristics and testing of piping material[12][13].

II. ANALYSIS OF PRESSRUE WAVE IN VISCUS MATERIAL CONVEYING PIPELI

When the viscous material conveying pipeline is blocked, the corresponding pressure change diagram is analyzed and shown in Fig .1. Pressure sensors are equipped in the two points of the O and A points of the slime conveying pipeline, the pressure distribution curve of the normal operation of the pipeline is shown in Fig. 1, then the pressure difference between the two ends of the OA is $vp1$. If the pipe is blocked, the pressure will increase before the block agep point and the pressure will drop after the blockage point, the pressure gradient of this process can be shown in curve 2.When the pipe blockage is relatively serious, the pressure gradient curve pipe as shown in curve 3. Here when the pipeline is blocked, the upstream pressure increases and the downstream pressure decreases, so that the pressure difference between upstream and downstream can be changed to $vp2$. Assuming the Po upstream sensor is installed at the O point, the downstream sensor is installed at the A point, so the pressure of the O point can be expressed as PO, the pressure of the A point is PA. the pressure at the point of O is expressed as po1 ,the pressure of the A point is PA1 when the fault occurs. the change relation of the points before and after the blockage can be expressed as follows formula (1):

$$\begin{cases} vP_1 = p_O - p_A \\ vP_2 = p_{O1} - p_{A1} \end{cases} \quad (1)$$

The variation of the pressure before and after the blockage can be obtained by the following formula (2):

$$vp_1 - vp_2 = E \quad (2)$$

If the E>T shows that the pipeline is blocked, the T is the threshold value of the detection, the general pipeline to the normal operation of the maximum pressure error.

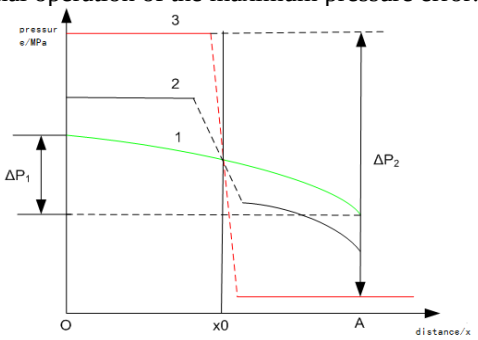

Figure 1. Schematic diagram of pressure variation in pipeline blockage

In summary, according to the variation of the pressure difference between the two ends of the pipeline before and after the pipeline blockage, the change of the difference E can be determined to detect whether the pipeline is blocked or not. According to the pressure change of the coal slurry pipeline, the pressure difference between the sensors is calculated with the measured pressure signals of each sensor, and then the blockage fault detection is realized.

III. PRESSURE WAVE DECOMPOSING BASED ON WAVELET TRANSFORMING AND ITS PARAMETER DETERMINATION

A. Determination of Time Difference of Pressure Wave Based on Wavelet Analysis

The boiler for the two phase of the project of 50MW unit in Shaanxi Huangling coal gangue power Generation Company. According to the proportion of 100:1, we built an experimental platform for coal slurry pipeline transport as shown in Fig .2.

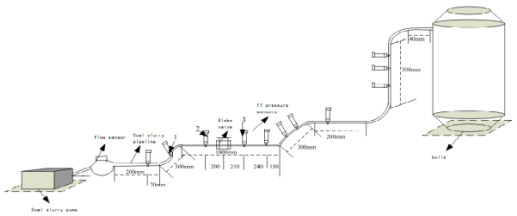

(a) experimental platform structure of coal slurry pipeline transportation

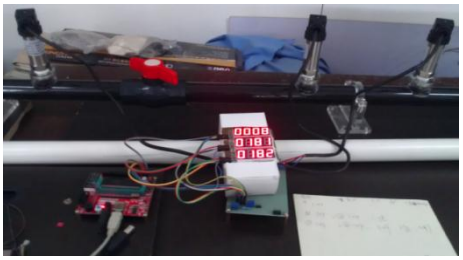

(b) part of the experimental platform for spherical valves between sensors 2 and 3

Figure 2. Experimental platform of coal slurry pipeline transportation

In the picture, in the case of the coal slurry pump open, The degree of slime blockage is simulated by the degree of the switch of the ball valve in the middle ofthe sensor 2 and the sensor 3 .When the coal slurry pipeline is blocked, the pressure value near the blockage point also changes.similar to the first singular point of the continuous signal, the pressure drop caused by the signal mutation caused, with the blockage is close to the vertical, the waveform of pressure drop signal can be collected by the pressure sensor installed on the pipeline, The wavelet transform can be used to obtain the abrupt change of pressure signal, Therefore the time difference of the pressure wave can be determined by detecting the pressure signal, that collected by the upstream sensor, and the

abrupt change of the pressure signal collected by the downstream sensor, the pressure signal collected by the upstream and downstream sensors is shown in Fig .2, and the wavelet transform is used to denoise the signal [14], the abrupt point of the signal can be detected as shown in Fig .3 and Fig .4. Wavelet transform to determine the time difference of the pressure wave signal can be divided into the following steps:

a) The pressure signals collected rely on the upstream and downstream sensors are decomposed by wavelet:

b) According to the different scale, the decomposed signal is reconstructed.

c) The reconstructed signals are compared and the maximum modulus points which the two groups are detected;

d)According to the maximum value of the model, the abrupt change point of the signal is determined, the two groups of signals is calculated and the time difference of pressure wave signal propagation can be obtained.

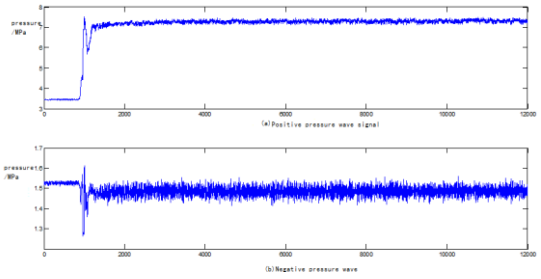

Figure 3. Positive pressure wave signal and negative pressure wave signal before and after the blockage

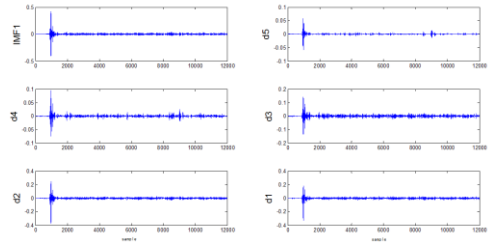

a. Detection of positive pressure wave in wavelet hierarchical mutation

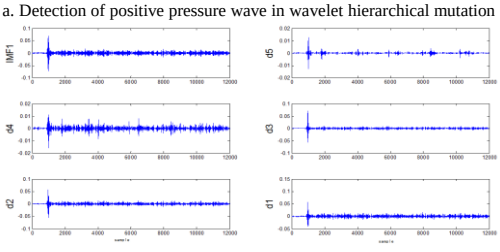

b. Detection of the negative pressure wave in wavelet hierarchical mutation

Figure 4. a, b

B. *Determination of Pressure Wave Velocity*

Pressure wave velocity formula (3) as shown in:

$$v=\sqrt{\frac{K/\rho}{1+\frac{K}{E}\frac{D}{e}C_1}} \tag{3}$$

Here,

K—Volume elasticity coefficient of fluid, Pa;

ρ—Density of fluid, kg/m3;

E—Elastic modulus of pipe, Pa;

D—Pipe diameter, m;

e—Tube wall thickness, m;

C_1—The correction factor related to the pipe constraint;

E, D, e, C_1 can be measured directly or obtained from empirical data. Both κ and ρ are functions of temperature for fixed pipes[15].

Bulk elastic coefficient of coal slurry κ: it indicates the change of the volume caused by the external pressure,its value is generally the reciprocal of the compression coefficient. Compressibility is the rate of change of the volume of the fluid when the fluid temperature is constanted.The formula is shown in formula (4).

$$\ln(F\times10^{10})=0.51992+0.0023662T+846596/\rho_0^{\,2}+2366.67T/\rho_0^{\,2} \tag{4}$$

Here,

F—Compressibility factor, 1/Pa

ρ_0— Standard density, kg/m3.

T—Fluid temperature, $^{\circ}C$;

Bulk modulus $K=\frac{1}{F}$.

The standard density refers to the material density under the standard conditions. For example, at a temperature of 273K (zero), the pressure at a standard atmospheric pressure of the gas standard density. The temperature in the standard density 20℃, the pressure in a standard under the pressure of liquid. For example, the density of water at different temperatures can be obtained by inquiring the general rules for the determination of density and relative density of chemical products, People's Republic of China national standard GB/T4472-2011.See Table I. The water in the 0-30℃ degrees, the maximum density value is 999.972 kg/m3, the minimum value is 992.591 kg/m3 and the maximum change is kg/m3, which it can be seen from the Table I, and it can be ignored in formula (4) calculation, its bulk elastic coefficient K=0.3787×1010.

Coal slurry pipeline is DN200 carbon steel pipe material, Therefore, the pipe diameter D=219mm, the pipe wall thickness of E =10mm, the pipe elastic modulus E=206×109Pa。

TABLE I. DENSITY AT DIFFERENT TEMPERATURE

t	0	1	2	...	8	9

0	999.84	999.89	999.96	999.84	999.78
10	999.69	999.60	999.37	998.59	998.40
20	998.20	997.99	997.53	996.23	995.94
30	995.64	995.34	995.02	992.96	992.59
40	992.12	991.83	991.43	988.92	988.49

Pipeline constraint coefficient C1 can be classified according to the different support conditions. If both ends of the pipe are fixed, there is no axial movement, that $C_1 = 1-\mu^2$, μ is the Poisson coefficient among them. The carbon steel material is used in the slime conveying pipeline,For carbon steel, $\mu = 0.26$. therefore $C_1 = 0.9324$

Substitution of F to formula (3), it can be obtained velocity formula (5) when the coal slurry in the water content of 30% wave .

$$v = \sqrt{\frac{K/\rho}{1+\frac{K}{E}\cdot\frac{D}{e}\cdot C_1}} = \sqrt{\frac{0.3787\times10^{10}/1450}{1+\frac{0.3787\times10^{10}\times0.219}{206\times10^{9}\times0.01}\times0.9324}} = 1.3781\times10^{3} m/s \tag{5}$$

IV. STUDY ON THE METHOD OF PRESSURE WAVE BLOCKAGE LOCATION BASED ON WAVELET TRANSFORM

A. *The Process of Pressure Wave Blockage Location Method Based on Wavelet Transform*

Its can be finded that the wavelet transform can detect the abrupt change point of the signal from the above analysis, Therefore, when the coal slurry pipeline is blocked, the pressure wave can be detected at the upstream and downstream pressure transmitter, the time difference Δt is obtained between the pressure wave and the two pressure transmitters. And through the formula (6) to locate the position, the formula (6) is as follows.

$$L_i = \frac{L \pm v\Delta t}{2} \tag{6}$$

In the formula, L represents the total length the conveying pipe; L_i indicates the blockage of the pipeline; '$\pm$' means the detection of positive pressure wave, the wavelet transform of the hierarchical point takes the '+', In the detection of the negative pressure wave, the wavelet layered mutation point takes the '-'; On the basis of the above analysis, The flow chart of the pressure wave blockage localization method based on wavelet transform is gived in this paper , as shown in Fig .5.

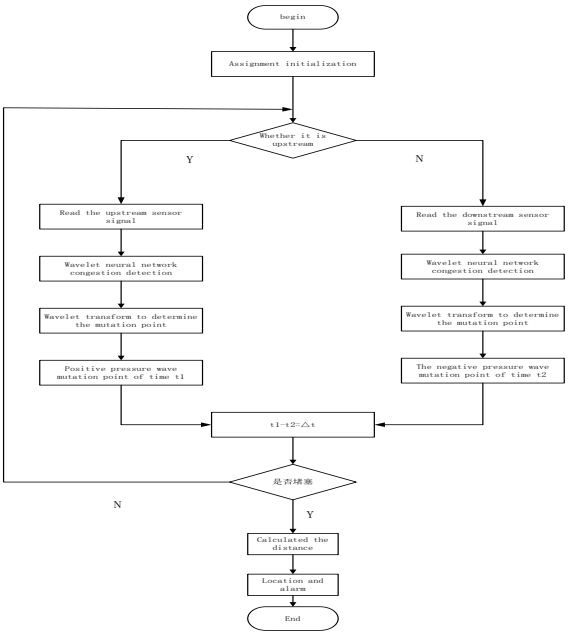

Figure 5. Blockage location flow of coal slurry transportation pipeline

B. *Experimental Verification of Pressure Wave Blockage Location Based on Wavelet Transform*

In the experiment, the length of the coal slurry pipeline L is 267m , the sensor installed upstream of the pipeline is called the upstream sensor, and the sensor installed downstream of the pipeline is called the downstream sensor, a ball valve is installed at a distance of 163.8 m from the upstream sensor to simulate the blockage of the pipeline, the wavelet transform can be used to obtain the position of the pressure signal when the pipeline is blocked from the point of view, that comes from the detection of the positive and negative pressure wave in Fig .3 and Fig .4, it is known that the abrupt change of barotropic wave occurs at 976th time points, and the negative pressure wave occurs at 968th time points, the difference of time between positive and negative pressure wave is 8, the sampling frequency of the system is 200Hz/s, so the time difference can be obtained as shown in formula (7)

$$\Delta t = t_1 - t_2 = \frac{976}{200} - \frac{968}{200} = 0.04s \tag{7}$$

Substitutio of the formula (6), the position of the blocking point of the positive pressure detection point can be obtained as a formula (8). The position of the blocking point of the negative pressure detection point is a formula (9)

$$L_1 = \frac{L+V\times\Delta t}{2} = \frac{267+1378.1\times0.04}{2} = 161.06\text{m} \tag{8}$$

$$L_2 = \frac{L-V\times\Delta t}{2} = \frac{167-1378.1\times0.04}{2} = 105.9\text{m} \tag{9}$$

The positioning error is as follows:

$$e_{x1} = \frac{163.8 - 161.06}{163.8} = 1.67\% \tag{10}$$

$$e_{x2} = \frac{108.1 - 105.9}{108.1} = 2.03\% \tag{11}$$

It is found that the location of the blockage of the pipeline can be determined by experiment, test, calculation and analysis.

V. CONCLUSION

Aimed at the difficult problem of the blocking location for viscous material pipeline transportation, a method of pipeline transportation jam location is discussed in this paper. Main research work is as follows:

a. Through the analysis of the pressure wave in the viscous pipeline, the mathematical model of the pressure change corresponding to the pipe blockage is established;

b. the method of pressure wave slime pipeline blockage location is proposed based on wavelet transform. Two factors that affect the positioning results are analyzed: the propagation velocity of pressure wave in the pipeline and the time of the pressure wave; then the velocity and time difference of pressure wave are determined, and the location of the blockage point is determined accurately.

c. On the basis of boiler of coal slurry pipeline of 50MW unit in Shanxi Huangling coal gangue power Generation Company's delivery system, the experimental platform is built according to the proportion of 100:1, simulation and experimental verification are finished. Results show that the blockage location error is less than 2.03%.

REFERENCES

[1] Wu Miao; Pan Yue; Zhao Guo-Rui et al.Pressure distribution of the coal slurry in the pipeline transportation[J]. Meitan Xuebao,2009,34(2):267-270

[2] Feng Li; LiuJiongtian; ZhangMingtian et al. Analy sis on Influencing Factors of Sedimentation Characteristics of Coal Slime Water[J]. Journal of China University of Mining and Technology,2010.9,39(5):672~675

[3] Gao Jie; Hao Xuedi; Wang Liang;etc.Resistance Characteristics of Coal Slime in Pipe Flow at High Pressure Resistance Characteristics of Coal Slime in Pipe Flow at High Pressure[J]. International Journal of Chemical Reactor Engineering,2016,14(1):299-307

[4] Lee Jong-Hwi; Chu Ick-Chan; Kim Hyun-Gi; etc.Evaluation of technology for preventing drainage pipe blockage in deteriorated tunnel[C]. 22nd International Offshore and Polar Engineering Conference,2012 606-611

[5] M R Khanarmuei; H Rahimzadeh; A R Kakuei et al.Effect of vortex formation on sediment transport at dual pipe intakes[J]. Indian Academy of Sciences, 2016,41(9):1055-1061

[6] Rushd, S.; Sanders, S. A parametric study of the hydrodynamic roughness produced by a wall-coating layer of oil during the pipeline transportation of heavy oil-water mixtures[C]. Society of Petroleum Engineers - SPE Canada Heavy Oil Technical Conference, Canada,2015:1035-1046

[7] Ulanov, A.M.; Bezborodov, S.A.Calculation Method of Pipeline Vibration with Damping Supports Made of the MR Material[C]. 2nd International Conference on Industrial Engineering,Russia, 2016: 101-106

[8] Lecreps, I.; Orozovic, O.; Erden, T. et al. Physical mechanisms involved in slug transport and pipe blockage during horizontal pneumatic conveying[J].Powder Technology,2014, 262(8):82-95

[9] Lining, Lei Hongbin, et al. Study on Key Technologies of coal slime resource utilization[J]. Coal engineering,2011(12):

[10] Li Ning. Research on Key Technologies of Safe Coal Gangue Power Generation[D]. Xi'an University of Science and Technology, 2012.6

[11] YangXuecun.Research on Blockage Prediction of Coal Slurry Transportation Pipeline in Gangue Power Plant Specialty[D].Xi'an University of Science and Technology, 2014.12

[12] Duan, Wenbo; Kirby, Ray; Prisutova, Jevgenija et al. On the use of power reflection ratio and phase change to determine the geometry of a blockage in a pipe[J].Applied Acoustics, 2015,87(1):190-197

[13] Tian Jinyi; Ni Long; Zhao, Jianing. Effect of underflow pipe diameter on performance of hydrocyclone anti-blockage device[J]. Huagong Xuebao,2016.67(10):4219-4224

[14] Dang jiao. Blockage Detection of Caol Slurry Pipeline[D].Xi'an University of Science and Technology, 2015.6

[15] Wang Long, Miao Qing, Cui Xiuguo, et al. Macroscopic characterization of the starting pressure wave velocity of crude oil pipeline [J]. Journal of Petrochemical University, 2011 .24(04):76-78

A New High-Precision Mode Acceleration Method for Calculating Frequency Response of Non-Classically Damped Systems

Jingfang Shen
School of Science
Huazhong Agricultural University
Wuhan, China
shenjingfang16@126.com

Peng Wang
School of Science
Huazhong Agricultural University
Wuhan, China
wangpeng505@foxmail.com

***Abstract*—The modal truncation problem of non-classically damped systems is constantly encountered in the dynamic analysis of engineering. The present study is designed to calculate the frequency response functions of the non-classically damping systems accurately on account of the Neumann expansion theory and the frequency shifting technique. Considering the first and the second term influence of the Neumann expansion equations in the frequency response analysis of the viscoelastic systems, we could correct the modal truncation problem of model displacement method. The property given in the study shows that this correcting method can reduce the high-order modes that can't be calculated to the lower-order modes that are easier to be computed. And the proposed method can also solve the problem causing by the singularity of stiffness matrix. The result of case given in the article shows that it can improve the accuracy of harmonic response effectively compared model displacement.**

Keywords-harmonic response analysis; frequency shifting technique; model displacement method

I. INTRODUCTION

In many engineering problems, dynamic analysis, vibration control, structural design and damage detection is always an important part of it. Thus, the design of the algorithm and error control during the process to calculate the frequency response function plays an important role. The design needs to be quick and accurate for calculating the system frequency response function and has a great practical significance. With the amount of degrees of the modes considered in dynamic response analysis increasing, the process of computing all the frequencies response functions can be extraordinarily time consumption. However, in fact, the only modes considered in the frequencies response analysis are the modes located in the range of frequencies of interest. Unfortunately, since the method neglect the contribution of the higher-order modes and the viscoelastic modes, there will be some error existing in the modal truncation. Thus, many modified methods are proposed to solve the error accounting in the modal truncation. In recent decades, lots of studies have been done centered on the model reduction by using dimensionality reduction techniques in many research orientations.

Mode displacement method is the most basic method to solve statically indeterminate structures for its simple calculating process and accurate calculation results. In addition, model superposition methods also have an extensively use in structural field. Since 19th century, model reduction technique is hot spot in the computing of frequency response functions and the structural dynamics response analysis, the most common method is mode superposition method (MSM) that was presented by Rayleigh [1]. However, this method can have some improvements of the original MSM by using different vectors in the procedure of Neumann expansion [2]. Craig and Bampton [3] also gave a method to increase the accuracy by analyzing the nonlinear dynamic stability of an actual large-scale rotor-bearing system, which is called the fixed-interface reduction method for the fixing boundary of mode of system. Based on the free vibration modes and the available modes of the engineering structure, the mode displacement method [4] have been proposed by representing the displacement in a harmonic way. But this condition will not be always satisfied, so this kind of will not be suitable for the forced system. Mode acceleration method (MAM) is put forward to solve this problem by considering the superposition of the available modes and the free vibration modes.

Therefore, the MAM is a static correction method because of zero frequency. The experiments showed that mode acceleration method can really enhance the accuracy of the frequency response and simplify calculation of the FRF. But in the real situation, these constraint conditions will not be always satisfied. It's means that the error of modal truncation still exists. To solve this problem, many scholars struggle for it year after year, and have achieved gratifying successes. For example, Mario and Giuseppe [5] proposed a modified method for dynamic frequency response analysis of the systems in the reference. And the numerical applications are also showing that the proposed method can improve calculating efficiency. Certainly, some other corrections method can also have a good performance in improving the accuracy of dynamic response including dynamic correction method [6], high-precision modal superposition methods, self-adapting superposition method, correction continuous systems methods and so on.

With the widely use of non-viscous damping to analyze mechanical systems and dynamic frequency response calculating. The calculating of frequency response of non-viscously damped system has become increasingly important. To enhance the accuracy of the frequency response functions

matrix, the articles proposed a method, which tries to estimate the influence of the modes that used to be irrespective and consider the nonviscously systems by taking the first one or two terms of Neumanm expansion into consideration. It's clear that with the number of modes used in the modal analysis of viscoelastic system increasing, the modal truncation error will accumulate gradually. A method is present to solve this problem by considering the lower mode and the firs terms' contribution in Neumann expansion. As to the non-proportionally systems, a method basing on the hybrid expansion is proposed to compute the response functions of the systems.

This study is devised to compute the harmonic responses of the available modes accurately. From the property obtained in the study on account of the Neumann expansion theorem and the frequency shifting technique, it's evident that the higher modes' frequency response function can express as equations consisting of the lower available modes and system matrices. We can use this property to simplify the higher modal truncation error. Certainly, we can use this method to improve the accuracy of frequency responses functions by dividing the frequency range into several sub-frequency ranges of interest and selecting different values for per sub-frequency range.

II. BACKGROUND OF THEORY

The equations of motion for a linear non-viscously damped system with zero Initialization, obeys the governing equation

$$M\ddot{u}(t)+C\dot{u}(t)+Ku(t)=f(t) \tag{1}$$

where M , C and $K\in R^{N\times N}$ are, the mass damping and stiffness matrices, $f(t)$ is the forcing vector. $u(t)$ is the displacement vector. In the sensitivity analysis of damped systems, $u(t)$ can also be called as the response vector.

In order to more aptly describe the phenomenon of "memory" of solid material or hysteresis effect, in 1874, Boltzmann put forward Boltzmann's superposition principle of linear viscoelastic materials. Later, in 1928, Volterra give the theory of hysteretic or memory in viscoelastic hereditary materials. So the damping force can be expressed as

$$f_d(t)=\int_0^t g(t-\tau)\dot{u}(t)d\tau \tag{2}$$

where $g(t)$ is a matrix of kernel function. Different places and areas have different choices of kernel function. Certainly, the theoretically how to choose kernel function remains unsolved. .

The equations of motion of a linear non-classically damped system with zero initial condition is

$$M\ddot{u}(t)+K_v\int_0^t g(t-\tau)\frac{\partial u(t)}{\partial\tau}dt+Ku(t)=f(t) \tag{3}$$

where K_v which is the damping coefficient matrix. $g(t)$ is a kernel function that has different names in the different places.

If the loading function is harmonic, that is $f(t)=F_h(s)\exp(st)$ with $s=iw$ and $F_h\in R^N$, the steady-state frequency response will also be harmonic, i.e. $u(t)=U_h(s)\exp(st)$. Taking the places of $u(t)$ and $f(t)$ in (3), we can obtain

$$(s^2M+sG(s)+K)U_h(s)=F_h \ \text{or} \ D(s)U_h(s)=F_h \tag{4}$$

Here $G(s)=K_VL[g(t)]$ and $L[]$ denotes the Laplace transform, we know that $G(s)$ can also be expressed as

$$G(s)=\sum_{k=1}^{n}\frac{c\mu_k}{s+\mu_k}K_v \tag{5}$$

Here c and μ_k are the relaxation parameters. And for the dynamic stiffness matrix, it can be expressed as

$$D(s)=s^2M+sG(s)+K \tag{6}$$

The accurate steady-state frequency response that we want to get can be acquired by utilizing the direct frequency response method. For the characteristic equation

$$\det\left|s^2M+sG(s)+K\right|=0 \tag{7}$$

The eigenvalue λ_j are the roots of it. And where φ_j denotes the j th eigenvector and can be rewritten in another way

$$(\lambda_j{}^2M+\lambda_jG(\lambda_j)+K)\varphi_j=0 \tag{8}$$

In addition, asymmetric-matrices problem may also arise for using the state-space approaches. However, these normal modes based on those approaches still have some error when computing the frequency response functions particularly for high-dimensionality damped systems. Furthermore, we can avoid the convergence problem by considering iterative strategy.

The complex FRF matrix and the response vector U_h can be obtained by

$$H(s)=\sum_{j=1}^{m}\frac{\varphi_j\varphi_j{}^T}{\theta_j(s-\lambda_j)}\ , \ U_h(s)=\sum_{j=1}^{m}\frac{\varphi_j{}^TF_h\varphi_j}{\theta_j(s-\lambda_j)} \tag{9}$$

where $\theta_j = \varphi_j^T \left.\frac{\partial D(s)}{\partial s}\right|_{s=\lambda_j} \varphi_j$

and $\left.\frac{\partial D(s)}{\partial s}\right|_{s=\lambda_j} = 2\lambda_j M + G(s) + \lambda_j \left.\frac{\partial D(s)}{\partial s}\right|_{s=\lambda_j}$

And this situation is suitable for the ideal situation that eigenvalues are separated or non-repeated. For the complexity of the non-viscously damped systems, the model will be presented by a large number of different equations. It's means that the modal-truncation error still exists.

To solve this problem, we introduce the modal truncation error. Given that the frequency from L_1 th to L_2 th of interest can be computed, the error of modal truncation of the modal displacement method can be obtained by

$$E_{MDM}(s) = \sum_{j=1}^{L_1-1} \frac{\varphi_j^T F_h \varphi_j}{(s-\lambda_j)\theta_j} + \sum_{j=L_2+1}^{m} \frac{\varphi_j^T F_h \varphi_j}{(s-\lambda_j)\theta_j} \tag{10}$$

For the inverse matrix, Neumann expansion can be expressed in the following way

$$(I_N - A)^{-1} = I_N + A + A^2 + A^3 + \cdots \tag{11}$$

Here $A \in R^{N\times N}$ and I on behalf of the unit matrix. Given that (9) meets converge condition, the power-series expansion can tend to the exact result. The FRF matrix presented can be rewritten into the matrix form as

$$H(s) = -U\Theta^{-1}(\Lambda - sI_m)^{-1}U^T \tag{12}$$

where $\Lambda=\text{diag}[\lambda_1,\lambda_2,\ldots,\lambda_m]$, $U=[\varphi_1,\varphi_2,\ldots,\varphi_m]$ and $\Theta=\text{diag}[\theta_1,\theta_2,\ldots,\theta_m]$.

Let $\bar{s} = s - \mu$ and using the Neumann expansion, the frequency response function matrix can be expressed by

$$H(s) = -\sum_{r=1}^{\infty} U\Theta^{-1}\bar{s}^{r-1}(\Lambda - \mu I_m)^{-r}U^T \tag{13}$$

where μ is a complex frequency shift constant.

The dynamic stiffness matrix $D(s)$ given in (6), can also be expressed as

$$\begin{aligned} D(s) = (s-\mu)^2 M + (s-\mu)(G(s)+2\mu M) \\ +(K+\mu G(s)+\mu^2 M) \end{aligned} \tag{14}$$

Let

$$\begin{aligned} \bar{K}(s) &= K + \mu G(s) + \mu^2 M \\ \bar{G}(s) &= G(s) + 2\mu M \end{aligned} \tag{15}$$

Comparing (12) and (13), let $\bar{s} \to 0 (s \to \mu)$, we can get

$$\begin{aligned} U\Theta^{-1}(\Lambda - \mu I_m)^{-1}U^T &= \lim_{s\to\mu} \bar{K}(s)^{-1} \\ &= (K + \mu G(\mu) + \mu^2 M)^{-1} \end{aligned} \tag{16}$$

III. A METHOD TO IMPROVE THE ACCURACY OF MODE ACCELERATION METHOD

Based on the free vibration modes and available of the structure, the mode displacement method have been presented by using a time-harmonic representation for the displacement of the unforced system. But this condition will not be always satisfied, so this kind of will not be suitable for the forced system. Mode acceleration method (MAM) is proposed to reduce the modal truncation error by considering the effect of higher modes. From the (16), we can see that this problem of singular problem of stiffness matrix have been overcome while incoming the frequency shift constant μ.

Substituting $\bar{K}(s)$ and $\bar{G}(s)$ in (15), the equation can be rewritten in the anther way as

$$\begin{aligned} U\Theta^{-1}(\Lambda - \mu I_m)^{-2}U^T &= (K + \mu G(\mu) + \mu^2 M)^{-1} \\ &\cdot (G(\mu) + 2\mu M)\cdot(K + \mu G(\mu) + \mu^2 M)^{-1} \end{aligned} \tag{17}$$

By using the Neumann expansion theorem and let $\bar{s} = s - \mu$, the FRF matrix given in (13) can be alternatively expressed as

$$H(s) = -\sum_{r=1}^{\infty}\sum_{j=1}^{m} \frac{\bar{s}^{r-1}\varphi_j\varphi_j^T}{\theta_j(\lambda_j - \mu)} \tag{18}$$

When $r = 1, 2$, considering the contribution of the first and second term of the Neumann expansion of the higher modes, (18) can be presented in the following way by utilizing the lower available modes

$$\begin{aligned} H_1(s) &= -\sum_{j=1}^{m} \frac{\varphi_j\varphi_j^T}{\theta_j(\lambda_j - \mu)} = (K + \mu G(\mu) + \mu^2 M)^{-1} \\ H_2(s) &= -\sum_{j=1}^{m} \frac{\bar{s}\varphi_j\varphi_j^T}{\theta_j(\lambda_j - \mu)^2} = (K + \mu G(\mu) + \mu^2 M)^{-1} \\ &\cdot (G(\mu) + 2\mu M)\cdot(K + \mu G(\mu) + \mu^2 M)^{-1} \end{aligned} \tag{19}$$

Assuming the frequency range from L_1 th to L_2 th of interest can be calculated, the response can be computed precisely in the following way

$$U_h(s)=\sum_{j=L_1}^{L_2}\frac{\varphi_j{}^T F_h\varphi_j}{(s-\lambda_j)\theta_j}+E_{MDM}(s) \tag{20}$$

The same process as (13), using Neumann expansion, we can obtain

$$E_{GMAM}(s)=-\sum_{k=0}^{\infty}(s-\mu)^k \cdot\left[\sum_{j=1}^{L_1-1}\frac{\varphi_j{}^T F_h\varphi_j}{\theta_j(\lambda_j-\mu)^{k+1}}+\sum_{j=L_2+1}^{m}\frac{\varphi_j{}^T F_h\varphi_j}{\theta_j(\lambda_j-\mu)^{k+1}}\right] \tag{21}$$

For the (21), it considers the first term of the right-hand equation. When $k=0$, the equation can be expressed as

$$E_{MDM}(s)\approx-\sum_{j=1}^{L_1-1}\frac{\varphi_j{}^T F_h\varphi_j}{\theta_j(\lambda_j-\mu)}-\sum_{j=L_2+1}^{m}\frac{\varphi_j{}^T F_h\varphi_j}{\theta_j(\lambda_j-\mu)} \tag{22}$$

Then give a frequency shift value μ to (22), we can obtain

$$\sum_{j=L+1}^{m}\frac{\varphi_j\varphi_j{}^T}{(\lambda_j-\mu)^2\theta_j}=(K+\mu G(\mu)+\mu^2M)^{-1} \cdot(G(\mu)+2\mu M)\cdot(K+\mu G(\mu)+\mu^2M)^{-1}-\sum_{j=1}^{L}\frac{\varphi_j\varphi_j{}^T}{(\lambda_j-\mu)^2\theta_j} \tag{23}$$

We can see that (23) can reduce the high modes to the lower modes. That is to say, we can use this equation to implement dimensionlity reduction. When $k=1$, the above equation will be rewritten in this way

$$E_{MDM}(s)\approx-\left[\sum_{j=1}^{L_1-1}\frac{\varphi_j{}^T F_h\varphi_j}{\theta_j(\lambda_j-\mu)}+\sum_{j=L_2+1}^{m}\frac{\varphi_j{}^T F_h\varphi_j}{\theta_j(\lambda_j-\mu)}\right] -(s-\mu)\left[\sum_{j=1}^{L_1-1}\frac{\varphi_j{}^T F_h\varphi_j}{\theta_j(\lambda_j-\mu)^2}+\sum_{j=L_2+1}^{m}\frac{\varphi_j{}^T F_h\varphi_j}{\theta_j(\lambda_j-\mu)^2}\right] \tag{24}$$

In order to compute efficiently, we remark the first term E_1 and the second term E_2. That is

$$E_1=-\sum_{j=1}^{L_1-1}\frac{\varphi_j{}^T F_h\varphi_j}{\theta_j(\lambda_j-\mu)}-\sum_{j=L_2+1}^{m}\frac{\varphi_j{}^T F_h\varphi_j}{\theta_j(\lambda_j-\mu)}$$
$$E_2=-(s-\mu)\sum_{j=1}^{L_1-1}\frac{\varphi_j{}^T F_h\varphi_j}{\theta_j(\lambda_j-\mu)^2}-(s-\mu)\sum_{j=L_2+1}^{m}\frac{\varphi_j{}^T F_h\varphi_j}{\theta_j(\lambda_j-\mu)^2} \tag{25}$$

In the equation, all parts can be computed. By considering the influence of the second term of the truncation error of model displacement method, it's no doubt that the error can be reduced in this way. For the singularity of stiffness matrix, the results in the number of terms that we can use are merely the first and the second one. Thus, the response in (9) can be calculated can be expressed by

$$U_h(s)=\sum_{j=L_1}^{L_2}\frac{\varphi_j{}^T F_h\varphi_j}{(s-\lambda_j)\theta_j}+E_{MDM}(s) =\sum_{j=L_1}^{L_2}\frac{\varphi_j{}^T F_h\varphi_j}{(s-\lambda_j)\theta_j}+E_1+E_2+E_e \tag{26}$$

Using the upper bound of the r th component of the error vector E_e, we can obtain the below equation

$$\left|E_e\right|_r\le\left|\sum_{k=2}^{\infty}\bar{s}^k\left[\sum_{j=1}^{L_1-1}\frac{\varphi_j{}^T F_h\varphi_j}{\theta_j(\lambda_j-\mu)^{k+1}}+\sum_{j=L_2+1}^{m}\frac{\varphi_j{}^T F_h\varphi_j}{\theta_j(\lambda_j-\mu)^{k+1}}\right]\right|_r \tag{27}$$

Here $\left|\varphi_j\right|_r$ represents the r th element of the vector. Comparing to the error of generalized mode acceleration method, we can know that the error is becoming smaller by considering the influence of the second term of the Neumann expansion of the model displacement error.

IV. EXAMPLE AND DISCUSS

In this present part, one case of the harmonic forced vibration of non-classically damped system is shown, which is a four DOF nonviscously system with free-free boundary condition [11].

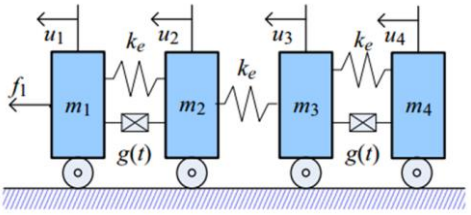

Figure 1. Four DOF non-classically damped system with free-free boundary condition

The system matrices of the nonviscously damped mode, shown in **Fig .1**, are M, K and G. It's obvious that the energy dissipation is not uniformly distributed in the whole system. That is say, the system is a non-classically damped system.

Suppose the interesting frequency range is 12-28 rad/s. According to the present theorem in [11], the frequency shift value is $\mu=20i$. Four elastic modes are covered in the frequency range of interest.

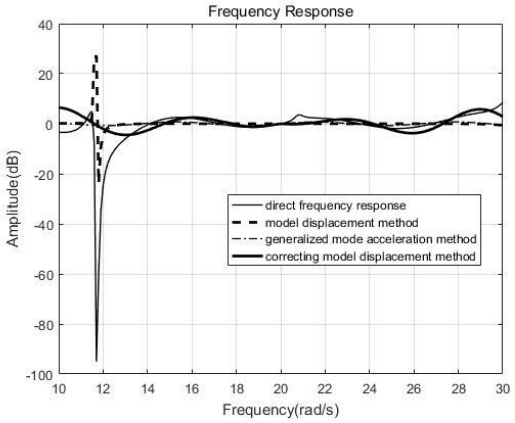

Figure 2. The FRF of the mode in the frequency range 10-30 rad/s

Fig .2 shows that the FRF of the second DOF in mode over the frequency range of interest. Since the frequency shift value $\mu = 20i$, it's evident that the modal truncation error caused by the model displacement method can be reduced when the considering frequency is located in the frequency range of interest. For example, in 14-30 rad/s, the correcting method presenting in this study can have a better accuracy that the generalized acceleration method proposed by Li et al. in [11]. That is say the results have a better performance when the frequency tends to the frequency shift μ .

V. CONCLUSIONS

You must submit the IEEE Electronic Copyright Form (ECF) per Step 7 of the CPS author kit's web page. This form Must be Submitted in Order to Publish Your Paper.

Please see Step 9 for ordering reprints of your paper. Reprints may be ordered using the form provided as <reprint.doc> or <reprint.pdf>.

ACKNOWLEDGMENT

This work was supported by the Fundamental Research Funds for the Central Universities (2662017JC024), National university students innovation project (2015310200731, 201610504076) and Higher school university mathematics teaching research and development center project (CMC20160408). Thanks to Peng Wang who is the corresponding author.

REFERENCES

[1] J.W.S. Rayleigh, The Theory of Sound, Dover Publications, New York, 1945.

[2] E.L. Wilson, M-W. Yuan, J.M. Dickens, Dynamic analysis by direct superposition of Ritz vectors, Earthquake Engineering & Structural Dynamics, 1982.

[3] R.R. Craig Jr., M.C.C. Bampton, Coupling of substructures for dynamic analyses, 1968.

[4] B. Besselink, U. Tabak, A. Lutowska, N. van de Wouw, H. Nijmeijer, D.J. Rixen, M.E. Hochstenbach, W.H.A. Schilders, A comparison of model reduction techniques from structural dynamics, numerical mathematics and systems and control, 2013.

[5] M. Di Paola, G. Failla, A correction method for dynamic analysis of linear systems, Comput. Struct. 82 (2004) 1217–1226.

[6] G. Borino, G. Muscolino, Mode-superposition methods in dynamic analysis of classically and non-classically damped linear systems, Earthquake Engineering & Structural Dynamics 14 (1986) 705–717.

Homotopy Analysis for Periodic Motion of Time-delayed Duffing system

You Xiangcheng
School of Petroleum Engineering, China University of Petroleum
Beijing 102249, China
E-mail: applexcyou@163.com

Abstract—In this paper, the periodic motions of local dynamics of time-delayed oscillators near a single Hopf bifurcation have been investigated by means of the homotopy analysis method (HAM). With this technique, analytical approximations with high accuracy for all possible solutions are captured, which match the numerical solutions in the whole time regions. Two examples of dynamic systems are considered, which focus on the periodic motions near a Hopf bifurcation of an equilibrium point. It is found that the current technique lead to higher accurate prediction on the local dynamics of time-delayed systems near a Hopf bifurcation than the energy analysis method or the traditional method of multiple scales with strongly nonlinear examples. We studied the temporal dynamics of time-delayed systems in various regimes characterized by the parameters of the oscillator and the time delay parameter. The results given in this paper show that the time delay plays very important role in the analysis of multiply periodic motions with time-delayed systems. This paper is presented a general approach to the analysis of periodic motions of time-delayed systems. Although here we only consider a non-autonomous Duffing system with linear and nonlinear time-delayed position feedback, HAM can be extended to solve other time-delayed systems, such as coupled oscillators with time-delayed, feedback control which may have significance for the control of some physical or engineering systems.

Keywords-Homotopy analysis method; Periodic motion; Time-delayed; Duffing system; Delayed differential equation

I. INTRODUCTION

In many applications, the time delays involved in nonlinear dynamics systems have to be considered even if they are very short. It is shown that the study of dynamic behavior usually get wrong conclusions because of simply ignoring small delays, moreover, some mechanical phenomena can be explained reasonably only considering the existence of time delay. The evolution of a time-delayed system depends on both the current and previous state of the system. So it is reasonable to describe the time-delayed dynamic systems by delayed differential equations (DDEs). On the other hand, the dynamics of time-delayed systems has also obtained great attention from the researchers in other fields such as machine tool dynamics, neural networks and biology, medicine and population dynamics [1-3].

Many studies [4,5] on the time-delayed systems have been done over the past several decades. Among these researches, the Van der Pol-Duffing oscillator has drawn considerable attention since it serves as a simple model in various engineering fields. For instance, some Van der Pol-Duffing oscillators with delayed feedback show the extremely simple dynamics if the time delay disappears, while infinite number of periodic motions even for very small time delays [6,7]. Furthermore, it is proved that the delayed feedback control is one of the most effective and flexible strategies in the fields of controlling chaos of nonlinear dynamics systems [8]. Obviously, the time-delay systems may exist abundant dynamics which involves chaotic motion and Hopf bifurcation [9-12]. However, the research on periodic motions is of special interest in engineering applications. Perturbation approaches, such as the method of multiple scales, the method of harmonic balance, are widely used to reveal the complex dynamics of nonlinear systems [13-16].

H. Khan et al. [17] investigated a nonlinear model in biology by means of HAM. A new discontinuous function is defined so as to express the piecewise continuous solutions of time-delay differential equations. It is shown that the proposed HAM method seems to be applicable to general systems that can be described using a general delay differential equation (DDE) of the form $x' = f\left(x, x\left(t-\tau\right)\right)$. The objective of this paper is to develop an effective analytical technique based on the homotopy analysis method (HAM, Refs.[18-23]) to give analytical approximations for periodic motion of Duffing system with delayed feedback. A Duffing oscillator with time-delayed feedback described by the second-order DDEs is used as an example to propose a general analytic approach for nonlinear time-delayed dynamic systems.

II. ANALYTICAL APPROXIMATIONS

Adding the terms of time-delayed position feedback in a Duffing system

$$\ddot{x} + \hat{\alpha}\dot{x} + \hat{\omega}_0^2 x + \hat{\beta}x^3 = \hat{A}x\left(t-\tau\right) + \hat{B}x^3\left(t-\tau\right). \quad (1)$$

Where $\hat{\alpha}$ is damping coefficient, $\hat{\omega}_0$ is system natural frequency, $\hat{\beta}$ is rigidity coefficient, $\hat{A}$ is the feedback-gain coefficient and τ is time-delay. $\hat{A}, \hat{B} > 0$ denotes positive feedback and $\hat{A}, \hat{B} < 0$ denotes negative feedback.

The initial conditions of Eq.(1) are

$$x(t)=a_0,\dot{x}(t)=0,-\tau\le t<0 \quad (2)$$

The system to be considered is the time-delayed position feedback control system, here we assume that the system has no signal feedback when t<0.
Under the transformations

$$\theta=\omega t, x(t)=au(\theta) \quad (3)$$

Where ω is frequency. Eq.(1) becomes

$$\begin{aligned}&\omega^2\ddot{u}(\theta)+\omega\hat{\alpha}\dot{u}(\theta)+\hat{\omega}_0^2u(\theta)+\hat{\beta}a^2u^3(\theta)\\&=\hat{A}u(\theta-\omega\tau)+\hat{B}u^3(\theta-\omega\tau)\end{aligned} \quad (4)$$

Subject to the initial conditions

$$u(0)=1,\dot{u}(0)=0. \quad (5)$$

Where the prime represents differentiation with respect to θ and $T=2\pi/\omega$ is period of system.

From the physical point of view, periodic motions of time-delayed dynamics systems can be expressed by periodic functions. Obviously, $u(\theta)$ may be expressed in this form:

$$u(\theta)=\tilde{a}_0+\sum_{n=1}^{+\infty}[\tilde{a}_n\cos(n\theta)+\tilde{b}_n\sin(n\theta)] \quad (6)$$

Where $\tilde{a}_n$ and $\tilde{b}_n$ are coefficients. This provides us with the rule of solution expression for $u(\theta)$.

We choose the initial guess of $u(\theta)$ based on the initial conditions (5) as

$$u_0(\theta)=\cos\theta \quad (7)$$

Besides, we choose

$$L[f]=\frac{\partial^2 f}{\partial\theta^2}+f \quad (8)$$

As the auxiliary linear operator, which has the following property

$$L[C_1\sin\theta+C_2\cos\theta]=0 \quad (9)$$

Where C_1 and C_2 are integral constants and f is a real function. The nonlinear operators are defined based on Eq.(4) as

$$\begin{aligned}N[U(\theta;q),\Omega(q),A(q)]&=\Omega^2(q)\frac{\partial^2U(\theta;q)}{\partial\theta^2}\\&+\hat{\alpha}\Omega(q)\frac{\partial U(\theta;q)}{\partial\theta}+\hat{\omega}_0^2U(\theta;q)\\&+\hat{B}A^2(q)U^3(\theta;q)\\&-\hat{A}U[\theta-\Omega(q)\tau;q]\\&-\hat{B}U^3[\theta-\Omega(q)\tau;q]\end{aligned} \quad (10)$$

Where $q\in[0,1]$ is the embedding parameter, $U(\theta;q)$ is a real function of θ and q, $\Omega(q)$ and $A(q)$ are the real function of q respectively.

Then, let η denote an auxiliary parameter. We construct the HAM deformation equation

$$\begin{aligned}&[1-B_1(q;c_1)]L[U(\theta;q)-u_0(\theta)]\\&=c_0A_1(q;c_2)H(\theta)N[U(\theta;q),\Omega(q),A(q)]\end{aligned} \quad (11)$$

Subject to the conditions

$$U(0;q)=1,\left.\frac{\partial U(\theta;q)}{\partial\theta}\right|_{\theta=0}=0 \quad (12)$$

Where $\theta\ge0$ and $H(\theta)=1$. Obviously, when $q=0$ and $q=1$, it is clear from Eq.(4) and the above zero-order deformation equation that

$$\begin{aligned}&U(\theta;0)=u_0(\theta),U(\theta;1)=u(\theta)\\&\Omega(0)=\omega_0,\Omega(1)=\omega\\&A(0)=a_0,A(1)=a\end{aligned} \quad (13)$$

So, as q increases from 0 to 1, $U(\theta;q)$ varies from the initial guess $u_0(\theta)$ to the exact solution $u(\theta)$, so do $\Omega(q)$ and $A(q)$ from the initial guesses ω_0 and a_0 to the corresponding exact values ω and a. Expanding $U(\theta;q),\Omega(q)$ and $A(q)$ in Taylor's series with respect to *q*. Differentiating the HAM deformation equation (11) *m* times with respect to *q*, then setting *q=0*, and finally dividing them by *m!*, the mth-order deformation equations can be used, then the analytical approximations for u,ω,a can be obtained.

III. RESULTS ANALYSIS

Many researchers have been made great efforts to investigate the stability of time-delayed dynamics systems over the past decades and many encouraging results have been obtained. However, most of these investigations were given by perturbation methods, which can hardly give results with high accuracy owing to its inherent limitation. Here, we re-examine the system of Duffing oscillator with time-delayed feedback by means of the homotopy analysis method. It is found the proposed technique can improve the accuracy for all captured solutions which are obtained from the analysis of periodic motions near a Hopf bifurcation of an equilibrium point.

When $\hat{\omega}_0 = 0, \beta = 0, \hat{A} = -1$, as an illustrative example is following

$$\ddot{x} + \hat{\alpha}\dot{x} = \hat{B}x^3(t-\tau) - x(t-\tau). \tag{14}$$

By means of the homotopy analysis method, the accurate analytical approximation of $x(t)$ is obtained, and the 10th-order approximation given by $\hat{\alpha} = -0.9, \hat{B} = -2,$ $\tau = 2$ and $\eta = -0.01$ reads

$$\begin{aligned} x(t) = {} & 0.57039\cos(\omega t) + 0.00114\cos(3\omega t) \\ & - 3.96212\times10^{-7}\cos(5\omega t) \\ & + 8.42288\times10^{-11}\cos(7\omega t) \\ & + 5.07591\times10^{-16}\cos(9\omega t) \\ & + 5.69177\times10^{-18}\cos(11\omega t) \end{aligned} \tag{15}$$

Where the frequency ω equals to 0.51545 in this case. As shown in Fig. 1, the 10th HAM approximation of periodic motion agrees well with the numerical results in the large region of time *t*. With 4-order Runge-Kutta numerical method, the computational domain of *t*, ranged from 0 to 1000, is divided into 1000000 intervals, namely fixed time step is 0.001. The convergence criterion used is based on the Root Mean Square error (RMS) which is 1×10^{-6} in the present work. It is worth noting that the approximate solution by using HAM contains an auxiliary parameter η, which provides a simple way to adjust and control the convergence region and rate of series solution. Mathematically, $x(t)$ is dependent on both of the physical variable *t* and the auxiliary parameter η when other parameters are given. So, from mathematical view points, given a value of *t*, $x(t)$ is a power series of η and thus its convergence is determined by η . For example, in the case of $\hat{\alpha} = -0.9, \hat{\omega}_0 = 0, \hat{\beta} = 0,$ $\hat{A} = -1, \hat{B} = -2, \tau = 2$, regarding η as a variable, we can plot the curves of $x(t) \sim \eta$ when *t=0*, as shown in Fig. 1.

As shown in TABLE I, the 10th HAM approximations of the amplitude of the bifurcation periodic solutions are in a very good agreement with numerical solutions. It can be found that the nonlinear becomes stronger and the amplitude becomes smaller as the value of parameters increasing. Furthermore, the approximate solutions are only more reliable with small parameters. As the value of parameters increases, the approximate solutions are gradually inaccurate. And the formula of approximation prediction is applied, which is a local method and it may fail for some DDEs. For example, the amplitude *a* simply equals to $2\sqrt{(\hat{\alpha} - \sin\tau)/3\hat{B}\sin\tau}$ in this case.

IV. CONCLUSION

In this paper, the periodic motions of the local dynamics of time-delayed oscillators near a single Hopf bifurcation have been investigated by means of the homotopy analysis method. With this technique, analytical approximations with high accuracy for all possible solutions are captured, which match the numerical solutions in the whole time regions. We studied the temporal dynamics of time-delayed systems in various regimes characterized by the parameters of the oscillator and the time delay parameter. The results given in this paper show that the time delay plays very important role in the analysis of multiply periodic motions with time-delayed systems.

It is well known that the time-delayed systems exhibit complex dynamics, including periodic, quasi-periodic and chaotic motions. This paper is presented a general approach to the analysis of periodic motions of time-delayed systems. Although here we only consider a non-autonomous Duffing system with linear and nonlinear time-delayed position feedback, the homotopy analysis method can be extended to solve other time-delayed systems, such as coupled oscillators with time-delayed, feedback control which may have significance for the control of some physical or engineering systems.

A. Figures and Tables

TABLE I. AMPLITUDE OF THE BIFURCATED PERIODIC SOLUTION OF EQ.(14)

Bifurc.param.	*Approx.sol.*	*Numer.sol.*	*S10th HAM sol.*
$\tau = 0.1, \hat{\alpha} = 0.05, \hat{B} = -0.1$	2.5798	2.7044	2.7045
$\tau = 0.1, \hat{\alpha} = 0.05, \hat{B} = -0.5$	1.1537	1.2094	1.2094
$\tau = 0.1, \hat{\alpha} = 0.05, \hat{B} = -2.0$	0.5769	0.6047	0.6047
$\tau = 1.0, \hat{\alpha} = 0.5, \hat{B} = -0.1$	2.3261	2.5944	2.5945
$\tau = 1.0, \hat{\alpha} = 0.5, \hat{B} = -0.5$	1.0403	1.1602	1.1602

Bifurc.param.	*Approx.sol.*	*Numer.sol.*	*S10th HAM sol.*
$\tau = 1.0, \hat{\alpha} = 0.5, \hat{B} = -2.0$	0.5201	0.5801	0.5801
$\tau = 2.0, \hat{\alpha} = 0.9, \hat{B} = -0.1$	0.3692	2.5530	2.5530
$\tau = 2.0, \hat{\alpha} = 0.9, \hat{B} = -0.5$	0.1651	1.1417	1.1417
$\tau = 2.0, \hat{\alpha} = 0.9, \hat{B} = -2.0$	0.0826	0.5709	0.5710

a. Sample of a Table footnote. (Table footnote)

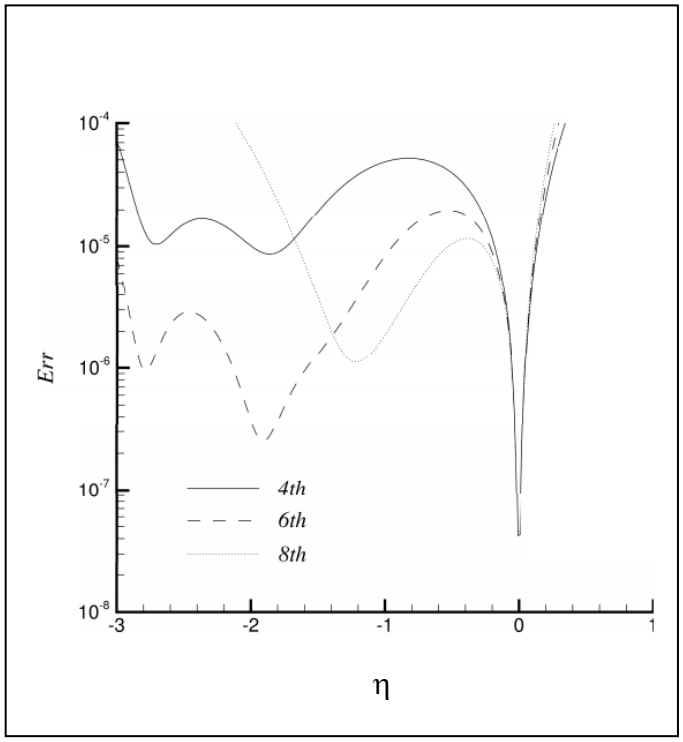

Figure 1. The curves of averaged residual error ~ η in the case of $\hat{\alpha} = 0.9, \hat{B} = -2, \tau = 2$. Solid line: 8th-order HAM solution; Dashed line: 6th-order HAM solution; Dash-dotted line: 4th-order HAM solution.

ACKNOWLEDGMENT

Thanks for the financial supports of the Science Foundation of China University of Petroleum, Beijing (No.2462015YQ0208).

REFERENCES

[1] D. Perioux, T. Erneux, A. Gavrielides, and V. Kovanis, "Hopf bifurcation subject to a large delay in a laser system,'' SIAM J. Appl. Math., vol. 61, pp.966-982, 2000.

[2] Shayer, and S.A. Campbell, "Stability, bifurcation, and multi-stability in a system of two coupled neurones with multiple time delays,'' SIAM J. Appl. Math., vol. 61, pp. 673-700, 2000.

[3] N. MacDonald, "Biological Delay Systems: Linear Stability Theory," Cambridge University Press, 1st ed., New York, 1989, pp.30-40.

[4] Y.X. Qin, Y.Q. Liu, L. Wang, and Z.X. Zheng, "Stability of dynamic systems with delays," Science Press, 1st ed., Beijing, 1989, pp.60-70.

[5] Y. Kuang, "Delay Differential Equations with Applications to Population Dynamics," Academic Press, 1st ed., New York, 1993, pp.10-25.

[6] F.M. Atay, "Van der pol's oscillator under delayed feedback," J. Sound Vibr., vol.218, pp.333-339, 1998.

[7] J.C.F. de Oliveira, "Oscillations in a van der Pol equation with delayed argument," J. Math. Analy. Appl., vol. 275, pp.789-803, 2002.

[8] S. Yamamoto, T. Hino, and T. Ushio, "Delayed feedback control with a minimal-order observer for stabilization of chaotic discrete-time systems," Inter. J. Bifur. Chaos, vol.12, pp.1047-1055, 2002.

[9] J. Belair, and S.A. Campbell, "Stability and bifurcations of equilibria in a multiple-delayed differential equation," SIAM J. Appl. Math., vol. 54, pp.1402-1424, 1994.

[10] D.V.R. Reddy, A. Sen, and G.L. Johnston, "Dynamics of a limit cycle oscillator under time delayed linear and nonlinear feedbacks," Phys. D: Nonlinear Phenom., vol. 44, pp.335-357, 2000.

[11] H.J. Dai, and J. Xu, "Effects of time delay on periodic motions in nonlinear system with parametric excitation," Chinese Quart. Mech., vol.25, pp.367-374, 2004.

[12] R. Xu, M.A.J. Chaplain, and F.A. Davidson, "Periodic solutions for a delayed predator-prey model of prey dispersal in two-patch environments," Nonlinear Analy.: Real World Appli., vol.5,pp.183-206, 2004.

[13] B.D. Hassard, N.D. Kazarinoff, and Y.H. Wan, "Counting roots of the characteristic equation for linear-delay differential systems," J. Differ. Eqn., vol.136, pp.222-235, 1997.

[14] Z.H. Wang, and H.Y. Hu, "Delay-independent stability of retarded dynamic systems of multiple degrees of freedom,"J. Sound Vibr., vol. 226, pp.57-81, 1999.

[15] P. Yu, Y. Yuan, and J. Xu, "Study of double Hopf bifurcation and chaos for an oscillator with time delayed feedback," Commun. Nonlinear Sci. Numer. Simul., vol.7, pp.69-91, 2002.

[16] Z.H. Wang, and H.Y. Hu, "An energy analysis of the local dynamics of a delayed oscillator near a Hopf bifurcation," Nonlinear Dyn., vol.46, pp.149-159, 2006.

[17] H. Khan, S.J. Liao, R.N. Mohapatra, and K. Vajravelu, "An analytical solution for a nonlinear time-delay model in biology," Commun. Nonlinear Sci. Numer. Simul., vol.14, pp.3141-3148, 2009.

[18] S.J. Liao, "Homotopy Analysis Method in Nonlinear Differential Equations," Springer, 1st ed., Heidelberg, pp.80-88, 2012.

[19] D.L. Xu, Z.L. Liu, S.J. Liao, and M. Stiassnie, "On the steady-state fully resonant progressive waves in water of finite depth," J. Fluid Mech., vol.710, pp.379-418, 2012.

[20] H. Xu, and I. Pop, "Mixed convection flow of a nanofluid over a stretching surface with uniform free stream in the presence of both nanoparticles and gyrotactic microorganisms," Int. J. Heat Mass Transf., vol.75, pp.610-623, 2014.

[21] H. Xu, and I. Pop, "Fully developed mixed convection flow in a horizontal channel filled by a nanofluid containing both nanoparticles and gyrotactic microorganisms," Eur. J. Mech. B/Fluids, vol.46, pp.37-45, 2014.

[22] Z.L. Liu, S.J. Liao, "Steady-state resonance of multiple wave interactions in deep water," J. Fluid Mech., vol.742, pp.664-700, 2014.

[23] D.L. Xu, Z.L. Liu, and S.J. Liao, "Equilibrium states of class-I Bragg resonant wave system," Eur. J. Mech. B/Fluids, vol.50, pp.38-51, 2015.

An Efficient Density-Based Clustering Algorithm for the Capacitated Vehicle Routing Problem

Jiashan Zhang
Chongqing vocational institute of engineering
Chongqing,402260,China;
zh_jiashan@163.com

***Abstract*—The capacitated vehicle routing problem (CVRP) is one of the most challenging problems in the optimization of distribution. Most approaches can solve case studies involving less than 100 nodes to optimality, but time-consuming. To overcome the limitation, this paper presents a novel two-phase heuristic approach for the capacitated vehicle routing problem. Phase I aims to identifying sets of cost-effective feasible clusters through an improved density-based clustering algorithm. Phase II assigns clusters to vehicles and sequences them on each tour. Max-min ant system is used to order nodes within clusters . The simulation results indicate efficiency of the proposed algorithm.**

Keywords-CVRP; Two-phase heuristic; Density-based clustering algorithm; Max-min ant system

I. INTRODUCTION

The Vehicle Routing Problem (VRP) has been proved to be NP-hard (Laporte 1992). In the past 50 years, hundreds of models and algorithms have been developed to obtain either optimal or heuristic solutions for different versions of VRP, in which the capacitated Vehicle Routing Problem (CVRP) is one of the most famous and widely studied problems. The CVRP involves designing the least cost delivery routes to service a geographically-dispersed customer set, while respecting vehicle-capacity constraints. The majority of current researches focus on the problems within a limited size of 200 customers[1]. Transportation logistics systems are usually large-scale in nature. It is common for real life vehicle routing applications ,such as waste collection, courier service , beverage distribution and milk collection and delivery, to involve the daily service of hundred or even thousand customers. According to the general diagram of the vehicle routing problem, these customers directly are treated as nodes, the street in the city the arc, the scale of the problem will be very large, the difficulty of solving the problem will become greater, the credibility of calculation lower, and the calculation time longer.

The exact algorithms and traditional heuristic algorithms are difficult, even impossible, to solve CVRP. First, the distance in a straight line isn't able to meet problem any longer. Second, calculating the distance matrix is time-consuming. Acctually, besides the distance between customers and the distribution center, the distances among adjacent customers are required, while customers away from each other usually don't belong to the same distribution route and there is little probability of using them. That's to say some (not all) of the distances matrix are used in the process of calculating. So Calculating all the distances between customers are unnecessary .

In the real-life vehicle routing applications, the customers are clustered according to different features, such as road information, customer information, vehicle information, and depot location. Besides simple sweep technology[2], there are several new customer clustering methods. In [3], the customers were firstly devided into districts according to the main road grid system. Then the customer districts were assigned to vehicles using the vehicle flow formulation model. Ouyang [4] proposed algorithms to automatically

discretize vehicle routing zones by utilizing a combination of spatial partitioning techniques to systematically obtain optimum zone designs. Ester et al. proposed a density-based clustering algorithm called DBSCAN[5],which is capable of finding arbitrarily shaped clusters. DBSCAN puts nodes with similary density into one cluster, otherwise into defferent clusters. However, in real life distribution, adjacent customers in the same district are seviced by the same vehicle, while customers away from each other are seviced by different vehicles. So, adjacent nodes should be serviced by one vehicle in spite of not reaching the density threshold.

In this literature, CVRP partitions two sub-problems: one is clustering problem ,for which improved DBSCAN is proposed and the other is travel salesman problem (TSP), which is solved by using MMAS.

The rest of this paper is organized as follows. Section 2 introduces the relevant literature. A mathematical programming formulation is developed in Section 3. Section 4 proposes the heuristic algorithm for solving CVRP. Computational results on benchmark instances are reported in Section 5. Finally, conclusions and future work are presented in Section 6.

II. LITERATURE REVIEW

Dantzig and Ramser [6] proposed the CVRP in 1959 at first. Great attention has been devoted on computational experimentation for CVRP since and a variety of algorithms have been developed to solve the CVRP.

Early, constructive heuristics are popular for CVRP. Saving method[7] (Clarke and Wright1964) starts from one dedicated trip for each customer, pairs of trips are merged as long as a saving is obtained. Sweeping method [8](Gillet and Miller 1974)is constructed to generate routes for goods delivery vehicles in which a solution to travelling salesman problem takes place in the second stage of the two stages which exist in Sweep Algorithm. The Mole and Jameson heuristic[9] is another classic in which routes are constructed using successive customer insertions (Mole and Jameson 1976). In general ,they provide solutions at 10-20% above the optimum, in negligible running times.

Tabu search that constituted the most competing algorithms in the 1990s is still present via variants that include sophisticated memory mechanisms. In 1996, Glover [10] presented the advances, applications, and challenges in tabu search and adaptive memory programming. The main idea is to extract a sequence of points (called bones) from a set of solutions and generate a route using adaptive memory. Further , the adaptive large neighborhood search (ALNLS) [11] is presented by Pisinger and Ropke (2007). However, the quality of tabu search depends on the quality of initial solution.

Evolutionary algorithms are proved efficient for the CVRP. [12] presents a grid-based hybrid cellular genetic algorithm for solving the largest existing benchmark instances of CVRP . [13] presents an Parallel Simulated Annealing for large-scale instances. However, the EA is slower than many TS algorithms.

Cluster first-route second methods , proposed by Fisher and Jaikumar [14],is an effective way to deal with CVRP, especially large scale CVRP. It decreases the problem's state space largely . The method first creates customer clusters, each having a total weight not exceeding the vehicle capacity Q and then optimizes the order of visits for each cluster as a TSP subproblem. In the method ,clustering is the key of problem.

III. PROBLEM DESCRIPTION AND FORMULATION

Let $G=(V,E)$ be a complete undirected graph with |V|=n+1 nodes. The node v0$\in$V represents a depot, where a fleet of m identical vehicles is based, and where the product to be distributed is stored. The other nodes vi$\in$V\{ v0},for i $\in${1, ..., n}, represent the customers, characterized by demands for non-negative amounts of product qi. Edges {i,j}$\in$E represent the possibility of traveling directly from a node (customer or depot) vi$\in$V to a different node vj$\in$V for a transportation cost of cij. The CVRP aims to find m or less vehicle routes, i.e. sequences of deliveries to customers, to visit each customer one time exactly while minimizing the total travel distance. The sum of demands should not exceed on any route a value Q assimilated to the vehicle capacity.

The decision variables of the model are:

$$x_{ij}^k = \begin{cases} 1, & \text{if customer j is supplied after visiting by vehicle k} \\ 0, & otherwise \end{cases}$$

$$y_{jk} = \begin{cases} 1, & if\ \text{vehicle k visit} \\ 0, & else \end{cases}$$

A vehicle has a capacity Q, a fixed cost fk and a per unit-distance variable cost gk. The cost of a vehicle of type k traversing the pair (i , j) is denoted by c_{ij}^k ,which is obtained by multiplying the distance dij and the variable cost gk.

The objective function can be written as follows:

$$\min \sum_{k=1}^{m} f_k \sum_{j=1}^{n} x_{oj}^k + \sum_{i=0}^{n} \sum_{j=1}^{n} \sum_{k=1}^{m} c_{ij}^k x_{ij}^k$$

Subjected to

$$\sum_{j=1}^{n} x_{oj}^k = 1, \quad k = 1,2,\text{K}\ ,\ m \tag{1}$$

$$\sum_{i=1}^{n} x_{ip}^k - \sum_{j=0}^{n} x_{pj}^k = 0, \quad p = 0,1\text{K}\ n; k = 1,2,\text{K}\ ,\ m \tag{2}$$

$$\sum_{i=1}^{n} q_i y_i^k \le Q, \quad k = 1,2,\text{K}\ ,\ m \tag{3}$$

$$\sum_{k=1}^{m} y_{ik} = \begin{cases} 1, & i = 1,2,..., \ n \\ m, & i = 0 \end{cases} \tag{4}$$

$$\sum_{j=0}^{n} x_{i\,jk} = y_{ik}, \quad i = 1,2,\text{K}\ ,\ n; \quad k = 1,2,\text{K}\ ,\ m \tag{5}$$

$$x_{ij}^k \in \{0,1\}, \forall i, j \in V; k = 1,2,\text{K}\ ,\ m$$

Constraints(1) and (2) state that each vehicle leaves the depot, after arriving at a customer, the vehicle leaves again, and finally returns to the depot. Constraint (3) guarantees that the vehicle capacity will not be exceeded. Constraint (4) and (5) ensure that each client's demand is fulfilled by exactly one vehicle.

IV. IMPROVED DENSITY-BASED CLUSTERING ALGORITHM

Phase I is intended to reduce the computational burden of the subsequent solution phase. By establishing the mathematical model in terms of a few clusters rather than a huge number of customers, the CVRP problem size can be decreased evidently. In this paper, improved density-based clustering algorithm is formulated as follows.

Four input parameters, neighborhood radius ε, the density threshold MinPts and the nearest distance ND, are required and the algorithm also supports the user in determining an appropriate value for the input parameters. They are introduced as follows.

A. *E-Neighborhood of a Node*

The ε-neighborhood of a node x is defined as

$$N_\varepsilon(x) = \{y \in D \mid d(x,y) < \varepsilon\}$$

Where ε is neighborhood radius, D is the data set and d(.,.) is a certain distance function.

The Density Threshold : MinPts

Minimum number of points in an ε-neighbourhood of that node.

P belongs to Nε(q) in fig. 1. q is core point only if |Nε(q)| ≥ MinPts.

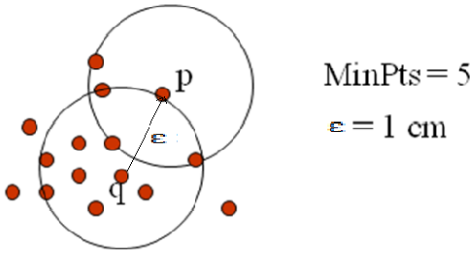

Figure 1. ε-neighborhood and core point

B. *The Nearest Distance : ND*

Two nodes x,y satisfy the nearest neighbor relationship only if d(x,y)<= ND. ND is constant, Usually ND<ε.

C. *Demand Threshold*

The total load of a route doesn't exceed the capacity of vehicle. Here, demand threshold W is introduced insuring that the total load of a cluster doesn't exceed W. Generally, w is one-fourth, one-third or half of the capacity q. That is uncertain.

In phase II, the customer clusters were assigned to vehicles using the vehicle flow formulation model. In this paper, saving method is used. So, the vehicle routes are determined as traveling salesman problem(TSP). The detailed routing and scheduling for each tour found is determined by ant colony algorithm (see [15]).

Improved density-based clustering algorithm is described as follows:

Let P be a node∈D, D is the data set. According to neighborhood radius ε and the density threshold MinPts , density-reachable nodes from P or nodes meeting the nearest neighbor relationship merge into one cluster. A cluster is then very intuitively defined as a set of density-connected points that is maximal with respect to density-reachability. If P is core node , nodes which are density-reachable from P or meeting the nearest neighbor relationship , are labelled the same cluster number. Further expansion goes on. If the node P is boundary object and not meeting the nearest neighbor relationship, or total load after merging P exceeds the capacity of vehicle, abandon p and calculate next node. Proceed in order till a cluster produced. Repeat the process till all nodes are labelled. Then , calculation steps into the second phase detailed above.

V. Experiments and Analysis

In this section, we report our computational results. The proposed algorithm has been executed on an Intel Pentium 4 machine with 2GB memory, running windows. Our computational experiment is based on the benchmark instances (1987),see table I.

In the first phase, customers are clustered through the improved strategy. We set $\varepsilon = \bar{D}/3, ND = \bar{D}/4, Minpts = 5, W = q/2$, $\bar{D}$ is the constant ,such as the average distance between customers. In the second phase, MMAS is executed for route scheming. We set $\alpha = 1, \beta = 3, \rho = 0.8$, the number of circulation $N_{c\max} = 200$. The clustering procedure is applied to the instances.

A-n45-k7 has been picked out to detail the computation. The 45 original nodes have been merged into 19 customer clusters(including discrete nodes) , see fig 2. The node size decreased by 56.8%. Cluster C1,C2 and C3 meet the density threshold : MinPts=5, C4, C5, C6, C7, C8, C9 and C10 meet the nearest distance. Others are discrete nodes , not merged into any cluster.

The routes are as follows, see figure 3.

Vehicle 1: 1-32-37-20-30-42-28--1; Vehicle 2: 1-15--6-34-45-25--1;

Vehicle 3: 1--2-38-31-23-11--1; Vehicle 4: 1-13-29-44-12--4--7--1;

Vehicle 5: 1--3--5-22-27-35-36-40--1; Vehicle 6: 1-39-18-26-24-43-16--9-10--1;

Vehicle 7:1-41-21-17--8-19-14-33—1.

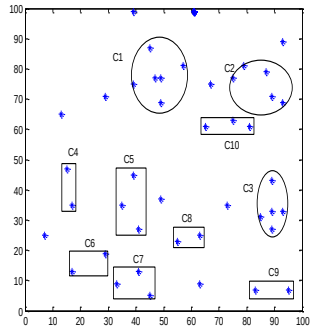

Figure 2. Cluster for problem A-n45-k7

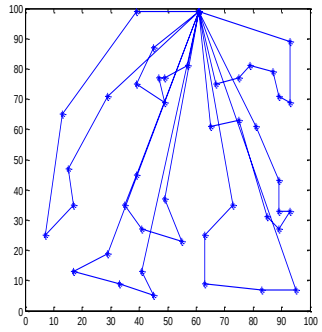

Figure 3. Best solution found for problem A-n45-k7

VI. Conclusion and Future Work

This paper introduces an efficient density-based clustering algorithm for the capacitated Vehicle Routing Problem. The method aims to integrate a heuristic clustering algorithm into an optimization framework.

The method is very successful for clustered examples and solve many of them to optimality. The introduce of preprocessing phase to gather nodes into a few clusters makes the CVRP size decreased sharply. The proposed method can retain optimum in a short time, especially doing well in solving large-scale CVRP. The optimization method is robust, too. Experiments show that density-based clustering algorithm can succeed in solving a variety of benchmark instances.

Real life vehicle routing application is more complicated. For example, the requirement of customers is often uncertain. The extension of the method to these more difficult problems is worth further research.

ACKNOWLEDGMENT

Foundation item: Supported by the National Natural Science Foundation of China (No. 50904032), Chongqing Education Department Science and Technology Project (No. KJ1603201),

Chongqing Association of Higher Education (No.CQGJ15387C) and Chongqing Educational Evaluation Institute (No.PJY2015-50).

REFERENCES

[1] PaoloT, Daniele V. Models, relaxations and exact approaches for the capacitated vehicle routing problem [J]. Discrete Applied Mathematics, 2002, 123: 487-512.

[2] Gillett B, Miller L. A heuristic for the vehicle dispatching problem. Operations Researeh,1974,22:340-349.

[3] Z. W. Qu, L. N. Cai et al, Solution framework for the large scale vehicle de-liver/collection problem, Journal of Tsinghua University (Sci. & Tech.), vol.44, no.5, pp.581-584,2004.

[4] Y. F. Ouyang, Design of vehicle routing zones for large-scale distribution systems,Transportation Research Part B: Methodological, vol.41, no.10, pp.1079-1093, 2014.

[5] Ester M. et al. A density-based algorithm for discovering clusters in large spatial databases with noise. Proceedings of 2nd Int'1 Conf, on Knowledge Discovery and Data Mining (KDD'96), Portland, Oregon, Aug. 1996, pp. 226-231.

[6] Dantzig, G., Ramser, J.. The truck dispatching problem. Management Science 6 (1), 80-91, 1959.

[7] CIarke G, Wright J.W .Scheduling of Vehicles from a Central Depot to a Number of Delivery Points. Operations Research, 1964,12:568-581.

[8] Gillett B, Miller L.A heuristic for the vehicle dispatching problem. Operations Researeh,1974,22:340-349.

[9] Mole R H, Jameson S R.A . Sequential Route-building Algorithm Employing Generalized Savings Criterion. Operational Research Quarterly,1976,27:503-511.

[10] F. Glover, Tabu search and adaptive memory programming-Advances, applications, and challenges,Interfaces in Computer Science and Operations Research, 1996.

[11] Pisinger D, Ropke S .A general heuristic for vehicle routing problems. Computers & Operations Research 2012,34:2403-2435.

[12] B. Dorronsoro, D. Arias, A Grid-based hybrid cellular genetic algorithm for very large instances of the VRP. Parallel and Grid Computing for Optimization, PGCO 2007.

[13] Czech Z. J, Czarnas P. Parallel Simulated Annealing for the Vehicle Routing Problem with Time Windows. Proceedings of the 10th Euromicro Workshop on Parallel, Distributed and Network-based Processing, 2015: 376-379.

[14] Fisher, M., Jaikumar, R.. A generalized assignment heuristic for vehicle routing. Networks 11 (2), 109-124, 1981.

[15] T. Stützle, H.H. Hoos, The MAX‐MIN ant system and local search for the traveling salesman problem, Proceedings of the IEEE International Conference on Evolutionary Computation (ICEC97), IEEE Press, Piscataway, USA, 1997, pp. 309-314.

TABLE I. SUMMARY OF COMPUTATION FOR BENCHMARK INSTANCES

Problems instance	Node_ number	Vehicle_ number	Computed cost	Cluster_ number	Node _size reduction	Vehicle_ number	Best Known cost	Deviation percentage(%)
A-n37-k5	36	5	709	21	41.7%	6	669	6.0%
A-n37-k6	36	6	980	22	38.9%	6	949	3.3%
A-n45-k7	44	7	1192	19	56.8%	7	1167	2.1%
A-n54-k7	53	7	1227	33	37.7%	7	1167	5.1%
A-n63-k9	62	9	1714	41	33.9%	9	1616	6.1%
A-n63-k10	62	10	1410	39	37.1%	11	1314	7.3%
E-n30-k3	29	3	527	17	41.4%	3	508	3.7%
E-n33-k4	32	4	858	19	40.6%	4	837	2.5%
E-n51-k5	50	5	538	28	44.0%	5	524	2.7%
E-n76-k7	75	7	713	43	42.7%	7	687	3.8%

Research on A Quantitative Assessment Model Based on Visual Perception in Low-Altitude Remote Sensing

Jianqiang Lu
College of Electronic Engineering
South China Agricultural University, Guangdong
Engineering Research Center for Monitoring Agricultural Information
Guangzhou,China
ljq@scau.edu.cn

Kexin Chen
College of Electronic Engineering
South China Agricultural University
Guangzhou,China
285078375@qq.com

Weixing Wang
College of Electronic Engineering
South China Agricultural University, Guangdong
Engineering Research Center for Monitoring Agricultural Information
Guangzhou,China
weixing@scau.edu.cn
Corresponding Author

Bing Jiang
College of Electronic Engineering
South China Agricultural University
Guangzhou,China
bing9783@163.com

***Abstract*—In order to evaluate the recovery effect of the visible light band in the low-altitude remote sensing, the sensitivity and significance of the visual perception of the restored image are selected and optimized by the perceptual characteristics of the human visual system. Finally, the effective detail retention ability, Structure information, multi - scale similarity and visual fidelity. A kind of image - based image fog quantification evaluation model QAMVP is proposed based on visual perception. The experimental results show that the model has a strong judgment force on the object group with obvious difference in the image quality evaluation. The accuracy rate of the sample group is 92%. In the aspect of visual perception, , The MSE of the model index curve is obviously lower than the comprehensive evaluation method and the PSNR measurement method, which indicates that the model has certain advantages in the degree of visual perception and the correlation with the visual perception of the human eye. The results of the study can provide theoretical basis and practical guidance for the objective evaluation of the visible image in the low-altitude remote sensing.**

Keywords—Low-altitude remote sensing; Visible band; Visual perception; Quantitative assessment; Precision agriculture

I. INTRODUCTION

Low-altitude remote sensing technology which has the advantages of low cost, high reliability and real-time acquisition that has attracted a wide spread attention in various application field. using unmanned aerial vehicles with wide-angle cameras to get multispectral remote sensing images in visible band to process remote sensing image and monitoring information of farmland rapidly has been one of the important means of precision agriculture. However, there still hasn't been a scientific and effective evaluation method on the quality of restored image. To provide reference, basis and improvement direction for the performance test of restoration processing of low-altitude remote sensing degraded image It's a key step in the research of the application of visible image in precision agriculture, which has important significance in the research of UAV low-altitude remote sensing.

II. DESIGN MOTIVATION

For the restoration of degraded image in visible, band so far the research has got different effect. As picture 1(b-f) showed, is He, MDCP, Retinex, Tarel, Zhu5 most popular algorithms' effect. However, how to evaluate the effect after restoration objectively and accurately, is still an important issue in the field of image processing. Based on the literature, objective evaluation methods of image quality are full reference type, half reference type and none reference type. UAVs taking the photos in visible band in Low-altitude remote sensing can't refers to Standard clear image, which is no reference quality evaluation category. Zhu pointed out that Image quality degradation duo to Atmospheric Scattering also can't refer to standard image, only can refer to degraded image.

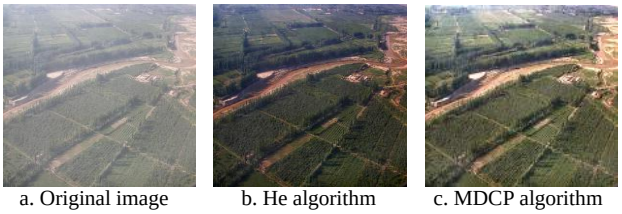

a. Original image b. He algorithm c. MDCP algorithm

d. Retinex algorithm e. Tarel algorithm f. Zhu algorithm

Figure 1. Restored results of classic algorithms

So far, Non - reference evaluation method is mainly Evaluate the unilateral performance of the image(such as PSNR, Information entropy and Average gradient ratio).Though Simple and targeted, but can not from the overall quality of the image to restore the effect of the judge. So the result can has a certain degree of deviation compared with the real comprehensive performance results of restore image.

For example, PSNR measurement method is an objective criterion for evaluating images, is one of the most common and extensive image evaluation objective measurement methods. But, many literature points out that PSNR measurement method's result can not be consistent with actual integrated visual quality. Using PSNR measurement method to evaluate picture 2(b-c), picture 2(b)'s PSNR value is 13.79, which is higher the picture 2(c)'s PSNR value's 12.25. But in human's eyes, picture 2(c) is better, which is Contrary to the results of the PSNR measurement method. Because PSNR measurement method only evaluates picture thought Image noise, ignoring the information contained by the picture.

a. Original image b. restore image (PSNR=13.79) c. restore image (PSNR=12.25)

Figure 2. Results of different method and its PSNR value

III. EAVALUATION MODEL DESIGN

A. *Evaluation and Optimization of Evaluation Factor*

The internal mechanism of HVS reveals the perception process of visual information, which can provide important guiding ideology for the comprehensive evaluation of image quality. Based on the study of human visual perception, this paper combines the auspicious knowledge of low-level remote sensing degradation image edge, contour distortion, low saturation, contrast reduction, overall brightness is large, and bionic simulation image visual perception,to propose a quantitative Assessment Model based on Visual Perception.

1) Image effective detail maintain ability

Human visual perception features show that the image contrast is not as high as possible, the contrast is too high for the recovery of the image is enhanced, the details are contrary to realism. Therefore, QAMVP defines an image effective detail retention capability factor L, which mainly reflects the ability of the restored image to eliminate noise and the "Halo" effect to influence the edge information.

The over-enhancement phenomena such as "Halo" effects of degraded image restoration processes, such as contours, depth of field, and so on, become wider and brighter. Therefore, the edge-enhanced detail intensity IHalo of the restored image can be obtained by summing the maximum pixel-point neighborhood of the corresponding region in the bright image of the restored image:

$$I_{Halo} = \frac{\sum_{x\in\phi}(\sum_{y\in\Omega(x)} I_{bright}(y))}{n} \tag{1}$$

Where Ω (x) is the field where the center point is x, n is the number of pixels in the neighborhood, and Ibright is the bright channel image. Similarly, the brightness intensity IiHalo of the region corresponding to the original image is:

$$I_{Halo}^{i} = \frac{\sum_{x\in\varnothing}(\sum_{y\in\Omega(x)} I_{bright}^{i}(x))}{n} \tag{2}$$

The over-enhanced approximation of the restored image is the difference between the two.

The total edge detail intensity LJ of the restored image can be solved by the Canny operator：

$$L_J = \sum I_J^{canny}(x) \tag{3}$$

Finally, the image effective detail retention capability factor L is reflected by the proportion of the edge of the restored image that enhances the detail intensity in the total edge detail intensity, which is:

$$L = \frac{(I_{Halo} - I_{Halo}^{i})}{L_J} \tag{4}$$

In equation (4), the smaller the L, the stronger the effective detail retention ability of the restored image, and the better the effect of suppressing the "Halo" effect.

2) The degree of tone reduction

When the restoration effect is good, the color of the image is truly coordinated, which is consistent with the degree of color shift in the visual perception. At this time, the histogram shape of the image before and after the restoration is substantially similar, so the histogram similarity can be used to measure the degree of hue offset of the restored image.

The Pasteur distance is used in statistics to measure the separability of two discrete probability distributions. In this paper, we define the calculation of histogram similarity from histDist. The mathematical expression is:

$$H = \sum \sqrt{p_1 \times p_2} \tag{5}$$

Where p1 and p2 are the probability distributions of the discrete points on the histogram before and after the restoration, respectively, and H is 1 when it is completely matched, and 0 is completely absent.

3) Structural information

The measure of the degree of change in scene structure is a good approximation of image perceived distortion. A large increase in the restoration of image structure information means over-enhancement and the introduction of noise, while a significant reduction represents the loss of detail information. Therefore, the structural information of the reconstructed image can be scientifically measured, and the realism and distortion of the restored image can be effectively evaluated.

An image I(x) can be expressed as a product of a reflection image R(x) and an illumination image L(x), which is:

$$I(x) = R(x) \cdot L(x) \tag{6}$$

The structure of the object in the scene is independent of the illuminance, so the texture information is extracted only for the reflected image R. The derivation of the reflection image R(x) is achieved by separating the illumination image by Gaussian kernel Gc(x):

$$R(x) = G_c(x) * I(x) \tag{7}$$

The similarity function is defined as S, and the reflection images R1 and R2 of the restored image are compared with the structural information, obtain:

$$S(R_1, R_2) = \frac{\sigma_{12}}{\sigma_1 \sigma_2} \tag{8}$$

among them,

$$\sigma_{12} = \frac{1}{M+1} \sum_{1}^{M} (R_{1,i} - \mu_1)(R_{2,i} - \mu_2) \tag{9}$$

M is the number of pixels; μ1 and σ1 are the mean and standard deviation of R1, respectively; μ2 and σ2 are the mean and standard deviation of R2 respectively.

4) Multi-scale structure similarity

Multi-scale Structural SIMilarity (MSSIM) is based on structural similar image quality evaluation factors, based on the HVS highly adaptable to natural vision systems. Compared with the single-scale structure similarity is only applicable to the specific situation, the multi-scale structure similarity has higher adaptability. The mathematical expression of MSSIM is:

$$MSSIM(x, y) = (l_M(x, y))^{\alpha_M} \prod_{i=1}^{M} \left[(c_i(x, y))^{\beta_i} (S_i(x, y))^{\gamma_i} \right] \tag{10}$$

In the above equation, the indices α_M, β_i and γ_i are used to adjust the relative importance of the different components of the formula.

5) Image visual fidelity

Visual Information Fidelity (VIF) reflects the perception that the image is the remake of the human eye by the HVS, similar to the process of extracting the valid information for the degraded image.

The traditional VIF carries out the fidelity calculation with the distortion less pattern as the reference pattern. In this paper, the original degraded image is used as the reference image, and the image information before and after the restoration is compared with the knowledge of the information theory. The results of the image fidelity evaluation are obtained. According to the above theory, VIF can be defined as:

$$VIF(x, y) = \frac{\sum_{j=1}^{s} \sum_{i=1}^{M_j} I(c_{i,j}, f_{i,j})}{\sum_{j=1}^{s} \sum_{i=1}^{M_j} I(c_{i,j}, e_{i,j})} \tag{11}$$

Where s is the number of scales of the image, Mj represents the number of image blocks on the scale j, and $I(c_{i,j}, f_{i,j})$ and $I(c_{i,j}, e_{i,j})$ are represented as mutual information. In general, the information obtained by the human eye is less than the original image, so the value range of VIF (x, y) is [0,1], the larger the value of VIF (x, y), the more the visual fidelity high.

B. The construction of the model

The above five visual sensory sensitive transcendental factors, from the aspects of the perception mechanism of HVS, and the characterization of degraded images of low-level remote sensing visible-band, the global weights and Measures of Image Quality Evaluation are carried out. Further ,By normalization and multivariate fitting analysis, we can come to the mathematical expression of QAMVP model as follows：

$$Q = \frac{(S)^{\alpha} \cdot (HistDist)^{\gamma} \cdot (MSSIM)^{\theta}}{(L)^{\beta} \cdot (1 - VIF)^{\varphi}} \tag{12}$$

In the above formula, Q is a comprehensive quantitative evaluation parameter, the larger the value of Q, the better the processing effect of the restored image. The five weight adjustment parameters,α， β， γ， θandφ,are the degree of sensitivity of the factors. According to the degree of

degradation of the original image，we make the value is less than 0.

IV. TEST RESULTS ANALYSIS

In order to verify the stability of the QAMVP model, the specific experimental method is as follows:

A. Test image sample library build

Through the network search, UAV sampling, etc. to establish low-altitude remote sensing visible light band degradation image sample library, a total of 600 images. Then, randomly extract 200 pictures to build the test image sample library

B. Evaluation of the sample map library building

The HE and DCP algorithm were used to reconstruct the test image sample database, and 200 restoration results were obtained. The construction of the sample library was evaluated. Herein, the reason for selecting the HE method is that although the method improves the contrast of the image to a certain extent in the restoration process, the recovery result is likely to be enhanced, the visual perception is not coordinated, and the comprehensive restoration effect is poor; , The choice of DCP algorithm is because the algorithm is currently recognized as one of the best algorithms for recovering visual effects. Therefore, the statistical results of the two algorithms on the restoration of large-volume image processing should be obvious.

C. Comparison of evaluation methods

The QAMVP model, the comprehensive evaluation method in and the PSNR measurement method were used for comparative analysis. By evaluating the probability of the highest value of the DCP algorithm in the scatter plot of each evaluation method, it can reflect the evaluation performance stability of each evaluation method. The detailed experimental data scatter plot is shown in Figure 3 to Figure 5.

In the figure, the abscissa indicates the evaluation sample group number; the ordinate indicates the evaluation index value, the same figure is large, indicating that the recovery effect is better. Figure 3 is the QAMVP model to evaluate the sample map library of the evaluation index value of the scatter plot, which DCP recovery results of the high value of 184 indicators, accounting for 92% of all the figure, can be seen as The QAMVP model has an accuracy rate of 92%. Figure 4 is a comprehensive evaluation method to evaluate the sample map library of the evaluation index value of the scatter plot, which DCP recovery results of the index value of the high group of 156, accounting for 78% of all the graph, the accuracy of this test is 78 %. Similarly, Figure 5 is the PSNR measurement method to evaluate the sample map library of the evaluation index value of the scatter plot, which DCP recovery results of high indicators of 44 groups, accounting for 22% of all graphs, that is, the test The accuracy rate is 22%.

It can be seen that the QAMVP model has a strong judgment on the objective group with obvious difference in the sample evaluation effect of the sample pool, and it can be deduced effectively. It is excellent in the evaluation experiment of 200 groups The stability of the. Through the data comparison and analysis, the comprehensive evaluation method can also get the correct evaluation result to a certain extent, but the accuracy rate is lower than the QAMVP model. PSNR measurement method evaluation accuracy is poor, the reason should be sensitive to PSNR HE method of a certain indicator of the upgrade. From the other side, it is pointed out that the objective evaluation method based on single factor is easy to fall into the trap of one-sided analysis in the evaluation process, and it is necessary to ignore the characteristics of the integrated information.

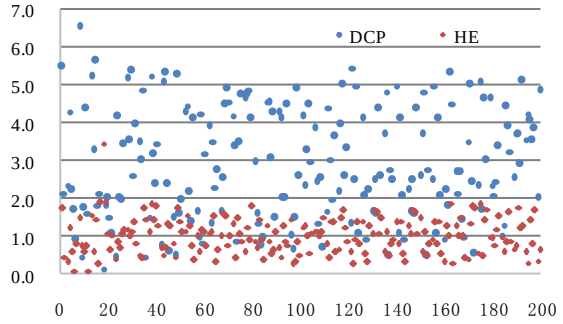

Figure 3. The evaluation scatter plot of QAMVP

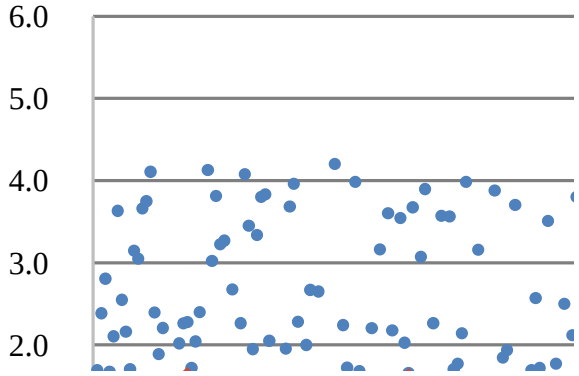

Figure 4. The evaluation scatter plot of comprehensive evaluation

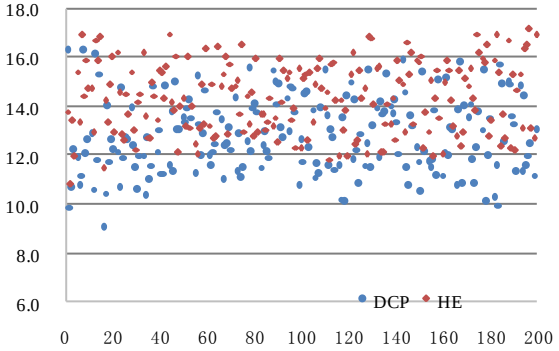

Figure 5. The evaluation scatter plot of PSNR evaluation method

V. CONCLUSION AND PROSPECT

low-altitude UAV remote sensing technology is one of the important means of fine agriculture, and it is of practical significance to carry out objective quantitative evaluation of the restoration of visible light band images in low-altitude remote sensing. Currently, in connection with the situation that the comprehensive quality evaluation of the reconstructed image is Emphasis on subjective evaluation, lacking of a scientific and objective quantitative evaluation system. Based on the perception of HVS, this article came up with an image quality evaluation model based on visual perception. The conclusion is as follows:

(1)The five low-altitude remote sensing degraded images visual perception sensitive a priori factors, which proposed by the QAMVP model, simulating the visual perception of the human eye, the subjective image performance evaluation, into a comprehensive factor to solve the mathematical problems, and it compensate for the single defect of the index in the traditional objective evaluation method. From the Visual perception perspective, a comprehensive evaluation analysis of the reconstructed image was made.

(2)Compared with the comprehensive evaluation method and PSNR measurement method, QAMVP model has its certain advantages in terms of evaluating performance stability, and obvious advantages in the aspect of visual perception as well as meeting performance.

(3)In this paper, the evaluation rate of 200 groups of evaluation samples is 92%,the value of MSE in two graphs of visual perception and meeting performance, are 0.075332 and 0.118076832 respectively, which shows that bases on visual perception, the model can evaluate the image of low-level remote sensing visible-band recovery effectively.

In the field of precision agriculture, application Technology of Low - level remote sensing visible light band image, will play an important role in the next period of time. With the involvement of large data acquisition and deep learning areas, the development of image quality evaluation methods, which based on visual perception ,will also get rapider and rapider..

ACKNOWLEDGMENT

The authors would like to gratefully acknowledge the financial support provided by Science and Technology Program of Guangzhou, China (201605030013).

REFERENCES

[1] Youlu Bai, Liping Yang, Lei Wang, et al.The Agriculture Low-altitude Remote Sensing Technology and Its Application Prospect[J]. Agriculture Network Information.2010(1):5-7. (in Chinese with English abstract)

[2] He K, Sun J, Tang X. Single image haze removal using dark channel prior[C]. 2011.

[3] Lu Jianqiang, Wang Weixing, Hu Ziang, et al. A front-end defogging system used for video image of basic farmland based on MDCP algorithm[J] Transactions of the CSAE,2016,32(10):143-148. (in Chinese with English abstract)

[4] Qian Liu, Xinhong Lu, Xianglin Li. Adaptive image enhancement method based on multi-scale Retinex algorithm. 2009,29(8):2077-2079. (in Chinese with English abstract)

[5] Tarel J P, Hautiere N. Fast visibility restoration from a single color or gray level image[C]. 2009.

[6] Zhu Q, Mai J, Shao L. A Fast Single Image Haze Removal Algorithm Using Color Attenuation Prior[J]. Image Processing IEEE Transactions on. 2015, 24(11): 3522-3533.

[7] Gangyi Jiang, Dajiang Huang, Xu Wang, et al. Review and prospect of image dehazing techniques[J]. Journal of Electronics and Information Technology,2010,32(1):219-226. (in Chinese with English abstract)

[8] Fan Guo, Zixing Cai, Bin Xie, et al. Review and prospect of image dehazing techniques[J]. Journal of Computer Applications,2010,30(9):2417-2421. (in Chinese with English abstract)

[9] Zhu Q, Hu Z, Ivanov K. Quantitative assessment mechanism transcending visual perceptual evaluation for image dehazing[C]. 2015.

[10] Zhang L, Zhang D, Mou X, et al. FSIM: A Feature Similarity Index for Image Quality Assessment[J]. IEEE Transactions on Image Processing. 2011, 20(8): 2378-2386.

[11] Shaoping Xu, Rongchang Yang, Xiaoping Liu. Information content weighted gradient salience structural similarity index for image quality assessment[J]. Journal of Image and Graphics ,2014,19(2):201-210. (in Chinese with English abstract)

[12] Zi'ang Hu, Weixing Wang, Jianqiang Lu, et al. Image dehazing using visual information loss prior[J]. Journal of Image and Graphics,2016(06):711-722. (in Chinese with English abstract)

[13] Automatica Sinica. 2011, 37(2): 143-149. Jing Yu, Dapeng Li, Qingmin Liao.Physics-based Fast Single Image Fog Removal[J]. Acta Automatica Sinica.2011,37(2):143-149. (in Chinese with English abstract)

[14] Hor é A, Ziou D. Image Quality Metrics: PSNR vs. SSIM[C]. 2010.

[15] Li Dapeng, Yu Jing,Xiao Chuangbai,No-reference quality assessment method for defogged images[J].Journal of Image and Graphics, 2011,16(9):1753-1757. (in Chinese with English abstract)

Design of Control System of Physical Fitness Treadmill Based on Embedded Technology

Jiujian Cui
Department of Physical Education and Military Theory
Suzhou Institute of Trade & Commerce
Suzhou, China
e-mail: 420356106@qq.com

Yan Wu
Department of Mechanical and Electrical Information
Suzhou Institute of Trade & Commerce
Suzhou, China
e-mail: 32676391@qq.com

***Abstract*—Treadmill is the commonest method to get a good health, but traditional treadmill has limited functions and low intelligence. While embedded technology implements special function and is controlled by internal computer system. Putting embedded technology into treadmill can enhance the intelligence and add extra functions. In this paper, system structure and work way of treadmill were analyzed scientifically through embedded technology and the design of controlling system. The system hardware structure was analyzed and designed effectively, combined with the application of embedded technology and serial communication technology, realizing the optimization of setting and motion parameters of the treadmill science display. Motion information was recorded, and multimedia entertainment function was also embedded in it. Finally, the system was tested and had a relatively stable and reliable working state. In addition, it also had a beautiful appearance and met the needs of consumers. Therefore, treadmill control system based on embedded technology has the features with cost-effective, low cost and relatively complete fashion and has a good prospect.**

Keywords-embedded technology; control system; sports fitness; treadmill control; system design.

I. INTRODUCTION

The traditional treadmill control system has a single function, which is mainly to set up and display the various state parameters of the treadmill, and the display mode is rare. It usually use the basic LED display, which is increasingly unable to meet the needs of today's consumers. Today, the embedded technology has developed rapidly, and has been widely used in industrial control, communications, information appliances, medical instruments, intelligent instruments and meters, automotive electronics, aerospace and other fields. Therefore, the embedded technology in the treadmill control system can make the control system more stable, the operation more concise and clear, and the additional multimedia functions will also meet the needs of consumers. In this paper, the embedded technology was integrated into the treadmill, and the control system of the treadmill was discussed in detail[1-3].

II. EMBEDDED TECHNOLOGY

Embedded technology pays attention to the reasonable control of the equipment, which realizes the effective monitoring of the equipment, and embodies the management function of the equipment comprehensively. Embedded system is adapted to a special computer system with higher requirements towards reliability, cost, volume and power consumption. It is composed of four parts, that is, embedded microprocessor, peripheral hardware device, embedded operating system and user application program. Usually, it is used to control, monitor and manage other devices, see Fig.1.

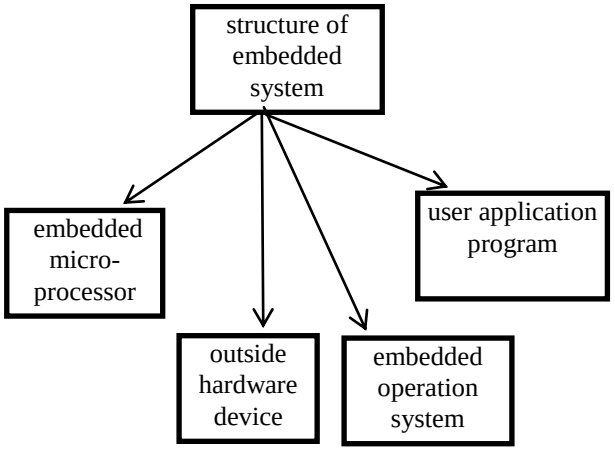

Figure 1. The structure of embedded system

III. STRUCTURE OF TREADMILL CONTROL SYSTEM

A. Hardware Structure

According to market research and user survey, the new control system has three main functions. One is the control function, which is used for a variety of state parameter setting and control of the treadmill. The second is the user motion information recording function, which is used for the historical record and compare the user's motion parameters. The third is the multimedia function for playing a variety of audio and video file. Based on this, the hardware design of the treadmill control system is shown in Fig.2[4-5].

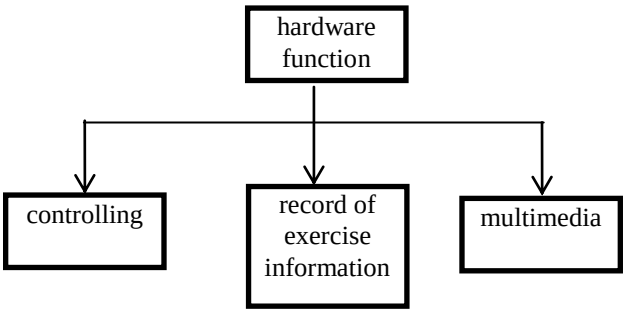

Figure 2. The hardware design of the treadmill control system

Control function is set and controlled based on condition parameter of treadmill. The realization of the user's motion information recording function is always focused on the reasonable settings of the user's historical motion parameters[6]. Multimedia functions are reflected to realize the effectiveness of audio and video files. The hardware structure of the control system is shown in Fig.3.

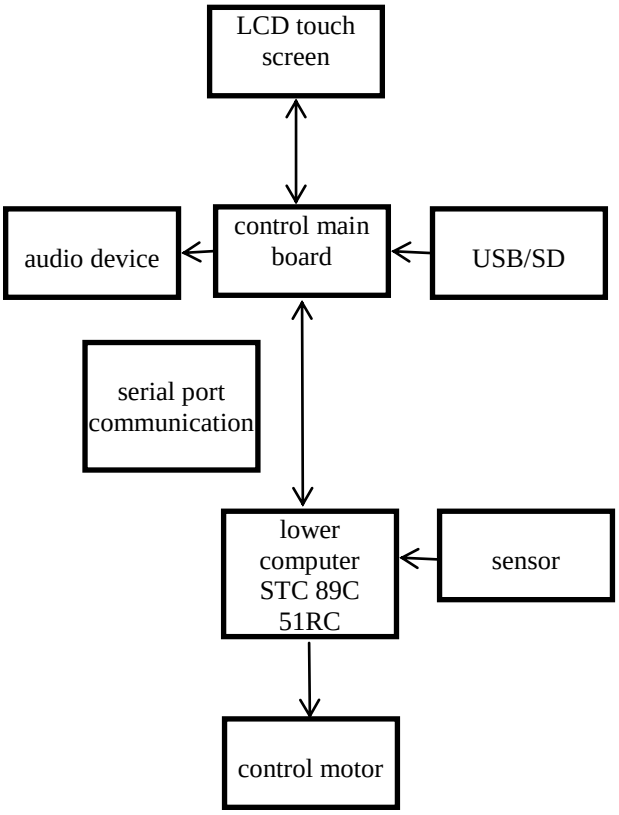

Figure 3. The hardware structure of the control system

LCD touch screen is mainly a link of man-machine interface. It will gradually realize information interaction between control system and user, and touch screen with the size of 4 inch is provided to get more wide field of vision. In addition, the control board is the core part of the host computer control system, which is based on the Samsung Corp ARM 926EJ embedded CPU as the core to expand the peripheral interface. Touch screen is the main part of man-machine interface, which realizes the information interaction between user and control system, and SHARP10.4 Inch Touch screen is adopted. The large screen not only brings wider vision, but also facilitates the operation of the user. Moreover, USB/SD interface is mainly used to connect external memory, such as USB device, SD card and so on[7].

The storage space available on the motherboard is very limited, and the addition of external storage devices is cheaper than of the motherboard, so external storage devices are a sure choice. An audio device is used for outputting sound, and audio interface is on the main board, which can play stereo. STC 89C 51RC is subordinate to the system's lower computer. It takes the chip STC, 89C, 51RC as the control core to realize the pulse signal reception and control of the motor, and use the serial port and the host computer control system for communication. Because positive logic is used in the upper and lower computer control circuit, TTL level communication mode is adopted in serial communication[8].

B. Software Structure

The system software mainly implements data processing, data communication, data display and man-machine graphic interface operation. The main process of the upper computer control system realizes the communication through the mechanism of shared memory, and the program reads the control information to the memory sharing area and completes the corresponding operation. The hardware system extends the external memory of 128M, the purpose of which is to store user data and software data, so as to facilitate the expansion of later functions. Finally, Windows CE 5.0 embedded operating system is selected as operating system[9].

As for the design of software system, the process of data processing and data communication is often paid attention to, and the data display function is provided to realize the man-machine graphical interface operation, as shown in Fig 4.

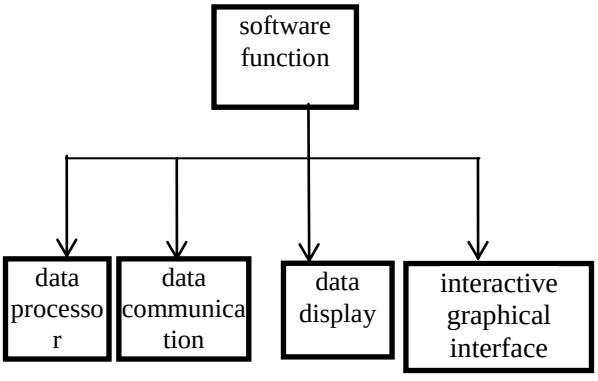

Figure 4. The function of software system

Process of data processing is to achieve the initial data and data processing optimization, as well as to achieve data communication and reasonable display of data. For the basic structure of the control system software, as shown in Fig.5.With regard to the software control process of the upper computer, combining the basic mechanism of memory, the communication process is realized gradually, and the corresponding operation is completed. The design of the hardware system pays more attention to the rational analysis of external memory, realizing the storage of user data, reasonable application of software data, and the expansion of function.

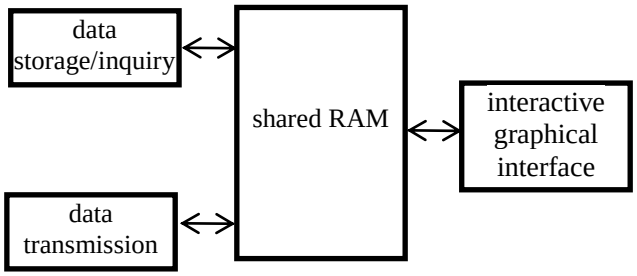

Figure 5. The basic structure of the control system software

IV. CONTROL SYSTEM DESIGN OF SPORTS FITNESS TREADMILL

A. *Hardware Design*

The hardware design of the control system of sports fitness treadmill is to choose a suitable chip according to a processor form on the motherboard, and focus on a variety of resources application interface controller to realize LCD controller module. For the application of the built-in hardware interface, wireless base band chip connection is implemented to realize other functional modules, and achieve stable and reliable system control, as well as provide powerful multimedia functions. With the participation of the system function module, the reasonable control of the LCD touch screen bus interface is needed, and the design of the power management module is effective. Z228 chip, developed by Shanghai Huarun electronics company, is selected as processor on the motherboard.The internal chip integrates the ARM 926EJ kernel, MPEG-4 hardware coder and a variety of controller and interface resources. Without the support of the peripheral chip, the system can achieve a variety of required functions. Among them, the built-in LCD controller can support up to XGA resolution true color liquid crystal display. A variety of built-in hardware interface can be easily connected to a wireless base band chip, memory expansion card, computer and other functional modules, and HDK, BSP and SDK of WinCE and Linux two versions are also provided. The application of Z228 chip in the control system of treadmill can not only realize stable and reliable control system, but also can provide powerful multimedia function. According to the functions needed by the system, LCD touch screen, bus interface, USB SD interface, UART interface, power management module and audio interface are extended in peripheral hardware devices..

B. *Software Design*

Main hardware structure of the system should be considered with regard to the realization of software design and gradual generation of the embedded operating system. Effective download on target board combined with the development process of main software in the system can achieve the system application in the platform. For the customization process of system platform, host computer control system adopts Windows CE 5.0 operating system to realize multiple thread task scheduling. The system has good tailoring and portability, and supports a variety of mainstream CPU, such as ARM, MIPS, X 86, SuperH. It has real-time functions on most occasions, rich API, friendly user interface, and rich application software. Moreover, it occupies a large proportion in today's consumer electronic products. According to the composition of system hardware, corresponding embedded operating system is generated by cutting the BSP provided by Z228. This system will be downloaded to the target board, and export specific software development kit SDK, which is used to compile applications that will run on the platform, as shown in Fig.6.

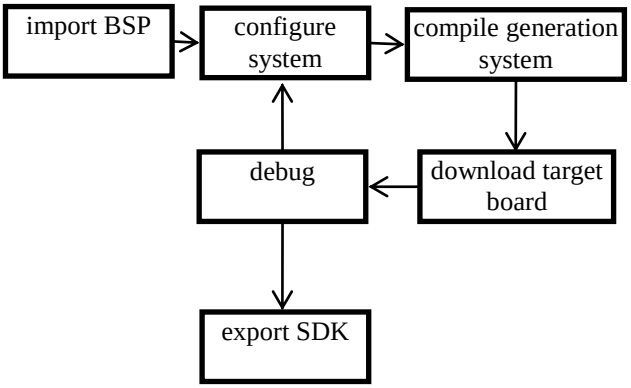

Figure 6. The customization of system platform

The application design process, combined with MPC multiple thread programming mechanism control, completes the design of multimedia function module and treadmill control module, and realizes the design of user information storage module and data communication module. The basic design of treadmill control module, combined with the application of motion parameters, pays attention to the direct monitoring of the movement state, and then realizes the effectiveness monitoring of the status thread. For the basic application of data communication module, it directly realizes data transmission of lower and upper computer, and focus on the special communication protocol, data communication and gradually realize the receiving and recognition of data communication. The design of multimedia function module pays more attention to the effective play of video files, and meets the needs of users gradually. The comprehensive application of the user

information storage module achieve programming and analysis through storage of effective record of the historical movement, and programming and analysis of the database, in order to get the effective and recycling use of space.

The data of sports fitness treadmill can be seen as table 1.

TABLE I. THE DATA OF SPORTS FITNESS TREADMILL

Parameter	Value		
	Data set 1	*Data set 2*	*Data set 3*
Time(s)	100	200	300
Distance(m)	10	40	90
Speed(m/s)	0.1	0.2	0.3
Heart rate(bpm)	70	90	120

V. WORK WAY OF TREADMILL

Once the system is in the state of power, automatic operation must be completed, main control interface is gradually opened, the reasonable application of LCD touch screen is realized, and reasonable motion parameters on the treadmill should be set. The application of motion module needs to combine the basic movement process of the subordinate computer feedback, which focus on the main interface screen and simulate the reasonable analysis of the user. In the actual movement stage, users can also enjoy the full enjoyment of the multimedia function. When the multimedia button is clicked, the multimedia player interface is opened.

First stage belt drive calculation is as follows.According to the calculation of power and speed, check the mechanical design manual and select the type of conveyor belt.Determine the diameter of the belt pulley and check the belt speed

The diameter of primary small round benchmark is $d_{d1} = 126mm$ and check the belt speed formula as

$$\upsilon = \frac{\pi d_{d1} n_1}{60 \times 1000} = \frac{126\pi \times 2600}{60 \times 1000} \tag{1}$$

The reference diameter of the large pulley d_{d2} can be calculate as formula(2)

$$d_{d2} = i_1 \cdot d_{d1} \tag{2}$$

The center distance a and reference length L_d of the belt are determined.When the initial center distance $a_0 = 900mm$ the required base length can be calculated as formula(3)

$$L_{d0} \approx 2a_0 + \frac{\pi}{2}(d_{d1} + d_{d2}) + \frac{(d_{d2} - d_{d1})^2}{4a_0} \tag{3}$$

Actual center distance a is calculated as formula

$$a \approx a_0 + \frac{(L_d - L_{d0})}{2} \tag{4}$$

$$a_{\min} = a - 0.015L_d$$
$$a_{\max} = a + 0.03L_d$$

The small wheel on the corner α_1 is checked as formula(5)

$$\alpha_1 \approx 180^0 - (d_{d2} - d_{d1})\frac{57.3^0}{a} \tag{5}$$

The minimum value $(F_0)_{\min}$ of the initial tension of a single V belt is calculated

$$(F_0)_{\min} = 886\frac{(2.5 - k_a)p_{ca}}{k_a z v} + qv^2 \tag{6}$$

Controlling of main interface of control system refers to effective observation of movement system with the help of U disk, and rationally use external memory. In addition, external storage space should be supported, and motion records should be reasonably selected. The system finally passed the test, and proved the design of control system of sports fitness treadmill based on the embedded technology not only has a relatively stable reliability, but also has a beautiful appearance, and will fully meet the needs of consumers.

VI. CONCLUSION

In a word, control system design of treadmill based on the embedded technology is different from the traditional treadmill control system. It not only improved the functional performance of the system, but also improved the appearance of the situation, and fully achieved the operation of touch screen. It gradually achieved user needs, and effectively recorded multiple information. Applications of embedded equipment has the features of cost-effective, low cost, relatively complete fashion, which meet the requirements of consumers. In this paper, design of embedded technology based sports treadmill control system provides a certain guiding significance in this field.

REFERENCES

[1] Eunsook Sung, "The effect of treadmill-based and track-based walking training on physical fitness in ankle-sprain experienced young people," Journal of Exercise Rehabilitation, vol. 13, pp. 84–88, Feb. 2017.

[2] CM Fairman,KL Kendall,BS Harris,KJ Crandall and M Jim, "Utilization of an anti-gravity treadmill in a physical activity program with female breast cancer survivors: a pilot study,"International Journal of Exercise Science, vol. 9, pp.101–109,January,2016.

[3] Pei Wang, "A software design of college students' physical fitness test based on mobile phone," Electronic Design Engineering, vol. 20, pp. 61–70, Nov. 2016.

[4] Mei Hong and Shen Junrong, "Software architecture research progress," Journal of software, vol. 12, pp. 1257-1275, Dec. 2015.

[5] Chu Wenkui and Zhang Fengming, "Based on the military software security problems of the COTS study, " Journal of Systems Engineering and Electronics,vol. 3, pp. 2166-2170, Aug. 2014.

[6] MK Edwards and PD Loprinzi, "Sedentary behavior, physical activity and cardiorespiratory fitness on leukocyte telomere length," Health Promotion Perspectives, vol.7, pp.22–27, August 2017.

[7] Han Lihong, "The embedded real-time operating system performance testing method," Journal of Command and Control and Simulation, vol.21, pp.98-101, Apr. 2015.

[8] Chen Zhuo, Wang Tian and Liang Xinyuan,The Embedded System Development. Beijing: Electronic Industry Press, 2015.

[9] Wang Jingang and Yang Ximai,The Vx Works BSP Developers Guide. Beijing: Tsinghua University Press, 2014.

[10] Tu Gang, zhang bo and Yang Fumin, "The research of embedded operating system transplant technology," Computer Application Research, vol. 56, pp. 83-85, Dec. 2014.

The Disease Assessment of Cucumber Downy Mildew Based on Image Processing

Jingzhu Li
The College of Engineering and Technology
Jilin Agricultural University
Changchun Jilin 130118, China
13234426475@163.com

Changxing Geng
Robotics and Microsystems Centre
Soochow University
Suzhou Jiangsu 215021,China
chxgeng@suda.edu.cn
251834198@qq.com

Peng Wang
Robotics and Microsystems Centre
Soochow University
Suzhou Jiangsu 215021,China

***Abstract*—Cucumber downy mildew is a kind of disease which spreads very fast and isdangerous, in order to prevent the disease, peoplealways spray plenty of pesticides indiscriminately. Accurate assessment of the level of cucumber downy mildew is very important to the disease prevention and control. In a cucumber growing season, this paper collected the typical cucumber downy mildew leaf samples, and developed the downy mildew spot extraction algorithm by using leaf image scanning method, calculated the index of the disease. The average identification accuracy of downy mildew image reaches 98.3%, and average image processing takes 10.9 ms/picture. By compared with human eyes assessment and basic value, the result shows that the human eyes assessment method have strong subjectivity, dramatic changes and bigger error, while the image analysis method get the correlation coefficient for disease index and basic value of 0.9417, has obvious linear correlation.**

Keywords-Cucumber downy mildew; Image processing; Disease assessment; human eyes assessment; linear correlation

I. INTRODUCTION

Crop disease identification based on crop leaf symptom is an important research content in plant protection [1-8]. In the middle of 80s, computer image processing and analysis technology was applied to disease detection and disease statistics. The image processing technology and fuzzy theory to preprocess the health and disease of pomegranate leaf image by SanjeevS [9], and they extract the features stored in the database, formatting the automatic recognition system of pomegranate disease recognition. The image processing technology and artificial neural network to extract treatment on Cucumber Downy Mildew and powdery mildew symptoms by Keyvan [10], via the back-propagation supervised learning method to train cucumber downy mildew and powdery mildew identification system. Dong [11] etuse the median filtering method to filter the noise ,separate the disease of cucumber downy mildew color, extractthe lesion surface color characteristic parameters and shape parameters, and format gray level co-occurrence matrix. the disease recognition rate is more than 96%. JiaJiannan [12] etseparatecucumber diseaseby using the method of Otsu image, indicating the feasibility of recognizing Cucumber Downy Mildew and cucumber by spot shape and neural network. XuLiangfeng[13]et proposed an adaptive weighted multiple classifier fusion method for identifying leaf diseases of maize. 7 common maize leaf disease pictures were tested, with an average recognition rate of 94.71%.Ye [14]et proposed an identification method of downy mildew of Cucumber Leaf based on visual saliency map, can identify the lesion of robust downy mildew from leaf color image accurately. Zhao [15] et eliminate the adverse effects of light used by Retinex algorithm for image enhancement, use automatic threshold method to separate spot imageinR-G gray space, extract color texture and invariant moments of the lesion, and used principal component analysis and support vector machine to classify common diseases of maize leaves.

According to the symptoms of crop leaves, image processing technology can be used to identify crop diseases. This paper optimizes the access to environmental disease leaf images, so as to get the image of good consistency, introducing dynamic variables to improve image quality and reduce the difficulty of image processing, using the linear operation of cucumber downy mildew. Based on the principles of disease evaluation and measurement, the baseline values are established and the validity of the image analysis algorithm is verified.

II. MATERIALS AND METHODS

A. Acquisition of Sample

The sample of cucumber for test was "Zhong Ke 958", and used the leaves of cucumber as the research object, and the 110 leaf samples of natural infection of downy mildew acquired from the greenhouse of Shang zhuang experiment station of China Agricultural University (acquisition time: 2012.8.2-10.2). The scanner for leaf image capture is Epson perfection 2480, and the maximum optical resolution is 2400×4800 dpi, select black scan background, increase the contrast of background and leaves, to reduce the

implementation difficulty of extraction algorithm, the experiment uses different resolution to scan leaf positive respectively. The images of leaf samples captured of typical different disease degree shown in figure1, the disease spot distribution of leaf 1 to 4 from less to more.

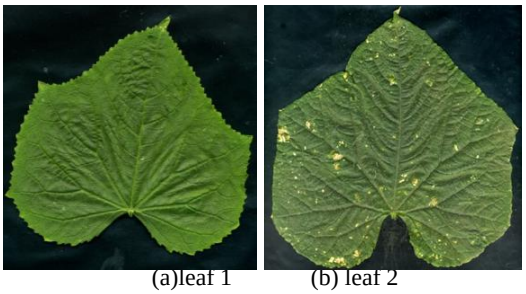

(a)leaf 1 (b) leaf 2

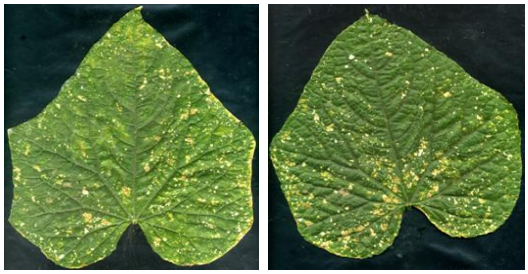

(c) leaf 3 (d) leaf 4

Figure 1. Cucumber leaves of different disease degree

B. *Image Analysis*

Analyzed the samples in Fig. 1 by the histogram analysis method, the results are shown in Fig. 2, it can be seen that blade R channel and G have bimodality, of which R channel trough distribution between 30-50 grey value, G channel trough distribution between 50-70 grey value, and obviously, the two peaks represent the black background and pixel concentrated areas of green leaves, rely on a single threshold is impossible to pick up the disease. From the curves in (a) to (d) of Fig. 2, it can be found that R channel and G channel increase with the distribution of disease spot, the part of grey value more than 200 appeared the trend of increase gradually, the entire waveform falling edge of the last shift to the right, and G channel growth significantly. It is consistent with the process of disease appeared, and it is the process of the disease spot characterized on leaves develop from nothing, from color, it is the process of pathological changes of leaf from green to yellow gradually, and the process is the grey value of the R channel and G channel increased gradually.

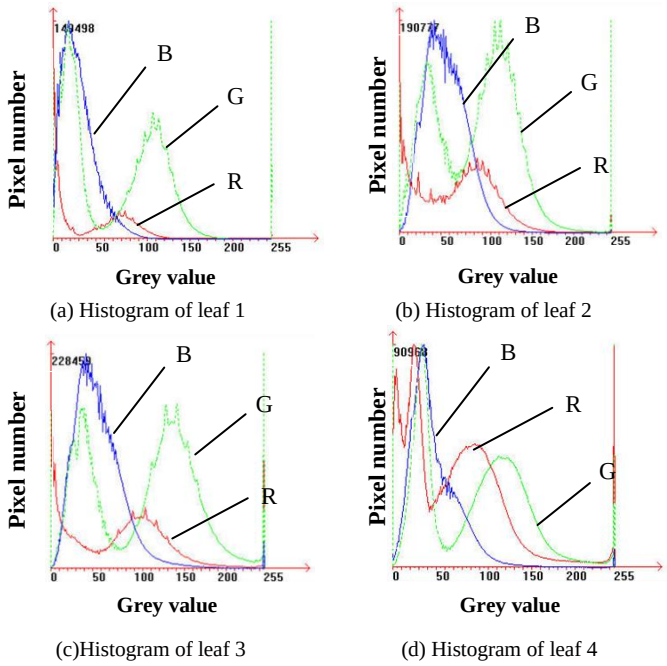

(a) Histogram of leaf 1 (b) Histogram of leaf 2

(c)Histogram of leaf 3 (d) Histogram of leaf 4

Figure 2. Histogram analysis of leaves of (a) to (d) in Figure1

C. *Extraction of Disease Image*

Given uniform image acquisition environment, image light change is small, it can be seen that the changes of color feature of disease spot is mainly caused by the composite value of R and G, so try to use simple combination of R and G to achieve the extraction of disease. To eliminate the leaf color difference of various plant growth period and different disease epidemic period, and to avoid unreasonable fixed threshold setting, by focusing on the analysis of disease spot in RGB space and the distribution of R and G on healthy leaf area, as shown in Fig. 3, extract normalized value of each image as a correction parameter can effectively reduce the color interference and false judgment. It can achieve effective separation by formula (1), and the results of image processing are shown in figure 4. By simple linear operation, extracts the disease spot in different disease distribution effectively, and implements fast separation of the disease spot and leaf and background.

$$B_{lack} = \begin{cases} 0 & 2 \times R - G > 80 \times (1 - N_I/3) \\ 255 & 2 \times R - G \le 80 \times (1 - N_I/3) \end{cases} \quad (1)$$

$$N_I = \frac{R+G+B}{3 \times 255} \quad (2)$$

In the formula Black—Pixel value after segmentation, disease information for 0, background information for 255

NI—Normalized value of image

R,G,B—R,G,B component value of image RGB space

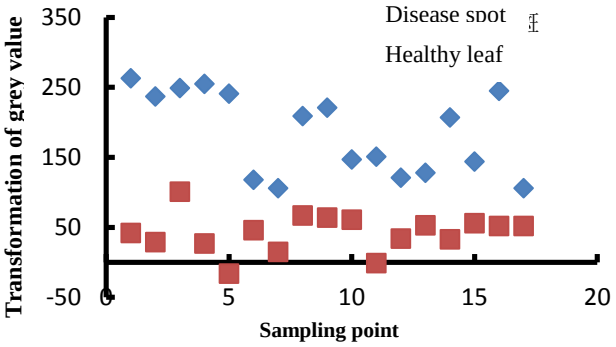

Figure 3. 2×R-G distributions of disease spot and healthy leaf

(a) Calibration image of leaf 1 (b) Calibration image of leaf

(c) Calibration image of leaf 3 (d) Calibration image of leaf

Figure 4. The calibration images of different condition of cucumber leaves

III. RESULTS AND DISCUSSION

A. *Disease Classification Method for Cucumber Leaf*

The determination of classification standard is the key of the direct impact on the illness unified analysis, but the classification standard of cucumber downy mildew is not the same for different countries. In China, the research started from the early 1960s, Fu Shuyun [18] introduced different classification standards of cucumber downy mildew, and the natural classification based on leaf, is divided into 5 levels. Yang Chongshi [19] and others introduced the development of classification standard of cucumber downy mildew in our country. The current national standard GB/T 17980.26-2000 [20] stipulated the classification standard of cucumber downy mildew (by leaf) as follows: level 0: without disease spot, Level 1: disease spot area below 5% of the total leaf area, Level 3: disease spot area is 6% - 10% of the total leaf area, Level 5: disease spot area is 11% - 25% of the total leaf area, Level 7: disease spot area is 26% - 50% of the total leaf area, level 9: disease spot cover more than 50% of the total leaf area. Considering that the standards above are expressed by the disease spot area percentage of the total leaf area, scanned leaf first in the following research, to process image analysis method(IAM), then selected 10 raters who have the experience of plant pathology management, to assess the disease by visual estimate method(VEM).

In order to avoid the error caused by single method, this paper set basic value for the disease condition of leaf, and the basic value use the national standard GB/T 17980.26-2000 [20] as a reference. Create the calibration images using the Boolean and operation with the processing result of leaf disease spot image, as shown in figure 4, and still select the same 10 raters to assess the calibration image after superposition. If they identify with the results of IAM, then use IAM result to replace the VEM result, otherwise retain their results or do the assessment again.

All the assessment results are calculated based on the disease condition, and the disease degree DS is the proportion of disease symptoms of leaf (percentage), as shown in formula (3).

$$D_S = \frac{D_A}{L_A} \cdot 100\% \quad (3)$$

In the formula D_A is the disease spot area on the leaf
L_A is the area of leaf

B. *Results Analysis*

Select 29 leaves of different disease degree as experimental samples. After using VEM to the leaves by the 10 raters, use the average (AVG) value as the assessment results, as shown in table 1.

Use the scanner to scan the positive side of leaves, the computer configuration for the analysis algorithm of image scanned as follows: CPU: Intel Pentium (R) 3.06 GHz, memory: 1 GB, and the software environment is Microsoft Visual C++ 6.0. Extract the disease spot of the 29 leaves using the algorithm shown in formula (1), and judge the accuracy of identification, the result shows that the average recognition accuracy of downy mildew image reaches 98.3%, and average image processing takes 10.9 ms/picture. Calculate the disease severity by formula (3), then the 10 raters judge the disease based on the calibration images, obtain the new assesement results, and use the AVG as the basic value, as shown in figure 5. The results suggest that the assessment results of VEM are always bigger than the assessment results of IAM, and the assessment results of VEM and the assessment results of IAM have big difference with the basic value especially when the disease degree is bigger. The assessment results of the same leaf assessed by each rater is obviously different as it is shown in table 1, for example, the maximum disparity of leaf 28 is more than 50%, but after the raters review the calibration images, the disparity turn smaller. And as it is shown in figure 5, the error of the assessment results of VEM is bigger than the

results of IAM, the results of IAM are similar to the basic value.

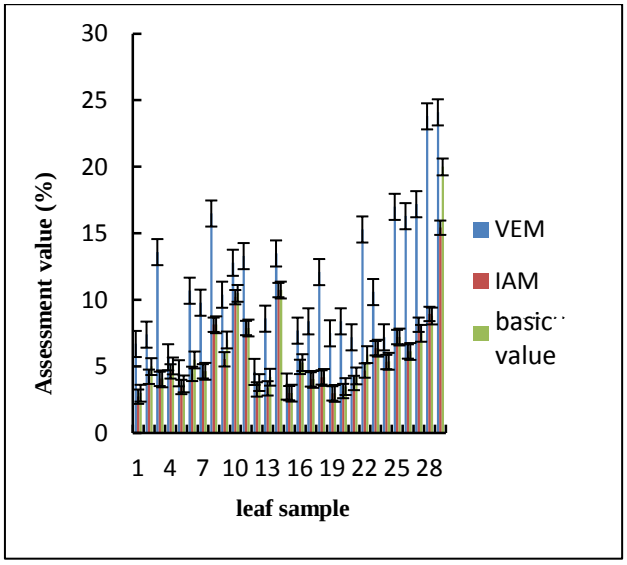

Figure 5. The assessment value of VEM and IAM and basic value

The differences mainly come from the followings:

The leaf color and disease condition degree of different plant growth period are different, which causes the characterization of color is different when the disease occurs, and it is easy to cause image segmentation errors. These results reflect the difference of the sample characteristics and the difference of the image characteristics. Light, surface reflection, saturation, hue, leaf age, symptoms, nutritional status, and even spraying time, may lead to the difference of leaf images.

The distribution of disease spot may lead to assessment error, for example leaf 28 and 29 shown in figure 6, due to the disease spot distributed full of leaf, and the assessment results of VEM are often exaggerated. But after assessing again based on IAM algorithm, the raters tend to agree with the IAM results or decline the VEM results.

In the processing of image capture, leaf folds cause the information missing, and in the processing of leaf acquisition, with no artificial cleaning, there will be pesticide residual and eluvial soil on the leaf surface, especially the lower leaves of plant, these bring the scatter noise of image, but the VEM can eliminate the noise.

Because the disease segmentation algorithm formula (1) is specific to the extraction of downy mildew information, so it may happen under segmentation when other disease occurs. Such as the leaf 4 shown in figure 6, it occurs the Liriomyza disease at the same time, by the VEM with the experience people can quickly rule out other diseases, but when using IAM to analyze the leaf with different kinds of diseases, there are potentially limiting factors, the features extracted are related to other disease features, and this need further research.

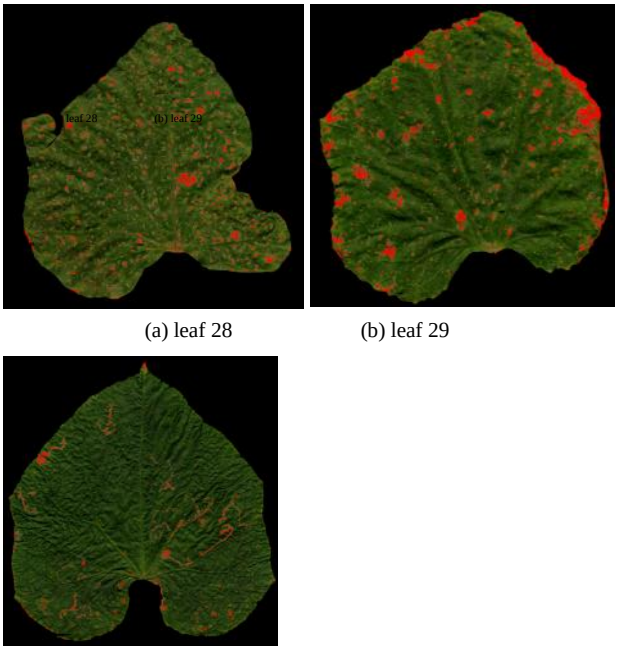

(a) leaf 28 (b) leaf 29

(c) leaf4

Figure 6. The calibration images of leaf 28 and 29

The correlation analysis results of the disease index obtained by IAM and basic value are shown in figure 7, the results show that the correlation coefficient R2 is 0.9417, have obvious linear correlation, but it still can be seen that the correlation in light disease degree is higher than in severe disease condition, the main reason is when the disease spot distributed full of leaf uniformly, the assessment results of VEM are big. Therefore, the IAM algorithm mentioned in this paper can be used in the disease feature extraction of cucumber downy mildew and as the assessment index of disease degree, comparing with VEM, IAM is rapid, simple, effective and low technical requirements for personnel, and has maneuverability and stability.

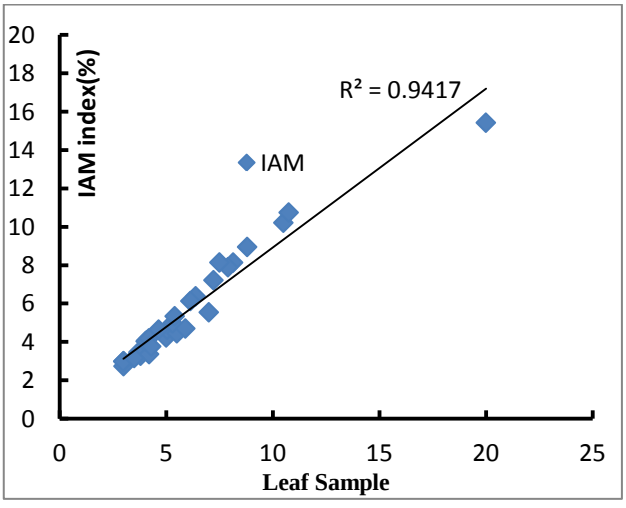

Figure 7. The correlation analysis of IAM and basic value

REFERENCES

[1] Zhan Wu Peng,Xue Wang. Study on the Method of Feature Extraction of Vegetable Diseases Based on Image Processing[J]. Advanced Materials Research,2014,3530(1044):.

[2] Xue Wang,Zhu Ma,Xin Wang,Dan Jiang,Xiaoxi Liu and Zhilei Jia. Study on automatic recognition of cucumber downy mildew based on color and shape features [J/OL]. Journal of Anhui Agriculture University, 2013 (06).

[3] Wang Xianfeng, Zhang Shanwen, Wang Zhen, Zhang Qiang. Identification method of cucumber diseases based on leaf images and environmental information [J]. Chinese Journal of agricultural engineering, 2014, (14): 148-153.R. Nicole, "Title of paper with only first word capitalized," J. Name Stand. Abbrev., in press.

[4] Wen Zhiyuan, Cao Leping. Citrus pest like hue multifractal and image recognition based on [J]. Journal of agricultural machinery, 2014, (03): 262-267.M. Young, The Technical Writer's Handbook. Mill Valley, CA: University Science, 1989.

[5] Zhao Yaochi, Hu Zhuhua, Bai Yong, Cao Fengqin. An accurate segmentation method of DRLSE disease and insect images based on texture difference guidance [J]. Acta Sinica, 2015, (02): 14-19.

[6] Wu Yuanyuan, Li Qingbo, Diao Hong. Study on color image feature extraction of wheat leaf diseases [J]. Agricultural Mechanization Research, 2015, (10): 79-82.

[7] Tian Kai, Zhang Liankuan, Huang Zhihao, Li Jiu, Xiong et, eggplant. Brown streak leaf spots feature recognition method based on [J]. Journal of agricultural engineering, 2016, (S1): 184-189.

[8] Xie Zeqi, Hu Xiaowei, Zhang Huimin, Zhang Shanwen, Zhang Yunlong. Grade recognition algorithm of crop leaf diseases based on environmental information and color features [J]., agricultural science, 2016, (07): 428-430..

[9] Sanjeev S. Sannakki,Vijay S. Rajpurohit,V. B. Nargund,R. Arunkumar. Disease Identification and Grading of Pomegranate Leaves Using Image Processing and Fuzzy Logic[J]. International Journal of Food Engineering,2013,9(4):.

[10] Jia Jiannan, Ji Haiyan. Journal of agricultural engineering, [J]. recognition of cucumber disease lesion shape based on neural network and S1:115-121. 2013.

[11] Xu Liangfeng, Xu Xiaobing, Hu Min, Wang Rujing, Xie Chengjun, Chen Hongbo. Identification of corn leaf diseases based on multiple classifier [J]. Journal of agricultural engineering, 2015, (14): 194-201+315.11-16.

[12] Keyvan Asefpour Vakilian,Jafar Massah. An artificial neural network approach to identify fungal diseases of cucumber (Cucumis sativus L.) plants using digital image processing[J]. Archives Of Phytopathology And Plant Protection,2013,46(13):.

[13] Dong Pixia,Wang Xiangdong. Recognition of Greenhouse Cucumber Disease Based on Image Processing Technology[J]. Open Journal of Applied Sciences,2013,03(01):.

[14] Ye Haijian, Lang Rui, Liu Chengqi, Li Li Zhen. Recognition of cucumber downy mildew based on visual saliency map [J]. proceedings of the Chinese society of Agricultural Mechanics, 2016,05:270-274.

[15] Qi Zhao, Jiang Zhaohui, Yang Chun he, Liu Lianzhong, Rao yuan. Identification of leaf diseases in Maize Based on image technology [J]. Journal of Anhui Agriculture University, 2016, (02): 325-330.

[16] Fu Shuyun, Yao Jianmin, Fu Junfan. Study on artificial inoculation technique of cucumber downy mildew [J]. Journal of Shenyang agricultural college. 1984 (02):11-16.

[17] Yang Chongshi, Wang Wanli, Liu Gengchun, et al. Progress and practice in bioassay of cucumber downy mildew [C]. 2000

[18] People's Republic of China national standard. Guidelines for field efficacy trials (1) Fungicides against cucumber downy mildew [S]. 2000.

TABLE I. THE DISEASE ASSESSMENT RESULTS OF VEM

Leaf \ Rater	1	2	3	4	5	6	7	8	9	10	AVG
1	5	5	6	10	10	5	6	5	5	10	6.7
2	4	3	6	10	5	6	10	5	10	15	7.4
3	7	5	8	30	5	10	15	6	20	30	13.6
4	4	2	6	10	2	10	8	5	5	5	5.7
5	2	1	5	5	5	8	5	4	5	5	4.5
6	6	3	10	20	10	15	15	8	10	10	10.7
7	5	2	15	15	10	10	12	9	10	10	9.8
8	8	2	20	30	20	15	20	10	20	20	16.5
9	4	2	10	20	15	8	15	10	10	10	10.4
10	6	10	10	20	15	10	16	9	10	22	12.8
11	5	5	15	30	10	15	18	10	10	15	13.3
12	1	2	8	10	5	3	5	2	5	5	4.6
13	6	5	4	10	10	10	8	5	20	8	8.6
14	8	8	15	20	10	20	20	6	20	8	13.5
15	1	1	0	10	5	5	5	5	0	3	3.5
16	2	3	3	30	10	4	6	6	5	8	7.7
17	3	4	10	20	5	5	10	7	10	10	8.4
18	3	5	10	20	5	10	20	8	20	20	12.1
19	2	5	8	15	5	8	10	7	10	5	7.5
20	3	3	8	20	5	8	10	7	10	10	8.4
21	2	2	10	10	5	8	12	7	10	6	7.2
22	4	4	25	20	5	20	15	10	20	30	15.3
23	3	3	15	20	5	15	20	7	10	8	10.6
24	2	2	5	10	3	8	25	6	5	6	7.2
25	4	4	35	30	10	20	25	10	20	12	17
26	4	6	30	30	5	20	20	8	20	20	16.3
27	5	5	20	40	10	20	25	7	20	20	17.2
28	10	9	25	60	15	25	30	9	30	25	23.8
29	12	12	25	50	20	25	40	15	20	22	24.1

Evaluation on Traffic Guidance Plan during Construction Period based on Vissim Simulation

Zheng Huimin
Qingdao Binhai University,
West Jialingjiang Road, Development Zone of Qingdao,
Qingdao, China
e-mail:zhmhappy@126.com

Sun Zhanxian
Qingdao Binhai University,
West Jialingjiang Road, Development Zone of Qingdao,
Qingdao, China
e-mail:1119828361@qq.com

Chen Xuan
Qingdao Binhai University,
West Jialingjiang Road, Development Zone of Qingdao,
Qingdao, China
e-mail: chenxuanjt@163.com

***Abstract*—With the urbanization process speeding up, the construction of City Road increased rapidly. So limited road resource is often occupied during the road construction, which makes road capacity of construction affected area greatly decrease. Then the contradiction of city original transport supply becomes more prominent. Therefore, it is very important to make a reasonable traffic organization plan. At first According to the present traffic investigation and construction site management program, combining with the OD（Origin - Destination） distribution principle, the traffic impact of construction section is analyzed, the scope of influence is determined. The Taihangshan Road of Qingdao No.1 subway line is taken as an example, three evaluation indicators, such as: average delays, queue length, number of vehicles between OD points are selected combined with current traffic flow. The available traffic guiding schemes include temporary widening of roads, traffic management measures and construction safety guarantee measures, and so on. Then VISSIM is used for the guidance measures simulation. Finally, According to the simulation results, quantitative guidance measures are evaluated. The choice of reasonable conduct measures is based on relevant data.**

Keywords-Traffic impact; OD distribution; Traffic Organization Plan; VISSIM Simulation; guidance measures

I. INTRODUCTION

Urban road is the main component of urban overall planning, with the rapid development of China's economy, the process of urban construction is speeding up. In order to promote urban development, urban road construction projects Such as road widening, subway construction, pipe lying are also increasing. The construction brings great pressure to the city traffic, and the big cities are more obvious.

In foreign countries, attention has been paid to the study of road maintenance operation and maintenance work area safety [1-2]. Most cities in China focus on the planning of artery in road network planning, Lack of attention to lower grade roads. There is not much research on intersections at construction stage. But many large construction projects, such as the construction of subway stations and viaducts are located near the intersection which lead to a decrease in traffic capacity of construction sections and intersections [3-4]. Road construction has a great influence on its residents' travel and traffic, especially the urban rail project with larger construction time and larger occupation area has more influence on it [5].

With the domestic experts and scholars on the traffic characteristics of the construction area of theoretical research, Construction area specifications and traffic guidance program design need to be further improved.

The Taihangshan Road of Qingdao No.1 subway line is taken as an example, the road and intersection traffic guidance scheme during the construction is explored, and Evaluate by Vissim simulation. It provides a basis for rational selection of traffic guiding scheme.

II. TRAFFIC IMPACT ANALYSIS DURING CONSTRUCTION

Within the scope of construction, the roads are mostly the main roads, and the traffic flow is relatively large. The speed and characteristics of motor vehicles, non-motorized vehicles and traffic flow are different because of the different traffic flow structure of expressways, main roads, secondary roads and branches [6].Construction takes up some sections of the road to reduce its traffic capacity, and the traffic pressure of the surrounding road network increases. Through the analysis of the changes of OD distribution during construction, the quantitative evaluation was carried out with Vissim simulation.

A. OD distribution principle

According to Wardrop's first principle, when the users of the road know the traffic state of the network exactly and try to choose the shortest path, the network will reach a balance

state. If there are a lot of roads between OD, and traffic between OD is very small, the vehicle will obviously walk along the shortest path. With the increase of traffic volume, the amount of traffic on the shortest route will increase accordingly. After increasing to a certain extent, the shortest route will travel longer because of congestion, and the shortest path will change. The vehicle will choose the road with shorter travel time, and as all traffic between OD continues to increase, all roads between OD are likely to be utilized [7-8]. If all the way users know exactly the roads needed to travel time and travel time of the shortest path, during construction as part of road traffic diversion needs, give full consideration to measures to guide traffic, the travel times between the points on the OD will be equal.

In 1956, Beckmann proposed the Wardrop principle to describe the traffic equilibrium assignment and created a mathematical programming model. It was not until 1975 that the Frank-Wolfe algorithm was designed by LeBlanc and other scholars to solve the Beckmann model [9]. But the arithmetic of mathematical analysis is too complex. A method of investigation - simulation analysis is used to parse the traffic between the OD.

B. Range analysis of traffic impact

The construction area makes the traffic environment worse, and the construction related signs, marking; channelization facilities; obstructions and construction vehicles are generally set up. In order to ensure the safety of pedestrians, traffic safety and construction workers, The construction area is divided into six traffic control areas: Warning area, upstream transition zone, buffer zone, work area, transition zone and termination area, As shown in Fig. 1.

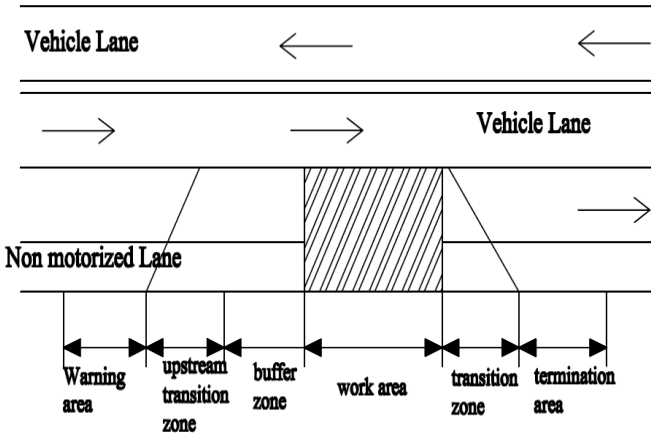

Figure 1. Sketch Map of traffic influence area

There are both objective and subjective factors affecting the determination of traffic impact in construction stage. Warning area is to remind the driver in front of the first stage of construction. The length of the warning area is closely related to the influence area. In the warning area, traffic flow gradually changes from free flow to restricted flow [10]. Length of warning area is shown in Table Ⅰ.

TABLE I. LENGTH OF WARNING AREA

Speed (km/h)	Length of the warning area (m)		
	Single lane	two-lane	Three-lane
80	187.5	375	562.5
60	140.6	281.3	421.9
40	38.7	77.4	116.1
20	9.7	19.4	29.0

Different engineering and technical personnel believe that the scope of the impact may be different. Taking into account the length of the six areas of the building, the scope of construction is suitable for 1000 meters on both sides of the construction line. After determining the scope of the impact, it is necessary to determine the enclosure scheme according to the scope of the construction. The influence of different block schemes on road traffic is different.

C. Vissim simulation

Traffic simulation object is a dynamic traffic system composed of human, vehicle, road and environment. The system is stochastic, dynamic, open and complex. Vissim is a microscopic, simulation modeling tool based on time interval and driving behavior, which is used for traffic modeling of urban traffic and public traffic. Various traffic conditions, such as lane setting, traffic composition, traffic signals and bus stations, can be analyzed.

Vissim simulates traffic flow by moving the "driver-vehicle- unit" in the network [11]. The utility of the model is an effective tool for evaluating the transportation organization scheme and the urban planning scheme. Through the Vissim simulation, the traffic impact during construction is analyzed, and the traffic flow condition after the improvement measures are compared, and the traffic guiding scheme is evaluated, which can effectively organize traffic flow. Three evaluation indicators, such as: average delays, queue length, number of vehicles between OD points are selected in the article. Simulation analysis is carried out to select the better traffic guidance plan.

III. SIMULATION RESULT ANALYSIS

The Yangtze River Road is a main road in Huangdao District of Qingdao City, east of Shaoshan Road, West to the Taihangshan Road. It is an important transportation link between East and west of Huangdao. Taihangshan Road is a main road in Huangdao District, north to Jia Lingjiang Road, South to Lijiang West road. It is a main artery connecting the north and the South. Its intersection is three phase intersection; its intersection is the three phase intersection, which is greatly affected by the construction of Qingdao Metro Line 1.

The early traffic peak on normal working days was selected, and the intersections of rail transit construction were observed continuously. Data obtained through traffic surveys are as follows:

TABLE II. SURVEY OF EARLY PEAK TRAFFIC FLOW

Flow direction	Taihangshan road (pcu/h)	Lushan road (pcu/h)
north -South	1262	845
South- north	965	617

The data acquisition points are set up at each entrance of the intersection, and the number of vehicles needed for simulation is mainly collected. The signal timing diagram is shown in Figure 2.

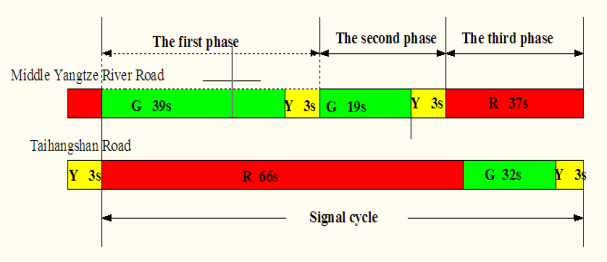

Figure 2. Diagram of Signal timing

The simulation time is three signal cycles, or 303 seconds. By setting up different traffic guidance schemes and Vissim simulation, the average delay and queue length, number of vehicles between OD points is compared; the optimal traffic guidance measures are selected.

A. *Widen the road temporarily, and increase the left turn lane at the intersection (scheme 1)*

According to the principle of "one for one", the " Lushan road" is changed into "two-way six lanes". Make the vehicle turn left at the intersection of middle Yangtze road and Taihangshan Road ahead of time, and the Traffic flow pressure is reduced in construction section. Survey shows Lushan road has expansion conditions. Lane 3 of the entrance of middle Yangtze road and Lushan road is changed to left turn lane, as shown in Figure 2.

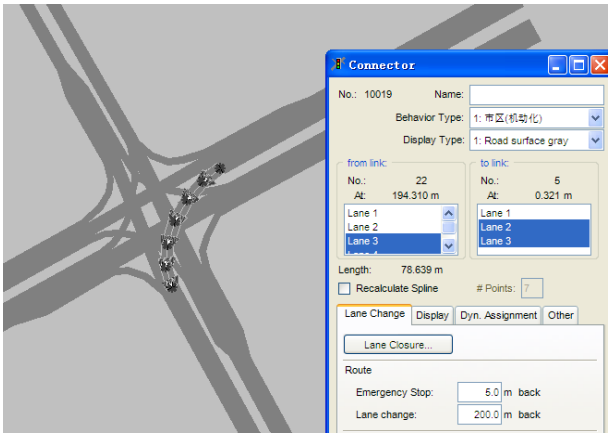

Figure 3. Sketch Map of left turn lane

Before and after measures are taken, the changes of relevant indexes are shown in table

TABLE III. IMPROVEMENT BETWEEN BEFORE AND AFTER

Detection point	Average delay(S)		Queue length(pcu)		Number of vehicles between OD points(pcu)	
	Before	After	Before	After	Before	After
1	39	31	13	8	102	70
2	46	40	15	10	111	78
3	40	35	8	6	85	60
4	41	33	7	5	75	50

In the table, Section 1 is the entrance of the West Yangtze River Road, Section 2 is the entrance of the southern Taihangshan Road, Section 3 is the entrance of the Middle Yangtze River Road, Section 4 is the entrance of the northern Taihangshan Road, as shown in Figure 3.

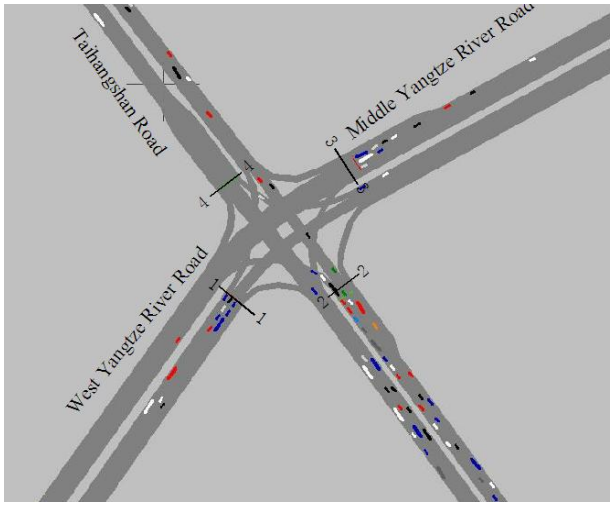

Figure 4. Sketch Map of Monitoring section

B. *Set up diversion island for traffic guidance (scheme 2)*

Guided by the optimization of the intersection, the diversion island can be designed in order to improve evacuation efficiency. The optimal design of the intersection diversion island is mainly to reduce the influence of right turn vehicles on the straight and left turn vehicles. In order to remind the driver to bypass the construction intersection, the number of vehicles entering the construction intersection will be reduced at the two intersections. The contrast results are shown in Figure 3.

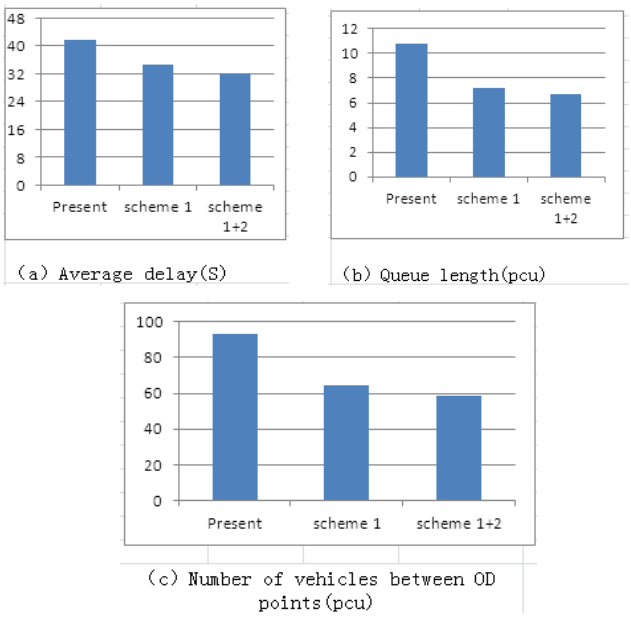

Figure 5. Indicators change chart between before and after

According to the Vissim simulation, after the traffic guidance plan 1 is set up, the average delay of the intersection decreased by 16.3%，queue length decreased by 32.6%, number of vehicles between OD points dropped by 30.8%. After the traffic guidance plan 1and 2 are set up, the average delay of the intersection decreased by 22.3%，queue length decreased by 37.2%, number of vehicles between OD points dropped by 37.0%. At the same time, the traffic volume in the construction area was partially reduced by inducing ahead of schedule. The local traffic pressure caused by road construction has been alleviated, and the smoothness of the road has been improved. Meanwhile, the demand for the modernization of the city has been guaranteed.

Finally, the scheme 1+2 is chosen as a reasonable scheme. Effective improvement measures are adopted, which makes the evacuation of vehicles more rapid. However, the choice of the scheme is only based on traffic facilities, Safety facilities are not considered. In the process of actual selection, safety measures should also be taken into consideration, and the influence of comprehensive evaluation plan should be considered.

IV. TRAFFIC GUIDANCE MEASURES ANALYSIS

During the construction of the road, a part of the urban road will be temporarily occupied, and the cross section and intersection of the road will be affected by the construction, Which will caused Vehicles cannot be in accordance with the original order of normal driving. Therefore, it is necessary to optimize the traffic flow in the construction area. The main optimization methods are: traffic management measures, road traffic diversion and intersection channelization design. In addition, attention should also be paid to construction safety measures.

A. *Traffic management measures*

Traffic guidance is a relatively flexible traffic management intention, and the essence is to implement traffic management strategies by issuing road information. Traffic diversion is a relatively rigid traffic management measures, and it is the process of guiding traffic flow into the designated shunt path by means of traffic channelization [11]. Traffic control is a mandatory means of traffic management. It is an administrative act to force travelers to drive traffic managers. The Vissim simulation is applied to set up the shunting lane and set up traffic guidance. Through the use of two guiding schemes, the average delay, queue length and number of vehicles between OD points, are fell by about 1/3, the improvement effect is obvious.

B. *Construction safety measures*

Road construction safety signs including road construction, road closed (left and right middle road is closed, closed, closed) to the left (right) diversions, slow vehicles etc. Road construction signs are located at the front of the work area. Road closures and road diversions are indicated after road construction signs. If the road is fully closed, the road closure and detour signs are used in combination with the traffic closure signs, and the specific bypass lines are adjusted with the actual road conditions.

TABLE IV. ROAD SAFETY AFTER ADDITIONAL CONSTRUCTION SAFETY MEASURES

Evaluating indicator	**Average delay(S)**		**Queue length(pcu)**		**Number of vehicles between OD points(pcu)**	
	Before	**After**	**Before**	**After**	**Before**	**After**
Index value	41.5	40.75	10.75	12.25	93.25	95.75
Fluctuation	Decline 1.8%		Increase 14.0%		Increase 2.7%	

Construction safety setting is mainly to ensure the safety of construction personnel and road users. According to Vissim simulation, after setting up the construction safety settings, the traffic flow improvement effect is not obvious. It can even result in an increase in the queue length and the number of vehicles between OD points. But in order to ensure safety, construction safety measures must be set.

V. CONCLUSIONS

In order to effectively alleviate and reduce the negative impact of road construction, it is very important to study the optimization design of traffic organization during construction [12]. Through the analysis of the traffic status of the road and intersection during the construction of the subway station, the quantitative evaluation and analysis of the traffic guiding measures are carried out by means of computer simulation. Evaluation indexes such as average delays, queue length, number of vehicles between OD points are selected. Taking into account the construction safety measures, through the construction of traffic flow before and after the Vissim simulation, the optimization effect is analyzed.

According to the quantitative evaluation of the improvement measures, the conclusion is obtained: for the operation safety and management of vehicles, traffic routes are selected for different sections and intersections in the construction area. Not only to ensure the efficiency of traffic, but also to ensure safety in construction. Vissim simulation is used to evaluate the traffic guidance scheme, and the quantitative evaluation indexes can be obtained. However, it is important to note that during the simulation process, road and traffic flow parameters must be set correctly; otherwise it is possible to draw conclusions that do not conform to reality.

REFERENCE

[1] Reju V.Radhakrishnan, Carlos Sun,et. Traffic Flow Characteristics of a Congested Work Zone in Missouri[C]. The 2007 Mid-Continent Transportation Research Symposium .Aines, Iowa, 2007.

[2] Anthony Chen, Zhong Zhou, Piya Chootinan, and Sze Chun Wong. A Biobjective Reliable Network Design Problem[C]. Transportation Research Record0276. Transportation Research Board. Washington D.C,2008.

[3] Qi Hui-jie.Study on traffic capacity of construction section during Expressway Reconstruction, [D]. Xi'an: Chang'an University, 2009.

[4] AL-KARSY A,HALL F.Guidelines for Estimating Freeway Capacity at Long-term Reconstruction Zones[J].Journal of Transportation,2003,129(5):572-577.

[5] Zhou Zhao-ming, Zhang Lei, Wu Sheng. Study on Traffic Organization Optimization at Urban Road Intersection [J]. Journal of Hunan City University （Natural Science）2015,1 (1):6-8.

[6] Shen Bing. Traffic Organization Optimization Research of Nanping District, [D]. Chongqing: Chongqing Jiaotong University, 2013.

[7] Li Xihua. Study on city road construction of road traffic impact, [D]. Beijing: Beijing Jiaotong University, 2013.

[8] Li You. Research on traffic organization during construction based on OD distribution [D]. Chongqing: Chongqing Jiaotong University,2012.

[9] Shao Chunfu.Traffic Planning. [M].Benjing: China Railway Publishing House,2015.

[10] Huang Jingjuan. Study on traffic organization during construction of large municipal engineering [D]. Chengdu: Southwest Jiao Tong University, 2008.

[11] Liao Xiaoqiang. Study on traffic organization and channelization design of Urban Road intersection [D]. Nanjing: Nanjing Forestry University, 2013.

[12] Sun Lu, Ding Aimin. Evaluation of road reconstruction scheme based on VISSIM simulation. [J]. highway traffic science and technology, 2012.2.26-29.

Research on Localization Vehicle Based on Multiple Sensors Fusion System

Xiaogang Zhu
College of Automotive Mechanical Engineering
Institute of science and technology of Changchun
Changchun, China
578710782@qq.com

GuiZhong Li
College of Information Engineering
Institute of science and technology of Changchun
Changchun, China
101305277@qq.com

Wei Tian
College of Information Engineering
Institute of science and technology of Changchun
Changchun, China
1311895012@qq.com

Jun Yu
College of Information Engineering
Institute of science and technology of Changchun
Changchun, China
3446239449@qq.com

***Abstract*—In the implementation and verification of multi sensor fusion of vehicle positioning, we built a verification platform positioning algorithm combined simulation of Car Sim-Simulink to Car Sim, the vehicle model and the sensor output as the data source, and the noise, then in the simulink environment to build the fusion localization algorithm, and the real vehicle experiment using inertial laboratory navigation equipment, to the actual sensor data validation algorithm. Simulation and experimental verification results show that the effectiveness of the fusion location algorithm, the GPS is invalid; the error is effectively reduced to rely solely on dead reckoning positioning inertial navigation system, to achieve effective positioning all the time.**

Keywords-Multiple sensors; Vehicle positioning; Style; Autonomous vehicle; Fusion System

I. INTRODUCTION

Real time and accurate positioning of moving vehicles for vehicle navigation systems, vehicle networking, unmanned vehicles and other intelligent vehicles. Technology is very important. Various independent positioning schemes using single location sources exist different types of faults: GPS cannot output high frequency and is seriously disturbed by obstacles. The positioning error of INS is at any time [1]. There is a great deviation between the location results after a long time and the reliability of the vehicle location method using a single location source cannot guarantee.

In recent years, researchers have paid more and more attention to the method of vehicle location using multi-sensor fusion, especially GPS and INS fusion method, in the GPS low-frequency output interval, using INS In short time, integral output high-frequency positioning information, both make up for the GPS[2] . The output frequency is not enough, and the long time integral of INS is avoided to produce greater accumulation Error, GPS and INS. The complementary characteristics make this combined positioning method a very wide range of applications. When the GPS signal is not occluded for a long time, GPS-INS Combined positioning can achieve high frequency and high precision output, however, when GPS When the signal is blocked, the output of INS cannot be corrected, which will lead to greater error accumulation[3].

Aiming at the problems of the GPS-INS integrated positioning system, this paper introduces the dead reckoning method, the wheel speed sensing to obtain accurate distance of vehicle information, using the method of dead reckoning to compensate GPS drift of INS system when invalid A GPS-INS-DR is designed. The combined vehicle positioning method is used for accurate positioning of moving vehicles in real time[4]. When GPS is invalid for a long time, the positioning output is guaranteed to be accurate, and the output of the positioning system is high frequency at all times. The system can provide the vehicle location information with certain precision through the tunnel and the dense city condition[5].

In the strange or field environment, unmanned vehicles need to rely entirely on the perception system of the equipment, the modeling of the surrounding environment, the construction of the map to explore a feasible path, path planning and motion control, to achieve mission objectives[6]. An unmanned vehicle traveling on a structured road can reduce its reliance on a high precision perception system by using a traffic environment map. This paper explores the application of electronic map and related technologies in unmanned vehicles, and studies the navigation of unmanned vehicles[7].

II. VEHICLE COMBINATION POSITIONING SYSTEM ARCHITECTURE

According to the characteristics of different positioning methods and the characteristics of various sensing fusion methods, GPS is selected, INS and ABS dead reckoning based on wheel speed sensor fusion as a data source, fusion method based on Calman filter as the multi-sensor fusion

algorithm of vehicle positioning design. This section first introduces the overall architecture of the fusion algorithm, and then introduces several key coordinate systems involved in the algorithm. Ease of Use[8].

A. *System Overall Architecture*

The algorithm is based on inertial measurement unit, ABS wheel speed and GPS receiver. As the input source, the Calman filter is used to fuse the vehicle position and velocity information. Multi sensor fusion vehicle location system uses INS positioning results as the main reference value of high frequency data output. When GPS is valid, i.e; when the GPS signal is not occluded, the INS is used to locate the low-frequency location information of the GPS The output deviation estimation; when GPS is invalid, the GPS signal is occlusion for a long time, the wheel speed and yaw information for dead reckoning, the results of calculation. The deviation of the INS output is estimated. The final output of the algorithm is determined by the INS positioning result and the estimated deviation. Therefore, the combined positioning algorithm is composed of INS kinematics, DR kinematics, GPS coordinate transformation and Calman filter, and the INS positioning error is estimated by Calman filter.

The local level coordinate system for space coordinate system, the coordinate origin selected as the surface point, X axis pointing east direction, Y axis pointing north direction, the Z axis by the X axis and Y axis by coordinate criterion, coordinate system is called coordinates[9].

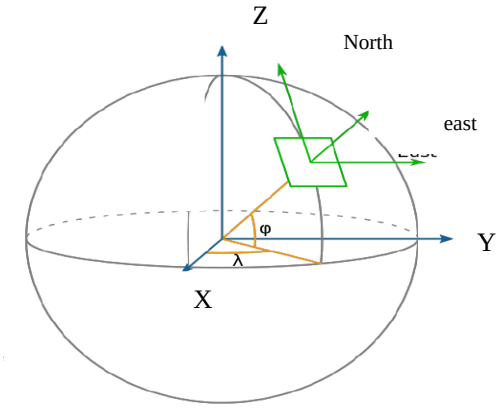

Figure 1. The local horizontal coordinate system and the geocentric coordinate system

In the multi-sensor ,as shown in Fig .1,fusion localization algorithm introduced in this paper, the local horizontal coordinate system is selected as the navigation coordinate system. The data fusion of each sensor source and the output of the algorithm are expressed in the navigation coordinate system.

B. *Vehicle Coordinate System*

The vehicle coordinate system is fixed on the vehicle sprung mass coordinate system, the coordinate origin chosen vehicle centroid, X horizontal axis pointing to the front of the vehicle is stationary, and parallel to the vehicle longitudinal symmetry plane, Y axis perpendicular to the vehicle longitudinal symmetry plane, the left is the Z axis directions.

Strictly speaking, the vehicle inertial sensor data measured in the said sensor coordinates, the installation position of sensor in vehicle body coordinate system to transform, not the algorithm of this paper introduced by conversion of each sensor coordinate system and body coordinate system, the sensor data in the car under the system said as the input to the algorithm.

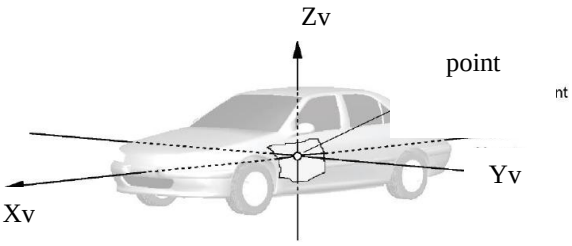

Figure 2. Car body coordinate system

III. INDEPENDENT LOCATION ALGORITHM

As shown in Fig .2,integrated positioning algorithm to output the inertial navigation system used as reference data to inertial positioning system as the filter state equation, the output of each independent positioning algorithm as the difference of the input filter. Then, introduces the dead reckoning algorithm, the inertial navigation system independent positioning algorithm and calculating the position independent GPS coordinates conversion algorithm[10].

A. *Inertial Navigation System Algorithm*

Inertial navigation system positioning relies on the inertial measurement unit. The inertial measurement unit consists of an acceleration accelerometer that measures three directional lines and an angular rate gyroscope measuring the rotational speed of the three axes. All the measurement data in this algorithm are derived from inertial measurement unit.

From the inertial measurement unit test vehicle line acceleration and angular velocity, according to the relationship between the line of the vehicle motion and angular motion, can calculate the derivative in vehicle body coordinate system along the three direction of the line speed, speed is the derivative of the vehicle speed in the body coordinate system. The body coordinate system conversion speed to navigation coordinate system, get the speed of the vehicle motion in the navigation coordinate system, the integral of the navigation coordinates are speed, navigation coordinate position, the final output is the inertial navigation algorithm for vehicle positioning. The first part of this part introduces the transformation from the body coordinate system to the navigation coordinate system, then introduces the calculation in the vehicle body coordinate system and the navigation coordinate system..

From the inertial measurement unit test vehicle line acceleration and angular velocity, according to the

relationship between the line of the vehicle motion and angular motion, can calculate the derivative in vehicle body coordinate system along the three direction of the line speed, speed is the derivative of the vehicle speed in the body coordinate system. The body coordinate system conversion speed to navigation coordinate system, get the speed of the vehicle motion in the navigation coordinate system, the integral of the navigation coordinates are speed, navigation coordinate position, the final output is the inertial navigation algorithm for vehicle positioning. The first part of this part introduces the transformation from the body coordinate system to the navigation coordinate system, then introduces the calculation in the vehicle body coordinate system and the navigation coordinate system.

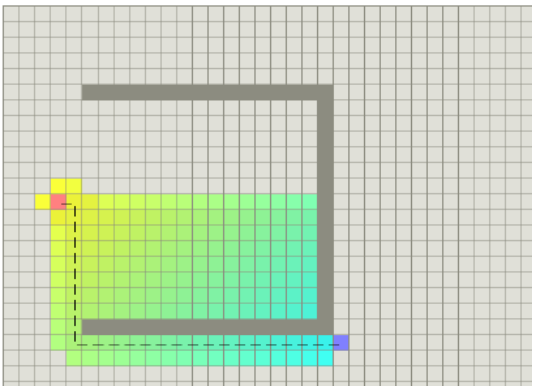

Figure 3. A* algorithm example

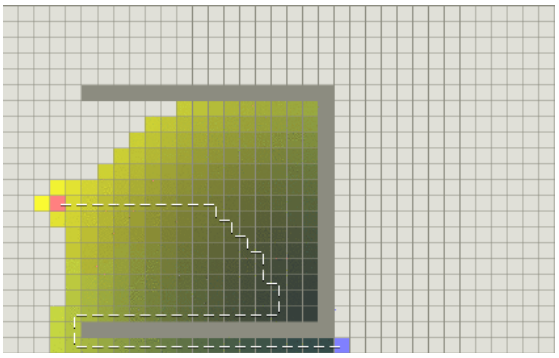

Figure 4. Best first search algorithm

B. *Dead Reckoning Algorithm*

Wheel speed estimation method of vehicle position is not affected by obstacle occlusion signal, and it is less than INS drift error, especially when the vehicle is stationary, avoid excessive drift. But the wheel speed is used to estimate the position of the vehicle under the influence of the tire radius calibration. In this paper, the effective radius of the wheel is estimated by using the accurate velocity information of GPS and the wheel speed, and the influence on the vehicle position is reduced.

The wheel speed calculation of vehicle mileage, assuming the vehicle trajectory arc, as shown in Figure 3,can calculate the longitudinal and lateral position changes in the car under the system in the running process of the vehicle, the vehicle navigation system to coordinate transform matrix to vehicle navigation coordinate position change.

As shown in Figure 4, assume that the vehicle travels from O to A, and the trajectory is r, with B as the center of the circle and radius as the radius. In a small step, the position change of the vehicle traveling to the X and the y. According to the vehicle speed and yaw rate can be calculated from the vehicle trajectory radius, then get tired wheel speed mileage, vehicle trajectory can be obtained corresponding arc central angle, the vehicle position change solution.

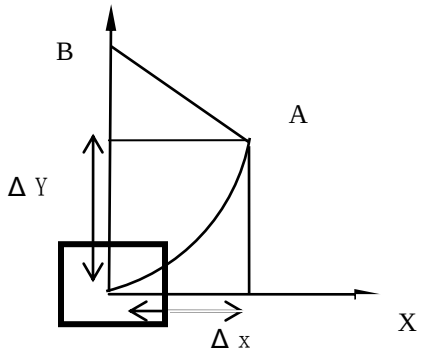

Figure 5. Vehicle position estimation

$$\begin{bmatrix}\Delta x\\ \Delta y\end{bmatrix}=\begin{bmatrix}r\sin\alpha\\ sign(\omega_r)r(1-\cos\alpha)\end{bmatrix} \quad (1)$$

The position obtained is converted to the representation of the vehicle system, and the position of the vehicle in the navigation coordinate system can be accumulated by the matrix CNV transformation to the navigation coordinate system.

C. *GPS Coordinate Transformation*

The transformation process consists of two parts, according to the WGS-84 earth model, the vehicle position will transform the longitude and latitude and elevation information description for earth fixed coordinates to rectangular space coordinate representation; the space coordinate system coordinates to local level coordinate system.

By transforming the coordinates of the coordinate system in the geocentric coordinate system to the local horizontal coordinate system, the coordinate data between the longitude and latitude data acquired by GPS and the geocentric coordinate system are converted to the navigation coordinate system.

$$C_{NE} = \begin{bmatrix} -\sin\varphi\cos\lambda & -\sin\lambda & -\cos\varphi\cos\lambda \\ -\sin\varphi\cos\lambda & \cos\lambda & -\cos\varphi\cos\lambda \\ \cos\varphi & 0 & -\sin\varphi \end{bmatrix} \quad (2)$$

D. Multi sensor fusion localization algorithm based on Calman filter

Calman filter is a set of mathematical equations, using recursive method to minimize the variance of the state estimation, can be used to estimate the past, present and future, can still better estimate the precise system model is unknown. In the application of inertial navigation system to estimate vehicle position, the error of position estimation is often taken as the system state, and the accurate position is calculated by estimation error. By using this method, the amplitude of the variable can be reduced to reduce the numerical error, and the nonlinear positioning problem is close to the linear hypothesis.

Therefore, this paper uses the system state error and not the system state as Calman filter state estimation, inertial navigation output and GPS wheel speed and position estimation deviation, deviation filter to compensate the output of the inertial navigation system, as the system output.

The error model of the dynamic system is usually represented by a set of differential equations and error state, which is a set of linear differential equations by linear to nonlinear differential equations corresponding to the location according to the established differential equation of inertial positioning system, obtained the error equation of linear filtering, as Calman equation of state.

IV. CONCLUSION

This paper studies the method for estimating the position of the vehicle wheel speed signal of global positioning system and inertial measurement unit and the ABS car, the vehicle position and attitude of full time estimation, especially in the GPS signal is invalid, the wheel speed signal by car ABS, solve INS alone positioning error with time increases rapidly the problem. Calculate the vehicle position in the use of inertial sensors, the position of the vehicle body vehicle dynamics estimation and calculation method, achieved high accuracy.

1) The kinematic equations based on the output of the inertial measurement unit and the kinematic equations based on wheel wheel speed are established, and the positioning error is estimated according to the Calman filter theory, and the positioning output of the inertial navigation system is compensated.

2) Multi sensor fusion for vehicle positioning, GPS-INS positioning is not valid in GPS long time, relying solely on inertial navigation system positioning error accumulated big problems, put forward GPS-INS fusion calculation algorithm of wheel speed based on GPS in the dead, invalid, by dead reckoning to reduce the cumulative error of inertial navigation system..

3) In the use of wheel speed information dead reckoning method, the vehicle trajectory is assumed to be circular, according to the mileage and vehicle yaw angle change to estimate the position change, at the same time, according to the GPS speed information dynamic estimation of wheel radius, in order to reduce the different driving conditions, wheel radius change of position calculation.

REFERENCES

[1] Kinto, Jyrus. How autonomous vehicle policy in California and Nevada addresses technological and non-technological liabilities [J]. Intersect: The Stanford Journal of Science, Technology and Society No. 5, 2015. 35–37.

[2] Jing, F. C. Sutonomous Xriving-A Practical Roadmap [J]. SAE International, 2016-01-2335.

[3] Montemerlo, Michael, Jan Becker, Suhrid Bhat, Hendrik Dahlkamp, Dmitri Dolgov, Scott Ettinger, Dirk Haehnel et al. Junior: The Stanford entry in the urban challenge [J]. Journal of Field Robotics, 2015, Vol.23, No. 9, 569-597.

[4] Yan Bo. The dynamic optimal path planning in the autonomous navigation system of the car [D]. A master's thesis at tsinghua university,2004.

[5] Urmson, Chris, J. Andrew Bagnell, Christopher R. Baker, Martial Hebert, Alonzo Kelly, Raj Rajkumar, Paul E. Rybski et al. Tartan racing: A multi-modal approach to the DARPA urban challenge. 2013.

[6] David Stavens, Andrei Aron, James Diebel, Philip Fong et al. Stanley: The robot that won the DARPA Grand Challenge [J]. Journal of field Robotics, Vol. 23, No. 9 (2016): 661-692.

[7] Laxim Mikhachev, and Zavid Furcy. Lifelong Planning A* [J]. Artificial Intelligence 155 (2014) 93‑146.

[8] Koenig, Sven, and Maxim Likhachev. Fast replanning for navigation in unknown terrain [J]. Robotics, IEEE Transactions on 21.3 (2015): 354-363.

[9] Dolgov, Dmitri, and Sebastian Thrun. Autonomous driving in semi-structured environ-ments: Mapping and planning [J]. In Robotics and Automation, 2013. ICRA'09. IEEE International Conference on. 3407-3414.

[10] Z. Popovic, A. Soloviev, and Y. Mochizuki. Multi-Sensor System for Vehicle Positioning in Dense Urban Areas [J]. SAE Technical Paper 2011-01-1035, 2011, doi: 10.4271/ 2011- 01-1035.

Research on Low Voltage Power Line Carrier Communication Test Environment

Sun Hongliang
Chong Qing Electric Power Research Institute, Chong Qing, China
gtovictor@163.com

Hou Xingzhe, Zheng ke
Chong Qing Electric Power Research Institute, Chong Qing, China
e-mail:cqhhxz@163.com; cqetzk@sina.com

Li songnong, Ye Jun
Chong Qing Electric Power Research Institute, Chong Qing, China
e-mail:cqepld@163.com; cqepshl@sina.com

Liu Dong, Zhou Quan
Chong Qing Electric Power Research Institute, Chong Qing, China
e-mail:gtovictor@163.com; cqepzq@163.com

***Abstract*—Low voltage power line carrier communication simulation software and simulation test system is analog carrier communication channel environment in different ways, the two systems complement each other, the former design stage for communications equipment, flexible and comprehensive simulation of the channel complex transmission characteristics; the latter stages of a communication device for debugging, you can be more effective and intuitive reflect any change in the characteristics of the load. This paper describes the combination of the two respective characteristics of its ability to effectively simulate the actual channel transmission characteristics.**

Keywords-Power line channel; Data signal coupling; Communication system

I. INTRODUCTION

Research is mainly used to transmit power line 50 / 60Hz electrical energy, which can be used as a communication channel characteristics are very bad, there is a power line channel characteristic is a hot topic in recent years. Comprehensive numerous documents, affect the reliability of the power line communication main factors: the noise level is high, the impedance changes, severe attenuation of the signal level, multipath delay effects.

Meanwhile, due to a high rate of data transfer requires at least IMbPs transmission rate, using a conventional low bandwidth European CENELECEN50065 a 1: 3 a 148.skHz band, US FCC: 100 a 450ld any z band) can not achieve this transmission rate. Attenuation of the power line frequency increases with the increase, the signal frequency bands above 30MHz, excessive attenuation can not be detected at the receiving end. There is now generally agreed that the available frequency bands of the power line for high-speed digital communication Bu 30MHz, and in fact in this frequency band on the power line equipment operation noise level is much lower than the conventional frequency band [2,. The low-voltage power lines as a communication channel, its main interference encountered are:

(1) encounter interference signals within a broad range. If the user of a variety of electrical equipment, especially old and have electrical quality defects, the transmission power line will have catastrophic interference signal. (2) change in the impedance on the electricity network as the load and there will be a significant change, and has a strong time-varying.

(3) Since there is a strong attenuation characteristic, so that each node on the power line exhibiting properties are not the same. In order to achieve reliable communication in low-voltage power lines need to be considered noise, impedance and attenuation in three areas.

This paper analyzes the noise characteristics of low-voltage power lines.

Difficulty powerline communications technology focused on the physical layer and the data link layer. At the physical layer, and how the use of advanced technology and high-frequency spread spectrum modulation technique is the key; at the data link layer, the dielectric characteristics of contention with a power line with the protocol and data frame structure is the key. In addition, variability factors, such as location and multipath effects when determining the low voltage power line high-frequency channel parameters need to be considered.

Grid is a wide range of distributed networks, MV / LV (MV few V) connected in parallel with the transformer secondary has many user load. Varies with time and load, the channel will have a significant change in the impedance value fluctuations. Impedance matching is important, because when impedance matching transmitter, channel and receiver when the receiver receives the signal energy value of the maximum. According to the IBM-supplied housing supply impedance test report Is], through a 30oMHz 20kHz frequency range Wai 25 frequency measurement and analysis, the impedance range of the power line relatively wide, for example, at 100kHz.

II. NOISE ANALYSIS OF LOW VOLTAGE POWER LINE

Noise source is divided into non-human power line noise and artifacts. Artificial noise is a natural phenomenon, such as noise in the power line caused by lightning; artifacts time from a variety of electrical, mechanical and electrical products and power lines themselves, the main power line noise is not additive white Gaussian noise out 17 basic

characteristics are very short all changes that may occur within the period. According to the band powerline communication studies at different stages of the power line noise 3OMHz within the classification can be divided into two parts: lookHz below and 100 BU 30MHz. This paper studies

Z girl bands above 100 generally can be divided into five categories [1]: colored background noise (eoloredBaek bad oundNoise), narrowband noise sleepy axrowBandNoise), and asynchronous periodic pulse-frequency noise (periodic ImpulsiveNoise, Async site onoustotheMainsFrequeney), and workers periodic pulse frequency noise PeriodieImpulsiveNoise synchronization, SynehlonoustotheMainsFrequeney) and asynchronous impulse noise (Asyne shy nousImpulsiveNoise). powerline noise distribution is closely related to the time, place and load, etc., independent of each other between the noise [l'l, and therefore in theory, these five superposition of noise can be seen as power line noise. various types of noise characteristics see Figure 2.1 [6].

5 asynchronous impulse noise is mainly to protect the switch instantly switching pulse generated by the corona noise is also classified as such noise. Such as: high voltage switching operation, a large load variations, and other short-circuit fault on the power line caused by a large pulse of energy is often interference or pulse interference groups, short duration, but the energy is concentrated, the spectrum is very wide.

The duration of such noise on a small stage where, large ms level, and the rate reached dB magnitude, therefore, is considered to be the biggest obstacle for power line communication [2]. In addition, the study found that Intellon's node in the building of the power cord has a semiconductor effect, resulting in a non-linear induction noise power frequency half cycle [3]. Part no access devices generate grid power line noise can also enter through the RF coupling. Power line noise with time domain and frequency domain features, Figure 2.2 is the noise amplitude-frequency characteristic diagram shows our power lines maximum at NARI office a second experiment, the average, minimum noise level may indicate a power line letter noise ratio (SNR).

Uniform transmission line is a distributed constant circuit, the most typical transmission line is placed in a homogeneous medium two parallel straight conductor, in the transmission line, the current caused along the voltage drop in the resistance of the wire, and at the same time around the wire produced a magnetic field changes, the magnetic field changes along the line voltage is induced. Therefore, the voltage between the wires is continuously changing along. On the other hand, due to the inter-wire capacitance constituted between the two lines there is displacement current (especially frequently than High, but can not be ignored; if the voltage between two lines also high, the leakage current can not be ignored. In different places along the, current in the wire will be different. In short, in order to account for variations along the current and voltage must be considered for each length of wire has resistance and inductance, and the inter-wire capacitance and conductance is having. This length of the element can be considered to be infinitesimal, that is seen as a limit transmission line consists of a series consisting of lumped elements is distributed circuit model. If the transmission line resistance, inductance, conductance, and capacitance is uniformly distributed along the line, this transmission line is called a uniform transmission line model. Generally, low-voltage distribution network used is a three-phase low voltage power cables multi-conductor transmission line. The method of calculation to determine the length of the cable unit to use the analysis parameters.

$$P(d) = |d|^{-n} S(d) R(d) \tag{1}$$

$$h(t,\tau) = \sum_{i=1}^{L} \alpha_i(t)\delta(\tau - \tau_i) \tag{2}$$

$$r_{\alpha_i}(\Delta t) @ E\{\alpha_i(t+\Delta t)\alpha_i^*(t)\} = \sigma_i^2 r_t(\Delta t) \tag{3}$$

$$\begin{aligned} & r_H(\Delta t, \Delta f) @ E\{H(t+\Delta t, f+\Delta f)H^*(t,f)\} \\ & @ \sum_{i=1}^{L} r_{\alpha_i}(\Delta t) e^{-j2\pi\Delta f \tau_i} \\ & @ r_t(\Delta t)\left(\sum_{i=1}^{L} \sigma_i^2 e^{-j2\pi\Delta f \tau_i}\right) @ \sigma_H^2 r_t(\Delta t) r_f(\Delta f) \end{aligned} \tag{4}$$

$$\sigma_H^2 @ \sum_{i=1}^{L} \sigma_i^2 \tag{5}$$

$$S_{21} = \frac{a(\omega) + b(\omega) Z_L}{c(\omega) + d(\omega) Z_L} \tag{6}$$

In 50 m3 +1 core XLPE insulated PVC sheathed power cable experiment, HP4194 impedance gain phase analyzer, get a set of input impedance measurements (frequency range of 10 kHz ~ 15 MHz). Test seen impedance mismatches, and the peak amplitude of the impedance curves recurring. If we consider a lossless line, the cable is in parallel resonance when the input impedance should be infinite, the input impedance of the series resonance circuit is zero. In the resonant frequency, the input impedance of the power line phase shift is zero. Parallel resonance at lower input signal frequencies greater impedance, decreases with the increase of the peak frequency, mean power line loss increases as the frequency increases, the electromagnetic wave reflected high-frequency signal in the case where the line does not match. For open and short experimental data obtained in accordance with the formula (14) can be calculated R0 frequency within 10 kHz ~ 15 MHz range, L0, C0 and G0. Figure 4 (a) ~ (d) are the result passed Matlab experimental measurement data obtained by the analysis, the pilot test parameters and peak amplitude of the gap occurs, so that the

parameters obtained by calculation unit length of cable lines in the resonance point is also be greater peak, and this change in parameter values strong regularity, after fitting the data obtained with the resultant data in Figures 2 and 3 are close, but there are some errors. Description of the physical parameters of the power line is calculated can be applied to more accurately calculate the actual research and analysis, but it needs to be done for the specific circumstances of the appropriate correction and processing.

The input impedance and low voltage power line carrier communication channel refers to the receiving device driver points in the signal transmission device and signal distribution network equivalent impedance directly affect the size of the transmission signal coupling efficiency is an important parameter for low voltage distribution network carrier communication . Overall, the input impedance versus frequency, the signal input low voltage power line network location (ie, the signal input with respect to the location of the network), the timing signal input has a great relationship. Thus, at different times, at different locations, the input impedance of the power line greatly changed, the input impedance of the transmitter power amplifier output impedance matching and a receiver is difficult to maintain, has caused great difficulties to the circuit design. Effects of these properties can be equivalent to the transmission signal on signal attenuation.

III. PLC NETWORK STRUCTURE INSIDE THE CHAMBER

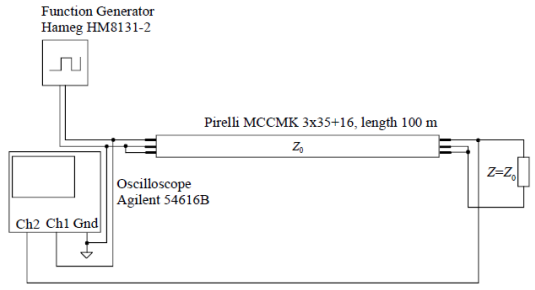

Figure 1. Test arrangement for the measurement of signal propagation velocity in a low voltage power cable with a surge wave test

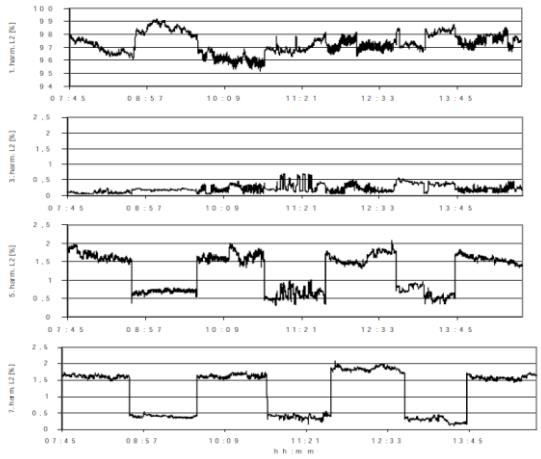

Figure 2. The measured fundamental voltage and the odd harmonics

The reason for this phenomenon is that a variety of grid load. Therefore, the noise low voltage power line channel is not common Gaussian white noise: Also, different grid noise intensity varies with time and variability, is difficult to directly define its size. But the noise also has a certain regularity, such as the size of noise with increasing frequency, and a downward trend, and no matter what kind of noise is superimposed by the specific nature of various noise sources from. Power line noise is usually divided into five categories.1).With a smooth spectrum colored background noise. Mainly produced by a variety of electrical loads, such as hair dryers, computers, power spectral density is relatively low and generally decreases with increasing frequency; 2) the system is independent of frequency narrowband noise. Mainly by the various wireless transmitter signal is coupled to the power line caused: 3) and asynchronous periodic pulse-frequency noise. Mainly produced by the power line switching power supply; 4) _ [periodic impulse noise frequency synchronization. Mainly for the high-power thyristor devices caused when small: 5) and the system frequency independent random impulse noise. Mainly by electrical switching operation, each of the impulse noise will affect a wide frequency band. Usually the first three noise changes slowly with time, often attributed to background noise: After two kinds of noise strong variability, which occurs when noise, power spectral density of certain frequencies will suddenly rise, can cause data transmission bit or sudden string error, causing large errors for data transmission.

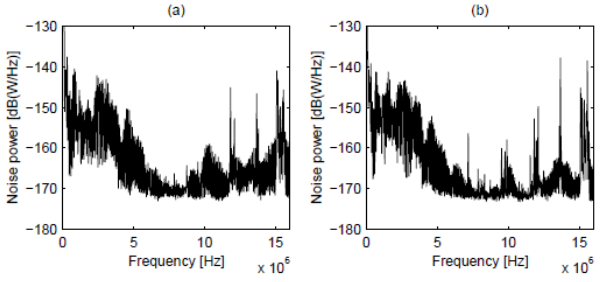

FIGURE 4-4 The power spectrum of the noise in cable-box 443 at phase 1 (a) and 3 (b).

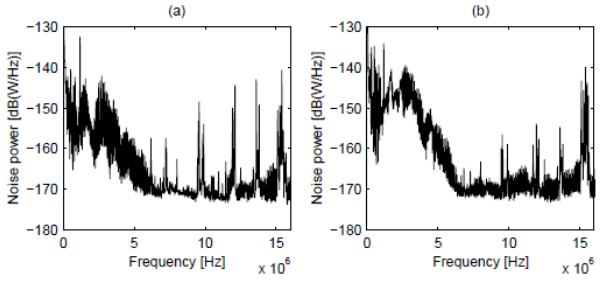

Figure 3. The power spectrum of the noise

IV. CONCLUSION

The results show that 443 and 444 can be considered as having relatively high-quality channels, on the contrary 447

is considered a low-quality channel. The PLC-P system, which is the system observed in that chapter, uses frequencies in the CENELEC A band (9-95 kHz), which is within the frequency band considered here. An objective with these measurements has also been to try to point out which parameters reduce the quality of some channels in the PLC-P system. Note that we do not evaluate PLC-P, but the quality of the channels that is used in the system.

ACKNOWLEDGMENT

This work is supported by State Grid Corporation of China technology project and cstc2016jcyjA0214

REFERENCES

[1] M. Zimmermann and K. Dostert, "A multipath model for the powerline channel," IEEE Trans. Commun., vol. 50, no. 4, pp. 553–559, Apr. 2002.

[2] D. Anastasiadou and T. Antonakopoulos, "Multipath characterization of indoor power-line networks," IEEE Trans. Power Del., vol. 20, no. 1, pp. 90–99, Jan. 2005.

[3] X. Ding and J. Meng, "Channel estimation and simulation of an indoor power-line network via a recursive time-domain solution," IEEE Trans. Power Del., vol. 24, no. 1, pp. 144–152, Jan. 2009.

[4] X. Ding and J. Meng, "Characterization and modeling of indoor powerline communication channels," presented at the 2nd Can. Solar Buildings Conf., Calgary, AB, Canada, Jun. 2007.

[5] J. Anatory, N. Theethayi, and R. Thottappillil, "Channel characterization for indoor power-line networks," IEEE Trans. Power Del., vol. 24, no. 4, pp. 1883–1888, Oct. 2009.

[6] J. Anatory, N. Theethayi, R. Thottappillil, M. Kissaka, and N. Mvungi, "The effects of load impedance, line length, and branches in the bplctransmission-line analysis for indoor voltage channel," IEEE Trans. Power Del., vol. 22, no. 4, pp. 2150–2155, Oct. 2007.

[7] J. Anatory, N. Theethayi, R. Thottappillil, M. Kissaka, and N. Mvungi, "The effects of load impedance, line length, and branches in typical low-voltage channels of the bplc systems of developing countries: Transmission-line analyses," IEEE Trans. Power Del., vol. 24, no. 2, pp. 621–629, Apr. 2009.

[8] H. Meng, S. Chen, Y. Guan, C. Law, P. So, E. Gunawan, and T. Lie, "Modeling of transfer characteristics for the broadband power line communication channel," IEEE Trans. Power Del., vol. 19, no. 3, pp. 1057–1064, Jul. 2004.

[9] S. Galli and T. Banwell, "A novel approach to the modeling of the indoor power line channel—Part II: Transfer function and its properties," IEEE Trans. Power Del., vol. 20, no. 3, pp. 1869–1878, Jul. 2005.

[10] S. Barmada, A. Musolino, and M. Raugi, "Innovative model for timevarying power line communication channel response evaluation," IEEE J. Sel. Areas Commun., vol. 24, no. 7, pp. 1317–1326, Jul. 2006.

[11] D. Sabolic, A. Bazant, and R. Malaric, "Signal propagation modeling in power-line communication networks," IEEE Trans. Power Del., vol. 20, no. 4, pp. 2429–2436, Oct. 2005.

Face Recognition of the Rhinopithecus Roxellana QinlingensisBased on Improved HOG and Sparse Representation

Cuan Ying
School of Computer Science, Xi'an Shiyou University
Xi'an, China
E-mail: ying_cuan@xsyu.edu.cn

Shi Yaojie
School of Computer Science, Xi'an Shiyou University
Xi'an, China
E-mail: 429553101@qq.com

***Abstract*—With the researches on face recognition of Rhinopithecusroxellanaqinlingensis, this thesis comes up with some methods that refining traditional HOG and Sparse Representation in order to improve the efficiency in recognizing golden monkeys. As we know, improved HOG is an optimal way to show partial information of an image. Besides, it can also plays an crucial role in staying stability in both optical and geometric distortion, which means the changes in expressions, postures and angles of golden monkeys can also be ignored. By using these characteristics as a alternation of original images to be a part of Sparse dictionary, and make a facial recognition on golden monkey with Sparse Representation, which can be a ideal method to erase many unnecessary messages and improve the accuracy on facial recognition of golden monkeys. Compared with mainstream method in recognition, this method is more reliable and effective and has a higher efficiency in recognition.**

Keywords-Rhinopithecus roxellana qinlingensis;Face recognition;Histogram of Oriented Gradient;Sparse Dictionary;Sparse Representation

I. INTRODUCTION

The Rhinopithecusroxellanaqinlingensis in the Qinling area is more precious and attracts people's attention [1 ~ 3], which is distributed in the Gansu, Sichuan, Hubei and Shaanxi regions, and is in the endangered state. In the recent years, the study of face recognition has been very mature [4 ~ 8], but, the animal recognition is less [9 ~ 10]. Especially for the monkey face recognition.

This paper presents a hybrid recognition algorithm based on improved histogram of Oriented Gradient (HOG) and sparse representation. The HOG can be used to maintain the invariance of the geometric and optical deformation of the image, and it is modified by the Gaussian smoothing filter and the cubic linear interpolation method [11]. On the other hand, the sparse representation algorithm is used to establish the Qinling Golden Monkey Face Recognition Model.

II. FACE RECOGNITION PROCESS OF THE RHINOPITHECUS ROXELLANA QINLINGENSIS

Golden monkey face recognition system consists of image acquisition, image preprocessing, HOG feature extraction, the classification of the sparse solution for improvement.Using the following steps to describe the specific process:

1) Take picture for the Rhinopithecusroxellanaqinlingensis using high pixel SLR cameras.

2) The golden monkey in the scene image need to denoisingand normalized .Next, we build the database for the Rhinopithecusroxellanaqinlingensis'face though face detection and segmentation.

3) With the Gaussian smoothing filter and the cubic linear interpolation method to improved the HOG, we can setup the characteristics of the samples which is texture feature extraction of golden monkey face.

4) Last,we can use the sparse representation based dictionary to get the recognition results .

A. Face Detection Location of the RhinopithecusRoxellana Qinlingensis

Golden monkey face detection is prerequisite for the identification of golden monkeys. State of the art uses the skin color to the animal face segmentation, skin color with the composition of melanin and saturation looks a bit different, but these differences are concentrated in the brightness, so the brightness of the skin in the analysis of skin plays a significant role [12]. In this paper, through the study of the brightness channel of the golden monkey picture, we found that there is a great difference in brightness between the golden monkey face image and the background of the brightness channel as shown in Fig .1.

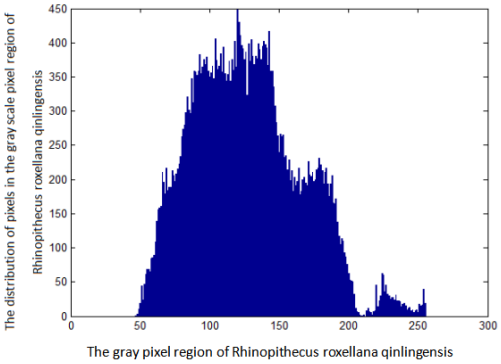

Figure 1. Luminance channel statistics of the Rhinopithecus roxellana qinlingensis

In Fig.1, the background pixels are basically concentrated between 50 ~ 200pix, while the golden monkey face pixels concentrated in the 200 ~ 250pix between. So the golden

monkey image is separated by YUV method [13] in this paper, divided into face and other regions by threshold segmentation. the golden monkey face data is normalize to the $N*N$. Golden monkey face detection are shown in Fig. 2:

(a)The sample images (b)YUV space(c)Face detection positing

Figure 2. Face Detection of the Rhinopithecus roxellana qinlingensis

The data of the correct positioning of the golden monkey face image is defined as a positive sample, others is defined as a negative sample due to the lighting, environment and so on. The result of dividing the positive and negative samples is shown in Fig .3.

(a) Positive samples

(b) Negative samples

Figure 3. Split positive and negative sample results

Remove negative samples and keep positive samples as test image data.

B. Improved HOG Feature Extraction Algorithm

HOG is a local descriptor whose features are the local gradient amplitude and direction.The traditional HOG feature extraction process is described below:

1) First,the gradient of the image abscissa and the ordinate direction is calculated on the local unit of the image. Next,the gradient direction value of each pixel position is calculated.

the gradient of the pixel (x, y) in the image is:

$$\begin{cases} G_x(x,y) = H(x+1,y) - H(x-1,y) \\ G_y(x,y) = H(x,y+1) - H(x,y-1) \end{cases} \tag{1}$$

In the formula(1), $G_x(x,y)$ is the horizontal direction gradient value of the pixel (x, y) in the input image; $G_y(x,y)$ is the vertical direction gradient value; $H(x,y)$ is the pixel values.

Thegradient at the pixel (x, y) amplitude and gradient direction are:

$$\begin{cases} G(x,y) = \sqrt{G_x(x,y)^2 + G_y(x,y)^2} \\ \mathrm{a}(x,y) = \tan^{-1}(\dfrac{G_x(x,y)}{G_y(x,y)}) \end{cases} \tag{2}$$

2) Construct the unit histogram. The target image is divided into small blocks of 16×16 pixels, each of which is called a unit. The gradient histogram of each cell is counted and form a block use each 9 gradient histogram .The gradient histogram of all the blocks is connected to form the HOG character descriptor of the image. As shown in Fig.5 (c), the traditional HOG feature extraction method is unbefitting in the golden monkey image. In this paper, the HOG characteristics of golden monkey were extracted by using the Gaussian smoothing filter and cubic linear interpolation to remove the color or change in the image.

The concrete description is as follows:

$$G(x,y) = \frac{1}{2\pi\sigma^2} \mathbf{e}^{-\frac{x^2+y^2}{2\sigma^2}} \tag{3}$$

x, y is the distance where the current point to the corresponding point. And the Gaussian filter binomial approximation σ, so the minimum variance of the binomial coefficients can be calculated by Gaussian function.

The cubic linear interpolation is used to poll the gradient direction in each cell, and the statistics of the gradient direction in the block are realized[14]. The cubic linear interpolation mathematical description is shown in equation (4):

$$h(x_1,y_1,\theta_1) \leftarrow h(x_1,y_1,\theta_1) + |\nabla f(x,y)|(1-\frac{x-x_1}{dx})$$
$$(1-\frac{y-y_1}{dy})(1-\frac{\theta-\theta_1}{d\theta})$$

$$h(x_1,y_1,\theta_2) \leftarrow h(x_1,y_1,\theta_2) + |\nabla f(x,y)|(1-\frac{x-x_1}{dx})$$
$$(1-\frac{y-y_1}{dy})(\frac{\theta-\theta_1}{d\theta})$$

$$h(x_2,y_1,\theta_1) \leftarrow h(x_2,y_1,\theta_1) + |\nabla f(x,y)|(\frac{x-x_1}{dx})(1-$$
$$\frac{y-y_1}{dy})(1-\frac{\theta-\theta_1}{d\theta})$$

$$h(x_2,y_1,\theta_2) \leftarrow h(x_2,y_1,\theta_2) + |\nabla f(x,y)|(\frac{x-x_1}{dx})(1-$$
$$\frac{y-y_1}{dy})(\frac{\theta-\theta_1}{d\theta})$$

$$h(x_1,y_2,\theta_1) \leftarrow h(x_1,y_2,\theta_1) + |\nabla f(x,y)|(1-\frac{x-x_1}{dx})$$
$$(\frac{y-y_1}{dy})(1-\frac{\theta-\theta_1}{d\theta})$$

$$h(x_1,y_2,\theta_2) \leftarrow h(x_1,y_2,\theta_2) + |\nabla f(x,y)|(1-\frac{x-x_1}{dx})$$
$$(\frac{y-y_1}{dy})(\frac{\theta-\theta_1}{d\theta})$$

$$h(x_2,y_2,\theta_1) \leftarrow h(x_2,y_2,\theta_1)+|\nabla f(x,y)|(\frac{x-x_1}{dx})(\frac{y-y_1}{dy})(1-\frac{\theta-\theta_1}{d\theta})$$

$$h(x_2,y_2,\theta_2) \leftarrow h(x_2,y_2,\theta_2)+|\nabla f(x,y)|(\frac{x-x_1}{dx})(\frac{y-y_1}{dy})(\frac{\theta-\theta_1}{d\theta}) \quad (4)$$

The three parameters of the cubic linear interpolation x,y,θ are the angular space of direction, direction and gradient. As shown in Fig. 4, when voting is done using the gradient amplitude as the weight, the pixel (x,y) is weighted according to the distance of the pixel from the center of the other lattice,as well as,the gradient direction of the pixel (x,y) is also interpolated in its adjacent interval.Improved Hog features of the golden monkey face are shown in Fig .5 (d).

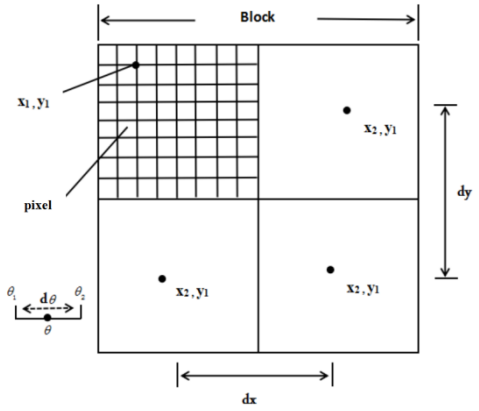

Figure 4. Three linear interpolation schemes of block

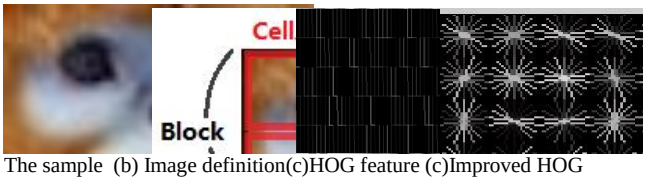

(a) The sample imagesextraction (b) Image definition(c)HOG feature feature extraction (c)Improved HOG extraction

Figure 5. HOG feature extraction

III. FACE RECOGNITION OF THE RHINOPITHECUS ROXELLANA QINLINGENSIS

Signal sparse representation is very important in the signal processing, and represent signals from as many atoms as possible in a given super-complete dictionary, making it easier to obtain information contained in the signal.

In the traditional sparse representation, the original image is input, and dictionary is establish by the sparseness of the image, Finally the images can be classified in the dictionary[15]. However, this simple way to build sparse tables not only contains a lot of redundant useless information, increased computing load, but also can not effectively to use the basic characteristics of the image. In order to solve these problems, this paper presents a hybrid method based on improved HOG and sparse dictionary to identify the golden monkey face. The sparse representation's input is the features by extracting the improved HOG feature of the golden monkey face image and creating a complete dictionary, the monkey face is effectively identified and classified. The specific process is as follows:

$$y = C * x \quad (5)$$

In the formula(5), y is the golden monkey face data information, C is the dictionary, x is the sparse coefficient. The algorithm description process is:

Firstly,We extracts the improved HOG feature in the golden monkey face image to establishment matrix C . Next, we uses the least squares method to perfect the dictionary represented by the matrix linearity [16].

$$C = \begin{bmatrix} a_{11} & a_{12} & a_{13} & \cdots & a_{1n} \\ a_{21} & a_{22} & a_{23} & \cdots & a_{2n} \\ a_{31} & a_{32} & a_{33} & \cdots & a_{3n} \\ \vdots & \vdots & \vdots & \ddots & \vdots \\ a_{m1} & a_{m2} & a_{m3} & \cdots & a_{mn} \end{bmatrix} \quad (6)$$

In the formula(6), m is the golden monkey; n is the HOG feature matrix ; a_{mn} is the Hog feature matrix of the n thphotograph of the m th golden monkey.

Secondly, the linear combination of the base vector is the test picture after pretreatment and feature extraction. A small number of non-zero elements in the sparse coefficient, and the other elements are zero, by this idea we can classify the golden monkey faces. In order to improve the accuracy of sparse solution classification, we can improve the sparse vector solution.

For each type of the golden monkey face,we can extract their HOG feature and define a feature function P to select the corresponding coefficient for the mth class, y is the golden monkey face data information,the non-zero sparse coefficients of the mth class form a new vector $P_m(y_m)$ .With this coefficient, the test sample Z can be reconstructed approximately:

$$Z_m = C * P_m(y_m) \quad (7)$$

Residual δ :

$$\delta = x - Z \quad (8)$$

In the formula(8),the residual δ is the difference value between the calculated value of the original test sample and

the component value of each object corresponding to the test sample.

Finally, calculate the residuals, output the results [17]. In this paper, the smaller the residual, the image sample which is reconstructed using the train sample is more similar to the original test sample,so we classify the two groups(one is test sample,other is train sample) with the least residuals as a class.

IV. ANALYSIS OF RESULTS

The entire experiment are completed on the computer in the frequency of 4 core 1.6GHz, 4G memory, code written in the matlab .

In this experiment, a total of 530 pieces of golden monkey data were collected in this experiment. A total of 504 pieces of golden monkey faces were detected, and 422 of them were positive samples, which obtained the golden monkey face pattern correctly Data, negative samples of 64; did not detect the golden monkey face data images a total of 44. false positive samples of 26(the image of the golden monkey is not facing the front, that means does not contain the golden monkey face image); false negative samples for 18(the golden monkey face image failed to detect). Fig .6 is the ratio of Qinling Golden Monkey face detection.

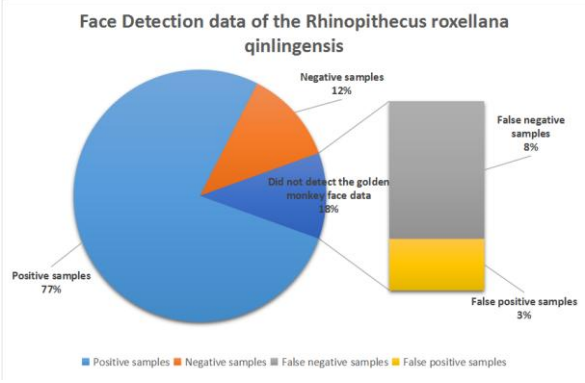

Figure 6. Face Detection data of the Rhinopithecus roxellana qinlingensis

Recall and Precise are two measures that are widely used in the statistical analysis and quality evaluation. From the above data we can see that the recall ratio of this experiment is about 95.91% (the number of positive samples/(the number of positive samples+the number of negative samples)). The accuracy is about 86.83% .

It contains 12 categories in the positive sample images of the golden monkeys, and each golden monkey have 30 images. For the experiment, a part of the images are used to establish sparse dictionary, and the other part of the image is used as test data. The stability test of the method is carried out according to the total data ratio and the recognition accuracy. The results are shown in Fig .(7).

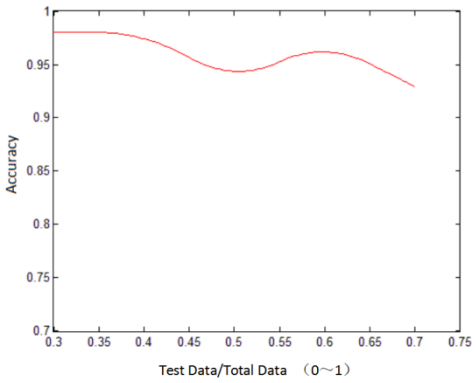

Figure 7. Face recognition stability test of the Rhinopithecusroxellanabase on Improved HOG feature extraction + Sparse Representation

It is found that the accuracy of the method is between 97.22% and 92.86%, which proves that the method has good robustness.

The following two experiments verify the recognition effect of the algorithm. Experiments were made in 70% (252 images)of the sample database for the data dictionary (or training data) ; 30% (108 images)of the image for testing data .

1) The image recognition experiment is carried out with the image sparse representation algorithm combined with different input data. The original image, the HOG feature and the improved HOG feature were used as input data in turn, and the results are shown in Table 1.

TABLE I. COMPARED WITH OTHER MAINSTREAM METHOD OF EXPERIMENTAL RESULTS

Recognition methods	Correctly identify the number of images	Accuracy
The original image+Sparse Representation	70	64.81%
HOG+Sparse Representation	87	80.56%
Improve HOG+Sparse Representation	105	97.22%

2) The image recognition experiment is carried out with the different algorithm combined the improved HOG feature as the input data. The support vector machine (SVM), BP neural network and image sparse representation were used to perform the golden monkey face recognition experiment, the results are shown in Table II.

TABLE II. COMPARED WITH OTHER MAINSTREAM METHOD OF EXPERIMENTAL RESULTS

Recognition methods	Correctly identify the number of images	Accuracy
Improve HOG+SVM	82	75.93%
Improve HOG+BP	61	56.48%
Improve HOG+Sparse Representation	105	97.22%

The results of experiments in Table 1 and Table 2 show that the recognition method based on the improved HOG feature and the sparse representation of the image is better in different input data and different recognition algorithms.

V. CONCLUSION

In this paper, a golden monkey face recognition algorithm is proposed based on an improved HOG feature and image sparse representation, which distinguishes individuals taking advantage of golden monkey images. Meanwhile, a sample library of wild golden monkeys in Qinling Mountains was established. This method is robust to the illumination andpose changes of the tested object. It can not only remove a large amount of redundant information, reduce the recognition speed, improve the accuracy of face recognition effectively, but also has a higher recognition accuracy.

ACKNOWLEDGMENT

China National Nature Science Funds (No.41301480).

REFERENCES

[1] YongYan-ge,LiuSi-yang,ZhangYong-wen.RhinopithecusRoxellana[J].Forest & Humankind,2013(2):40-47.

[2] Wang Xiao-wei,Lv Jiu-quan,Guo Song-tao et al.Foraging biology of the Foraging biology[J].Bulletin of Biology, 2006, 41(3):13-14.

[3] Zhang Peng,Li Bao-guo,.Kazuo WADA et al.Social structure of a group of Sichuan snub-nosed monkeys(Rhinopithecus roxellana)in the Qinling Mountains of China[J].Current Zoology,2003, 49(6):727-735.

[4] Yang S, Luo P, Loy C C, et al. From Facial Parts Responses to Face Detection: A Deep Learning Approach[C]// IEEE International Conference on Computer Vision. IEEE Computer Society, 2015:3676-3684.

[5] Lu J, Liong V E, Zhou J. Simultaneous Local Binary Feature Learning and Encoding for Face Recognition[C]// IEEE International Conference on Computer Vision. 2015:3721-3729.

[6] Huang Z, Wang R, Shan S, et al. Projection Metric Learning on Grassmann Manifold with Application to Video based Face Recognition[J]. 2015:140-149.

[7] Klare B F, Klein B, Taborsky E, et al. Pushing the frontiers of unconstrained face detection and recognition: IARPA Janus Benchmark A[J]. 2015:1931-1939.

[8] Wei Dong-mei,Zhou Wei-dong.Face recognition using collaborative representation with neighbors[J].Journal of Xidian University:Science and Technology,2015,42(3):115-121.

[9] Zeng Chen-ying Research of Image Monitoring and Identification Oriented to Rare Wild Animals Protection[D].Beijing Forestry University,2015.

[10] Xie Su-yi.Research on Pet-Cat Face Detection Algorithm[D].Shanghai Jiaotong University,2015.

[11] Dalal N, Triggs B. Triggs, B.: Histograms of Oriented Gradients for Human Detection. In: CVPR[J]. 2005, 1(12):886-893.

[12] Mao Hui-yun.Feature Analysis and Machine Learning of Facial Beauty Attractiveness[D].South China University of Technology, 2011

[13] Zhao Qian,Zhu Hua-wei,Zeng Zhao-hui,et al.Target Tracking Fusion Algorithm Based on YUV Color Space Characteristic[J].Video Engineering,2013,37(9): 187-191.

[14] Tian Xian-xian,Bao Hong,Xu Cheng.Improved HOG Algorithm of Pedestrian Detection[J].Computer Science, 2014,41(9):320-324.

[15] Cheng Jian,Li Lan,Wang Hai-xu.SAR Target Recognition under the Framework of Sparse Representation[J].Journal of University of Electronic Science and Technology of China,2014(4):524-529.

[16] Zhou Jian-cheng,Zhang Wen-ting.A New Algorithm of Image Super-Resolution Reconstruction Based on MOD Dictionary-Learning.[J]Journal of Graphics,2015(3):402-406.

[17] Zhang Mu-fan.Appliance of Sparse Representation based Face Recognition[D].Nanjing University of Posts and Telecommunications,2014.

Study on Modeling and Simulation of Logistics Sorting System Based on Flexsim

Fan Zhang
Business School,Gannan Normal University
Ganzhou City, Jiangxi Province, China;
Electronic Commerce Research Center, Gannan Normal University,
Ganzhou City, Jiangxi Province, China
E-mail: maggie820812@163.com

Chun Tian
Business School,Gannan Normal University
Ganzhou City, Jiangxi Province, China
E-mail: 25504283@qq.com

***Abstract*—Applying Flexsim system simulation software to build the simulation model of logistics sorting system. Before the introduction of automatic sorting equipment and technology in the sorting system, through the establishment of the Flexsim simulation model to simulate, analyze and evaluate the design scheme.**

Keywords-Sorting system; Flexsim; Simulation

I. INTRODUCTION OF FLEXSIM SYSTEM SIMULATION SOFTWARE

Flexsim system simulation software is a set of processing technology gathering computer three-dimensional image processing technology, simulation technology, artificial intelligence technology, data processing technology as a whole, which can establish object system three-dimensional model in the inner of computer, and then make a variety of system analysis and engineering validation for the model, and ultimately get the optimal design and transformation program. Software provides a wealth of physical units, the establishment of the physical simulation model can be used to show three-dimensional animation, providing an effective means of visualization for planning design or transformation of the logistics center. Because Flexsim provides a realistic graphical animation for displaying a complete operational performance report, and through operation of the model to provide related feedback information of a variety of programs for analyst, so analysts can compare the merits and inferior in a short period of time on the of various programs, to assess various pre-selection programs.

II. DESIGN THOUGHT OF LOGISTICS SORTING SYSTEM

Logistics sorting system is widely used in an automated operating system, directly impacting on the cost, efficiency and quality of service of the entire logistics center. Therefore, to improve the overall efficiency of the logistics center, the design and development of the sorting system is the key. But if the entire logistics center are introduced the automated sorting equipment in one-time, then the beginning of the fixed investment is relatively high, with big capital pressure. In view of this, this article takes express business for example, putting forward this design idea "automatic sorting file class express, manual sorting non-file class express" to ease the introduction of automated sorting equipment in the beginning of the higher investment pressure. The establishment of a sorting system model with Flexsim software allows you to validate the viability of its operational strategy before introducing automated sorting equipment, enabling business decision makers to make a feasibility assessment of the operational plan in a shorter period of time.

III. ESTABLISHING A SORTING SYSTEM MODEL

A. Sorting Process

Based on the above "automatically sorting file type express, manually sorting non-file tyep express" vision, as well as the express sorting process analysis, designing sorting process as shown in Fig. 1:

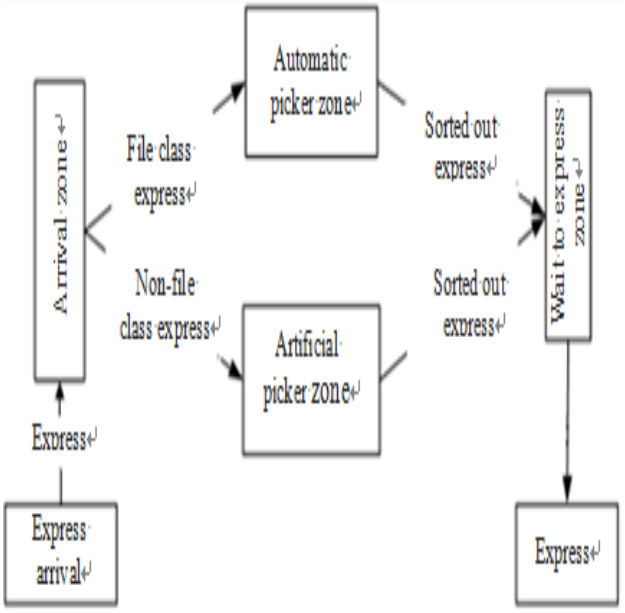

Figure 1. Sorting process

B. In The System Model, The Main Used Entity And Its Role In The Model Shown In Table 1:

TABLE I. MAIN SUBSTANCE DESCRIPTION

Name	Notes
generator	Used to generate express mail
storage cache	Temporary storage of express mail
Conveyor belt	Send express mail
Sorting conveyor belt	Sorting express mail
Operator	Handling, sorting, processing and so on
Resolver	Classification express
Handling machine	Carry sort of good shipment
Absorber	Release temporary entity (express)

C. System-Related Parameters are as Follows:

*1) Express arrival part:*The arrival frequency of the sorting center express (8 hours of peak hours) follows the normal distribution function: normal (0.38,0.1,0) s;

For all express, 60% of them are the file class express, the others are the package or special pieces. The Express category ("File Class Express" or "Non-File Class Express") is subject to the Bernoulli Distribution Function: bernoulli (60,1,2);

Assuming that all the express in the sorting center are sent to 36 large areas and they are random, the target destination of the express is subject to an integer uniform distribution function: duniform (1,36).

2) Automatic sorting part and manual sorting part: The "preset" time of the sorting tray follows the normal distribution function: normal (45,10,0);

Time of Sorting the shipment of the express and packaging obeys the normal distribution function: normal (60,10,0);

Automatic sorting conveyor speed is 1.5 m / s; manual sorting zone conveyor speed is 1 m / s;

The operator's parameters are based on the system default settings.

IV. BUILDING FLEXSIM SIMULATION MODEL

Combined with our established sorting system model and related system parameters, using Flexsim software to design simulation model, sorting system simulation model is shown in Fig. 2:

A. Purchase Area

In the model, the generator area is placed with a generator for generating various categories of "express" (temporary entities) that convey the resulting "express" to the sorting area via the conveyor.

We define the generation model, type, and label of express (Temporary Entity) by system attribute and custom code. The key code is as follows:

(*38, 0.1, 0); / * "Express" arrival time interval is a normal distribution with a mean of 0.38 and a standard deviation is 0.1 *

Setitemtype(item,bernoulli(60,1,2)); / * generated "Express" have 60% chance of being a file class Express * /:

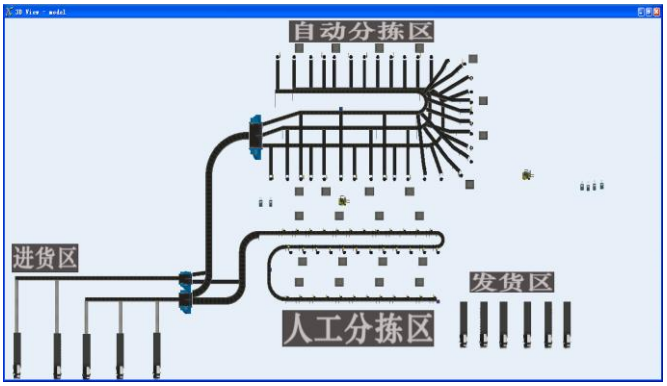

Figure 2. Flexsim 3D simulation model view

B. File Class And Non-File Class Separation

Because this link of the "file class and non-file class separation" are not the focus of this model discussion, so in the process of setting the model we will set this part of the automatic processing, that is, "file class and non-file class separation" is done automatically by the resolver with the following key code:

```
Int value = getitemtype (item);
switch (value) {
case 1: return 1;
case 2: return 2;
default: return 0;
}
```

C. Automatic Sorting Area

There are three main automatic sorting conveyors (automatic picking conveyor 01,02,03) in the automatic sorting area. A total of 36 sorting outlets are set up, which means sorting the express mail sent to 36 different areas.

Resolver temporary entity flow in the auto sorter properties - The key code sent to the port is as follows:

```
Int value = getlabelnum (item, "letters");
Double mod_01 = fmod (value, 3); / * The tag value labeled "letters" is sent to port 1, dividing 3 to modulo, if 1, it is the temporary entity, and 2 for the temporary entity to port 2, It is sent to port 3 for other situations * /
```

D. Manual Sorting Area

The manual sorting area has only one main picking belt, with 36 sorting outlets, which means sorting the shipment to 36 different areas. In the "artificial _ main sort conveyor" sending conditions, preparing the following code:

```
Int port = parval (2);
Int label_value = getlabelnum (item, "no_letters");
Switch (port) {
```

```
Case 1: return label_value == 1; / * means that the temporary entity with the label name "label_value" of 1 is sent to port 1, the following synonyms. * /
... / * here omitted the middle part of the similar code * /
Case 36: return label_value == 36;
Case 37: return 1 == 1;
Case 38: return 1;
Default: return 1; / ** /
}
Return 1;
```

V. Simulation Model Operation and Result Analysis

Carrying out Simulation of the above sorting system, setting the simulation time of 10000s, run the simulation model several times, after each run, it generated the corresponding data, we extracted a sample from a number of data, then do data analysis.

A. The Output Results for Part of the Operation was Shown in Table 2:

TABLE II. Artificial sorting and automatic sorting simulation results

Simulation time	10000s		
Object	Type	Input amount	Output amount
Artificial _ main sort conveyor belt	MergeSort	10097	10002
Artificial error picking	Sink	1234	0
Automatic Pickup Conveyor 01	MergeSort	5249	5237
Automatic Pickup Conveyor 01	MergeSort	5167	5151
Automatic Pickup Conveyor 01	MergeSort	5306	5283
Artificial error picking	Sink	173	0

As shown in the above table, the manual sorting 10002 pieces of express mail in 1000s, the number of wrong picking is 1234, the wrong rate is $\frac{1234}{10002} \approx 12.3\%$, the automatic sorting in 10000s sorting 5237 +5151 + 5283 = 15671 pieces, the number of wrong picking is 173, the wrong rate is $\frac{173}{15671} \approx 1.2\%$. The sorting rate of automatic sorting is 11.1% lower than that of manual sorting, and the accuracy rate is greatly improved. And the wrong picking rate of the entire sorting center is $\frac{1407}{25673} \approx 5.5\%$. Obviously, the overall rate of wrong picking of the sorting center has decreased compared to 12.3% of the total picking rate. Besides, in the same 10000s, the automatic sorting can sort 15,671 pieces, while manual sorting can sort 10002 pieces, the number of automatic sorting is 1.5 times of the number of manual sorting, sorting efficiency has been greatly improved.

B. In the Manual Sorting Area, the Artificial Picker Needs to Identify, Sort and Classify the Express Mail.

In the automatic sorting area, the sorting personnel can only pack the express and the middle links are different, resulting in its showing a different state, the final amount of processing express is also a big difference, the specific situation shown in Table III:

TABLE III. Manual Picker VS Auto Picker Status

Report statue	Artificial picker	Automatic picker
Simulation time	10000s	
idle(free time)	5987s(59.9%)	5734.7s(57.3%)
utilize(working time)	2791.5s(27.9%)	4161.1s(41.6%)
travel_loaded（return）	138.2s(1.4%)	
loading（pick up express）	544.7s(5.4%)	
unloading（place）	296.7s(3%)	

This table reflects the status of the artificial picker and the automatic picker in the set time. The simulation results for artificial picker are: idle (idle time) is 5987s, the proportion is 59.9% (working time) is 2791.5s, the proportion is 27.9%; while the status of the automatic picker is: idle (idle time) is 5734.7s, the proportion is 57.3%, the service time is 4161.1s, the proportion is 41.6% of the total. The date of utilize is different greatly, the reason is that the middle part of the manual selection taking a lot of time, such as travel_loaded (return) need 138.2s, loading (picking up), unloading (placed) 544.7s and 296.7s, respectively. Through the analysis, compared with the artificial picker, automatic sorting staff work less with lower strength.

VI. Conclusion

In the overall planning and design, logistics center is one of the most important part of sorting system design. Application of Flexsim system simulation software can carry out effective simulation analysis before investing and constructing logistics center, analyzing the design deficiencies in order to find a reasonable design strategy will be able to greatly reduce the investment risk, bring more big benefit to the enterprise and the whole society. Flexsim system simulation software has great potential in the sorting system and the auxiliary design research field of the entire logistics center.

References

[1] T.B. Qin. Practical system simulation modeling and analysis - using Flexsim [M]. Beijing: Tsinghua University Press, 2016

[2] F. Zhang, T. Chun. Application of Flexsim System Simulation Software in Sorting System Design [J]. Journal of Gannan Normal University, 2012 (3): 68-71

A Study and Simulation on Thermal Cycling System of CFB Boiler

Yingtao Hou
State Grid Jibei Electric Power Company Limite
Skills Training Center
Baoding Electric Power VOC.& TECH. College
Baoding, China
E-mail: huangt410128@yeah.net

Xiuhua Jiang
State Grid Jibei Electric Power Company Limited
Skills Training Center
Baoding Electric Power VOC.& TECH. College
Baoding, China
E-mail: jiangxiuhua54322@126.com

***Abstract*—Energy is the main resource for our country to survive. However, in recent years, the excessive consumption of energy has made the environment worse and worse, and made the development of our country restricted. Technology of circulating fluid-bed boiler is the main way of general clean coal at present, and is a hot topic for each country in the world. However, the experimental process of the technology often spend a great cost, therefore is not suitable in practice. So simulation technology of circulating fluid-bed was used in this paper to solve practical problems. This paper established a circulating fluid-bed (CFB) boiler simulation system based on XinXiang HG-440 CFB, and analyzed final simulation system. Simulation process from thermal efficiency to thermal energy transformation were researched based on rules of thermal cycling and outlet of improving thermal energy utilization.This technology can not only improved the efficiency of energy, but also effectively reduced the energy generated in the process of burning gas pollution. Moreover, it has played an important role in China's energy construction.**

Keywords-Thermal cycling; Heat transfer model; Thermal energy utilization; Cyclone separator; CFB boiler.

I. INTRODUCTION

China is a great energy power in the world. It would be not easy for China to develop its economy in a high speed without the support of energy. Energy is the base for economic growth. However recent years resulting from over-expanding coal and other energy environment in China gets worse and worse day by day, which greatly threatens sustainable development. In order to efficiently guarantee sustainable development of environment coordinated development of energy production clean coal technology comes into being consequently. This kind of technology not only improves the efficiency of energy, but also efficiently decreases inventory of total polluted gases produced in the process of energy combustion. As the main technology gets to hot topic in the world CFB technology gets to hot topic in the world. Nevertheless objective experiment of CFB technology often costs too much, which is unfit to process in practice. Therefore CFB simulation takes great advantage in the field[1-2].

XinXiang HG-440 CFB boiler is the simulation object in this paper. This kind of boiler is produced by Harbin boiler factory integrating German ALSTOM company's EVT technology. It can further optimize coal clean on the condition of high temperature and high pressure. Besides it, this kind of boiler is widely used in daily life and produces more varied types of CFB boilers, such as HG-440 which is a representative figure.

II. THERMAL MODEL OF CFB BOILER

In the combustion process of CFB boiler qualities of its intrinsic energy and power energy produces both observe law of conservation of mass. So mathematical model of CFB boiler which has been established includes all kinds of energy conservation, such as solid and gas. Mass conservation of energy becomes the base to build boiler model. Mathematical model of CFB boiler consists in various sub-models. Analyzing of sub-models is as following.

A. Boiler Components Model

The most important part in designing CFB boiler is to design separating device. In practical working cyclone separator is the most common separating device. When cyclone separator works, energy stream of gas and solid in its inner part is an extremely complex and magnified process. In order to easily express it this paper assumes： when energy existing as gas exercises in separator its trajectory could be seen as the same area among slug stream along with gas energy and cross selection of separator entrance ignoring coal particle's vertical disintegrating in the process of rotating with gas, namely it only happens at the bottom of gas stream in the process of vertical disintegrating. In addition, in this assumption it should also ignore slip velocity and other shear forcing to gas and solid, which' s only considered to cross section area of separator entrance. Through simplifying practical condition material balance of coal particles in separator can be gained as following:

$$\frac{d(VpiCi)}{dI} = Dspi\frac{d2Ci}{dI2} + Gspi \tag{1}$$

Among them Ci stands for permeation flux of coal particles i; Vpi stands for the velocity of coal particles; Dspi stands for vertical disintegration models of coal particles; Gspi stands for the production rate of coal particles; I stands for the height when gas spires along separator.

B. Combustion Model of Coal Particles

Combustion of coal particles is a complex process which constantly happens chemical change energy change,

especially in CFB boiler. In order to have a better research the combustion process coal particles into CFN boiler can be summarized as: particles go into the inner part of CFB boiler, then dry coal particles, further exhaust all kind of volatile compounds in coal particles, moreover combustion coal particles, finally process post-combustion of rest coal particles[3].

In order to explain coal particles in the process of its its combustion assumption is needed: carbon monoxide and carbon dioxide both belong to production of primary combustion in the process of coal particles' combustion. Carbon monoxide will stay in the furnace in primary combustion. As for different ash coal particles, they can be generally divided into three types: high ash particles, low ash particles and aerosol coal particles. They exist in the forms of double-retract, retract and none- retract in combustion.

In the process of coal particle combustion, in order to explain the gas coming during combustion in CFB boiler, an assumption is needed: as for different volatile contents in coal particles combustion, it only needs to be represented as one volatile content; Chemical reaction among varied gases is only controlled by dynamic stress in furnace, then calculation formula for coal particles firing in CFB boiler can be gained as:

$$Ks = \frac{Fs \cdot CO_2, \infty}{\frac{1}{Kc} + \frac{1}{\beta_0} \cdot \left(\frac{R}{R_1} \right)^2 + \frac{R}{R_1} \cdot \frac{\delta}{D_K}} \tag{2}$$

Among them, Fs stands for ratio between carbon content and oxygen content in coal particles' overall reaction; CO2 and ∞ stand for oxygen concentration in pretty far area; K3 stands for carbon combustion rate in coal particles; R stands for radius of coal particles; R1 stands for radius of coal particles post- combustion; δ stands for ash thickness of coal particles; Kc stands for chemical reaction's rate in coal particles combustion; $\beta 0$ stands for quality motion modules when fluid and furnace happens in coal particles combustion; Dx stands for oxygen diffusion coefficient[4-5].

C. Thermal Model of CFB Boiler

CFB boiler is affected by furnace heating surface area thermal conductivity, material of furnace heating surface, and shape of furnace heating surface in combustion. At the same time it relates to flow velocity of coal particles in furnace, density of coal particles and size of coal particles. Compared with data collected from practical life data through calculating furnace heating surface modules in combustion, range of error within $\pm 5\%$. As a result, it's relatively reasonable to apply CFB in practical life. So this kind of heat transfer in furnace has been successfully applied to practical production[6].

Heat transfer between fluidized bed and furnace internal wall processes through spiral gas in fluidized bed and impure coal particles together with energy transfer in furnace internal wall. Energy exchange can be divided into convection and scattering after the mixture of gas and material in furnace internal wall. Thereby, total energy of heat transfer in CFB and linear sum of convection and scattering can be represented as:

$$\begin{cases} \gamma_b = \gamma_r + \gamma_c \\ \gamma_r = \varepsilon\sigma(T_b + T_w) \cdot (T_b^{\,2} + T_w^{\,2}) \\ \gamma_c = \gamma_{gc} + \gamma_{pc} \end{cases} \tag{3}$$

Among them γ_r stands for scattering heat transfer modules of coal particles; γ_c stands for convection heat transfer modules; ε stands for system emissivity of fluidized bed and furnace internal wall; σ stands for Boltzmann costant; γ_{gc} stands for smoke convection energy transfer modules after coal particles combustion; γ_{pc} stands for convection energy transfer modules in coal particles combustion.

III. Analysis of CFB Combustion System Module

A. Mass Balance of Gas and Solid Energy

In interior combustion system gas would not disappear assuming its interior part is tight. Value for energy transfer is the sum of convection and scattering energy in steady CFB interior combustion system.

The detailed information of configuration and operation procedures for the 30 kW CFB combustor had been reported in previous publications elsewhere as shown in Fig .1.

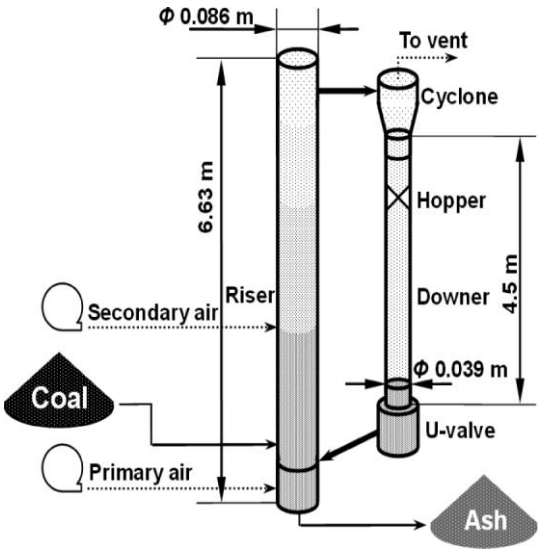

Figure 1. Schematic illustration of a 30 kW circulating fluidized bed combustor

B. Simulation of CFB Combustion System

This paper simulates the effect of different air concentration having on CFB combustion., CFB furnace

combustion ares and CFB furnace separator in CFB combustion by designing HG-440 model, through which CFB combustion can be clearly and straightly observed and it contributes to promoting CFB simulation research.

The calculated voidage profile along the CFB riser height in the 30 kW CFB combustor is illustrated in Fig. 2. The voidage in turbulent region 1 is considered as the same as that in turbulent region 2, and the average voidage in acceleration region 3,acceleration region 4, and completely fluidized region 5 is assigned to be equal to that at an appropriate height hi (i= 3, 4, 5) in each region, respectively.The constructed flow sheet of CFB coal combustion process is illustrated in Fig. 3.based on Aspen Plus.

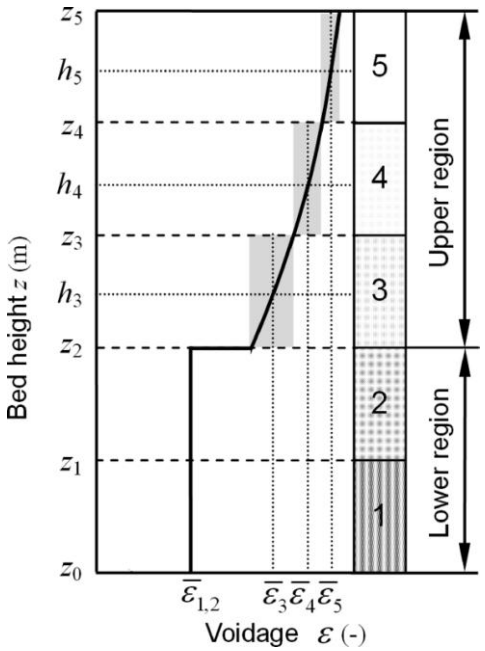

Figure 2. Schematic illustration of relationship between voidage and height in five different subunits along CFB riser height in a 30 kW CFB combustor.

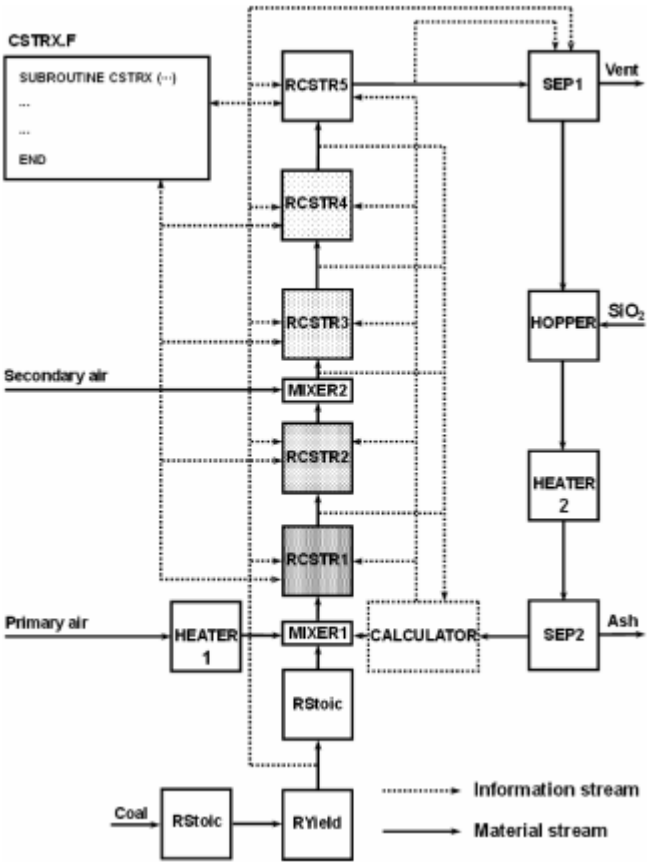

Figure 3. Constructed flow sheet of CFB coal combustion process based on Aspen Plus.

The thermal cycling test parameters were shown in table I.

TABLE I. INITIAL VALUES OF RELATED PARAMETERS IN EACH MODULE FOR SIMULATION OF CFB COAL COMBUSTION BY ASPEN PLUS

upper cycling temperature	temperature changing rates (℃/min)	cycle times
200	5	1
200	5	3
200	5	6
200	5	9

IV. THERMAL CYCLING BEHAVIORS

A. Thermal Cycling Curves

The shapes and sizes of the hysteresis loop and the dimensional stability of materials had a direct relationship. The dimensional stability of the material became better when the hysteresis loop was narrow and the area was large; By contrast, the dimensional stability became worse when the hysteresis loop was wide and the area was large during deformation.The diagrams of the relatively linear length variations versus times were shown in Fig. 4. The obvious serrated phenomenon did not see from Fig. 4. The net change in size almost maintained a certain amount after the thermal

cycling. It was indicated that the symmetry of stress relaxation was very good in the thermal cycle process.

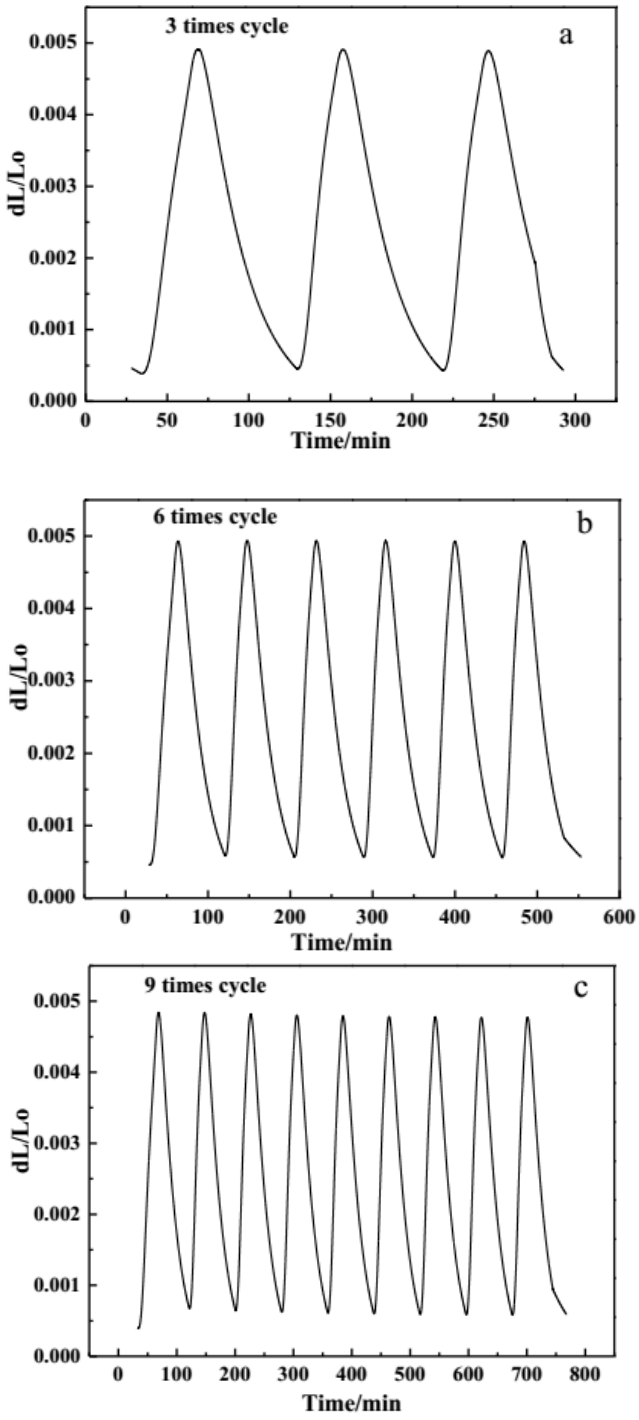

Figure 4. The diagrams of the relatively linear length variations versus times:(a) 3 Thermal cycles (b) 6 Thermal cycles (c) 9 Thermal cycles

The above curves of the relatively linear length variation versus time were converted into the relatively linear length variation versus temperature in order to make it easier to analyze.

The warming and cooling stages during the thermal cycling were distinguished by NETZSCH Proteus Thermal Analysis software and shown in Fig. 5. From Fig. 5 it can be observed that the relatively linear length variations of the warming stage were smaller than the cooling stage.

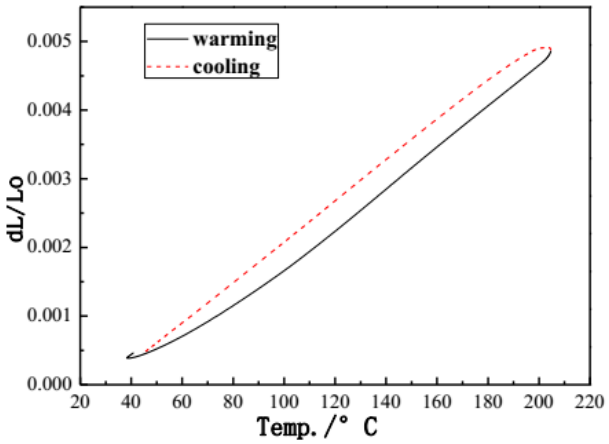

Figure 5. The diagram of the thermal cycling process

B. *The Coefficient of Thermal Expansion*

The CTE-T curves of the 1st, 3rd, 6th warming stages were shown in Fig. 6. It can be seen that the coefficient of the thermal expansion during the first warming stage was significantly larger than the later several warming stages, and the coefficient of the expansion during the later warming stages were basically the same as. This explains the reason that the hysteresis loops of the first warming stage is higher than that of the later warming stages.

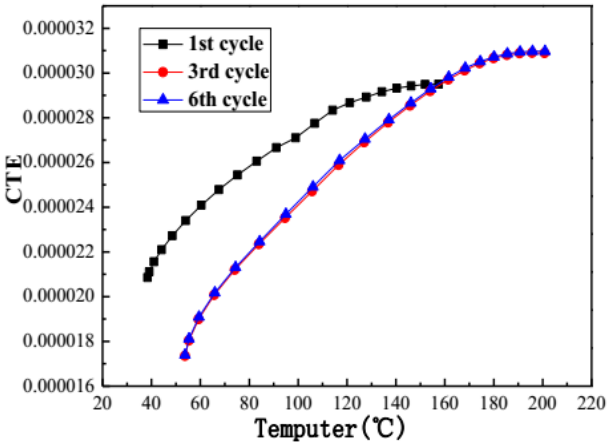

Figure 6. Curve coefficient of thermal expansion

V. CONCLUSION

As a kind of low energy consumption and low coal consumption technology which rises rapidly in recent years, CFB has been widely used in heavy industry, such as electric power industry and thermal power industry, and made great progress because of its unique advantage. This paper aims to implant new thoughts in designing simulation through

analyzing and designing the model in CFB combustion as well as simulating CFB combustion process.

REFERENCES

[1] S. Kumar, A. K. Mondal, H.Dieringa and K. Kainer, "Analysing hysteresis and residual strains in thermal cycling curves of short fibre reinforced Mg-MMCs,"Composites Science and Technology,vol.64 ,pp.1179-1189,2014.

[2] Wang Jinhui, Duo Jun and Ding Yanlin, "Thermal cycling behavior of Mg-4%Sn-2.5%Pb alloy," Journal of Residuals Science & Technology, vol.14,pp.420-425,2017.

[3] T.W.Clyne and W.J.Withers, Introduction Metal Matrix Composite. Beijing: Metallurgic Industry Press, 2016.

[4] Bing Liu,Xuemin Yang,Wenli Song and Weigang Lin, "Process simulation development of coal combustion in a circulating fluidized bed combustor based on aspen plus,"Energy & Fuels,vol.25,pp.1721-1730,2015.

[5] J Pan ,G Wu and D Yang, "Thermal-hydraulic calculation and analysis on water wall system of 600MW supercritical CFB boiler,"Applied Thermal Engineering, vol.82,pp.225-236,2015.

[6] S.Y.Chang, SJ. Flemings, M.C Lin, "Thermal expansion behavior of silver matrix composites,"Metallurgical and Materials Transactions A, vol.31,pp.291-298,2014.

[7] P.L.Wu,L.D. Wang,W.D. Fei, "Interfacial reaction in Al matrix composites reinforced by Mg borate whisker," Materials Science Forum, vol.33,pp.643-648,2016.

[8] Rong Zhou,Thermal Cycling System.Beijing: Electronic Industry Press, 2015.

[9] J Pettersson, C Pettersson and N Folkeson, "The influence of sulfur additions on the corrosive environments in a waste-fired CFB boiler,"Materials Science Forum,vol.55,pp.563-570,2016.

[10] J Pan ,D Yang and G Chen, "Thermal-hydraulic analysis of a 600MW supercritical CFB boiler with low mass flux,"Applied Thermal Engineering, vol.32,pp.41-48,2014.

Fine-grained Access Control Scheme Based on Cloud Storage

Xiaojie Niu
Deptment of IT Services,
Computer Application Institute of Nuclear Industry
Beijing,China
E-Mail:shybull@163.com

***Abstract*—Cloud storage originates from cloud computing, and brings new model of data sharing and storage, which provided great convenience for users. However, cloud environment confronts with many problems, and one of the most important problems is the security problem. This paper researched on security problem based on encryption, and proposed a secure and efficient scheme according to system characteristics of data storage on cloud platform, and applied it in cloud storage system with fine-grained access control based on CP-ABE. Through the analysis and comparison, the experimental results showed that the proposed scheme optimized the user revocation, reduced the time of data owner to manage data, and realized the safe sharing and efficient storage of sensitive data in the public cloud storage. Finally, the technology in this paper was an optimization both on security and the whole expense, and it must have a good prospect in the future.**

Keywords-access control; cloud computing; attribute encryption algorithm; CP-ABE encryption; cloud storage.

I. INTRODUCTION

According to the security problem of cloud storage, users need to encrypt data, and in the cloud storage system to achieve access control. In the current storage system, security and performance are always opposite. When the introduction of security means that will spend more time. However, you can make a balance between the security of the system and the overall overhead by reducing the storage space. So this paper proposes a cloud storage system with high efficient user revocation based on CP-ABE[1].

In the 90s of last century, the network as a novel and convenient information media, gradually being recognized. People realize that it has a huge scale of computing resources, fascinated by its huge application prospects, and to study how to use these resources efficiently and easily. With the popularization and application of cloud computing technology, people have the ability to use large-scale distributed computing resources in the network. Cloud computing as a hot topic of research and application in recent years, most IT companies and industry insiders believe that the next generation of computer network application technology core architecture. Under the cloud computing environment, users do not have to spend the high cost of hardware and software to powerful computing resources and huge storage capacity, all of which can be handed over to the cloud computing service providers to complete. Not only saves the cost, but also does not need to expend the massive energy.The threat of network security is increasing, the network has a strong dependence on cloud computing is inevitable in the application process there are many security risks. In the traditional IT service solution, the vast majority of application software and data information is running or stored in the user's local physical equipment, in the user's absolute controllable range [2].

II. CP-ABE ALGORITHM AND SECRET SHARING SCHEME

A. CP-ABE Algorithm

Goyal et al.[3] proposed a new method of Attribute-Based Encryption (ABE) algorithm, which is a new method of access control under the condition of encryption. Later, ABE is divided into key policy attribute based encryption and CP-ABE. In the KP-ABE system, the access policy is made by DU. On the contrary, in the CP-ABE system, the access policy is formulated by DO, so the CP-ABE algorithm is more suitable for application in access control applications.

CP-ABE algorithm mainly includes the following four steps:

Step1 Generate a main (Key, MK) and public key PK.

Step2 C = Encrypt (PK, F, T): the data F using PK and access structure tree T encryption to get the cipher text C.

Step3 SK = Gen Key (MK, S): enter the main key MK and the property set S, the output of a private key (Key Secret, SK).

Step4 Decrypt (C, SK): as long as the SK contains the attribute set S to meet the access structure tree T, you can decrypt the encrypted C SK data obtained by F; otherwise into Step2.

B. Secret Sharing Scheme

Secret sharing scheme, also called (k, n) threshold scheme. As follows the secret s is divided into n blocks, S1,S2,…,Sn:Knowing any k or more Si data blocks, S can be easily calculated;Know any k - 1 or less Si data blocks, it is completely unable to get S.

This paper will use a method called All-Or-Nothing Transform-reed Solomon,AONT-RS. This method is to use All-Or-Nothing Transform,AONT to process before using Information Dispersal Algorithm to divide the data. The AONT scheme can be seen as a (n + 1, n + 1) threshold scheme, a document encoding divided into n + 1, can guarantee any number of slice less than the threshold will not able to decrypt data. IDA algorithm is a data slicing

algorithm, similar to the same SSS configuring a threshold, but the results of the slice will not increase with the factor. For example, the threshold scheme is (10, 15), then the total slice size is (15 /10) times as much as the original data[4].The related formulas are as follows,

$$f(x) = W_u \frac{r^3 \tan^3 \delta_0 \cos \delta_0}{\pi} x(\sin \delta_0 \cos \delta_0 + \frac{\pi}{2}) - \delta_0 (x2 + r^2 \tan^2 \delta_0)^2 \quad (1)$$

$$f(x) = W_0 \frac{3r^2}{\pi}(1 - \frac{x^2}{r^2}) \quad (2)$$

$$f(x) = W_0 \frac{2}{\sqrt{\pi^3} rx} e^{-4\frac{x^2}{r^2}}, n = 1 \quad (3)$$

$$f(x) = W_0 \frac{0.216x}{r} e^{-4\frac{x^6}{r^6}}, n = 3 \quad (4)$$

$$f(x) = W_0 \frac{2}{r^2} e^{-2\pi\frac{x^2}{r^2}}, n = 1 \quad (5)$$

$$f(x) = W_0 \frac{2}{r^2} e^{-2\pi\frac{x^2}{r^2}}, n = 2 \quad (6)$$

III. SECURE AND EFFICIENT CLOUD STORAGE SYSTEM FRAMEWORK

The secure and efficient cloud storage system is proposed in this paper, which is based on CP-ABE, and the AONT-RS scheme is used to optimize the performance. The framework of the cloud storage system is shown in Figure 1, where there are three participants: data owners, data users, and CSP. The main process of the system can be divided into three stages: data publishing, data retrieval and user revocation.

At the beginning of the data release phase, DO runs the Setup algorithm to generate public key PK and a master key MK. Then running the Key Gen algorithm to get the private key SK of each DU, and then SK send to DU through a secure channel. As the analysis in the introduction, the program needs to divide the original data F (assuming that the data F contains T words, each word has w bit) into pieces. Therefore DO will run the data slice (Splitting Data, DS) algorithm to segment the data. The corresponding algorithm is shown in algorithm 1. In this algorithm, the original data F first through the AONT method will code the original t into t + 1 words, of which the t + 1 word and CT+1 was used to check the integrity of the reconstructed data. The generated key K1 is used to reconstruct the phase, and is encrypted by the CP-ABE algorithm during the data release phase. And then through the (k, n) IDA algorithm will handle the data into n slices. Through Data Publishing, the data will be issued by DU to cloud random selection of N - (k - 1) a slice encryption, such unauthorized Du cannot recover the data through the rest of the (k - 1) slice, also in the cloud saving a copy of the data[4].

At present, although the cloud computing service providers through stable high-speed Internet connection allows users to access remote data storage, convenient and efficient access to services, but because of the cloud computing has virtual, large-scale, dynamic configuration and scalability and other characteristics, and has brought many security risks and challenges for the calculation of large-scale data storage service environment under the cloud. In order to improve the utilization rate of the storage efficiency and storage space, large data files are usually stored in the cloud computing service providers is split into a plurality of small blocks of data, location and storage of each data block of the user state is unknown, the user may doubt the integrity and consistency of your data file. As a key index to measure the data storage service, how to ensure the integrity and consistency of user data files stored in the geographic unknown huge server in the cluster, has always been a major problem in cloud computing and data storage services are facing. Especially after the Amazon Simple Storage Service and Google Docs service interruption and other accidents have occurred, users of cloud computing service providers is to save resources and reduce the cost of concealing safety accidents more had a great distrust. Users want to have a complete set of mechanisms so that they do not spend too much computing resources and time under the premise of a data file integrity and consistency of the ability to review. Related research has been carried out a long time ago, and has achieved good results in the design of efficiency, verifiability, query and recovery. Currently, there are two common solutions for data integrity and consistency: private audit and open audit. Private audit as the name implies is the users own commitment to the data file audit work, public audit is the audit trusted third party audit institutions to complete. Although the private audit because of its simple logic has higher efficiency of auditing, but public audit can not only provide safe and reliable data for the user, but also to a large extent for the user to save a lot of computing resources and time. In the cloud computing environment, users are unlikely to have a lot of time and energy to carry out frequent audit work on their own data files, will this time-consuming task by having reliable and complete audit protocol to solve the trusted third party audit plan to complete can be said to be a very good choice. Data storage research attention verification in terms of long ago already by the industry, the solution proposed by scholars in efficiency, verifiability, query and recoverability etc. also have achieved certain results. Unfortunately, most scholars' research is limited to the operation of static data files, many research results cannot meet the dynamic operation of data files frequently. The following will be scholars before the relevant research results are summarized. Based on the previous research results, this paper solves the verification problem of user data file integrity and consistency in cloud computing environment by using special tree structure of Merkle Hash Tree. Not only effectively support cloud computing basic data dynamic operation of all environments (including data add, delete and modify etc.), also give full consideration to the storage of data in a distributed environment the geographical location of influence on the

computational efficiency, the validation of the Merkle Hash based on Tree to make a certain contribution [5].

A. *Safety Assumption*

The scheme assumes that all communication channels do not exist in the case of large packet loss (communication channels include between USER and CDC, between CDC and TPA and between three parts of TPA and USER). At the same time, the TPA in the program is unbiased, fully trusted third party audit institutions, able to faithfully complete all tasks entrusted by USER. The security assumption of CDC in the scheme is slightly different from previous research, CDC is no longer completely non trust, but has a certain curiosity but can faithfully complete all tasks. CDC ensures that all parameters of their commitment to the correctness of calculation, no deceptive and non-repudiation, and unconditional response at any time for any user data file audit request. After all user data files are pretreated, there is no possibility of mutual interference between data blocks. In addition, the focus of the scheme is how to support the integrity and consistency verification of user data files stored in CDC and dynamic operation of data. Therefore, other securities issues such as user access control, data file recovery and so on are not within the scope of this chapter, this section will not be described in detail. Before the file is processed, USER will forward the data file storage request to CDC. CDC authentication of USER in accordance with its predefined access control rules. CDC authentication by legitimate users will get permission to file storage. In order to location only a block of data, for added position label to a size of 5 bytes for each data block (LTag), which is composed of a machine frame tag tag information sequence marking information, 2 bytes of the 1 byte and 2 byte node tag information composition. Sequence tag information record is the data blocks in all data blocks in the order number, frame marker information recording is the specific piece of data is stored in the data center frame number, node number specific server node tag information indicating the data block storage [6]. CDC maintains a LTag tag list for each data file, recording the LTag tag information for all data blocks of the file. File block sketch map shown in Fig.1.

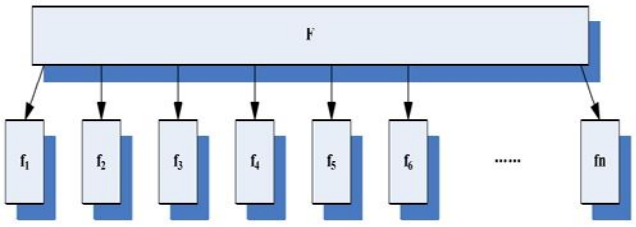

Figure 1. File block diagram

B. *Verification of Data Files*

In the process of file preprocessing, the Merkle Hash Tree of nodes, racks and files are constructed, and their corresponding root node values are calculated. All root node values will be the primary validation information for the solution. Program provides that the data file all validation information will not only be saved in CDC, but also in TPA backup. CDC is responsible for the latest authentication information to update the data file in real time through the communication network with TPA so that TPA can complete the data integrity and consistency verification of USER delegation. The program provides TPA file Merkle Hash Tree to the root node update data file with the latest LTag list information, stored data files of all the nodes Merkle Hash Tree root node value, the stored data files of all Merkle Hash Tree frame the root node value and the value of the stored data file. In addition, TPA clearly generates rules and methods for all validation information in a data file. First, CDC completes the USER data file storage, and submits to TPA the relevant verification data stored by USER. Data files before being deleted by USER, as long as the changes have occurred, CDC will be responsible for the data file to generate the latest validation information, and real-time updates with TPA. Then, CDC notification USER data file storage and verification information generation work has been completed, and told USER can begin to entrust TPA data file integrity and consistency of the verification. USER can choose immediately or try other time to communicate with the TPA, to entrust TPA to verify the integrity and consistency of data files. TPA from USER in the Audit Commission after the request, will carry out audit verification regularly or irregularly on the data file according to the requirement of USER, and all the audit operations retain verification log for USER days after the inspection. In the verification process, if the data file authentication fails, TPA will inform the USER by e-mail or SMS and other communications, while requiring CDC to recover data files and other remedies. Cloud computing environment, most of the data files carried out frequently three basic dynamic operations are: data insertion, data modification and data deletion. In this scheme, after the three dynamic operations of the data file, all the verification information related to the data file must be re generated by CDC.

IV. EXPERIMENTAL RESULTS

The encryption algorithm based on attribute by adding the user identity attribute description, use and gate, or gate and gate contains threshold function as constraint condition, significantly improve the ability of sharing data file, the system in a distributed environment, access control efficiency is better than the traditional use of unique identity label identity based encryption algorithm is very suitable. In the cloud computing environment data file sharing rate is very high. To research attention access control scheme in long before there has been the application of encryption algorithm based on attribute, the solution proposed by scholars in the permission revocation, threshold function support and proxy re encryption and other aspects also have achieved certain results. Unfortunately, most of the scholars of the research content are limited to the use of encryption algorithm based on attribute to solve the control problems of the traditional computing model in which access, most research are not able to meet the application requirements in cloud computing environment. The following first of

scholars before the relevant research results are summarized. The scheme assumes that all communication channels do not exist in the case of malicious packet loss . At the same time, the TPA in the program is unbiased, completely trusted third party audit institutions, able to faithfully complete all tasks entrusted by USER. The CDC in this paper is slightly different from the CDC in the previous scheme, although the CDC in the scheme has the curiosity, but can faithfully complete the task, no longer completely unreliable. All parameters of the CDC calculation, and bear the encryption key generation and distribution of work tasks, can guarantee the absolute correctness, no deceptive and non-repudiation. CDC can unconditionally respond to any USER file access request issued at any time, and strictly comply with the protocol formulated by the protocol key generation, change and distribution work. In addition, TPA can update real-time CDC access control and file information, CDC supervision. Cloud computing data storage security architecture, creative trusted third party audit agency into cloud computing access control operations. Therefore, the access control operation of the data file is slightly different from the traditional access control strategy. The program provides has write permissions for USER as long as the data file is modified, all have the data file access to the private key of the USER Merkle Hash Tree will file with the root node value change and failure, all USER access control permissions will be granted. When the USER key is proposed using failure data file access request, CDC will request to TPA for processing TPA, after confirming the identity of the USER, according to new data file access control permissions for the re issuance of private key operations. If USER still has access to the data files, then TPA will release a new private key for USER, so that USER can operate the corresponding data file; otherwise, TPA USER refused to file access request [10].

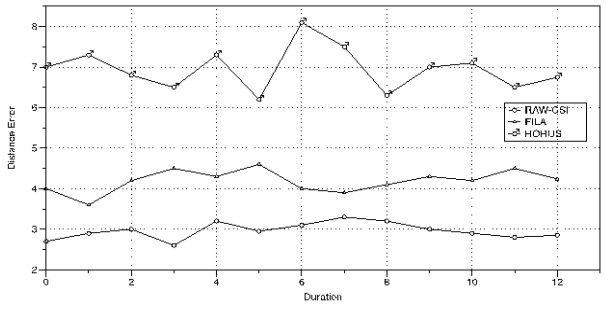

Figure 2. Mean Errors

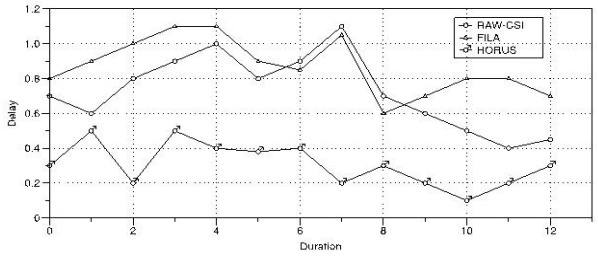

Figure 3. Mean Delays

Fig. 2 shows the comparison result among the three algorithms, RAW-CSI, HORUS and FILA. Apparently, in Fig. 2, RAW-CSI and FILA, both based on CSI, are superior to RSSI-as-fingerprint HROUS. Meanwhile, as shown in Fig.3, compared with FILA, because of the simplicity of RAW-CSI, its positioning delay is similar as FILA. i.e., RAW-CSI can reach a higher positioning accuracy than FILA without the breakdown of computing complication and positioning delay.

V. CONCLUSION

A secure and efficient cloud storage system is proposed in this paper. This system is an access control system based on CP-ABE, and puts forward a high efficient storage scheme based on data sharing and secret sharing, while only keeping a copy of the data. This scheme can significantly reduce the workload of DO and the storage space overhead of CSP, which can effectively promote the use of cryptography in the cloud storage system. At the same time, the security analysis proves that the system is safe. From the theoretical analysis and the actual test results, it can be seen that SECSS in the user revocation and storage space overhead is more efficient than OSCSS. Therefore, in the case where frequent and large amount of data is revoked, CSP and DO will benefit from that. Overall, the optimization scheme of this paper is to make an optimal balance between the system security and the overall overhead.

REFERENCES

[1] Kelejian H H and Prucha I R,“Estimation of simultaneous systems of spatially interrelated cross sectional equations,”Journal of Econometrics, vol.118, pp.27-50, Jul. 2014.

[2] Gebremariam G H, Gebremedhin T G and Schaeffer P V,“A simultaneous spatial panel data model of regional growth variation: An empirical analysis of employment, income, migration and local public services,”Computer Knowledge & Technology, vol.21, pp.34-38, Apr. 2015.

[3] Guangnan Zhang, Computer Technology.Beijing: Metallurgic Industry Press, 2016.

[4] Gebremariam G H, Gebremedhin T G, and Schaeffer P V,“Employment, income, migration and public services: A simultaneous spatial panel data model of regional growth,”Papers in Regional Science, vol.91, pp.275–297, Jun. 2014.

[5] Cherubini U, Mulinacci S and Gobbi F. Dynamic Copula Methods Infinance,New York:John Wiley & Sons, 2015.

[6] Fantazzini D. ,“Dynamic Copula Modelling for Value at Risk,” Frontiers in Finance & Economics, vol.45, pp.45-49, Jun. 2015.

[7] Patton A J. ,“Modeling Asymmetric Exchange Rate Dependence,” International economic review, vol. 34, pp.80 -85, Jul. 2014.

[8] Nelsen R B. An Introduction to Copulas.Springer,2014.

[9] Chu Wenkui and zhang Fengming,“Based on the military software security problems of the COTS study,”Journal of Systems Engineering and Electronics, vol. 3, pp.2166-2170, Aug. 2014.

[10] Tu Gang, zhang bo and Yang Fumin,“The research of embedded operating system transplant technology,”Computer application research, vol. 56, pp.83-85, Dec. 2014.